GEOPHYSICAL MONOGRAPH SERIES

AGU
ADVANCING EARTH AND SPACE SCIENCE

Hydrogeology, Chemical Weathering, and Soil Formation

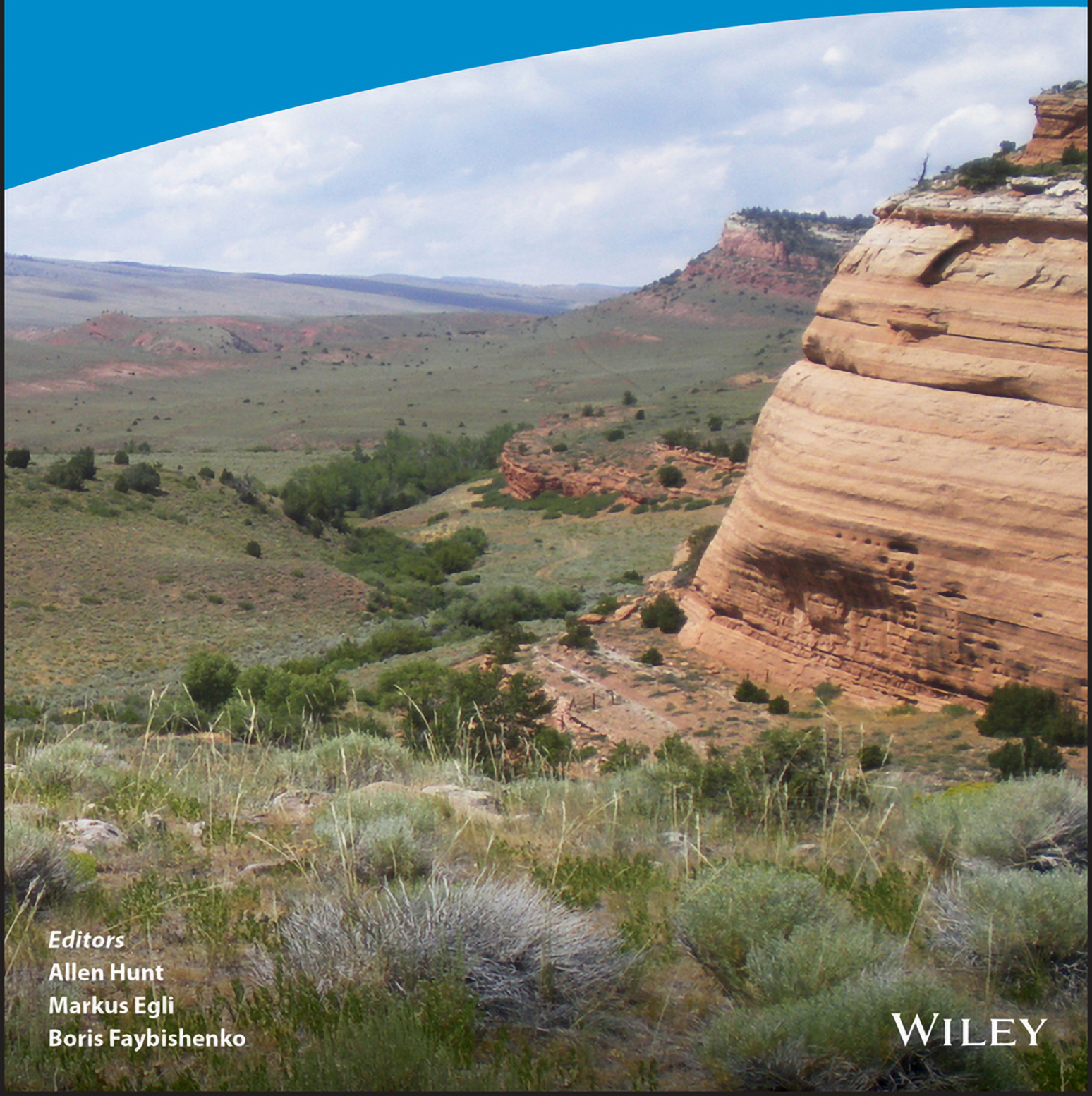

Editors
Allen Hunt
Markus Egli
Boris Faybishenko

WILEY

Geophysical Monograph Series

206 **Remote Sensing of the Terrestrial Water Cycle** *Venkat Lakshmi (Ed.)*
207 **Magnetotails in the Solar System** *Andreas Keiling, Caitriona Jackman, and Peter Delamere (Eds.)*
208 **Hawaiian Volcanoes: From Source to Surface Rebecca** *Carey, Valerie Cayol, Michael Poland, and Dominique Weis (Eds.)*
209 **Sea Ice: Physics, Mechanics, and Remote Sensing** *Mohammed Shokr and Nirmal Sinha (Eds.)*
210 **Fluid Dynamics in Complex Fractured-Porous Systems** *Boris Faybishenko, Sally M. Benson, and John E. Gale (Eds.)*
211 **Subduction Dynamics: From Mantle Flow to Mega Disasters** *Gabriele Morra, David A. Yuen, Scott King, Sang Mook Lee, and Seth Stein (Eds.)*
212 **The Early Earth: Accretion and Differentiation** *James Badro and Michael Walter (Eds.)*
213 **Global Vegetation Dynamics: Concepts and Applications in the MC1 Model** *Dominique Bachelet and David Turner (Eds.)*
214 **Extreme Events: Observations, Modeling and Economics** *Mario Chavez, Michael Ghil, and Jaime Urrutia-Fucugauchi (Eds.)*
215 **Auroral Dynamics and Space Weather** *Yongliang Zhang and Larry Paxton (Eds.)*
216 **Low-Frequency Waves in Space Plasmas** *Andreas Keiling, Dong-Hun Lee, and Valery Nakariakov (Eds.)*
217 **Deep Earth: Physics and Chemistry of the Lower Mantle and Core** *Hidenori Terasaki and Rebecca A. Fischer (Eds.)*
218 **Integrated Imaging of the Earth: Theory and Applications** *Max Moorkamp, Peter G. Lelievre, Niklas Linde, and Amir Khan (Eds.)*
219 **Plate Boundaries and Natural Hazards** *Joao Duarte and Wouter Schellart (Eds.)*
220 **Ionospheric Space Weather: Longitude and Hemispheric Dependences and Lower Atmosphere Forcing Timothy Fuller-Rowell,** *Endawoke Yizengaw, Patricia H. Doherty, and Sunanda Basu (Eds.)*
221 **Terrestrial Water Cycle and Climate Change Natural and Human-Induced Impacts** *Qiuhong Tang and Taikan Oki (Eds.)*
222 **Magnetosphere-Ionosphere Coupling in the Solar System** *Charles R. Chappell, Robert W. Schunk, Peter M. Banks, James L. Burch, and Richard M. Thorne (Eds.)*
223 **Natural Hazard Uncertainty Assessment: Modeling and Decision Support** *Karin Riley, Peter Webley, and Matthew Thompson (Eds.)*
224 **Hydrodynamics of Time-Periodic Groundwater Flow: Diffusion Waves in Porous Media** *Joe S. Depner and Todd C. Rasmussen (Auth.)*
225 **Active Global Seismology** *Ibrahim Cemen and Yucel Yilmaz (Eds.)*
226 **Climate Extremes** *Simon Wang (Ed.)*
227 **Fault Zone Dynamic Processes** *Marion Thomas (Ed.)*
228 **Flood Damage Survey and Assessment: New Insights from Research and Practice** *Daniela Molinari, Scira Menoni, and Francesco Ballio (Eds.)*
229 **Water-Energy-Food Nexus – Principles and Practices** *P. Abdul Salam, Sangam Shrestha, Vishnu Prasad Pandey, and Anil K Anal (Eds.)*
230 **Dawn–Dusk Asymmetries in Planetary Plasma Environments** *Stein Haaland, Andrei Rounov, and Colin Forsyth (Eds.)*
231 **Bioenergy and Land Use Change** *Zhangcai Qin, Umakant Mishra, and Astley Hastings (Eds.)*
232 **Microstructural Geochronology: Planetary Records Down to Atom Scale** *Desmond Moser, Fernando Corfu, James Darling, Steven Reddy, and Kimberly Tait (Eds.)*
233 **Global Flood Hazard: Applications in Modeling, Mapping and Forecasting** *Guy Schumann, Paul D. Bates, Giuseppe T. Aronica, and Heiko Apel (Eds.)*
234 **Pre-Earthquake Processes: A Multidisciplinary Approach to Earthquake Prediction Studies** *Dimitar Ouzounov, Sergey Pulinets, Katsumi Hattori, and Patrick Taylor (Eds.)*
235 **Electric Currents in Geospace and Beyond** *Andreas Keiling, Octav Marghitu, and Michael Wheatland (Eds.)*
236 **Quantifying Uncertainty in Subsurface Systems** *Celine Scheidt, Lewis Li, and Jef Caers (Eds.)*
237 **Petroleum Engineering** *Moshood Sanni (Ed.)*
238 **Geological Carbon Storage: Subsurface Seals and Caprock Integrity** *Stephanie Vialle, Jonathan Ajo-Franklin, and J. William Carey (Eds.)*
239 **Lithospheric Discontinuities** *Huaiyu Yuan and Barbara Romanowicz (Eds.)*
240 **Chemostratigraphy Across Major Chronological Eras** *Alcides N.Sial, Claudio Gaucher, Muthuvairavasamy Ramkumar, and Valderez Pinto Ferreira (Eds.)*
241 **Mathematical Geoenergy: Discovery, Depletion, and Renewal** *Paul Pukite, Dennis Coyne, and Daniel Challou (Eds.)*
242 **Ore Deposits: Origin, Exploration, and Exploitation** *Sophie Decree and Laurence Robb (Eds.)*
243 **Kuroshio Current: Physical, Biogeochemical and Ecosystem Dynamics** *Takeyoshi Nagai, Hiroaki Saito, Koji Suzuki, and Motomitsu Takahashi (Eds.)*
244 **Geomagnetically Induced Currents from the Sun to the Power Grid** *Jennifer L. Gannon, Andrei Swidinsky, and Zhonghua Xu (Eds.)*
245 **Shale: Subsurface Science and Engineering** *Thomas Dewers, Jason Heath, and Marcelo Sánchez (Eds.)*
246 **Submarine Landslides: Subaqueous Mass Transport Deposits From Outcrops to Seismic Profiles** *Kei Ogata, Andrea Festa, and Gian Andrea Pini (Eds.)*
247 **Iceland: Tectonics, Volcanics, and Glacial Features** *Tamie J. Jovanelly*
248 **Dayside Magnetosphere Interactions** *Quigang Zong, Philippe Escoubet, David Sibeck, Guan Le, and Hui Zhang (Eds.)*
249 **Carbon in Earth's Interior** *Craig E. Manning, Jung-Fu Lin, and Wendy L. Mao (Eds.)*
250 **Nitrogen Overload: Environmental Degradation, Ramifications, and Economic Costs** *Brian G. Katz*
251 **Biogeochemical Cycles: Ecological Drivers and Environmental Impact** *Katerina Dontsova, Zsuzsanna Balogh-Brunstad, and Gaël Le Roux (Eds.)*
252 **Seismoelectric Exploration: Theory, Experiments, and Applications** *Niels Grobbe, André Revil, Zhenya Zhu, and Evert Slob (Eds.)*
253 **El Niño Southern Oscillation in a Changing Climate** *Michael J. McPhaden, Agus Santoso, Wenju Cai (Eds.)*
254 **Dynamic Magma Evolution** *Francesco Vetere (Ed.)*
255 **Large Igneous Provinces: A Driver of Global Environmental and Biotic Changes** *Richard. E. Ernst, Alexander J. Dickson, Andrey Bekker (Eds.)*
256 **Coastal Ecosystems in Transition: A Comparative Analysis of the Northern Adriatic and Chesapeake Bay** *Thomas C. Malone, Alenka Malej, Jadran Faganeli (Eds.)*

Geophysical Monograph 257

Hydrogeology, Chemical Weathering, and Soil Formation

Allen Hunt
Markus Egli
Boris Faybishenko
Editors

This Work is a co-publication of the American Geophysical Union and John Wiley and Sons, Inc.

AGU
ADVANCING EARTH AND SPACE SCIENCE

WILEY

This Work is a co-publication between the American Geophysical Union and John Wiley & Sons, Inc.

This edition first published 2021 by John Wiley & Sons, Inc., 111 River Street, Hoboken, NJ 07030, USA and the American Geophysical Union, 2000 Florida Avenue, N.W., Washington, D.C. 20009

Published under the aegis of the AGU Publications Committee

Brooks Hanson, Executive Vice President, Science
Carol Frost, Chair, Publications Committee
For details about the American Geophysical Union visit us at www.agu.org.

Wiley Global Headquarters
111 River Street, Hoboken, NJ 07030, USA

For details of our global editorial offices, customer services, and more information about Wiley products visit us at www.wiley.com.

Library of Congress Cataloging-in-Publication Data

Names: Hunt, Allen G. (Allen Gerhard), editor. | Egli, Markus, editor. | Faybishenko, Boris, editor. | John Wiley & Sons.
Title: Hydrogeology, chemical weathering, and soil formation / Allen Hunt, Markus Egli, Boris Faybishenko, editors.
Description: First Edition. | Hoboken : Wiley, 2020. | Series: Geophysical monograph series | Includes index.
Identifiers: LCCN 2020029283 (print) | LCCN 2020029284 (ebook) | ISBN 9781119563969 (Hardback) | ISBN 9781119563990 (Adobe PDF) | ISBN 9781119564003 (eBook)
Subjects: LCSH: Hydrogeology. | Chemical weathering. | Soil formation.
Classification: LCC GB1003.2 .H939 2020 (print) | LCC GB1003.2 (ebook) | DDC 551.49–dc23
LC record available at https://lccn.loc.gov/2020029283
LC ebook record available at https://lccn.loc.gov/2020029284

Cover Design: Wiley
Cover Images: © Haupt Verlag, Bern

Set in 10/12pt Times New Roman by SPi Global, Pondicherry, India

10 9 8 7 6 5 4 3 2 1

DEDICATION

We dedicate this volume to Jeannie Dixon, who missed out on contributing due to illness. We hope that she enjoys the book during her recovery and is contributing to our science again soon.

CONTENTS

LIST OF CONTRIBUTORS

Suzanne P. Anderson
Institute of Arctic and Alpine Research and Department of Geological Sciences, University of Colorado, Boulder, Colorado, USA

Keerthika Nirmani Ranathunga Arachchige
Department of Soil Management, Ghent University, Ghent, Belgium

Katherine Barnhart
Cooperative Institute for Research in Environmental Sciences, University of Colorado, Boulder, Colorado, USA

Renée-Claire Le Bayon
Laboratory of Functional Ecology, Institute of Biology, University of Neuchâtel, Neuchâtel, Switzerland

Kevin Befus
Department of Civil and Architectural Engineering, University of Wyoming, Laramie, Wyoming, USA

Philip Brunner
Center for Hydrogeology and Geothermics, CHYN, University of Neuchâtel, Neuchâtel, Switzerland

Géraldine Bullinger
Institute of Construction and Environmental Technology, Haute école d'ingénierie et d'architecture, Fribourg, Switzerland

Steven G. Driese
Department of Geosciences, Baylor University, Waco, Texas, USA

Markus Egli
Department of Geography, University of Zürich, Zürich, Switzerland

Boris Faybishenko
Earth and Environmental Sciences Area, E. O. Lawrence Berkeley Laboratory, Berkeley, California, USA

Peter A. Finke
Department of Soil Management, Ghent University, Ghent, Belgium

Maryam Foroughi
Warnell School of Forestry and Natural Resources, University of Georgia, Athens, Georgia, USA

Michael N. Gooseff
Hydrology, Water Resources and Environmental Fluid Mechanics, Environmental Engineering, University of Colorado, Boulder, Colorado, USA

Claire Guenat
Laboratory of Ecological Systems, ECOS & WSL, Ecole Polytechnique Fédérale, Lausanne, Switzerland

Noah Hoffman
INSTAAR and Dept. of Geography, University of Colorado, Boulder, Colorado, USA

Rainer Horn
Institute for Plant Nutrition and Soil Science, Christian Albrechts University, Kiel, Germany

Richard J. Huggett
School of Environment, Education, and Development, University of Manchester, Manchester, UK

Allen Hunt
Department of Physics and Department of Earth & Environmental Sciences, Wright State University, Dayton, Ohio, USA

Patrick J. Kelly
INSTAAR and Dept. of Geography, University of Colorado, Boulder, Colorado, USA

Rattan Lal
Carbon Management and Sequestration Center, The Ohio State University, Columbus, Ohio, USA

Deborah L. Leslie
Department of Earth Sciences, University of Memphis, Memphis, Tennessee, USA

Claire E. Lukens
Department of Life and Environmental Sciences, University of California, Merced, California, USA

W. Berry Lyons
School of Earth Sciences and Byrd Polar & Climate Research Center, The Ohio State University, Columbus, Ohio, USA

Daniel Markewitz
Warnell School of Forestry and Natural Resources, University of Georgia, Athens, Georgia, USA

Aldo Mirabella
Piazza S. Nicolò 23, 95036 Randazzo, Italy

Lee C. Nordt
Department of Geosciences, Baylor University, Waco, Texas, USA

Kevin P. Norton
Te Herenga Waka/Victoria University of Wellington, Wellington, New Zealand

William Ouimet
Department of Geography and Center for Integrative Geosciences, University of Connecticut, Storrs, Connecticut, USA

Todd C. Rasmussen
Warnell School of Forestry and Natural Resources, University of Georgia, Athens, Georgia, USA

Peter B. Sak
Department of Earth Sciences, Dickinson College, Carlisle, PA, USA
Earth and Environmental Systems Institute and Dept. of Geosciences, Pennsylvania State University, University Park, PA, USA

Rodolphe Schlaepfer
Laboratory of Ecological Systems, ECOS & WSL, Ecole Polytechnique Fédérale, Lausanne, Switzerland

Andreas Schomburg
Laboratory of Functional Ecology, Institute of Biology, University of Neuchâtel, Neuchâtel, Switzerland

Gary E. Stinchcomb
Watershed Studies Institute & Department of Earth and Environmental Sciences, Murray State University, Murray, Kentucky, USA

Arnaud J.A.M. Temme
Department of Geography and Geospatial Sciences, Kansas State University, Manhattan, Kansas, USA

Pascal Turberg
Laboratory of Ecological Systems, ECOS & WSL, Ecole Polytechnique Fédérale, Lausanne, Switzerland

Ann Verdoodt
Department of Soil Management, Ghent University, Ghent, Belgium

Qiuzhen Yin
Earth and Life Institute, Georges Lemaitre Center for Earth and Climate Research, Université Catholique de Louvain, Louvain-la-Neuve, Belgium

Yanyan Yu
Institute of Geology and Geophysics, Chinese Academy of Sciences, Beijing, China

PREFACE

The soil is a nexus for water, chemicals, and biologically coupled nutrient cycling; it is an upper bound of the sediment and rock cycle and constitutes a lower bound for water and carbon recycling through the atmosphere. Our choice of title, "Hydrogeology, Chemical Weathering, and Soil Formation," emphasizes the linkage of the topics of soil formation and chemical weathering through water cycling. Of course, biological processes are a foundation of all three of these topics and work on many levels, from nitrogen fixation and soil zonation through bioturbation to large-scale ecology. The importance of the chemical weathering of silicate minerals to soil formation, the composition of the atmosphere and Earth's biological history, has been studied for more than a century (e.g. Darwin, 1881; Dokuchaev, 1883) and extensively reviewed (e.g. Berner, 1992).

According to the Urey reaction, taken to represent a general model of the carbonate-silicate cycle and weathering of silicate minerals, calcium silicate (wollastonite) is converted to calcium carbonate, while simultaneously gaseous CO_2 is replaced by solid SiO_2. Thus is atmospheric carbon dioxide sequestered in the reservoir of carbonate rocks. Removal of large quantities of atmospheric CO_2 by this reaction is the basis of its relevance to climate change and the history of Earth's atmosphere, as well as to the evolution of life (chapter 2 of this volume). In other words, without silicate weathering, the Earth would likely have become a runaway greenhouse with an unhabitable climate (Frings & Buss, 2019). No long-term effect on atmospheric CO_2 results from subsequent weathering of carbonate rocks, which merely triggers renewed sequestration of the same quantity of carbon, even though a short-term CO_2 drawdown may result from an increase in carbonate weathering rates.

The silicate weathering reaction is effective only in the presence of water. While the role of water in kinetics is clarified in the expression for the reaction of plagioclase, its typically even more important role in the actual rate of weathering near the Earth's surface is still largely hidden from view. The rate at which chemical weathering of silicate minerals actually occurs is proportional to the flux of water through Earth's surface, meaning that the reaction rate of minerals such as plagioclase is often limited not by its reaction kinetics but by transport of either the reacting species into, or reaction products out of, the chemical weathering zone (Blättler & Higgins, 2017; Maher, 2010). Thus, the reaction rate is proportional to the water throughflow within the Earth's skin (i.e. the soil or regolith), and quantification of the partitioning of the water at the interface between the terrestrial surface and the atmosphere becomes key to understanding the rates of weathering around the world. Chemical weathering and soil formation intersect in this way the cycles of water and of carbon at the terrestrial surface.

The release of P as well as ions such as K^+ and Ca^{2+} (or likewise Mg^{2+} and related species) turns out to be critical for soil formation, as such mineral nutrients are essential for the functions of vascular plants, whose respiration, for example, provides a significant part of the CO_2 required to continue the silicate weathering. The process by which plants are established and form communities with microorganisms, leading to the development of soil, is quite complex and is the subject of a great deal of research. In any case, more mature soils are differentiated in depth, with plant roots, litter, and other organic material near the surface, a primarily mineral layer rich in carbon (the A horizon) just below, and a weathered layer with much lower organic content (the B horizon) below that. The rate at which these layers form and differentiate, together with the processes by which they form, is important in a range of human activities as well as geologic processes too wide to list here. The rate at which predominantly the A horizon is lost to erosion is important in agriculture, water quality, river management, and geomorphology, as well as other areas. Most important for the present volume is that the process of chemical weathering appears to be water flow-rate limited overall. Yet the history of the study of soil formation, tracing back to Darwin and to Dokuchaev in the 19th century, has left an imprint on the study of soils, even while modern understanding places the single process of chemical weathering at the center of examination. While Dokuchaev emphasized the soil formation factors, which can be related to silicate weathering, Darwin's emphasis was rather on bioturbation. A contrasting approach to soil is discussed by Huggett in the introductory chapter. Here, rather than focusing on rate-limiting processes or controlling reactions, a unifying picture of a collection of mutually interacting constituents is presented.

Looked at from a deep-Earth perspective, the formation of soil feeds back into the deep rock hydrologic cycles, potentially providing a limitation on the rate at which sediment can be transported from its source regions on the continents and islands to regions of deposition along rivers, in lakebeds, and especially in oceans. Variable ranges of soil formation in time and space relate to landforms and their changes, as well as to the isostatic adjustments in the Earth's crust from erosion and deposition. The volume of sediment subducted in trenches is closely related to its water content through its porosity, described through porosity-depth relationships, linking the subaerial and subsurface water cycles.

Why should we wish to bring out this volume on soil formation and chemical weathering now? Standard interpretations of soil formation and chemical weathering have been challenged in the 21st century. White and Brantley's (2003) summary of the chemical weathering of silicate minerals has

shown that results of laboratory experiments often bear little resemblance to field results, where silicate substrates may be weathering at a rate as much as six orders of magnitude more slowly. These authors showed that the decline in chemical weathering rates conformed to a power law for periods from weeks to about 6 Myr. The decline in weathering rates tracks rather closely the decline in soil formation rates, which have been known for a long time to slow with time, though no consensus had been reached regarding an associated time-dependence. Field studies (e.g. Blättler & Higgins, 2017; Maher, 2010; White & Brantley, 2003) provide evidence of the relevance of water fluxes to chemical weathering rates and require development of a compatible theoretical framework. Ultimately, interpretations of the development of paleosols together with the evolution of the atmosphere need to be revised accordingly, with possible relevance to such far-flung topics as extinctions. Partitioning of carbon between ocean, atmosphere, and biosphere has varied drastically over glacial-interglacial cycles. The resulting swings in atmospheric CO_2 and climate are particularly instructive for learning how the weathering feedback works (Frings, 2019).

This volume attempts to place the problem of chemical weathering and soil formation in its geological, climatological, biological, and hydrological perspective. The way in which this is approached is reflected in the organization of the book, which, following Huggett's defining chapter, continues with a perspective based on Earth's history (Driese and coauthors). The authors trace the evolution of soils over 3.25 billion years together with geology, paleoclimate and atmospheric composition, and the evolution of life. The following section emphasizes that several basic processes compete for importance in soil formation, namely soil production with its relationship to chemical (and physical) weathering, bioturbation, and aeolian deposition. Chemical weathering and soil formation are related to water and energy fluxes (Hunt), where theoretical approaches of the interactions between the hydrological cycle, soil formation, and net primary production are provided. Le Bayon and coauthors address some of the fundamental aspects of soil formation and development associated with bioturbation, which harks back to Charles Darwin's initial hypothesis. Clay minerals are important agents in providing nutrients and water to plants. Egli and Mirabella discuss the evolution of clay minerals in alpine soils also in the light of kinetic limitation and percolation. Lukens and Norton depict the role of aeolian deposition in soil formation, as not only water and carbon are transported through the atmosphere, but dust as well. Related to this topic is the chapter of Finke and coauthors in the next section, where loess records are shown to be important climate indicators.

Weathering rinds are indicative of the exposure age of a rock (Sak). In fact, rinds can be considered as microsoils and obey the same weathering principles that also depend on climate. Soil trajectories related to compression from agriculture are discussed in the chapter of Horn and Lal. The role of pedogenesis in geomorphology is discussed in the example of landsliding (Temme). Finally, a cross-section of integrative field studies is presented with results from several critical zone observatories (CZOs). These include the contribution of Lyons and coauthors on soil formation in the Antarctic dry valleys, Rasmussen and coauthors on the impacts of land-use change on soils in the southeastern piedmont of the USA, and Suzanne Anderson and coauthors' discussion of Gordon Gulch from the Boulder Creek CZO. The book closes with a summary of the current state of affairs.

Allen Hunt
Wright State University, USA

Markus Egli
University of Zürich, Switzerland

Boris Faybishenko
Lawrence Berkeley National Laboratory, USA

REFERENCES

Berner, R. A. (1992). Weathering, plants, and the long-term carbon-cycle. *Geochimica et Cosmochimica Acta*, *56*, 3225–3231.

Blättler, C. L., & Higgins, J. A. (2017). Testing Urey's carbonate–silicate cycle using the calcium isotopic composition of sedimentary carbonates. *Earth and Planetary Science Letters*, *479*, 241–251. https://doi.org/10.1016/j.epsl.2017.09.033

Darwin, C. (1881). The formation of vegetable mould through the action of worms, with observations on their habits. London: John Murray. (Source: http://darwin-online.org.uk/converted/pdf/1881_Worms_F1357.pdf)

Dokuchaev, V. V. (1883/1948/1967). Russian Chernozem. In *Selected works of V. V. Dokuchaev, Moscow, 1948* (vol. 1, pp. 14–419). Jerusalem: Israel Program for Scientific Translations Ltd. (for USDA-NSF), Publ. by S. Monson, 1967. (Transl. into English by N. Kaner).

Frings, P. J. (2019). Palaeoweathering: How do weathering rates vary with climate? *Elements*, *15*, 259–265. DOI: 10.2138/gselements.15.4.259

Frings, P. J., & Buss, H. L. (2019). The central role of weathering in the geosciences. *Elements*, *15*, 229–234. DOI: 10.2138/gselements.15.4.229

Maher, K. (2010). The dependence of chemical weathering rates on fluid residence time. *Earth Planetary Science Letters*, *294*, 101–110. DOI: 10.1016/j.epsl.2010.03.010

White, A. F., & Brantley, S. L. (2003). The effect of time on the weathering rates of silicate minerals. Why do weathering rates differ in the lab and in the field? *Chemical Geology*, *202*, 479–506. https://doi.org/10.1016/j.chemgeo.2003.03.001

Part I
Soil Definition

1

Soil as a System: A History

Richard J. Huggett

ABSTRACT

The idea of soil as a system is not yet a hundred years old. Its origins lie in Dokuchaev's view of soil as an independent object, an idea promoted so successfully and eloquently by Hans Jenny. It was Jenny who first thought of soil as a system. His CLORPT equation focused on state factors (external drivers) of the soil system and, later, ecosystems. His approach was largely statistical and empirical. Later, a few researchers investigated energy as a soil-system driver. A different line of investigation, spurred by Milne's catena concept, saw soil as a spatial system. Research in this field began in earnest with Simonson's concept of soil as an open system, which at first involved one-dimensional soil profiles but was later extended to catenas and three-dimensional soil landscapes, all researched using a rich variety of statistical and deterministic models. Last came the recognition that soil is part of an interdependent system. This line of enquiry began with conceptual models of the ecosphere. Since the millennium it has made big advances from cross-disciplinary enquiries focusing on the Earth's critical zone and interactions between soils and geomorphology, soils and hydrology, soils and life, and soils and humans.

1.1. INTRODUCTION

Ideas about soil have a long and rich history. It is perhaps easy to dismiss older notions as outmoded, but the foundations of soil science laid down by the creators of the subject still have currency, even though later thinkers have refined them and added new elements. Expanding a metaphor, if Isaac Newton could see further by standing on the shoulders of giants, then modern soil scientists can see further by standing in the soil pits of their predecessors. This chapter will explore the view taken by Hans Jenny, a veritable giant among soil scientists, that soil may be regarded as a system. Jenny mooted this idea in 1930, but soil concepts developed in the five decades before that date provide an essential background and they will be discussed first, before considering soil as a system, soil as a spatial system, and soil as an interdependent system. The chapter will end with a brief look at prospects for the systems approach in pedology.

In developing ideas about soil and soil formation, Jenny, his predecessors, and later researchers have put forward various models that attempt to explain the structure and function of soil systems and their component parts. Table 1.1 summarizes some of these models and serves as a guide for the discussion that follows.

1.2. SOIL AS AN INDEPENDENT BODY

As a discipline in its own right, soil science emerged and flowered during the second half of the nineteenth century when a few researchers proposed the idea of soil as an independent entity (Brevik & Cerdà, 2016). This radical idea was presaged by Friedrich Albert Fallou (1862), who argued that soil was distinct from the underlying geology, and who also coined the term *pedology*.

School of Environment, Education, and Development, University of Manchester, Manchester, UK

Hydrogeology, Chemical Weathering, and Soil Formation, Geophysical Monograph 257, First Edition.
Edited by Allen Hunt, Markus Egli, and Boris Faybishenko.

DOI: 10.1002/9781119563952.ch1

Table 1.1 Soil models with selected examples.

	Type of Model		
	Qualitative	Quantitative	
Subject of Model	Conceptual	Statistical and Empirical	Deterministic
Soil as an independent system			
System drivers (state factors)	Dokuchaev (1899) Zakharov (1927) Shaw (1930) Jenny's (1941) CLORPT equation Wilde (1946) Stephens (1947) Major (1951) Lin (2011)	Climofunctions, biofunctions, topofunctions, lithofunctions, chronofunctions (Jenny 1946, 1958, 1980) Yaalon (1975) Birkeland (1999)	Kline (1973) Huggett's (1991, 1995) BRASH equation Phillips (1993a, 1993b, 1998)
Energy as a system driver	Runge (1973) Lin (2011)	Volobuyev (1963) Rasmussen et al. (2005) Rasmussen and Tabor (2007) Rasmussen et al. (2015) Shepard et al. (2017)	Regan (1977) Quijano and Lin (2014)
Soil as a spatial system			
1D soil profile	Simonson (1959, 1968) Runge (1973) Johnson and Watson-Stenger (1987)	Parton et al. (1987)	Kline (1973) Salvador-Blanes et al. (2007) Finke and Hutson (2008)
2D hillslope	Milne (1935a, 1935b) Ruhe and Walker (1968) Conacher and Dalrymple (1977)	Huggett (1976) Brown et al. (2004) Grealish and Fitzpatrick (2014) Brillante et al. (2017)	Heimsath et al. (1997) Minsany and McBratney (1999) Yoo et al. (2007) Wackett et al. (2018)
3D landscape	Ruhe and Walker (1968) Huggett (1975)	McBratney et al.'s (2003) SCORPAN equation Shepard et al. (2017) Iticha and Takele (2018)	Ahnert (1967) Huggett (1975) Sommer (2006) Vanwalleghem et al. (2013)
Soil as an interdependent system			
Ecosphere	Vernadsky (1926, 1929, 1998) Cole (1958)		Huggett (1991, 1995, 1997) Phillips (1993b)
Critical zone	National Research Council (2001) Chorover et al. (2007)	Banwart et al. (2017)	Banwart et al. (2017)
Biopedology	Darwin (1881) Johnson (1990) Johnson et al. (2005a) Johnson and Schaetzl (2015)	Peacock and Fant (2002) Johnson et al. (2005b)	Saco and Moreno-de las Heras (2013) Gabet et al. (2014)
Geopedology and topopedology	Zinck et al. (2016)	Brillante et al. (2017)	Temme and Vanwalleghem (2016) Willgoose (2018)
Hydropedology	Lin (2003)	Pereira et al. (2018)	Ma et al. (2017)
Anthropopedology	Yaalon and Yaron (1966) Amundson and Jenny (1991)		Barton et al. (2016) Leguédois et al. (2016)

Source. Partly inspired by discussion in Hoosbeek and Bryant (1992) and discussion and tables in Minasny et al. (2008).
Note. The boundaries between the three types of model are often blurred, with some actual models having characteristics of more than one type; the terms *geopedology* and so on are explained in Figure 1.2.

Arguably, Eugene Woldemar Hilgard recognized the independent nature of soil in his *Report on the Geology and Agriculture of Mississippi* published in 1860 (Jenny, 1961b). But it is undeniably the case that modern soil science was born in the early 1880s when Dokuchaev published his *Russian Chernozem* in 1883.

1.2.1. Dokuchaev's Formula for Soil Formation

Vasilii V. Dokuchaev was a Russian geologist turned pedologist who surveyed large stretches of the chernozems underlying the Russian steppes. This work led him to express the view that soil is an independent object and not simply a geological formation; it is a surficial body of mineral and organic substances produced by the combined activity of animals and plants, parent material, climate, and relief (Dokuchaev, 1880, 1883). In taking this view, he rejected the then-prevalent agrogeological definition of soil, the chemical approach to soil classification, and the agronomic view of soils (Krupenikov, 1992). In their place, he put forward two seminal ideas: (1) that soil is an independent natural body worthy of study in its own right and (2) that five soil-forming factors determine the course of soil genesis.

Dokuchaev's original formula for soil formation appeared in an 1899 publication (Florinsky, 2011, 2012; see also Stockman et al., 2011) and read

$$\Pi = f(\text{К, О, Г})\text{В},$$

where Π is soil or soil properties, К is climate, О is organisms, Г is parent material, and В is age of the soil. Topography was not included in the expression, most likely owing to a stenographer's mistake in the original text, in which a discussion of the role of topography preceded the equation (Florinsky, 2012). Using English symbols, Dokuchaev's equation becomes

$$s = f(cl, o, p)t.$$

This became known as the factorial or state-factor approach to soil genesis (Table 1.1).

In 1927, Sergey Zakharov, building on Dokuchaev's work, presented a general soil formation equation in his textbook on soils. In English, the equation reads

soil = *f* (parent rock material, plant and animal organisms, climate, age of the terrain, topography) or using symbols:

$$s = f(p, o, cl, t, r)$$

1.2.2. Shaw's Elaboration

Another major elaboration of the state-factor approach initiated by Dokuchaev was due to Charles F. Shaw (1930). Shaw argued that soils are formed by the modification, and partial decomposition and disintegration, of parent material owing to the action of water, air, temperature change, and organic life. He expressed soil formation according to the formula

$$S = M(C + V)^T + D,$$

which states that soil, S, is formed from parent material, M, by the work of climatic factors, C, and vegetation, V, over a time, T, but the process may be modified by erosion of, or deposition upon, the soil surface, D. Shaw noted that each of the factors in soil formation is important in determining the character of soil, though under local conditions any one factor may exert a dominant influence.

1.2.3. Jenny's CLORPT Equation

The most famous and lasting development of Dokuchaev's approach was the CLORPT equation given by Hans Jenny (1941). This equation expresses any soil or soil property, s, as a function of soil-forming factors:

$$s = f(cl, o, r, p, t, \ldots),$$

where *cl* is environmental climate; *o* is organisms (the fauna and flora originally in the system and that entering later); *r* is topography, including hydrological features such as the water table; *p* is parent material, defined as the initial state of soil when pedogenesis starts; *t* is the age of the soil, or absolute period of soil formation; and the dots are additional factors such as fire. In short, the state of the soil or specific soil properties is a function of the external environment.

It is clear that this CLORPT equation is the same as Zakharov's equation but with the soil-forming factors appearing in a different order. For this reason, and given the earlier date of Zakharov's formulation, Igor V. Florinski (2011, 2012) suggested it should be called the Zakharov–Jenny equation. However, Jenny "framed and expanded the existing theory and lifted it to a level that is the accepted to the present day," which explains his influence (Hartemink, 2016, 88).

Several researchers proposed modifications of Jenny's original formula. Sergius A. Wilde (1946, 13) recast Dokuchaev's formula so that time was expressed as a differential:

$$s = \int (g, e, b)\, dt,$$

where s is soil, g is geological (parent) material, e is environmental influences, and b is biological activity. This model was further modified by Charles G. Stephens (1947) who split environmental influences into climate, c,

relief, r, and water table, w, and changed the g and b factors into parent material, p, and organisms, o:

$$s = \int (c, o, r, w, p)\, dt,$$

which is almost identical to the CLORPT equation except time is seen to influence all factors and the factors can have dependent and independent status.

Jack Major (1951) extended the CLORPT equation to embrace the entire ecosystem: soils, vegetation, and animal life. Jenny (1961a, 1980) offered his own extension that included ecosystems (entire sections of landscapes). He derived a general state-factor equation of the form

$$l, s, v, a = f(L_0, P_x, t),$$

where l is ecosystem properties such as total carbon content, primary production, and respiration; v is vegetation properties such as biomass, species frequency, and sodium content; a is animal properties such as size, growth rate, and color; s is soil properties such as pH, texture, humus content; L_0 is the initial state of the system, that is, the assemblage of properties at time zero when development starts (the L stands for the ecosystem, or larger system as Jenny styled it, of which the soil is part); P_x are external flux potentials; and t is the age of the system.

The state factors are groups of variables associated with L_0 and P_x. The initial state of the system is defined by parent material, p, and by the original topography and water table, r. The external flux potentials are environmental properties that lead to additions and subtractions of matter and energy to and from the system. They include environmental climate, cl, a biotic factor, o, comprising fauna and flora as a pool of species or genes, active or dormant, that happen to be in the ecosystem at time zero or that enter it later. The biotic factor is thus distinct from the vegetation that grows as the system develops; this appears as a system property on the left-hand side of the equation. Other external fluxes would include dust storms, floods, and the additions of fertilizers; these could be given symbols and entered separately in the equation if so desired. In an extended form, the general state-factor equation becomes

$$l, s, v, a = f(cl, o, r, p, t, \ldots).$$

That brings us back to the CLORPT equation, only this time it applies to ecosystems and not just soils. An even later version of the CLORPT equation considered the place of the human species in the state-factor theory of ecosystems (Amundson & Jenny, 1991).

Henry Lin (2011) pointed out that climate, organisms, relief, and parent material vary across geographical space and all change with time, which in turn means that soil environments change continuously through time, a point stressed by Dokuchaev and others (e.g. Johnson et al., 1990). To address this problem, Lin suggested an equation for the total change of a soil profile over a pedogenic time period $t = t_n - t_0$ (where t_n is the current time and t_0 is the beginning of pedogenesis) to capture the cumulative effects of all four time-dependent spatial factors on pedogenesis:

$$s = \int_{t_0}^{t_n} f\left[cl(t), o(t), r(t), p(t)\right] dt.$$

Grouping the spatial soil-forming factors into flux factors (cl and o) and site factors (p and r), Lin writes this equation more succinctly as:

$$s = \int_{t_0}^{t_n} f\left[cl(t), o(t)\right] dt\,|_{p(t),r(t)},$$

which specifies the cumulative effects of climate and organisms on pedogenesis conditioned by parent material and topography.

Jenny's formulation has proved itself exceedingly valuable, both as a conceptual and a research tool. It has deepened understanding of soil variation across individual state factors (see below), although attempts to tackle the combined effects of all state factors using multivariate techniques have had little success (Yaalon, 1975; Amundson & Jenny, 1997). Nevertheless, the CLORPT equation is still cited and used, albeit in slightly modified forms, by pedologists and, to a lesser degree, ecologists. And it has acted as a springboard for later concepts regarding the soil as a system, a development instigated by Jenny himself.

1.3. SOIL AS A SYSTEM

Figure 1.1 depicts the soil system and its connections to the other terrestrial spheres. It serves to illustrate the various concepts about the soil system that have appeared since Hans Jenny first suggested that soil could be usefully conceived in that manner. Jenny's earliest ideas seem to have been first set down in 1930 when he approached soils from a general theory of state, in which "soil properties, soil processes, and soil-forming factors are united into a comprehensive system" (Jenny, 1930, 1053). Later, in his classic book *Factors of Soil Formation* (1941), he treated soil as a physical system to underline its status as a natural body. He also recognized that the soil system is an open system to which substances may be added or removed, a point taken up by later pedologists.

1.3.1. Jenny's Soil System

To characterize a soil system, Jenny used the symbols s_1, s_2, s_3, and so forth to stand for soil properties (nitrogen content, acidity, clay content, or whatever). In modern parlance, these properties are state variables, a term adopted by Jenny in his 1980 book. The soil properties are interrelated, such that if one changes the others may also change:

$$s = f(s_1, s_2, s_3, \ldots).$$

In Jenny's original discussion of the soil as a system, he distinguished soil formers or soil-forming factors (climate, relief, parent material, organisms, and time) and explored their relationships to the soil system itself. He later styled them state factors and stressed that they are "independent" variables that condition the state of the soil system (e.g. Jenny, 1980, 10). In Figure 1.1, these variables are shown as atmosphere and hydrosphere (climate), biosphere (organisms), toposphere (relief), and lithosphere (parent material); the entire system changes through time. Jonathan D. Phillips (1989) argued that the purpose and scope of Jenny's state factors is sometimes misunderstood: they are not intended to describe pedogenetic processes or components of the soil itself; rather, they provide the context and the boundary conditions within which soil formation and development occurs. As Jenny (1961a, 385) put it, "The factors are not formers, or creators, or forces: they are the variables (state factors) that define the state of the soil system." Jenny made it clear that his factorial approach is very much an ecological approach in which the soil component cannot be considered in isolation from its physical and biotic environment (Jenny, 1961a, 1980). However, it is true to say that Jenny's work tended to consider the effect of one state factor on a single soil property, all other factors being held constant, and then expressing the relationship as a mathematical function of some kind, usually a linear or curvilinear regression equation. In Figure 1.1, this means that the arrows from the external or driving variables to the soil system are investigated one at a time, and that no interaction between the driving variables or feedback from the soil state variables to the driving variables is considered. Given five state factors, Jenny proposed five broad groups of functions or sequences: climofunctions or climosequences, biofunctions or biosequences, topofunctions or toposequences, lithofunctions or lithosequences, and chronofunctions or chronosequences. He also included dotfunctions and dotsequences to allow for the effects of other factors such as fire. Subsequent work has established a host of such functions and sequences (see Yaalon, 1975; Huggett, 1998; Birkeland, 1999).

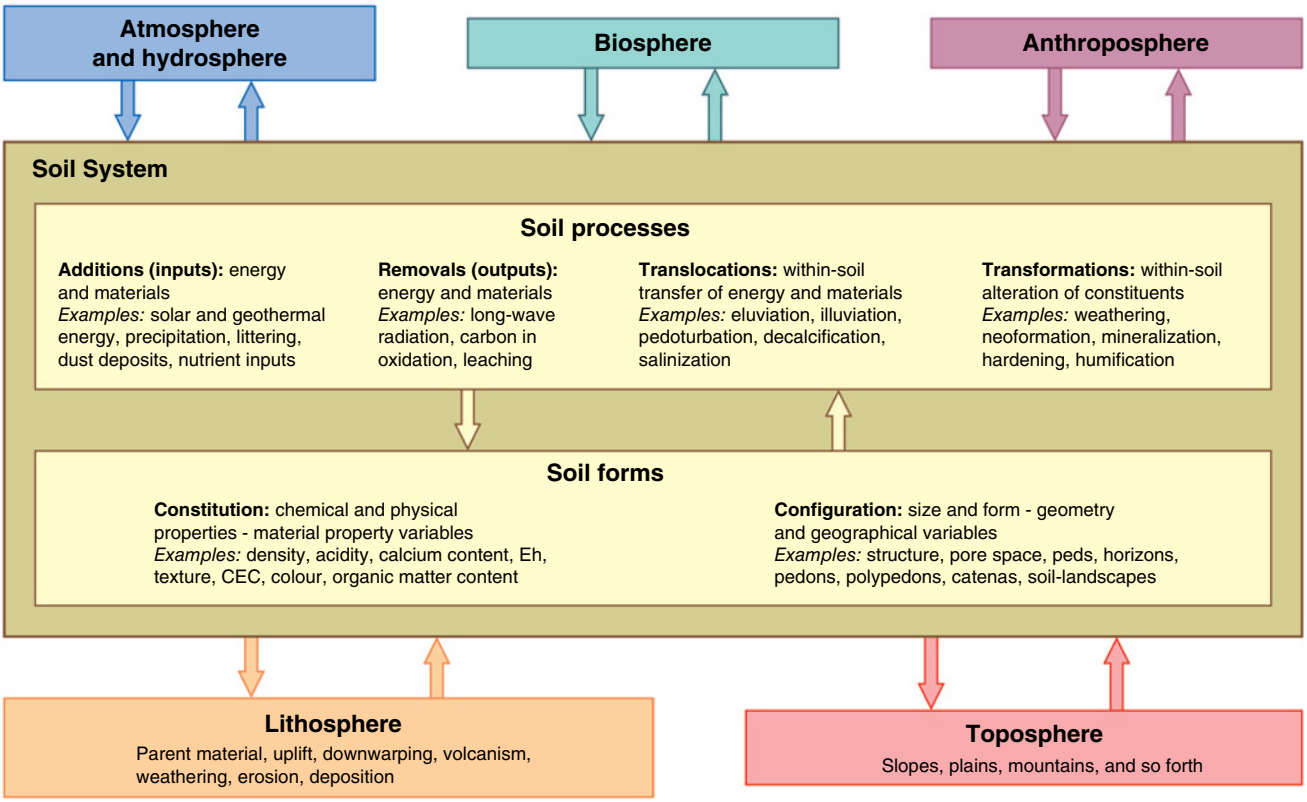

Figure 1.1 The soil system.

1.3.2. Simonson's Soil System

Roy W. Simonson's (1959) generalized theory of soil genesis took a decidedly systems view of soils and elaborated upon Jenny's view of the soil as an open system. He described four groups of physical, chemical, and biological processes common to all soils: additions of organic and mineral matter as solids, liquids, and gases; their removal; their transfer or translocation; and their transformation:

$$s = f\,(additions, removals, translocations, transformations).$$

Simonson argued that the changing balances between these processes differentiate one soil from another. For example, mineralization and humification of plant litter engage more or less the same processes of transformation in all environments, but different process rates may lead to different end products.

Stanley Buol et al. (1980) categorized processes of soil formation using Simonson's general scheme: enrichment, deposition on the soil surface, and littering are additions; leaching and surface erosion are removes; eluviation, lessivage, and pedoturbation are examples of transfers; and humification, mineralization, and weathering involve transformations. In Figure 1.1, Simonson's model would engage the internal soil processes and forms with energy and material inputs from, and outputs to, the atmosphere, hydrosphere, biosphere, and anthroposphere. For the soil system to persist, incoming material must at least replace outgoing material. This fact was recognized by Constantin C. Nikiforoff (1959), who likened the situation to a section of an aggraded stream between two bends: water enters from upstream, water leaves downstream, but between the two bends nothing is lost and work is done. The corresponding "stream" in the soil system is the collection of surficial materials which constitute the soil. In the words of Buol et al. (1980, 11), "A soil is an evolving entity maintained in the midst of a stream of geologic, biologic, hydrologic, and meteorologic material."

1.3.3. Soil Energy System

Coexisting with the material soil system is an energy exchange and storage system (Lin, 2011). Thermal energy (heat) is stored in the soil. The soil system gains heat from incoming solar radiation, terrestrial radiation emitted by the atmosphere, possibly from incoming soil materials and from exothermic reactions; it loses thermal energy in emitting radiation, by conduction out of the system, in outgoing soil materials and in endothermic reactions. Potential energy of a chemical or elevational nature is also stored, imported, and exported. Energy transfers in the soil are brought about by heat conduction, by convection associated with water and air movements, and by translocation of materials. Energy transformations in the system occur in chemical alterations, biological activity, wetting and drying, freezing and thawing, and evaporation and condensation in the soil atmosphere.

The soil energy system is not as well studied as the soil material system, but there are some interesting investigations (Table 1.1). A few researchers have developed models that considered the energy involved in weathering and soil formation, and in doing so quantify the climatic factor of soil formation though such measures as organic matter production and the amount of water available for leaching (Runge, 1973); the energy expended in soil formation (Volobuyev, 1963; Regan, 1977); a measure of the effective energy and mass transfer to the subsurface that accounts for local variations in topography, water and energy balances, and primary production (Rasmussen et al., 2005; Rasmussen & Tabor, 2007; Rasmussen et al., 2015); a probabilistic approach for quantifying soil property variability through integrating energy and mass inputs over time (Shepard et al., 2017); and a review of energy and entropy in near-surface Earth systems (Quijano & Lin, 2014).

1.4. SOIL AS A SPATIAL SYSTEM

Soil may be viewed as a one-dimensional, two-dimensional, or three-dimensional object. The soil profile concept, introduced to western soil scientists by Curtis F. Marbut in 1921 (see Tandarich et al., 2002; Brevik et al., 2016), is one dimensional, defining soil as the vertical cross-section from the surface downward through all the soil horizons and into the parent material. It was adopted as the basic unit for soil survey. During the 1920s and first half of the 1930s, soil surveyors mapped the spatial distribution of soils and in doing so were assuredly aware that soils were part of landscapes, but they did not consider soil as a three-dimensional functional landscape unit. Concepts of that nature appeared first with the two-dimensional soil catena and later with the three-dimensional soil landscape, both of which, along with the soil profile, were to lend themselves to a systems approach.

1.4.1. Soil Profiles

As explained above, Simonson (1959) suggested the concept of the soil profile as an open system. Quantitative models of soil profile development followed. An example was the CENTURY model used to simulate the formation of soil organic matter (Parton et al., 1987). It established statistical relationships between production

and decomposition rates of soil organic matter and four driving variables (annual precipitation, temperature controls on decomposition, soil texture, and plant lignin content) and then predicted soil carbon and nitrogen levels for 24 grassland locations in the Great Plains of the USA. Donald Sasscer and his colleagues (1971) built a deterministic model to study stable and titrated water through an old-field system in Argonne, Illinois; the system consisted of a vegetation compartment and 49 soil compartments, each 1 cm thick. Jerry Kline (1973) used the same basic model to investigate soil–plant relationships and soil genesis.

Donald Lee Johnson (1985) devised an evolutionary model of profile pedogenesis that considered soil thickness changes:

$$T = f\left(D + U + R\right),$$

where T is soil thickness, D is profile deepening, U is soil upbuilding, and R is soil removal. An important feature of this model, and what makes it "evolutionary," is that soil thickness is dynamic and may ebb or flow over time. This model formed the basis of Johnson and Watson-Stegner's (1987) comprehensive soil evolution model, which suggested that phenomena such as erosion, deposition, and pedoturbation can influence the soil formation processes. The model posited that soils may evolve along either progressive or regressive pathways:

$$S = f\left(P, R\right),$$

where S is soil; P is progressive pedogenesis and includes processes, factors, and conditions that promote differentiated profiles; and R is retrogressive pedogenesis and includes processes, factors, and conditions that promote simplified profiles. This model was an attempt to allow for the fact that soil evolves in an ever-changing environment so that polygenetic soils are the norm. Its keynote is polygenesis and stands in antithesis to monogenetic models and notions of zonal soils, normal soils, and climax soils.

Johnson and his colleagues (1990) developed a related evolutionary model. In summary, it assumed that

$$s = f\left(D, P, \frac{dD}{dt}, \frac{dP}{dt}\right),$$

where s is a soil property or the degree of pedogenesis, D is a set of dynamic vectors and dD/dt their rate of change through time, P is a set of passive vectors and dP/dt their rate of change through time. The dynamic vectors include energy fluxes, mass fluxes, the frequency of wetting and drying events, organisms, and pedoturbation. The passive vectors include parent material, the chemical environment of the soil, permanently low water tables, the stability of slopes, and pedogenetic accessions such as fragipans, natric horizons, and histic horizons.

Jonathan D. Phillips (1993a) explored the idea of progressive–regressive pedogenic changes in his own numerical model that incorporated relative rates of progressive and retrogressive pedogenesis and feedbacks between the rate and the degree of soil development:

$$\frac{d\boldsymbol{s}}{dt} = \frac{dP}{dt} - \frac{dR}{dt},$$

where $\boldsymbol{s}$ is soil development (degree of pedogenic alternation and profile organization), P is progressive pathways, and R is regressive pathways. The time differentials of P and R are defined as follows:

$$\frac{dP}{dt} = c_1\ exp^{-k_1\boldsymbol{s}} \text{ and } \frac{dR}{dt} = c_2\ exp^{-k_2\boldsymbol{s}},$$

where c_1 is the maximum rate of progressive pedogenesis and k_1 a coefficient describing the decrease in P rates as soil develops; c_2 is the maximum rate of regressive pedogenesis and k_2 a coefficient describing the decrease in R rates as soil develops (negligible). Phillips's analysis revealed that soil development may display deterministic chaos, with soil profile state at any time being unique to the interplay of progressive and retrogressive soil-forming processes and sensitive to initial conditions, rather than simply the age of the deposit in which the soil is formed. This possibility challenges the classic view of soil developing unidirectionally to an increasingly differentiated state. Rather, it shows that pedogenesis can proceed in different directions due internal dynamics and thresholds, a point first made by Daniel Muhs (1982, 1984; see also Phillips, 1993b, 2001, 2013, 2017; Chadwick & Chorover, 2001).

1.4.2. Soil Catenas

In 1935, Geoffrey Milne, inspired by an idea of his colleague W. S. Martin (Brown, 2006), put forward the concept of the catena as a unified framework within which to study functional aspects of soils on hilly terrain. Milne was based at the East African Agricultural Research Station, Amani. A problem he faced was to map on a small piece of paper the complex entanglement of soils in a large piece of country. To surmount the problem, he took advantage of the fact that in many parts of East Africa, the topography over large tracts consists of little else but a repetition of crests and hollows, and a transect running from crest to hollow traverses very different soil profiles. Mapping the individual soils along the transect would be impossible in all but the most detailed of surveys. Nor, he reasoned, would it be necessary to do so

because "they are not, properly speaking, individual soils at all, but are a compound soil unit of another kind in which a chain of profile-differences occurs in a regular manner" (Milne 1935a, 192).

Milne used the term *catena* (the Latin word for "chain") to describe the regular repetition of soil profiles on crest–hollow topography. He considered adopting the word *suite*, as used by Gilbert Wooding Robinson (1936) to describe a range of differing soils related by topography in Wales. Robinson confined his suites to soils formed in the same parent material; he did not deal with such extreme differences in soils on hills and in valleys as Milne did. In summary, Milne proposed the term *catena* to describe the lateral variation of soils on a hillslope and reasoned that, owing to the agency of geomorphological and pedological processes, all soils occurring along a hillslope are related to one another. He was quite explicit that the topographic relationships of the soils were the prime concern, and that the uniformity of parent material was of subsidiary interest.

At the time of its inception, the idea of a soil catena had a mixed reception, but it was generally hailed a valuable, if radical, idea. Its radicality stemmed from Milne's contention that soils of the bottomlands are as important as soils on the ridges and his conclusion, shared by Sergei Neustruev (1915) before him, that soil-climatic zones comprise zonal complexes rather than zonal soil types. At the time, it was mainly the well-drained soils of a region that were singled out as characteristic zonal soil types and displayed on maps; the ill-drained soils in valley bottoms were demoted to intrazonal status (see Gennadiyev & Bockheim, 2006).

The catena concept was embellished by Thomas M. Bushnell (1942, 1946), who also identified precedents to it, though the term *catena* was assuredly first adopted by Milne. Bushnell (1942) argued that differences in soil drainage classes along a catena create a hydrological sequence, which suggestion led eventually to the idea of the soil association in USA's Soil Survey. Some researchers believe that Bushnell narrowed the catena concept to slopes on which all soils have formed in the same parent material; however, that was only the case for his "simple catenas," in which all soil-forming factors were the same except for drainage conditions; in his "multiple catenas," soil-forming factors, including parent material, could vary. Even so, Bushnell's emphasis on catenas as hydrological soil sequences did lead to the playing down of the role of slope-influenced transport and depositional processes that had been held previously as important to the explanation of soil development along slopes (cf. Schaetzl, 2013, 146). Indeed, David Brown (2006, 79) went as far as to say, 'The U.S. soil survey community distorted and confused Milne's catena, and only through the work of Robert Ruhe in the 1950s and 1960s," which re-energized thinking about connections and interactions between soils and hillslope processes, "was the concept saved from scientific obscurity."

Topography was one of Jenny's state factors of soil formation, and he termed variations in soil properties due to topography a toposequence (a contraction of topographical sequence). Unfortunately, partly owing to Bushnell, confusion surrounds the words *toposequence* and *catena*. Technically speaking, a toposequence involves variations of soils and soil properties in relation to topography (a state factor) with all other state factors held constant, which means that parent material should be uniform along the sequence; that would make a toposequence equivalent to Bushnell's narrower definition of a catena. Jenny (1980, 280) suggested that a catena runs from crest to crest across an intervening valley, with the sequence from crest to valley bottom (what he called a half catena) being a toposequence (on uniform parent material). It seems helpful to use *catena* as originally defined by Milne and distinguish it from *toposequence*, where slope properties vary but parent material and all other state factors are constant.

Back in Africa, a potent development that underscored the connection between hillslope soils and hillslope hydrology came from Cecil Morison (Morison et al., 1948; Morison, 1949), then at the Department of Agriculture, University of Oxford. Morison and his colleagues went on several expeditions to the Anglo-Egyptian Sudan to investigate the soil–vegetation units. Preliminary work suggested that the catena concept could be usefully adopted as a framework of study in this area. He found it helpful to distinguish three zones (he termed them complexes) along a catena, each associated with a broad topographic site: the eluvial zone, the colluvial zone, and the illuvial zone. The eluvial zone is a high-level site that loses water and soluble and suspended matter. Material washed from it is used to build up the colluvial and illuvial zones. The colluvial zone occupies slope sites. It receives material from soils in the eluvial zone and loses some of it to the illuvial zone. The illuvial zone occupies low-level sites. In many cases it has very mixed parentage, consisting of either a simple mosaic or else a mosaic of zoned patterns, depending upon the amount and nature of drainage. It has three distinguishing characteristics: it receives more water than the climatic normal site, it receives much dissolved and suspended matter, and water is lost from it by surface movement, by drainage, or by evaporation.

Interestingly, at around the same time as Milne proposed the soil catena, Boris B. Polynov put forward the notion of geochemical landscapes. Polynov believed in the integrity of the landscape in producing, transporting, and removing rock debris. Two ideas were central to his thesis: first, that there are three basic landscape types

relevant to chemical migration and second, that each chemical has a characteristic mobility in the landscape (Polynov, 1935, 1937). His basic landscape types were eluvial, superaqual, and aqual. In eluvial landscapes, the water table is always, or nearly always, below the ground surface; in superaqual landscapes, the water table and the ground surface coincide; in aqual landscapes, free water rests on the land surface as in lakes. From Polynov's pioneering studies have evolved several conceptual schemes of geochemical landscapes. Notable contributions have come from Mariya A. Glazovskaya (1963, 1968).

During the 1960s, researchers started to take up Milne's and Morison's seminal ideas and investigate soil evolution in the context of hillslopes. Indeed, Vance T. Holliday (2006) argued that Milne's unique contribution was actually in his linking of soil–catenary patterns to specific slope-related processes: wetness, solute transport, and erosion and deposition. A consensus grew that soils on lower slopes are potential sumps for the drainage of soils upslope of them (Hallsworth, 1965); that, on hilly terrain, water movement connects soils with one another and differentiates their properties (Blume, 1968); and that adjacent soils at different elevations are linked by a lateral migration of chemical elements to form a single geochemical landscape (Glazovskaya, 1968). A key point in this work is that solution and water transport act selectively so that, as vertical movement in soil profiles produces A and B horizons, the lateral concatenation of soils leads to a differentiation of soil materials along a slope: hill-top soils are analogues of A horizons, and the valley-bottom soils are analogues of B horizons (Blume & Schlichting, 1965; Sommer & Schlichting, 1997). Subsequently, the burgeoning sophistication of hillslope hydrological investigations has prompted increasingly detailed and revealing examinations of slope soils using statistical models (e.g. Brown et al., 2004; Brillante et al., 2017) and deterministic models (e.g. Heimsath et al., 1997; Minasny & McBratney, 1999; Yoo et al., 2007; Wackett et al., 2018), although researchers now tend to extend their analysis to the third dimension and consider soil landscapes.

1.4.3. Soil Landscapes

Soil catenas are two-dimensional transects along hillslopes. They form part of a geomorphic system, the flows of material and energy within which are characteristically three-dimensional. In moving down slopes, weathering products tend to move at right angles to land-surface contours. Flowlines of material converge and diverge according to the curvature of contours. The pattern of vergency influences the amounts of water, solutes, colloids, and clastic sediments held in store at different landscape positions. Of course, the movement of weathering products alters the topography, which in turn influences the movement of the weathering products; there is feedback between the two systems.

As soil evolution takes place within a three-dimensional mantle of material, the spatial pattern of many soil properties will reflect the three-dimensional topography of the land surface. Indeed, according to the concept of soil-landscape systems, the dispersion of all the debris of weathering, solids, colloids, and solutes, is, in a general and basic way, influenced hugely by land surface (and phreatic surface) form and organized in three dimensions within the framework imposed by the drainage network (Huggett, 1975).

Investigating the effect of landscape setting on pedogenesis requires a characterization of topography in three dimensions. Early attempts to describe the three-dimensional character of topography was made by Andrew R. Aandahl (1948) and Frederick Troeh (1964). Later, geographers and geomorphologists explored methods of terrain description (e.g. Moore et al., 1991). Topographic attributes that appear to be important are those that apply to a two-dimensional catena (elevation, slope, gradient, slope curvature, and slope length), plus those pertaining to three-dimensional landform (slope direction, contour curvature, and specific catchment area).

In distilling previous work on digital soil models, Alex McBratney and his colleagues (2003) proposed that soil is a function of seven factors (the so-called SCORPAN factors), as follows:

$$S = f\left(s, c, o, r, p, a, n\right),$$

where S is soil (*Sc* for soil classes or *Sa* for soil attributes or properties) at a point; s is existing soil information; c represents climate; o represents organisms or biological activity; r represents topographic or landscape attributes; p represents parent material; a represents age; n represents spatial position. Nathan Odgers et al. (2008) emphasized the strong influence of topography on soil characteristics and soil formation processes, noting that such topographic variables (terrain parameters, topographic attributes) as slope, landscape curvature, and flow direction are readily derived from a digital elevation model. They demonstrated how toposequences can be generated from such models.

Three-dimensional topographic influences on soil properties were considered in small drainage basins by the present author (Huggett, 1973, 1975) and Willem J. Vreeken (1973), while André G. Roy and his colleagues (1980) considered soil–slope relationships within a drainage basin. Later work has confirmed that a three-dimensional topographic influence does exist, and that some soil properties are very sensitive to minor variations in the topographic field (e.g. Moore et al., 1991, 1993; Fissore et al., 2017; Li et al., 2018; Iticha & Takele, 2018).

1.4.4. Soil-Landscape Modeling

Soil-landscape models seek to integrate soils, parent material, topography, land use and land cover, and human activities with the aim of understanding the spatial distribution of soil attributes, characteristics of soils, and their behavior through time (Grunwald, 2006, 6). They build on earlier soil models, starting with the factorial models instigated by Dokuchaev, Zacharov, and Jenny, and the later soil system models (Table 1.1).

Soil landscapes are complex, involving geomorphological, biological, and hydrological processes acting over hundreds, thousands, or even millions of years. For this reason, understanding how soil landscapes function and evolve demands an interdisciplinary holistic approach and has benefitted hugely from the appearance of new and powerful technologies over the last few decades: satellite remote sensing, geographic information systems (GISs), global positioning systems (GPSs), digital elevation models (DEMs), and landscape evolution models (LEMs; cf. Brown, 2006). Pedologists have combined these technologies to tackle questions about soil landscapes. The value of digital terrain modeling to hydrology, geomorphology, and ecology was recognized by the early 1990s (e.g. Moore et al., 1991). More recently, pedometrics has attempted to integrate knowledge from numerous disciplines, including soil science, statistics, and GIS.

Early numerical models of landscapes in geomorphology included soil depth as a state variable (e.g. Ahnert, 1967; Armstrong, 1980). Huggett (1975) simulated the movement of solutes on slopes within a drainage basin. The model of the soil–landscape continuum built by Kevin McSweeney and his colleagues (1994) benefitted from technical advances made through linking hydrology and land-surface form for terrain-based modeling of hydrological processes. In their model of soil-landscape systems, various sources of spatial data (e.g. vegetation and geological substrate) and attribute data (e.g. soil organic-matter content and particle-size distribution) are integrated through GIS technology. Four interrelated and iterative stages are applied in the model: physiographic domain characterization; geomorphometric characterization; soil horizon characterization; and soil property characterization. Many subsequent models have appeared, each adding refinements (e.g. Heimsath et al., 1997; Sommer, 2006; Vanwalleghem et al., 2013; Willgoose, 2018).

1.5. SOIL AS AN INTERDEPENDENT SYSTEM

Ideas about the interdependence of environmental factors were mooted in the late eighteenth century, principally by Johann Reinhold Forster and Alexander von Humboldt. Dokuchaev (1899) stressed the importance of interactions between the zones of the Earth, arguing a that a special discipline was needed to study the integrity of the natural sciences (geology, orography, climatology, botany, zoology) and offering genetic soil science (pedology) as a candidate for such a role (Bockheim & Gennadiyev, 2010). To be sure, his categorical statement of the factors of soil formation provided a basis for exploring in a formal way the connections between ecosystems and their environmental influences. The terrestrial spheres are not mentioned specifically in this formulation, but they are there by implication: climate involves the atmosphere and hydrosphere; animals and plants (plus the three kingdoms of micro-organisms) are the biosphere; parent material is connected to the lithosphere; and relief is part of the toposphere.

Vladimir I. Vernadsky, a follower of Dokuchaev, made explicit the interconnectedness of the terrestrial spheres in his concept of the biosphere, a term he adopted from Eduard Suess after having read Die Antlitz der Erde (Suess, 1883–1909). Vernadsky (1926, 1929, 1998) developed original ideas on biogeochemistry and promulgated his own take on the biosphere, suggesting that living organisms and all life and life-support systems (living organisms and their planetary environment) evolve together and form the media in which they live (air, water, soil, sediment). Some later workers argued that the biosphere should be confined to living things and the totality of life and life-support systems be called the ecosphere (Cole, 1958; Gillard, 1969), a view to which the present author subscribes (see Huggett, 1999).

In 1938, Sante Mattson (1938) considered all possible interactions between the lithosphere, atmosphere, hydrosphere, pedosphere, and biosphere (Figure 1.2). Three years later, Jenny listed the components of the ecosphere in his CLORPT equation, but his focus was the influence of environmental factors on soils and ecosystem properties rather than on the interrelationships between the environmental factors themselves.

With the advent of Earth systems science and the notion that "everything is connected to everything else," a new integrative ecosystem approach emerged that addressed the interdependence of life, soils, climate, rocks, and relief (Figure 1.3). The BRASH model was an attempt to express these interdependencies as a general dynamic systems equation (Huggett, 1991, 1995):

$$\frac{d\boldsymbol{x}}{dt} = \boldsymbol{f}(\boldsymbol{x}) + \boldsymbol{z},$$

where $\boldsymbol{x}$ is a vector of all state variables describing the system considered, $\boldsymbol{f}(\boldsymbol{x})$ is a matrix defining interactions between the state variables, $\boldsymbol{z}$ is a vector of driving

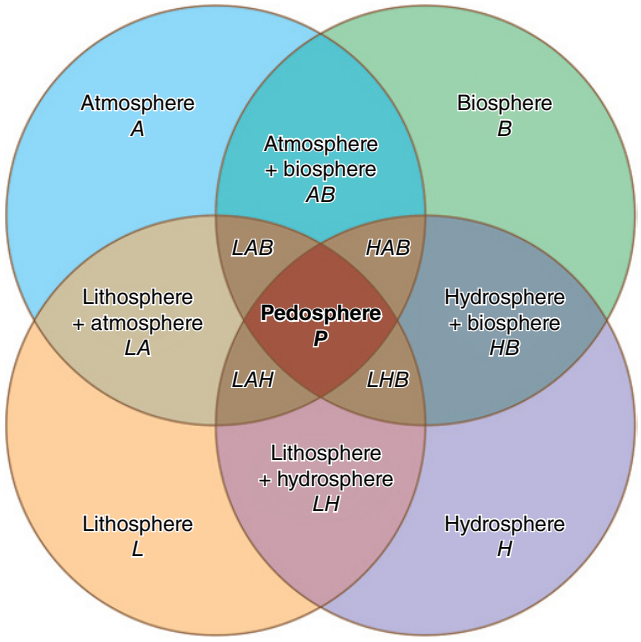

Figure 1.2 Terrestrial spheres and their interaction as envisioned by Sante Mattson. The shaded portion is the ecosphere, a term unknown to Mattson. *Source:* Adapted from Mattson (1938).

variables, and t is time. For the whole ecosphere, the state variables are biosphere, b, relief, r, atmosphere, a, hydrosphere, h, and $\boldsymbol{z}$ is external driving forces (geological or cosmic). Adding the five state variables to the general interaction matrix gives the BRASH equation:

$$\frac{d\boldsymbol{x}}{dt} = f\left(b, r, a, s, h\right) + \boldsymbol{z}.$$

Huggett (1995) argued that this approach reformulates the factorial model into mathematically solvable equations and models soil properties as a function of processes. Applications of these system equations can be found in Phillips (1993b), where it was shown in a numerical example that changes in the initial condition and parameter values can trigger the creation of chaotic behavior of soil development (see also Phillips, 1998).

The rise of Earth system science has led to an evaluation of the pedosphere's role in the global system, both as a vital component of what has become known as the Earth's critical zone and as a two-way interactor with the other terrestrial spheres, the study of which has given rise to some new pedologies (Figure 1.4). These topics will conclude the chapter.

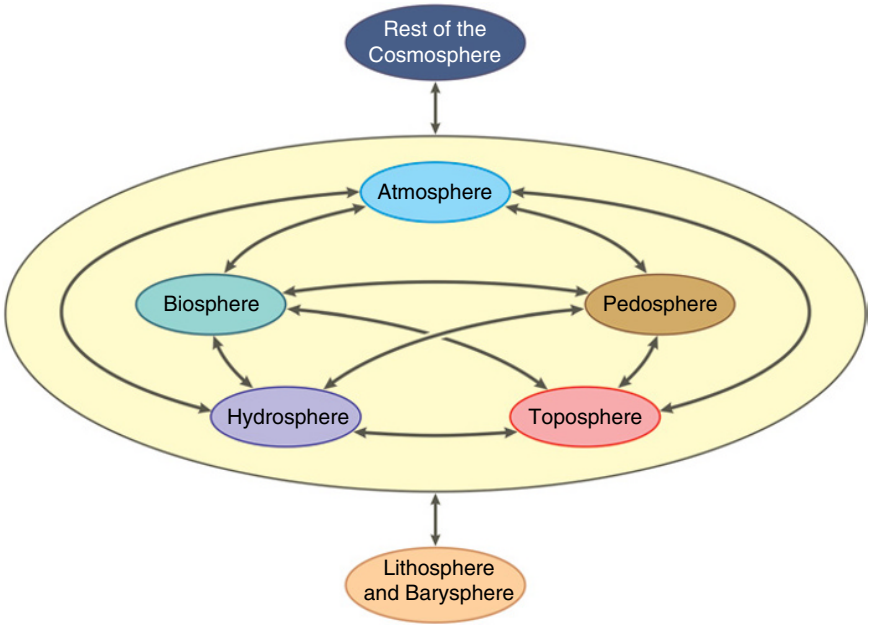

Figure 1.3 A schema for the terrestrial spheres: their interactions and external influences. Before 1875, the only terrestrial sphere given a special name was the atmosphere. Then the Austrian geologist Eduard Suess (1875), in the last and most general chapter of a slim volume titled *Die Entstehung der Alpen* (*The Origin of the Alps*), invented the eminently helpful terms *hydrosphere*, *lithosphere*, and *biosphere*, with the Swedish agricultural chemist Sante Mattson adding the term *pedosphere* in 1938. The present author suggested the word *toposphere* as substitute for Julius Büdel's (1982) *relief sphere*, which Büdel used to describe the totality of the Earth's topography (Huggett, 1995, 1997; Huggett & Cheesman, 2002). The toposphere sits at the interfaces of the pedosphere and atmosphere and the pedosphere and hydrosphere; it is a complex surface separating the predominantly solid body of the Earth from its mainly gaseous and liquid outer envelopes. *Source:* Adapted from Huggett (1995).

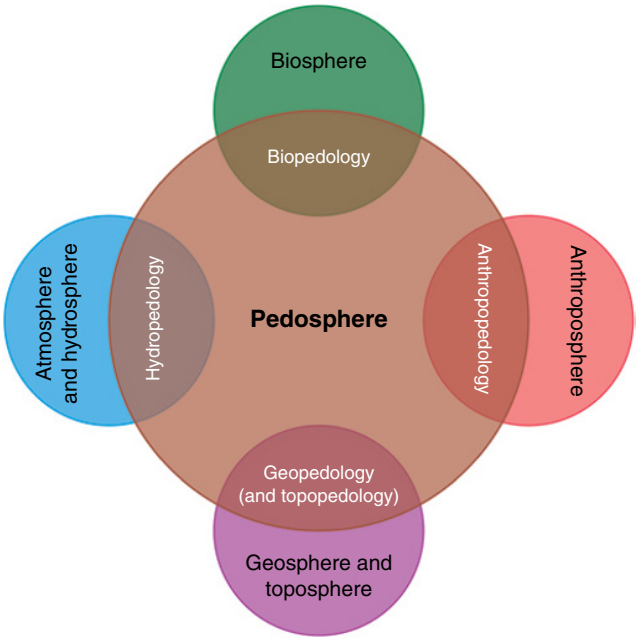

Figure 1.4 Research areas straddling the pedosphere and individual components of the Earth system. The word *topopedology* is suggested here, although there is a precedence for its use (Brillante et al., 2017).

1.5.1. The Critical Zone

As defined by the National Research Council (2001, 37), the critical zone is

> a dynamic interface between the solid Earth and its fluid envelopes, governed by complex linkages and feedbacks among a vast range of physical, chemical, and biological processes. These processes can be organized into four main categories: (1) *tectonics* driven by energy in the mantle, which modifies the surface by magmatism, faulting, uplift, and subsidence; (2) *weathering* driven by the dynamics of the atmosphere and hydrosphere, which controls soil development, erosion, and the chemical mobilization of near-surface rocks; (3) *fluid transport* driven by pressure gradients, which shapes landscapes and redistributes materials; and (4) *biological activity* driven by the need for nutrients, which controls many aspects of the chemical cycling among soil, rock, air, and water. [italics in original]

Henry Lin (2011) rightly pointed out that soils can be literally called the critical component of the Earth's critical zone (see also Wilding & Lin, 2006).

A key feature of critical zone research is its integrative nature. The multifarious components of the critical zone have engaged scientists from distinct and often isolated disciplines: vegetation by botanists, soils by soil scientists, groundwater by hydrogeologists, and substrate by geologists. Important though such separate studies be, predicting the overall behavior of the critical zone demands a combined effort, not least because the functional, emergent properties of such a complex system are the result not only of its various parts but also of the interactions among its parts (Chorover et al., 2007). Recent publications point to the value of integrative modeling (e.g. Banwart et al., 2017). Critical zone research has gained enormously from National Science Foundation funding, and it has led to the increased inclusion of geochemical reaction models and concepts in soil science.

1.5.2. New Pedologies

Biopedology, the oldest of the new pedologies, considers interactions between soils and life. Its origins lie with Charles Darwin and his work on earthworms (e.g. Darwin, 1881). Darwin was also the first to recognize the importance of faunal mixing in soil formation and the textural sorting it can produce (Johnson, 2002; Brevik & Hartemink, 2010). Biopedology has made a strong comeback in the last few decades with research into bioturbation and biomantle theory (e.g. Hole, 1961; Johnson, 1990; Peacock & Fant, 2002; Johnson et al., 2005a, 2005b; Saco & Moreno-de las Heras, 2013; Gabet et al., 2014; Fleming et al., 2014; Johnson & Schaetzl, 2015); it is also benefitting from research in biogeomorphology (e.g. Verboom & Pate, 2013; Pawlika & Šamonil, 2018; see also Huggett, 2017).

The second oldest of the new pedologies is geopedology, which is short for geomorphopedology and focuses on the interdependency between soils and geomorphology. The argument is that soils and vegetation seldom develop in a totally inactive geomorphological environment: the landscapes in which soils and vegetation develop normally change. Thus, the development of terrestrial ecosystems and the geomorphological development of landscapes take place at the same time and influence one another. Pedologists were alerted to this fact by Shaw (1930), Robinson (1936), and Milne (1936), who discussed the role of erosion and deposition in soil evolution (see above). Indeed, soil geomorphology began in the USA in the 1930s with a spate of soil erosion studies made under the auspices of the USDA (Effland & Effland, 1992). In 1952, the USDA set up a Soil-Geomorphology Group that included Robert V. Ruhe, who championed the process dimension of Milne's catena concept (e.g. Ruhe, 1960), arguing that it is the clearest general systems statement about soil geomorphology, integrating the factors in explaining soil differences while focusing on past history of the land surface, geohydrology, erosion, sediment transport, and pedogenic processes (Ruhe, 1975; Birkeland, 1990; Johnson & Hole, 1994). Geopedology has blossomed over the last couple

of decades (see Zinck et al., 2016) and the advent of sophisticated soilscape–landscape deterministic models has given it a new impetus (e.g. Willgoose, 2018).

Hydropedology is one of the latest pedologies. It is "an emerging intertwined branch of soil science and hydrology that studies interactive pedologic and hydrologic processes and properties in the Earth's Critical Zone [and that] aims to bridge disciplines, scales, and data, connect soils with the landscape, link fast and slow processes, and integrate mapping with monitoring and modeling to provide a holistic understanding of the interactions between the pedosphere and the hydrosphere" (Ma et al., 2017). Unlike conventional soil science, it emphasizes in situ soils in the landscape, which have distinct pedogenic features and varying environmental settings (Lin et al., 2012). In doing so, it yields a more realistic and integrated understanding of real-world soil and hydrological processes.

Anthropopedology is the study of the human impact on soils. It has a long history. Dan Yaalon and Bruno Yaron (1966) used the term *metapedogenesis* to cover human-made soil changes; Ron Amundson and Jenny (1991) considered the place of the human species in the state-factor theory of ecosystems. But two-way interactions between soils and the human sphere (anthroposphere) have been the subject of increased research over the last few decades owing to the recognition of soil as an indispensable resource (e.g. Richter & Yaalon, 2011). Topics investigated include coupled human–natural landscapes (Barton et al., 2016) and the evolution of technosols (soils subjected to a strong human influence and containing significant amounts of artefacts, characteristic of the Anthropocene; Leguédois et al., 2016). Research in anthropopedology becomes ever-more pressing as human security comes to rely increasingly on Earth's diverse soil resources. As Amundson et al. (2015) point out:

> Soil is the living epidermis of the planet. Globally, soil is the medium through which a number of atmospheric gases are biologically cycled and through which waters are filtered and stored as they pass through the global hydrological cycle. Soil is a large and dynamic reservoir of carbon and the physical substrate for most of our food production. Profound changes are on the horizon for these interconnected functions—particularly sparked by changes to climate and food production—that will likely reverberate through society this century.

1.6. PROSPECT

Big gains have come from viewing the soil as a system. From the early ideas on state factors, inputs and outputs, and transfers and transformation have evolved sophisticated models of soil landscapes and soils as a key component of the Earth system, and in particular of its critical zone. Of course, challenging questions in pedology remain, and it may take fresh approaches to answer them, but a systems approach still offers a powerful method of investigation. Indeed, Henry Lin (2011) demonstrates the value of such an approach in understanding spatial and temporal changes in soil systems and advancing forecasts and plans for changes related to critical societal needs. To do so, he brings together three general principles of soil change and pedogenesis in time and space (especially time):

First is the *principle of conservation plus evolution*, which provides the reconciliation of fast and slow changes in multiphase soil systems. Incomplete closure and partial irreversibility of many cyclic processes involved in soil functioning produce a range of residual solid products that accumulate over time, meaning that soil profiles record their own history, at least to an extent; this idea was first put forward by Aleksei A. Rode (1947) and later called "soil memory" (Targulian & Sokolova, 1996). Fast and slow changes in complex soil systems thus require an evolutionary and holistic approach to account for their connections and to quantify structural and informational accumulation alongside energy and matter conservation.

Second is the *principle of dissipation plus organization*, which explains the simultaneous processes of dissipation (that create the soil matrix) and organization (that create soil structure) that occur in the formation and evolution of natural soil systems. The idea is consistent with the theory of dissipative structure and self-organization: soil entropy changes provide potential indices for the degree of soil weathering (residuals) and soil structural development (fluxes) once appropriate quantification is made. In addition to energy and mass changes, entropy change and its link to a complex system's orderliness and information need to be quantified to gain a fuller understanding of soil complexity.

Third is the *principle of space plus time*, which highlights the fundamental differences and intimate links between time and space. Space is reversible (you can return to a location already visited), conservative in the sense that energy and matter cannot be created or destroyed but can be transformed and transferred, and structured in three dimensions; time is irreversible, evolutionary, and nonstructured (always moving in one direction); however, time and space both share the common characteristics of preferentiality (preference for different spatial locations and preference for different stable states through time) and thresholds (abrupt changes) that govern soil functions and soil evolution.

Lin admits that there are many unknowns in the workings of the soil system, but he argues that his three principles offer useful perspectives for modeling and predicting soil change and pedogenesis. They are certainly areas where the systems approach may provide new pedological

insights that build upon the foundations laid by Dokuchaev, Jenny, Simonson, and the other giants of the discipline.

ACKNOWLEDGMENTS

I would like to thank Allen G. Hunt for inviting me to write this chapter and two anonymous reviewers for their helpful and encouraging comments. My doctoral thesis dealt with soil-landscape systems, but my interests have shifted to other areas during my career, mainly to aspects of ecology and geomorphology, so revisiting the old soil literature (including my own!) and updating myself on the latest research has proved to be at once a nostalgic, educational, and rewarding adventure.

REFERENCES

Aandahl, A. R. (1948). The characterization of slope positions and their influence on the total nitrogen content of a few virgin soils of western Iowa. *Soil Science Society of America Proceedings*, *13*, 449–454.

Ahnert, F. (1967). The role of the equilibrium concept in the interpretation of landforms of fluvial erosion and deposition. In P. Macra (Ed.), *L'evolution des versants* (pp. 23–41). Liège: L'Université de Liège.

Amundson, R., & Jenny, H. (1991). The place of humans in the state factor theory of ecosystems and their soils. *Soil Science*, *151*, 99–109.

Amundson, R., & Jenny, H. (1997). On a state factor model of ecosystems. *BioScience*, *47*, 536–543.

Amundson, R., Berhe, A. A., Hopmans, J. W., Olson, C., Sztein, A. E., & Sparks, D. L. (2015). Soil and human security in the 21st century. *Science*, *348*, 1261071. doi:10.1126/science.1261071

Armstrong, A. D. (1980). Soils and slopes in a humid temperate environment: A simulation study. *Catena*, *7*, 327–338.

Banwart, S. A., Bernasconi, S. M., Blum, W. E. H., de Souza, D. M., Chabaux, F., Duffy, C., et al. (2017). Soil functions in Earth's Critical Zone: Key results and conclusions. *Advances in Agronomy*, *142*, 1–27.

Barton, C. M., Ullah, I. I. T., Bergin, S. M., Sarjoughian, H. S., Mayer, G. R., Bernabeu-Auban, J. E., et al. (2016). Experimental socioecology: Integrative science for Anthropocene landscape dynamics. *Anthropocene*, *13*, 34–45.

Birkeland, P. W. (1990). Soil–geomorphic research: A selective review. *Geomorphology*, *3*, 207–224.

Birkeland, P. W. (1999). *Soils and geomorphology*, 3rd ed. Oxford: Oxford University Press.

Blume, H.-P. (1968). Die pedogenetische Deutung einer Catena durch die Untersuchung der Bodendynamik. *Transactions of the Ninth International Congress of Soil Science, Adelaide*, *4*, 441–449.

Blume, H.-P., & Schlichting, E. (1965). The relationships between historical and experimental pedology. In E. G. Hallsworth & D. V. Crawford (Eds.), *Experimental Pedology* (pp. 340–353). London: Butterworths.

Bockheim J. G., & Gennadiyev, A. N. (2010). Soil-factorial models and Earth-system science: A review. *Geoderma 159*, 243–251.

Brevik, E. C., Calzolari, C., Miller, B. A., Pereira, P., Kabala, C., Baumgarten, A., & Jordán, A. (2016). Soil mapping, classification, and modeling: History and future directions. *Geoderma*, *264*, 256–274.

Brevik, E. C., & Cerdà, A. (2016). History of soil science. In R. Lal (Ed.), *Encyclopedia of soil science*, 3rd ed. (pp. 1093–1097). Boca Raton, Florida: CRC Press.

Brevik, E. C., & Hartemink, A. E. (2010). Early soil knowledge and the birth and development of soil science. *Catena*, *83*, 23–33.

Brillante, L., Mathieu, O., Lévêque, J., van Leeuwenc, C., & Boisa, B. (2017). Water status and must composition in grapevine cv. Chardonnay with different soils and topography and a mini meta-analysis of the δ^{13}C/water potentials correlation. *Journal of the Science of Food and Agriculture*, *98*, 691–697.

Brown, D. J. (2006). A historical perspective on soil–landscape modeling. In S. Grunwald (Ed.), *Environmental soil–landscape modeling: Geographic information technologies and pedometrics* (pp. 61–103). Boca Raton, Florida: CRC Press.

Brown, D. J., Clayton, M. K., & McSweeney, K. (2004). Potential terrain controls on soil color, texture contrast and grain-size deposition for the original catena landscape in Uganda. *Catena*, *122*, 51–72.

Büdel, J. (1982). *Climatic geomorphology*, transl. by L. Fischer & D. Busche. Princeton, NJ: Princeton University Press.

Buol, S. W., Hole, F. D., and McCracken, R. J. (1980). *Soil Genesis and Classification*, 2nd ed. Ames: Iowa State University Press.

Bushnell, T. M. (1942). Some aspects of the soil catena concept. *Soil Science Society of America Proceedings*, *7*, 466–476.

Bushnell, T. M. (1946). The catena cauldron. *Soil Science Society of America Proceedings*, *10*, 335–340.

Chadwick, O. A., & Chorover, J. (2001). The chemistry of pedogenic thresholds. *Geoderma*, *100*, 321–353.

Chorover, J., Kretzschmar, R., Garcia-Pichel, F., and Sparks, D. L. (2007). Soil biogeochemical processes within the Critical Zone. *Elements*, *3*, 321–326.

Cole, L. C. (1958). The ecosphere. *Scientific American*, *198*, 83–96.

Conacher, A. J., & Dalrymple, J. B. (1977). The nine-unit landsurface model: An approach to pedogeomorphic research. *Geoderma*, *18*, 1–154.

Darwin, C. R. (1881). *The formation of vegetable mould through the action of worms, with observations on their habits*. London: John Murray.

Dokuchaev, V. V. (1880). Protocol of the meeting of the branch of geology and mineralogy of the St. Petersburg Society of Naturalists. [Translated by the Department of Soils and Plant Nutrition, University of California, Berkeley and cited by Amundson & Jenny (1997)]. *Transactions of the St. Petersburg Society of Naturalists*, *XII*, 65–97.

Dokuchaev, V. V. (1883). *Russian Chernozem: Selected Works of V. V. Dokuchaev*, vol. *1*. Jerusalem: Israel Program for Scientific Translations (translated in 1967).

Dokuchaev, V. V. (1899). *Report to the Transcaucasian Statistical Committee on Land Evaluation in General and*

Especially for the Transcaucasia. Horizontal and Vertical Soil Zones (Tipogr. kantselyarii Glavnonachal'stvuyushchego grazhdanskoi chast'yu na Kavkaze, Tiflis, 1899) [in Russian].

Effland, A. B. W., & Effland, W. R. (1992). Soil geomorphology studies in the U.S. Soil Survey Program. *Agricultural History*, *66*, 189–212.

Fallou, F. A. (1862). *Pedologie; oder allgemeine und besondere Bodenkunde*. Dresden: Schönfeld Buchhandlung.

Finke, P. A., & Hutson, J. L. (2008). Modelling soil genesis in calcareous loess. *Geoderma*, *145*, 462–479.

Fissore, C., Dalzell, B. J., Berhe, A. A., Voegtle, M., Evans, M, & Wu, A. (2017). Influence of topography on soil organic carbon dynamics in a Southern California grassland. *Catena*, *149*, 140–149.

Fleming, P. A., Anderson, H., Prendergast, A. S., Bretz, M. R., Valentine, L. E., & Hardy, G. E. S. (2014). Is the loss of Australian digging mammals contributing to a deterioration in ecosystem function? *Mammal Review*, *44*, 94–108.

Florinski, I. V. (2011). The soil formation equation: Imaginary priority of Hans Jenny. *Pedometron*, *30*, 1–3.

Florinski, I. V. (2012). The Dokuchaev hypothesis as a basis for predictive digital soil mapping (on the 125th anniversary of its publication). *Eurasian Soil Science*, *45*, 445–451.

Gabet, E. J., Perron, J. T., & Johnson, D. L. (2014). Biotic origin for Mima mounds supported by numerical modeling. *Geomorphology*, *206*, 58–66.

Gennadiyev, A. N., & Bockheim, J. G. (2006). Development of the soil cover pattern and soil catena concepts. In B. P. Warketin (Ed.), *Footprints in the soil: People and ideas in soil history* (pp. 167–186). Amsterdam and Oxford: Elsevier.

Gillard, A. (1969). On terminology of biosphere and ecosphere. *Nature*, *223*, 500–501.

Glazovskaya, M. A. (1963). On geochemical principles of the classification of natural landscapes. *International Geology Review*, *5*, 1403–1431.

Glazovskaya, M. A. (1968). Geochemical landscapes and geochemical soil sequences. *Transactions of the Ninth International Congress of Soil Science, Adelaide*, *4*, 303–312.

Grealish, G. J., & Fitzpatrick, R. W. (2014). Assisting nonsoil specialists to identify soil types for land management: An approach using a soil identification key and toposequence models. *Soil Use and Management*, *30*, 251–262.

Grunwald, S. (2006). What do we really know about the space–time continuum of soil–landscapes? In S. Grunwald (Ed.), *Environmental soil–landscape modeling: Geographic information technologies and pedometrics* (pp. 3–36). Boca Raton, Florida: CRC Press.

Hallsworth, E. G. (1965). The relationship between experimental pedology and soil classification. In E. G. Hallsworth & D. V. Crawford (Eds.), *Experimental Pedology* (pp. 354–374). London: Butterworths.

Hartemink, A. E. (2016). The definition of soil since the early 1800s. *Advances in Agronomy*, *137*, 73–126.

Heimsath, A. M., Dietrich, W. E., Nishiizumi, K., & Finkel, R. C. (1997). The soil production function and landscape equilibrium. *Nature*, *388*, 358–361.

Hilgard, E. W. (1860). *Report on the geology and agriculture of Mississippi*. Jackson, MS: E. Barksdale, State Printer.

Hole, F. D. (1961). A classification of pedoturbation and some other processes and factors of soil formation in relation to isotropism and anisotropism. *Soil Science*, *91*, 375–377.

Holliday, V. T., 2006. A history of soil geomorphology in the United States. In B. P. Warkentin (Ed.), *Footprints in the soil: People and ideas in soil history* (pp. 187–254). Amsterdam: Elsevier Press.

Hoosbeek, M. R., & Bryant, R. B. (1992). Towards the quantitative modeling of pedogenesis: A review. *Geoderma*, *55*, 183–210.

Huggett, R. J. (1973). *Soil landscape systems: Theory and field evidence*. (Ph.D. thesis). University of London.

Huggett, R. J. (1975). Soil landscape systems: A model of soil genesis. *Geoderma*, *13*, 1–22.

Huggett, R. J. (1976). Lateral translocation of soil plasma through a small valley basin in the Northaw Great Wood, Hertfordshire. *Earth Surface Processes*, *1*, 99–109.

Huggett, R. J. (1991). *Climate, Earth processes and Earth history*. Heidelberg: Springer.

Huggett, R. J. (1995). *Geoecology: An evolutionary approach*. London: Routledge.

Huggett, R. J. (1997). *Environmental change: The evolving ecosphere*. London: Routledge.

Huggett, R. J. (1998). Soil chronosequences, soil development, and soil evolution: A critical review. *Catena*, *32*, 155–172.

Huggett, R. J. (1999). Ecosphere, biosphere, or Gaia? What to call the global ecosystem. *Global Ecology and Biogeography*, *8*, 425–431.

Huggett, R. J. (2017). *Fundamentals of geomorphology*, 4th ed. Abingdon: Routledge.

Huggett, R. J., & Cheesman, J. E. (2002). *Topography and the environment*. Harlow, Essex: Prentice Hall.

Iticha, B., & Takele, A. (2018). Soil–landscape variability: Mapping and building detail information for soil management. *Soil Use and Management*, *34*, 111–123.

Jenny, H. (1930). An equation of state for soil nitrogen. *Journal of Physical Chemistry*, *34*, 1053–1057.

Jenny, H. (1941). *Factors of soil formation: A system of quantitative pedology*. New York: McGraw-Hill.

Jenny, H. (1946). Arrangement of soil series and types according to functions of soil forming factors. *Soil Science*, *61*, 375–391.

Jenny, H. (1958). The role of the plant factor in pedogenic functions. *Ecology*, *39*, 5–16.

Jenny, H. (1961a). Derivation of state factor equations of soil and ecosystems. *Soil Science Society of America Proceedings*, *25*, 385–388.

Jenny, H. (1961b). *E. W. Hilgard and the birth of modern soil science*. Pisa, Italy: Collana della Rivista 'Agrochimica' and Berkeley, California: Farallon.

Jenny, H. (1980). *The soil resource: Origin and behaviour* (Ecological Studies, vol. *37*). New York: Springer.

Johnson, D. L. (1985). Soil thickness processes. In P. Jongerius (Ed.), *Soils and geomorphology* (Catena Supplement 6, pp. 29–40). Braunschweig: Catena Verlag.

Johnson, D. L. (1990). Biomantle evolution and the redistribution of earth materials and artifacts. *Soil Science 149*, 84–102.

Johnson, D. L. (2002). Darwin would be proud: Bioturbation, dynamic denudation, and the power of theory in science. *Geoarchaeology: An International Journal*, *17*, 7–40.

Johnson, D. L., Domier, J. E. J., & Johnson, D. N. (2005a). Reflections on the nature of soil and its biomantle. *Annals of the Association of American Geographers*, *95*, 11–31.

Johnson, D. L., Domier, J. E. J., & Johnson, D. N. (2005b). Animating the biodynamics of soil thickness using process analysis: A dynamic denudation approach to soil formation. *Geomorphology*, *67*, 23–46.

Johnson, D. L., & Hole, F. D. (1994). Soil formation theory: A summary of its principal impacts on geography, geomorphology, soil–geomorphology, Quaternary geology and paleopedology. In R. Amundson (Ed.), *Factors of soil formation: A fiftieth anniversary retrospective* (Soil Science Society of America Special Publication 33, pp. 111–126). Madison, WI: Soil Science Society of America.

Johnson D. L., Keller, E. A., & Rockwell T. K. (1990). Dynamic pedogenesis: New views on some key soil concepts, and a model for interpreting Quaternary soils. *Quaternary Research*, *33*, 306–319.

Johnson, D. L., & Schaetzl, R. J. (2015). Differing views of soil and pedogenesis by two masters: Darwin and Dokuchaev. *Geoderma*, *237–238*, 176–189.

Johnson D. L., & Watson-Stegner, D. (1987). Evolution model of pedogenesis. *Soil Science*, *143*, 349–366.

Kline, J. R. (1973). Mathematical simulation of soil–plant relationships and soil genesis. *Soil Science*, *115*, 240–249.

Krupenikov, I. A. (1992). *History of soil science: From its inception to the present*. New Delhi: Oxonian Press.

Leguédois, S., Séré, G., Auclerc, A., Cortet, J., Huot, H., Ouvrard, S., et al. (2016). Modelling pedogenesis of Technosols. *Geoderma*, *262*, 199–212.

Li, X., McCarty, G. W., Karlenc, D. L., & Cambardellac, C. A. (2018). Topographic metric predictions of soil redistribution and organic carbon in Iowa cropland fields. *Catena*, *120*, 222–232.

Lin, H. S. (2003). Hydropedology. *Vadose Zone Journal*, *2*, 1–11.

Lin, H. S. (2011). Three principles of soil change and pedogenesis in time and space. *Soil Science Society of America Journal*, *75*, 2049–2070.

Lin, H. S. (2012). Hydropedology: Addressing fundamentals and building bridges to understand complex pedologic and hydrologic interactions. In H. Lin (Ed.), *Hydropedology: Synergistic integration of soil science and hydrology* (pp. 3–40). Amsterdam: Academic Press.

Ma, Y., Lia, X., Guo, Li, & Lin, H. (2017). Hydropedology: Interactions between pedologic and hydrologic processes across spatiotemporal scales. *Earth-Science Reviews*, *171*, 181–195.

Major, J. (1951). A functional factorial approach to plant ecology. *Ecology*, *32*, 392–412.

Mattson, S. (1938). The constitution of the pedosphere. *Annals of the Agricultural College of Sweden*, *5*, 261–276.

McBratney, A. B., Mendonça Santos, M. L., & Minasny, B. (2003). On digital soil mapping. *Geoderma*, *117*, 3–52.

McSweeney, K., Slater, B. K., Hammer, R. D., Bell, J. C., Gessler, P. E., & Petersen, G. W. (1994). Towards a new framework for modeling the soil–landscape continuum. In R. Amundson, J. Harden, & M. Singer (Eds.), *Factors of soil formation: A fiftieth anniversary retrospective* (Soil Science Society of America Special Publication Number 33, pp. 127–145). Madison, WI: Soil Science Society of America.

Milne, G. (1935a). Some suggested units of classification and mapping, particularly for East African soils. *Soil Research*, *4*, 183–198.

Milne, G. (1935b). Composite units for the mapping of complex soil associations. *Transactions of the Third International Congress of Soil Science, Oxford, England*, *1935*. 1, 345–7.

Milne, G. (1936). Normal erosion as a factor in soil profile development. *Nature*, *138*, 548–549.

Minasny, B., & McBratney, A. B. (1999). A rudimentary mechanistic model for soil production and landscape development. *Geoderma*, *90*, 3–21.

Minasny, B., McBratney, A. B., & Salvador-Blanes, S. (2008). Quantitative models for pedogenesis: A review. *Geoderma*, *144*, 140–157.

Moore, I. D., Gessler, P. E., Nielsen, G. A., & Peterson, G. A. (1993). Soil attribute prediction using terrain analysis. *Soil Science Society of America Journal*, *57*, 443–452.

Moore, I. D., Grayson, R. B., & Ladson, A. R. (1991). Digital terrain modelling: A review of hydrological, geomorphological, and biological applications. *Hydrological Processes*, *5*, 3–30.

Morison, C. G. T. (1949). The catena concept and the classification of tropical soils. In *Proceedings of the First Commonwealth Conference on Tropical and Sub-Tropical Soils*, *1948* (Commonwealth Bureau of Soil Science, Technical Communication No. 46, pp. 124–128). Harpenden, England: Commonwealth Bureau of Soil Science.

Morison, C. G. T., Hoyle, A. C., & Hope-Smith, J. F. (1948). Tropical soil–vegetation catenas and mosaics: A study in the south-western part of the Anglo-Egyptian Sudan. *Journal of Ecology*, *36*, 1–84.

Muhs, D. R. (1982). The influence of topography on the spatial variability of soils in Mediterranean climates. In C.E. Thorn (Ed.), *Space and time in geomorphology* (pp. 269–284). London: George Allen & Unwin.

Muhs, D. R. (1984). Intrinsc thresholds in soil systems. *Physical Geography*, *5*, 99–110.

National Research Council (2001). *Basic research opportunities in Earth science*. Washington, DC: National Academy Press.

Neustruev, S. S. (1915). On soil combination of plains and uplands [in Russian]. *Pochvovednie [Soil Science]*, *1*, 62–73.

Nikiforoff, C. C. (1959). Reappraisal of the soil. *Science*, *129*, 186–196.

Odgers, N. P., McBratney, A. B., & Minasny, B. (2008). Generation of *k*th-order random toposequences. *Computers & Geosciences*, *34*, 479–490.

Parton, W. J., Schimel, D. S., Cole, C. V., & Ojima, D. S. (1987). Analysis of factors controlling soil organic matter levels in Great Plains grasslands. *Soil Science Society of America Journal*, *51*, 1173–1179.

Pawlika, Ł., & Šamonil, P. (2018). Soil creep: The driving factors, evidence and significance for biogeomorphic and pedogenic domains and systems – A critical literature review. *Earth-Science Reviews*, *178*, 257–278.

Peacock, E., & Fant, D. W. (2002). Biomantle formation and artifact translocation in upland sandy soils: An example from the Holly Springs National Forest, North-Central Mississippi,

U.S.A. *Geoarchaeology: An International Journal*, *17*, 91–114.

Pereira, T. T. C., Almeida, I. C. C., de Oliveira, F. S., Schaefer, C. E. G. R., de Souza Pinheiro, L., & Matuk, F. A. (2018). Hydropedology of a high tableland with cerrado, Brazilian Central Plateau: The Frutal Catchment case study. *Revista Brasileira de Ciência do Solo*, *42*, e0160523. https://dx.doi.org/10.1590/18069657rbcs20160523

Phillips, J. D. (1989). An evaluation of the state factor model of soil ecosystems. *Ecological Modelling*, *45*, 165–177.

Phillips, J. D. (1993a). Progressive and regressive pedogenesis and complex soil evolution. *Quaternary Research*, *40*, 169–176.

Phillips, J. D. (1993b). Stability implications of the state factor model of soils as a nonlinear dynamical system. *Geoderma*, *58*, 1–15.

Phillips, J. D. (1998). On the relations between complex systems and the factorial model of soil formation (with discussion). *Geoderma*, *86*, 1–21.

Phillips, J. D. (2001). The relative importance of intrinsic and extrinsic factors in pedodiversity. *Annals of the Association of American Geographers*, *91*, 609–621.

Phillips, J. D. (2013). Nonlinear dynamics, divergent evolution, and pedodiversity. In J. J. Ibãnez & J. Bockheim (Eds.), *Pedodiversity* (pp. 59–78). Boca Raton, Florida: CRC Press.

Phillips, J. D. (2017). Soil complexity and pedogenesis. *Soil Science*, *182*, 117–127.

Polynov, B. B. (*1935*). Types of weathering crust. *Transactions of the Third International Congress of Soil Science, Oxford, England*, 1935, *1*, 327–330.

Polynov, B. B. (1937). *The cycle of weathering*. Translated from Russian by A. Muir; foreword by W. G. Ogg. London: Thomas Murby.

Quijano, J., & Lin H. (2014). Entropy in the critical zone: A comprehensive review. *Entropy*, *16*, 3482–3536.

Rasmussen, C., Pelletier, J. D., Troch, P. A., Swetnam, T. L., & Chorover, J. (2015). Quantifying topographic and vegetation effects on the transfer of energy and mass to the critical zone. *Vadose Zone Journal*, *14*(11). doi: https://doi.org/10.2136/vzj2014.07.0102

Rasmussen, C., Southard, R. J., & Horwath, W. R. (2005). Modeling energy inputs to predict pedogenic environments using regional environmental databases. *Soil Science Society of America Journal*, *69*, 1266–1274.

Rasmussen, C., & Tabor, N. J. (2007). Applying a quantitative pedogenic energy model across a range of environmental gradients. *Soil Science Society of America Journal*, *71*, 1719–1729.

Regan, E. J. (1977). *A natural energy basis for soils and urban growth in Florida* (master's thesis). University of Florida.

Richter, D. deB., & Yaalon, D. H. (2011). "The Changing Model of Soil" revisited. *Soil Science Society of America Journal*, *76*, 766–778.

Robinson, G. W. (1936). Normal erosion as a factor in soil profile development. *Nature*, *137*, 950.

Rode, A. A. (1947). *The soil-forming process and soil evolution*. Jerusalem: Israel Program for Scientific Translations (Translated into English by J. S. Joffe, 1961).

Roy, A. G., Jarvis, R. S., & Arnett, R. R. (1980). Soil-slope relationships within a drainage basin. *Annals of the Association of American Geographers*, *70*, 397–412.

Ruhe, R. V. (1960). Elements of the soil landscape. *Transactions of the Seventh International Congress of Soil Science, Madison*, *4*, 165–170.

Ruhe, R. V. (1975). Review of "Pedology, Weathering and Geomorphological Research" by P. W. Birkeland. *Geoderma*, *14*, 176–177.

Ruhe, R. V., & Walker, P. H. (1968). Hillslope models and soil formation: I. Open systems. *Transactions of the Ninth International Congress of Soil Science, Adelaide*, *4*, 551–560.

Runge, E. C. A. (1973). Soil development sequences and energy models. *Soil Science*, *115*, 183–193.

Saco, P. M., & Moreno-de las Heras, M. (2013). Ecogeomorphic coevolution of semiarid hillslopes: Emergence of banded and striped vegetation patterns through interaction of biotic and abiotic processes. *Water Resources Research*, *49*, 115–126.

Salvador-Blanes, S., Minasny, B., and McBratney, A. B. (2007). Modelling long-term in situ soil profile evolution: Application to the genesis of soil profiles containing stone layers. *European Journal of Soil Science*, *58*, 1535–1548.

Sasscer, D. C., Jordan, C. F., & Kline, J. R. (1971). A mathematical model of tritiated and stable water movement in and old-field system. In D. J. Nelson (Ed.), *Radionuclides in Ecosystems. Proceedings of the Third National Symposium on Radioecology* (pp. 915–923). CONF-710501-P1, US Atomic Energy Commission.

Schaetzl, R. J. (2013). Catenas and soils. In J. Shroder (Ed. in Chief), Pope, G.A. (Ed.), *Treatise on geomorphology: Vol. 4. Weathering and soils geomorphology* (pp. 145–158). San Diego, CA: Academic Press.

Shaw, C. F. (1930). Potent factors in soil formation. *Ecology*, *11*, 239–245.

Shepard, C., Schaap, M. G, Pelletier, J. D., & Rasmussen, C. (2017). A probabilistic approach to quantifying soil property change through time integration of energy and mass input. *SOIL*, *3*, 67–82.

Simonson, R. W. (1959). Outline of a generalized theory of soil genesis. *Soil Science Society of America Proceedings*, *23*, 152–156.

Simonson, R. W. (1968). Concept of soil. *Advances in Agronomy 20*, 1–47.

Sommer, M. (2006). Influence of soil pattern on matter transport in and from terrestrial biogeosystems: A new concept for landscape pedology. *Geoderma*, *133*, 107–123.

Sommer, M., & Schlichting, E. (1997). Archetypes of catenas in respect to matter a concept for structuring and grouping catenas. *Geoderma*, *76*, 1–33.

Stephens, C. G. (1947). Functional synthesis in pedogenesis. *Transactions of the Royal Society of South Australia*, *71*, 168–181.

Stockmann, U., Minasny, B., & McBratney, A. B. (2011). Quantifying processes of pedogenesis. *Advances in Agronomy*, *113*, 1–74.

Suess, E. (1875). *Die Entstehung der Alpen*. Wien: Wilhelm Braunmüller.

Suess, E. (1883–1909). *Das Antlitz der Erde*, *5* vols. Wien: Gustav Freytag.

Tandarich, J. P., Darmody, R. G., Follmer, L. R., & Johnson, D. L. (2002). Historical development of soil and weathering

profile concepts from Europe to the United States of America. *Soil Science Society of America Journal*, *66*, 335–346.

Targulian, V. O., & Sokolova, T. A. (1996). Soil as a bio-abiotic natural system: A reactor, memory and regulator of biospheric interactions. *Eurasian Soil Science*, *29*, 34–47.

Temme, A.J.A.M., & Vanwalleghem, T. (2016). LORICA – A new model for linking landscape and soil profile evolution: Development and sensitivity analysis. *Computers & Geosciences*, *90*, 131–143.

Troeh, F. R. (1964). Landform parameters correlated to soil drainage. *Soil Science Society of America Proceedings*, *28*, 808–812.

Vanwalleghem, T., Stockmann, U., Minasny, B., & McBratney, A. B. (2013). A quantitative model for integrating landscape evolution and soil formation. *Journal of Geophysical Research: Earth Surface*, *118*, 331–347.

Verboom, W. H., & Pate, J. S. (2013). Exploring the biological dimension to pedogenesis with emphasis on the ecosystems, soils and landscapes of southwestern Australia. *Geoderma*, 211–212, 154–183.

Vernadsky, V. I. (1926). *Biosfera*. Leningrad: Nauchoe Khimikoteknicheskoe Izdatelstvo.

Vernadsky, V. I. (1929). *La biosphère*. Paris: Félix Alcan.

Vernadsky, V. I. (1998). *The biosphere*, translated by David B. Langmuir. Heidelberg: Springer-Verlag.

Volobuyev, V. R. (1963). *Ecology of soils*. Academy of Sciences of the Azerbaidzan SSR. Institute of Soil Science and Agrochemistry. Israel Program for Scientific Translations, Jerusalem (Translated into English by A. Gourevich, 1964).

Vreeken, W. J. (1973). Soil variability in small loess watersheds: Clay and organic matter content. *Catena*, *2*, 321–336.

Wackett, A. A., Yoo, K., Amundson, R., Heimsath, A. M., & Jelinski, N. A. (2018). Climate controls on coupled processes of chemical weathering, bioturbation, and sediment transport across hillslopes. *Earth Surface Processes and Landforms, 43*, 1575–1590 doi: 10.1002/esp.4337

Wilde, S. A. (1946). *Forest soils and forest growth*. Waltham, MA: Chronica Botanica.

Wilding, L. P., & Lin, H. (2006). Advancing the frontiers of soil science towards a geoscience. *Geoderma*, *131*, 257–274.

Willgoose, G. (2018). *Principles of soilscape and landscape evolution*. Cambridge: Cambridge University Press.

Yaalon, D. H. (1975). Conceptual models in pedogenesis: Can soil-forming functions be solved? *Geoderma*, *14*, 189–205.

Yaalon, D. H., & Yaron, B. (1966). Framework for man-made soil changes: An outline of metapedogenesis. *Soil Science*, *102*, 272–277.

Yoo, K., Amundson, R., Heimsath, A. M., Dietrich, W. E., & Brimhall, G. H. (2007). Integration of geochemical mass balance with sediment transport to calculate rates of soil chemical weathering and transport on hillslopes. *Journal of Geophysical Research: Earth Surface*, *112*, F02013.

Zakharov, S. A. (1927). *A course of soil science* [in Russian]. Moscow: Gosizdat.

Zinck, J. A., Metternicht, G., Bocco Verdinelli, G. H. R., & Del Valle, H. F. (Eds.) (2016). *Geopedology: An integration of geomorphology and pedology for soil and landscape studies*. Cham: Springer.

Part II
Soil History

2

Soils, Chemical Weathering, and Climate Change in Earth History

Steven G. Driese[1], Lee C. Nordt[1], and Gary E. Stinchcomb[2]

ABSTRACT

Earth's changing climates, landscapes, and atmospheres are recorded in paleosols, which form in the Earth's critical zone by interactions between the lithosphere/pedosphere, biosphere, atmosphere and hydrosphere. Weathering during much of the Precambrian Eon was dominated by very high pCO_2 (10x to >20x present atmospheric level, PAL) leading to acidic chemical weathering, with additional and very poorly constrained weathering influences of primitive biota. The Great Oxidation Event at 2.0–2.2 Ga was marked by a major increase in pO_2, which was still very low compared to modern conditions. Towards the end of the Precambrian (Neoproterozoic) at least two major Snowball Earth glaciations occurred, punctuated by rapid warming, which intensified weathering processes, leading to releases of nutrients to oceans and the Cambrian Explosion and diversification of life. By the early Paleozoic the first nonvascular land plants evolved; these were small in stature, lacked deep root systems, were spore-reproducing, and were limited to wet soil environments. They were followed by the arrival of invertebrate terrestrial soil organisms. By the Middle to Late Devonian, trees with deep-penetrating root systems evolved that accelerated weathering and soil formation through the release of organic acids, which enhanced clay production. Coincident with afforestation, a significant drop in pCO_2 (at or below PAL) and concomitant rise in pO_2 (for a time exceeding PAL) culminated at the end of the Paleozoic Era with widespread Carboniferous coal swamps. Paleosols record the end-Permian mass extinction and the Cretaceous-Paleogene mass extinction and complement the marine records of these events. The Paleocene-Eocene Thermal Maximum (PETM), a transient 200 kyr warming spike attributed to release of methane hydrates, is considered the closest ancient analog to modern climate change. Evolution of angiosperms (flowering plants) in the Cretaceous, and C_4 grasses in the Miocene, record increasing diversification of land plant strategies and ability to occupy all known major terrestrial ecological niches.

2.1. INTRODUCTION

2.1.1. Definition of Paleosols

Paleosols are "fossil" soils that have been buried and preserved as part of the sedimentary rock record (Retallack, 2001a). In Quaternary deposits, the paleosols are commonly referred to as "buried soils" and are relatively soft and unconsolidated, with properties like those of modern soils (Birkeland, 1999). For older (pre-Quaternary) paleosols, the processes of burial compaction and diagenesis (cementation and mineral alteration) contribute to lithification, resulting in a paleosol with rock properties. Retallack (1988) proposed that three primary criteria identify paleosols: root traces, soil horizons, and soil structures (peds).

Root traces are the most unequivocal evidence for a fossil soil (Retallack, 1988, 2001b). Such traces satisfy even a soil scientist's definition of soil as material that supports, or once supported, plant life. However, roots

[1]*Department of Geosciences, Baylor University, Waco, Texas, USA*

[2]*Watershed Studies Institute & Department of Earth and Environmental Sciences, Murray State University, Murray, Kentucky, USA*

Hydrogeology, Chemical Weathering, and Soil Formation, Geophysical Monograph 257, First Edition.
Edited by Allen Hunt, Markus Egli, and Boris Faybishenko.

DOI: 10.1002/9781119563952.ch2

are rarely preserved as fossil organic tissues. More commonly, "drab-haloed" root traces are preserved in paleosols because of organic decomposition of root tissues and redox changes occurring within the root pore. Rhizoliths and rhizocretions composed of calcium carbonate have high preservation potential. Root casts are infilled with soil/sediment due to preferential stages of periderm and endoderm decay. Permineralization/petrifaction of tissues is possible in some circumstances, as is carbonization of organic tissues. Problems arise because of secular changes in plants and plant root systems, and the fact that many older paleosols must have formed without vascular land plants. Pre-Devonian soils had no true roots, as indicated by studies by Driese and Foreman (1992), Driese and Mora (2001), and Driese et al. (1992, 1997, 2000), which have shown evidence for pre-Silurian lichenous (or algal) mats (but no roots), and Silurian rhizomatous structures (2–3 cm deep). The Devonian exhibits the transition to "true roots," with Early Devonian paleosols showing evidence of roots 10–15 cm deep and Late Devonian taproots 2–3 m deep.

Soil horizons are very diagnostic when identifiable, because they indicate specific genetic processes of soil formation (e.g. clay or carbonate accumulation); however, boundaries (and horizons per se) are commonly quite obscure due to loss of organic matter during diagenesis, loss of original soil colors during burial diagenesis and loss of soil structures during cementation (Retallack, 1988, 2001b). Soil horizons do not always equate with changes in rock color nor with changes in grain size.

Soil structures (peds) are diagnostic because parent materials, such as mudrocks, are typically fissile or bioturbated when deposited, but ped formation imparts a different weathering pattern that is distinctive in the field (i.e., ped structures), which have different sizes and shapes indicative of specific pedogenic processes (Retallack, 1988, 2001b). Peds commonly are the result of episodic soil wetting and drying, as well as soil disturbance by plant roots and soil animals. Peds appear to survive physical compaction during burial diagenesis, but secondary cementation may make peds very obscure.

Other supplementary criteria include micromorphology (thin-section analysis), geochemical patterns of elemental gains or losses attributable to weathering, stable isotopes of organic matter and carbonate, depositional or paleoenvironmental "context," such as association with paleocatenary relationships of a past landscape, sequence-stratigraphic boundaries, exposure surfaces, etc. (e.g. Atchley et al., 2013a; Birkeland, 1999; Retallack, 2001b; Sheldon & Tabor, 2009; Stoops, 2003). In particular, mineral weathering has been evaluated geochemically using the Chemical Index of Alteration (CIA) of Nesbitt and Young (1982): $100 \times [(Al_2O_3)/ (Al_2O_3 + CaO + Na_2O + K_2O)]$, and a K-free version defined as the Chemical Index of Alteration minus Potash (CIA-K) by Maynard (1992): $100 \times [(Al_2O_3/ (Al_2O_3 + Na_2O + CaO)$.

2.1.2. Soil-Forming Factors

Very early work by the British naturalist Charles Darwin and the Russian soil scientist Dokuchaev was conducted to determine the relative importance of plants versus animals in soil formation (Johnson & Schaetzl, 2015). These efforts were followed by development of the Environmental Factor Model of Hans Jenny (1941), written as: S = f (cl, o, r, p, t). The original model states the soil (S), is a function of the "soil-forming" factors of climate (cl), organisms (o), relief (or topography/drainage) (r), parent material (p), and time (t). As it turns out, Jenny did not consider these so much as variables and factors of soil formation, but rather as "state factors" whose interrelationships and fluxes define the evolution of the soil system. Nevertheless, as a conceptual model, the Jenny (1941) soil state factors concept is still very useful, and changes in soils and weathering as functions of changes in climate and organisms are the foci for our discussion. If several of these factors can be isolated, then one can be examined: for example, for climosequences the attempt is to try to isolate and hold constant all the state functions except for climate. Similarly, for a chronosequence, the attempt is to try to isolate and hold constant all the state functions except for time. For a toposequence, one isolates all the state functions except for relief or landscape position/drainage. A lithosequence compares soils formed on different parent material lithologies. For a biosequence, one would compare soils in which all the state factors are constant except for soil organisms (plants and animals). As should also be apparent to the reader, identifying an ideal soil system for study that isolates a single state factor (climo-, bio-, topo-, litho- or chronosequence) is exceedingly difficult (Birkeland, 1999).

2.1.3. Paleosols as Potential Records of "Paleo-Critical Zones"?

As originally defined by the National Science Foundation (NSF) Geosciences Beyond 2000 Report, the "Critical Zone" highlighted challenges to the Earth sciences community to expand its capability to predict future changes in the Earth climate system (NSF, 2000). The National Research Council and National Academy of Sciences subsequently identified integrative studies of the critical zone as one of the six compelling opportunities for earth scientists in the next decade (National Research Council, 2001, 2003). In 2006 NSF created and funded a national Critical Zone Observatory (CZO)

program, which now consists of 10 active observatories stationed throughout the US (http://criticalzone.org/).

Why is the critical zone (CZ) so important? The CZ is defined as the near-surface environment in which complex interactions involving rock, soil, water, air, and living organisms regulate the natural habitat from the top of the vegetation canopy to the groundwater table below (Brantley et al., 2007; National Research Council, 2001). Critical zones are actualistic environmental laboratories designed to study the biogeochemical byproducts of the interactions of the atmosphere (energy, gases) and hydrosphere (water flux, mineral weathering) acting on the lithosphere (chemical elements, physical substrate) to produce the pedosphere (weathered lithosphere, nutrient storage) and biosphere (floral/faunal, nutrient cycling). Critical zone studies provide a framework for studying the response of Earth systems to the effects of tectonic, climatic, and anthropogenic perturbations at multiple temporal and spatial scales. CZOs are designed to study the interface of Earth systems within a defined area by monitoring climate with weather stations and for water, chemical, and gas flux; assessing vegetation dynamics from the landscape to molecular level; and performing thermodynamic and kinetic modeling of the integrated system.

However, the sedimentary geology community, and the smaller subset community interested in paleosols (i.e. paleopedology), has largely been excluded from the CZ discussion, which is unfortunate because it is the deep-time sedimentary record that informs us about past CZ systems and provides important information useful for predicting future changes in the Earth climate system. An NSF "Transitions" report (Parrish et al., 2011) argued that the deep-time critical zone (DTCZ) concept is important because future climate states will appear unlike anything we have seen during the last glacial epoch (last 2 Ma years). Further, climates of the past are often examined using general circulation models (GCMs); however, the only test of the validity of any proposed GCM is to use actual data obtained from ancient geologic records of climate preserved in rocks, including ancient soil deposits known as paleosols. Geoscientists researching paleoclimate are thus positioning themselves to study critical transitions of the past to better understand our future (Montañez & Isaacson, 2013; Parrish & Soreghan, 2013). Nordt and Driese (2013) proposed to extend the CZ concept to deep time, arbitrarily defined as pre-Quaternary (>2 Ma).

The preservation potential of CZ properties in the deep-time sedimentary record is under examination; however, because of recent advances in the study of paleosols, and especially in the development of refined geochemical paleoclimate proxies and pedotransfer functions for certain soil types, it is now possible to reconstruct biogeochemical cycles from paleosols preserved in the sedimentary record in deep time (Nordt et al., 2011). Nordt and Driese (2013) presented a case study of a DTCZ as investigated within the framework of a DTCZ observatory. A broad compilation of geochemical approaches to paleoclimate study using paleosols is provided in Sheldon and Tabor (2009). Advances in interpretations derived from modern soil geochemical databases have greatly improved our understanding of the geochemistry of weathering; in addition, better methods for estimating mean annual precipitation (MAP) and mean annual temperature (MAT) have been found using the bulk geochemistry of paleosols (e.g. Gallagher & Sheldon, 2013; Lukens et al., 2018; Nordt & Driese, 2010a, 2010b; Sheldon et al., 2002; Stinchcomb et al., 2016).

2.1.4. Paleosol Taxonomy

Taxonomic systems provide a means of consistent identification, classification and communication of key attributes of natural phenomena. The most commonly used modern taxonomy is the US system that employs 12 soil orders at the highest categorical level (Soil Survey Staff, 1999). This system has been applied more than any other to paleosols, even though because of burial diagenesis it is difficult measuring some of the properties in the same way as in modern soils. A commonly used alternative system designed specifically for paleosols uses only observable field properties, which is not as robust from an interpretive standpoint, but easier to use (Mack et al., 1993).

To assist with referencing of paleosol types, and as a proxy for the soil-forming factors, we refer to both taxonomic systems in this chapter. Table 2.1 provides a summary of key properties for the modern US soil taxonomy, and Table 2.2 key properties developed specifically as a paleosol taxonomy.

2.2. PRECAMBRIAN EON (4.55–0.54 GA)

2.2.1. General History

The Precambrian comprises seven-eighths of Earth history and ended circa 540 million years ago; it is generally subdivided into two formal geologic time units, the Archean and Proterozoic eons, with the boundary at 2.5 Ga, and inclusion of a pre-Archean unit known as the Hadean for time (not represented by preserved rock) extending from the initial formation of the Earth at 4.55 Ga and ending at about 4.1 Ga (Figure 2.1). During this vast interval of time, the first continental crust formed, as well as the first water bodies and first atmosphere on Earth. Paleosols, although commonly cryptic and metamorphosed, are routinely used to interpret the pO_2 and pCO_2 of the Precambrian atmosphere, as well as providing

Table 2.1 Summary properties of modern soil orders.

Soil Order	Common Horizons	Diagnostics	Interpretation
Entisols	A	Ochric surface horizon, no subsurface diagnostics	Weakly developed
Inceptisols	Bw, Bk, By, Bg	Cambic, calcic, gypsic horizons, differential drainage	Weakly to moderately developed subsoil (structure, salts)
Mollisols	A	Mollic surface horizon, variable subsoil horizons	Grassland surface horizon, weakly to moderately developed subsoil (structure, salts)
Alfisols	Bt, Btg, Btk, Bty	Argillic horizon, differential subsoil horizons	Well-developed subsoil (silicate clay), hardwood forests or savannas
Spodosols	Bhs, E	Spodic, albic horizons	Sandy subsoil (sesquioxides), coniferous forests
Ultisols	Bt, Btg, E	Argillic, albic horizons	Well developed (silicate clay), few weatherable minerals, hardwood or coniferous forests
Oxisols	Bo	Oxic horizon	Very well developed (sesquioxide/kaolinitic clay), tropical forests/savannas
Vertisols	Bss, Bssk, Bssy, Bssg	Shrink-swell properties	Weak to well developed, slickensides
Andisols	Bw, (Bk, By)	Andic properties	Weakly to moderately developed, volcanic ash
Gelisols	Bf, Bj	Gelic properties	Weakly developed, permafrost
Aridisols	Bw, Bk, By, Bz, Btn	Climate regime	Weakly to well developed, arid
Histosols	O	Organic materials	Bogs, swamps

Source. Data from Soil Survey Staff (1999).

Table 2.2 Paleosol orders, associated properties, and equivalents to the U.S. Soil Taxonomy.

Soil Order	Common Horizons	Diagnostics	Interpretive Equivalents
Protosols	A	No subsoil	Entisols, some Inceptisols
Calcisols	Bk	Calcic (presence of pedogenic calcite)	Aridisols, Inceptisols, Mollisols, Vertisols, Alfisols, Andisols
Gypsisols	By	Gypsic (presence of pedogenic gypsum)	Aridisols, Inceptisols, Mollisols, Vertisols, Alfisols, Andisols
Argillisol	Bt	Argillic (increase in clay)	Alfisols, Ultisols, and some Mollisols, Aridisols
Spodosols	Bhs	Spodic, albic (translocation of OM and Al/Fe complexes;	Spodosols
Oxisols	Bo	Oxic (highly weathered, mostly Al and Fe)	Oxisols
Vertisols	Bss	Vertic (shrink-swell) properties	Vertisols
Gleysols	Bg	Wetness (Fe reduction)	Aquic moisture regime of most soil orders (e.g. Aqualfs)
Histosols	O	Organic materials	Histosols

Source. Data from Mack et al. (1993).

evidence for the presence of terrestrial (generally microbial) life on Earth (Rye & Holland, 1998). Although a detailed summary of Precambrian history is outside the scope of this paper, in what follows we touch upon a few high points.

2.2.1.1. Plate tectonic "styles"

The traditional view is that Precambrian plate tectonics was dominated by at least three "cycles" of supercontinent formation associated with superplume formation and episodes of juvenile crust formation at 2.7, 1.9, and 1.2 Ga, interspersed with supercontinent breakups (Condie, 1998, 2004). The Archean-Proterozoic 2.5 Ga boundary corresponds to a major worldwide unconformity and was accompanied by a change from a more primitive form of plate tectonics (characterized by small plates dominated by rapid subduction beneath trenches of island arcs) to modern-style plate tectonics (characterized by large plates that interacted more slowly) (Cawood et al., 2006; Korenaga, 2013). Proterozoic plates had a wider "freeboard" and increased shallow-marine and terrestrial deposits. However, recent work by Dygert et al. (2018) suggests that plate tectonics could have been active from the Earth's very beginning.

2.2.1.2. Geology and sedimentary deposits

Archean rocks are dominated by (1) granite-gneiss terrains (complexly deformed and metamorphosed granite

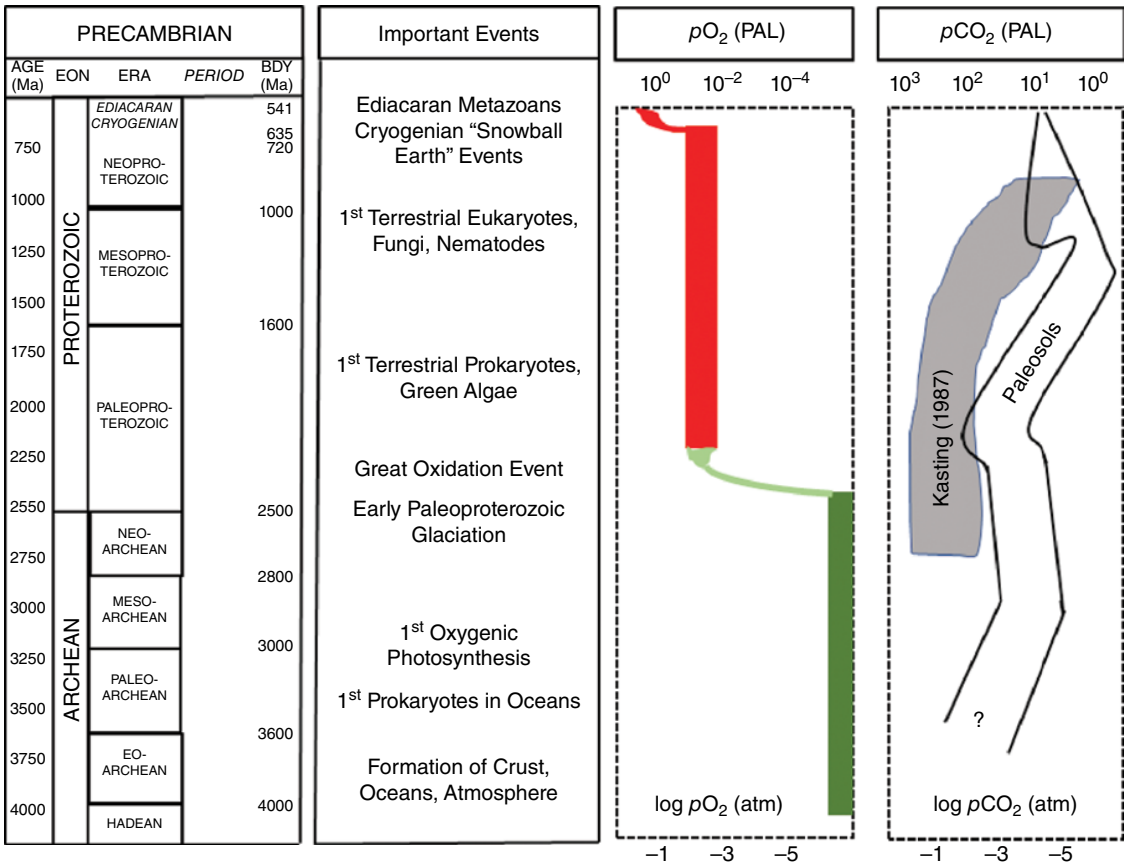

Figure 2.1 Changes in climate, organisms, and atmospheric chemistry important to chemical weathering during the Precambrian. Geologic timescale after Walker et al. (2018). *Sources:* Kasting (1987, 1993), Rye and Holland (1998), Sheldon (2006), Mitchell and Sheldon (2010), Driese et al. (2011), Kanzaki and Murakami (2015, 2016), Mills et al. (2019).

and gneiss, which are the oldest basement rocks dated on Earth) and by (2) greenstone belts (less deformed sequences of rocks composed of, from bottom to top: ultramafic rocks such as peridotites, overlain by pillow basalts, which are in turn overlain by deepwater (turbidite) greywacke (dirty, clay-rich) sandstones and shales (Wiemer et al., 2018). Paleosols are notably rare (Rye & Holland, 1998). The formation of cratonic lithosphere coincided with the initiation of plate tectonics determined as circa 3 Ga by Beall et al. (2018). Proterozoic sedimentary rocks are more diverse and include shallow-water sandstone, shale, and carbonate rocks; extensive evaporite deposits; terrestrial red-bed deposits; banded iron formations containing mainly oxidized Fe; and more abundant paleosols. The amount of continental crust was extensive by this time, and the Earth's plates were approaching the sizes of today.

Problems invariably arise when examining Precambrian paleosols for use as paleoclimate proxies because of metamorphism involving textural, mineralogical, and chemical changes (Retallack, 1992). Nearly all Precambrian paleosols have been metamorphosed to varying degrees, some as high as garnet and sillimanite grade, but most are greenschist grade or lower. Resulting reconstitution of chemistry, new crystal growth, and new minerals make it difficult to infer the original weathering profile, and thin-section micromorphological assessment of original pedogenic features is difficult. Potassium metasomatism, which is the wholesale addition of large quantities of K_2O to the profiles by warm to hot burial fluids, also presents a major problem. Most Precambrian paleosols are enriched in K, and some are enriched in Na_2O as well. Therefore, chemical indices of alteration (CIA) calculated from bulk chemical data must be corrected before considering applications of weathering or MAP proxies to the profiles (Driese et al., 2007; Fedo et al., 1995). Finally, absence of body fossils is problematic, and there may not even be any isotopic or biogeochemical traces of organisms (microbes) that were involved in the weathering processes.

2.2.2. Paleosol Records of Atmospheric CO_2

The early atmosphere of Earth originated by a combination of volcanic exhalations, plus gases and ice captured from passing comets. Precambrian atmospheres were *not* identical to those of modern Earth's (Canfield, 2005; Catling & Claire, 2005; Zahnle, 2006). Astronomic constraints, referred to as the "faint young-sun paradox," are known from solar evolutionary models that predict an early Archean sun that was 30% less luminous than today. With a weaker sun and an atmosphere like that of today, the entire surface of the Earth should have been frozen (frozen oceans). The "paradox" is that the geological record indicates that liquid water was abundant, that weathering was occurring on the surface, and that there were at least two major intervals of glaciation (2.3–2.5 Ga, 800–650 Ma) (von Paris et al., 2008), and possibly a third at 2.9 Ga (Kopp et al., 2005). The solution to the paradox is that Earth must have had an early atmosphere that was enriched in greenhouse gases, such as CO_2, methane, and water vapor; early calculations by Kasting (1993) suggested that CO_2 concentrations were as high as 50x–100x present atmospheric levels (PAL), which would have provided the necessary greenhouse effect. More recent modeling by Kanzaki and Murakami (2018a, 2018b) suggested that the Archean pCO_2 levels need not have been nearly this high to maintain ice-free conditions, which is also supported by estimates derived from paleosols placing conditions at ≈10x–20x PAL during the Archean and between ≈1x and 10x PAL during the Proterozoic (Driese et al., 2011, 2018; Kanzaki & Murakami, 2015; Mitchell & Sheldon, 2010; Sheldon, 2006, 2013).

2.2.3. Paleosol Records of Atmospheric Oxygen

Rye and Holland (1998) examined published reports of more than 50 Precambrian paleosols described in the literature, ranging in age from the 2.75 Ga Mt. Roe paleosol in Australia to the 1.1 Ga Sturgeon Falls paleosol from Michigan. Paleosols were classified as definite, likely, possible, or unlikely, depending on whether they satisfied what the authors proposed to be five diagnostic criteria: (1) The paleosol must be developed on homogeneous parent rock and have been preserved in place (not on transported material). (2, 3, 4) The paleosol must exhibit changes in mineralogy (2), texture (3), and chemical composition (4) from the parent material to top of paleosol that are consistent with soil-forming processes. (5) There must be identifiable soft-sediment features along the contact between the paleosol and immediately overlying rocks, indicating that it was initially unlithified.

Rye and Holland's (1998) interpretations were that the chemical profiles in the 15 identified "definite" paleosols clearly indicated that atmospheric pO_2 rose between 2.75 and 2.0 Ga. The Σ Fe/Al ratio profiles suggest that atmospheric pO_2 rose from $< 8 \times 10^{-4}$ atm to >0.03 atm by around 2.2 Ga, termed the Great Oxidation Event. Kanzaki and Murakami (2016), in contrast, have estimated lower pO_2 levels for four previously published Archean and Proterozoic paleosols: $10^{-7.1}$–$10^{-5.4}$ atm at ≈2.46 Ga, $10^{-5.0}$–$10^{-2.5}$ atm at ≈2.15 Ga, $10^{-5.2}$–$10^{-1.7}$ atm at ≈2.08 Ga, and more than $10^{-4.6}$–$10^{-2.0}$ atm at ≈1.85 Ga. Comparison of their calculated pO_2 levels to the previously proposed quantitative patterns of oxygen rise in the literature suggests that a drastic rise of oxygen would not have occurred at ≈2.4 Ga, instead supporting a slightly rapid rise of oxygen at ≈2.4 Ga and a gradual rise of oxygen in the Paleoproterozoic over the long term. Two case studies are mentioned here: (1) the 2.2 Ga Hekpoort paleosol at Waterval Onder, South Africa, which is the youngest Precambrian paleosol for which Fe is mainly reduced, which would seem to indicate lower oxygenation (Driese, 2004; Retallack, 1986a; Rye & Holland, 2000), and (2) the 1.8 Ga Mt. Isa paleosols of Queensland in northeastern Australia, for which the Fe in the paleosols is completely oxidized (Driese et al., 1995). The Mt. Isa paleosols contain prominent redoximorphic features that suggest warm to cool temperate paleoclimate (mean annual soil temperature 5–20 °C) characterized by seasonal saturation, with a minimal concentration of organic C (at least 1 wt%, possibly of microbial or bacterial origin) to allow for Fe reduction.

2.2.4. Neoproterozoic "Snowball Earth" Events, 570–680 Ma, and Paleosols

The "snowball Earth" hypothesis posits that the Earth's surface became entirely or nearly entirely frozen at least once, sometime earlier than 650 Ma (Hoffman et al., 1998; Hoffman & Schrag, 2002). Proponents of the hypothesis argue that it best explains sedimentary deposits generally regarded as of glacial origin at tropical paleolatitudes, and other otherwise enigmatic features in the geological record. Opponents of the hypothesis contest the implications of the geological evidence for global glaciation, the geophysical feasibility of an ice- or slush-covered ocean, and the difficulty of escaping an all-frozen condition. There are several unanswered questions, including whether the Earth was a full snowball or a "slushball" with a thin equatorial band of open (or seasonally open) water. The geological time frames under consideration come before the sudden multiplication of life forms on Earth known as the Cambrian explosion, and the most recent snowball episode may have triggered the evolution of multicellular life on Earth. Another, much earlier and longer, snowball episode, the Huronian

glaciation, which occurred 2400 to 2100 Ma, may have been triggered by the oxygen catastrophe.

One well-studied paleosol formed between Cryogenian glaciations is the Baltic paleosol of Estonia (Driese et al., 2018; Liivamägi et al., 2014, 2015). The Neoproterozoic record of paleosols is generally sparse; however, the weathering intensity as well the depth of the weathering of the Baltic paleosol is remarkably higher/deeper compared to about 570 Ma weathering profiles described in the Gaskiers Formation, Newfoundland, Canada (Retallack, 2013c), which are thin and weakly developed, with maximum CIA values of 60 and clay content between 30% and 40%. In contrast, the 980 Ma sub-Torridonian Group weathering profile in Scotland more closely resembles the Baltic paleosol and is characterized by significant oxidation and pedogenic clay formation (including smectite) at the expense of primary silicate phases, indicating formation in a subhumid and probably seasonal temperate to tropical environmental setting (Retallack & Mindszenty, 1994). Also, well-preserved Mesoproterozoic paleosol profiles (Sturgeon Falls and Good Harbor Bay, Michigan, USA) described by Mitchell and Sheldon (2009; 2010) have lower CIA values, up to 50 in Good Harbor Bay and 58 in Sturgeon Falls, as compared to the higher values of the Baltic paleosol.

The climate during Neoproterozoic time was characterized by episodic "snowball Earth" cooling events (Harland, 2007), whereby the cool climate states were punctuated by warm-humid periods (Pierrehumbert et al., 2011). It has been suggested that highly cyclic CO_2 levels accumulated over the glacial periods triggered intense continental weathering "consuming" the elevated atmospheric CO_2 (Ridgwell et al., 2003). Effects on paleosol development should have been pronounced: for example, periglacial paleosols representing the oldest paleo-Gelisols that are evidence for a cold Cryogenian paleoclimate were reported near Adelaide, South Australia, by Retallack et al. (2015), and these paleosols, which clearly formed in a much colder paleoclimate, are quite unlike the Baltic paleosol. MAP estimates of circa 1500–1600 mm/yr for the Baltic paleosol are based on the CIA-K geochemical proxy of Sheldon et al. (2002) and MAT estimates of 13–15 °C based on their Na/K salinization model (Driese et al., 2018; Liivamägi et al., 2015). The duration of paleoweathering for the Baltic paleosol could not be constrained except to <40 million years.

2.2.5. Primitive State of Terrestrial Biotic Conditions and Cryptic Preservation

The traditional view of Precambrian life on land has been described by some as a microbial "slime-world" dominated by cyanobacteria, bacteria, and fungi. But this is perhaps too simplistic, and what if we are underestimating the role of terrestrial biota in Precambrian weathering processes? Arbuscular mycorrhizal fungi are the most ancient of the mycorrhizal fungi, with fossil evidence going back to the Ordovician period (Redecker et al., 2000). However, molecular clock studies indicate that they may have originated much earlier, possibly 1.2–1.4 Ga (Heckman et al., 2001). Increasing evidence points to the origin of eukaryotes after the Great Oxidation Event of 2.0–2.2 Ga (Beraldi-Campesi, 2013). Modern studies in South Africa show a diverse biosphere that consists of microbes and eukaryotes (Eukaryota, Bacteria, and Archaea), which occupy fractures and other micropores at great depths below the current surface (1–2 km) under conditions of elevated temperature, unusual water chemistry, and in which the organisms are either sulfur-reducing bacteria (under low oxygen) or eukaryotes that mainly feed on fungal mycelia coating the fractures and mineral surfaces (Borgonie et al., 2011, 2015). The estimated biomass in these deep terrestrial systems must be significant. Documentation of such ecosystems in the paleo (rock) record is currently lacking. But is it because of lack of preservation, or because researchers have not been looking hard enough?

Biotic enhancement of weathering and changes in atmospheric oxygen and carbon dioxide across the Neoproterozoic (1000–544 Ma) were proposed by Lenton and Watson (2004) and linked to selective weathering of phosphorus from rocks. Kump (2014) hypothesized a link between Neoproterozoic "greening" of the land surface and formation of a more oxygen-rich paleoatmosphere, starting at circa 850 Ma, which reflected the establishment of the first terrestrial fungal-lichen ecosystems. Mitchell and Sheldon (2010) used the chemical composition of the ~1.1 Ga Sturgeon Falls profile in Michigan to calculate an atmospheric pCO_2 value of 4–6x PAL, which is like previous estimates for the 980 Ma Sheigra paleosols in Scotland (Sheldon, 2006). A new study links the rise in atmospheric oxygen in the Precambrian to cooling mantle and crystallization temperatures, which also lead to the rise of crystallization of igneous rocks with increasing P; phosphorus is an essential nutrient that became increasingly available to organisms in the Precambrian (Cox et al., 2018).

Examining the Earth system more broadly, the appearance of eukaryotic macrofossils, according to Beraldi-Campesi's (2013) compilation, could have been as early as the Paleoproterozoic, which was well after the preservation of paleosols, terrestrial microfossils, and paleosol organic matter. Raman spectroscopy has been shown to be very useful for interpreting types of organic matter in geologic materials. In a recent study by Homann et al. (2018) kerogen was identified in 3.2 Ga terrestrial organic mats. Molecular-clock studies by Heckman et al. (2001) suggested that among eukaryotes, nematodes were likely

the first soil animals, appearing in the late Proterozoic at 1.2 Ga, before arthropods and vertebrates, and coincident with fungi and early plants such as green algae. Interestingly, nematodes have been filtered by Borgonie et al. (2011, 2015) from water pumped or seeping out of fractures in gold mines in South Africa, at depths of 1–2 km, and thus they are clearly able to survive under extreme environmental conditions of elevated temperatures and unusual water chemistries.

2.3. PHANEROZOIC EON (540 MA TO PRESENT)

Boucot et al. (2013) provided a comprehensive analysis of Phanerozoic paleoclimate in the form of an atlas of lithologic indicators of climate. It utilized geophysical data to establish the paleo-positions of the Earth's tectonic plates through geologic time, at the same time using the spatial distributions of sedimentary lithologies indicative of specific climate conditions, some of which are paleosols or related materials (e.g. coal, laterite, bauxite, kaolinite, calcretes, etc.). Mack and James (1994) proposed a global relationship between paleoclimate and paleosols, using the Mack et al. (1993) paleosol taxonomy (described previously) for the Phanerozoic. Retallack (2001b, 1986b) predicted changes in paleosols corresponding to changes in climate as well as in biota (flora and fauna) over Earth history. For example, prior to the Devonian, he predicted that only Entisols, Inceptisols, Vertisols, Aridisols and Oxisols were present, but after the Devonian-Carboniferous transition, Histosols (the dominant soil type of modern swamps), Alfisols, Ultisols, and Spodosols (soil types associated with modern forests) appeared; the last major change was the appearance of Mollisols in the Cenozoic associated with the appearance of grasses and grassland ecosystems (see Tables 2.1 and 2.2). In what follows, we present a brief overview of changes in weathering as related to evolutionary changes in biotic (flora, fauna) conditions, as well as changes in climate and paleoatmospheric pCO_2 and pO_2 (summarized in Figures 2.2–2.5).

2.3.1. Early Paleozoic Era

2.3.1.1. Early life on land

The early Paleozoic era was the time of the origination of terrestrial plant and animal life on Earth. The

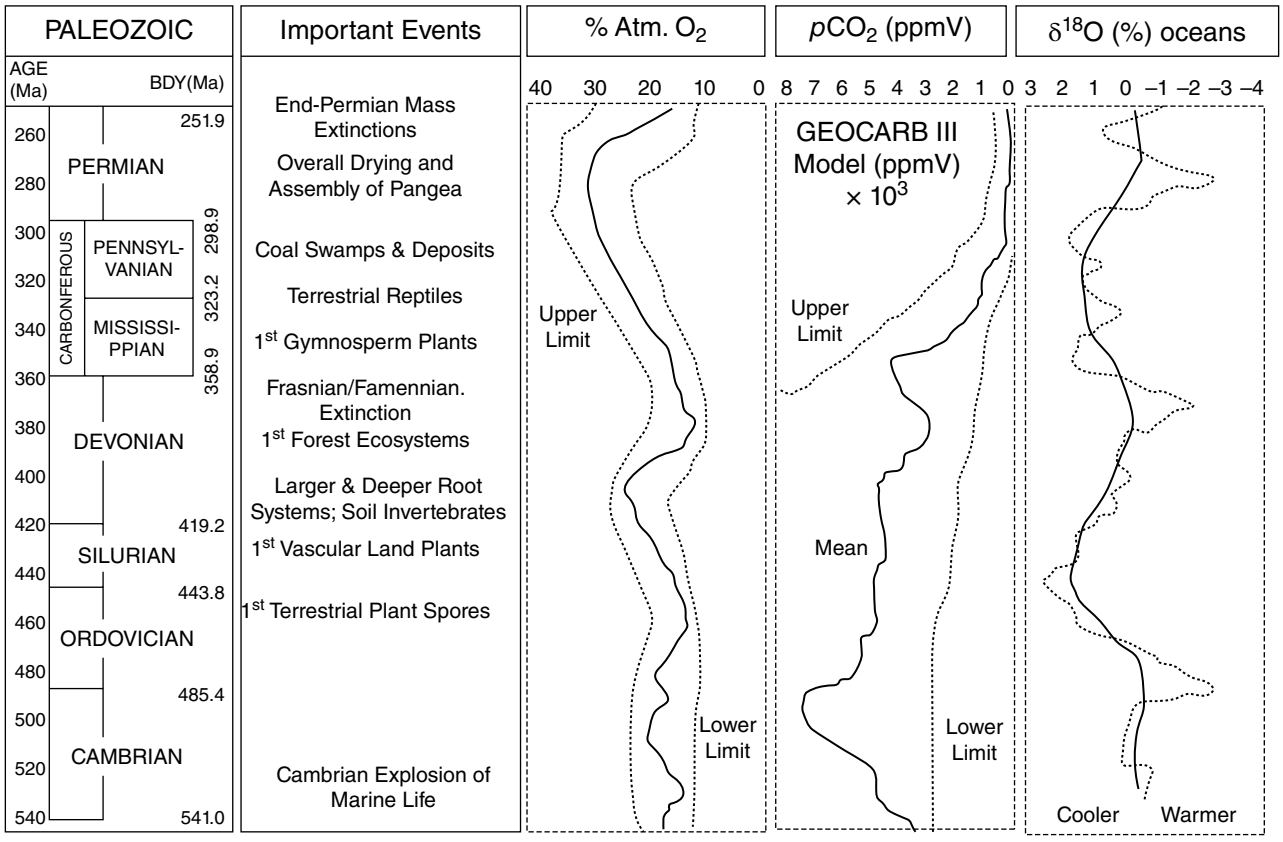

Figure 2.2 Changes in climate, organisms, and atmospheric chemistry important to chemical weathering during the Paleozoic. Geologic timescale after Walker et al. (2018). *Sources:* Veizer et al. (1999), Berner and Kothavala (2001), Berner (2006, 2009), Glasspool and Scott (2010), Veizer and Prokoph (2015).

conventional wisdom is that (1) aquatic life migrated out of the oceans and out of freshwater bodies into the terrestrial environment, and that (2) land plants were followed, temporally, by land animals, because the animals would have utilized plants as a food source (Beerbower, 1985; Gray & Boucot, 1978; Gray & Shear, 1992; Morris et al., 2018). Soils and paleosols have been used extensively to evaluate the evidence for the presence of early terrestrial life on Earth; Retallack (1985, 1986b, 2000) has proposed that paleosols provide an important archive of terrestrialization in the early to mid-Paleozoic.

Molecular phylogeny suggests that land plants had a common ancestor in aquatic green algae, and that there are four major groups of plants: the liverworts, hornworts, and mosses comprise the bryophytes, or so-called "nonvascular" plants, and the fourth group includes the tracheophytes, or "vascular" plants. The transition from the aquatic realm to the terrestrial realm was a difficult one and involved the following adaptive innovations: (1) development of a waxy outer coating, or cuticle, to prevent loss of water, (2) development of pores, called stomata, to allow for gas exchange, (3) development of reproductive structures and strategies that could function on land, such as spores and seeds, that could be dispersed by wind or later by animals, (4) development of a water and food conducting system, and the ability to stand erect and thereby overcome the Earth's gravity field, and (5) progressive differentiation of specialized parts, such as stems, leaves, and roots, that each served different functions (Gensel & Andrews, 1987). The search for evidence of the timing of these disparate developments in the geologic record has been challenging.

2.3.1.2. Timing and sequence of terrestrial colonization by plants

Gray (1985) proposed that terrestrial plants without vascular tissue, or bryophytes, were present by the mid-Ordovician, as evidenced by terrestrial spores with a tetrad morphology identified in terrestrial and nearshore marine deposits, which was confirmed by later work by Steemans et al. (2009) and Salamon et al. (2018). Gensel and Andrews (1987) were more conservative and suggested Late Ordovician to Early Silurian time, based on both coexisting fossil spores and plant cuticle. Early land plants with vascular tissue, or tracheophytes, bore trilete spores and are subdivided into four major groups. Gensel and Andrews (1987) and Stewart and Rothwell (1993) proposed that the major morphological radiation of vascular land plants occurred in Early Devonian time, as follows. Gensel and Andrews (1987) and Hotton et al. (2001) developed detailed reconstructions of Early Devonian landscapes in the Gaspé region of Québec, Canada, that suggest an affinity for water and wet soil environments.

Rhyniophytes are the oldest line of vascular plants and appear in the mid-Silurian, represented by the genus *Cooksonia*, which was very small (2–3 cm tall), had simple dichotomous branching, no leaves, no true roots (only rhizomes), true xylem and phloem, and reproduced by spores borne on terminal sporangia (E. Edwards & Wellman, 2001). *Renalia* is a related rhyniophyte that was larger than *Cooksonia*, measuring 20–30 cm in height, and was distinguished by a main axis with branches bearing kidney-shaped sporangia. *Renalia* had no leaves but was covered by spiny or thorny emergences. This plant had rhizomes with unicellular rhizoids but still lacked true roots.

Zosterophyllophytes first appear in the Early Devonian and are exemplified by the genus *Sawdonia*, which was up to 50 cm tall and had both trailing and upright stems as well as a very thick and resistant cuticle; sporangia were borne on the sides of the stem, and leaves were spines attached to the stems (Hotton et al., 2001). Zosterophyllopytes in the Early Devonian gave rise to the Lycophytes. The Devonian genus *Baragwanathia* was a Lycophyte characterized by the presence of abundant microphyllous leaves, which are usually small in size, exhibiting one unbranched vein, and sporangia that are borne either on the leaves or on the axils. Microphyllous leaves evolved through the enlargement and progressive vascularization of thorns or other emergences, such as occur on the related *Renalia*. By Middle to Late Devonian time, Lycophytes bore leaves with 2–3 forks, and by Late Devonian time they had become arborescent, with trunks up to a half meter in diameter and heights of 8–10 meters. By Carboniferous (Mississippian-Pennsylvanian) time, some Lycophytes achieved heights of 30 m, and they were a dominant element of coal swamps, represented by *Lepidodendron* (trunk) and *Stigmaria* (roots).

The third major line of early land plants, the **Trimerophytes**, is important for its possible role in the evolution of megaphyllous leaves (seen in modern ferns) and as the probable ancestor of both ferns and seed plants. *Psilophyton* best characterizes this group; it grew up to 30 cm high, with many branches terminating in masses of paired sporangia producing large numbers of spores, and with needle-like, spine-like, or forked emergences. *Pertica* is an excellent example of an advanced Trimerophyte, with a very complexly branched 3-D structure, standing 1–2 m tall, with sporangia borne on terminal axes, and with thorny leaves. The genus *Chaleuria* is exceptional in its preservation of evidence of heterospory; that is, it bore two types of spores that were of different sizes and sexes. This was antecedent to the development of sex cells in plants and to the formation of the first seeds. The heterosporous **Progymnosperm** line of plants apparently arose from the Trimerophytes and was important as the first plants exhibiting arborescence or tree-like body plan (Gensel & Andrews, 1987).

2.3.1.3. Origin of roots

Roots are one of the three fundamental organ systems of vascular plants, serving functions involving anchorage, water and nutrient uptake, and important symbiosis with mycorrhizal fungi (Hetherington & Dolan, 2018). The oldest true roots are in *Asteroxylon*, an Early Devonian lycophyte from the Rhynie Chert of Scotland (D. Edwards et al., 2017; Kidston & Lang, 1920, 1921), which has been interpreted as silicified peat and thus potentially represents the oldest paleo-Histosol. Root evolution appears to have paralleled other plant innovations but has been largely ignored by paleobotanists because actual fossilized root tissues preserved in paleosols are relatively rare (Gensel et al., 2001). Algeo et al. (1995, 2001) provided an excellent overview of this transformation of soils and terrestrial weathering processes as related to advances in the size and depth of rooting coinciding with plant evolution. Driese et al. (2000) and Driese and Mora (2001) proposed a "pedological signature" of root evolution, characterized by progressive increases in rooting depth and morphological complexity from the Silurian through the Devonian, as evidenced by root traces and root casts observed in Appalachian basin paleosols. By Late Devonian time, trees with taproots exhibiting a very modern aspect are common, and there appear to be fewer morphological changes in roots since that time (Driese et al., 1997).

2.3.1.4. Environments of colonization

A major question is whether early land plants were bound by their poor root systems, lack of efficient vascular tissues, and poor reproductive strategy (namely spores) to life in wet, soggy soil environments? A problem with addressing this issue is that plant fossils are typically best preserved in greenish-gray, reduced sedimentary deposits, rather than in red, oxidized paleosol deposits. Indeed, many of the plants appear to have been transported some distance from where they might have lived. However, paleosols and plant fossils preserved in the Gaspé region of northeastern Québec show unusually large numbers of plants preserved in growth position in paleosols and buried by event deposits. This relationship is documented in papers by Elick et al. (1998) and Hotton et al. (2001), which suggest that some plants were water-loving and lived in saturated soils near water bodies, whereas other plants were adapted to drier and better-drained soil conditions.

2.3.1.5. Early animal advances within the terrestrial realm

The problems faced by aquatic animals in making the transition to dry land were like those faced by aquatic plants (Beerbower, 1985; Gray & Boucot, 1978; Gray & Shear, 1992; Shear & Selden, 2001). Special environmental problems that needed to be solved included (1) the need to convert from water breathing with gills to air breathing with primitive lungs or other adaptive structures and (2) the need to overcome drying out, which was solved by growing an exoskeleton made of organic-mineral mixtures such as cuticle or scleratin. Gray and Shear (1992) proposed that plants did, indeed, precede land animals, at least based on the fossil record for each. Retallack and Feakes (1987), Feakes and Retallack (1988), and Retallack (2000) presented evidence for the presence of trace fossils of soil animals, such as millipedes and centipedes, in the Juniata Fm. (Upper Ordovician) of central Pennsylvania. Driese and Foreman (1991, 1992) examined an approximately time-equivalent paleosol succession (also Juniata Fm.) in eastern Tennessee and found no evidence of soil animals, only marine *Glossifungites* trace fossils that penetrated the top of the paleosol after marine flooding and transgression. A more conservative interpretation is that the earliest body fossil record of invertebrate soil animals are the trigonotarbids, which first appear in the Middle Silurian and go extinct by the Early Permian (Gray & Shear, 1992; Shear & Selden, 2001). They were 1–14 mm predatory animals that were encased in armor and bore distinctive fangs. Though spider-like, they did not have any specialized structures for spinning silk to make webs.

Fossil centipedes first appear in Upper Silurian deposits of the Old Red Sandstone at Ludford Lane, Ludlow, in the Welsh Borderland. Fossil millipedes first appear in Lower Devonian Rhynie Chert deposits of Scotland. Being herbivores, both organisms were undoubtedly important to soil-forming processes, as they fed upon microbes and plant detritus. If Retallack and Feakes (1987), Feakes and Retallack (1988), and Retallack (2000) are correct in their trace fossil interpretations, then these types of organisms may have been present in Late Ordovician soils as well. Middle Devonian deposits at Gilboa, in upstate New York, have yielded fossils of non-flying insects, such as earwigs, as well as true fossil spiders with preserved spinnerets (Gray & Shear, 1992; Shear & Selden, 2001). Land scorpions and flying insects do not appear in the fossil record until the Carboniferous Period, often exquisitely preserved in carbonate concretions known as coal balls, such as in the famous Mazon Creek site in Illinois. Interestingly, the oldest fossil oligochaetes, or earthworms, are Carboniferous, but the fossil record is very poor. So it is likely that soft-bodied soil animals are seriously underrepresented in the geologic record due to poor preservation potential.

An interesting case study on early Paleozoic terrestrialization includes the Vertisol paleosols in the Bloomsburg Formation (Upper Silurian) of central Pennsylvania (Driese et al., 1992). No vascular plant body fossils have been recovered, and there is very poor spore preservation in redbed paleosols. Cryptic pedogenic carbonate deposits

with peculiar horizontal, branching, rhizomatous structures that are either a rhizome structure or the actual body parts themselves (Driese et al., 1992; Driese & Mora, 2001). They have moderately negative $\delta^{13}C$ values ranging from −4 to −6 ‰ PDB, as compared with coeval marine calcite that ranges from −0.5 to +1.5 ‰ PDB. Soil organic matter is sparse but averages about −26.5 ‰ PDB. The pCO_2 estimates based on these carbon isotope values suggest elevated levels of CO_2 that are as much as 10–12 times present atmospheric level (Mora et al., 1996). The animal traces that are present are large, up to 2 cm in diameter, and are deeply penetrating, to over 50 cm. They could be soil animal traces of large millipedes and centipedes, as proposed by Retallack (1986b), or possible marine invertebrate traces.

2.3.2. Middle Paleozoic Paleosols and Interpretations of Early Forest Ecosystems

2.3.2.1. The dawn of arborescence

The Middle Devonian was marked by the appearance of arborescence in plants, and thus the appearance of the first true forest ecosystems. Arborescence only became possible as plants developed woody tissue, known as secondary xylem, as a means of rigidifying the trunk and allowing the plant to be large and still stand upright to resist the effects of gravity. There are apparently physical limitations as to how large a plant can be and be able to hold itself upright by relying solely on turgor, or water pressure maintained through vascular tissue. Development of deeper and stouter root systems occurred concomitantly with development of arborescence, and this permitted plants to occupy progressively drier and better-drained soil environments in more upland geomorphic settings. Mägdefrau (1952) provided an intriguing series of hypothesized paleoecosystem reconstructions for the Lower, Middle, and Upper Devonian that show remarkable changes in the additions of forests to what were herbaceous-dominated paleocommunities.

2.3.2.2. Innovative new plant groups

The innovation of arborescence in terrestrial communities arose in at least several plant groups derived from ancestral trimerophytes, simultaneously in the Middle to Late Devonian. The earliest true trees are likely represented by the cladoxylaleans, as exemplified by the genus *Eospermatoperis* from the Gilboa Formation of upstate New York. Driese et al. (1997) described sandstone-filled stump casts of these large trees up to 50 cm in diameter and over 1 m tall, preserved rooted in drab, gleyed, pyritic siltstone and silty claystone paleosols that represent a wet, poorly drained swamp environment. The trees were buried by a rapid influx of sand associated with crevasse splay or avulsion processes. Their root systems were surprisingly shallow and strap-like, extending to several meters from the base of the stump, which was probably an adaptation to living in a wet soil environment.

Progymnosperms are the most widespread arborescent group in the Late Devonian fossil record and are exemplified by the genus *Archaeopteris* of the Catskill Formation of upstate New York and Pennsylvania. This tree is reconstructed to have had trunk diameters of up to 1 m and heights of up to 30 m. It had very well-developed woody tissue, differentiated leaves and stems, and was heterosporous, meaning that it bore two sizes and sexes of spores. This was antecedent to the development of sex cells and sexual reproduction via seeds in later groups such as the seed ferns and conifer-type seed plants. Driese et al. (1997) described sandstone-filled stump casts of *Archaeopteris*, up to 50 cm in diameter and 1 m tall, with attached deep primary and secondary taproots up to 1.5 m deep, from fluvial channel-margin or levee deposits in the Upper Devonian Catskill Fm. of Pennsylvania. The soils were sandy and well drained, as evidenced by the red colors and lack of redoximorphic features. Snigirevskaya (1988) described permineralized stumps and root masses of *Callixylon* from the Upper Devonian of the Donetz region of Russia that measured 40-50 cm at the base, and which were very morphologically like the sandstone-filled stump casts from the Catskill Fm. described by Driese et al. (1997) and Mintz et al. (2010).

Lycophytes, as mentioned earlier, were spore-reproducing plants that had humble beginnings in the Late Silurian to Early Devonian. By Middle to Late Devonian time, Lycophytes bore leaves with 2–3 forks, and by Late Devonian time they had become arborescent, with trunks up to a half meter in diameter and heights of 8–10 meters. By Carboniferous (Mississippian-Pennsylvanian) time, some Lycophytes achieved heights of 30 m and were a dominant element of coal swamps, represented by *Lepidodendron* (trunk) and *Stigmaria* (roots) (Gensel & Andrews, 1987; Stewart & Rothwell, 1993). These plants probably constituted the main biomass of coal deposits (Histosols) formed in Pennsylvanian coal swamps in the eastern US.

Conifers and conifer-bearing seed plants had their origins during the Mississippian period (Gensel & Andrews, 1987; Stewart & Rothwell, 1993). The development of a seed was a significant adaptation for plants for two reasons: (1) it allowed plants to recombine genes during sexual reproduction, thereby permitting more evolutionary innovations, and (2) it allowed plants to extend their range into drier soil environments because their seeds were more viable than spores, which must be shed onto moist substrates to germinate. Unfortunately, the fossil and trace fossil record for early conifers preserved in paleosols is exceedingly poor, and we know of no good examples in the literature or from rocks that we ourselves have examined.

2.3.2.3. Ramifications of the emergence of early forest ecosystems

2.3.2.3.1 Drawdown of atmospheric pCO_2 and acceleration of rates of silicate weathering. Berner (1994, 1997, 2001) addressed the geochemical significance of developing forests on the long-term mass-balance carbon model for the Earth using his GEOCARB model. Ibarra et al. (2019) examined the consequences of land plant evolution on silicate weathering. The activities of trees and forests should have resulted in enhanced silicate weathering and thus enhanced removal of atmospheric CO_2. There are several reasons for this enhancement: (i) Rootlets (plus symbiotic microflora) with high surface area secrete organic acids and chelates, which attack minerals in order to gain nutrients; (ii) organic litter decomposes to H_2CO_3 and organic acids, providing additional acid for weathering; (iii) on a regional scale, forests recirculate water by means of transpiration followed by rainfall, and thereby increase water-mineral contact time; and (iv) forests anchor clay-rich soil, retarding erosion and allowing for retention of water and continued weathering of primary minerals between rainfall events (Algeo et al., 1995, 2001). The model predicts a sevenfold drop in pCO_2 during the Devonian period, which coincides with afforestation of the land surface. Mora et al. (1991, 1996), Mora and Driese (1993), Driese et al. (1992, 2000), and Driese and Mora (2001) provided independent estimates for the Silurian-Devonian to Permian pCO_2 reduction using the $\delta^{13}C$ values of pedogenic carbonate sampled from a variety of paleosols from the Appalachian Basin of the U.S. and Canada. Their data showed that Late Silurian pCO_2 was 10–16x PAL, declining only slightly to 8–14x PAL by the Early Devonian, and by early Late Devonian time had declined to 2–6x PAL. There is a marked step drop at about the Middle Devonian/Late Devonian boundary, which may relate to the propagation of forests and C sequestration in biomass. By Mississippian and Pennsylvanian time, pCO_2 had dropped to 2–4x PAL, and by Permian time was at or below PAL. The stomatal density data of Chaloner and McElwain (1997) are in general agreement with these interpretations; high stomatal densities reflect times when plants were CO_2 starved because of low atmospheric pCO_2, whereas low stomatal densities correlate with times of CO_2 surplus because of high pCO_2.

2.3.2.3.2. Fuel source for wildfires. Cressler (2001) considered evidence of the earliest known wildfires in the Upper Devonian Catskill Fm. exposed near Red Hill in north-central Pennsylvania. The presence of the charcoal indicates that the Late Devonian paleoatmospheric O_2 level was at least 13%, the lower limit for combustion. Oxygen levels in the atmosphere may have reached this level earlier in the Paleozoic Era or possibly in the Proterozoic Eon, but the fuel source for combustion may only have reached enough biomass by the Late Devonian for charcoal to be readily evident. Charcoal fragments of a zygopterid fern, *Rhacophyton*, are abundant, but there are no burned fragments of the progymosperm tree *Archaeopteris*. Apparently, the ferns composed the understory of the forest and were ignited by lightning, but the open structure of the forest, combined with the deep root structure of the trees, precluded a substantial burn of the forest canopy. The charcoal thus generated was then washed into an oxbow lake, where saturation prevented decay of the organic matter. There are some thin coals (with enough organic matter to qualify as paleo-Histosols) as early as Frasnian age in Canada and thicker ones in West Virginia by Famennian time (Retallack et al., 1996).

2.3.2.3.3. Oceanic anoxic events and biotic crises. Algeo et al. (1995, 2001) proposed that the rise of early land plants, and especially trees with deep rooting systems, also had drastic consequences for marine organisms and ecosystems. The higher degree of weathering on land (i.e. intensified pedogenesis) associated with arborescence and the seed habit had both transient as well as long-term effects, such as (1) increased fine-grained clay sediment yields as more feldspars weathered to clay minerals and (2) increased nutrient flux to the world's oceans as more organic matter was generated, which resulted in eutrophication and development of oceanic anoxia (these, in turn, caused extinction events and widespread black shale deposition, which increased C_{org} burial and enriched $\delta^{13}C$ marine carbonate values, and increased sulfide burial, which enriched sulfate $\delta^{34}S$ values); (3) increased development of modern soil profiles, with attendant increased kaolinite and smectite abundances and compositional maturity of sand and silt deposits coming off of the continents; and (4) decreased atmospheric and oceanic CO_2, which increased global cooling, leading to Permo-Carboniferous glaciation, and changed oceanic chemistry affecting calcite solubility and dolomite abundances. Retallack and Huang (2011) presented an alternative interpretation, proposing that the widespread black shales were due to enhanced weathering caused by greenhouse spikes from Large Igneous Province (LIP) volcanic processes.

2.3.2.3.4. Sequestration of organic C. Although forests represent an enormous organic C sink, second only to modern grasslands in terms of total biomass, the Devonian forests did not give rise to formation of Histosols and extensive coal deposits. There was apparently a lag time until the Carboniferous before organic C sequestration in coals became widespread. This may have

to do with plants developing organic compounds more resistant to microbial degradation. This is discussed next when the Pennsylvanian coal swamp floras and soils are described and characterized.

2.3.3. Carboniferous Coal Swamps and Glaciations, Gondwana Supercontinent

2.3.3.1. Coal and clastic swamp and fluvial-deltaic environments

The Pennsylvanian was marked by the appearance of two major kinds of tropical swamps, as described in DiMichele et al. (1986): (1) coal swamps, or paleo-Histosols, represented by most thicker coal seams, and (2) clastic swamps, represented by mineral paleosols. Controlling the tempo of environmental change driving ecosystem change were advances and retreats of Gondwana glaciers, which affected global sea level, which in turn controls base level. Gastaldo et al. (1996) provided an important assessment of these conditions in relation to modern changes in flora.

Coal swamps were described morphologically as either planar (filling topographic lows on landscape), topogenous (which are higher in ash and sulfur, and formed during drier climate phases), or domed (forming topographic highs on landscape); ombrogenous coal swamps are lower in ash and sulfur and formed during wettest climate phases. Coal swamps were semienclosed ecological islands limited in species exchange with non-peat-forming habitats, had low pH, low-nutrient and low-oxygen availability, had low species diversity due to biotically stressful conditions, and were distributed in a broad equatorial belt, extending from the eastern half of the US into Europe and China. The floral components are best known from "coal balls," which are permineralized masses of plants preserved in carbonate concretions, with exquisite preservation of cell structure, tissues, and reproductive organs. Five major groups of plants comprise 95% of the biomass of coals (described later).

Clastic swamps were composed of broad ecological bands with much greater species exchange than peat-forming habitats and were better drained than coal swamps, with moderate pH, moderate to high nutrients, and moderate to high oxygen availability. They had a higher species diversity than coal swamps due to less stressful conditions. Floral components are best known from "compression flora," which are flattened masses of plants preserved as coalified masses, carbonized films, or as sandstone-filled tree stump and root casts; plant distribution was controlled by subtle changes in topography and nutrient supply: *Lepidophiolos* in swampy lows, *Lepidodendron* was slightly higher, and *Sigillaria*/*Calamites*/ferns and pteridosperms grew on channel-margin levees (Gastaldo, 1987).

2.3.3.2. Important floristic components

Lycopods were dominated by tree-like forms such as *Lepidodendron* with *Stigmaria* root systems. The major tissues were a very thick bark (periderm) and parenchyma (rootlets and stems). They dominated poorly drained habitats and may have had deterministic growth (one cycle or season of reproduction, followed by death) (DiMichele & DeMaris, 1987; Gastaldo, 1986). *Psaronius* tree ferns produced mainly parenchymous tissues and roots with abundant air chambers, which were very compressible upon conversion to peat, so an abundance of plants was needed to form an accumulation of organic matter. Their "cheap tree construction" was characteristic of an opportunistic "weed" species that took advantage of physical or climatic disturbances to produce openings. Pteridosperms, also known as seed ferns, consisting mainly of medullosans, produced parenchyma that was highly compressible and subject to decay, therefore not contributing much to peat formation. These species tended to live in better-drained habitats of the clastic swamps. Sphenopsids are represented by "giant horsetails" such as *Calamites* and by sphenophylls. These two major groups produced mainly woody tissues. *Cordaites* are ancestors of the modern gymnosperms, or coniferous plants, and produced mainly woody tissues. These tended to live in better-drained habitats of the clastic swamps.

2.3.3.3. Major floral patterns

Basic patterns in tropical wetland mires were established in the Early Pennsylvanian; coal swamps were lycopod dominated during the Early and Middle Pennsylvanian, and secondarily by *Cordaites*; ferns then took over remainder of the Late Pennsylvanian, as lycopods severely declined (Gastaldo et al., 1996). In tropical clastic wetlands, pteridosperms dominated initially but were replaced by tree ferns and gymnosperms, at about the same time that the lycopods turned over and declined in the coal swamps. There was also a Northern Temperate Angaran Flora and a Southern Temperate Gondwana Flora, with slightly different floral components. By Permian time, and especially into Triassic time, there is a tremendous floral turnover in favor of gymnosperms and especially conifers (Kerp, 2000). Seed reproduction apparently won out over spore reproduction, and conifers could endure the better-drained, drier conditions on the new paleolandscapes.

2.3.3.4. Carboniferous climate patterns interpreted from mineral paleosols

Cecil (1990) proposed predictable sedimentological responses to Mississippian, Pennsylvanian, and Permian climate changes, and that these should be recorded by both the distributions of coal and by paleosols through time and space. Clastic sediment transport is low for both

arid and tropical rainy climate regimes but is maximized under seasonal wet-dry climates. Pedogenic carbonates and evaporates form under lower precipitation and humidity, clastics under intermediate conditions, and peat and coal under the highest precipitation and humidity. Domed peat swamps dominate during the wettest conditions, whereas planar peat swamps dominate during drier phases. Cecil (1990) showed that the long-term patterns of sparsely developed coals during the Late Devonian to Late Mississippian, with abundant redbed paleosols, indicating semi-arid to wet-dry tropical conditions, was followed by a dramatic shift in the Early Pennsylvanian to wet-dry tropical to tropical rainy climates, marked by well-developed coals and gleyed paleosols. Kahmann and Driese (2008) documented the abrupt paleosol transition from drier, better-drained, highly calcareous red paleosols of the Pennington Formation (Upper Mississippian) to the wetter, reduced, and coal-bearing basal Pennsylvanian paleosols at Pound Gap in eastern Kentucky, USA.

Early and early Middle Pennsylvanian siliciclastic paleosols were dominated by low-chroma, gleyed, strongly chemically leached, kaolinitic "seat earths," or "paleo-Oxisols," which were characterized by Gardner et al. (1988) as mineral soils formed beneath peat swamps in poorly drained environments. Driese and Ober (2005) later determined that many of these seat-earth paleosols began as well-drained reddish Vertisols that later became poorly drained and saturated because of rising sea-level or rising groundwater table; hence, paleosols are mostly gleyed paleo-Vertisols with "sphaerosiderite" (sensu Ludvigson et al., 1998) formed after pedogenic calcite and typically preserved beneath Histosols (now coal seams). These paleosols commonly also contain siderite-rich rhizoconcretions and root masses, indicating poorly drained, moderately low Eh conditions. Coal seams are very thick and are correlative over large areas (Cecil, 1990). Paleoclimate was interpreted as wet tropical, with high water table and a very short dry season. Middle and Late Pennsylvanian siliciclastic paleosols are dominated by high-chroma, well-drained, slickensided, smectitic-illitic paleo-Vertisols or paleo-Aridisols that may be gleyed at paleosol tops but red in the middle and base, due to a rising water table associated with climate change to wetter conditions, or to rising sea level, or both (Joeckel, 1995, 1999). These paleosols are calcite rich, with well-developed rhizoliths and rhizocretions, indicating moderately high Eh conditions and high evapotranspiration. Coal seams are very thin, or absent, and therefore are not correlative over large areas. The paleoclimate was interpreted as drier, with lower water table, and strong wet-dry seasonality.

By Late Pennsylvanian time, the climate shifted back to one that was drier and not favoring coal development but favoring red paleosol formation. Heckel (1995) and Cecil (2013) discussed how glacial-eustatic sea-level changes were likely the driving mechanism for climate changes of various types during the Late Pennsylvanian. Heckel (1995) presented paleogeographic reconstructions and general circulation models (GCMs) that indicate that the megacontinent Pangea was prone to a megamonsoonal seasonal circulation. The Appalachian basin region, though predicted to receive 550–730 mm yr^{-1} MAP, would have had summer temperatures greater than 30 °C, and a seasonal soil moisture deficit of 30–50 mm yr^{-1} due to high evapotranspiration. The predominance of paleo-Vertisols during this time is consistent with the climate models.

Montañez et al. (2007) analyzed the carbon isotopic values from mature and well-drained late Paleozoic paleosols using pedogenic calcite and soil organic matter as well as shallow-water gastropods ($\delta^{18}O$) to reconstruct paleoatmospheric pCO_2 and tropical marine surface temperatures during the Late Paleozoic Ice Age (LPIA). Terrestrial samples were obtained from the Midland, Pedregosa, Anadarko, and Paradox basins and the Grand Canyon embayment of western paleoequatorial Euramerica. Overall, they showed a strong CO_2-climate-glaciation linkage during the Permian, which is consistent with generally accepted deglaciation of continental masses and warmer climatic conditions. Their results also show short-lived periods of glaciation during an overall warming climate, raising the importance of understanding greenhouse/icehouse dynamics and linking it to the climatic challenges we are facing today. Montañez et al. (2016) used soil carbonate-based and fossil leaf-based proxies to reconstruct paleoatmospheric pCO_2 for a 16 myr duration period during the late Paleozoic. Their model showed substantial fluctuations in paleoatmospheric CO_2 ranging from 200 to 700 ppm and reflecting alternation of glacial/interglacial periods in very different climatic and environmental conditions as we know them today. They also correlated these fluctuations with expansion and recession of the largest paleotropical wetland forests on Earth and posited on the impact that this might have had on atmospheric pO_2 and the soil carbon pool.

2.3.4. End-Permian Extinctions and Climate Changes, Pangea Supercontinent

By the end of the Permian Laurasia and Gondwana had collided and sutured to form a single large landmass, termed Pangea. This land mass extended from the extreme southerly latitudes, through the equator and into high northerly latitudes, with a large region characterized as arid to semiarid based on paleosols, estimates of MAP, GCMs, and fossil assemblages (Poulsen et al., 2007; Tabor et al., 2017). The extinction event termed by some "the mother of all extinctions" resulted in major losses (up to 90% of species) of both terrestrial and marine

biodiversity (Erwin, 1994, 1996). These extinctions have been attributed by some authors to abrupt climate change and severe losses of shallow-marine habitats, and in marine carbon isotope records there is an abrupt shift in heavier $\delta^{13}C$ values that record this event. The paleosol record includes numerous sites in the Karoo Basin in South Africa (Smith, 1995) as well as the Dunkard Group (Lower Permian) rocks preserved in the US Appalachian Basin (Fedorko & Skema, 2013). Overall, the terrestrial record is of drying and warming climate, and of diminished habitat (Veevers et al., 1994). A global "coal gap" exists between the Permian-Triassic extinction and the Middle Triassic recovery of peat-forming plants (Retallack et al., 1996). Krull and Retallack (2000) described a profound carbon isotope excursion of up to 10‰ across terrestrial successions in Antarctica, which they attributed to methane release.

2.4. MESOZOIC

The Mesozoic Era encompasses the Triassic, Jurassic, and Cretaceous Periods, which range in age from ~250 to 66 Ma (F. M. Gradstein et al., 2012; Skelton et al., 2003; Sues & Fraser, 2006) (Figures 2.3 and 2.4). The Mesozoic represents a continuum of biogeochemical weathering processes from the late Paleozoic, although with some differences. Mass extinctions, massive basalt flows, the rifting of the supercontinent Pangea, the rise and fall of the dinosaurs, diversification of gymnosperms, and the appearance of angiosperms all define this important interval of geological time. Gondwana and Laurasia had merged to form the supercontinent Pangea by the Permian Period of the Paleozoic, which persisted until Cretaceous times when continental rifting accelerated (G. O. Klein, 1994; Scotese, 2001). Pangea was also migrating slowly northward during most of the Mesozoic. There were relatively narrow mountain chains across some continental margins of Pangea, and sea level was relatively low during the Triassic and Jurassic because of the presence of the large land mass. Sea level increased substantially from sea floor spreading during the greenhouse world of the Cretaceous (Haq et al., 1988).

The Mesozoic is bracketed by two of the greatest mass extinctions of the Phanerozoic. The end-Permian event was a response to the massive Siberian Traps basalt flows that led to the destruction of vast terrestrial ecosystems from elevated atmospheric CO_2 concentrations and greenhouse warming. The K-T bolide impact is believed to have ended the Mesozoic Era and the age of the dinosaurs. Within the Mesozoic, the Triassic-Jurassic boundary chronicles another mass extinction possibly related to basalt flows and elevated pCO_2 from rifting in the Newark Basin (Central Atlantic Magmatic Province). Paleogeographically during the Mesozoic, Pangea began

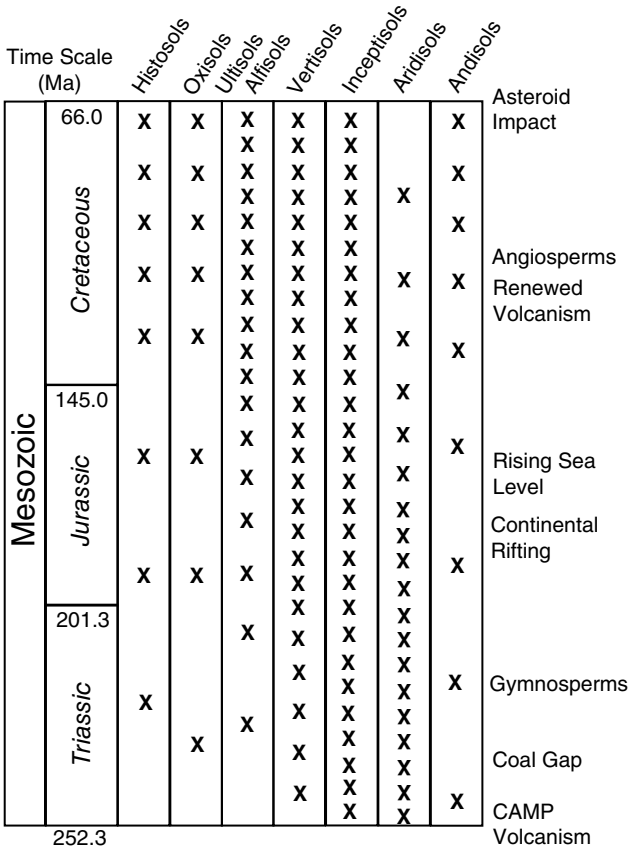

Figure 2.3 Geologic timescale for the Mesozoic in association with relative climate shifts and frequency of documented and predicted paleosol types. (Modified from F. M. Gradstein et al., 2012)

to break apart, first into Laurasia and Gondwana and then into multiple terrestrial continents during the Cretaceous, which led to one of the great greenhouse climates of the Phanerozoic because of escalating pCO_2. After the flourishing of gymnosperms during the Triassic and Jurassic, the Cretaceous saw the arrival of the angiosperms and new ecosystems, shifting weathering rates and carbon turnover rates, and the coevolution of insects and flowering plants.

The evolving continents, climates, and ecosystems shaped the formation and distribution of the soilscape in new ways during the Mesozoic. The temporal and spatial magnitude of the different soil-forming factors during the Mesozoic is critical to understanding the kinds and distributions of paleosols preserved during this interval.

2.4.1. Atmospheric Gases

After the end-Permian extinction, atmospheric CO_2 concentrations during the Triassic dropped to near 1000 ppmV based on both geochemical modeling and proxy

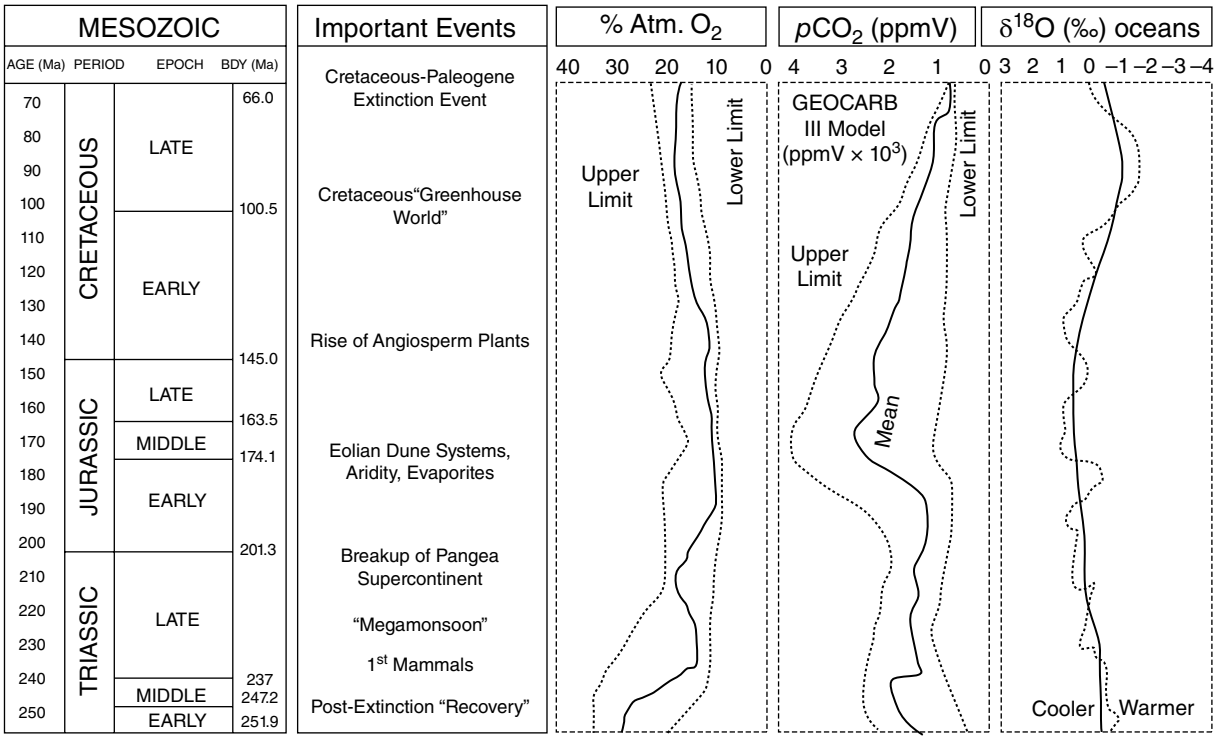

Figure 2.4 Changes in climate, organisms, and atmospheric chemistry important to chemical weathering during the Mesozoic. Geologic timescale after Walker et al. (2018). *Sources:* Veizer et al. (1999), Berner and Kothavala (2001), Berner (2006, 2009), Glasspool and Scott (2010), Veizer & Prokoph (2015).

estimates of the earliest Triassic (Royer et al., 2014), in large part because of low carbon sequestration from disturbed terrestrial and marine ecosystems and the absence of glaciers (Figure 2.3). As terrestrial ecosystems, including swamps, began to recover, pCO_2 slowly declined in the Middle to Late Triassic as more carbon was sequestered in terrestrial environments. After a brief increase near the Triassic-Jurassic boundary in response to widespread tectonic activity and incipient continental plate rifting, atmospheric CO_2 concentrations decreased to 400–700 ppmV. During the Cretaceous, pCO_2 increased again from accelerated tectonic forcing, although it remained between 500 and 1000 ppmV. Global temperatures generally followed the concentration of pCO_2 as a key greenhouse gas. Because of the emergence of volcanic rocks, silicate weathering rates may have increased and kept pCO_2 at modest levels during the Cretaceous (Berner, 2006).

According to the GEOCARBSULF model (Royer et al., 2014) and the work of Lenton et al. (2018), pO_2 was approximately 20% to 25% during the Triassic before declining to 13% to 15% during the Jurassic and then back to nearly 25% during the Cretaceous. This is supported by long-term changes in Corg:P ratios (Algeo & Ingall, 2007). Oxygen concentrations were near modern-day levels during most of the Triassic, in part because so little carbon was stored on land from the ecosystem collapse at the end of the Permian and because of arid conditions (Lenton et al., 2018). Oxygen was high enough to support wildfires but not so high as to limit photosynthesis through excess photorespiration during this time interval (Berner, 2009).

2.4.2. Megamonsoon

The climate during the maximum expression of the monsoon during the Triassic and much of the Jurassic is characterized as a hothouse world with low latitudinal temperature gradients in the absence of polar ice. The extreme climate seasonality during much of the Triassic and much of the Jurassic governed the distribution of weathering phenomena across the Pangean supercontinent where MATs were relatively high and MAP variable (Parrish, 1993). The megamonsoon intensified during the Middle to Late Triassic as the continental mass in its slow migration northward became divided equally on either side of the equator. For example, north westerlies in the equatorial tropics of the southern hemisphere originated on land in the winter, but upon entering warm tropical waters off the western coast of Pangea, they would

eventually be drawn back to the northeast and onto land north of the equator in response to extremely low atmospheric pressure (Dubiel et al., 1991; Wilson et al., 1994). Consequently, seasonal rainfall during the megamonsoons of the Late Triassic was as high as 1200 mm (Nordt et al., 2015). The tropical to subtropical megamonsoon began to breakdown during the Jurassic as continents continued moving northward, and in the case of western equatorial Pangea where monsoon winds were blocked by an emerging coastal volcanic belt (Nordt et al., 2015).

2.4.3. Biota

The deleterious effects of the end-Permian mass extinction of plants and animals significantly altered and even destroyed many terrestrial ecosystems (Retallack, 2013a). During the Early Triassic, there were remnants of the low-diversity lycopod and fern communities in lowland settings that had flourished during the late Paleozoic, which eventually led to the radiation and spread of gymnosperm forests during the Middle Triassic when the tropical to subtropical megamonsoon emerged (S. R. Gradstein & Kerp, 2012; Greb et al., 2006). By the Middle Triassic, peatlands had appeared, particularly in Antarctica, and were dominated by gymnosperms, ferns, seed ferns, ginkgos, and cycads. Gymnosperm forests reached their peak global extent during the Jurassic and were accompanied by savannas and deserts in drier regions (Parrish et al., 2004). The rise and then dominance of angiosperms occurred during the middle to late Cretaceous. After this time, angiosperms dominated all regions except polar, where gymnosperms still flourished (Royer, 2010).

Forests, savannas, mangrove, desert, and woodland plant formations were widespread during the Mesozoic. These ecosystems reflected the regional climates and distribution of paleosols and associated biological features. Much of the Triassic was characterized by cosmopolitan vertebrates with the advent of the first crocodiles, turtles, a new breed of mammals, and of course the arrival of dinosaurs (Hasiotis, 2004). Trace fossils in paleosols reflected environments of deposition and facies within related to hydrolytic tiering (Bedatou et al., 2008; Genise et al., 2000; Hasiotis, 2004) when many of the soil fauna became tillers. Examples include adhesive meniscate and back-filled burrows, beetle traces, ant trails, bee nests, and burrows in sediment and on plant debris, large and small vertebrate burrows, and large to small root traces as burrows, casts, and infills (Buatois & Mángano, 2011; Genise et al., 2000; Hasiotis, 2002; Hasiotis & Dubiel, 1993, 1994). These burrows contributed to soil infiltration, ped structure, and nutrient cycling, with contributions from the spread of crayfish and lungfish in palustrine terrestrial settings.

2.4.4. Paleosols

2.4.4.1. Triassic

Weathering rates accelerated across the Permian-Triassic boundary based on marine strontium and osmium isotopes and marine sedimentation (Algeo et al., 2011; Sedlacek et al., 2014). Sun et al. (2018) show through marine lithium isotopes that the emission of CO_2 from the Siberian Traps led to abrupt global warming in the Early Triassic and that for a time excessive continental weathering from exposure of basalts led to additional runoff and pulses of ocean anoxia delaying the response of ecosystems on both land and in water (Zhang et al., 2016). These observations are supported by advanced weathering indexes of sedimentary rocks during this interval (Cao et al., 2018) as many Paleozoic forests shifted to herbaceous cover and warmer temperatures (Berner, 2005, 2006).

The paleosol record of this remarkable event is spotty, in part because of associated erosional events, but also because the actual Permo-Triassic crisis was relatively short in terms of soil-forming intervals (Figure 2.4). However, for the first 10 Ma of the Triassic, terrestrial ecosystems were so disrupted that coal deposits never formed, creating the well-documented "coal gap" (Retallack et al., 1996). Afterward, but still within the Early Triassic, Boucot et al. (2013) mapped much of Pangea as hot and arid from the presence and distribution of evaporites and calcretes throughout most of the continental interior. Aridisols, calcic Inceptisols, and calcic Vertisols dominated, as supported by widespread documentation of paleosols with aridic properties in the western interior (Lawton & Buck, 2006; Mack & Cole, 2005). However, a few coal deposits formed (Histosols) in the warm temperate subpolar regions of the north and along the equatorial island chain on the more humid east side of Pangea (Retallack & Alonso-Zarza, 1998). The mapping of a few bauxite and laterite deposits in the eastern tropics also suggests that other weathered soils such as Oxisols, Ultisols, and Alfisols may have been present. It is unclear whether the kind of coniferous vegetation to support Spodosols was present at this time, although acid, sandy substrates in humid regions were likely present. Donnadieu et al. (2009) mapped a 5° latitudinal swath of tropical broadleaf forest and herbaceous vegetation during the Early Triassic, needleleaf evergreen in subpolar temperate regions above 70° N and S, and vast arid regions between.

During the middle to Late Triassic, arid lands were shrinking as warm-temperate climates expanded into high latitudes (Boucot et al., 2013). The east coast of Pangea contained some coals (Histosols) in low-lying areas likely interspersed with tropical to subtropical gymnosperm forests. Peat-forming plants that eventually recovered were mainly lycopods, equisetalians, and

conifers, as forests persisted in polar latitudes. As the trade winds strengthened in response to the intensifying megamonsoon, subhumid conditions emerged in the tropics along the west coast of Pangea. Overall, weathered Inceptisols, Vertisols, and possibly Alfisols and Ultisols spread at the expense of Aridisols (Nordt et al., 2015; Trendell et al., 2013a, b). Here Donnadieu et al. (2009) modeled the expansion of tropical evergreen forests from 10° to 15° latitude on either side of the equator reflecting maximum expression of the tropical monsoon.

However, from field studies of the western equatorial region and the Newark Basin of Pangea, the monsoon climate of the Middle to Late Triassic (Blodgett, 1988; Hubert, 1977; LeTourneau & Huber, 2006; Nordt et al., 2015; Prochnow et al., 2006; Retallack, 1997; Tabor et al., 2004; Therrien & Fastovsky, 2000) began to accelerate near the end of the Triassic as more soils became enriched in carbonate and in some cases evaporites (Blodgett, 1988; Cleveland et al., 2008; Driese & Mora, 2002; Hubert, 1977; Nordt et al., 2015; Prochnow et al., 2006; Retallack, 2009; Schaller et al., 2015; Tanner, 2000; Tanner & Lucas, 2012). In contrast, subpolar regions remained warm and temperate supporting humid to subhumid soils. The cause of the shift in the western interior is inconclusive, as some believe Pangea had shifted far enough to the north by this time to break the monsoon cycle (Dubiel, 1994; Dubiel et al., 1991; Parrish, 1993), whereas others provide evidence that tectonic uplift along the west coast (Sonoma orogeny) may have blocked warm, moist tropic air from penetrating inland (Atchley et al., 2013b; Nordt et al., 2015).

The end-Triassic mass extinction was apparently brought on by increasingly warm temperatures accompanied by an increase in pCO_2 associated with initial rifting of Pangea, i.e. the Newark Basin, producing the Central Atlantic Magmatic Province (CAMP) (Huynh & Poulsen, 2005; McElwain et al., 1999; Schaller et al., 2011). Accelerated continental weathering and runoff based on osmium isotopic ratios (i.e. ratio of radiogenic influxes of fluvial sediment vs. weathering of juvenile basalts) may have led to anoxia similar to the Triassic-Jurassic transition (Percival et al., 2016; Them et al., 2017). Many faunal clades, including species of tetrapods (reptile and amphibian), went extinct, as well as many kinds of megaflora. The imprint of this event on soils at the time was probably more in their geochemistry, such as stable carbon isotopes, than other properties that might have shifted development of one soil type into another (e.g. Inceptisol to Alfisol).

2.4.4.2. Jurassic

The Jurassic soilscapes and weathering zones were an extension of the Late Triassic because Pangea was still largely intact, the distribution of monsoonal and non-monsoonal climates persisted, plant and animal evolution was gradualistic, and glaciers were absent (Figures 2.3 and 2.4). But because the supercontinent, although still largely intact, was migrating northward through the latitudes, and some plate rifting was beginning, some climate changes were beginning to occur.

According to paleogeographic maps (Boucot et al., 2013), Jurassic climate indicators were similar to the Late Triassic except that the western equatorial monsoon system had shifted northward by some 10° latitude because of continental drift. For example, the continental interior in the tropical to subtropical latitude of the Newark Basin (northeastern North America) consisted of intercalated eolian deposits and calcic paleosols attesting to seasonal climate extremes (Gierlowski-Kordesch, 1991; Hubert, 1977; LeTourneau & Huber, 2006; Suchecki et al., 1988), consistent with observations in large areas of the western interior of Pangea and in the southern margins of Gondwana associated with sand dunes and Aridisols (Parrish et al., 2004; Smith & Kitching, 1997; Smith et al., 2009). However, in northern subpolar latitudes of the Early Jurassic, as during the Late Triassic, Histosols, Alfisols, Ultisols, and poorly drained counterparts (Gleysols) likely occurred, and leached basalts were present in persistently warm and temperate climates of both subpolar regions (Petersen & Nielsen, 1995; Rees et al., 2004; Retallack, 2009; Singer et al., 1994). Included in the northern temperate zone and its counterpart in the subpolar southern hemisphere were a few bauxites and kaolinite beds (Boucot et al., 2013), also suggesting the presence of Alfisols, Ultisols, and Oxisols. Ahlerg et al. (2003) showed that in Sweden on Laurasia, smectitic clays turned to kaolinites in deep weathering profiles, in part because of plate migration northward from the arid tropical zone to the temperate warm and humid zone. Donnadieu et al. (2009) mapped similar ecosystems during the Early to Middle Jurassic that were present in the Late Triassic.

The Late Jurassic was accompanied by an escalation of rifting of Pangea and the breakdown of the tropical to subtropical megamonsoon as aridlands in the continental interior persisted. Arid to semiarid climates remained in the tropical to subtropical region of Gondwana in Argentina based on the presence of calcic and gypsic paleosols (Myers et al., 2014). Late Jurassic paleosols with carbonate in the western interior of the Colorado Plateau indicate arid to subtropical wet/dry climates as remnants of the megamonsoon persisted, consistent with observations in similar latitudes of China, Patagonia, Spain, and central Africa based on the presence of Aridisols, calcic to gypsic Inceptisols, and calcic Vertisols (Cabaleri et al., 2005; Currie, 1998; Demko et al., 2004; Demko & Parrish, 1998; Gutierrez & Sheldon, 2012; Kirkland, 2006; Liu et al., 2018; Myers et al., 2011; Roca & Nadon, 2007; Tanner et al., 2014; Vincent & Allen, 1999). Further, soils in the western interior supported

authigenic illites and smectites in association with carbonate nodules interpreted as having formed in a semiarid climate (Jennings & Hasiotis, 2006). However, the warm temperate subpolar northerly latitudes still supported gymnosperm forests (Matthewman et al., 2012), and southern high latitudes supported forests in floodplains that were carbonate free, indicative of a continuation of seasonally humid to subhumid climates (Liu et al., 2018; Pole, 2001). The Late Jurassic climate became progressively more humid towards the Cretaceous boundary as tectonic activity increased and interior aridlands began to shrink in favor of a greater distribution of Inceptisols and Alfisols (Demko et al., 2004; Gutierrez & Sheldon, 2012; Myers et al., 2014; Parrish et al., 2004).

Whereas Histosols began to spread during the Late Jurassic, organic carbon sequestration rates were like the Late Triassic. Gymnosperm forests were spreading in the polar regions of the island arc and there were some bauxites, suggesting the continuation of true tropical conditions that included Oxisols, Ultisols, and Alfisols in eastern Pangea and in both polar hemispheres (Bata, 2016).

2.4.4.3. Cretaceous

During the Cretaceous, intensified rifting of Pangea and the formation of the continental plates as we now know them brought forth a greenhouse world that reduced the distribution of arid climates across the globe. Even so, soil distributions were similar to what we see today, except for the absence of Gelisols (permafrost tundras) and Mollisols (grasslands). During this time, Donnadieu et al. (2009) modeled the breakup of Pangea, the breakdown of the megamonsoon, the migration and proliferation of tropical evergreen ecosystems around the equator, the spread of boreal forests into subpolar regions, and the shift of arid zones from the tropics to zones of persistently high pressure at 30° N and S latitude. Because of the greenhouse climate and rising sea-level inundating shallow coastlines, the early Cretaceous preserves vast coal deposits that were accompanied by bauxites, laterites, and kaolinites in stable interior landscapes. The greenhouse climate reached its maximum extent during the middle Cretaceous in response to elevated pCO_2 from tectonic activity, which also increased the hydrological cycle (Berner & Kothavala, 2001; Gibbs et al., 1999; White et al., 2001). As weathering of newly exposed silicate substrates from mountain building by the latter part of the Cretaceous intensified, pCO_2 and temperatures began to decline.

Early Cretaceous paleosols across Canada, Alaska, and northern Europe in ancient fluvial settings are typically carbonate free and with coal seams (Histosols) interbedded with paleosols having slickensides, sphaerosiderites, and mottles from differential hydromorphic conditions (Leckie et al., 2004; Wright et al., 2000). Most of these soils are classified as Alfisols (cutans) dominated by smectite and illitic clay minerals, and possibly Ultisols (kaolinites) in association with Entisols, Inceptisols, and Vertisols, with many preserving aquic conditions (McCarthy et al., 1999; Ufnar et al., 2001, 2005). These soil types extended down into more southerly latitudes of central to north-central North America where Alfisols and Ultisols with E horizons containing an abundance of kaolinite were present (Joeckel, 1995). Vitali et al. (2002), in mid-Cretaceous interfluve soils of British Columbia, described carbonate-free paleosols with detrital kaolinite and illite in association with clay skins, indicating the presence of Alfisols and Ultisols. The Albian of Antarctica contains fluvial paleosols with in situ tree stumps and surface horizons that are somewhat organically enriched A (melanic like) over B horizons with blocky peds, clay cutans, and mottling (cambic or argillic). These decalcified Alfisols and Inceptisols formed in a temperate high-latitude warm climate under a broad-leaved evergreen forest (Howe & Francis, 2005).

However, seasonal climates producing soils containing pedogenic carbonate nodules were still common across much of the globe during the early Cretaceous in the regions of the newly formed subtropical high-pressure gyres. Thus, many paleosols in fluvial paleosols of Spain (Clemente & Pérez-Arlucea, 1993), south-central China, Japan, and Korea (Eberth et al., 2001; C. Huang et al., 2013; Lee, 1999; Lee & Hisada, 1999; Lee et al., 2003; Li et al., 2016; Pan & Huang, 2014) classify as Inceptisols (Calcisols), Vertisols, and Aridisols with carbonate nodules. Nevertheless, there is some evidence for Alfisols (clay cutans) because these climates were still seasonal in some areas. Argentina at the time was also in the subtropical high-pressure cell of the southern hemisphere recording similar soil types typical of seasonally dry climates formed in fluvial sediments (Paredes et al., 2007). As a testament to the presence of tropical wet climates during the early Cretaceous, Suarez et al. (2010) documented paleosols formed in alluvium of Columbia as Entisols, Inceptisols and Alfisols, with the possibility that some soils contained very few weatherable minerals. Most of the karst bauxites of Europe and the deep weathering profiles of Alabama are early Cretaceous paleo-Oxisols (Bárdossy, 1982; Sigleo & Reinhardt, 1988).

By the middle to late Cretaceous, the continents had separated sufficiently that zonal climate patterns had emerged, with tropical wet regions along the equator from merging trade winds, subtropical gyres promoting aridity at 30° N and S latitude, warm temperate regions between 40° and 60° N latitude, and temperate climates reaching into polar regions consistent with the absence of glaciers. Fricke et al. (2010) modeled climate and biome types for the late Cretaceous, showing open-canopy mixed forests in North America and Canada, deciduous

broadleaf forests in the mid-continent, and moist savannas in the southern regions, reflective of a lingering monsoonal-type climate. Consistent with this modeling effort, deep weathering profiles occurred up to 60° N and S, based on the presence of bauxites, laterites, and kaolinites (Bata, 2016) because climates were hot and humid (Föllmi, 2012). In general, paleosols in mid- to high-latitude North America were decalcified and often poorly drained along the western interior seaway in the form of Inceptisols, Histosols, and a few Vertisols and Alfisols (Flaig et al., 2011; Flood & Hampson, 2014; McCarthy & Plint, 2003; Retallack, 1994). In Alberta, Canada, paleosols were mainly well to poorly drained and decalcified Inceptisols with smectite and illite as the dominant clay minerals, some with overlying Histics and some with coals thick enough to classify as Histosols (Fanti & Miyashita, 2009; Quinney et al., 2013). Jaramillo et al. (2015) identified one of the few Andisols during this time in Alaska because of Fe-Al humus complexes and low bulk densities together with evidence of volcanic ash. In central Utah during the latest Cretaceous, Famubode and Bhattacharya (2016) documented carbonate-free Entisols, Inceptisols, Vertisols, and Alfisols in floodplain successions based on slickensides and clay cutans, interspersed with coals. In southern Italy extending into the tropical zone at the time, red ferruginous paleosols with kaolinite, goethite, hematite, and quartz formed in tropical wet climates (Oxisols) (Vacca et al., 2012).

Along the southern margins of Texas where the subtropical gyre was located similar to today, soils accumulated carbonate nodules in these subhumid to semiarid climates (Buck & Mack, 1995; Nordt et al., 2003; Nordt et al., 2011). Mack (1992) and Mack and Cole (2005) reported paleosols in New Mexico ranging from arid to subhumid during the early to late Cretaceous tracking Aridisols (various Inceptisols and Calcisols) to woodland Alfisols and Inceptisols without carbonate. These observations are consistent with the subtropical gyre (Hadley cell) of China, Korea, Japan, Nepal, Thailand, and Iran during the late Cretaceous (Buck et al., 2004; Horiuchi et al., 2009, 2012; Kim et al., 2009; Leier et al., 2009; Moussavi-Harami et al., 2009; Paik et al., 2001, 2012; Zhang et al., 2016) and in the southern hemisphere of Brazil (Dal'Bó et al., 2010; Fernandes & Basilici, 2009; Hong & Lee, 2012), as soils ranging from Aridisols and calcic Inceptisols and Vertisols were interspersed in some areas with Alfisols. Therrien (2005) and Therrien et al. (2009) in Romanian rocks of Maastrichtian age showed paleosols mainly with carbonate nodules and red beds with slickensides, indicating the presence of Vertisols and probably Inceptisols in a seasonally semiarid to subhumid climate. In France, Cojan and Moreau (2006) interpreted subhumid intervals forming calcareous Vertisols with illite-smectite. Ghosh (1997) mapped calcic Inceptisols and Aridisols in arid to semiarid climates in India at the time it was still in the southern hemisphere but located on the margins of the subtropical high. Also, in the southern hemisphere of Brazil during late Cretaceous, floodplains intercalated with dunes show a dominance of sandy soils enriched in carbonate and sometimes with silica in association with other regions of northeastern Brazil having calcic Vertisols (Batezelli & Ladeira, 2016; Nascimento et al., 2017).

Although angiosperms were believed to have increased weathering intensity and carbon turnover rates during the Cretaceous, recent work indicates that their influence may not have been that great, especially in terms of pCO_2 drawdown (M. Y. Andrews et al., 2008). However, weathering intensity may have increased because of the increased hydrological cycle.

2.4.5. Weathering Rates

Pangea during the Triassic and Jurassic is known for low weathering rates because of continental aridity, limited tropical wet climates, low outgassing, and low chemical and sediment erosion fluxes to groundwater and oceans (Figures 2.3 and 2.4). For example, the weathering potential was reduced as evidenced by the low abundance of lateritic bauxites and kaolins (Mindszenty, 2016) and the overall decrease in clay production during this time (Weaver, 1989). Even though pCO_2 was relatively high during the Early Triassic, weathering rates were relatively low because of the slow ecosystem recovery from the Permo-Triassic extinction event. Arid conditions discouraged biogeochemical weathering and nutrient flux and promoted less runoff and more evaporation. Inorganic carbon sequestration was particularly high during this time because of vast arid regions. By the Middle Triassic, however, organic carbon sequestration increased as gymnosperm forests spread across many landscapes and as bogs and other organic deposits spread.

Organic acid production increased with the return of peatlands and the continued spread of angiosperm and gymnosperm forests in response to rising pCO_2 from reactivated tectonic activity during the Cretaceous (Figure 2.3). Not only had arid climates decreased in areal coverage by about 6% (see Boucot et al., 2013, maps), they had shifted largely from the tropics to subtropics with the breakdown of the megamonsoon. Last, whereas the temperate regions remained about the same geographically overall during the Cretaceous, the warm temperate climates became split between warm and cool temperate with the drawdown of atmospheric CO_2 from silicate weathering. Because of these differences in climate regime, Histosols and advanced carbon sequestration occurred through the Mesozoic, as did the distribution of Oxisols, Ultisols (Argillisols), and Alfisols (Argillisols). During the Cretaceous there was

greater overall weathering and runoff of ions to groundwater, rivers, and the oceans than at any other time during the Mesozoic (Nordt et al., 2011). In contrast, Aridisols (Calcisols), although more abundant in the early Mesozoic, declined in distribution during the Cretaceous, thereby reducing the sequestration of inorganic carbon. Vertisols and Inceptisols are cosmopolitan soil orders in thick sedimentary basins, and Andisols likely increased somewhat during the Cretaceous with accelerated volcanic activity.

2.5. CENOZOIC

The Cenozoic (66 Ma to present) marks the most recent geologic era, which includes the current Holocene Epoch (F. M. Gradstein et al., 2012) (Figure 2.5). Modern critical zones and critical zone observatories monitor weathering phenomena occurring in the Cenozoic. Compared to the more distant geologic past, more Cenozoic Era geologic deposits and their details are preserved, due to their young age and thus higher likelihood of preservation. More geochronological techniques are available for dating and correlating these younger deposits. This enhanced preservation and the fact that the Cenozoic deposits as archives of information about past biota and climate change are from a tectonic configuration similar to that of the present day has made it an ideal era for testing and comparing modern atmospheric gas levels, climates, biota, and weathering rates (Beerling & Royer, 2011; Hansen et al., 2008; Maher & Chamberlain, 2014; Willenbring & von Blanckenburg, 2010; Zachos et al., 2008).

The Cenozoic is divided into three geologic periods: Paleogene (66 to 23.03 Ma), Neogene (23.03 to 2.58 Ma), and Quaternary (2.58 to 0 Ma). These periods are divided into several geologic epochs in which the plate tectonic configuration, paleoatmosphere, paleoclimate, and paleobiota are more well known compared to previous geologic eras (Scotese, 2001; Zachos et al., 2001; Zachos et al., 2008).

2.5.1. Plate Tectonics

Cenozoic cooling resulted in large global continental ice sheet growth. This cooling coincided with the collision of India and Asia and the development of the Tibetan plateau uplift, along with other high-altitude plateaus and mountainous areas. The Tibetan uplift is thought to have attained its current elevation during the mid-Eocene (Rohrmann et al., 2012; Wang et al., 2008) and may have

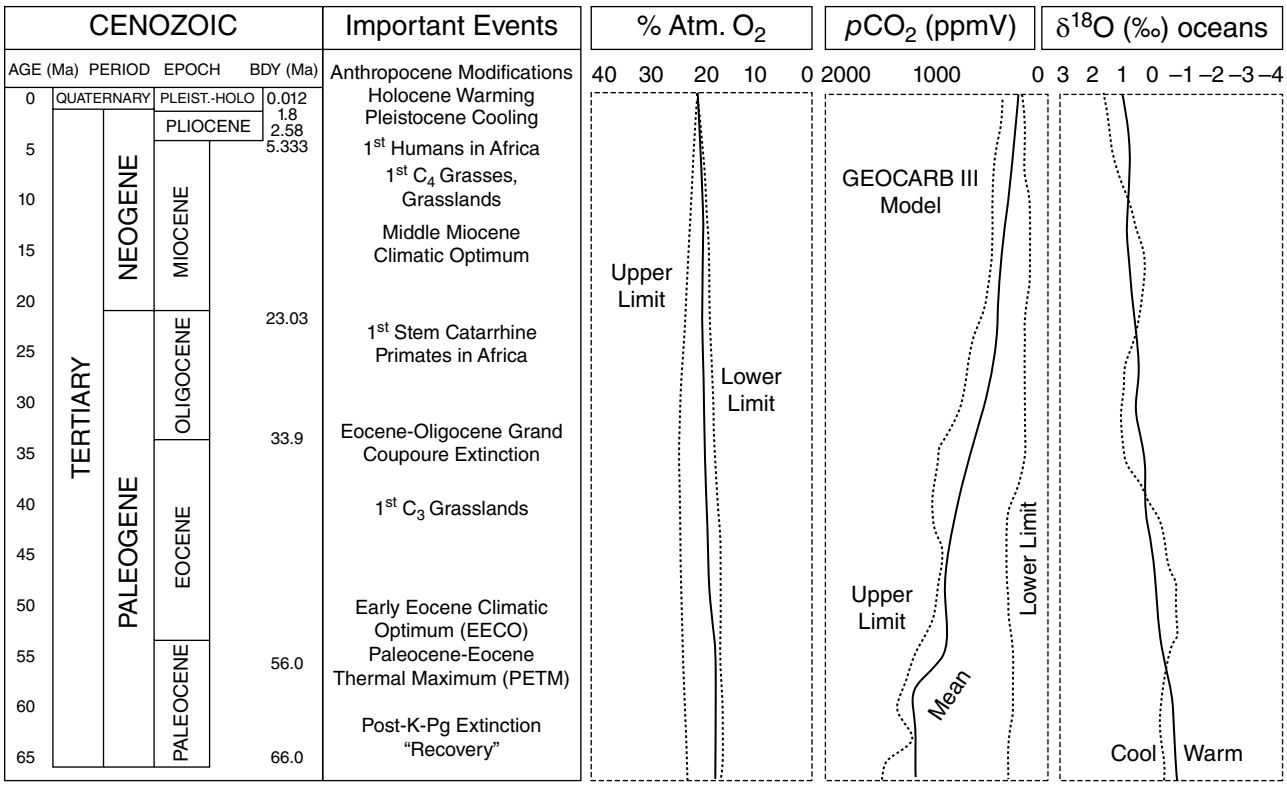

Figure 2.5 Changes in climate, organisms, and atmospheric chemistry important to chemical weathering during the Cenozoic. Geologic timescale after Walker et al. (2018). *Sources:* Veizer et al. (1999), Berner and Kothavala (2001), Berner (2006, 2009), Glasspool and Scott (2010), Veizer and Prokoph (2015).

initiated a positive feedback whereby this uplift drove increased chemical weathering and consumption of pCO_2 during the past 40 million years (Raymo & Ruddiman, 1992). Thermochronometric ages from 18,000 bedrock samples suggest an increase in global sediment flux associated with increased cooling during the Pliocene and Pleistocene epochs (Herman et al., 2013). However, increased denudation related to global cooling has been called into question for the Late Cenozoic because more recent work showed a stable weathering flux (Willenbring & von Blanckenburg, 2010). Alternatively, Molnar and England (1990) argued the inverse of tectonic-induced cooling, namely, that the expansion of glaciers led to scouring of mountainous areas, which facilitated glacio-isostatic uplift. In Molnar and England's scenario, cooling precedes uplift. More recent work showed that extensive growth of the Maritime Continent since 5 Ma contributed to Plio-Pleistocene cooling and the recurrence of Ice Ages. Basic calculations showed that resulting climate change and CO_2 consumption during basalt weathering of Maritime Continent rocks would have affected pCO_2 and lowered global temperatures by 0.25 °C (Molnar & Cronin, 2015).

Ocean currents during the Oligocene Epoch began to resemble modern ocean currents. The opening of the Tasmanian Gateway during the Eocene-Oligocene transition and Drake Passage during the early Oligocene triggered the Antarctic Circumpolar Current flow, facilitating the formation of permanent ice sheets on Antarctica (Lyle et al., 2008; Mackensen, 2004). The collision of India and Asia resulted in significant closure of the Tethys Seaway (Lyle et al., 2008), and subsequent plate movement and shrinkage of the Tethys amplified the response of the Middle Miocene climate transition to pCO_2 drawdown (Hamon et al., 2013). The closing of the Tethys is also thought to be a key driver in the onset of aridification and formation of the Sahara (Zhang et al., 2014).

Although uplift of the Tibetan Plateau occurred during the Eocene and continued into the Neogene, a major pulse and significant increase in altitude occurred during the late Miocene (10–8 Ma) (Zhisheng et al., 2001). This event triggered the intensification of the East Asian summer and winter monsoons, enhanced dust transport to the northern Pacific Ocean, and is linked to the development of Northern Hemisphere glaciations (Zhisheng et al., 2001). An alternative interpretation by Retallack et al. (2018) suggests an earlier monsoon onset at 20 Ma, based on paleosols, that is apparently not linked to cooling by Himalayan uplift.

One of the most pronounced oceanic changes in the past 20 million years was the complete desiccation of the Mediterranean that occurred during the Messinian (5.96 to 5.33 Ma), known as the Messinian salinity crisis (Krijgsman et al., 1999). This desiccation event is thought to have been driven by a combination of tectonic, glacio-eustatic sea-level and processional changes, where the complete desiccation of the Mediterranean drove biogeographic change in Northern Africa (Flecker et al., 2015; Van der Made et al., 2006).

The connection of the North and South American continents by means of the Isthmus of Panama during the Pliocene (O'Dea et al., 2016) blocked warm Pacific currents from flowing into the Atlantic and intensified the Gulf Stream, which delivered warm waters to high northern latitudes (Haug & Tiedemann, 1998). By the Pleistocene Epoch, the continents were in a position very similar to today. Plio-Pleistocene glaciations and concomitant sea-level fall created land bridges between Africa and Eurasia and Eurasia and North America, which affected the genetic structure of floral and faunal populations (Hewitt, 2000; Rohling et al., 1998).

2.5.2. Atmospheric Gases

Atmospheric pCO_2 declined over the course of the Cenozoic Era to modern-day values of ~300–400 ppmV, whereas, pO_2 increased slightly over the Cenozoic Era to modern-day values of 210,000 ppmV (Berner, 2006). Current model estimates of pCO_2 during the early Cenozoic underpredict concentrations when compared to proxy records that document pCO_2 from 1000 to 2500 ppmV, whereas boron proxies indicate up to 4000 ppmV (Royer, 2006; Royer et al., 2014; Zachos et al., 2008).

Overprinted on the long-term Cenozoic decline of pCO_2 are short-term fluctuations, most notably the Paleocene-Eocene Thermal Maximum (PETM), when more than 2,000 Gt of C as CO_2 entered the ocean and atmosphere, triggering a global temperature increase of 5 °C in less than 10,000 years (Zachos et al., 2001, 2008). The pCO_2 fluctuations during the latter part of the Cenozoic, even though well below 1,000 ppmV, are significant and coincide with notable climate transitions. For example, stomatal frequency data show pCO_2 fluctuations during the Miocene ranging from 300 to 600 ppmV, whereas Miocene Climatic Optimum (18 to 14 Ma) CO_2 levels were 500 ppmV (Kürschner et al., 2008). Kürschner et al. (2008) showed that intervals of lower pCO_2 (~300 ppmV) coincide with major glaciations, and intervals of high pCO_2 (~500 ppmV) coincide with the climatic optimum. Ice cores from the middle and late Pleistocene document CO_2 variability ranging from 180 ppmV during glacial and 280–300 ppmV during interglacial stages (Lüthi et al., 2008).

2.5.3. Environments, Climates, and Weathering during the Cenozoic

The Cenozoic climate cooled from greenhouse to icehouse conditions, ice sheets developed and expanded, and mammals and other biota evolved into modern

forms. The diversity of mammals increased in the Cenozoic due in part to extinction of nonavian dinosaurs. These long-term trends of the Cenozoic are marked by more prominent short-term events, notably: the Cretaceous-Paleogene extinction event, the Paleocene-Eocene Thermal Maximum, the Early Eocene Climatic Optimum and associated hyperthermals, the Eocene-Oligocene transition, the Miocene expansion of grasslands and the Middle Miocene Climatic Optimum, Plio-Pleistocene glaciations, abrupt and millennial-scale climate changes, and anthropogenic effects.

2.5.3.1. Cretaceous-Paleogene extinction event (66 Ma)

The Cretaceous-Paleogene extinction (K-Pg) event coincided with a large asteroid impact at Chicxulub, Mexico, and enhanced effects of volcanism associated with the Deccan flood basalts (Schulte et al., 2010). Catastrophic environmental effects included prolonged darkness (nuclear winter), cooling, and acid rain (Kring, 2007). Three-quarters of plant and animal life went extinct during the K-Pg, some 66 Ma (Barnosky et al., 2011).

Retallack et al. (1987) noted changes from Late Cretaceous lowland forest soil ecosystems to early Paleocene swampy soil ecosystems that are consistent with the catastrophic change in biota that coincided with the K-Pg. However, in a later, more detailed pedotype analysis, Retallack (1994) noted little change in paleosol types from the latest Cretaceous to earliest Paleogene in the Hell Creek Formation of northern Montana. Most paleosols in the lower Paleocene were characterized as Histosols, gleyed Inceptisols, or Entisols that formed under cypress in swamp environments in a humid climate with MAP exceeding 1200 mm (Retallack, 1994). This subtle variation in paleosols is in stark contrast to the more marked transition in floral and faunal communities (Kring, 2007; Labandeira et al., 2002; Schulte et al., 2010). These more marked changes in faunal communities are consistent with recent work that showed a reduction in soil-dwelling insect body size observed in Paleogene deposits from Texas, USA, suggesting that continental ecosystems, like marine, experienced a reduction in body size following a mass extinction event (Wiest et al., 2018). Significant changes in vegetation were also documented in the $\delta^{13}C$ of soil carbonates across the K-Pg boundary (C. Huang et al., 2013; Nordt et al., 2002).

2.5.3.2. Paleocene and Eocene hothouse conditions

2.5.3.2.1. Paleocene-Eocene thermal maximum: Climate and biota. The early Paleocene Epoch (66 to 56 Ma) of the Paleogene Period was cooler and drier than the previous Cretaceous Period, but temperatures increased to 5 to >8 °C warmer than the current global mean annual temperature. Short-lived increases in temperature and precipitation are documented in Inceptisols from South America during the mid-Paleocene (Hyland et al., 2015). The general warming during the Paleocene culminated in an abrupt increase in pCO_2 and MAT, known as the Paleocene Eocene Thermal Maximum (PETM) (McInerney & Wing, 2011; Zachos et al., 2001, 2008). This transient 200,000 yearlong warming event is attributed to the sudden release of methane hydrates (Dickens et al., 1995). More recent work shows two large and rapid releases of C during the onset of the PETM (Bowen et al., 2015). Following the PETM, warm greenhouse conditions prevailed during the Paleocene with cool and temperate poles and warm-humid midlatitudes, i.e. equitable climate of the early Eocene, 53 to 51 Ma (Hyland et al., 2018; Zachos et al., 2008). The PETM coincided with a mass extinction of benthic foraminifera and the evolution of land mammals in the form of dispersal events and short-lived decreases in body size (Clyde & Gingerich, 1998; Gingerich, 2003; Koch et al., 1992; Zachos et al., 2001).

2.5.3.2.2. Paleocene-Eocene thermal maximum: Weathering. Direct paleosol evidence of the PETM is largely constrained to midlatitude settings. Warming during the PETM coincides with a significant carbon isotope excursion (CIE) in the marine record, whereas CIEs documented in soil-forming carbonates in northern midlatitudes are consistently ~3‰ more negative than age-equivalent marine records (Bowen et al., 2004). This was explained as a 20%–25% increase in soil and atmospheric moisture and a near-doubling of the rate of terrestrial carbon cycling. This increase in humidity, promoting a prolonged wet climate state, would have enhanced silicate weathering. Paleosols from North Dakota and Texas, USA, Argentina, and central China show an increase in weathering from pre-PETM to PETM time (E. Andrews et al., 2017; Z. Chen et al., 2016; Clechenko et al., 2007; White & Schiebout, 2008). This increase in weathering, as documented using CIA, is consistent with the clay mineralogy, which transitions from smectite dominated to more kaolinite, the occurrence of Oxisols (and some calcic Vertisols) and increase in clay translocation and $CaCO_3$ leaching (Clechenko et al., 2007; Do Campo et al., 2018).

Several paleosols studied in the northern midlatitudes show less chemical weathering and evidence of water stress when compared to pre- and post-PETM paleosols (Bowen & Bowen, 2008; Kraus et al., 2013; Kraus & Riggins, 2007). Work in the Bighorn Basin shows $CaCO_3$ accumulation and drying related to pre-CIE warming, where evidence of this drying continues up-section into the body of the PETM (Kraus et al., 2013). Consistent with this trend in the Bighorn Basin, enhanced kaolinitization is followed by intense pedogenesis (lateritic materials) manifested during the PETM by an "orange zone" of the Golden Valley Formation from the Williston Basin in North Dakota (Clechenko et al., 2007). The

kaolinitization is thought to relate to an early drying phase in the Williston Basin during the onset of the PETM, similar to the Bighorn Basin (Kraus et al., 2013; Kraus & Riggins, 2007). Evidence of wetter soils occurs during the recovery phase of the PETM and persists into post-PETM time. These observations led some to suggest that an increase in the seasonality of precipitation, rather than an increase in total precipitation, characterized midlatitude continental settings during the PETM (McInerney & Wing, 2011). Simultaneous with the PETM, shifts towards enhanced transport and storage of sediment from upland catchments are documented in western Colorado and northern Spain, consistent with modeling that shows increased sediment flux related to rapid vegetation turnover and increased monsoonal precipitation (Colombera et al., 2017; Foreman et al., 2012). Modeling efforts suggest that discharge increased up to 14x normal Paleocene discharge and extreme flooding and channel mobility eroded nearby soils, leading to a large export of terrigenous sediment to the ocean (C. Chen et al., 2018). An erosional event of this magnitude would have exposed large areas of fresh rock, which would have potentially facilitated silicate weathering and long-term CO_2 drawdown.

2.5.3.2.3. Early Eocene climatic optimum and hyperthermals: Climate and biota. The Early Eocene Climatic Optimum (EECO) is a period when temperatures were significantly warmer than modern, especially at higher latitudes. In addition to the PETM, several short-lived warming events (hyperthermals) occurred during the early Eocene (Cramer et al., 2003; Lauretano et al., 2015; Littler et al., 2014; Nicolo et al., 2007; Slotnick et al., 2012), which likely aided in the poleward transfer of heat. The PETM and early Eocene hyperthermal events are considered potential analogs for modern and near-future warming (Anagnostou et al., 2016; Zachos et al., 2008; Zeebe et al., 2016). More recent work showed evidence of increased continental runoff (John et al., 2008; Nicolo et al., 2007; Slotnick et al., 2012). Some have suggested that extreme precipitation events occurred during hyperthermal events and may be decoupled from mean annual precipitation trends, which has important implications for how we interpret hydrological proxies during the PETM and early Eocene (Carmichael et al., 2018).

Unlike today's polar deserts, warm climates promoted conifer-broadleaf rain forests in high latitudes, where *Metasequoia* are found in Eocene swamp deposits in the Canadian Arctic (Eberle & Greenwood, 2012; Kumagai et al., 1995) and tropical mangroves in Tasmania and England (Carpenter, 1994; Macphail et al., 1994). Fossil wood in Antarctica shows cool-wet and warm climates during the Paleocene and Eocene, with MAT estimates ranging from 7 to 15 °C (Francis & Poole, 2002). Biota in these arctic environments included alligators, turtles, primates, tapirs, and brontotheres (Eberle & Greenwood, 2012).

2.5.3.2.4. Early Eocene climatic optimum and hyperthermals: Weathering. The prevalence of warm-wet climates during the EECO enabled the development of highly weathered kaolinitic soils that include bauxites and laterites (Mindszenty, 2016; Retallack, 2010). Early Eocene bauxitic and lateritic paleosols (Oxisols and Ultisols) from the Monaro succession in southeastern Australia document warm-wet climate conditions and are thought to be associated with the short-lived EECO hyperthermals (Retallack, 2008). These Monaro paleosols weather basalt flows and are largely devoid of bases and enriched in Al and Fe. Mineralogy from a coeval ferralitic paleosol, the Ngaiur paleosol, in Australia is dominated by gibbsite and kaolinite, typical of Oxisols weathering in modern-day perhumid climates (Zhou et al., 2015). Lateritic paleosols have been documented in northern high latitude Late Paleocene rocks in Ireland (Tabor & Yapp, 2005). Detrital laterites were documented in Central Oregon (Bestland et al., 1996), where saprolitic rhyolites are overlain with conglomeratic ironstones, where the latter are thought to be detrital laterites from eroded Ultisols. In contrast, multiple proxies from calcic paleosols and paleoflora of the Green River Basin (Wyoming, USA) document amplified seasonality during early Eocene hyperthermal events (Hyland et al., 2018), which may confirm signals like those found in PETM paleosols in the continental interior of the US (Kraus et al., 2013).

2.5.3.3. Eocene-Oligocene transition into the icehouse world

2.5.3.3.1. Eocene-Oligocene transition: Climate and biota. The hothouse to icehouse transition, and thus global climate cooling, followed the EECO, when pCO_2 declined and mountain and sheet glaciers developed in Antarctica. The middle Eocene saw the extinction of archaic forest-dwelling mammals (Prothero, 1994). The Eocene-Oligocene transition (E-O) (33.9 Ma) is marked by a prominent change in marine oxygen isotopes that record a change in water temperature, Oi-1 (Zachos et al., 2001), and a large temperature drop in the continental interior of the US (Zanazzi et al., 2007). This isotope event coincides with the occurrence of several glacial deposits in the rock record and a large-scale extinction event and floral and faunal turnover, where broadleaf forests declined and mammals adapted to eating tough vegetation thrived (Prothero, 1994; Zachos et al., 2001). More recent terrestrial isotope geochemistry shows pronounced ~7 °C cooling in air temperature in the continental interior of the US (Fan et al., 2018).

The Oligocene Epoch (33.9 to 23.03 Ma) marks this continued transition from the greenhouse conditions of the Eocene to more modern conditions and ecosystems of the Miocene Epoch (23.03 to 5.33 Ma). Cooling and drying during the Oligocene resulted in the development and expansion of desert grasslands in central Oregon and the North American Great Plains (Retallack, 2001a). The upper boundary of the Oligocene is less prominent than the Grand Coupoure of the lower boundary, simply marking cooler conditions approaching the Miocene.

2.5.3.3.2. Eocene-Oligocene transition: Weathering. The terrestrial transition from warm-wet hothouse conditions during the Paleocene and Eocene to cool-dry conditions and ice sheets during the latter Cenozoic is perhaps nowhere better documented than in North America (Bestland, 2000; Bestland et al., 1996; Fan et al., 2018; Retallack, 2007; Sheldon et al., 2002; Sheldon & Retallack, 2004; Terry Jr, 2001). This transition to cooler-drier conditions on land coincides with the appearance and expansion of C_3 grasslands during the late Eocene and E-O, and C_4 grasses during the Miocene (Sheldon & Retallack, 2004; Strömberg, 2004). The North American paleosol record of Cenozoic weathering is consistent with a gradual transition towards cooler-drier climates. Eocene paleosols from central Oregon and southwestern South Dakota are characterized as well-developed Ultisols and Oxisols weathering in humid forests, and in some cases tropical forests (Retallack, 1983; Retallack et al., 1999). Paleosols from northwestern Nebraska, which include Alfisols, Mollisols, and petrocalcic horizons, document a change from humid forested environments during the late Eocene to semiarid and seasonal open-range environments during the early Oligocene, 33.2 Ma (Terry Jr, 2001).

Paleoprecipitation data from the E-O in Montana show no long-term precipitation change, whereas the Oregon and Nebraska records show long-term drying trends associated with the transition (Sheldon & Retallack, 2004). Rain shadow expansion due to the Cascade and Laramide orogenies was implicated as the long-term driver of the east and west drying trends during the E-O in Oregon and Nebraska (Sheldon & Retallack, 2004). However, these orographic rain shadows do not explain the short-term paleoclimate variability observed in the North American paleosols records, such as the Middle Miocene warm-wet spikes (Retallack, 2007).

Unlike most paleosol studies, Bestland (2000) calculated weathering flux estimates for the Central Oregon E-O paleosol succession and considered the record as a reservoir of both upland (hinterland) soil weathering and erosion and alluvial system sedimentation and weathering. Bestland (2000) showed that although the degree of weathering decreased from the Eocene to the Oligocene, the rate of sediment accumulation increased, which suggested increased aggradation due to changes in sediment supply from the uplands. Because of this state change in sediment accumulation, the calculated weathering flux increased into the Oligocene because greater erosion of soils contributed freshly deposited and more chemically reactive sediment. From this, Bestland (2000) inferred that drier climate and sparser vegetation during the Oligocene caused higher sediment yields in the lowlands and thus more reactive sediments for weathering and CO_2 sequestration. These inferences seem consistent with modern work showing that increased mountain building can deliver more reactive sediment to the lowlands, which would facilitate weathering and CO_2 sequestration (Bouchez et al., 2012; Maher & Chamberlain, 2014; West et al., 2002).

2.5.3.4. Miocene Epoch and the expansion of grasslands

2.5.3.4.1. Miocene Epoch: Climate and biota. The late Oligocene was characterized by warming and reduction in ice volume. This warming continued into the Miocene and peaked during the Middle Miocene Climatic Optimum (17 to 15 Ma) (Zachos et al., 2001). The Middle Miocene Climatic Optimum (MMCO) was a global warming event where the MAT was ~3 °C higher than modern-day MAT, which is similar to worst-case IPCC projections of projected long-term warming by the year 2100 (Solomon et al., 2007; You et al., 2009). Although the cause(s) of warming during the MMCO and pCO_2 concentrations are heavily debated, proxy records from the Miocene suggest a warmer climate than modern, despite having pCO_2 similar to preindustrial concentrations (Knorr et al., 2011). The climate gradually cooled following the MMCO, and major ice sheet development resumed in Antarctica (Zachos et al., 2001).

Vegetation structure studies (fauna, phytoliths, paleosols, isotopes, tooth wear) show that canopies opened and C_3 grasslands expanded during the Oligocene-Miocene transition and during the early Miocene (23 to 16 Ma) (E. J. Edwards et al., 2010; Strömberg, 2004). This C_3 grassland expansion preceded the worldwide expansion of C_4 grasses during the late Miocene and Pliocene (8 to 3 Ma) (Cerling et al., 1997). This forest-to-grassland transition was likely driven by some combination of tectonically driven aridification (Y. Huang et al., 2007; Sepulchre et al., 2006) and disturbance mechanisms (e.g., fire, increased herbivory) (Retallack, 2001a). However, as noted by E. J. Edwards et al. (2010), scenarios used to explain forest-to-grassland transition during the late Miocene and Pliocene rely on modern mechanisms found in C_4-dominated systems. The earlier forest-to-grassland transition involved mostly C_3 grasses, and it is not clear whether processes responsible for the rise of C_4-dominated systems were responsible for this expansion.

2.5.3.4.2. Miocene Epoch: Weathering. Several paleosol studies document evidence of the forest-to-grassland transition and its attendant effects on weathering. Early Miocene deposits near Lake Victoria, Kenya, have a polypedogenic Vertisol that likely weathered under a tropical seasonal forest and retains oxisolic characteristics, including very high Fe_d and evidence of laterization and extreme kaolinitization (Driese et al., 2016). Paleosol geochemistry suggests that this oxisolic paleo-Vertisol weathered under a humid, tropical climate with MAP of ~1800 mm yr^{-1} and a MAT of up to 25 °C (Stinchcomb et al., 2016). Intriguingly, this interval of intense pedogenesis coincides with relatively high pCO_2 (500–600 ppmV) during the earliest Miocene (Kürschner et al., 2008). This oxisolic Vertisol is overlain by less well-developed paleosols, where the morphology, isotopic geochemistry from soil carbonates, and microcharcoal and microvertebrate fauna suggest open-canopy conditions during the early Miocene in western Kenya (Lukens, Lehmann, et al., 2017), consistent with previous interpretations (Bonnefille, 2010; Kingston et al., 1994).

Neogene Siwalik paleosols from Pakistan record the emergence and expansion of C4 grasses during the late Miocene (Quade & Cerling, 1995). Prior to 7.3 Ma, the paleosols are characterized as Alfisols or Mollisols supporting C_3 vegetation, whereas after 7.3 Ma, Mollisols supported C_4-dominated vegetation. Subsequent work on lateral Siwalik paleosol variability showed that during the transition to a C_4-dominated ecosystem, C_3 and C_4 plants occupied different environments in the Siwalik valley bottom, largely a function of local topography and moisture dynamics (Behrensmeyer et al., 2007). Late Miocene paleosols from the Texas Panhandle range from Entisols and Inceptisols to Vertisols, included pedogenic carbonate and yield a mean annual rainfall reconstruction that is notably wetter than today's average annual rainfall. These data suggest that the Late Miocene climate was not sufficiently arid to select for grasses utilizing C_4 photosynthesis (Lukens, Driese, et al., 2017). This could suggest that another mechanism (herbivory or fire) was a primary driver of C_4 expansion in North America.

Long-term aridification as documented in the continental interior of North America facilitated the development and expansion of desert grasslands during late Oligocene to short- and tall-sod grasslands and paleo-Mollisols in the Miocene (Retallack, 2001a). The development of these sod-forming grasslands, which includes near-mollic to mollic epipedons, led to the development of deep crumb-structured C-rich soil matrix. These sod grasslands would have increased albedo, soil-water retention and the storage of C. As a result, the evolution and expansion of these sod grasslands has been invoked as a driver of climate cooling during Cenozoic (Retallack, 2001a). More recent work shows that a worldwide increase in $\delta^{18}O$ in paleosol carbonates and fossil teeth from the Neogene is consistent with an increase in soil-water evaporative and transpirative flux (Chamberlain et al., 2014), which is consistent with Retallack's (2013b) hypothesis that the widespread expansion of grassland soils altered the albedo and soil water retention properties on large spatial scales.

2.5.3.5. Pliocene-Pleistocene glaciations

Plio-Pleistocene paleosol archives of climate, hydrology, and weathering are extensive. Paleosol archives that have been the subject of decades of research are successions of loess and paleosols found in the mid-continent of North America (Grimley et al., 2003; Mason et al., 2008; Muhs et al., 2003, 2008; Ruhe, 1965), Eurasian Steppe (Bronger, 2003; Buggle et al., 2014; Fitzsimmons et al., 2012; Marković et al., 2009), Chinese Loess Plateau (Bronger & Heinkele, 1989; Gallet et al., 1996; Kemp, 1995; Kemp et al., 1995; Maher & Thompson, 1995) and the Chaco-Pampean plains of Argentina (Kemp et al., 2006; Zárate, 2003). Space does not permit discussion of each of these regions; however, some review of the Chinese Loess Plateau (CLP) is pertinent.

One of the more significant advances in paleosols, climate, and hydrology was the linking of terrestrial paleoenvironmental and paleoclimate records of the CLP to marine and ice core records (Heller & Liu, 1982; Kukla, 1987). This work, and many more subsequent studies, showed that variations in loess and paleosol development archived in the CLP track orbital and shorter-term millennial-scale changes in intensity of the East Asian Monsoon (An, 2000). These records also match orbital variations in ice sheet growth and ocean temperatures as inferred from oxygen isotopes from ice- and marine-core records. Loess deposition at the CLP coincided with glacial times and a stronger winter monsoon, and these deposits have massive to weakly developed ped structure and primary carbonates. Weathering, and paleosol formation, at the CLP dominated interglacial times and stronger summer monsoon, whereby these fossil soils have Ah horizons with spongy microfabrics and pedogenic carbonates. Paleosols older than 0.374 Ma in the Louchuan section of the CLP have argillic subsoil horizons in addition to pedogenic carbonates (Bronger & Heinkele, 1989). These associations highlight the connections between long-term atmospheric pressure differences driven by ocean vs. land temperatures (monsoon) which drove hydroclimatic variability and silicate weathering and calcification in the CLP during the Plio-Pleistocene (An, 2000). Recent model simulations of soil development on calcareous European loess showed that late glacial (0.013–0.01 Ma) bioturbation affected topsoil decarbonization rates and clay migration (Finke & Hutson, 2008).

Also notable are the many paleosol studies from East Africa, largely driven by paleoanthropological and

archaeological studies of hominin evolution. Many of the Plio-Pleistocene paleosol records from East Africa document increasing aridity, C_4 vegetation and opening of canopy (Cerling et al., 2011; Cerling & Hay, 1986; Levin et al., 2011; Wynn, 2004). However, there is considerable variability in these paleoclimate proxies for any given time interval, which has been attributed to pedofacies, where the physical, biogeochemical, and mineralogical properties of paleosols change systematically with proximity to the paleo-channel (Bown & Kraus, 1987). This concept of paleosol diversity as a function of depositional environment, groundwater effects, geomorphic position, and parent material has been documented in the Plio-Pleistocene rocks from Tanzania and Ethiopia (Ashley et al., 2014; Levin et al., 2004).

Wynn (2000) documented a range of Pliocene paleosols and environments associated with *Australopithecus anamensis* in the Turkana Basin of northern Kenya. These types include Vertisols, Inceptisols, Entisols, and Aridisols that weathered in semiarid to arid seasonal climates under low tree-shrub/savanna vegetation. A later, more extensive, Plio-Pleistocene paleosol record from western and eastern Turkana showed evidence of aridification events at 3.58, 3.35, 2.52–2, and 1.81–1.58 Ma that coincided with bovid and hominin turnover events, suggesting that evolution of these mammals was driven by climate and habitat instability (Wynn, 2000).

2.5.3.6. Late Pleistocene and Holocene transition: The Younger Dryas

The transition from the Late Pleistocene to the Holocene Epoch (0.0117 Ma) marks a geologically rapid (10^3 years) change from cold glacial to warmer interglacial conditions. The warming interval leading up to this boundary, the Allerød oscillation, 0.0139 to 0.0129 Ma, was interrupted by an abrupt return to glacial conditions between 0.0129 and 0.0117 Ma (Alley, 2000). This cold interval is known as the Younger Dryas (YD). Although the YD was first recognized in Europe, it has now been documented in marine and ice records worldwide (Bard et al., 1993; Fairbanks, 1990; Taylor et al., 1993). The triggers for this abrupt climate change event are complex and likely consisted of a shutdown of the Atlantic Meridional Overturn Current caused by meltwater discharge into the North Atlantic, more negative radiative forcing and a changing atmospheric circulation (Broecker et al., 1988; Fairbanks, 1989; Renssen et al., 2015). Although some have advocated an asteroid impact that triggered YD cooling (Firestone et al., 2007), this hypothesis has been met with resistance and remains controversial (Holliday et al., 2016; Pinter et al., 2011).

These abrupt YD climate changes in the Northern Hemisphere had a global impact on Earth's surface. Black mats from the southern Great Basin and throughout much of the Northern Hemisphere were once wet meadow and shallow pond environments (wetlands) likely formed in response to YD-age recharge (Haynes, 2008; Quade et al., 1998). These black mats have also been classified as Aquolls, Mollisols that formed in aquic soil moisture regimes. The parent material for these Aquolls was eolian silt or fine sand (Haynes, 2008). A micromorphological analysis of these organic-rich sediments and soils showed remnants of humic acids, plant fragments, diatoms, phytoliths, and gastropods (Harris-Parks, 2016). These paleosols varied as a function of topography and relation to the water table, ranging from organic horizons, moist soils, or ponded sediments and suggest that during the YD this environment had greater effective moisture than the modern desert climate of Arizona and Nevada (Harris-Parks, 2016). Younger Dryas black mat paleosols, interpreted as paleo-Mollisols, weathered and were buried by eolian sediments and therefore document a brief interval of mesic conditions. The YDs interval also corresponds with notable changes in human adaptation during the Clovis-to-Folsom transition, notably a decline in mammoth hunting and increased regionalization (Ballenger et al., 2011).

This type of abrupt climate change impact on Earth's surface is perhaps nowhere more dramatic than in one of the driest places on Earth today: the Atacama Desert. Paleowetlands were mapped throughout the central Atacama Desert and document elevated groundwater levels during two periods: 0.0159 to ~0.0138 and 0.0127 to ~0.0097 Ma (Quade et al., 2008). These wet intervals are likely related to the strengthening of the South American Monsoon, whereas links to the YD effects in the North Atlantic are not firmly established.

2.5.3.7. Anthropocene

Although the Anthropocene is not a formal geologic time unit and there are controversies associated with this proposed boundary (Autin & Holbrook, 2012; Gale & Hoare, 2012), its approximate delineation is useful when discussing human impacts on Earth's surface and the sedimentary record (Zalasiewicz et al., 2008, 2015). Evidence suggests that A.D. 1610 or 1964 (e.g. atmospheric fallout from nuclear tests) may serve as useful geochronological markers for the beginning of the Anthropocene; however, human impacts to climate, biota, and weathering are documented several thousand years earlier (Ruddiman, 2003; Smith & Zeder, 2013; Stinchcomb et al., 2011). Anthropogenic soil horizons and the modern pedosphere have been considered as ideal candidates for delineating the "golden spike" of the proposed Anthropocene (Certini & Scalenghe, 2011), where some have also advocated the implementation of an anthro-pedostratigraphy (Richter et al., 2015). Furthermore, lithologic discontinuities have been proposed as a useful concept for delineating anthropogenic deposits (and soil) overlying older, possibly preanthropogenic soil because these discontinuities are

defined by marking the boundary between two geologic layers in a soil profile (Ahr et al., 2016; Stinchcomb et al., 2013).

2.5.3.7.1. Anthropogenic effects on climate and biota. Recent Anthropogenic impacts on climate have caused global temperatures to increase, especially northern polar regions where temperature increases are twice the global average from AD 1965 to 2005 (Solomon et al., 2007). In addition to these temperature changes, snow cover has declined for many regions, arctic sea ice extent has decreased, and temperatures at the top of permafrost have increased by 3 °C since the 1980s (Solomon et al., 2007). Associated human impacts on Earth's surface have resulted in a significant loss in range area for several mammals, which is a threat to species diversity (Ceballos & Ehrlich, 2002) and also related generally to biodiversity decline (Butchart et al., 2010). Recent estimates show that this rapid loss in biodiversity is sufficiently severe to be called the "sixth mass extinction" (Ceballos et al., 2015) and suggest that biodiversity will continue to decline over the 21st century (Pereira et al., 2010).

If the most recent anthropogenic impacts are any indicator, then evidence of earlier anthropogenic impacts would lead one to surmise that these effects also altered earlier climates and biota (Ruddiman, 2003, 2013). Middle Holocene changes in pCO_2 and pCH_4 have been linked to land-use practices like forest clearance and rice agriculture (Ruddiman, 2003, 2013), and so in this regard, humans already altered the surrounding biota millennia prior to the present. Between 0.011 and 0.009 Ma, animal domestication arose independently in many parts of the world and this would have also directly affected biota (Smith & Zeder, 2013).

2.5.3.7.2. Anthropogenic effects on weathering. Human impacts on Earth's surface and sedimentary record are time-transgressive, and therefore, soils may record these multiple impacts as polypedogenesis (Richter et al., 2015). Technosols, a soil group in the World Reference Base for Soil Resources (FAO, 1998), are soils characterized by human creation, where pedogenesis is operating on reactive human discard (i.e. artifacts) and kinetics of reactions are rapid (Leguédois et al., 2016). This latter observation is related to the fact that humans can quickly create or transfer reactive materials to the soil. It has been proposed that the addition of these artifacts to soil could be quantified to an approximate degree through human history using a simple mass-transfer equation (Stinchcomb, 2018).

The degree of anthropogenic effects on soil can vary widely and may range from the addition of industrial aerosols concentrated in heavy elements (e.g. Mn, Pb, Zn) (Herndon et al., 2010; Ma et al., 2014; Stinchcomb et al., 2014), to the addition of human-altered organic matter and artifacts (e.g. Terra Preta) (Glaser et al., 2001; Lima et al., 2002; Mann, 2008), to complete removal or manipulation of the soil surface by large-scale machinery or labor practices (Hooke, 2000; Wilkinson, 2005). Compiling these observations into a pedostratigraphy in order to more systemically document human impacts on soil is an ongoing effort (Richter et al., 2015).

2.6. SUMMARY AND CONCLUSIONS

2.6.1. Climate, Terrestrial Biota, and Weathering Are Inextricably Linked

The preceding review of weathering over Earth history, as elucidated by paleosols, clearly demonstrates that climate, biota and weathering are inextricably linked. Availability of water and warmer temperatures enhance rates of weathering. Land plants with deeply penetrating root systems advance the depth and rates of weathering as plants excrete organic acids, weather mineral grains, and physically mix weathered rock and soil material (e.g. Ibarra et al., 2019). Likewise, soil animals function importantly in mixing weathered rock and soil material through bioturbation. Atmospheric chemistry, especially pCO_2 and pO_2, are important chemical constituents affecting hydrolysis and silicate weathering in general, as well as oxidation-reduction reactions. The fact that these controlling factors of the Earth system have changed significantly over time, through changes in plate tectonic processes, such as subduction, sea-floor spreading and volcanism, and through biological and botanical evolution, are expressed as variable weathering conditions over Earth history and recorded in paleosols.

2.6.2. Paleosols Are Important for Inferring Changes in Climate, Terrestrial Biota, and Weathering Over Time

Because paleosols form in the critical zone, at the interface between the biosphere-atmosphere-hydrosphere, lithosphere, and pedosphere, they are a primary record of these processes. Paleosol recognition requires identification of specific features and properties through the veil of diagenesis and deep-time, and it is up to paleopedologists to use the identified paleosols to reconstruct paleoclimate, paleolandscape, and paleoatmospheric chemistry. The majority of paleosol studies (reviewed here) were aimed at reconstructing past climates and environments. Few of these studies attempted to more directly reconstruct variations in weathering flux through time. More work like this could help modern CZ

research by providing longer term view of weathering flux and potential drivers (tectonics, climate, biota).

ACKNOWLEDGMENTS

We gratefully acknowledge the volume editors (A. Hunt and M. Egli) for inviting us to submit this overview, the reviewers G. Retallack and T. Algeo for their insightful comments and suggestions for improving the manuscript, and the Baylor Geosciences Department, the U.S. National Science Foundation, and the American Chemical Society-Petroleum Research Fund, which over the years have supported various aspects of our research.

REFERENCES

Ahlberg, A., Olsson, I., & Šimkevičius, P. (2003). Triassic–Jurassic weathering and clay mineral dispersal in basement areas and sedimentary basins of southern Sweden. *Sedimentary Geology*, *161*(1–2), 15–29.

Ahr, S. W., Nordt, L. C., & Schaetzl, R. J. (2016). Lithologic discontinuities in soils. *International Encyclopedia of Geography: People, the Earth, Environment and Technology*, 1–8.

Algeo, T. J., Berner, R. A., Maynard, J. B., & Scheckler, S. E. (1995). Late Devonian oceanic anoxic events and biotic crises: "Rooted" in the evolution of vascular land plants. *GSA Today*, *5*(3), 45–66.

Algeo, T. J., Chen, Z. Q., Fraiser, M. L., & Twitchett, R. J. (2011). Terrestrial–marine teleconnections in the collapse and rebuilding of early Triassic marine ecosystems. *Palaeogeography, Palaeoclimatology, Palaeoecology*, *308*(1–2), 1–11.

Algeo, T. J. & Ingall, E. (2007). Sedimentary C_{org}:P ratios, paleocean ventilation, and Phanerozoic atmospheric pO_2. *Palaeogeography, Palaeoclimatology, Palaeoecology*, *256*, 130–155.

Algeo, T. J., Scheckler, S. E., & Maynard, J. B. (2001). Effects of the Middle to Late Devonian spread of vascular land plants on weathering regimes, marine biotas, and global climate. *Plants Invade the Land: Evolutionary and Environmental Perspectives*. New York: Columbia University Press, 213–236.

Alley, R. B. (2000). The Younger Dryas cold interval as viewed from central Greenland. *Quaternary Science Reviews*, *19*(1–5), 213–226.

An, Z. (2000). The history and variability of the East Asian paleomonsoon climate. *Quaternary Science Reviews*, *19*(1–5), 171–187.

Anagnostou, E., John, E. H., Edgar, K. M., Foster, G. L., Ridgwell, A., Inglis, G. N., et al. (2016). Changing atmospheric CO_2 concentration was the primary driver of early Cenozoic climate. *Nature*, *533*(7603), 380–384.

Andrews, E., White, T., & del Papa, C. (2017). Paleosol-based paleoclimate reconstruction of the Paleocene-Eocene Thermal Maximum, northern Argentina. *Palaeogeography, Palaeoclimatology, Palaeoecology*, *471*, 181–195.

Andrews, M. Y., Ague, J. J., & Berner, R. A. (2008). Weathering of soil minerals by angiosperm and gymnosperm trees. *Mineralogical Magazine*, *72*(1), 11–14.

Ashley, G. M., Beverly, E. J., Sikes, N. E., & Driese, S. G. (2014). Paleosol diversity in the Olduvai Basin, Tanzania: Effects of geomorphology, parent material, depositional environment, and groundwater on soil development. *Quaternary International*, *322*, 66–77. https://doi.org/10.1016/j.quaint.2013.12.047

Atchley, S. C., Nordt, L. C., Dworkin, S. I., Cleveland, D. M., Mintz, J. S., Harlow, H., et al. (2013). Alluvial stacking pattern analysis and sequence stratigraphy: concepts and case studies. *New Frontiers in Paleopedology and Terrestrial Paleoclimatology: SEPM, Special Publication*, *104*, 109–130.

Atchley, S. C., Nordt, L. C., Dworkin, S. I., Ramezani, J., Parker, W. G., Ash, S. R., & Bowring, S. A. (2013). A linkage among Pangean tectonism, cyclic alluviation, climate change, and biologic turnover in the Late Triassic: The record from the Chinle Formation, southwestern United States. *Journal of Sedimentary Research*, *83*(11–12), 1147–1161. https://doi.org/10.2110/jsr.2013.89

Autin, W. J., & Holbrook, J. M. (2012). Is the Anthropocene an issue of stratigraphy or pop culture? *GSA Today*, *22*(7), 60–61.

Ballenger, J. A., Holliday, V. T., Kowler, A. L., Reitze, W. T., Prasciunas, M. M., Miller, D. S., & Windingstad, J. D. (2011). Evidence for Younger Dryas global climate oscillation and human response in the American Southwest. *Quaternary International*, *242*(2), 502–519.

Bard, E., Arnold, M., Fairbanks, R. G., & Hamelin, B. (1993). 230 Th-234 U and 14 C ages obtained by mass spectrometry on corals. *Radiocarbon*, *35*(1), 191–199.

Bárdossy, G. (1982) *Karst bauxites*. Amsterdam: Elsevier.

Barnosky, A. D., Matzke, N., Tomiya, S., Wogan, G. O., Swartz, B., Quental, T. B., et al. (2011). Has the Earth's sixth mass extinction already arrived? *Nature*, *471*(7336), 51.

Bata, T. (2016). Evidences of widespread Cretaceous deep weathering and its consequences: A review. *Earth Sciences Research*, *5*(2), 148–155.

Batezelli, A., & Ladeira, F. S. B. (2016). Stratigraphic framework and evolution of the Cretaceous continental sequences of the Bauru, Sanfranciscana, and Parecis basins, Brazil. *Journal of South American Earth Sciences*, *65*, 1–24.

Beall, A. P., Moresi, L., & Cooper, C. M. (2018). Formation of cratonic lithosphere during the initiation of plate tectonics. *Geology*, *46*(6), 487–490.

Bedatou, E., Melchor, R. N., Bellosi, E., & Genise, J. F. (2008). Crayfish burrows from Late Jurassic–Late Cretaceous continental deposits of Patagonia: Argentina. Their palaeoecological, palaeoclimatic and palaeobiogeographical significance. *Palaeogeography, Palaeoclimatology, Palaeoecology*, *257*(1–2), 169–184.

Beerbower, R. (1985). Early development of continental ecosystems. *Geological Factors and the Evolution of Plants*, 47–91.

Beerling, D. J., & Royer, D. L. (2011). Convergent cenozoic CO2 history. *Nature Geoscience*, *4*(7), 418–420.

Behrensmeyer, A. K., Quade, J., Cerling, T. E., Kappelman, J., Khan, I. A., Copeland, P., et al. (2007). The structure and rate of late Miocene expansion of C4 plants: Evidence from

lateral variation in stable isotopes in paleosols of the Siwalik Group, northern Pakistan. *Geological Society of America Bulletin*, *119*(11–12), 1486–1505.

Beraldi-Campesi, H. (2013). Early life on land and the first terrestrial ecosystems. *Ecological Processes*, *2*, 2192–1709.

Berner, R. A. (1994). GEOCARB II: A revised model of atmospheric CO2 levels over Phanerozoic time. *Science*, *249*, 1382–1386.

Berner, R. A. (1997). The rise of plants and their effect on weathering and atmospheric CO2. *Science*, *276*(5312), 544–546.

Berner, R. A. (2001). The effect of the rise of land plants on atmospheric CO2 during the Paleozoic. *Plants Invade the Land: Evolutionary and Environmental Perspectives, Critical Moments and Perspectives in Earth History and Paleobiology*. New York: Columbia University Press, 173–178.

Berner, R. A. (2005). The carbon and sulfur cycles and atmospheric oxygen from middle Permian to middle Triassic. *Geochimica et Cosmochimica Acta*, *69*(13), 3211–3217.

Berner, R. A. (2006). GEOCARBSULF: A combined model for Phanerozoic atmospheric O2 and CO2. *Geochimica et Cosmochimica Acta*, *70*(23), 5653–5664.

Berner, R. A. (2009). Phanerozoic atmospheric oxygen: New results using the GEOCARBSULF model. *American Journal of Science*, *309*(7), 603–606.

Berner, R. A., & Kothavala, Z. (2001). GEOCARB III: a revised model of atmospheric CO2 over Phanerozoic time. *American Journal of Science*, *301*(2), 182–204.

Bestland, E. A. (2000). Weathering flux and CO2 consumption determined from palaeosol sequences across the Eocene–Oligocene transition. *Palaeogeography, Palaeoclimatology, Palaeoecology*, *156*(3–4), 301–326.

Bestland, E. A., Retallack, G. J., Rice, A. E., & Mindszenty, A. (1996). Late Eocene detrital laterites in central Oregon: Mass balance geochemistry, depositional setting, and landscape evolution. *Geological Society of America Bulletin*, *108*(3), 285–302.

Birkeland, P. W. (1999). *Soils and geomorphology* (vol. 3). Oxford: Oxford University Press.

Blodgett, R. H. (1988). Calcareous paleosols in the Triassic Dolores Formation. *Paleosols and weathering through time—Principles and applications. Geological Society of America Special Papers*, *216*, 103–121.

Bonnefille, R. (2010). Cenozoic vegetation, climate changes and hominid evolution in tropical Africa. *Global and Planetary Change*, *72*(4), 390–411.

Borgonie, G., García-Moyano, A., Litthauer, D., Bert, W., Bester, A., van Heerden, E., et al. (2011). Nematoda from the terrestrial deep subsurface of South Africa. *Nature*, *474*(7349), 79.

Borgonie, G., Linage-Alvarez, B., Ojo, A. O., Mundle, S. O. C., Freese, L. B., Van Rooyen, C., et al. (2015). Eukaryotic opportunists dominate the deep-subsurface biosphere in South Africa. *Nature Communications*, *6*, 8952.

Bouchez, J., Gaillardet, J., Lupker, M., Louvat, P., France-Lanord, C., Maurice, L., et al. (2012). Floodplains of large rivers: Weathering reactors or simple silos? *Chemical Geology*, *332*, 166–184.

Boucot, A. J., Xu, C., Scotese, C. R., & Morley, R. J. (2013). *Phanerozoic paleoclimate: an atlas of lithologic indicators of climate*. SEPM (Society for Sedimentary Geology).

Bowen, G. J., Beerling, D. J., Koch, P. L., Zachos, J. C., & Quattlebaum, T. (2004). A humid climate state during the Palaeocene/Eocene thermal maximum. *Nature*, *432*(7016), 495–499.

Bowen, G. J., & Beitler Bowen, B. (2008). Mechanisms of PETM global change constrained by a new record from central Utah. *Geology*, *36*(5), 379–382.

Bowen, G. J., Maibauer, B. J., Kraus, M. J., Röhl, U., Westerhold, T., Steimke, A., et al. (2015). Two massive, rapid releases of carbon during the onset of the Palaeocene–Eocene thermal maximum. *Nature Geoscience*, *8*(1), 44.

Bown, T. M., & Kraus, M. J. (1987). Integration of channel and floodplain suites, I. Developmental sequence and lateral relations of alluvial paleosols. *Journal of Sedimentary Research*, *57*(4).

Brantley, S. L., Goldhaber, M. B., & Ragnarsdottir, K. V. (2007). Crossing Disciplines and Scales to Understand the Critical Zone. *Elements*, *3*(5), 307. https://doi.org/10.2113/gselements.3.5.307

Broecker, W. S., Andree, M., Wolfli, W., Oeschger, H., Bonani, G., Kennett, J., & Peteet, D. (1988). The chronology of the last deglaciation: Implications to the cause of the Younger Dryas event. *Paleoceanography and Paleoclimatology*, *3*(1), 1–19.

Bronger, A. (2003). Correlation of loess–paleosol sequences in East and Central Asia with SE Central Europe: Towards a continental Quaternary pedostratigraphy and paleoclimatic history. *Quaternary International*, *106*, 11–31.

Bronger, A., & Heinkele, T. (1989). Micromorphology and genesis of paleosols in the Luochuan loess section, China: Pedostratigraphic and environmental implications. *Geoderma*, *45*(2), 123–143.

Buatois, L. A., & Mángano, M. G. (2011). *Ichnology: Organism-substrate interactions in space and time*. Cambridge University Press.

Buck, B. J., & Mack, G. H. (1995). Latest Cretaceous (Maastrichtian) aridity indicated by paleosols in the McRae Formation, south-central New Mexico. *Cretaceous Research*, *16*(5), 559–572.

Buck, B. J., Hanson, A. D., Hengst, R. A., & Shu-Sheng, H. (2004). "Tertiary Dinosaurs" in the Nanxiong Basin, southern China, are reworked from the Cretaceous. *The Journal of Geology*, *112*(1), 111–118.

Buggle, B., Hambach, U., Müller, K., Zöller, L., Marković, S. B., & Glaser, B. (2014). Iron mineralogical proxies and Quaternary climate change in SE-European loess–paleosol sequences. *Catena*, *117*, 4–22.

Butchart, S. H., Walpole, M., Collen, B., Van Strien, A., Scharlemann, J. P., Almond, R. E., et al. (2010). Global biodiversity: indicators of recent declines. *Science*, *328*(5982), 1164–1168.

Cabaleri, N. G., Armella, C., & Nieto, D. G. S. (2005). Saline paleolake of the Cañadón Asfalto Formation (Middle-Upper Jurassic), Cerro Cóndor, Chubut province (Patagonia), Argentina. *Facies*, *51*(1–4), 350–364.

Canfield, D. E. (2005). The early history of atmospheric oxygen: Homage to Robert M. Garrels. *Annu. Rev. Earth Planet. Sci.*, *33*, 1–36.

Cao, Y., Song, H., Algeo, T. J., Chu, D., Du, Y., Tian, L., et al. (2018). Intensified chemical weathering during the Permian-Triassic transition recorded in terrestrial and marine successions. *Palaeogeography, Palaeoclimatology, Palaeoecology*, *519*, 166–177.

Carmichael, M. J., Pancost, R. D., & Lunt, D. J. (2018). Changes in the occurrence of extreme precipitation events at the Paleocene–Eocene thermal maximum. *Earth and Planetary Science Letters*, *501*, 24–36.

Carpenter, R. J. (1994). Cenozoic vegetation in Tasmania: Macrofossil evidence. In R. S. Hill (Ed.), *Australian vegetation history: Cretaceous to recent* (pp. 276–298). Cambridge: Cambridge University Press.

Catling, D. C., & Claire, M. W. (2005). How Earth's atmosphere evolved to an oxic state: S status report. *Earth and Planetary Science Letters*, *237*(1–2), 1–20.

Cawood, P. A., Kroner, A., & Pisarevsky, S. (2006). Precambrian plate tectonics: criteria and evidence. *GSA Today*, *16*(7), 4.

Ceballos, G., & Ehrlich, P. R. (2002). Mammal population losses and the extinction crisis. *Science*, *296*(5569), 904–907.

Ceballos, G., Ehrlich, P. R., Barnosky, A. D., García, A., Pringle, R. M., & Palmer, T. M. (2015). Accelerated modern human–induced species losses: Entering the sixth mass extinction. *Science Advances*, *1*(5), e1400253.

Cecil, C. B. (1990). Paleoclimate controls on stratigraphic repetition of chemical and siliciclastic rocks. *Geology*, *18*(6), 533–536.

Cecil, C. B. (2013). An overview and interpretation of autocyclic and allocyclic processes and the accumulation of strata during the Pennsylvanian–Permian transition in the central Appalachian Basin, USA. *International Journal of Coal Geology*, *119*, 21–31.

Cerling, T. E., Harris, J. M., MacFadden, B. J., Leakey, M. G., Quade, J., Eisenmann, V., & Ehleringer, J. R. (1997). Global vegetation change through the Miocene/Pliocene boundary. *Nature*, *389*(6647), 153.

Cerling, T. E., & Hay, R. L. (1986). An isotopic study of paleosol carbonates from Olduvai Gorge. *Quaternary Research*, *25*(1), 63–78.

Cerling, T. E., Wynn, J. G., Andanje, S. A., Bird, M. I., Korir, D. K., Levin, N. E., et al. (2011). Woody cover and hominin environments in the past 6 million years. *Nature*, *476*(7358), 51.

Certini, G., & Scalenghe, R. (2011). Anthropogenic soils are the golden spikes for the Anthropocene. *Holocene (Sevenoaks)*, *21*(8), 1269–1274.

Chaloner, W. G., & McElwain, J. (1997). The fossil plant record and global climatic change. *Review of Palaeobotany and Palynology*, *95*(1–4), 73–82.

Chamberlain, C. P., Winnick, M. J., Mix, H. T., Chamberlain, S. D., & Maher, K. (2014). The impact of Neogene grassland expansion and aridification on the isotopic composition of continental precipitation. *Global Biogeochemical Cycles*, *28*(9), 992–1004.

Chen, C., Guerit, L., Foreman, B. Z., Hassenruck-Gudipati, H. J., Adatte, T., Honegger, L., et al. (2018). Estimating regional flood discharge during Palaeocene-Eocene global warming. *Scientific Reports*, *8*(1), 13391.

Chen, Z., Ding, Z., Yang, S., Zhang, C., & Wang, X. (2016). Increased precipitation and weathering across the Paleocene-Eocene Thermal Maximum in central China. *Geochemistry, Geophysics, Geosystems*, *17*(6), 2286–2297.

Clechenko, E. R., Kelly, D. C., Harrington, G. J., & Stiles, C. A. (2007). Terrestrial records of a regional weathering profile at the Paleocene-Eocene boundary in the Williston Basin of North Dakota. *GSA Bulletin*, *119*(3–4), 428–442.

Clemente, P., & Pérez-Arlucea, M. (1993). Depositional architecture of the Cuerda del Pozo Formation, Lower Cretaceous of the extensional Cameros Basin, north-central Spain. *Journal of Sedimentary Research*, *63*(3), 437–452.

Cleveland, D. M., Nordt, L. C., & Atchley, S. C. (2008). Paleosols, trace fossils, and precipitation estimates of the uppermost Triassic strata in northern New Mexico. *Palaeogeography, Palaeoclimatology, Palaeoecology*, *257*(4), 421–444.

Clyde, W. C., & Gingerich, P. D. (1998). Mammalian community response to the latest Paleocene thermal maximum: An isotaphonomic study in the northern Bighorn Basin, Wyoming. *Geology*, *26*(11), 1011–1014.

Cojan, I., & Moreau, M.-G. (2006). Correlation of terrestrial climatic fluctuations with global signals during the upper Cretaceous–Danian in a compressive setting (Provence, France). *Journal of Sedimentary Research*, *76*(3), 589–604.

Colombera, L., Arévalo, O. J., & Mountney, N. P. (2017). Fluvial-system response to climate change: The Paleocene-Eocene Tremp Group, Pyrenees, Spain. *Global and Planetary Change*, *157*, 1–17.

Condie, K. C. (1998). Episodic continental growth and supercontinents: A mantle avalanche connection? *Earth and Planetary Science Letters*, *163*(1–4), 97–108.

Condie, K. C. (2004). Supercontinents and superplume events: Distinguishing signals in the geologic record. *Physics of the Earth and Planetary Interiors*, *146*(1–2), 319–332.

Cox, G. M., Lyons, T. W., Mitchell, R. N., Hasterok, D., & Gard, M. (2018). Linking the rise of atmospheric oxygen to growth in the continental phosphorus inventory. *Earth and Planetary Science Letters*, *489*, 28–36.

Cramer, B. S., Wright, J. D., Kent, D. V., & Aubry, M.-P. (2003). Orbital climate forcing of δ13C excursions in the late Paleocene–early Eocene (chrons C24n–C25n). *Paleoceanography*, *18*(4).

Cressler III, W. L. (2001). Evidence of earliest known wildfires. *Palaios*, *16*(2), 171–174.

Currie, B. S. (1998). Upper Jurassic-Lower Cretaceous Morrison and Cedar Mountain formations, NE Utah–NW Colorado: Relationships between nonmarine deposition and early Cordilleran foreland-basin development. *Journal of Sedimentary Research*, *68*(4), 632–652.

Dal'Bó, P. F. F., Basilici, G., & Angélica, R. S. (2010). Factors of paleosol formation in a Late Cretaceous eolian sand sheet paleoenvironment, Marília Formation, Southeastern Brazil. *Palaeogeography, Palaeoclimatology, Palaeoecology*, *292*(1–2), 349–365.

Demko, T. M., Currie, B. S., & Nicoll, K. A. (2004). Regional paleoclimatic and stratigraphic implications of paleosols and fluvial/overbank architecture in the Morrison Formation

(Upper Jurassic), Western Interior, USA. *Sedimentary Geology*, *167*(3–4), 115–135.

Demko, T. M., & Parrish, J. T. (1998). Paleoclimatic setting of the Upper Jurassic Morrison formation. *Modern Geology*, *22*, 283–296.

Dickens, G. R., O'Neil, J. R., Rea, D. K., & Owen, R. M. (1995). Dissociation of oceanic methane hydrate as a cause of the carbon isotope excursion at the end of the Paleocene. *Paleoceanography and Paleoclimatology*, *10*(6), 965–971.

DiMichele, W. A., & DeMaris, P. J. (1987). Structure and dynamics of a Pennsylvanian-age Lepidodendron forest: Colonizers of a disturbed swamp habitat in the Herrin (No. 6) Coal of Illinois. *Palaios*, 146–157.

DiMichele, W. A., Phillips, T. L., & Willard, D. A. (1986). Morphology and paleoecology of Pennsylvanian-age coal-swamp plants. *Studies in Geology, Notes for a Short Course*, *15*, 97–114.

Do Campo, M., Bauluz, B., del Papa, C., White, T., Yuste, A., & Mayayo, M. J. (2018). Evidence of cyclic climatic changes recorded in clay mineral assemblages from a continental Paleocene-Eocene sequence, northwestern Argentina. *Sedimentary Geology*, *368*, 44–57.

Donnadieu, Y., Goddéris, Y., & Bouttes, N. (2009). Exploring the climatic impact of the continental vegetation on the Mezosoic atmospheric CO2 and climate history. *Climate of the Past*, *5*(1), 85–96.

Driese, S.G. (2004). Pedogenic translocation of Fe in modern and ancient Vertisols and implications for interpretations of the Hekpoort paleosol (2.25 Ga). *The Journal of Geology*, *112*(5), 543–560.

Driese, S.G., & Foreman, J. L. (1991). Traces and related chemical changes in a Late Ordovician paleosol, Glossifungites ichnofacies, southern Appalachians, USA. *Ichnos: An International Journal of Plant & Animal*, *1*(3), 207–219.

Driese, S.G., & Foreman, J. L. (1992). Paleopedology and paleoclimatic implications of Late Ordovician vertic paleosols, Juniata Formation, southern Appalachians. *Journal of Sedimentary Research*, *62*(1), 71–83.

Driese, S.G., Jirsa, M. A., Ren, M., Brantley, S. L., Sheldon, N. D., Parker, D., & Schmitz, M. (2011). Neoarchean paleoweathering of tonalite and metabasalt: Implications for reconstructions of 2.69 Ga early terrestrial ecosystems and paleoatmospheric chemistry. *Precambrian Research*, *189*(1–2), 1–17.

Driese, S.G., Medaris Jr, L. G., Kirsimäe, K., Somelar, P., & Stinchcomb, G. E. (2018). Oxisolic processes and geochemical constraints on duration of weathering for Neoproterozoic Baltic paleosol. *Precambrian Research*, *310*, 165–178.

Driese, S.G., Medaris Jr, L. G., Ren, M., Runkel, A. C., & Langford, R. P. (2007). Differentiating pedogenesis from diagenesis in early terrestrial paleoweathering surfaces formed on granitic composition parent materials. *The Journal of Geology*, *115*(4), 387–406.

Driese, S.G., & Mora, C. I. (2001). Diversification of Siluro-Devonian plant traces in paleosols and influence on estimates of paleoatmospheric CO2 levels. *Plants Invade the Land: Evolutionary and Environmental Perspectives*, 237–253.

Driese, S.G., & Mora, C. I. (2002). Paleopedology and stable-isotope geochemistry of Late Triassic (Carnian-Norian) paleosols, Durham Sub-basin, North Carolina, USA: Implications for paleoclimate and paleoatmospheric pCO2.

Driese, S.G., Mora, C. I., Cotter, E., & Foreman, J. L. (1992). Paleopedology and stable isotope chemistry of Late Silurian vertic Paleosols, Bloomsburg Formation, central Pennsylvania. *Journal of Sedimentary Research*, *62*(5), 825–841.

Driese, S.G., Mora, C. I., & Elick, J. M. (1997). Morphology and taphonomy of root and stump casts of the earliest trees (Middle to Late Devonian), Pennsylvania and New York, USA. *Palaios*, *12*(6), 524–537.

Driese, S.G., Mora, C. I., & Elick, J. M. (2000). The paleosol record of increasing plant diversity and depth of rooting and changes in atmospheric pCO 2 in the Siluro-Devonian. *The Paleontological Society Papers*, *6*, 47–62.

Driese, S. G., & Ober, E. G. (2005). Paleopedologic and paleohydrologic records of precipitation seasonality from early Pennsylvanian "underclay" Paleosols, USA. *Journal of Sedimentary Research*, *75*(6), 997–1010. https://doi.org/10.2110/jsr.2005.075

Driese, S.G., Peppe, D. J., Beverly, E. J., DiPietro, L. M., Arellano, L. N., & Lehmann, T. (2016). Paleosols and paleoenvironments of the early Miocene deposits near Karungu, Lake Victoria, Kenya. *Palaeogeography, Palaeoclimatology, Palaeoecology*, *443*, 167–182.

Driese, S.G., Simpson, E. L., & Eriksson, K. A. (1995). Redoximorphic Paleosols in alluvial and lacustrine deposits, 1.8 Ga Lochness Formation, Mount Isa, Australia: Pedogenic processes and implications for paleoclimate. *Journal of Sedimentary Research*, *65*(4a), 675–689.

Dubiel, R. F. (1994). Triassic deposystems, paleogeography, and paleoclimate of the Western Interior. Rocky Mountain Section (SEPM).

Dubiel, R. F., Parrish, J. T., Parrish, J. M., & Good, S. C. (1991). The Pangaean megamonsoon-evidence from the Upper Triassic Chinle Formation, Colorado Plateau.

Dygert, N., Jackson, C. R., Hesse, M. A., Tremblay, M. M., Shuster, D. L., & Gu, J. T. (2018). Plate tectonic cycling modulates Earth's 3He/22Ne ratio. *Earth and Planetary Science Letters*, *498*, 309–321.

Eberle, J. J., & Greenwood, D. R. (2012). Life at the top of the greenhouse Eocene world—A review of the Eocene flora and vertebrate fauna from Canada's High Arctic. *Bulletin*, *124*(1–2), 3–23.

Eberth, D. A., Brinkman, D. B., Chen, P.-J., Yuan, F.-T., Wu, S.-Z., Li, G., & Cheng, X.-S. (2001). Sequence stratigraphy, paleoclimate patterns, and vertebrate fossil preservation in Jurassic Cretaceous strata of the Junggar Basin, Xinjiang Autonomous Region, People's Republic of China. *Canadian Journal of Earth Sciences*, *38*(12), 1627–1644.

Edwards, D., & Wellman, C. H. (2001). Embryophytes on land: The Ordovician to Lochkovian (Lower Devonian) record. In P.G. Gensel & D. Edwards (Eds.), *Plants invade the land: Evolutionary and environmental perspectives* (pp. 3–28). Columbia University Press New York.

Edwards, D., Kenrick, P., & Dolan, L. (2017). *History and contemporary significance of the Rhynie cherts—our earliest preserved terrestrial ecosystem*. The Royal Society.

Edwards, E. J., Osborne, C. P., Strömberg, C. A., Smith, S. A., & Consortium, C. G. (2010). The origins of C4 grasslands:

Integrating evolutionary and ecosystem science. *Science*, *328*(5978), 587–591.

Elick, J. M., Driese, S. G., & Mora, C. I. (1998). Very large plant and root traces from the Early to Middle Devonian: Implications for early terrestrial ecosystems and atmospheric p (CO2). *Geology*, *26*(2), 143–146.

Erwin, D. H. (1994). The Permo–Triassic extinction. *Nature*, *367*(6460), 231.

Erwin, D. H. (1996). The mother of mass extinctions. *Scientific American*, *275*(1), 72–78.

Fairbanks, R. G. (1989). A 17,000-year glacio-eustatic sea level record: Influence of glacial melting rates on the Younger Dryas event and deep-ocean circulation. *Nature*, *342*(6250), 637.

Fairbanks, R. G. (1990). The age and origin of the "Younger Dryas climate event" in Greenland ice cores. *Paleoceanography and Paleoclimatology*, *5*(6), 937–948.

Famubode, O., & Bhattacharya, J. (2016). Sequence stratigraphic analysis of the youngest nonmarine sequence in the Cretaceous Ferron Notom Delta, south central Utah, U.S.A. *Journal of Sedimentary Research*, *86*(3), 168–198.

Fan, M., Ayyash, S. A., Tripati, A., Passey, B. H., & Griffith, E. M. (2018). Terrestrial cooling and changes in hydroclimate in the continental interior of the United States across the Eocene-Oligocene boundary. *GSA Bulletin*, *130*(7–8), 1073–1084.

Fanti, F., & Miyashita, T. (2009). A high latitude vertebrate fossil assemblage from the Late Cretaceous of west-central Alberta, Canada: Evidence for dinosaur nesting and vertebrate latitudinal gradient. *Palaeogeography, Palaeoclimatology, Palaeoecology*, *275*(1–4), 37–53.

Feakes, C. R., & Retallack, G. J. (1988). Recognition and chemical characterization of fossil soils developed on alluvium: A Late Ordovician example. *Paleosols and Weathering through Geologic Time: Principles and Applications: Geological Society of America Special Paper*, *216*, 35–48.

Fedo, C. M., Wayne Nesbitt, H., & Young, G. M. (1995). Unraveling the effects of potassium metasomatism in sedimentary rocks and paleosols, with implications for paleoweathering conditions and provenance. *Geology*, *23*(10), 921–924.

Fedorko, N., & Skema, V. (2013). A review of the stratigraphy and stratigraphic nomenclature of the Dunkard Group in West Virginia and Pennsylvania, USA. *International Journal of Coal Geology*, *119*, 2–20.

Fernandes, L. A., & Basilici, G. (2009). Transition of ephemeral palustrine to aeolian deposits in a continental arid–semi-arid environment (Upper Cretaceous Bauru Basin, Brazil). *Cretaceous Research*, *30*(3), 605–614.

Finke, P. A., & Hutson, J. L. (2008). Modelling soil genesis in calcareous loess. *Geoderma*, *145*(3–4), 462–479.

Firestone, R. B., West, A., Kennett, J. P., Becker, L., Bunch, T. E., Revay, Z. S., et al. (2007). Evidence for an extraterrestrial impact 12,900 years ago that contributed to the megafaunal extinctions and the Younger Dryas cooling. *Proceedings of the National Academy of Sciences*, *104*(41), 16016–16021.

Fitzsimmons, K. E., Marković, S. B., & Hambach, U. (2012). Pleistocene environmental dynamics recorded in the loess of the middle and lower Danube basin. *Quaternary Science Reviews*, *41*, 104–118.

Flaig, P. P., McCarthy, P. J., Fiorillo, A. R., Davidson, S. K., & Leleu, S. (2011). A tidally influenced, high-latitude coastal-plain: The upper Cretaceous (Maastrichtian) Prince Creek Formation, North Slope, Alaska. In *From River to Rock Record: The Preservation of Fluvial Sediments and Their Subsequent Interpretation* (Vol. *97*, pp. 233–264). SEPM (Society for Sedimentary Geology), Tulsa.

Flecker, R., Krijgsman, W., Capella, W., de Castro Martíns, C., Dmitrieva, E., Mayser, J. P., et al. (2015). *Evolution of the Late Miocene Mediterranean–Atlantic gateways and their impact on regional and global environmental change*. Elsevier.

Flood, Y. S., & Hampson, G. J. (2014). Facies and architectural analysis to interpret avulsion style and variability: Upper Cretaceous Blackhawk Formation, Wasatch Plateau, Central Utah, USA. *Journal of Sedimentary Research*, *84*(9), 743–762.

Föllmi, K. B. (2012). Early Cretaceous life, climate and anoxia. *Cretaceous Research*, *35*, 230–257.

Food and Agriculture Organization of the United Nations (FAO) (1998). *World reference base for soil resources* (Vol. *3*). Food & Agriculture Org.

Foreman, B. Z., Heller, P. L., & Clementz, M. T. (2012). Fluvial response to abrupt global warming at the Palaeocene/Eocene boundary. *Nature*, *491*(7422), 92.

Francis, J. E., & Poole, I. (2002). Cretaceous and early Tertiary climates of Antarctica: Evidence from fossil wood. *Palaeogeography, Palaeoclimatology, Palaeoecology*, *182*(1–2), 47–64.

Fricke, H. C., Foreman, B. Z., & Sewall, J. O. (2010). Integrated climate model-oxygen isotope evidence for a North American monsoon during the Late Cretaceous. *Earth and Planetary Science Letters*, *289*(1–2), 11–21.

Gale, S., & Hoare, P. (2012). The stratigraphic status of the Anthropocene. *The Holocene*, *22*(12), 1491–1494. https://doi.org/10.1177/0959683612449764

Gallagher, T. M., & Sheldon, N. D. (2013). A new paleothermometer for forest paleosols and its implications for Cenozoic climate. *Geology*, *41*(6), 647–650. https://doi.org/10.1130/G34074.1

Gallet, S., Jahn, B., & Torii, M. (1996). Geochemical characterization of the Luochuan loess-paleosol sequence, China, and paleoclimatic implications. *Chemical Geology*, *133*(1–4), 67–88.

Gardner, T. W., Williams, E. G., & Holbrook. (1988). Pedogenesis of some Pennsylvanian underclays; Groundwater, topographic, and tectonic controls. In J. Reinhardt & W. R. Sigleo (Eds.), *Paleosols and weathering through geologic time* (pp. 81–101).

Gastaldo, R. A. (1986). Implications on the paleoecology of autochthonous lycopods in clastic sedimentary environments of the Early Pennsylvanian of Alabama. *Palaeogeography, Palaeoclimatology, Palaeoecology*, *53*(2–4), 191–212.

Gastaldo, R. A. (1987). Confirmation of Carboniferous clastic swamp communities. *Nature*, *326*(6116), 869.

Gastaldo, R. A., DiMichele, W. A., & Pfefferkorn, H. W. (1996). Out of the icehouse into the greenhouse: A late Paleozoic analogue for modern global vegetational change. *GSA Today*.

Genise, J. F., Mángano, M. G., Buatois, L. A., Laza, J. H., & Verde, M. (2000). Insect trace fossil associations in paleosols: The Coprinisphaera ichnofacies. *Palaios*, *15*(1), 49–64.

Gensel, Patricia G., & Andrews, H. N. (1987). The evolution of early land plants. *American Scientist*, *75*(5), 478–489.

Gensel, Patricia G., Kotyk, M. E., & Basinger, J. F. (2001). Morphology of above-and below-ground structures in Early Devonian (Pragian–Emsian) plants. *Plants Invade the Land: Evolutionary and Environmental Perspectives*, *83*.

Ghosh, P. (1997). Geomorphology and palaeoclimatology of some Upper Cretaceous palaeosols in central India. *Sedimentary Geology*, *110*(1–2), 25–49.

Gibbs, M. T., Bluth, G. J., Fawcett, P. J., & Kump, L. R. (1999). Global chemical erosion over the last 250 my: Variations due to changes in paleogeography, paleoclimate, and paleogeology. *American Journal of Science*, *299*(7–9), 611–651.

Gierlowski-Kordesch, E. (1991). Ichnology of an ephemeral lacustrine/alluvial plain system: Jurassic East Berlin Formation, Hartford Basin, USA. *Ichnos: An International Journal of Plant & Animal*, *1*(3), 221–232.

Gingerich, P. D. (2003). Mammalian responses to climate change at the Paleocene-Eocene boundary: Polecat Bench record in the northern Bighorn Basin, Wyoming. *Special Papers—Geological Society of America*, 463–478.

Glaser, B., Haumaier, L., Guggenberger, G., & Zech, W. (2001). The "Terra Preta" phenomenon: A model for sustainable agriculture in the humid tropics. *Naturwissenschaften*, *88*(1), 37–41.

Glasspool, I. J. & Scott, A. C. (2010). Phanerozoic concentrations of atmospheric oxygen reconstructed from sedimentary charcoal. *Nature Geoscience*, *3*, 627–630.

Gradstein, F. M., Ogg, J. G., Schmitz, M., & Ogg, G. (2012). *The geologic time scale 2012*. Elsevier.

Gradstein, S. R., & Kerp, H. (2012). A brief history of plants on Earth. *The Geologic Time Scale*, *29*, 233–237.

Gray, J. (1985). The microfossil record of early land plants: Advances in understanding of early terrestrialization, 1970–1984. *Philosophical Transactions of the Royal Society of London. B, Biological Sciences*, *309*(1138), 167–195.

Gray, J., & Boucot, A. J. (1978). The advent of land plant life. *Geology*, *6*(8), 489–492.

Gray, J., & Shear, W. (1992). Early life on land. *American Scientist*, *80*, 444.

Greb, S. F., DiMichele, W. A., & Gastaldo, R. A. (2006). *Evolution and importance of wetlands in earth history*. *Special Papers—Geological Society of America*, *399*, 1.

Grimley, D. A., Follmer, L. R., Hughes, R. E., & Solheid, P. A. (2003). Modern, Sangamon and Yarmouth soil development in loess of unglaciated southwestern Illinois. *Quaternary Science Reviews*, *22*(2–4), 225–244.

Gutierrez, K., & Sheldon, N. D. (2012). Paleoenvironmental reconstruction of Jurassic dinosaur habitats of the Vega Formation, Asturias, Spain. *GSA Bulletin*, *124*(3–4), 596–610.

Hamon, N., Sepulchre, P., Lefebvre, V., & Ramstein, G. (2013). The role of eastern Tethys seaway closure in the Middle Miocene Climatic Transition (ca. 14 Ma). *Climate of the Past*, *9*(6), 2687–2702.

Hansen, J., Sato, M., Kharecha, P., Beerling, D., Berner, R., Masson-Delmotte, V., et al. (2008). Target atmospheric CO2: Where should humanity aim? *ArXiv Preprint ArXiv:0804.1126*.

Haq, B. U., Hardenbol, J., & Vail, P. R. (1988). Mesozoic and Cenozoic chronostratigraphy and cycles of sea-level change.

Harland, W. B. (2007). Origins and assessment of snowball Earth hypotheses. *Geological Magazine*, *144*(4), 633–642.

Harris-Parks, E. (2016). The micromorphology of Younger Dryas–aged black mats from Nevada, Arizona, Texas and New Mexico. *Quaternary Research*, *85*(1), 94–106.

Hasiotis, S. T. (2002). *Continental Trace Fossil Atlas* (Vol. *51*). Tulsa, OK: SEPM Short Course Notes.

Hasiotis, S. T. (2004). Reconnaissance of Upper Jurassic Morrison Formation ichnofossils, Rocky Mountain Region, USA: Paleoenvironmental, stratigraphic, and paleoclimatic significance of terrestrial and freshwater ichnocoenoses. *Sedimentary Geology*, *167*(3–4), 177–268.

Hasiotis, S. T., & Dubiel, R. F. (1993). Trace fossil assemblages in Chinle Formation alluvial deposits at the Tepees, Petrified Forest National Park, Arizona. *The Nonmarine Triassic, Bulletin of the New Mexico Museum of Natural History and Science*, *3*, G42–G43.

Hasiotis, S. T., & Dubiel, R. F. (1994). Ichnofossil tiering in Triassic alluvial paleosols: Implications for Pangean continental rocks and paleoclimate.

Haug, G. H., & Tiedemann, R. (1998). Effect of the formation of the Isthmus of Panama on Atlantic Ocean thermohaline circulation. *Nature*, *393*(6686), 673.

Haynes, C. V. (2008). Younger Dryas "black mats" and the Rancholabrean termination in North America. *Proceedings of the National Academy of Sciences*, *105*(18), 6520–6525.

Heckel, P. H. (1995). Glacial-eustatic base-level–Climatic model for late Middle to Late Pennsylvanian coal-bed formation in the Appalachian basin. *Journal of Sedimentary Research*, *65*(3).

Heckman, D. S., Geiser, D. M., Eidell, B. R., Stauffer, R. L., Kardos, N. L., & Hedges, S. B. (2001). Molecular evidence for the early colonization of land by fungi and plants. *Science*, *293*(5532), 1129–1133.

Heller, F., & Liu, T.-S. (1982). Magnetostratigraphical dating of loess deposits in China. *Nature*, *300*(5891), 431.

Herman, F., Seward, D., Valla, P. G., Carter, A., Kohn, B., Willett, S. D., & Ehlers, T. A. (2013). Worldwide acceleration of mountain erosion under a cooling climate. *Nature*, *504*(7480), 423.

Herndon, E. M., Jin, L., & Brantley, S. L. (2010). Soils reveal widespread manganese enrichment from industrial inputs. *Environmental Science & Technology*, *45*(1), 241–247.

Hetherington, A. J., & Dolan, L. (2018). Stepwise and independent origins of roots among land plants. *Nature*, *561*(7722), 235.

Hewitt, G. (2000). The genetic legacy of the Quaternary ice ages. *Nature*, *405*(6789), 907.

Hoffman, P. F., Kaufman, A. J., Halverson, G. P., & Schrag, D. P. (1998). A Neoproterozoic snowball Earth. *Science*, *281*(5381), 1342–1346.

Hoffman, P. F., & Schrag, D. P. (2002). The snowball Earth hypothesis: Testing the limits of global change. *Terra Nova*, *14*(3), 129–155.

Holliday, V., Surovell, T., & Johnson, E. (2016). A blind test of the Younger Dryas impact hypothesis. *PloS One*, *11*(7), e0155470.

Homann, M., Sansjofre, P., Van Zuilen, M., Heubeck, C., Gong, J., Killingsworth, B., et al. (2018). Microbial life and

biogeochemical cycling on land 3,220 million years ago. *Nature Geoscience*, *11*(9), 665.

Hong, S. K., & Lee, Y. I. (2012). Evaluation of atmospheric carbon dioxide concentrations during the Cretaceous. *Earth and Planetary Science Letters*, *327*, 23–28.

Hooke, R. L. (2000). On the history of humans as geomorphic agents. *Geology*, *28*(9), 843–846.

Horiuchi, Y., Charusiri, P., & Hisada, K. (2012). Identification of an anastomosing river system in the Early Cretaceous Khorat Basin, northeastern Thailand, using stratigraphy and paleosols. *Journal of Asian Earth Sciences*, *61*, 62–77.

Horiuchi, Y., Hisada, K., & Lee, Y. I. (2009). Paleosol profiles in the Shiohama Formation of the Lower Cretaceous Kanmon Group, Southwest Japan and implications for sediment supply frequency. *Cretaceous Research*, *30*(5), 1313–1324.

Hotton, C. L., Hueber, F. M., Griffing, D. H., Bridge, J. S., Gensel, P. G., & Edwards, D. (2001). Early terrestrial plant environments: An example from the Emsian of Gaspé, Canada. *Plants Invade the Land: Evolutionary and Environmental Perspectives*, 179–212.

Howe, J., & Francis, J. E. (2005). Metamorphosed palaeosols associated with Cretaceous fossil forests, Alexander Island, Antarctica. *Journal of the Geological Society*, *162*(6), 951–957.

Huang, C., Retallack, G. J., Wang, C., & Huang, Q. (2013). Paleoatmospheric pCO2 fluctuations across the Cretaceous–Tertiary boundary recorded from paleosol carbonates in NE China. *Palaeogeography, Palaeoclimatology, Palaeoecology*, *385*, 95–105.

Huang, Y., Clemens, S. C., Liu, W., Wang, Y., & Prell, W. L. (2007). Large-scale hydrological change drove the late Miocene C4 plant expansion in the Himalayan foreland and Arabian Peninsula. *Geology*, *35*(6), 531–534.

Hubert, J. F. (1977). Paleosol caliche in the New Haven Arkose, Connecticut: Record of semiaridity in Late Triassic–Early Jurassic Time. *Geology*, *5*(5), 302–304.

Huynh, T. T., & Poulsen, C. J. (2005). Rising atmospheric CO2 as a possible trigger for the end-Triassic mass extinction. *Palaeogeography, Palaeoclimatology, Palaeoecology*, *217*(3–4), 223–242.

Hyland, E. G., Huntington, K. W., Sheldon, N. D., & Reichgelt, T. (2018). Temperature seasonality in the North American continental interior during the Early Eocene Climatic Optimum. *Climate of the Past*, *14*(10), 1391–1404.

Ibarra, D. E., Rugenstein, J. K. C., Bachan, A., Baresch, A., Lau, K. V., Thomas, D. L., et al. (2019). Modeling the consequences of land plant evolution on silicate weathering. *American Journal of Science*, *319*(1), 1–43.

Jaramillo, S. S., McCarthy, P. J., Trainor, T. P., Fowell, S. J., & Fiorillo, A. R. (2015). Origin of clay minerals in alluvial paleosols, Prince Creek Formation, North Slope, Alaska, USA: Influence of volcanic ash on pedogenesis in the Late Cretaceous Arctic. *Journal of Sedimentary Research*, *85*(2), 192–208.

Jennings, D. S., & Hasiotis, S. T. (2006). Paleoenvironmental and stratigraphic implications of authigenic clay distributions in Morrison Formation deposits, Bighorn Basin, Wyoming. In J. R. Foster & S. G. Lucas (Eds.), *Paleontology and geology of the Upper Jurassic Morrison Formation* (pp. 25–34).

Jenny, H. (1941). *Factors of soil formation: A system of quantitative pedology*. McGraw-Hill.

Joeckel, R. M. (1995). Paleosols below the Ames Marine Unit (Upper Pennsylvanian, Conemaugh Group) in the Appalachian Basin, USA: Variability on an ancient depositional landscape. *Journal of Sedimentary Research*, *65*(2a), 393–407.

Joeckel, R. M. (1999). Paleosol in Galesburg Formation (Kansas City Group, Upper Pennsylvanian), northern Midcontinent, USA: Evidence for climate change and mechanisms of marine transgression. *Journal of Sedimentary Research*, *69*(3), 720–737.

John, C. M., Bohaty, S. M., Zachos, J. C., Sluijs, A., Gibbs, S., Brinkhuis, H., & Bralower, T. J. (2008). North American continental margin records of the Paleocene-Eocene thermal maximum: Implications for global carbon and hydrological cycling. *Paleoceanography*, *23*(2).

Johnson, D. L., & Schaetzl, R. J. (2015). Differing views of soil and pedogenesis by two masters: Darwin and Dokuchaev. *Geoderma*, *237*, 176–189.

Kahmann, J. A., & Driese, S. G. (2008). Paleopedology and geochemistry of Late Mississippian (Chesterian) Pennington Formation paleosols at Pound Gap, Kentucky, USA: Implications for high-frequency climate variations. *Palaeogeography, Palaeoclimatology, Palaeoecology*, *259*(4), 357–381.

Kanzaki, Y., & Murakami, T. (2015). Estimates of atmospheric CO2 in the Neoarchean–Paleoproterozoic from paleosols. *Geochimica et Cosmochimica Acta*, *159*, 190–219.

Kanzaki, Y., & Murakami, T. (2016). Estimates of atmospheric O2 in the Paleoproterozoic from paleosols. *Geochimica et Cosmochimica Acta*, *174*, 263–290.

Kanzaki, Y., & Murakami, T. (2018a). Effects of atmospheric composition on apparent activation energy of silicate weathering: I. Model formulation. *Geochimica et Cosmochimica Acta*, *233*, 159–186.

Kanzaki, Y., & Murakami, T. (2018b). Effects of atmospheric composition on apparent activation energy of silicate weathering: II. Implications for evolution of atmospheric CO2 in the Precambrian. *Geochimica et Cosmochimica Acta*, *240*, 314–330.

Kasting, J. F. (1987). Theoretical constraints on oxygen and carbon dioxide concentrations in the Precambrian atmosphere. *Precambrian Research*, *34*, 205–228.

Kasting, J. F. (1993). Earth's early atmosphere. *Science*, *259*(5097), 920–926.

Kemp, R. A. (1995). Distribution and genesis of calcitic pedofeatures within a rapidly aggrading loess-paleosol sequence in China. *Geoderma*, *65*(3–4), 303–316.

Kemp, R. A., Derbyshire, E., Xingmin, M., Fahu, C., & Baotian, P. (1995). Pedosedimentary reconstruction of a thick loess-paleosol sequence near Lanzhou in north-central China. *Quaternary Research*, *43*(1), 30–45.

Kemp, R. A., Zárate, M., Toms, P., King, M., Sanabria, J., & Arguello, G. (2006). Late Quaternary paleosols, stratigraphy and landscape evolution in the Northern Pampa, Argentina. *Quaternary Research*, *66*(1), 119–132.

Kerp, H. (2000). The modernization of landscapes during the Late Paleozoic-Early Mesozoic. In R. A. Gastaldo & W. A.

DiMichele (Eds.), *Phanerozoic terrestrial ecosystems, a short course* (Vol. *6*, pp. 79–113). New Haven: The Paleontological Society Papers.

Kidston, R., & Lang, W. H. (1920). XXIV.—On Old Red Sandstone plants showing structure, from the Rhynie Chert Bed, Aberdeenshire. Part II. Additional Notes on Rhynia Gwynne-Vaughani, Kidston and Lang; with Descriptions of *Rhynia major*, n. sp., and *Hornea Lignieri*, ng, n. sp. *Earth and Environmental Science Transactions of The Royal Society of Edinburgh*, *52*(3), 603–627.

Kidston, R., & Lang, W. H. (1921). XXXII.—On Old Red Sandstone plants showing structure, from the Rhynie Chert Bed, Aberdeenshire. Part IV. Restorations of the vascular cryptogams, and discussion of their bearing on the general morphology of the Pteridophyta and the origin of the organisation of land-plants. *Earth and Environmental Science Transactions of the Royal Society of Edinburgh*, *52*(4), 831–854.

Kim, C.-B., Al-Aasm, I. S., Ghazban, F., & Chang, H.-W. (2009). Stable isotopic composition of dinosaur eggshells and pedogenic carbonates in the upper cretaceous Seonso formation, South Korea: Paleoenvironmental and diagenetic implications. *Cretaceous Research*, *30*(1), 93–99.

Kingston, J. D., Hill, A., & Marino, B. D. (1994). Isotopic evidence for Neogene hominid paleoenvironments in the Kenya Rift Valley. *Science*, *264*(5161), 955–959.

Kirkland, J. I. (2006). Fruita paleontological area (Upper Jurassic, Morrison Formation), western Colorado: An example of terrestrial taphofacies analysis. *New Mexico Museum of Natural History and Science Bulletin*, *36*, 67–95.

Klein, G. O. (1994). *Pangea: Paleoclimate, tectonics, and sedimentation during accretion, zenith, and breakup of a supercontinent* (Vol. *288*). Geological Society of America.

Knorr, G., Butzin, M., Micheels, A., & Lohmann, G. (2011). A warm Miocene climate at low atmospheric CO2 levels. *Geophysical Research Letters*, *38*(20).

Koch, P. L., Zachos, J. C., & Gingerich, P. D. (1992). Correlation between isotope records in marine and continental carbon reservoirs near the Palaeocene/Eocene boundary. *Nature*, *358*(6384), 319.

Kopp, R. E., Kirschvink, J. L., Hilburn, I. A., & Nash, C. Z. (2005). The Paleoproterozoic snowball Earth: A climate disaster triggered by the evolution of oxygenic photosynthesis. *Proc. Natl. Acad. Sci. U.S.A.*, *102* (32), 11131–11136.

Korenaga, J. (2013). Initiation and evolution of plate tectonics on Earth: Theories and observations. *Annual Review of Earth and Planetary Sciences*, *41*, 117–151.

Kraus, M. J., McInerney, F. A., Wing, S. L., Secord, R., Baczynski, A. A., & Bloch, J. I. (2013). Paleohydrologic response to continental warming during the Paleocene–Eocene Thermal Maximum, Bighorn Basin, Wyoming. *Palaeogeography, Palaeoclimatology, Palaeoecology*, *370*, 196–208.

Kraus, M. J., & Riggins, S. (2007). Transient drying during the Paleocene–Eocene Thermal Maximum (PETM): Analysis of paleosols in the Bighorn Basin, Wyoming. *Palaeogeography, Palaeoclimatology, Palaeoecology*, *245*(3–4), 444–461.

Krijgsman, W., Hilgen, F. J., Raffi, I., Sierro, F. J., & Wilson, D. S. (1999). Chronology, causes and progression of the Messinian salinity crisis. *Nature*, *400*(6745), 652.

Kring, D. A. (2007). The Chicxulub impact event and its environmental consequences at the Cretaceous–Tertiary boundary. *Palaeogeography, Palaeoclimatology, Palaeoecology*, *255*(1–2), 4–21.

Krull, E. S., & Retallack, G. J. (2000). Delta C-13 depth profiles from paleosols across the Permian-Triassic boundary: Evidence for methane release. *Geological Society of America Bulletin*, *112*(9), 1459–1472. https://doi.org/10.1130/0016-7606(2000)112<1459:CDPFPA>2.0.CO;2

Kukla, G. (1987). Loess stratigraphy in central China. *Quaternary Science Reviews*, *6*(3–4), 191–219.

Kumagai, H., Sweda, T., Hayashi, K., Kojima, S., Basinger, J. F., Shibuya, M., & Fukaoa, Y. (1995). Growth-ring analysis of Early Tertiary conifer woods from the Canadian High Arctic and its paleoclimatic interpretation. *Palaeogeography, Palaeoclimatology, Palaeoecology*, *116*(3–4), 247–262.

Kump, L. R. (2014). Hypothesized link between Neoproterozoic greening of the land surface and the establishment of an oxygen-rich atmosphere. *Proceedings of the National Academy of Sciences*, *111*(39), 14062–14065.

Kürschner, W. M., Kvaček, Z., & Dilcher, D. L. (2008). The impact of Miocene atmospheric carbon dioxide fluctuations on climate and the evolution of terrestrial ecosystems. *Proceedings of the National Academy of Sciences*, *105*(2), 449–453.

Labandeira, C. C., Johnson, K. R., & Wilf, P. (2002). Impact of the terminal Cretaceous event on plant–insect associations. *Proceedings of the National Academy of Sciences*, *99*(4), 2061–2066.

Lauretano, V., Littler, K., Polling, M., Zachos, J. C., & Lourens, L. J. (2015). Frequency, magnitude and character of hyperthermal events at the onset of the Early Eocene Climatic Optimum. *Clim. Past*, *11*(10), 1313–1324. https://doi.org/10.5194/cp-11-1313-2015

Lawton, T. F., & Buck, B. J. (2006). Implications of diapir-derived detritus and gypsic paleosols in Lower Triassic strata near the Castle Valley salt wall, Paradox Basin, Utah. *Geology*, *34*(10), 885–888.

Leckie, D. A., Wallace-Dudley, K. E., Vanbeselaere, N. A., & James, D. P. (2004). Sedimentation in a low-accommodation setting: Nonmarine (Cretaceous) Mannville and marine (Jurassic) Ellis Groups, Manyberries Field, southeastern Alberta. *AAPG Bulletin*, *88*(10), 1391–1418.

Lee, Y. I. (1999). Stable isotopic composition of calcic paleosols of the Early Cretaceous Hasandong Formation, southeastern Korea. *Palaeogeography, Palaeoclimatology, Palaeoecology*, *150*(1–2), 123–133.

Lee, Y. I., & Hisada, K. (1999). Stable isotopic composition of pedogenic carbonates of the Early Cretaceous Shimonoseki Subgroup, western Honshu, Japan. *Palaeogeography, Palaeoclimatology, Palaeoecology*, *153*(1–4), 127–138.

Lee, Y. W., Lee, Y. I., & Hisada, K. (2003). Paleosols in the Cretaceous Goshoura and Mifune groups, SW Japan and their paleoclimate implications. *Palaeogeography, Palaeoclimatology, Palaeoecology*, *199*(3–4), 265–282.

Leguédois, S., Séré, G., Auclerc, A., Cortet, J., Huot, H., Ouvrard, S., et al. (2016). Modelling pedogenesis of Technosols. *Geoderma*, *262*, 199–212.

Leier, A., Quade, J., DeCelles, P., & Kapp, P. (2009). Stable isotopic results from paleosol carbonate in South Asia: Paleoenvironmental reconstructions and selective alteration. *Earth and Planetary Science Letters*, *279*(3–4), 242–254.

Lenton, T. M., Daines, S. J., & Mills, B. J. (2018). COPSE reloaded: An improved model of biogeochemical cycling over Phanerozoic time. *Earth-Science Reviews*, *178*, 1–28.

Lenton, T. M., & Watson, A. J. (2004). Biotic enhancement of weathering, atmospheric oxygen and carbon dioxide in the Neoproterozoic. *Geophysical Research Letters*, *31*(5).

LeTourneau, P. M., & Huber, P. (2006). Early Jurassic eolian dune field, Pomperaug basin, Connecticut and related synrift deposits: Stratigraphic framework and paleoclimatic context. *Sedimentary Geology*, *187*(1–2), 63–81.

Levin, N. E., Brown, F. H., Behrensmeyer, A. K., Bobe, R., & Cerling, T. E. (2011). Paleosol carbonates from the Omo Group: Isotopic records of local and regional environmental change in East Africa. *Palaeogeography, Palaeoclimatology, Palaeoecology*, *307*(1), 75–89.

Levin, N. E., Quade, J., Simpson, S. W., Semaw, S., & Rogers, M. (2004). Isotopic evidence for Plio–Pleistocene environmental change at Gona, Ethiopia. *Earth and Planetary Science Letters*, *219*(1), 93–110.

Li, J., Wen, X. Y., & Huang, C. M. (2016). Lower Cretaceous paleosols and paleoclimate in Sichuan Basin, China. *Cretaceous Research*, *62*, 154–171.

Liivamägi, S., Somelar, P., Mahaney, W. C., Kirs, J., Vircava, I., & Kirsimäe, K. (2014). Late Neoproterozoic Baltic paleosol: Intense weathering at high latitude? *Geology*, *42*(4), 323–326.

Liivamägi, S., Somelar, P., Vircava, I., Mahaney, W. C., Kirs, J., & Kirsimäe, K. (2015). Petrology, mineralogy and geochemical climofunctions of the Neoproterozoic Baltic paleosol. *Precambrian Research*, *256*, 170–188.

Lima, H. N., Schaefer, C. E., Mello, J. W., Gilkes, R. J., & Ker, J. C. (2002). Pedogenesis and pre-Colombian land use of "Terra Preta Anthrosols" ("Indian black earth") of Western Amazonia. *Geoderma*, *110*(1–2), 1–17.

Littler, K., Röhl, U., Westerhold, T., & Zachos, J. C. (2014). A high-resolution benthic stable-isotope record for the South Atlantic: Implications for orbital-scale changes in Late Paleocene–Early Eocene climate and carbon cycling. *Earth and Planetary Science Letters*, *401*, 18–30. https://doi.org/10.1016/j.epsl.2014.05.054

Liu, L., Qin, M., Tian, N., Zhou, C., Wang, D., Basinger, J. F., & Xue, J. (2018). Belowground rhizomes and roots in waterlogged paleosols: Examples from the Middle Jurassic of Beijing, China. *Geobios*, *51*(5), 419–433.

Ludvigson, G. A., Gonzalez, L. A., Metzger, R. A., Witzke, B. J., Brenner, R. L., Murillo, A. P., & White, T. S. (1998). Meteoric sphaerosiderite lines and their use for paleohydrology and paleoclimatology. *Geology*, *26*(11), 1039–1042. https://doi.org/10.1130/0091-7613(1998)026<1039:MSLATU>2.3.CO;2

Lukens, W. E., Driese, S. G., Peppe, D. J., & Loudermilk, M. (2017). Sedimentology, stratigraphy, and paleoclimate at the late Miocene Coffee Ranch fossil site in the Texas Panhandle. *Palaeogeography, Palaeoclimatology, Palaeoecology*, *485*(Supplement C), 361–376. https://doi.org/10.1016/j.palaeo.2017.06.026

Lukens, W. E., Lehmann, T., Peppe, D. J., Fox, D. L., Driese, S. G., & McNulty, K. P. (2017). The Early Miocene Critical Zone at Karungu, western Kenya: An equatorial, open habitat with few primate remains. *Frontiers in Earth Science*, *5*, 87. https://doi.org/10.3389/feart.2017.00087

Lukens, W. E., Nordt, L. C., Stinchcomb, G. E., Driese, S. G., & Tubbs, J. D. (2018). Reconstructing pH of paleosols using geochemical proxies. *The Journal of Geology*, *126*(4), 427–449.

Lüthi, D., Le Floch, M., Bereiter, B., Blunier, T., Barnola, J.-M., Siegenthaler, U., et al. (2008). High-resolution carbon dioxide concentration record 650,000–800,000 years before present. *Nature*, *453*(7193), 379.

Lyle, M., Barron, J., Bralower, T. J., Huber, M., Lyle, A. O., Ravelo, A. C., et al. (2008). Pacific Ocean and Cenozoic evolution of climate. *Reviews of Geophysics*, *46*(2).

Ma, L., Konter, J., Herndon, E., Jin, L., Steinhoefel, G., Sanchez, D., & Brantley, S. (2014). Quantifying an early signature of the industrial revolution from lead concentrations and isotopes in soils of Pennsylvania, USA. *Anthropocene*, *7*, 16–29.

Mack, G. H. (1992). Paleosols as an indicator of climatic change at the early-late Cretaceous boundary, southwestern New Mexico. *Journal of Sedimentary Research*, *62*(3), 483–494.

Mack, G. H., & Cole, D. R. (2005). Geochemical model of δ18O of pedogenic calcite versus latitude and its application to Cretaceous palaeoclimate. *Sedimentary Geology*, *174*(1–2), 115–122.

Mack, G. H., & James, W. C. (1994). Paleoclimate and the global distribution of paleosols. *The Journal of Geology*, *102*(3), 360–366.

Mack, G. H., James, W. C., & Monger, H. C. (1993). Classification of paleosols. *Geological Society of America Bulletin*, *105*(2), 129–136.

Mackensen, A. (2004). Changing Southern Ocean palaeocirculation and effects on global climate. *Antarctic Science*, *16*(4), 369–386.

Macphail, M. K., Alley, N. F., Truswell, E. M., & Sluiter, I. R. K. (1994). Early Tertiary vegetation: evidence from spores and pollen. In R. S. Hill (Ed.), *History of the Australian vegetation: Cretaceous to Recent* (pp. 189–261). Cambridge: Cambridge University Press.

Mägdefrau, K. (1952). *Vegetationsbilder der vorzeit*. Jena, Germany: Gustav Fischer.

Maher, B. A., & Thompson, R. (1995). Paleorainfall reconstructions from pedogenic magnetic susceptibility variations in the Chinese loess and paleosols. *Quaternary Research*, *44*(3), 383–391. https://doi.org/10.1006/qres.1995.1083

Maher, K., & Chamberlain, C. P. (2014). Hydrologic regulation of chemical weathering and the geologic carbon cycle. *Science*, *343*(6178), 1502–1504.

Mann, C. C. (2008). *Ancient earthmovers of the Amazon*. American Association for the Advancement of Science.

Marković, S. B., Hambach, U., Catto, N., Jovanović, M., Buggle, B., Machalett, B., et al. (2009). Middle and late Pleistocene loess sequences at Batajnica, Vojvodina, Serbia. *Quaternary International*, *198*(1–2), 255–266.

Mason, J. A., Miao, X., Hanson, P. R., Johnson, W. C., Jacobs, P. M., & Goble, R. J. (2008). Loess record of the Pleistocene–

Holocene transition on the northern and central Great Plains, USA. *Quaternary Science Reviews*, *27*(17–18), 1772–1783.

Matthewman, R., Cotton, L. J., Martins, Z., & Sephton, M. A. (2012). Organic geochemistry of late Jurassic paleosols (dirt beds) of Dorset, UK. *Marine and Petroleum Geology*, *37*(1), 41–52.

Maynard, J. B. (1992). Chemistry of modern soils as a guide to interpreting Precambrian paleosols. *The Journal of Geology*, *100*(3), 279–289.

McCarthy, P. J., Martini, I. P., & Leckie, D. A. (1999). Pedogenic and diagenetic influences on void coating formation in Lower Cretaceous paleosols of the Mill Creek Formation, southwestern Alberta, Canada. *Geoderma*, *87*(3–4), 209–237.

McCarthy, P. J., & Plint, A. G. (2003). Spatial variability of palaeosols across Cretaceous interfluves in the Dunvegan Formation, NE British Columbia, Canada: Palaeohydrological, palaeogeomorphological and stratigraphic implications. *Sedimentology*, *50*(6), 1187–1220.

McElwain, J. C., Beerling, D. J., & Woodward, F. I. (1999). Fossil plants and global warming at the Triassic-Jurassic boundary. *Science*, *285*(5432), 1386–1390.

McInerney, F. A., & Wing, S. L. (2011). The Paleocene-Eocene thermal maximum: A perturbation of carbon cycle, climate, and biosphere with implications for the future. *Annual Review of Earth and Planetary Sciences*, *39*, 489–516.

Mills, B.J.W., Krause, A. J., Scotese, C. R., Hill, D. J., Shields, G. A., & Lenton, T. M. (2019). Modelling the long-term carbon cycle, atmospheric CO2, and Earth surface temperature from late Neoproterozoic to present day. *Gondwana Research*, *67*, 172–186.

Mindszenty, A. (2016). Bauxites: Feedbacks of system Earth at greenhouse times. *Geologia Croatica*, *69*(1), 79–87.

Mintz, J. S., Driese, S. G., & White, J. D. (2010). Environmental and ecological variability of Middle Devonian (Givetian) forests in Appalachian Basin paleosols, New York, United States. *Palaios*, *25*(2), 85–96.

Mitchell, R. L., & Sheldon, N. D. (2009). Weathering and paleosol formation in the 1.1 Ga Keweenawan Rift. *Precambrian Research*, *168*(3–4), 271–283.

Mitchell, R. L., & Sheldon, N. D. (2010). The 1100 Ma Sturgeon Falls paleosol revisited: Implications for Mesoproterozoic weathering environments and atmospheric CO2 levels. *Precambrian Research*, *183*(4), 738–748.

Molnar, P., & Cronin, T. W. (2015). Growth of the Maritime Continent and its possible contribution to recurring Ice Ages. *Paleoceanography*, *30*(3), 196–225.

Molnar, P., & England, P. (1990). Late Cenozoic uplift of mountain ranges and global climate change: Chicken or egg? *Nature*, *346*(6279), 29.

Montañez, I. P., & Isaacson, P. E. (2013). A sedimentary record of opportunities. *The Sedimentary Record*, *11*(1), 4.

Montañez, I. P., McElwain, J. C., Poulsen, C. J., White, J. D., DiMichele, W. A., Wilson, J. P., et al. (2016). Climate, pCO2 and terrestrial carbon cycle linkages during late Palaeozoic glacial–interglacial cycles. *Nature Geoscience*, *9*(11), 824.

Montañez, I. P., Tabor, N. J., Niemeier, D., DiMichele, W. A., Frank, T. D., Fielding, C. R., et al. (2007). CO2-forced climate and vegetation instability during Late Paleozoic deglaciation. *Science*, *315*(5808), 87–91.

Mora, C. I., & Driese, S. G. (1993). A steep, mid-to late Paleozoic decline in atmospheric CO2: Evidence from the soil carbonate CO2 paleobarometer. *Chemical Geology*, *107*(3–4), 217–219.

Mora, C. I., Driese, S. G., & Colarusso, L. A. (1996). Middle to late Paleozoic atmospheric CO2 levels from soil carbonate and organic matter. *Science*, *271*(5252), 1105–1107.

Mora, C. I., Driese, S. G., & Seager, P. G. (1991). Carbon dioxide in the Paleozoic atmosphere: Evidence from carbon-isotope compositions of pedogenic carbonate. *Geology*, *19*(10), 1017–1020.

Morris, J. L., Puttick, M. N., Clark, J. W., Edwards, D., Kenrick, P., Pressel, S., et al. (2018). The timescale of early land plant evolution. *U.S. National Academy of Sciences Proceedings*, *115*, e2274–2283.

Moussavi-Harami, R., Mahboubi, A., Nadjafi, M., Brenner, R. L., & Mortazavi, M. (2009). Mechanism of calcrete formation in the Lower Cretaceous (Neocomian) fluvial deposits, northeastern Iran based on petrographic, geochemical data. *Cretaceous Research*, *30*(5), 1146–1156.

Muhs, D. R., Bettis III, E. A., Aleinikoff, J. N., McGeehin, J. P., Beann, J., Skipp, G., et al. (2008). Origin and paleoclimatic significance of late Quaternary loess in Nebraska: Evidence from stratigraphy, chronology, sedimentology, and geochemistry. *Geological Society of America Bulletin*, *120*(11–12), 1378–1407.

Muhs, D. R., Bettis, E. A., Chan, M. A., & Archer, A. W. (2003). Quaternary loess-paleosol sequences as examples of climate-driven sedimentary extremes. *Special Papers-Geological Society of America*, 53–74.

Myers, T. S., Tabor, N. J., & Jacobs, L. L. (2011). Late Jurassic paleoclimate of central Africa. *Palaeogeography, Palaeoclimatology, Palaeoecology*, *311*(1–2), 111–125.

Myers, T. S., Tabor, N. J., & Rosenau, N. A. (2014). Multiproxy approach reveals evidence of highly variable paleoprecipitation in the Upper Jurassic Morrison Formation (western United States). *Bulletin*, *126*(7–8), 1105–1116.

Nascimento, D. L. do, Ladeira, F. S. B., & Batezelli, A. (2017). Pedodiagenetic characterization of cretaceous paleosols in southwest Minas Gerais, Brazil. *Revista Brasileira de Ciência Do Solo*, *41*.

National Research Council. (2001). *Basic research opportunities in Earth science*. National Academies Press.

National Research Council. (2003). Basic research opportunities in Earth sciences. Commission on Geosciences, Environment, and Resources. For web-accessible executive summary, see http://books.nap.edu/catalog/9981.html

National Science Foundation. (2000). *NSF geosciences beyond 2000: Understanding and predicting Earth's environment and habitability*. Washington, DC: Directorate for Geosciences, National Science Foundation. Retrieved from http://www.nsf.gov/geo/adgeo/geo2000.jsp

Nesbitt, H. W., & Young, G. M. (1982). Early Proterozoic climates and plate motions inferred from major element chemistry of lutites. *Nature*, *299*(5885), 715.

Nicolo, M. J., Dickens, G. R., Hollis, C. J., & Zachos, J. C. (2007). Multiple early Eocene hyperthermals: Their sedimentary expression on the New Zealand continental margin and in the deep sea. *Geology*, *35*(8), 699–702.

Nordt, L., Atchley, S., & Dworkin, S. I. (2002). Paleosol barometer indicates extreme fluctuations in atmospheric CO2 across the Cretaceous-Tertiary boundary. *Geology*, *30*(8), 703–706.

Nordt, L., Atchley, S., & Dworkin, S. (2003). Terrestrial evidence for two greenhouse events in the latest Cretaceous. *GSA Today*, *13*(12), 4–9.

Nordt, L., Atchley, S., & Dworkin, S. (2015). Collapse of the Late Triassic megamonsoon in western equatorial Pangea, present-day American Southwest. *Bulletin*, *127*(11–12), 1798–1815.

Nordt, L. C., & Driese, S. D. (2010a). New weathering index improves paleorainfall estimates from Vertisols. *Geology*, *38*(5), 407–410. https://doi.org/10.1130/G30689.1

Nordt, L. C., & Driese, S. G. (2010b). A modern soil characterization approach to reconstructing physical and chemical properties of Paleo-Vertisols. *American Journal of Science*, *310*(1), 37–64. https://doi.org/10.2475/01.2010.02

Nordt, L. C., & Driese, S. G. (2013). Application of the critical zone concept to the deep-time sedimentary record. *Sedimentary Record*, *11*(3), 4–9.

Nordt, L. C., Dworkin, S. I., & Atchley, S. C. (2011). Ecosystem response to soil biogeochemical behavior during the Late Cretaceous and early Paleocene within the western interior of North America. *Geological Society of America Bulletin*, *123*(9–10), 1745–1762. https://doi.org/10.1130/B30365.1

O'Dea, A., Lessios, H. A., Coates, A. G., Eytan, R. I., Restrepo-Moreno, S. A., Cione, A. L., et al. (2016). Formation of the Isthmus of Panama. *Science Advances*, *2*(8), e1600883.

Paik, I. S., Kim, H. J., & Huh, M. (2012). Dinosaur egg deposits in the Cretaceous Gyeongsang Supergroup, Korea: Diversity and paleobiological implications. *Journal of Asian Earth Sciences*, *56*, 135–146.

Paik, I. S., Kim, H. J., Park, K. H., Song, Y. S., Lee, Y. I., Hwang, J. Y., & Huh, M. (2001). Palaeoenvironments and taphonomic preservation of dinosaur bone-bearing deposits in the Lower Cretaceous Hasandong Formation, Korea. *Cretaceous Research*, *22*(5), 627–642.

Pan, Y., & Huang, C. (2014). Quantitative reconstruction of early cretaceous paleoclimate using paleosol carbonates in China. *Carbonates and Evaporites*, *29*(3), 327–335.

Paredes, J. M., Foix, N., Piñol, F. C., Nillni, A., Allard, J. O., & Marquillas, R. A. (2007). Volcanic and climatic controls on fluvial style in a high-energy system: The Lower Cretaceous Matasiete Formation, Golfo San Jorge basin, Argentina. *Sedimentary Geology*, *202*(1–2), 96–123.

Parrish, J. T. (2011). *Transitions Workshop Report* (p. 62). Washington, DC: Directorate for Geosciences, *National Science Foundation.*

Parrish, J. T. (1993). Climate of the supercontinent Pangea. *The Journal of Geology*, *101*(2), 215–233.

Parrish, J. T., Peterson, F., & Turner, C. E. (2004). Jurassic "savannah"—plant taphonomy and climate of the Morrison Formation (Upper Jurassic, Western USA). *Sedimentary Geology*, *167*(3–4), 137–162.

Parrish, J. T., & Soreghan, G. S. (2013). Sedimentary geology and the future of paleoclimate studies. *Sedimentary Record*, *11*, 4–10.

Percival, L. M., Cohen, A. S., Davies, M. K., Dickson, A. J., Hesselbo, S. P., Jenkyns, H. C., et al. (2016). Osmium isotope evidence for two pulses of increased continental weathering linked to Early Jurassic volcanism and climate change. *Geology*, *44*(9), 759–762.

Pereira, H. M., Leadley, P. W., Proença, V., Alkemade, R., Scharlemann, J. P., Fernandez-Manjarrés, J. F., et al. (2010). Scenarios for global biodiversity in the 21st century. *Science*, *330*(6010), 1496–1501.

Petersen, H. I., & Nielsen, L. H. (1995). Controls on peat accumulation and depositional environments of a coal-bearing coastal plain succession of a pull-apart basin: A petrographic, geochemical and sedimentological study, Lower Jurassic, Denmark. *International Journal of Coal Geology*, *27*(2–4), 99–129.

Pierrehumbert, R. T., Abbot, D. S., Voigt, A., & Koll, D. (2011). Climate of the Neoproterozoic. *Annual Review of Earth and Planetary Sciences*, *39*, 417–460.

Pinter, N., Scott, A. C., Daulton, T. L., Podoll, A., Koeberl, C., Anderson, R. S., & Ishman, S. E. (2011). The Younger Dryas impact hypothesis: A requiem. *Earth-Science Reviews*, *106*(3–4), 247–264.

Pole, M. (2001). Repeated flood events and fossil forests at Curio Bay (Middle Jurassic), New Zealand. *Sedimentary Geology*, *144*(3–4), 223–242.

Poulsen, C. J., Pollard, D., Montañez, I. P., & Rowley, D. (2007). Late Paleozoic tropical climate response to Gondwanan deglaciation. *Geology*, *35*(9), 771–774.

Prochnow, S. J., Nordt, L. C., Atchley, S. C., & Hudec, M. R. (2006). Multi-proxy paleosol evidence for middle and late Triassic climate trends in eastern Utah. *Palaeogeography, Palaeoclimatology, Palaeoecology*, *232*(1), 53–72.

Prothero, D. R. (1994). *The Eocene-Oligocene transition: Paradise lost*. Columbia University Press.

Quade, J., & Cerling, T. E. (1995). Expansion of C4 grasses in the late Miocene of northern Pakistan: Evidence from stable isotopes in paleosols. *Palaeogeography, Palaeoclimatology, Palaeoecology*, *115*(1–4), 91–116.

Quade, J., Forester, R. M., Pratt, W. L., & Carter, C. (1998). Black mats, spring-fed streams, and late-glacial-age recharge in the southern Great Basin. *Quaternary Research*, *49*(2), 129–148.

Quade, J., Rech, J. A., Betancourt, J. L., Latorre, C., Quade, B., Rylander, K. A., & Fisher, T. (2008). Paleowetlands and regional climate change in the central Atacama Desert, northern Chile. *Quaternary Research*, *69*(3), 343–360.

Quinney, A., Therrien, F., Zelenitsky, D. K., & Eberth, D. A. (2013). Palaeoenvironmental and palaeoclimatic reconstruction of the Upper Cretaceous (late Campanian–early Maastrichtian) Horseshoe Canyon Formation, Alberta, Canada. *Palaeogeography, Palaeoclimatology, Palaeoecology*, *371*, 26–44.

Raymo, M. E., & Ruddiman, W. F. (1992). Tectonic forcing of late Cenozoic climate. *Nature*, *359*(6391), 117.

Redecker, D., Kodner, R., & Graham, L. E. (2000). Glomalean fungi from the Ordovician. *Science*, *289*(5486), 1920–1921.

Rees, P. M., Noto, C. R., Parrish, J. M., & Parrish, J. T. (2004). Late Jurassic climates, vegetation, and dinosaur distributions. *The Journal of Geology*, *112*(6), 643–653.

Renssen, H., Mairesse, A., Goosse, H., Mathiot, P., Heiri, O., Roche, D. M., et al. (2015). Multiple causes of the Younger Dryas cold period. *Nature Geoscience*, *8*(12), 946.

Retallack, G. J. (1983). *Late Eocene and Oligocene paleosols from Badlands National Park, South Dakota* (Vol. 193). Geological Society of America.

Retallack, G. J. (1985). Fossil soils as grounds for interpreting the advent of large plants and animals on land. *Philosophical Transactions of the Royal Society of London. B, Biological Sciences*, *309*(1138), 105–142.

Retallack, G. J. (1986a). Reappraisal of a 2200 Ma-old paleosol near Waterval Onder, South Africa. *Precambrian Research*, *32*(2–3), 195–232.

Retallack, G. J. (1986b). The fossil record of soils. *Paleosols: Their Recognition and Interpretation*, 1–57.

Retallack, G. J. (1988). Field recognition of paleosols. *Geological Society of America Special Paper*, *216*, 1–20.

Retallack, G. J. (1992). How to find a Precambrian paleosol. In *Early Organic Evolution* (pp. 16–30). Springer.

Retallack, G. J. (1994). A pedotype approach to latest Cretaceous and earliest Tertiary paleosols in eastern Montana. *Geological Society of America Bulletin*, *106*(11), 1377–1397.

Retallack, G. J. (1997). Dinosaurs and dirt. In D. L. Wolberg, E. Stump, & G. D. Rosenberg (Eds.), *Dinofest International Proceedings* (pp. 345–359). Philadelphia: Academy of Natural Sciences.

Retallack, G. J. (2000). Ordovician life on land and early Paleozoic global change. *The Paleontological Society Papers*, *6*, 21–46.

Retallack, G. J. (2001a). Cenozoic expansion of grasslands and climatic cooling. *The Journal of Geology*, *109*(4), 407–426.

Retallack, G. J. (2001b). *Soils of the past: An introduction to paleopedology* (2nd ed.). Malden, MA, Oxford: Blackwell Science.

Retallack, G. J. (2007). Cenozoic paleoclimate on land in North America. *Journal of Geology*, *115*(3), 271–294. https://doi.org/10.1086/512753

Retallack, G. J. (2008). Cool-climate or warm-spike lateritic bauxites at high latitudes? *The Journal of Geology*, *116*(6), 558–570.

Retallack, G. J. (2009). Greenhouse crises of the past 300 million years. *Geological Society of America Bulletin*, *121*(9–10), 1441–1455. https://doi.org/10.1130/B26341.1

Retallack, G. J. (2010). Lateritization and bauxitization events. *Economic Geology*, *105*(3), 655–667.

Retallack, G. J. (2013a). Permian and Triassic greenhouse crises. *Gondwana Research*, *24*(1), 90–103. https://doi.org/10.1016/j.gr.2012.03.003

Retallack, G. J. (2013b). Global cooling by grasslands in the geological past and near future. *Annual Reviews of Earth and Planetary Science*, *41*, 69–86.

Retallack, G. J. (2013c). Ediacaran Gaskiers glaciation of Newfoundland reconsidered. *Journal of the Geological Society*, *170*(1), 19–36.

Retallack, G. J., & Alonso-Zarza, A. M. (1998). Middle Triassic paleosols and paleoclimate of Antarctica. *Journal of Sedimentary Research*, *68*(1), 169–184.

Retallack, G. J., Bajpai, S., Liu, X., Kapur, V. V., & Pandey. S. K. (2018). Advent of strong Indian monsoon by 20 million years ago. *Journal of Geology*, *126*, 1–24.

Retallack, G. J., Bestland, E. A., & Fremd, T. J. (1999). *Eocene and Oligocene paleosols of central Oregon*, *344*. Geological Society of America.

Retallack, G. J., & Feakes, C. R. (1987). Trace fossil evidence for Late Ordovician animals on land. *Science*, *235*(4784), 61–63.

Retallack, G. J., Gose, B. N., & Osterhout, J. T. (2015). Periglacial paleosols and Cryogenian paleoclimate near Adelaide, South Australia. *Precambrian Research*, *263*, 1–18.

Retallack G. J. & Huang, C.-M. (2011). Ecology and evolution of Devonian trees in New York, USA. *Palaeogeography Paleoclimatology Paleoecology*, *299*, 110–128.

Retallack, G. J., Leahy, G. D., & Spoon, M. D. (1987). Evidence from paleosols for ecosystem changes across the Cretaceous/Tertiary boundary in eastern Montana. *Geology*, *15*(12), 1090–1093.

Retallack, G. J., & Mindszenty, A. (1994). Well preserved late Precambrian paleosols from northwest Scotland. *Journal of Sedimentary Research*, *64*(2a), 264–281.

Retallack, G. J., Veevers, J. J., & Morante, R. (1996). Global coal gap between Permian–Triassic extinction and Middle Triassic recovery of peat-forming plants. *Geological Society of America Bulletin*, *108*(2), 195–207.

Richter, D. D., Bacon, A. R., Brecheisen, Z., & Mobley, M. L. (2015). Soil in the Anthropocene. In *IOP Conference Series: Earth and Environmental Science* (Vol. *25*, p. 012010). IOP Publishing.

Ridgwell, A. J., Kennedy, M. J., & Caldeira, K. (2003). Carbonate deposition, climate stability, and Neoproterozoic ice ages. *Science*, *302*(5646), 859–862.

Roca, X., & Nadon, G. C. (2007). Tectonic control on the sequence stratigraphy of nonmarine retroarc foreland basin fills: Insights from the Upper Jurassic of central Utah, *USA. Journal of Sedimentary Research*, *77*(3), 239–255.

Rohling, E. J., Fenton, M., Jorissen, F. J., Bertrand, P., Ganssen, G., & Caulet, J. P. (1998). Magnitudes of sea-level lowstands of the past 500,000 years. *Nature*, *394*(6689), 162.

Rohrmann, A., Kapp, P., Carrapa, B., Reiners, P. W., Guynn, J., Ding, L., & Heizler, M. (2012). Thermochronologic evidence for plateau formation in central Tibet by 45 Ma. *Geology*, *40*(2), 187–190.

Royer, D. L. (2006). CO2-forced climate thresholds during the Phanerozoic. *Geochimica et Cosmochimica Acta*, *70*(23), 5665–5675.

Royer, D. L. (2010). Fossil soils constrain ancient climate sensitivity. *Proceedings of the National Academy of Sciences*, *107*(2), 517–518.

Royer, D. L., Donnadieu, Y., Park, J., Kowalczyk, J., & Godderis, Y. (2014). Error analysis of CO2 and O2 estimates from the long-term geochemical model GEOCARBSULF. *American Journal of Science*, *314*(9), 1259–1283.

Ruddiman, W. F. (2003). The anthropogenic greenhouse era began thousands of years ago. *Climatic Change*, *61*(3), 261–293.

Ruddiman, W. F. (2013). The anthropocene. *Annual Review of Earth and Planetary Sciences*, *41*, 45–68.

Ruhe, R. V. (1965). Quaternary Paleopedology. In H. E. Wright & D. G. Frey (Eds.), *Quaternary of the United States* (pp. 755–764). Princeton, NJ: Princeton University Press.

Rye, R., & Holland, H. D. (1998). Paleosols and the evolution of atmospheric oxygen: A critical review. *American Journal of Science*, *298*(8), 621–672.

Rye, R., & Holland, H. D. (2000). Geology and geochemistry of paleosols developed on the Hekpoort Basalt, Pretoria Group, South Africa. *American Journal of Science*, *300*(2), 85–141.

Salamon, M.A., Gerrienne, P., Steemans, P., Gorzelak, P., Filipiak, P., Le Hérissé, A., et al. (2018). Putative Late Ordovician land plants. *New Phytologist*, *218*, 1305–1309.

Schaller, M. F., Wright, J. D., & Kent, D. V. (2011). Atmospheric pCO2 perturbations associated with the Central Atlantic magmatic province. *Science*, *331*(6023), 1404–1409.

Schaller, M. F., Wright, J. D., & Kent, D. V. (2015). A 30 Myr record of Late Triassic atmospheric p CO2 variation reflects a fundamental control of the carbon cycle by changes in continental weathering. *Bulletin*, *127*(5–6), 661–671.

Schulte, P., Alegret, L., Arenillas, I., Arz, J. A., Barton, P. J., Bown, P. R., et al. (2010). The Chicxulub asteroid impact and mass extinction at the Cretaceous-Paleogene boundary. *Science*, *327*(5970), 1214–1218.

Scotese, C. R. (2001). *Paleomap project*. Paleomap Project.

Sedlacek, A. R., Saltzman, M. R., Algeo, T. J., Horacek, M., Brandner, R., Foland, K., & Denniston, R. F. (2014). $^{87}Sr/^{86}Sr$ stratigraphy from the Early Triassic of Zal, Iran: Linking temperature to weathering rates and the tempo of ecosystem recovery. *Geology*, *42*(9), 779–782.

Sepulchre, P., Ramstein, G., Fluteau, F., Schuster, M., Tiercelin, J.-J., & Brunet, M. (2006). Tectonic uplift and Eastern Africa aridification. *Science*, *313*(5792), 1419–1423.

Shear, W. A., & Selden, P. A. (2001). Rustling in the undergrowth: Animals in early terrestrial ecosystems. In P. G. Gensel & D. Edwards (Eds.), *Plants invade the land: Evolutionary and environmental perspectives* (pp. 29–51). New York: Columbia University Press.

Sheldon, N. D. (2006). Precambrian paleosols and atmospheric CO2 levels. *Precambrian Research*, *147*(1–2), 148–155. https://doi.org/10.1016/j.precamres.2006.02.004

Sheldon, N. D. (2013). Causes and consequences of low atmospheric pCO2 in the Late Mesoproterozoic. *Chemical Geology*, *362*, 224–231.

Sheldon, N. D., & Retallack, G. J. (2004). Regional paleoprecipitation records from the late Eocene and Oligocene of North America. *The Journal of Geology*, *112*(4), 487–494.

Sheldon, N. D., Retallack, G. J., & Tanaka, S. (2002). Geochemical climofunctions from North American soils and application to paleosols across the Eocene-Oligocene boundary in Oregon. *The Journal of Geology*, *110*(6), 687–696.

Sheldon, N. D., & Tabor, N. J. (2009). Quantitative paleoenvironmental and paleoclimatic reconstruction using paleosols. *Earth-Science Reviews*, *95*(1–2), 1–52. https://doi.org/10.1016/j.earscirev.2009.03.004

Sigleo, W., & Reinhardt, J. (1988). Paleosols from some Cretaceous environments in the southeastern United States. In J. Reinhardt & W. Sigleo (Eds.), *Paleosols and weathering through geologic time: Principles and applications*. Geological Society of America Special Paper, 216, 123–142.

Singer, A., Wieder, M., & Gvirtzman, G. (1994). Paleoclimate deduced from some early Jurassic basalt-derived paleosols from northern Israel. *Palaeogeography, Palaeoclimatology, Palaeoecology*, *111*(1–2), 73–82.

Skelton, P. W., Spicer, R. A., Kelley, S. P., & Gilmour, I. (2003). *The Cretaceous world*. Cambridge, UK: Cambridge University Press.

Slotnick, B. S., Dickens, G. R., Nicolo, M. J., Hollis, C. J., Crampton, J. S., Zachos, J. C., & Sluijs, A. (2012). Large-amplitude variations in carbon cycling and terrestrial weathering during the latest Paleocene and earliest Eocene: The record at Mead Stream, New Zealand. *The Journal of Geology*, *120*(5), 487–505.

Smith, B. D., & Zeder, M. A. (2013). The onset of the Anthropocene. *Anthropocene*, *4*, 8–13.

Smith, R. M. (1995). Changing fluvial environments across the Permian-Triassic boundary in the Karoo Basin, South Africa and possible causes of tetrapod extinctions. *Palaeogeography, Palaeoclimatology, Palaeoecology*, *117*(1–2), 81–104.

Smith, R., & Kitching, J. (1997). Sedimentology and vertebrate taphonomy of the Tritylodon acme zone: A reworked palaeosol in the Lower Jurassic Elliot Formation, Karoo Supergroup, South Africa. *Palaeogeography, Palaeoclimatology, Palaeoecology*, *131*(1–2), 29–50.

Smith, R. M., Marsicano, C. A., & Wilson, J. A. (2009). Sedimentology and paleoecology of a diverse Early Jurassic tetrapod tracksite in Lesotho, southern Africa. *Palaios*, *24*(10), 672–684.

Snigirevskaya, N. S. (1988). The Late Devonian: The time of the appearance of forests as a natural phenomenon. *Contributed Papers: The Formation and Evolution of the Continental Biotas, L.: 31st Session of the All-Union Palaeontological Society*, 115–124.

Soil Survey Staff. (1999). *Keys to soil taxonomy*. Washington, DC: U.S. Department of Agriculture, Natural Resources Conservation Service.

Solomon, S., Qin, D., Manning, M., Averyt, K., & Marquis, M. (2007). *Climate change 2007: The physical science basis. Working Group I contribution to the fourth assessment report of the IPCC* (Vol. *4*). Cambridge University Press.

Steemans, P., Le Hérissé, A., Melvin, J., Miller, M.A., Paris, F., Verniers, J., & Wellman, C.H. (2009). Origin and radiation of the earliest vascular land plants. *Science*, *324*, 353–353.

Stewart, W. N., & Rothwell, G. W. (1993). *Paleobotany and the evolution of plants*. Cambridge University Press.

Stinchcomb, G. E. (2018). Quantifying past hominin interactions with Earth's surface using the mass flux of artifacts. *Zeitschrift Für Geomorphologie*, *62*(1), 57–71.

Stinchcomb, G. E., Messner, T. C., Stewart, R. M., & Driese, S. G. (2014). Estimating fluxes in anthropogenic lead using alluvial soil mass-balance geochemistry, geochronology and archaeology in eastern USA. *Anthropocene*, *8*, 25–38.

Stinchcomb, G. E., Nordt, L. C., Driese, S. G., Lukens, W. E., Williamson, F. C., & Tubbs, J. D. (2016). A data-driven spline model designed to predict paleoclimate using paleosol geochemistry. *American Journal of Science*, *316*(8), 746–777.

Stinchcomb, G. E., Stewart, R. M., Messner, T. C., Nordt, L. C., Driese, S. G., & Allen, P. M. (2013). Using event stratigraphy to map the Anthropocene: An example from the historic coal mining region in eastern Pennsylvania, USA.

Geomorphology of the Anthropocene: Understanding the Surficial Legacy of Past and Present Human Activities, *2*, 42–50. https://doi.org/10.1016/j.ancene.2013.06.001

Stinchcomb, G., Stinchcomb, G. E., Messner, T. C., Driese, S. G., & Nordt, L. C. (2011). Pre-colonial (A.D. 1100–1600) sedimentation related to prehistoric maize agriculture and climate change in eastern North America. *Geology (Boulder)*, *39*(4), 363.

Stoops, G. (2003). *Guidelines for analysis and description of soil and regolith thin sections*. Wisconsin, USA: Soil Science Society of America, Inc.

Strömberg, C. A. (2004). Using phytolith assemblages to reconstruct the origin and spread of grass-dominated habitats in the great plains of North America during the late Eocene to early Miocene. *Palaeogeography, Palaeoclimatology, Palaeoecology*, *207*(3–4), 239–275.

Suarez, M. B., Gonzalez, L. A., & Ludvigson, G. A. (2010). Estimating the oxygen isotopic composition of equatorial precipitation during the mid-Cretaceous. *Journal of Sedimentary Research*, *80*(5), 480–491.

Suchecki, R. K., Hubert, J. F., & Birney de Wet, C. C. (1988). Isotopic imprint of climate and hydrogeochemistry on terrestrial strata of the Triassic-Jurassic Hartford and Fundy rift basins. *Journal of Sedimentary Research*, *58*(5), 801–811.

Sues, H.-D., & Fraser, N. C. (2006). *Triassic life on land: The great transition*. Columbia University Press.

Sun, H., Xiao, Y., Gao, Y., Zhang, G., Casey, J. F., & Shen, Y. (2018). Rapid enhancement of chemical weathering recorded by extremely light seawater lithium isotopes at the Permian–Triassic boundary. *Proceedings of the National Academy of Sciences*, *115*(15), 3782–3787.

Tabor, N. J., Sidor, C. A., Smith, R. M., Nesbitt, S. J., & Angielczyk, K. D. (2017). Paleosols of the Permian-Triassic: Proxies for rainfall, climate change and major changes in terrestrial tetrapod diversity. *Journal of Vertebrate Paleontology*, *37*(sup1), 240–253.

Tabor, N. J., & Yapp, C. J. (2005). Coexisting goethite and gibbsite from a high-paleolatitude (55 N) Late Paleocene laterite: Concentration and 13 C/12 C ratios of occluded CO 2 and associated organic matter. *Geochimica et Cosmochimica Acta*, *69*(23), 5495–5510.

Tabor, N. J., Yapp, C. J., & Montañez, I. P. (2004). Goethite, calcite, and organic matter from Permian and Triassic soils: Carbon isotopes and CO2 concentrations. *Geochimica et Cosmochimica Acta*, *68*(7), 1503–1517.

Tanner, L. H. (2000). Palustrine-lacustrine and alluvial facies of the (Norian) Owl Rock Formation (Chinle Group), Four Corners region, southwestern USA: Implications for Late Triassic paleoclimate. *Journal of Sedimentary Research*, *70*(6), 1280–1289.

Tanner, L. H., Galli, K. G., & Lucas, S. G. (2014). Pedogenic and lacustrine features of the Brushy Basin Member of the Upper Jurassic Morrison Formation in western Colorado: Reassessing the paleoclimatic interpretations. *Volumina Jurassica*, *12*(2), 115–130.

Tanner, L. H., & Lucas, S. G. (2012). Carbonate facies of the Upper Triassic Ojo Huelos Member, San Pedro Arroyo Formation (Chinle Group), southern New Mexico: Paleoclimatic implications. *Sedimentary Geology*, *273*, 73–90.

Taylor, K. C., Lamorey, G. W., Doyle, G. A., Alley, R. B., Grootes, P. M., Mayewski, P. A., et al. (1993). The "flickering switch" of late Pleistocene climate change. *Nature*, *361*(6411), 432.

Terry Jr, D. O. (2001). Paleopedology of the Chadron Formation of Northwestern Nebraska: Implications for paleoclimatic change in the North American midcontinent across the Eocene–Oligocene boundary. *Palaeogeography, Palaeoclimatology, Palaeoecology*, *168*(1–2), 1–38.

Them, T. R., Gill, B. C., Selby, D., Gröcke, D. R., Friedman, R. M., & Owens, J. D. (2017). Evidence for rapid weathering response to climatic warming during the Toarcian Oceanic Anoxic Event. *Scientific Reports*, *7*(1), 5003.

Therrien, F. (2005). Palaeoenvironments of the latest Cretaceous (Maastrichtian) dinosaurs of Romania: Insights from fluvial deposits and paleosols of the Transylvanian and Haţeg basins. *Palaeogeography, Palaeoclimatology, Palaeoecology*, *218*(1–2), 15–56.

Therrien, F., & Fastovsky, D. E. (2000). Paleoenvironments of early theropods, Chinle Formation (Late Triassic), Petrified Forest National Park, Arizona. *Palaios*, *15*(3), 194–211.

Therrien, F., Zelenitsky, D. K., & Weishampel, D. B. (2009). Palaeoenvironmental reconstruction of the Late Cretaceous Sânpetru Formation (Haţeg Basin, Romania) using paleosols and implications for the "disappearance" of dinosaurs. *Palaeogeography, Palaeoclimatology, Palaeoecology*, *272*(1–2), 37–52.

Trendell, A. M., Atchley, S. C., & Nordt, L. C. (2013a). Facies analysis of a probable large-fluvial-fan depositional system: The Upper Triassic Chinle Formation at Petrified Forest National Park, Arizona, USA. *Journal of Sedimentary Research*, *83*(10), 873–895.

Trendell, A. M., Nordt, L. C., Atchley, S. C., Leblanc, S. L., & Dworkin, S. I. (2013b). Determining floodplain plant distributions and populations using paleopedology and fossil root traces: Upper Triassic Sonsela Member of the Chinle Formation at Petrified Forest National Park, Arizona Upper Triassic Chinle Rhizoliths and Paleosols. *Palaios*, *28*(7), 471–490.

Ufnar, D. F., González, L. A., Ludvigson, G. A., Brenner, R. L., & Witzke, B. J. (2001). Stratigraphic implications of meteoric sphaerosiderite δ18O values in paleosols of the Cretaceous (Albian) Boulder Creek Formation, NE British Columbia foothills, Canada. *Journal of Sedimentary Research*, *71*(6), 1017–1028.

Ufnar, D. F., González, L. A., Ludvigson, G. A., Brenner, R. L., Witzke, B. J., & Leckie, D. (2005). Reconstructing a mid-Cretaceous landscape from paleosols in western Canada. *Journal of Sedimentary Research*, *75*(6), 984–996.

Vacca, A., Ferrara, C., Matteucci, R., & Murru, M. (2012). Ferruginous paleosols around the Cretaceous-Paleocene boundary in central-southern Sardinia (Italy) and their potential as pedostratigraphic markers. *Quaternary International*, *265*, 179–190.

Van der Made, J., Morales, J., & Montoya, P. (2006). Late Miocene turnover in the Spanish mammal record in relation to palaeoclimate and the Messinian Salinity Crisis. *Palaeogeography, Palaeoclimatology, Palaeoecology*, *238*(1–4), 228–246.

Veevers, J. J., Conaghan, P. J., & Shaw, S. E. (1994). Turning point in Pangean environmental history at the Permian/Triassic (P/Tr) boundary. *Pangea: Paleoclimate, tectonics, and sedimentation during accretion, zenith, and breakup of a supercontinent. Geological Society of America Special Paper*, *288*, 187–196.

Veizer, J., Ala, D., Azmy, K., Bruckschen, P., Buhl, D., Bruhn, F., et al. (1999). $^{87}Sr/^{86}Sr$, $\delta^{13}C$ and $\delta^{18}O$ evolution of Phanerozoic seawater. *Chemical Geology*, *161*, 59–88.

Veizer, J., & Prokoph, A. (2015). Temperatures and oxygen isotopic composition of Phanerozoic oceans. *Earth Science Reviews*, *146*, 92–104.

Vincent, S. J., & Allen, M. B. (1999). Evolution of the Minle and Chaoshui Basins, China: Implications for Mesozoic strike-slip basin formation in Central Asia. *Geological Society of America Bulletin*, *111*(5), 725–742.

Vitali, F., Longstaffe, F. J., McCarthy, P. J., Plint, A. G., & Caldwell, W. G. E. (2002). Stable isotopic investigation of clay minerals and pedogenesis in an interfluve paleosol from the Cenomanian Dunvegan Formation, NE British Columbia, Canada. *Chemical Geology*, *192*(3–4), 269–287.

von Paris, P., Rauer, H., Grenfell, J. L., Patzer, B., Hedelt, P., Stracke, B., et al. (2008). Warming the early Earth—CO2 reconsidered. *Planetary and Space Science*, *56*(9), 1244–1259.

Walker, J. D., Geissman, J. W., Bowring, S. A., & Babcock, L. E. (Compilers) (2018). *Geologic time scale v. 5.0*. Geological Society of America. https://doi.org/10.1130/2018.CTS005R3C

Wang, C., Zhao, X., Liu, Z., Lippert, P. C., Graham, S. A., Coe, R. S., et al. (2008). Constraints on the early uplift history of the Tibetan Plateau. *Proceedings of the National Academy of Sciences*, *105*(13), 4987–4992.

Weaver, C. E. (1989). *Clays, muds, and shales* (Vol. 44). Elsevier.

West, A. J., Bickle, M. J., Collins, R., & Brasington, J. (2002). Small-catchment perspective on Himalayan weathering fluxes. *Geology*, *30*(4), 355–358.

White, P. D., & Schiebout, J. (2008). Paleogene paleosols and changes in pedogenesis during the initial Eocene thermal maximum: Big Bend National Park, Texas, USA. *Geological Society of America Bulletin*, *120*(11–12), 1347–1361.

White, T., González, L., Ludvigson, G., & Poulsen, C. (2001). Middle Cretaceous greenhouse hydrologic cycle of North America. *Geology*, *29*(4), 363–366.

Wiemer, D., Schrank, C. E., Murphy, D. T., Wenham, L., & Allen, C. M. (2018). Earth's oldest stable crust in the Pilbara Craton formed by cyclic gravitational overturns. *Nature Geoscience*, *11*(5), 357.

Wiest, L. A., Lukens, W. E., Peppe, D. J., Driese, S. G., & Tubbs, J. (2018). Terrestrial evidence for the Lilliput effect across the Cretaceous-Paleogene (K-Pg) boundary. *Palaeogeography, Palaeoclimatology, Palaeoecology*, *491*, 161–169.

Wilkinson, B. H. (2005). Humans as geologic agents: A deep-time perspective. *Geology*, *33*(3), 161–164.

Willenbring, J. K., & von Blanckenburg, F. (2010). Long-term stability of global erosion rates and weathering during late-Cenozoic cooling. *Nature*, *465*(7295), 211.

Wilson, K. M., Pollard, D., Hay, W. W., Thompson, S. L., & Wold, C. N. (1994). General circulation model simulations of Triassic climates: Preliminary results. In G. D. Klein (Ed.), *Pangea: Paleoclimate, tectonics, and sedimentation during accretion, zenith, and breakup of a supercontinent* (pp. 91–116). Boulder, CO: The Geological Society of America.

Wright, V. P., Taylor, K. G., & Beck, V. H. (2000). The paleohydrology of Lower Cretaceous seasonal wetlands, Isle of Wight, southern England. *Journal of Sedimentary Research*, *70*(3), 619–632.

Wynn, J. G. (2000). Paleosols, stable carbon isotopes, and paleoenvironmental interpretation of Kanapoi, Northern Kenya. *Journal of Human Evolution*, *39*(4), 411–432.

Wynn, J. G. (2004). Influence of Plio-Pleistocene aridification on human evolution: Evidence from paleosols of the Turkana Basin, Kenya. *American Journal of Physical Anthropology*, *123*(2), 106–118.

You, Y., Huber, M., Müller, R. D., Poulsen, C. J., & Ribbe, J. (2009). Simulation of the middle Miocene climate optimum. *Geophysical Research Letters*, *36*(4).

Zachos, J. C., Dickens, G. R., & Zeebe, R. E. (2008). An early Cenozoic perspective on greenhouse warming and carbon-cycle dynamics. *Nature*, *451*(7176), 279–283.

Zachos, J. C., Pagani, M., Sloan, L., Thomas, E., & Billups, K. (2001). Trends, rhythms, and aberrations in global climate 65 Ma to present. *Science*, *292*(5517), 686–693.

Zahnle, K. J. (2006). Earth's earliest atmosphere. *Elements*, *2*(4), 217–222.

Zalasiewicz, J., Waters, C. N., Williams, M., Barnosky, A. D., Cearreta, A., Crutzen, P., et al. (2015). When did the Anthropocene begin? A mid-twentieth century boundary level is stratigraphically optimal. *Quaternary International*, *383*, 196–203.

Zalasiewicz, J., Williams, M., Smith, A., Barry, T. L., Coe, A. L., Bown, P. R., et al. (2008). Are we now living in the Anthropocene? *GSA Today*, *18*(2), 4.

Zanazzi, A., Kohn, M. J., MacFadden, B. J., & Terry, D. O. (2007). Large temperature drop across the Eocene–Oligocene transition in central North America. *Nature*, *445*(7128), 639.

Zárate, M. A. (2003). Loess of southern South America. *Quaternary Science Reviews*, *22*(18–19), 1987–2006.

Zeebe, R. E., Ridgwell, A., & Zachos, J. C. (2016). Anthropogenic carbon release rate unprecedented during the past 66 million years. *Nature Geosci*, *9*(4), 325–329.

Zhang, L., Wang, C., Cao, K., Wang, Q., Tan, J., & Gao, Y. (2016). High elevation of Jiaolai Basin during the Late Cretaceous: Implication for the coastal mountains along the East Asian margin. *Earth and Planetary Science Letters*, *456*, 112–123.

Zhang, Z., Ramstein, G., Schuster, M., Li, C., Contoux, C., & Yan, Q. (2014). Aridification of the Sahara desert caused by Tethys Sea shrinkage during the Late Miocene. *Nature*, *513*(7518), 401.

Zhisheng, A., Kutzbach, J. E., Prell, W. L., & Porter, S. C. (2001). Evolution of Asian monsoons and phased uplift of the Himalaya–Tibetan plateau since Late Miocene times. *Nature*, *411*(6833), 62.

Zhou, Y., Retallack, G. J., & Huang, C. (2015). Early Eocene paleosol developed from basalt in southeastern Australia: implications for paleoclimate. *Arabian Journal of Geosciences*, *8*(3), 1281–1290.

Part III
Soil Formation Processes

3

Soil Formation, Vegetation Growth, and Water Balance: A Theory for Budyko

Allen Hunt

ABSTRACT

Percolation theory can be used to generate expressions for solute transport distances and velocities as a function of time. Previous studies have shown that the solute velocity can be used to predict soil production rates. Steady-state conditions allow prediction of a soil depth nearly proportional to the ratio of the infiltration rate, I, and the erosion rate. Other results from percolation theory have been used to find the dependence of the net primary productivity, NPP, on transpiration, T. In Budyko theory, the two relevant fluxes, evapotranspiration, ET, and runoff, Q, are different from I and T, but it is nevertheless reasonable to approximate I as Q and T as ET. Here it is argued that NPP is also proportional to the soil depth. Since the water fluxes (Q) that produce soil and correspond to transpiration (ET) are complementary to each other, i.e. add up to the precipitation, P, the new result allows an optimization of NPP with respect to ET. The predicted result, using the percolation prediction for root fractal dimensionality, is $ET = 0.623P$, which compares very well with the global average, variously given as between $0.63P$ and $0.65P$. Using 55 published values of the root fractal dimensionality of forbs and grasses grown under ideal conditions of moisture and energy (i.e. aridity index $ET_0/P = 1$, where ET_0 is the potential evapotranspiration) maps out the spread of observed values of ET/P at aridity index 1.

3.1. INTRODUCTION

3.1.1. Water Partitioning at the Terrestrial Earth Surface

When water falls as rain on the continents, some may evaporate directly back to the atmosphere, some may be used by plants, some runs off along the surface, and some infiltrates deeply into the subsurface, only to re-emerge in, for example, streams, and flow to the ocean (e.g. Manabe, 1969). The sum of the surface and subsurface components of the runoff is typically denoted by Q. Finally, some of what goes into the ground increases subsurface water storage, including reservoirs that have been drawn down, often to satisfy human requirements. Although any changes in underground water storage will be ignored in the following, each of these water pathways has consequences for a wide range of scientific disciplines, such as ecology, hydrology, climate studies, geomorphology, and soil science, as well as for society, such as water power from rivers, flooding, future water reserves, agriculture, and soil loss.

How to predict the partitioning of water (water balance) that lands on the terrestrial Earth surface is a question of central importance (Budyko, 1958; Milly, 1994; Williams et al., 2012). Plant productivity clearly depends on how much water the plants use (Lieth, 1972; Rosenzweig, 1968), and it has recently also become clear that the formation of the soil requires the passage of water through the solid Earth surface (whether bedrock or unconsolidated materials) and on into stream flow (Maher, 2010). Indeed, both observation (Maher, 2010) and theory

Department of Physics and Department of Earth & Environmental Sciences, Wright State University, Dayton, Ohio, USA

Hydrogeology, Chemical Weathering, and Soil Formation, Geophysical Monograph 257, First Edition.
Edited by Allen Hunt, Markus Egli, and Boris Faybishenko.

DOI: 10.1002/9781119563952.ch3

(Hunt & Ghanbarian 2016) indicate that the rate of chemical weathering as well as of soil formation should be proportional to the fluid flow rate. Predicting what fraction of precipitation, P, goes into soil formation and how much into vegetation growth (i.e. the water balance), however, has presented difficulties. Because the first useful description of this process is due to Budyko (1958, 1974), it is also often referred to as the Budyko problem and its solution as Budyko theory. In his work, Budyko clearly identified the limiting behavior of the evapotranspiration, ET, in both hydrologic limits: (1) water-limited ecosystems and (2) energy-limited ecosystems.

Water balance models have appealed to the water usage strategies of plants and the physical properties of soils (Porporato et al., 2004; Rodriguez-Iturbe et al., 1999), a system driven by the vagaries of climate and the details of the precipitation. Shortages of either precipitation or solar energy will hinder the use of water by plants, for example. Some of these models are quite simplified and yield general curves of ET as a function of potential evapotranspiration, ET_0, which measures how much water could be evaporated by the incoming radiation. Porporato et al. (2004) predicted a dependence of ET on soil depth which is linear, or close to it. Some models are more complex, requiring substantial characterization of any particular ecosystem. Other methods to generate the water partitioning include optimization principles from energy and entropy (Milne & Gupta, 2017; D. Wang et al., 2014), the balance of carbon cost and water benefit (Guswa, 2008, 2010), or optimal vegetation growth from maximum water content (Eagleson, 1978a, 1978b).

Budyko generated an ad hoc function that describes the fraction of water returned to the atmosphere by ET, which has proved reasonably reliable and, indeed, the more accurate the longer the period of observation considered (Gentine et al., 2012). Finally, Sposito (2017) has emphasized the interrelatedness of combinations of variables of water and radiation within a framework of homogeneous functions, a set of guidelines from statistical and thermal physics. The above discussion constitutes a brief overview of existing general strategies for estimating water partitioning at the terrestrial surface.

The present Budyko treatment falls into the category of optimization strategies. It exploits new results on soil formation rates (Egli et al., 2018; Hunt & Ghanbarian, 2016; Yu & Hunt, 2017a, 2017b), as well as of plant growth rates and net primary productivity, NPP (Hunt, 2017). Use of predictive relationships for soil formation and NPP allows optimization of productivity with respect to the actual water partitioning, as long as energy is not the limiting factor. Combined with existing arguments regarding the behavior of ET in the energy-limited regime, we generate a reasonable upper bound on ET throughout the spectrum of environments. The relevance of this upper bound becomes clearer when compared with datasets compiled over longer periods of time. That many points nevertheless fall below the predicted curve, but very few above, is at least consistent with the assertion that we generate an optimal ET. Failure to reach the upper bound suggests that the theoretical optimization has not been achieved in a basin with its particular plant community and existing soil characteristics.

3.1.2. Water and Energy Conservation Foundation: The Budyko Approach

In its fundamental partitioning, Budyko theory (Budyko, 1958, 1974; Sposito, 2017; D. Wang et al., 2014) does not distinguish between the various evaporation pathways, nor even between evaporation and transpiration, which become linked into evapotranspiration, ET. Further, the water flow, called runoff, can travel either on the surface or through the soil and bedrock. This latter consideration is somewhat problematic for the present treatment, based on steady-state soil formation rates (Yu & Hunt, 2017a), since only the subsurface component of Q contributes to soil formation, while both contribute to soil erosion. We remind also that changes in storage are considered to be negligible over longer periods of time (Budyko, 1958, 1974). With these definitions and approximations, water conservation requires that

$$P = ET + Q. \tag{1}$$

Radiation, R, impinging on the Earth's surface can contribute either to sensible heat flux, H, or to latent heat flux through ET. Regardless of whether water changes phase through direct evaporation or through transpiration, the water flux, ET, must be multiplied by the latent heat, L, of water to generate an energy flux, and energy conservation then requires that

$$R = L\,ET + H. \tag{2}$$

Division through both sides of this equation by L leads to

$$ET_0 \equiv \frac{R}{L} = ET + \frac{H}{L}. \tag{3}$$

ET_0 is how much water vapor would be released if all incoming radiant energy were converted to latent heat, and it is thus termed potential evapotranspiration. When $ET = ET_0$, $H = 0$, and such systems are designated "energy limited." When $Q = 0$, however, increases in ET with increasing radiation cannot occur, since there is no additional water to evaporate, and these systems are termed "water limited." The analogous forms of

equation (1) and equation (3) inspired Budyko's original formulation (1958) as well as the thermodynamic basis proposed by Sposito (2017).

3.1.3. Fundamental Relationships Between *ET* and ET_0: Climate Influences

In climate zones where there is ample water but little solar radiation, transpiration of plants may be limited by very low evaporation rates, a situation called energy limited. In the opposite extreme, where there is a great deal of solar radiation but limited precipitation, as is common in arid regions, ecosystems are called water limited. In the water-limited case, *ET* cannot exceed *P,* but in the energy-limited case, *ET* cannot exceed ET_0. In the energy-limited case, if plants are utilizing energy optimally for growth and productivity is a monotonically increasing function of transpiration, then *ET* will equal ET_0 and $H = 0$. In the water-limited case, at sufficiently high ET_0, *ET* will equal *P* and there will be no water left for surface or subsurface flow, making $Q = 0$. Specific advances beyond this point are, as yet, uncertain, even though many approaches have been tried. This is partly a result of the wide range of experimental results reported, including the conditions of their measurement, but indicates as well an uncertainty in the best way to approach a problem of such high complexity and potential variability. The latter uncertainty is exacerbated by our limited knowledge of which secondary variables control the variability in data. Significantly, Budyko's original guess as to the functional form of *ET* (ET_0/P) appears to work as well as later modifications made to increase flexibility (Gentine et al., 2012).

3.2. HYPOTHESIS

Our working hypothesis: *NPP* has a complex and potentially optimizable dependence on *ET* and *Q*. Ecosystems that exploit this relationship to maximize productivity will have an adaptive advantage.

NPP depends sensitively on *ET* (Rosenzweig, 1968). But *ET* depends on soil depth (Porporato et al., 2004), while soil depth depends on *Q* (Maher, 2010). Recent research has shown it is possible to express soil formation rates (Egli et al., 2018; Yu & Hunt, 2017a, 2017b) and vegetation growth rates (Hunt, 2017) as proportional to the fundamental fluxes of deep infiltration (the major part of *Q*) and transpiration (the major part of *ET*), respectively. Both faster growth rates and deeper soils will contribute to greater primary productivity of the plants. Thus, how the water is partitioned at the Earth's surface controls the rates of plant growth and soil formation. The more water that plants take from the earth, the faster they can grow, but the slower soil will form. Such a competition for water can be optimized.

Should our hypothesis be satisfied, we will have demonstrated that the soil/vegetation system is not merely a passive responder to climate, topography, and parent materials; rather, it exploits its advantages in controlling water fluxes to optimize productivity. This result would provide a theoretical basis for the view expressed in the report (National Research Council, 1991) on hydrologic sciences (HS) that triggered the establishment of the HS program at NSF: "The more we learn about our desiccated, and apparently barren, neighboring planets, the more we wonder if our good fortune is not a result as well as the cause of life on the earth," which echoes early statements from Eagleson (1978a, 1978b) and from Eagleson and Tellers (1982).

Thus, we assert that a knowledge of the fundamental spatiotemporal scaling behavior of plant growth and soil formation allows a first estimate of the partitioning of the water in the hydrologic cycle, making Budyko theory an output of the models for vegetation and soils rather than merely an input factor. This coupling adds an important facet of relevance to the discussion of the principle hydrologic fluxes in the context of a volume on hydrogeology, chemical weathering, and soil formation. As pointed out by Dietrich and Perron (2006) (and reiterated by Gentine et al., 2012), soil, topography, vegetation, and climate are intimately interconnected. The relevance of water balance at the Earth's surface can be used to couple these processes theoretically.

3.3. THEORETICAL APPROACH AND STEADY-STATE RESTRICTIONS

Application of Budyko theory is usually restricted to steady-state conditions, such that year-to-year (and interannual) variations in water storage can be ignored. The restriction on time scales of observation introduced by this constraint has been assumed to be 50 years (Gentine et al., 2012), though an argument based on climate variability might also be made, in which case a better choice could be the corresponding definition of climate as an average over weather, i.e. ca. 30 years. Variations in average weather (thus climate) over longer periods would then be considered climate change and could trigger steady-state changes in vegetation. Either way, decades of data should be used. A yet longer time scale may be introduced by adaptation of vegetation to climate change. In some cases, it may take centuries, or even millennia, before local vegetation can adapt to new climates, such as required by the expanding deserts at the beginning of the Holocene (Hunt & Wu, 2004). Limitations in plant adaptation are placed by the efficacy of seed dispersal mechanisms. More pertinently, similar complications may arise from human impacts on climate in the Anthropocene today. Rates of poleward migration of climate zones today may exceed the ability of ecosystems to follow. To the extent that soil

depth influences vegetation productivity, it also becomes necessary to consider the impact that changing climate or vegetation properties exerts on soil depth. Times to reach steady-state soil depth vary but can reach a million years, depending on what erosion rates are, as the time required to reach steady-state is inversely proportional to the erosion rate (Yu & Hunt, 2017a). In regions of active tectonics, where erosion rates reach mm/yr, this equilibration time may be 100 years or less, but in continental interiors with three orders of magnitude slower erosion rates, such times can easily exceed 100,000 years. Under such extreme conditions, steady-state assumptions may not be relevant to calculations.

Porporato et al. (2004) cite Knapp et al. (2002) and summarize: "There is growing evidence that the predicted changes in rainfall regime due to climate change will reduce ecosystem net primary productivity and possibly induce shifts in community composition." Finding a reliable optimization of NPP that describes an upper bound of ET, and thus NPP, across climate zones would be a good start in developing a predictive treatment of the effects of climate and land-use change on plant-related productivity. Further advances will also be possible if any discrepancies between the predicted upper bound of *ET* and observation can be interpreted in terms of specific failures of actual behavior of the biosphere to reach optimality.

The strategy for solution is as follows: (1) Use the first of the two Budyko equations, equation (1), to write $ET = P - Q$. (2) Import the equation for *NPP* as a function of *ET*. (3) Modify the equation by multiplying by the soil depth as a function of Q. (4) Optimize *NPP* as a function of Q.

3.3.1. Percolation Theory, Solute Transport, and Chemical Weathering: Relevance to Soil Formation

Although soil formation is certainly a very complex process, an increasing body of research (Anderson & Anderson, 2010; Burke et al., 2006, 2009; Dixon et al., 2009a, 2009b; Egli et al., 2014; Maher, 2010) suggests that chemical weathering of the substrate is the component that most commonly limits the rate of formation of soil. At the same time, evidence has been accumulating that field measured values of the chemical weathering rate are consistent with the assumption that the weathering process is solute transport limited. Solute transport limitations are introduced by the tendency of chemical reactions to go to equilibrium if the reaction products are not removed efficiently. Thus, it has been proposed that it is possible to calculate weathering rates from (non-Gaussian) solute transport rates. Because solute transport velocities diminish with time, under field conditions solute transport will always become limiting after sufficient time has passed. If chemical weathering is also the limiting component of soil formation, then the solute transport velocity should generate the rate of soil formation. Egli et al. (2018) investigated the world's largest relevant soil database, finding that in Mediterranean sites soil formation rates were given by solute transport rates at all timescales. At alpine sites, reaction kinetics could dominate at timescales up to 100 years or so, but at larger timescales, solute transport was found to control chemical weathering and soil formation rates.

Since soil formation rates decay with time (or increasing depth), if soil erosion rates remain constant, eventually soil formation and erosion rates can coincide, at which point a steady-state soil production has been achieved. In the large majority of the soils considered by Egli et al. (2018), steady-state conditions were reached by a few tens of thousands of years. The equation derived for the steady-state soil depth, x, was

$$x = d_{50}\left[\frac{I}{D_b \varnothing E}\right]^{\frac{1}{D_b - 1}} = d_{50}\left[\frac{I}{1.87 \varnothing E}\right]^{1.15}. \qquad (4)$$

Here d_{50} is the median particle diameter, $\varnothing$ the porosity, E the erosion rate, and I the deep infiltration rate. The numerical constants $D_b = 1.87$ and $1/(D_b - 1) = 1.15$ relate to the fractal dimensionality of the percolation backbone, $D_b = 1.87$. The value 1.87 is appropriate for both saturated and wetting conditions with 3D connectivity (Hunt & Sahimi, 2017), a degree of universality sufficient for most soil development, though questionable for development within fractures, for which pore-space connectivity is more likely 2D. We will use equation (4) for the soil depth but with the substitution of Q for I. This is not entirely justified for two reasons: (1) It assumes that the entire runoff is through the subsurface, and (2) it takes the erosion rate, E, as an input value independent of I (or Q). The first assumption is consistent with zero runoff by overland flow. The second is generally consistent with erosion rates that are slope controlled and less sensitive to minor changes in precipitation, P. In any case, erosion rates do depend less sensitively on the fraction of Q given by I; increases of infiltration at the expense of overland flow increase erosion by chemical weathering (removal of the products in solution) at the expense of physical erosion. The direct physical source of this constraint can be analyzed through a comparison of the ratio of the hydraulic conductivity with the porosity and the rainfall rate, a detail which we prefer to neglect in this initial investigation. Using Q for I, we find

$$x = d_{50}\left[\frac{Q}{1.87 \varnothing E}\right]^{1.15}. \qquad (5)$$

A number of problems in soil formation and geomorphology are amenable to solution using the described approach (Egli et al., 2018; Yu & Hunt, 2017a, 2017b), while a wide range of data (Hunt, 2017) have been found consistent with equation (4). Although the depth evolution of some soils was, at short timescales (less than 100 years), shown to be limited by reaction kinetics (Egli et al., 2018) rather than solute transport, this timescale was considerably less than the time required to reach steady state, which was typically 10,00 to 100,000 years.

Here we compare soil depths obtained from equation (4) using typical values of particle sizes, erosion rates, porosity, and infiltration rates with the results of Gentine et al. (2012) for rooting depth. Thus, we check to see if the magnitudes of x using known values of Q are reasonable. Later, we check to see if known values of Q are generated from an optimization of our results for soil depth and vegetation growth.

For comparison with rooting depth, it is important that estimates of the actual depth of the soil do not use the value for $Q = 0.377\ P$, derived below, but only that portion which actually infiltrates rather than running off on the surface, which is closer to $0.22\ P$ (Lvovitch, 1973). Estimates (Yu et al., 2017) of typical global soil depths using equation (4) and $I/\varphi = 0.22P/\varphi$ approximately 0.5, ranged from about 0.45 m to 1.67 m. In those estimations, d_{50} was taken to be 0.00003 m, a typical porosity of 0.4 was chosen, and the typical erosion rate was given as 0.000029 m/yr (Montgomery, 2007). Mean precipitation rates from the literature varied from a little over 800 mm/yr to approximately 1100 mm/yr, while there was an even greater range in approximate fractions of P that infiltrated deeply. For comparison, consider that the rooting depths obtained by Gentine et al. (2012) ranged from 0.32 to 0.8 m (their Figure 2). In our calculation below, 62% of the water transiting the root zone returns to the atmosphere. In accord with this effective water content, one could define an equivalent depth of nearly full saturation, but which is only 62% as deep, as the source of water for transpiration. Using this factor of 0.62, the range of values from Yu et al. (2017) for the soil depth are transformed to 0.30 to 1.03 m, rooting depths which are roughly equivalent to those of Gentine et al. (2012).

3.3.2. Vegetation Growth and Net Primary Productivity (NPP)

Here it is important to state at the outset that we have not developed a steady-state expression for *NPP*. Rather, it was shown that *NPP* is proportional to a specific, non-integral power of *ET* at any time scale (Hunt, 2017). Elsewhere it will be shown that both *NPP* and *ET* decrease with increasing mean age of vegetation. However, it is presumed that in natural ecosystems, at least, barring such events as fire, a steady state in population has been reached, i.e. that the number of woody plants entering any specific age class in a given time period due to increasing individual age is equal to the number removed from that age class, either by death or further aging.

Hunt (2017) showed that data support the theoretical proposition that *NPP* is proportional to T (transpiration) to the 1.9 power, i.e. $NPP = C\ T^{1.9}$, with C a constant of proportionality, which was at that time undiagnosed. The argument for this choice of power was that roots were following optimal paths (least resistance and maximum nutrient and water fluxes) near the surface that were constrained to a medium that was effectively two-dimensional (2D). Thus, the mass fractal dimensionality of the root systems should be equal to the mass fractal dimensionality of large clusters near the percolation threshold in 2D. This argument was influenced by descriptions of forest systems. However, particularly in arid systems, it has been suggested that the root mass can be more isotropic, and it is possible that the appropriate mass fractal dimensionality is actually 2.5, the percolation value associated with a 3D medium. One data set by Seeley (1978), as described in Hunt (2017), may support this suggestion at the far dry end of the transpiration range in the Namibian desert.

Some variability in *NPP* values at a given transpiration existed (the constant C) and was not accounted for (Hunt, 2017). The present hypothesis may supply some of the source of variability in a dependence on soil depth, but part might be traced to simply to constants required by dimensional analysis. Dimensional analysis, since *NPP* is measured in grams of carbon in the dry weight of vegetation that has developed over 1 year in a specified area, A (1 m square), requires the additional presence of a density factor, which we have not explicitly included. Thus, a volume per unit area, A, must be multiplied by the density to generate the carbon content. Not all plant matter has the same carbon density. In addition, volume is not generated by the horizontal root development alone but also through multiplication by the rooting depth, suggested to be roughly a constant and equal to the soil depth. Equating the soil depth with the rooting depth arose in combination with the result that the soil depth, as calculated from equation (4), is usually about 1 m, whereas most roots are confined within the top meter or two of the surface. Additional support is provided by a range of authors (Hillel, 2005; Jenny, 1941), who describe the world's soils as being typically about 1 m in depth. As explanation, we cite the argument (Lynch, 1995) that roots seek nutrients in the top ~1 m of soil, which tends to lie in the vadose zone above the water table. This portion of the subsurface is also where water contents tend to change most drastically. In fact, the rooting depth is the focus of other studies

of Budyko theory (Yang et al., 2016), who state explicitly, "In terrestrial ecosystems, the plant rooting depth (Z) primarily determines the active soil zone that has potential to return water back into the atmosphere via plant transpiration." The rooting depth is typically restricted to a maximum of 1 to 2 meters (Fan et al., 2017), except in highly water-limited environments.

The quoted result for NPP (ET) is based on below-ground productivity and the assumption of equivalence between below-ground and above-ground productivity. Differences in above- and below-ground productivity can also account for some of the variability in the NPP (ET) relationship.

We now write the net primary productivity, NPP, as

$$NPP = \frac{x\,ET^{d_f}}{A}. \tag{6}$$

Although A, as stated, represents a reference surface area (1 m square), its interpretation becomes important when, for large aridity index, plant separation becomes very large. The proportionality of NPP to soil depth in equation (6) corresponds closely to the result of Porporato et al. (2004). Equation (6) applies the assumption that d_f, the mass fractal dimensionality of percolation theory, is appropriate for the root mass. The value of d_f depends only on whether the percolation cluster is constructed in 2D or in 3D; in the former case $d_f = 1.9$; in the latter, $d_f = 2.5$ (and the density factor is still neglected). The choice depends on the degree of confinement of the root mass to a shallow soil layer. The below-ground productivity is confined mostly within the soil with depth x. Owing to the relatively small thickness of soil compared with the heights and root radial extent of most plants, we use the value $d_f = 1.9$ appropriate for 2D, except when we formulate alternate hypotheses. Dimensional analysis requires, in addition to a length scale to the d_f power, also a length scale (or scales) to the power $3 - d_f$. Since we chose x^1, we point out that equation (6) is missing a factor proportional to a length scale to the $3 - (1 + 1.9) = 0.1$ power.

3.3.3. Optimization of *NPP* and Result for *ET* (*P*) for Steady-State Soil Conditions

The first step towards optimization of NPP with respect to the water partitioning is substitution of the result for x as a function of Q from equation (5) into equation (6). Then use $P = Q + ET$ to represent NPP as a function of only Q, rather than ET and Q:

$$NPP = KQ^{\frac{1}{D_b-1}}ET^{d_f} = KQ^{\frac{1}{D_b-1}}\left[P-Q\right]^{d_f}. \tag{7}$$

Here K is another constant, independent of the fluxes. In order to optimize NPP (Q), the derivative of equation (7) with respect to Q may be set equal to zero, generating the equation

$$\frac{1}{D_b-1}\left(P-Q\right) = d_f Q. \tag{8}$$

The solution of equation (8) is

$$Q = \frac{P}{1+d_f\left(D_b-1\right)}. \tag{9}$$

For $d_f = 1.9$ and $D_b = 1.87$, as in the published predictions of NPP and soil depths, equation (9) yields $Q = 0.377\,P$ and $ET = 0.623\,P$.

Start from equation (7), but apply the assumption that roots spread equivalently in all directions ($d_f = 2.5$). Now, dimensional analysis does not allow a root mass to be proportional to the product of the root radial extent to the 2.5 power and the rooting depth, since the combination of powers of lengths is greater than 3. Thus, the factor x is replaced by x^{3-df} and the optimization procedure analogous to that performed on equation (7) yields

$$Q = \frac{3-d_f}{3-d_f+\left(D_b-1\right)d_f}P = 0.187P. \tag{10}$$

The result $ET = 0.813\,P$ follows for $d_f = 2.5$. Isotropic root systems are thus more effective at removing water from the soil, enhancing ET. In arid regions, applicability of either equation (5) or equation (10) is likely restricted to the immediate subsurface beneath plants, where soil and the rooting depth is greater than the average value (Yang et al., 2016).

Two special cases of equation (10) may be considered. In one case, $d_f = 3$, making $Q = 0$, leaving $ET = P$. In the second case, $D_b = 1$ (Gaussian conditions, where solute transport and water flow velocities are the same). Then $Q = P$ and $ET = 0$. This latter condition, however, is not relevant, since in that case solute transport is so rapid that it does not limit chemical weathering and soil formation. Indeed, soil formation is then reaction kinetics limited (Yu & Hunt, 2018).

3.3.4. Optimization for the Case of Transient Soil Development

In many areas in the world, nascent soils are forming in regions where ice sheets or glaciers have retreated (e.g., Mavris et al., 2010). In the first few hundred years (Egli et al., 2018), soil depths increase rather rapidly and

according to the following equation (Yu & Hunt, 2017a, 2017b; Egli et al., 2018):

$$x = d_{50}\left[\frac{t}{\varnothing d_{50}\,/\,I}\right]^{\frac{1}{D_b}}. \tag{11}$$

Note that requiring equivalence of the time derivative of equation (11) (rate of increase of soil depth is the soil production function) and the denudation rate generates equation (5) for the steady-state soil depth (Yu & Hunt, 2017a, 2017b; Egli et al., 2018). In other regions, where erosion rates may be very small, the relevance of such a relationship to much longer timescales has also been documented (Yu & Hunt, 2017a). Examples include central Australia.

Carrying through the analogous optimization of *NPP* (*Q*) as with equation (7) leads to the result

$$Q = \frac{P}{1 + d_f D_b}. \tag{12}$$

The validity of equation (12) is restricted to areas with vegetation. Choosing the 2D value, $d_f = 1.9$ leads to $Q = 0.22\,P$ and $ET = 0.78\,P$. Using the analogous procedure in 3D (following the modifications in the derivation of equation [10]), one finds

$$Q = \frac{3 - d_f}{3 - d_f + D_b d_f} P. \tag{13}$$

Equation (13) yields $Q = 0.097$P and $ET = 0.903\,P$. The larger fractions of the precipitation that go into *ET* reflect the more efficient soil formation at shorter times, consistent with the smaller fraction of *P* represented by *Q*. Thus, it is possible for vegetation to extract more water from young soils without hindering the soil development so strongly, since the soil production rates are higher. It is important that even surfaces that have been exposed for 100,000 years or more may not reach steady-state soil depths if climates are sufficiently arid, such as in central Australia.

3.3.5. Predicted Variability in *ET*

One can address the observed variability *ET* with our formulation, even though it allows, in principle, variability only in a single variable parameter, the mass fractal dimensionality of the root system. Thus, one can use the observed variability in root fractal dimensionality for the parameter d_f, rather than the optimal value from percolation theory, in order to estimate *variability* in *ET*, rather than the optimal value of *ET*.

3.3.6. Variation of *ET*(*P*) with Dryness Index

The result from equation (9), $ET = 0.623\,P$, does not account for constraints on evaporation due either to water limitations or energy limitations. Williams et al. (2012) found that 62% of the variability in *ET* values could be attributed to variations in the ratio of ET_0/P, but only about 13% was due to climate. Thus, it is necessary at least to develop a means to treat the variation of *ET* with ET_0.

In the limit of $ET_0/P << 1$, Budyko (1958) found that $ET = ET_0$, while in the limit $P/ET_0 << 1$, $ET = P$. Below, we develop a framework to address the variability of *ET* with solar radiation in terms of the so-called dryness index for water-limited conditions, expanding the range of conditions that we can consider.

In arid regions, roots may extend vertically as easily as horizontally. Rooting depths are deeper (Fan et al., 2017), and examples of root fractal dimensionality similar to 2.5 are not infrequent for grassland plant species (Levang-Brilz & Biondini, 2002). Substitution of $d_f = 2.5$ into equation (11) yields $Q = 0.187\,P$, implying $ET = 0.813\,P$. However, in water-limited environments, particularly warm deserts, separations between plants can be very large. In such cases, Yang et al. (2016) have emphasized the need to account for the plant separation in an "effective rooting depth." In between plants, where soil can be virtually absent (Yang et al., 2016), we suggest that evaporation is simply equal to *P* and no water goes into soil formation. Such an assumption is in general accord with both adaptive behavior of plants, which may grow best in regions with higher infiltration, such as along fractures (Stothoff et al., 1999), or the result of surface armoring by small clasts (rocks) between plants, which strongly inhibits water infiltration (Wells et al., 2014). A quick estimate of the aerial density of dominant vegetation yields the quotient of *P* and ET_0. Then one could write the total *ET* as equal to $(0.817)\,P\,(P/ET_0) + P\,(1 - P\,/\,ET_0) = P - (0.183)\,P\,(P/ET_0)$. Division by *P* yields $ET/P = 1 - 0.183\,(P/ET_0)$.

A reasonable approach to defining a predicted upper bound for optimization of vegetative capacity for transpiration is to combine the two results, $ET = ET_0$ for values of $ET/ET_0 < 0.623$ and $P - 0.183\,P/ET_0$ for dryness index greater than or equal to 1. However, this would leave a region of dryness index between 0.62 and 1 without any predicted upper bound. A second possible strategy is to continue the approximation for water-limited systems down to a dryness index value where the large *ET*/P prediction coincides with the small *ET*/*P* result ($ET = ET_0$), thereby ensuring continuity of the ratio of *ET*/P everywhere, although not of the slope. Nevertheless, the result for the intermediate dryness

regime, $0.623 < ET_0/P < 1$, is not specifically justifiable, and a better treatment might well differ from our prediction in this region.

3.3.7. Qualitative Modeling of *NPP* Across Climate Zones

At low aridity index, the optimal *ET* of ecosystems is ET_0, since all radiation can be utilized without any limitations from water. Given the modeled, and observed, power-law dependence of *NPP* on *ET*, one should expect that, in this range, $NPP = x^1\ ET^{1.9}$ would generate the same dependence on ET_0, i.e. $NPP = x^1\ ET_0^{1.9}$. In contrast, at high values of ET_0/P one would expect the areal density of plants to control *NPP* in conjunction with *ET*. This areal density was assumed to be P/ET_0; thus, one finds an ecosystem productivity proportional to $ET^{2.5}ET$, or $ET^{3.5}$. In the water-limited regime, however, *ET* becomes very nearly *P*, so that to a good approximation, *NPP* is expected to be proportional to $P^{3.5}$.

The behavior of *NPP* for a given *P* but increasing ET_0 can now be addressed. The prediction is that for low ET_0, *NPP* increases as $ET_0^{1.9}$ through aridity index 1 but diminishes as $1/ET_0$ as ET_0 continues to increase. Consider next the same transit of the aridity index, from small to large, but for ever-increasing *P* values. *NPP* can rise to ever-larger values for increasing *P* as the aridity index approaches 1. Eventually, the maximum *NPP*, reached at $P/ET_0 = 1$, will equal 3500 gC/m^{2}yr, which is recognized as (approximately) the maximum possible *NPP* for the largest solar radiation available at the Earth's surface (de Wit, 1965; Krause-Jensen & Sand-Jensen, 1998). Further increases in *P* will not produce greater values of *NPP*, even at aridity index of 1. According to the present theoretical construct, they will thus also not produce larger values of *ET*. Yet ET/ET_0 will not change, simply because ET_0 has reached its maximum. Thus, as revealed by the concept of the aridity index and the reality of the Budyko curve, such further increases in *P* will simply translate ecosystems to smaller aridity indices, for which the approximation $ET = ET_0$ becomes more precise.

3.4. COMPARISONS WITH DATA

3.4.1. Global Terrestrial Mean Value of *ET*

The global average for *ET* in terrestrial ecosystems is given by various sources as 0.633 *P* (vegetation mean) or 0.635 *P* (climate mean, with two additional sites) (Williams et al., 2012), 0.64 *P* (Schlesinger & Jasechko, 2014) or 0.65 *P* (Lvovitch, 1973). Our numerical result of 0.623 *P* differs from these three quoted results by 1%, 3%, and 5%, respectively.

3.4.2. Variation in *ET* with Aridity Index

We have digitized the data from Gentine et al. (2012) and compare our predicted functional form to the results. We maintain their distinctions of "in phase," when the precipitation maximum is simultaneous with the maximum in irradiance, "out of phase," when these maxima are not simultaneous, and "non-seasonal," when precipitation is not principally defined by the season but spread out over much of the year. The comparison with our prediction is shown in Figure 3.1.

Over most of the region of aridity index values, we provide an excellent upper bound, but in areas of large aridity, we tend to underestimate the actual *ET*. It is possible that the discrepancy is due to our underestimation of the ability of plants to adapt to arid environments, including extraction of water from sources not considered (such as dew or fog). It is also possible that, particularly in very arid environments, soils are continuing to deepen (Yu & Hunt, 2017a) and the optimization procedure for transient, rather than steady-state, soil conditions is appropriate. When soils are still deepening, our derivation implies that a greater fraction of *P* is lost to *ET*. Whether measurement error can contribute to the discrepancy is not clear. Certainly, measured values of $ET > ET_0$, when they occur, do not appear to fit with the Budyko framework.

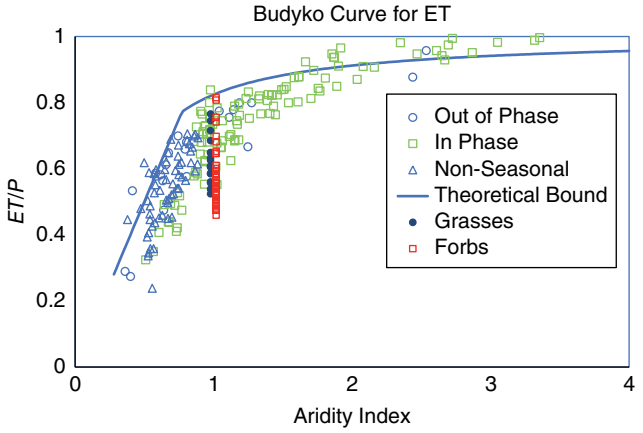

Figure 3.1 Plot of data compiled by Gentine et al. (2012) for *ET*/P as a function of aridity index, ET_0/P. Theoretical upper bound derivation for large aridity index uses the steady-state result for soil depth and 3D root fractal dimensionality of 2.5. "Grasses" and "Forbs" represent the fraction of *ET/P* predicted using all experimentally determined values (Levang-Brilz & Biondini, 2002) of the root fractal dimensionality in grasses and forbs. Experimental parameters are compatible with an aridity index of 1, since either the water-limited or energy-limited regime would preclude the optimal growth conditions described in Levang-Brilz and Biondini (2002).

3.4.3. Variability in *ET* for Specific Aridity Index

In a greenhouse study of Great Plains vegetation, Levang-Brilz and Biondini (2002) planted 38 species of forbs and 17 of grasses in large pots and allowed them to grow over a season. One half the studied plants were given a prescribed drip irrigation regimen with fertilization and adequate light. In the second half, all parameters were adjusted to generate a "maximum growth rate." Our interpretation is that a maximum growth rate implies that the plants were neither energy limited nor water limited (or even nutrient limited), and we therefore suggest that the appropriate experimental aridity index for this experiment is 1 ($P = ET_0$). Even in the first case, optimal conditions were likely approached, since adequate light was guaranteed and drip irrigation was used. Although by far the dominant vegetation type in the Great Plains is grass (e.g. Barker & Whitman, 1988), we reproduce both results for forbs and grasses here. Levang-Brilz and Biondini (2002) measured the root fractal dimensionalities of each species using multiple individuals under each range of experimental conditions. This fractal dimensionality was measured by determining the exponent in the relationship between root mass and root radial extent, exactly as defined here. We used all their species of both forbs and grasses, as shown in Figure 3.1. The observed variability in *ET* is predicted almost exactly by the variability in d_f for the steady-state thin soil (2D) case (equation (9); assumed to be the most common), as shown in the figure.

3.4.4. Climate Dependence of *NPP*(*ET*)

Above, it was suggested that at the very dry end of the spectrum, *NPP* should be proportional to $P^{2.5}$ P^1, or $P^{3.5}$, rather than $P^{1.9}$. Here the first factor in *P* reflects individual plant transpiration, whereas the second factor accounts for the plant density. Evidence for such a crossover from a lower exponent to a higher exponent with increasing aridity is seen in Figure 3.2, although the extracted powers in the two data sets, 3.14 and 1.64, are about 15% and 50% smaller, respectively, than the predicted values of 3.5 and 2.5, respectively, and may be more easily reconciled with the 2D predicted exponents of 2.9 and 1.9.

Note that the transition to a more rapid reduction of productivity with decreasing precipitation has some similarity to the complementary principle of Bouchet (1963) discussed in Carmona et al. (2016), that as ET_0 increases, soil water content decreases, producing a decrease in *ET*. In the present case, a transition from $P > 100$ mm yr^{-1} to $P < 100$ mm yr^{-1} produces such a decrease in *NPP*, that *ET* decreases faster than would be anticipated from extrapolating the Chihuahuan desert to lower *P* values,

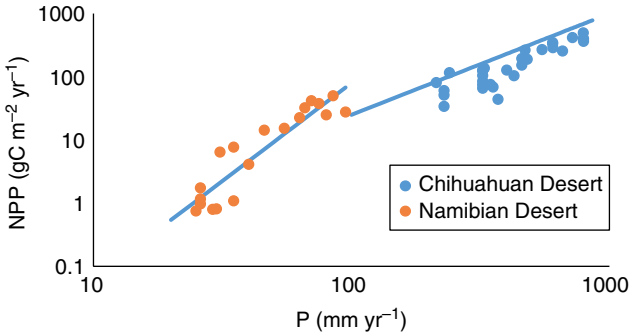

Figure 3.2 Dependence of net primary productivity, *NPP*, on precipitation, *P*, in arid ecosystems. The data from the Namibian desert are from Seeley (1978) and from the Chihuahuan desert from Muldavin et al. (2008). Note that, at precipitation values approaching 100 mm/yr, the dependence on *P* of *NPP* in the Namib may be compatible with that of *NPP*(*P*) in the Chihuahuan desert, which would imply that the spatial separation of growing plants only becomes significant at very low precipitation values, significantly less than 100 mm/yr.

meaning that *ET*/*P* may be a function of the actual values of ET_0 and *P*, and not just their ratio. In the study of Carmona et al. (2016), this eventuality is also anticipated, and the authors define three relevant ratios.

3.5. DISCUSSION AND POTENTIAL STRATEGIES FOR IMPROVEMENT

A potentially important result of this study relates to using the observed values of the root fractal dimensionality, d_f, as a means to predict the fraction of *P* represented by *ET*, which can be defined as α, i.e. $ET = \alpha P$. This was represented graphically in Figure 3.1. It is also useful to give the mean and standard deviation of α. For grasses, the predicted value turns out to be $\alpha = 0.63 \pm 0.07$, while for forbs, $\alpha = 0.58 \pm 0.09$. It is perhaps no surprise, given their dominance, that grasses appear to have more nearly attained the optimal α of approximately 0.63 to 0.64, and with a smaller variance than that of the forb species. What the larger variance of α implies, from Figure 3.1, is that forbs show up more at both small and large *ET* values, making it appear as though they are capable of exploiting conditions that deviate more from the norm. But since their predicted mean *ET* is lower than that of the grasses, and since *NPP* depends so strongly on *ET*, one can surmise that grasses have an important overall advantage in growth and productivity. Nevertheless, our comparison with the variability in *ET* at aridity index 1 in terms of the variability of d_f does not constitute a proof that the variability in observed d_f is the cause of the variability in *ET*. More studies are needed for greater confidence.

Our predictions for ET as a function of ET_0/P are mostly for steady-state conditions, with vegetation adapted to soil conditions after having contributed to its development. In the large ET_0 regime, we have also used non-steady-state conditions for soil development. This adaptation takes place under specific conditions of topography, aspect, and climate. Since conditions of steady state may not, for example, be reached during any intervals between landslides, regions susceptible to landsliding cannot be expected to conform closely to the predictions here. Other important conditions that may be expected to invalidate the assumption of a steady-state optimization of NPP by ecosystems include locations degraded by human impacts or those for which fire produces periodic disturbances. During periods of rapid climate change, perhaps no place on Earth could be considered to be in steady state. Nevertheless, it is not the focus of this work to trace discrepancies to conditions out of steady state. Other factors may also be responsible. We have considered one such factor, that vegetation may not always be able to take advantage of the optimal strategy for growth and carbon conversion. Other possibilities are addressed more quantitatively next.

Our full derivation (Egli et al., 2018) for soil depth, for example, clearly takes into account that both surface runoff and infiltration contribute to erosion, whereas only infiltration contributes to soil formation. However, this distinction is not preserved in Budyko formulations. Nevertheless, it is important to distinguish between surface (Q_a) and subsurface (Q_b) runoff, with chemical weathering losses in solution proportional to Q_b, and (primarily) physical erosion proportional to Q_a. (Even with this increase in care in treating water and erosional fluxes, aeolian deposition and erosion are neglected!) Neglecting aeolian inputs, the soil depth should thus be proportional to $(Q_b/[aQ_a + bQ_b])^{1.15}$, with a an b constants of proportionality, rather than a simple ratio of $(Q_b/E)^{1.15}$. In the case that surface runoff is a relatively small fraction of Q, but $b >> a$, the approximation that we chose here can be accurate. For most of the world's rivers, sediment in suspension greatly exceeds sediment in solution, supporting such an approximation. But in areas where chemical weathering is particularly important, our approximation would be expected to break down. There, greater infiltration leads simultaneously to a greater denominator as well as a larger numerator in the expression for soil depth, and the importance of soil in the optimization of NPP is reduced. Indeed, the soil thickness is reduced as well, which should be expected to lead to a reduction in NPP as well as a reduction in ET. One situation where one might expect to see such effects is in karst topography. B. Wang et al. (2009), for example, isolated substrate as a variable and found that the NPP of drainage basins in nonkarstic regions in Guizhou province in China was 13.3% higher than in karstic regions. This implies a 7% higher value of ET (proportional to the 0.53 power of NPP) in nonkarstic regions, in view of the proportionality of NPP to $ET^{1.9}$. A variation of 7% is about half the typical variation of ET over long periods of time, as shown in the data of Gentine et al. (2012) (Figure 3.1).

Just as the Budyko framework does not distinguish adequately between surface and subsurface runoff, neither does it distinguish sufficiently between evaporation and transpiration. It is true that Rosenzweig (1968) also did not distinguish between these two fluxes in his original work addressing the dependence of $NPP(ET)$. However, logic dictates that the water lost through evaporation directly from the ground surface, rather than through plant transpiration, does not contribute to plant productivity. Thus, the assumed equivalence between NPP and ET values is not sound. A variability in the fraction of ET represented by the transpiration would complicate the entire derivation. We have, to some degree, taken such a variability systematically into account in desert climates, but any fluctuations in adaptability that could lead to a variable ratio of transpiration to ET would introduce variability into the fraction of P represented by ET, since the purely evaporative component would not directly influence the optimization of ET except by its absence.

The current results may help to resolve a puzzle noted by Egli et al. (2018), namely that the model of equation (5) and equation (10) appeared to overpredict soil depths for alpine surroundings, particularly at early times, by approximately 40%. The predicted fraction of P given by ET increases from approximately 0.62 for steady-state conditions (equation [5]) to 0.78 for transient conditions (equation [10]), thus implying a reduction in Q from $0.38P$ to $0.22P$. The corresponding reduction in soil depth would be approximately 25%.

3.6. CONCLUSIONS

We have developed a theoretical approach to find the fraction of precipitation, P, falling on the continents that is returned to the atmosphere as evapotranspiration, ET. This approach is based on percolation theoretical results for soil depth in terms of runoff, and net primary productivity as a function of transpiration. Our prediction for the global average ET (P) = 0.623 P appears to be within 1%–3% of observed values. Our prediction for the variability of ET (P) for a single value of the aridity index ($ET_0/P = 1$) is nearly identical to the observed variability. In this case, the variability in ET relates to the variability of a single parameter, the root mass fractal dimensionality. Our prediction for the variation of the maximum value of ET with aridity index appears to bound relatively well the actual dependence of this variable when only

long-term averages of *ET* as a fraction of *P* are considered. At this time, evidence suggests that our framework for the Budyko problem may have wide applications in future studies.

ACKNOWLEDGMENTS

The research reported here benefited greatly from extended discussions with Garrison Sposito and Bruce Milne. Dr. Milne emphasized the Rosenzweig (1968) study on *NPP* (*ET*) as well as the importance overall of analyzing the principal hydrologic fluxes. Dr. Sposito pointed out the relevance of the data compiled by Gentine et al. (2012) and insisted on the significance of being able to predict the soil depth within the same framework that predicts net primary productivity. This significance appears to derive from the results of the work of Porporato et al. (2004) in finding a correspondence between soil depth and ecosystem productivity.

REFERENCES

Anderson, R. S., & Anderson, S. P. (2010). *Geomorphology: The mechanics and chemistry of landscapes*. New York: Cambridge University Press.

Barker, W. T., & Whitman, W. C. (1988). Vegetation of the northern Great Plains. *Rangelands*, *10*, 266–272.

Bouchet, R. J. (1963). Evaptranspiration reele et potentielle signification climatique. *General Assembly Berkley, Int. Assoc. Sci. Hydrol. Pub*, *62*, 134–142.

Budyko, M. I. (1958). The heat balance of the Earth's surface. Washington, DC: US Dept. of Commerce, Weather Bureau.

Budyko, M. I. (1974). *Climate and life* (English ed.). San Diego, CA: Academic.

Burke, B. C., Heimsath, A. M., Chappell, J., & Yoo, K. (2009). Weathering the escarpment: Chemical and physical rates and processes, southeastern Australia. *Earth Surface Processes and Landforms*, *34*, 768–785. doi: 10.1002/esp.1764

Burke, B. C., Heimsath, A. M., & White, A. F. (2006). Coupling chemical weathering with soil production across soil-mantled landscapes. *Earth Surface Processes and Landforms*, *32*, 853–873. doi: 10.1002/esp.1443

Carmona, A. M., Poveda, G., Sivapalan, M., Vallejo-Bernal, S. M., & Bustamante, E. (2016). A scaling approach to Budyko and the complementary relationship of evapotranspiration in humid environments: Case study of the Amazon river basin. *Hydrol. Earth System Science*, *20*, 589–603.

de Wit (1965). Photosynthesis of leaf canopies, Agricultural Research Report no. 663 PUDOC Wageningen.

Dietrich, W. E., & Perron, J. (2006). The search for a topographic signature of life. *Nature*, *439*(7075), 411–418, doi: 10.1038/nature04452.

Dixon, J. L., Heimsath, A. M., & Amundson, R. (2009b). The critical role of climate and saprolite weathering in landscape evolution. *Earth Surface Processes and Landforms*, *34*, 1507–1521. doi: 10.1002/esp.1836

Dixon, J. L., Heimsath, A. M., Kaste, J., & Amundson, R. (2009a). Climate-driven processes of hillslope weathering. *Geology*, *37*, 975–978. doi: 10.1130/G30045A.1

Eagleson, P. S. (1978a). Climate, soil, and vegetation: 1. Introduction to water balance dynamics. *Water Resour. Res.*, *14*(5), 705–712, doi: 10.1029/WR014i005p00705.

Eagleson, P. S. (1978b). Climate, soil, and vegetation: 2. The distribution of annual precipitation derived from observed storm sequences. *Water Resour. Res.*, *14*(5), 713–721.

Eagleson, P., & Tellers, T. (1982). Ecological optimality in water-limited natural soil-vegetation systems: 2. Tests and applications. *Water Resour. Res.*, *18*(2), 341–354. doi: 10.1029/WR018i002p00341.

Egli, M., Dahms, D., & Norton, K. (2014). Soil formation rates on silicate parent material in alpine environments: Different approaches—different results? *Geoderma*, *213*, 320–333. doi: 10.1016/j.geoderma.2013.08.016

Egli, M., Hunt, A. G., Dahms, D., Raab, G., Derungs, C., Raimondi, S., & Yu, F. (2018). Prediction of soil formation as a function of age using the percolation theory approach. *Frontiers in Environmental Sciences*, *28*. https://doi.org/10.3389/fenvs.2018.00108

Fan, Y., Miguez-Macho, G., Jobbágy, E. G., Jackson, R. B., & Otero-Casal, C. (2017). Hydrologic regulation of plant rooting depth. *Proceedings of the National Academy of Sciences*, *114*. doi/10.1073/pnas.1712381114

Gentine, P., D'Pdorico, P., Linter, B. R., Sivandran, G., & Salvucci, G. (2012). Interdependence of climate, soil, and vegetation as constrained by the Budyko curve. *Geophys. Res. Lett.*, *39*, L19404. doi: 10.1029/2012GL053492

Guswa, A. (2008). The influence of climate on root depth: A carbon cost-benefit analysis. *Water Resources Research*, *44*, W02427.

Guswa, A. (2010). Effect of plant uptake strategy on the water-optimal root depth. *Water Resources Research*, *46*, W09601.

Hillel, D. (2005). Soil: Crucible of life. *J. Nat. Resour. Life Sci. Educ.*, *34*, 60–61.

Hunt, A. G. (2017). Spatio-temporal scaling of vegetation growth and soil formation: Explicit predictions. *Vadose Zone Journal.* doi:10.2136/vzj2016.06.0055

Hunt, A. G., & Ghanbarian, B. (2016). Percolation theory for solute transport in porous media: Geochemistry, geomorphology, and carbon cycling. *Water Resources Res.*, *52*, 7444–7459.

Hunt, A. G., & Sahimi, M. (2017). Flow, transport, and reaction in porous media: Percolation scaling, critical path analysis and effective-medium approximation. *Reviews of Geophysics*, *55*, 993–1078. doi: 10.1002/2017RG000558

Hunt, A. G., & Wu, Q. J. (2004). Climatic influences on Holocene variations in soil erosion rates on a small hill in the Mojave Desert. *Geomorphology*, *58*, 263–289.

Jenny, H. (1941). *Factors of soil formation: A system of quantitative pedology*. New York: Dover.

Knapp, A. K., Fay, P. A., Blair, J. M., Collins, S. L., Smith, M. D., Carlisle, J. D., et al. (2002). Rainfall variability, carbon cycling, and plant species diversity in a mesic grassland. *Science*, *298*, 2202–2205.

Krause-Jensen, D., & Sand-Jensen, K. (1998). Light attenuation and photosynthesis of aquatic plant communities. *Limnology and Oceanography*, *43*, 396–407.

Levang-Brilz, N., & Biondini, M. E. (2002). Growth rate, root development and nutrient uptake of 55 plant species from the Great Plains Grasslands, *USA. Plant Ecology*, *165*, 117–144.

Lieth, H. (1972). Modelling the primary productivity of the world. UNESCO, *Pads. Nature Res. 8*, 5–10.

Lvovitch, M. I. (1973). The global water balance: U.S. National Committee for the International Hydrological Decade. *U.S. National Committee for the International Hydrological Decade Bulletin*, *23*, 28–42. doi: 10.1029/EO054i001p00028

Lynch, J. (1995). Root architecture and plant productivity. *Plant Physiology*, *109*, 7–13.

Maher, K. (2010). The dependence of chemical weathering rates on fluid residence time. *Earth Plan. Sci. Lett.*, *294*, 101–110. doi: 10.1016/j.epsl.2010.03.010

Manabe, S. (1969). Climate and ocean circulation: I. Atmospheric circulation and hydrology of the Earth's surface. *Mon. Weather Rev.*, *97*(11), 739–774. doi: 10.1175/1520-0493(1969)0972.3.CO;2

Mavris, C., Egli, M., Plötze, M., Blum, J., Mirabella, A., Giaccai, D., & Haeberli, W. (2010). Initial stages of weathering and soil formation in the Morteratsch proglacial area (Upper Engadine, Switzerland). *Geoderma*, *155*, 359–371.

Milly, P. (1994). Climate, soil-water storage, and the average annual water balance. *Water Resour. Res.*, *30*(7), 2143–2156. doi: 10.1029/94WR00586

Milne, B., & Gupta, V. (2017). Horton ratios link self-similarity with maximum entropy of eco-geomorphological properties in stream networks. *Entropy*, *19*(6), 249. doi: 10.3390/e19060249

Montgomery, D. (2007). Soil erosion and agricultural sustainability. *Proc. Natl. Acad. Sci.*, *104*, 13268–13272.

Muldavin, E. H., Moore, D. I., Collins, S. L., Wetherill, K. R., & Lightfoot, D. C. (2008). Aboveground net primary production dynamics in a northern Chihuahuan desert ecosystem. *Oecologia*, *155*, 123–132.

National Research Council (1991). *Opportunities in the hydrologic sciences*. Washington, DC: National Academies Press. https://doi.org/10.17226/1543

Porporato, A., Daly, E., & Rodriguez-Iturbe, I. A. (2004). Soil water balance and ecosystem response to climate change. *The American Naturalist*, *164*, 625–632.

Rodriguez-Iturbe, I., Porporato, A., Ridolfi, L., Isham, V., & Cox, D. R. (1999). Probabilistic modelling of water balance at a point: the role of climate, soil and vegetation. *Proceedings of the Royal Society of London A*, *455*, 3789–3805.

Rosenzweig, M. L. (1968). Net primary productivity of terrestrial communities: Prediction from climatological data. *The American Naturalist*, *102*, 67–74.

Schlesinger, W. H., & Jasechko, S. (2014). Transpiration in the global water cycle. *Agricultural and Forest Meteorology*, *189*, 115–117. doi: 10.1016/j.agrformet.2014.01.011

Seeley, M. K. (1978). Grassland productivity: The desert end of the curve. *South African Journal of Science*, *74*, 295–297.

Sposito, G. (2017). Understanding the Budyko equation. *Water*, *9*(4), 236. doi: 10.3390/w9040236

Stothoff, S. A., Or, D., Groeneveld, D. P., & Jones, S. B. (1999). The effect of vegetation on infiltration in shallow soils underlain by fissured bedrock. *J. Hydrology*, *218*, 169–190.

Wang, B., Yang, S., Lu C. Zhang, J., & Wang, Y. (2009). Comparison of net primary productivity in karst and non-karst areas: A case study in Guizhou Province, *China. Environmental Earth Sciences*, *59*(6), 1337–1347l. doi: 10.1007/s12665-009-0121-6

Wang, D., Zhao, J., Tan, Y., & Sivapalan, M. (2014). A thermodynamic interpretation of Budyko and L'vovich formulations of annual water balance: Proportionality hypothesis and maximum entropy production. *Water Resources Research*, *51*, 3007–3016. doi:10.1002/2014WR016857

Wells, S. G., McFadden, L. D., McDonald, E. V., Eppes, M. C., Young, M. H., & Wood, Y. A., (2014). Desert pavement process and form: Modes and scales of landscape stability and instability in arid regions. *Geophysical Research Abstracts*, *16*, EGU2014–8060-1.

Williams, C. A., Reichstein, M., Buchmann, N., Baldocchi, D., Beer, C., Schwalm, C., et al. (2012). Climate and vegetation controls on the surface water balance: Synthesis of evapotranspiration measured across a global network of flux towers. *Water Resources Research*, *48*, W06523. doi: 10.1029/2011WR011586.

Yang, Y., Donohue, R. J., & T. R. McVicar (2016). Global estimation of effective plant rooting depth: Implications for hydrological modeling. *Water Resources Research*, *52*. doi: 10.1002/2016WR019392

Yu, F., Faybishenko, B., Hunt, A. G., & Ghanbarian, B. (2017). A simple model of the variability of topsoil depths. *Water*, *9*(7), 460. doi: 10.3390/w9070460

Yu, F., & Hunt, A. G. (2017a). An examination of the steady-state assumption in certain soil production models with application to landscape evolution. *Earth Surface Processes and Landforms*. doi: 10.1002/esp.4209

Yu, F. & Hunt, A. G. (2017b). Predicting soil formation on the basis of transport-limited chemical weathering. *Geomorphology*. https://doi.org/10.1016/j.geomorph.2017.10.027

Yu F., & Hunt, A. G. (2018). Damköhler number input to transport-limited chemical weathering calculations. *ACS Earth and Space Chemistry*, *1*, 30–38. doi: 10.1021/acsearthspacechem.6b00007

4

Earthworms, Plants, and Soils

Renée-Claire Le Bayon[1], Géraldine Bullinger[2], Andreas Schomburg[1], Pascal Turberg[3], Philip Brunner[4], Rodolphe Schlaepfer[3], and Claire Guenat[3]

ABSTRACT

The importance of engineers is increasingly recognized in soil science because of their implication in most important pedological processes. Furthermore, they contribute to ecological functions provided by soils in both natural and human-modified environments. In this review, we focus on the role of two ecosystem engineers: (1) plants, their root system, and associated microorganisms and (2) earthworms. First, we explain why they are considered as major soil engineers, and which variables (texture, porosity, nutrient, and moisture dynamics) control their activities in space and time (hotspots and hot moments). Then, their roles in three processes of soil formation are reviewed, namely, rock and mineral weathering, soil structure (formation, stabilization, and disintegration), and bioturbation. For each of them, the involved mechanisms that occur at different spatial scales (from local to landscape) are presented. On one hand, tree uprooting plays a key role in rock weathering and soil profile bioturbation. In addition, living and dead roots also contribute to rock alteration and aggregation. On the other hand, earthworms are mainly involved in the formation of aggregates and burrows through their bioturbation activities and to a less extent in weathering processes. The long-term effects of such mechanisms on soil heterogeneity, soil development, and pathways of pedogenesis are discussed. Finally, we show how these two main ecosystem engineers contribute to provisioning and regulating services. Through their physical activities of burrowing and soil aggregation, earthworms and plants increase plant productivity, water infiltration, and climate warming mitigation. They act as catalysts and provide, transform, and translocate organic matter and nutrients throughout the soil profile. Finally, due to inter- and intraspecific interactions and/or symbiosis with microorganisms (arbuscular fungi, bacteria), they enhance soil fertility, decrease parasitic action, and bioremediate some pollutants. Future research is, however, still needed for a better understanding of the relationships between adequate soil management, agricultural practices, and soil biota in a perspective of relevant maintenance and durability of ecological services.

[1]*Laboratory of Functional Ecology, Institute of Biology, University of Neuchâtel, Neuchâtel, Switzerland*

[2]*Institute of Construction and Environmental Technology, Haute école d'ingénierie et d'architecture, Fribourg, Switzerland*

[3]*Laboratory of Ecological Systems, ECOS & WSL, Ecole Polytechnique Fédérale, Lausanne, Switzerland*

[4]*Center for Hydrogeology and Geothermics, CHYN, University of Neuchâtel, Neuchâtel, Switzerland*

4.1. PLANTS AND EARTHWORMS ARE ECOSYSTEM ENGINEERS

4.1.1. Why Are Plants and Earthworms Called Ecosystem Engineers?

Ecosystem functioning and stability mainly depend on living organisms (biocenosis) being in equilibrium with their abiotic environment (biotope). The higher

Hydrogeology, Chemical Weathering, and Soil Formation, Geophysical Monograph 257, First Edition.
Edited by Allen Hunt, Markus Egli, and Boris Faybishenko.

DOI: 10.1002/9781119563952.ch4

biodiversity is, the greater are resistance and resilience of ecosystems facing disturbances. Organisms themselves affect their own habitat through their activities and then modulate species richness and heterogeneity of the environment, and thus the ecosystem functions at several spatiotemporal scales. Such ecological interactions are usually distinguished in (1) trophic relationships encountered in ecological networks such as food webs (Ings et al., 2009) and (2) nontrophic relationships implying organisms that affect others by creating, modifying, maintaining, or destroying habitats, called "ecosystem engineers" (C. G. Jones et al., 1997, 1994; Wright & Jones, 2006). Independently from their origin and their location, ecosystem engineers initiate habitat formation in the abiotic environment, therefore creating a modified structural state. Environmental heterogeneity is then enhanced with new ecological niche opportunities and increased biodiversity (C. G. Jones et al., 2010). Moreover, ecosystem engineers contribute not only to structural changes but also to abiotic and biotic changes, processes that are interdependent with feedback effects (C. G. Jones et al., 2010). Allogenic engineers thus modify living or non-living materials from one state to another, whereas autogenic engineers modify their own structure and morphology; some engineers are both allogenic and autogenic at the same time (Berke et al., 2010; C. G. Jones et al., 1994, 1997).

Focusing on terrestrial ecosystems, soils play a central role in major global biogeochemical cycles and host the largest diversity of organisms (Smith et al., 2015). Among these organisms, plants and invertebrates are key components of soil genesis, functions, and properties, and their occurrence in the pedon is crucial, focusing on their engineering activities. This is particularly the case in the so-called "humipedon," the upper soil layers enriched in organic matter (mainly O and A) that experience interactions between vegetation and soil (Zanella et al., 2018). The activity of soil organisms is particularly high in humipedons and is strongly involved in organic matter recycling and provisioning, as well as the formation of biogenic structures such as burrows and aggregates. Earthworms and plant roots are particularly involved in these processes that result in aggregates of different size, shape, and water stability. They act mainly as allogenic engineers and are responsible for physical modifications but may also be involved in biological and biochemical processes (see sections 4.1.2 and 4.1.3). Plants and earthworms also share common features regarding their engineering activities. For instance, both contribute to aggregate and burrow formation, especially in the top 30 cm of soil. In temperate ecosystems, they are thus the main soil engineers creating habitats for other organisms, such as small arthropods like springtails or mites (Cameron et al., 2013; Eisenhauer, 2010; Liu et al., 2013).

Both plants and earthworms produce also chemical substances: exudates (Bais et al., 2006) and mucus, respectively (Salmon, 2001), which are enriched in water, carbon (C), and nitrogen (N). These secretions are major drivers of bacterial diversity and activities (Wu et al., 2017) and contribute to enhanced enzymatic activities (Gianfreda, 2015; Le Bayon & Binet, 2006) but also modulate the attraction of small arthropods (Salmon, 2001). Plant roots interact with earthworms, and their concomitant activity increases aggregate stability (Fonte et al., 2012; Schomburg, Schilling, et al., 2018; Schomburg, Verrecchia, et al., 2018).

4.1.2. Relationships Between Selected Soil Properties, Plants, and Earthworms

4.1.2.1. Soil texture

Texture is one of the main soil properties driving the general behavior of ecosystem engineers. For plants, the optimum spatial distribution of roots depends mainly on soil water and nutrients, whose retention is largely influenced by soil texture. Higher clay fractions promote retention of water and sorption of nutrients, whereas a high sand content tends to enhance drainage (Weil & Brady, 2017). On the other hand, high clay contents can lead to soil compaction and prevent root development, or even access of water, whereas sharp sand grains may cause abrasion of fine root tips (Coleman et al., 2004). Lipiec et al. (2016) showed that rough sand increases the tortuosity of wheat roots and decreases root length, diameter, and even root dry weight. Whereas most cultivated plants require soil with balanced proportions of silt, sand, and clay, some plants tolerate more severe constraints, such as shrubs living in desert or coastal dunes, where sand is predominant. In northern California, a native shrub (*Ericameria ericoides*) is well adapted to its sandy environment by developing an efficient root network that helps to retain coarse organic matter and decreases aeolian erosion. In a coastal dune system, shrub species (*Lupinus chamissonis* and *Ericameria ericoides*) serve also as ecosystem engineers acting at multiple levels of biological organization through both positive and negative effects on richness and biomass of herbaceous plants (Cushmann et al., 2010). *Phalaris arundinacea* is also well known to grow up in alluvial sandy soils. This pioneer herbaceous species is especially resistant to drought conditions and has an efficient root system that protects riverbanks from erosion (Schomburg, Schilling, et al., 2018). In these alluvial ecosystems with regular erosion and/or deposits of sediments during flood events, riparian trees act both as allogenic and autogenic engineers. By trapping sand and organic matter, they can modulate soil moisture and accelerate landform formation, particularly island growth (Gurnell & Petts, 2006).

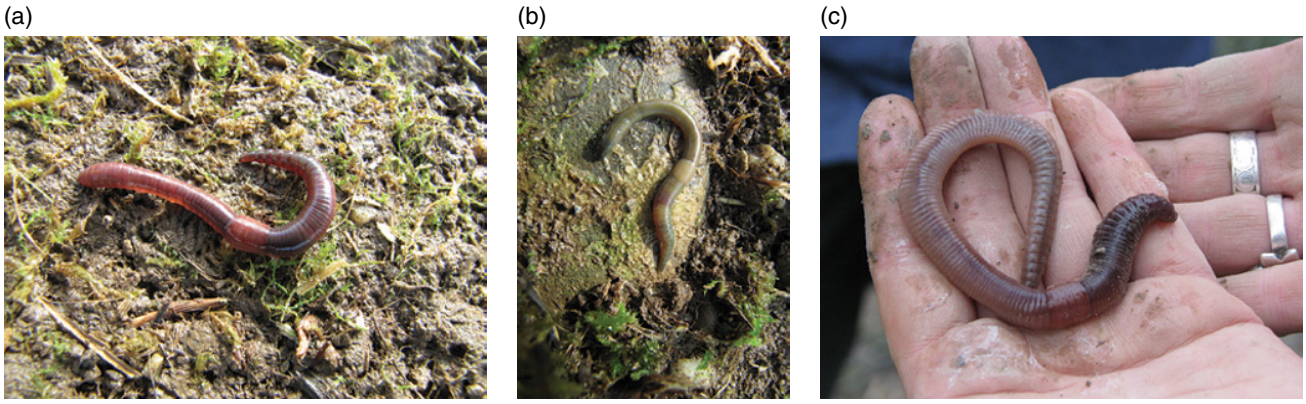

Figure 4.1 Ecological categories of earthworms. (a) Epigeic species, *Lumbricus rubellus*. (b) Endogeic species, *Allolobophora chlorotica* (c) Anecic species, *Lumbricus terrestris* (sometimes also classified as epi-anecic). Photos a and b, Claire Le Bayon; photo c, Géraldine Bullinger.

Soil texture also directly influences pedofauna. Indeed, soil macrofauna need material to construct biogenic structures (Bardgett, 2005; Coleman et al., 2004; Edwards & Bohlen, 1996; Lavelle et al., 1997, 2016), and through their selective choice of building components they often create gradients of organic and mineral particles in their living space (Edwards, 2004; Frouz et al., 2003; Jouquet et al., 2014, 2018; Véle et al., 2011). Earthworms select mainly both fine organic and mineral particles that they ingest and usually avoid soils with a high proportion of sand due to potential skin damages (Blouin, Hodson, et al., 2013; Blouin, Sery, et al., 2013; Curry & Schmidt, 2007; Lee, 1985). However, earthworms may also select sand grains that improve the grinding of leaf litter in their muscular gizzard (Marhan & Scheu, 2005; Schulmann & Tiunov, 1999). Depending on their ecological category, epigeic, endogeic, or anecic species as defined by Bouché (1977), earthworms differ in their habitat, not only in relation to soil depth but also to texture distribution in the soil profile.

Epigeics (Figure 4.1a) usually live in holorganic humus layers, dead wood, or composts, consuming and digesting organic matter without mixing it with mineral particles. They increase organic matter decomposition rates and act as ecosystem engineers by strongly affecting other litter-inhabiting organisms such as microfauna and microorganisms (Edwards, 2004). Endogeic species (Figure 4.1b) are mostly located in the shallow part of the soil and feed on soil and associated organic matter. To satisfy their dietary requirements, they actively move into the soil profile and build up long and dense horizontal branching burrows filled with their casts (Edwards & Bohlen, 1996). Endogeics prefer silty-clay soils, and their burrows and casts serve both as nutrient and habitat resources for plant roots (Lee, 1985). Anecic earthworms (Figure 4.1c) dig large vertical burrows that may extend several meters into the soil profile and thus prefer deep soils with fine texture (Bullinger-Weber et al., 2012; Salomé et al., 2011). These worms are especially efficient at burying fresh organic matter into their burrows using the strong muscles of their prostomium. By doing this, they largely contribute to the incorporation and the storage of organic materials in the subsoil. Through their bioturbation activity, and like endogeics, anecic earthworms excrete casts inside their permanent burrows, lining their walls with C-enriched mineral-organic material, but they may also seal their burrow openings with surface casts (middens). All these biogenic structures (burrows, casts, and middens) may serve as habitats for plant roots (and vice versa, as previously mentioned), but also for microfauna (springtails, mites, enchytraeids) and microorganisms (Eisenhauer, 2010). Besides these three ecological categories of earthworms, intermediate situations exist as epi-endogeic (*Lumbricus rubellus*) or endo-anecic ones (*Aporrectodea longa*), increasing the complexity of their role as ecosystem engineers.

4.1.2.2. Soil porosity

Soil porosity is the ratio between the volume of pores and the total soil volume. This porosity depends on several factors, including the size, shape, and arrangement of primary particles, as well as their cementing (Nimmo, 2004). Both burrowing by soil-dwelling animals and expansion of the root network create the largest biopores in soil. Soil aggregates also contribute to generating spaces into the soil; the intimate mixing of organic matter and mineral particles occurs either in the digestive system of animals, in particular earthworms, or by enmeshment of soil particles by roots, hyphae, and their exudates (Coleman et al., 2004; Milleret, Le Bayon, & Gobat, 2009; Milleret, LeBayon, Lamy, et al., 2009; Six et al., 2002; Tisdall & Oades, 1982). Consequently, vegetation

and earthworms largely contribute to forming porosity in the humipedon, where their activities prevail.

Roots influence the soil pore system, but they are controlled by both soil and root characteristics. Bodner et al. (2014) showed that coarse root systems increase macroporosity by 30%, whereas plants with dense, fine root systems heterogenize the pore space and increase microporosity. Therefore, not only plants but also their lifetimes (perennial versus annual) influence the formation and the permanence of root systems (Yunusa & Newton, 2003). After root decay, which varies according to plant communities, several size classes of biopores are freed up, becoming then available for air and water transport (Bodner et al., 2014; Horn & Smucker, 2005; Mitchell et al., 1995).

Earthworms are well known to enhance porosity as they move through the soil, thus decreasing soil density (Johnson-Maynard et al., 2007) and improving soil aeration (Edwards & Bohlen, 1996) and water infiltration (Capowiez et al., 2014; Shipitalo & Le Bayon, 2004). The number of burrows, as well as their length, diameter, and above all their connectivity, are essential to ensure an efficient hydraulic conductivity (Johnson-Maynard et al., 2002; Pérès et al., 2010). The amount of organic matter, the diet type of the worms, and the soil texture are the main components that drive length and branching of earthworm burrows (Amossé, Le Bayon, et al., 2015; Amossé, Turlberg, et al., 2015; Lavelle & Spain, 2001). These burrow systems then depend on soil features but also on earthworm species that construct burrows of different length, diameter, and branching (Amossé, Le Bayon, et al., 2015; Amossé, Turlberg, et al., 2015; Bastardie et al., 2005; Capowiez et al., 2014). Moreover, Felten and Emmerling (2009) showed that species interactions may occur between anecic and endogeic earthworms. For instance, the burrowing activity of the endogeic *Octolasion tyrtaeum* is significantly reduced in the presence of the anecic *Lumbricus terrestris* compared to the specific single treatment, revealing potential interspecific competition and trophic niche separation (Felten & Emmerling, 2009).

4.1.2.3. Soil nutrient balance

In the vicinity of roots. The soil directly in contact with roots (i.e., the rhizosphere, see section 1.3) has very different physical, chemical, and biological properties compared with the bulk soil. Through their multiple activities of ecosystem engineering, plants create a gradient of soil water content and nutrient availability around their root system (Gilad et al., 2007; Guttierez & Jones, 2006). Moreover, carbohydrates formed by photosynthesis are transferred into rhizospheric soil where they stimulate microbial activity; in turn, microbial enzymes decompose soil organic matter, thus releasing nutrients through priming effects (Bengtson et al., 2012; Finzi et al., 2015). Huang et al. (2014) showed that plant exudates modulate fungal and bacterial activities, which also influence root exudation. Consequences on soil nutrient balances are obvious, and Finzi et al. (2015) showed that root-accelerated mineralization and priming effect can account for up to one third of the total C and N mineralized in temperate forest soils. As most of the plants have symbiotic relationships, arbuscular mycorrhizal fungi also contribute to nutrient availability by facilitating interplant nutrient transfer (Le Bayon & Milleret, 2009; Wilson et al., 2006). Mimmo et al. (2018) focused on how chemical, biochemical, and physical interactions occurring in the rhizosphere affect nutrient availability. They showed that qualitative and quantitative composition of root exudates depends on many factors (plant species, plant age, environmental conditions, etc.) and influences the mobilization of nutrients.

In casts and burrows. The selective ingestion of organic material contributes to the concentration of organic matter in casts compared to the surrounding soil (Edwards & Bohlen, 1996; Le Bayon et al., 2017; Lee, 1985; van Groenigen et al., 2019). The addition of mucus during the gut transit stimulates microorganisms and consequently enzyme activities, which enhance organic matter mineralization (Blouin, Hodson, et al., 2013; Chapuis-Lardy et al., 2011; Shipitalo & Le Bayon, 2004). A meta-analysis on cast fertility (van Groenigen et al., 2019) highlighted that nutrient availability is higher in casts than in bulk soil (total elemental concentrations increased by 241% and 84% for mineral N and available P, respectively). In addition, pH, cation exchange capacity, and base saturation are also increased. Earthworm burrow linings are also enriched in organic matter and nutrients compared to non-ingested soil (Jégou et al., 1998). Mucus, composed mainly of water, C, and N, serves as a lubricant to improve the displacement of earthworms. This resource enrichment leads to the presence of specific and active communities of microflora and microfauna directly located in the burrow walls (Jégou et al., 1998; Savin et al., 2004; Tiunov & Scheu, 1999), and enzyme activities are enhanced over 2–3 mm all along the linings (Le Bayon & Binet, 2006). Consequently, casts and burrows are major sources of bio-avaiblable nutrients that could directly be absorbed by plant roots (Milleret, Le Bayon, & Gobat, 2009; Hoang et al., 2016). As an example, roots of *Achillea millefolium* preferentially occupy burrows of the anecic *Lumbricus terrestris* (Cameron et al., 2014). Moreover, earthworm burrows provide interconnected channels that make easier the penetration of roots into the soil and serve as a regeneration niche for plants in grassland ecosystems (Milcu et al., 2006).

4.1.3. Hotspots, Hot Moments in the Soil: Rhizosphere and Drilosphere

The soil biota modulates physical, chemical, and biological properties of soils in several ways (Blouin, Hodson, et al., 2013; Coleman et al., 2004; Lavelle et al., 1997). Five areas in the soil with specific properties were thus defined by Beare et al. (1995): (1) the rhizosphere in the vicinity of plant roots, (2) the detritusphere in the organic layers, (3) the aggregatusphere encompassing soil aggregates, (4) the porosphere considering voids, and finally (5) the drilosphere, e.g. the soil under the influence of earthworms. Such "hotspots" of intense biological activity, also called "hotspheres," may represent more than 90% of the total biological activity concentrated in less than 10% of the total soil volume (Beare et al., 1995). Kuzyakov and Blagodatskaya (2015) underlined that hotspots located in rhizosphere and drilosphere can be associated with "hot moments" defined as short-term events or sequences of events inducing accelerated process rates, as compared to average rates. Hot moments induce successions in microbial communities and intense intra- and interspecific competition, thus affecting C use efficiency, microbial growth, and turnover. Consequently, the intensification of fluxes increases and such hot moments result in priming effects localized in microbial hotspots (Kuzyakov & Blagodatskaya, 2015).

4.1.3.1. Rhizosphere

The rhizosphere is the soil volume that interacts directly and immediately with living plant roots, from nanometers to centimeters in radial distance from the root surface (Richter et al., 2007). Organisms found in the rhizosphere include bacteria, fungi, nematodes, protozoa, algae, and microarthropods (Lynch, 1990; Raaijmakers et al., 2009). This diversity is mainly due to rhizodeposits released by plant roots, and these deposits are the main food source for microorganisms that modulate population density and activities of other organisms. Rhizodeposition is a mixture of several compounds such as lysis products of root cells, insoluble mucilages, soluble root exudates, and volatile organic C (D. L. Jones et al., 2009). Soil microorganisms are chemotactically attracted to these spots enriched in C and tend to proliferate in this particular environment (Lugtenberg & Kamilova, 2009). In return, microbial activity in the rhizosphere is essential for plant functioning, as it assists plants in nutrients uptake and offers protection against pathogen attack (Berendsen et al., 2012; see section 4.3.2). Therefore, the rhizosphere is a zone of communication between soil microorganisms and roots that occurs and changes continuously due to nutrient solubility, soil transport, or plant uptake (Mimmo et al., 2018). Huang et al. (2014) reviewed interactions between plants and rhizosphere microbes, focusing on how root exudates are involved in these processes. Regarding soil structure at a smaller scale, Foster (1998) and Bruand et al. (1996) showed the importance of bacteria and roots in rearranging and stabilizing soil properties. Feeney et al. (2006) discovered that soil microbes and plant roots modify their habitats by changing size and clustering properties (i.e. spatial correlation) of soil pores. Consequently, the rhizosphere is not only a hotspot of biochemical processes and fluxes but also a hotspot and a hot moment regarding aggregate formation.

4.1.3.2. Drilosphere

The drilosphere is the part of soil the influenced by earthworm burrowing and casting activities (Blouin, Hodson, et al., 2013; Johnson-Maynard & Strawn, 2016). Earthworm burrows, surface casts, and casts produced within the soil profile belong to the drilosphere, but also earthworm gut contents, as well as symbionts (Ojha & Devkota, 2014). Hence, the drilosphere displays a high degree of relationship between microorganisms and micro-, meso-, and macroinvertebrates. Generally, anecics and endogeics are involved in the drilosphere formation due to their ecological behavior and selective ingestion of particles (Curry & Schmidt, 2007). The permanent burrow system of anecic species (about 2 to 3 m depth) is an important network of root growth activity and microbial dispersal, while endogeic species are more located around the rhizospheric region (Hirth et al., 1998). As a consequence, soil biogeochemical properties within the drilosphere differ from those of the bulk soil, similar to the rhizosphere (Lipiec et al., 2016). Linking drilosphere and rhizosphere functioning is then obvious. Earthworms enhance plant growth and plant quality (van Groenigen et al., 2014) that is closely linked to drilosphere-rhizosphere interactions. Kim et al. (2017) also showed that some combinations of earthworm-mediated soil aeration, modification of moisture conditions in the rhizosphere and drilosphere, and comminution of organic matter modify microbial communities and significantly affect the N cycle.

4.2. PLANTS AND EARTHWORMS ARE IMPLIED IN SOIL FORMATION

Among biota, plants and earthworms mainly contribute to pedogenetic processes as ecosystems engineers. According to Blum et al. (2018), pedogenesis is defined as "the processes of formation and development of soils, resulting in many different soil bodies. Soils with common particular characteristics form a distinctive soil group or soil type or soil unit." Processes of soil formation are subdivided into two main groups: transformation and

translocation. Transformation (weathering and formation of new minerals, decomposition and stabilization of organic matter, development of soil structure, ion exchange and redox processes, etc.) operates *in situ* and may involve some movement of substances over a very short distance (microns to millimeters). Translocation processes (transport of salts, organic and mineral substances, turbation, etc.) lead to displacement, sorting and mixing of solid matter within the soil profile (centimeters to meters). Both transformation and translocation are controlled by five main factors: climate, parental material, relief, biota, and time, resulting in the development of distinctive soil horizons with particular properties. These soil-forming factors determine both direction (pathways) and speed of pedogenesis.

In this section, we analyze the role of biota, in particular plants and earthworms, in key transformation and translocation processes during pedogenesis, namely, weathering of rocks and minerals, structure formation, and bioturbation. Although these processes can occur simultaneously and interact with each other, they are presented successively to facilitate understanding. In addition, for each process, the main impacts of earthworms, plants, roots, and their associated microorganisms are discussed. Nevertheless, the interactions between these two ecosystem engineers are not detailed.

4.2.1. Rock and Mineral Weathering

Weathering is a process involving both the breakdown of rocks and minerals and the formation of new secondary products. This cascade process creates continuous changes in the environment and gathers physical or mechanical disintegration, but also chemical alteration. The contribution of soil organisms is widely recognized, but it is difficult to disentangle the effects of purely mechanical from chemical weathering because they frequently act synergistically.

4.2.1.1. Plants

4.2.1.1.1. Mechanical weathering. Mechanical weathering is mainly due to root growth in length and girth, which causes axial and radial pressures during rock penetration. Swelling of roots, promoted by water absorption, can exert a huge pressure, slowly splitting a rock apart (Gabet et al., 2003). Fine roots penetrate joints and fractures of rocks, widen them, and contribute to the conversion of bedrock to regolith (fractured soil parental material), or to deepening/thickening regolith. However, the efficiency of this mechanism remains unclear because the tensile strength of most unweathered rock exceeds the pressure that growing roots can reach. Pawlik et al. (2016) reported that maximum radial pressures of root growth range from 0.51 to 0.9 MPa, while the tensile strength of crustal rocks ranges from 1 to 25 MPa. Tree uprooting also contributes to rock weathering and soil formation at different spatial scales, from landscape to fine scales such as pits and mounds (Šamonil, Král, et al., 2010; Šamonil, Tejnecký, et al., 2010). Mechanical and biochemical weathering processes are also closely linked because when roots have entered rocks, moisture fluxes along roots are then modified, and physiological functions of plants (respiration, nutrition, transpiration) immediately induce chemical weathering. Roots subsequently play a role of transmission pathways for moisture, nutrients, microorganisms, and heat. There is also an indirect input of water, organic matter, and bioconstructions in places presently or previously occupied by roots (Pawlik et al., 2016).

4.2.1.1.2. Chemical weathering. Soil organisms (lichens, mosses, plants, fungi, bacteria) greatly accelerate chemical weathering and mediate the formation of secondary minerals, but their relative *in situ* contribution is difficult to identify (Taylor et al., 2009). According to Pawlik et al. (2016), biochemical weathering prevails on mechanical weathering for two reasons. First, the main microorganisms implied in this process are widespread, can survive under extreme conditions, and can colonize niches unattainable by other organisms. Second, the fungal hyphal network associated with roots highly increases the space potentially subjected to biochemical weathering. Soil organisms act both directly and/or indirectly on weathering, either by producing compounds (organic acids, phenolic compounds, and protons) and/or by stimulating the activities of microorganisms that further accelerate weathering. Five key mechanisms of weathering exist: (1) root exudates containing protons and organic acids, (2) CO_2 release from root respiration, (3) organic acids and chelators from organic matter decomposition, (4) evapotranspiration that increases the flow of water bearing base cations and other nutrients to plants, and (5) reduction of erosion that also allows further soil development (see section 4.2.2).

Focusing on exudates, Landeweert et al. (2001) reported that low molecular weight organic acids produced by plant roots, bacteria, and fungi are considered to be the most important biological weathering agents in soils, driven by their acidifying and complexing capacities. Due to their high acid strength, citrate, malate, and oxalate are the strongest chelators of metals, including Al^{3+}, a central element in most mineral crystal lattices. All these organic acids are largely produced by fungi, bacteria, and roots, especially proteoid roots (Weisskopf et al., 2008). By contrast, medium- to high-molecular-weight organic acids, such as humic substances, are less effective for the dissolution of minerals.

Schulz et al. (2013) underlined that most of the studies on the role of microorganisms in weathering were

obtained through laboratory experiments and do not allow predicting the rates of weathering under field conditions. The rare field researches were conducted in pioneer stages of soil formation, as for example in the forefields of retreating glaciers, where biofilms of bacteria dissolve the siliceous bedrock by exuding organic acids (Schulz et al., 2013). Lichens also enhance the transformation of feldspars to clay, and mosses generally produce a great abundance of expandable clay minerals. Finally, Pawlik et al. (2016) suggested that mycorrhizal and saprotrophic fungi participate in weathering of feldspars and hornblends in granitic bedrocks and E horizons of podzolic soils.

4.2.1.2. Earthworms

4.2.1.2.1. Mineral weathering. The mean grain size of minerals in aggregates produced by earthworms is generally smaller than in the surrounding soil. This difference results from (1) a mechanical breakdown of mineral grains during their passage through the earthworm gut, or (2) a selective ingestion by earthworms (Curry & Schmidt, 2007; Edwards & Bohlen, 1996; see section 4.1.2). Actually, several experimental studies have shown the ability of earthworms to mediate mineral weathering. Suzuki et al. (2003) showed that pellets produced by epigeic earthworms (*Eisena fetida*) contain smaller and rounder grains than noningested grains. Moreover, due to its hardness, the disintegration of quartz is slower than that of K-feldspath. The mechanism of mineral weathering is, however, still unclear. It is unlikely due to proton dissolution because the earthworm's gut is at near neutral pH, probably promoted by a ligand produced by a digestive enzyme of the earthworm or by microbes contained in the earthworm's gut (Carpenter et al., 2007). However, earthworm species may play a role as demonstrated by Hodson et al. (2014). In this study, the anecic *Lumbricus terrestris* seems not to affect mineralogy, whereas both the epigeic *Eisenia veneta* and the endogeic *Allobophora chlorotica* clearly accelerate mineral weathering, especially on primary silicates (anorthite, biotite, and olivine) compared to secondary minerals (kaolinite, illite, and smectite).

4.2.1.2.2. Calcium cycling. Several authors underlined the role of earthworms in the biogeochemical cycling of calcium in soil. Many species secrete granules of calcium carbonate ranging from single calcite crystals to agglomerated granules up to 2.5 mm in diameter (Canti & Piearce, 2003). The rate of granule production differs between species and varies according to physico-chemical properties of the surrounding soil. Under suitable conditions, such granules are often preserved from dissolution, remain in soils for decades to thousands of years, and constitute a small but significant component of calcium storage in soil (Lambkin et al., 2011).

4.2.2. Soil Structure Formation, Stabilization, and Disintegration

Soil structure relates to the spatial arrangement of mineral and organic particles and their associated pores into groupings called aggregates or peds (Oades, 1993). Churchman (2010) considers that aggregation is a specific feature of soils and plays a fundamental role in terms of soil functioning. In fact, a well-developed structure can improve biodiversity in ecosystems; positively affect water storage capacity, infiltration, and aeration in soil; promote plant uptake and root growth; and increase the resistance to soil erosion.

There is a long history of research about aggregation processes (Six et al., 2004). In 1982, Tisdall and Oades proposed the concept of aggregate hierarchy that distinguishes primary particles (< 20 microns), microaggregates (20–250 microns) and macroaggregates (> 250 microns). This hierarchical concept is used worldwide (Totsche et al., 2018; Lehmann, Leifheit, et al., 2017; Lehmann, Zheng, et al., 2017), but soil aggregation is still a complex process that is controlled by an interplay of physical processes affecting the ecosystem, soil physico-chemical parameters (texture, amount of organic matter, calcium carbonate content, etc.), soil organisms, and interrelated factors: physical (drying-wetting, freezing-thawing), chemical (binding agents), and biological (fauna, roots, and microorganisms).

4.2.2.1. Soil structure and biota The chemical, physical, and biological effects of different key organisms (earthworms, termites, fungi, plant roots) in the formation, stabilization, and disintegration of soil structure has been recognized for decades. Biochemical mechanisms include particle adhering and orientation, surface sealing, and particle surface hydrophobicity. Biophysical mechanisms refer to soil compaction and compression, particle grinding and remolding, changes in water content, and particle entanglement by fungal hyphae.

4.2.2.2. Plants and soil aggregation Aggregation processes can be divided into five mechanisms that can interact and are dependent on the size of aggregates, namely, (1) root penetration, (2) changes in soil water regime, (3) agglutination, (4) dead root decomposition, and (5) root entanglement (Six et al., 2004). Several reviews discuss root-related processes that affect soil structure formation, stabilization, and disintegration (Angers & Caron, 1998; Degens, 1997; Six et al., 2004).

4.2.2.2.1. Root penetration. Root growth in pores and the soil matrix generates compressive and shear stresses, which can reach up to 2 MPa (Angers & Caron, 1998). Radial compression may reorient clay particles in the close

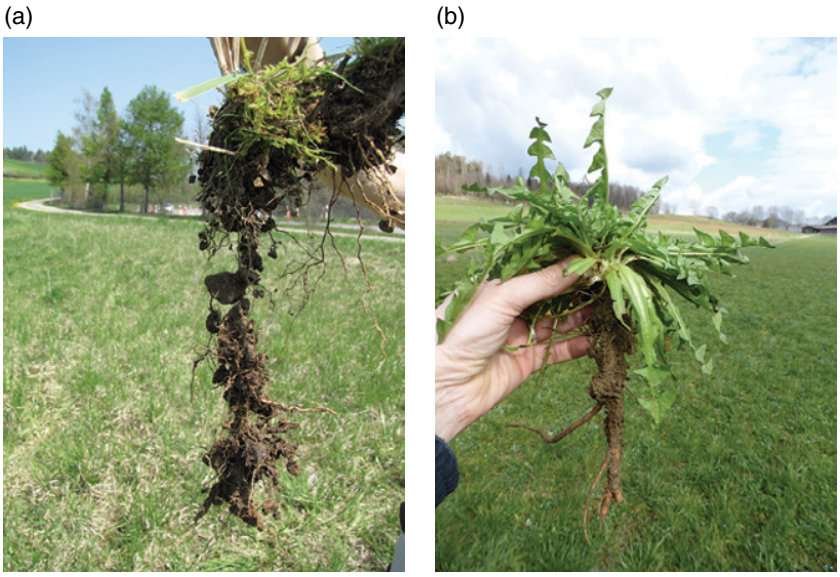

Figure 4.2 Two different root systems. (a) Well-branched roots of *Lolium sp*. (b) Taproot system of *Taraxacum sp*. Photos: Claire Le Bayon.

vicinity of roots, mostly in a 50–200 μm zone. These clay particles are then bound together by extracellular polysaccharides secreted by roots that induce the formation of microaggregates. By contrast, root penetration into relatively unstable macroaggregates may divide them in small units, thus decreasing the proportion of large aggregates. Depending on the type of vegetation, and especially root architecture (Figure 4.2), the overall influence of root penetration on aggregation may vary (Six et al., 2004). Similarly, the growth of fungal hyphae exerts a pressure on the surrounding soil and can potentially push and move particles and aggregates. However, there is still no report on this mechanism in either mycorrhizal or nonmycorrhizal fungi (Lehmann, Leifheit, et al., 2017).

4.2.2.2.2. Changes in soil water regime. Variations in frequency and amplitude of dry-wet cycles generally promote the formation of aggregates in soils. Six et al. (2004) cited a decrease (in the order of 10% to 20%) in aggregation due to changes in soil water status, for instance: (1) the water absorption by plants induces localized drying effects, which can promote bonds between root exudates and clays; (2) root exudates reduce the wetting rate by occluding pores or increasing pore tortuosity; (3) a preferential water flow occurs along living roots. Consequently, the shape of aggregates may differ; hence, physicogenic macroaggregates formed under sterilized, moist (20% of water holding capacity) conditions appear planar and angular at both macro- and microscales (Blankinship et al., 2016). In contrast, biogenic macroaggregates formed under live, dry (10% of water holding capacity) conditions are spherical with rounded edges. Lehmann, Leifheit, et al. (2017) hypothesized that mycorrhizal fungi may also affect the aggregation process by changing the soil water status. Water fluxes between the host plant and its symbionts can alternatively result in dampening or drying the soil of mycorrhizosphere.

4.2.2.2.3. Agglutination of particles and aggregates. Many products act as agents capable of gluing, or agglutinating, particles or aggregates. Transient (e.g. organic materials), temporary (e.g. roots, hyphae, and bacteria), and persistent compounds (e.g. amorphous iron and aluminum, aromatic humic material, complexes of clay-polyvalent metal-organic matter) perform as binding agents for aggregates (Tisdall & Oades, 1982). Anyway, their composition and origin have not yet been fully established.

According to Totsche et al. (2018), "gluing agents include all organic substances (e.g. polysaccharides, proteins, extracellular polymeric substances) responsible for the agglutination of subunits forming a micro-aggregate or a composite building unit". Fungi and bacteria secrete mucilaginous products containing polysaccharides and root exudates, which stimulate microbial activity and tight interactions between roots and microbes in the rhizosphere.

4.2.2.2.4. Dead roots. The decomposition of dead roots also promotes both aggregation and macropores, which can significantly influence moisture dynamics. Six et al. (2004) reported that most of the stable aggregates are formed after the senescence phase and not during the vegetative one. The magnitude of this effect depends on both the amount and decomposability of organic material.

4.2.2.2.5. Entanglement by root and fungal hyphae. Lehmann, Leifheit, et al. (2017) underlined that despite the evidence of this mechanism for both formation and stabilization of macroaggregates, entanglement by roots and fungi is still very poorly documented. One of the reasons is the difficulty of disentangling the influence of entanglement from other associated processes, in particular exudation promoted by roots and fungi. The mycelial meshwork helps to stabilize enmeshed soil and aggregates, and hyphae confer shear resistance and tensile strength to soil units. In addition, the regenerative capacity and longevity of mycelia increase their resistance against disturbances. With time, soil structure changes and unstable macroaggregates can thus disintegrate into microaggregates due to the penetration of roots. In addition, vesicular arbuscular mycorrhizae (VAM) could also participate to degrade mucilages and thus destabilize aggregates. However, data measuring the turnover of aggregates are still rare.

4.2.2.3. Implication of plants in organic matter stabilization

According to traditional viewpoints, organic matter persists in soil for a longer or shorter time depending on its chemical complexity and composition. New models about the persistence of organic matter in soil have recently emerged (Schmidt et al., 2011). Indeed, molecular structure alone does not control C residence times, as C stability mainly depends on the physicochemical and biological environment (water availability, pH, presence of degraders, etc.). The key role of roots and rhizosphere in the dynamics of organic matter is also emphasized. First, plant roots and rhizosphere inputs make a large contribution to soil organic matter. Second, root-derived C would be more retained than aboveground inputs (leaves or needles). Third, root and mycorrhizae are very efficient in physicochemical interactions with soil particles. Finally, the fresh root inputs could be considered as primers leading to a more rapid decomposition of older organic matter.

4.2.2.4. Earthworms and soil aggregation

By moving in the soil matrix and mixing, ingesting, and excreting soil and organic matter particles, earthworms create biogenic structures, such as burrows and casts (Lavelle et al., 1997). Through their selective feeding behavior, earthworms ingest fine organic and/or mineral particles and contribute to organic matter degradation and intimate incorporation to clay and silt (Brown et al., 2000). Casts and burrows thus form new habitats usually enriched in organic matter and nutrients that act as hotspots of biological activity. Endogeic and anecic earthworms are particularly implied in aggregate and burrow buildup, whereas epigeic species localized in holorganic layers create mainly organic pellets (Bouché, 1977; Lee, 1985). Earthworm activity depends on both soil temperature (Uvarov et al., 2011; Whalen et al., 2004) and moisture (Edwards & Bohlen, 1996; Kanianska et al., 2016), and they tend to decrease their activity substantially in summer (Potvin & Lilleskov, 2017). However, species such as *Lumbricus terrestris* may remain active throughout winter.

4.2.2.4.1. Mucus and gut processes. At the body surface and in the forepart of the gut, earthworms secrete polysaccharide compounds called mucus (Chapuis-Lardy et al., 2011; Lee, 1985). The amount or quality of the epidermal mucus may vary according to ecological earthworm categories and ingested substrates (Trigo et al., 1999). The mucus of *Allolobophora chaetophora* is, for instance, composed of 69% proteins and peptides and 31% carbohydrates (Cortez & Bouché, 1987). Zhang et al. (2016) demonstrated that mucus samples from three earthworm species (*Eisenia fetida*, *Aporrectodea trapezoides*, and *Amynthas pingi*) may contain 16 amino acids that could activate microorganisms (Bityutskii et al., 2012; Blouin, Hodson, et al., 2013; Chapuis-Lardy et al., 2011; Shipitalo & Le Bayon, 2004). The exoenzymes produced by ingested microorganisms enhance the degradation of complex organic matter during its passage through the gut and thus enhance the capacity of the worm to assimilate nutrients (Edwards, 2004). Moreover, *Lumbricus terrestris* has its own enzyme pool, independent from the microorganisms present in the ingested soil; this is notably the case for alcaline phosphatases implied in organic phosphorus mineralization (Le Bayon & Binet, 2006).

4.2.2.4.2. Cast production. According to Lee (1985), earthworms can process up to 25% of the A horizon in 1 year through the production of casts within the soil profile and onto the surface (often called surface casts or middens when particularly enriched in organic matter debris; see Figure 4.3). Most of the studies focused on surface casts whose amount of production may reach a mean of 40,000 kg/ha/yr (based on 19 studies; Feller et al., 2003). In a maize plot, Le Bayon and Binet (1999) calculated that surface-cast production may reach 34 kg dwt/yr per kg of earthworms (fwt) in the presence of anecic *Lumbricus terrestris* and the endogeic *Aporrectodea caliginosa* as the dominant species. In a grassland in Luxembourg, a total amount of 195.6 ton/ha of casts was measured, 58% from endogeic earthworms and 42% from anecics (Zangerlé et al., 2016). According to Zorn et al. (2008), endogeic species may deposit up to 95% casts underground. Therefore, earthworms act as a living bioreactor, and the duration of digestion probably affects the first step of microaggregate disruption before being remoulded in larger aggregates (Six et al., 2002, 2004). As example, the pressure applied to soil may reach 259 Pa in

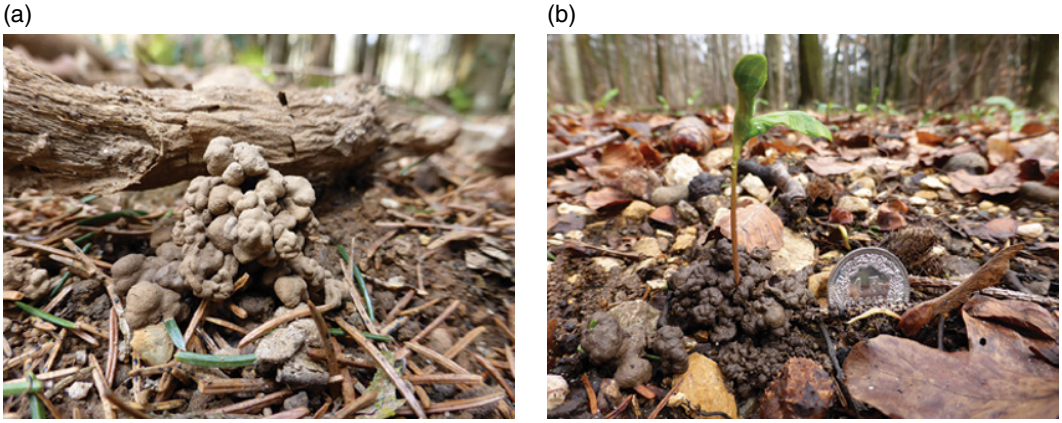

Figure 4.3 Surface-casts of anecic earthworms. (a) Different colors of structures indicate the variable organic matter content. (b) Casts constitute hotspots of available nutrients for plant growth, here beneficial for a seedling of *Fagus sylvatica*. Photos: Claire Le Bayon.

the gut of *Aporrectodea rosea* (McKenzie & Dexter, 1987) and, concomitant to the addition of mucus, can lead to the disruption of existing interparticle water and cation bridges within aggregates (Shipitalo & Protz, 1988, 1989). Consequently, the soil fabric is reorganized in the intestines of earthworms (Barois et al., 1993), and this remolding, combined with the high water content, may explain why fresh, moist casts are usually less water-stable than non-ingested soil (Le Bayon & Binet, 2001; Le Bayon et al., 2002; Marinissen & Dexter, 1990; Shipitalo & Protz, 1988). With time, casts are stabilized by a combination of physical (thixotropic hardening), chemical (secretion of amorphous calcium carbonate as a binding agent), and biological processes (microbial polysaccharides). This stabilization also depends on earthworm species, and Schrader and Zhang (1997) noted that water-stable aggregation is significantly higher in casts of *Lumbricus terrestris* than in casts of *Aporrectodea caliginosa*. They also noticed that the tensile strength of casts is positively correlated with the clay and carbonate content of the parent soil, while for water-stable aggregation the correlation is inverse. The initial soil texture also plays a major role in cast content (see section 4.1.2). In pioneer environments such as floodplains with regular sediment deposits, epigeic earthworms (mainly *Lumbricus rubellus*) are the first engineers involved in soil structure in the short term. If the texture is favorable (mostly silt dominated), anecic and endogeic earthworms may then colonize the different soil layers, improving physical and nutrient conditions and creating long-term stable aggregates (Bullinger-Weber et al., 2007).

4.2.2.4.3. Burrowing. Burrows (Figure 4.4) result from two main processes: (1) the soil is crumbly enough to allow earthworms to dig into it without ingesting it or (2) the soil is so compact that they have to ingest it before excreting casts. Through peristaltic movements (Lee, 1985), earthworms exert a strong lateral pressure to push particles aside during burrow construction, and anecic species such as *Lumbricus terrestris* and *Aporrectodea nocturna* but also the endogeic *Aporrectodea caliginosa* are especially efficient in this process (Edwards & Bohlen, 1996). The speed of burrowing depends on soil texture, a silty texture being more favorable than a clayish one (Edwards, 2004), but also on temperature, water content, and topography, as well as on ecological categories (Bastardie et al., 2005; Perreault & Whalen, 2006). Capowiez et al. (2015) showed that endogeic earthworms make more extended burrow systems, which are more highly branched, less continuous, and of smaller diameter than those of anecic earthworms. Three main characteristics significantly influence water infiltration: burrow length, burrow number, and bioturbation volume, but the connectivity of galleries seems also essential to ensure efficient hydraulic conductivity (Pérès et al., 2010).

Estimations of the number of burrows in temperate regions range from 100 to 800 per square meter (Lavelle, 1988), with a mean ranging between 50 to 200 burrows per square meter (Edwards & Bohlen, 1996). Some species such as *Lumbricus terrestris* make nearly vertical permanent burrows up to 12 mm in diameter and 2.4 m deep in which they can live over several years (Edwards & Bohlen, 1996; Lavelle & Spain, 2001; Lee, 1985). *Lumbricus terrestris* intensively reuses its continuous, vertical burrows (Grigoropoulou & Butt, 2012; Nuutinen, 2011). These burrows can have several entrances, as they are directly underneath surface casts, which can block the entrance. Earthworm burrows function as soil macropores, improving soil aeration (Knight et al., 1992), infiltration (Stockdill, 1966), and water-holding capacity, especially in casts and burrow linings. Quantifying the number of burrows or soil macropores might thus be a

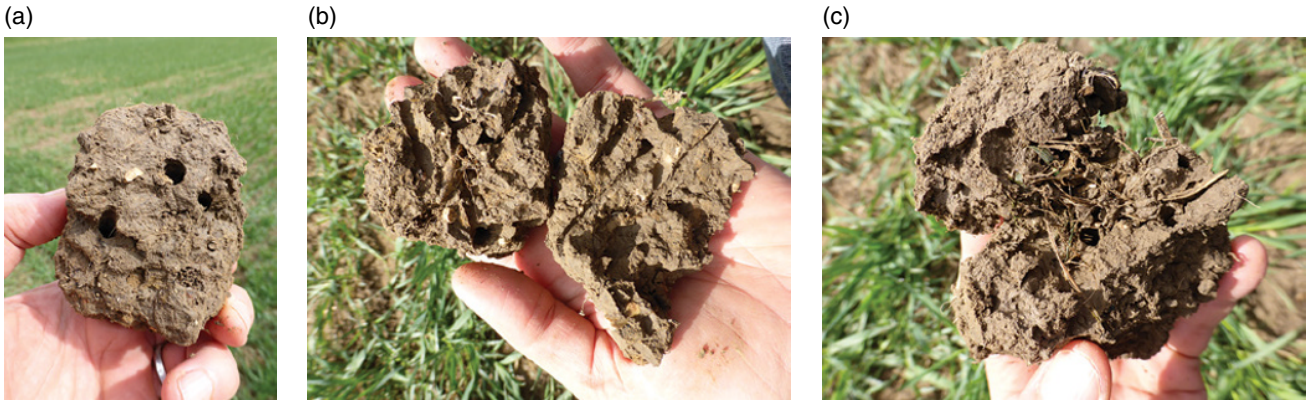

Figure 4.4 Burrows of anecic earthworms. (a) Burrow openings of anecic earthworms. (b) Burrow linings when the soil clod is cut in two parts. (c) Coarse fragments of organic matter are clearly visible inside worm galleries. Photos: Claire Le Bayon.

good indicator of current or past earthworm activity (Pérès et al., 2010).

4.2.2.4.4. Aggregate disintegration. When polysaccharides and other organic gluing agents are mineralized, the breakdown of soil macroaggregates increases over time (Ge et al., 2001; Guggenberger et al., 1996). Surface casts are primarily disrupted by climatic events, such as raindrop impacts and wet-dry cycles (Binet & Le Bayon, 1998; Le Bayon et al., 2002), by cattle trampling (Decaëns, 2000), when small earthworms such as Eudrilidae and enchytraeids dig burrows into the casts (Blanchart et al., 1997; Topoliantz et al., 2000), or if casts themselves come unstable as soon as they are produced. The case of belowground casts of *Metaphire posthuma* was highlighted by Botinelli et al. (2010). As they disintegrate, these weak casts are more susceptible to dispersion and may lead to a rapid compaction of the soil after rainfall events, especially in Asia due to the high intensity of monsoon rainfall. This subsequent formation of a compact and impermeable layer was well studied in tropical regions by Blanchart et al. (1997, 1999) and Chauvel et al. (1999). Blanchart et al. (1997) and Rossi (2003) also showed the existence of "compacting" earthworm species versus "decompacting" species that play a key role in the regulation of savannah soil structure. Compacting species produce large globular casts that are expected to compact the soil, whereas decompacting species produce fine granular casts that can decrease soil bulk density (Blanchart et al., 1993, 1997). Guéi et al. (2012) demonstrated that despite the presence of both, soil water infiltration rate may increase. Thus, the preservation of earthworm species belonging to contrasting functional groups appears essential for the maintenance of stable soil structure in agro-tropical ecosystems (Guéi et al., 2012).

4.2.3. Bioturbation due to Plant and Earthworm Activities: Impacts on Soil Differentiation and Development

The concept of bioturbation in soil was initially introduced by Darwin (1881) for earthworms and Schaler (1891, in Wilkinson et al., 2009) for plants. Bioturbation by terrestrial organisms generates the physical displacement of materials and results in a redistribution and reorganization of these components, as well as a dissemination of organisms in soil. Wilkinson et al. (2009) classified bioturbation into primary processes (soil production, soil mixing) and secondary processes (mounding) resulting from previous ones. Soil production occurs both directly by mass displacement and indirectly by weathering of parental material. Soil mixing refers to material movements within or between soil horizons, and mounding to depositions on the soil surface (Wilkinson et al., 2009). Moreover, abiotic processes (aeolian and water erosion) and biotic ones (dismantlement of mounds by predators or by cattle trampling) affect redistribution of soil in mounds. In addition, secondary fabric features (burrows, root channels) result from recent and/or past bioturbation within or between horizons (Wilkinson et al., 2009).

Present at different spatio-temporal scales, bioturbation can contribute to a progressive or a regressive pathway of soil development (Gobat & Le Bayon, 2013), but until now only few models integrate the calculation of soil development rates. Alexandrovskiy (2007) applied such a turbational model to Chernozems, soils in which horizon mixing by burrowing animals is particularly remarkable.

For each ecosystem engineer (first plants and then earthworms), we describe in the following sections (1) the mechanisms of bioturbation taken in consideration, (2) the effects of bioturbation on soil heterogeneity at different spatial scales, and (3) the effects of bioturbation on

soil development. Finally, a discussion about their effects on pedogenesis pathways (trajectories) is tackled.

4.2.3.1. Bioturbation by plants: Mechanisms

Gabet et al. (2003) identified five mechanisms of bioturbation performed by plants: (1) root expansion during growth, (2) decay and infilling of former root channels, (3) settling of the soil due to water extraction by roots, (4) agitation of the plant during storms, and (5) uprooting. The first three mechanisms occur within a horizon at different spatial scales, ranging from mineral particles to aggregates (see sections 4.2.1 and 4.2.2). While agitation is poorly known, uprooting is better understood. This mechanical process is due to wind, snow overload, root decomposition, or fall of adjacent trees. The probability that trees are uprooted is a function of soil depth, and is maximum for shallow soils (about 35 cm depth), and then decreases to nil for soils over 1.5 m depth (Gabet et al., 2003). This phenomenon has been especially studied in Podzols, whereas little research was conducted on Cambisols or on soils with hydromorphic features (Kooch et al., 2015; Kooch, Hosseini, et al., 2014; Kooch, Zaccone, et al., 2014; Šamonil et al., 2015; Šamonil, Král, et al., 2010; Šamonil, Tejnecký, et al., 2010; 2015; Schaetzl et al., 1990). The uprooting and fall of a tree usually creates a pit where the roots were previously located and an adjacent mound resulting from slumping of the displaced and decaying root plate (Figure 4.5). Slump and erosion of material from the root plate are known as bioturbation processes. The paired pit/mound system is highly variable in size and longevity and the study of its chronosequences provides a good understanding of the effects of uprooting over time (Bormann et al., 1995; Coyle et al., 2017; Kooch et al., 2015; Kooch, Hosseini, et al., 2014; Kooch, Zaccone, et al., 2014; Pawlik et al., 2016; Šamonil et al., 2015; Samonil, Král, et al., 2010; Šamonil, Tejnecký, et al., 2010; Schaetzl et al., 1990; Valtera & Schaetzl, 2017). Moreover, cross-sectional drawings of pit/mound pairs describe changes in spatial patterns. Depending on climatic conditions and site characteristics, this system covers from 0.1% to 90% of the forest area and its total disintegration can be very rapid (5 to 10 years in humid tropics) or can exceed 500 to 1000 years in many other environments. Consequently, the effects of uprooting on soil heterogeneity and soil development are thus highly variable (Schaetzl et al., 1990).

Figure 4.5 Tree uprooted following a wind event two years ago. Soil (Cambisol) and calcareous stones are still attached to the roots (east of France). Photo: Claire Guenat.

4.2.3.2. Bioturbation by plants: Effects on soil heterogeneity and soil development

According to Pierret et al. (2007), root growth reorients and packs particles, and enhances macroporosity. By (re) using paths of less mechanical resistance, including former root channels, root growth leads to the formation of a specific environment, which significantly differs both chemically and biologically from the bulk soil. Water uptake by plants can also induce moisture gradients that, depending on soil texture and mineralogy, contribute to increase soil heterogeneity. These *in situ* mechanisms generate transformations leading to displacement of materials over a very short distance (Blum et al., 2018). At the pedon scale, tree uprooting can change the spatial arrangement of soil, from single horizons to the entire soil profile, which can be completely reversed or even destroyed. Moreover, the heterogeneity of the soil profile is increased by the displacement of stones, brought to the soil surface and then buried under deposits produced by collapse of the root plate and erosion (Schaetzl et al., 1990). Uprooting may also modify chemical and biological properties, especially in pits and mounds that differ compared to adjacent and undisturbed soils. For example, in a beech forest in northern Iran, Kooch, Hosseini, et al. (2014) showed that organic C, total N, water content, microbial respiration, texture, density, and biomass of earthworms are significantly greater in pits than in mounds and undisturbed soils.

4.2.3.3. Postuprooting pedogenesis

The effects of uprooting diminish over time and new sequences of horizons, reflecting the process of postuprooting pedogenesis, are gradually developed. According to Šamonil et al. (2015), progressive soil development is generally observed, whereas regressive development is rare, but pedogenetic processes in pits and mounds can show diverse evolutionary trajectories. The evolution is nonlinear, and postuprooting pedogenesis is more rapid in pits because weathering is generally more efficient (Šamonil et al., 2015; Schaetzl et al., 1990). In podzolic soils, postuprooting pedogenesis is determined by C

dynamics (accumulation versus decomposition) driven by the frequency of disturbance (Bormann et al., 1995). Similar divergences of pedogenetic trajectories are also reported by Schaetzl et al. (1990) for other types of soils (Inceptisols instead of Podzosols) and extrapolations, as well as simulations of soil development, thus remain challenging (Šamonil et al., 2015).

4.2.3.4. Bioturbation by earthworms: Mechanisms and rates

All processes of bioturbation are carried out by earthworms relative to ecological activity, species, and also abundance and biomass. The first assessments come from Darwin (1881) in the United Kingdom, with annual rates (ton/ha) of 19–40 for mounding, 26 for mixing, and 2–152 for burial of soil. Also in the United Kingdom, Evans (1948) estimated mounding rates from 3 to 63 tons/ha/yr and mixing rates from 5 to 53 tons/ha/yr. In France, Bouché (1981) obtained equivalent rates (20 tons/ha/yr) for mounding and mixing. Finally, in Australia, under humid subtropical conditions, mixing rates reach 127 tons/ha/yr, while mound rates are very low (5–6 tons/ha/yr).

4.2.3.5. Bioturbation by earthworms and pedogenesis

According to Cunha et al. (2016), earthworms affect pedogenesis in two main ways: first by modifying soil profile through bioturbation and second by their effects on decomposition and nutrient cycling. Earthworms need from 5 to 20 years to turn over once the topsoil (0–30 cm) in grasslands under temperate climate. For the same climate conditions, Feller et al. (2003) suggested that earthworms can potentially move about 40 cm of soil to the surface each century. As burrows facilitate the transfer of water, air, and nutrients, earthworm bioturbation enhances organic matter incorporation and microorganisms' redistribution, which in turn enhances the homogenization of the soil's profile and properties. However, material movements by earthworms is greater in the uppermost layers than in deeper soil layers (Muller-Lemans & van Dorp, 1996). Consequently, both structuration and accumulation of organic matter occur mainly in topsoil. Besides, the composition of casts differs from the surrounding soil, increasing thus soil heterogeneity (Pierret et al., 2007). Finally, as coarse materials (gravels, stones) cannot be ingested by earthworms, they tend to be gradually buried under topsoil casts and may thus form a stone layer, increasing soil profile differentiation (Wilkinson et al., 2009).

4.3. PLANTS AND EARTHWORMS CONTRIBUTE TO SOIL ECOSYSTEM SERVICES

The notion of ecosystem service (ES) is increasingly used in the evaluation of environmental sustainability. ESs are commonly defined as the "benefits people obtain from the ecosphere and its ecosystems" (MEA, 2005) and are listed in four broad categories: provisioning (e.g. production of food and water), regulating (control of water, climate and disease, C sequestration), cultural (spiritual and recreational benefits), and supporting services (e.g. habitat, biodiversity, nutrient cycles). The first three categories directly affect people, whereas the supporting services are there to maintain the other services (Dominati et al., 2010).

4.3.1. Provisioning Services

There is a strong link between soil and agricultural productivity, and therefore most studies about soil-related ESs include an assessment of provisioning ES such as biomass production (da Silva et al., 2018). Many components of biodiversity affect ES delivery. For example, earthworms act as catalysts in improving crop yield, but their performance depends on the amount of crop residues, earthworm density, and rate of fertilization (Sharma et al., 2017). On their side, plants influence soil by the vast majority of organic matter upon which the rest of soil life depends, and they also deform the soil under the mechanical action of roots by elongation or radial growth (Briat & Job, 2017).

In a meta-analysis about the effect of earthworms on plant production across the globe, van Groenigen et al. (2014) showed that earthworms favor the availability of N from crop residues that stimulate plant growth. In this case, organic fertilizers prevail over inorganic ones. In another study reporting an inoculation of *Lumbricus terrestris*, the effect on plant productivity was increased by 20% to 60% of both plant cover and biomass (Forey et al., 2018). van Groenigen et al. (2014) also mentioned that in pastures with presence of plants capable of symbiotic N_2 fixation such as legumes, the positive effect of earthworms was smaller, and their influence on pasture productivity disappeared. Earthworms are also known to increase phosphorus availability in their casts and burrows (Le Bayon & Milleret, 2009). Earthworm density also has a significant effect on aboveground plant biomass, particularly at high densities (> 400 individuals per m^2; van Groenigen et al., 2014). In pots containing homogenized and repacked soil, the earthworm effect on aboveground biomass was almost twice as high as in undisturbed soils, meaning a positive effect on plant growth and thus on productivity (van Groenigen et al., 2014). Management practices with objectives of sustainable intensification of agriculture should be encouraged to maintain earthworm populations in good health. For example, low-input farming systems in the tropics, and to a lesser extent organic farming systems, vary in terms of habitat quality for earthworms (van Groenigen et al., 2014), and large application rates of organic manure of

high-quality crop residues provide excellent conditions for bioturbation. Tillage can also have detrimental effects on soil life, especially when the soil is inverted, leading to strong effects on soil organisms such as epigeic earthworms (Orgiazzi et al., 2016). No-till systems may thus support larger and more diverse earthworm communities. Epigeic and anecic species particularly benefit from no-till, as endogeic ones may support tillage systems that incorporate crop residues. Earthworms are also affected by tillage frequency: physical injuries or death by tools, exposure to predators and/or desiccation or frost by soil inversion, destruction of burrows, changes in soil physical conditions, and soil compaction (Orgiazzi et al., 2016).

Plants also contribute meaningfully to provisioning ESs because they are the major source of C inputs into the soil through litterfall and whole-plant senescence, as well as root-derived C loss by living plants (Bowsher et al., 2018). In fact, root exudates and sloughed-off cells influence N availability (mainly nitrates) and thus plant growth (Jackson et al., 2008). Therefore, when N supply and access is high through nitrification, N losses may be lower, thereby increasing the provisioning services provided by plant-microbes-soil transformations without any application of fertilizers (Jackson et al., 2008). Moreover, plant roots in up to 80% of plant families may establish symbiotic interactions with VAM that not only improve the growth of plants through uptake of available soil phosphorus and other mineral nutrients but also prevent erosion by stabilizing aggregates (Gianinazzi et al., 2010). However, management practices as soil tillage negatively affects VAM through different mechanisms such as propagation, extraradical hyphae, and colonized root segments. Tillage also destroys the mycelial network and affects nutrient acquisition, especially during early stages of crop growth (Orgiazzi et al., 2016). In this context, future prospects on sustainable management have to be considered. In fact, by 2050, the global population is projected to be 50% larger than now with a global grain demand that follows this trend. Further increases in agricultural yields are essential but not at the cost of losing important ecosystem functions. Due to their great diversity, soil organisms such as earthworms and plants offer many resources, but this natural capital must be further investigated in order to preserve them and evaluate the range of possible strategies.

4.3.2. Regulating Services

4.3.2.1. Health and soil fertility

According to FAO (2015), "healthy soils are a basic prerequisite to meeting varied needs for food, biomass (energy), fiber, fodder, and other products and to ensuring the provision of essential ecosystem services in all regions of the world." In this context, biodiversity is among the main factors responsible for the provision of regulating and supporting ESs. Earthworms and plants are important in maintaining soil health, and higher plants are the major primary producers of biomass, C, and energy released into the soil. According to FAO (2015), earthworms could give general indications of relative changes in soils and may thus be considered as indicators and should be included in the global soil health monitoring scheme. Moreover, they have been shown to enhance soil fertility through a variety of mechanisms including increased nutrient availability, enhanced soil aggregation, and water availability, as well as improved stress tolerance and pest regulation (Fonte et al., 2019). Earthworms also degrade and decompose dead organic matter through mineralization that takes place in their guts, thus enhancing natural stocks of nutrients available for soil biota for chemical reactions, which enables humans to live in a stable, healthy, and resilient environment (Dominati et al., 2010).

4.3.2.2. Water infiltration

Plant roots and earthworms greatly influence soil formation and maintenance by the creation of soil structure (see section 4.2), particularly at the very first stages of pedogenesis, providing physical support to plants, animals, and human infrastructures. Pioneer plants allow accumulation of organic matter from their dead materials essential for the development of a first soil horizon, the A layer, and contribute to soil stabilization through the physical action of very fine roots. Earthworm burrows in the upper layer are suitable for root growth. With their foraging activity, earthworms create preferential flow paths for water, thus decreasing propensity for overland flow, which leads to a reduction of erosion risk, especially in mature soils where large amounts of water infiltrate and are retained in the pore spaces.

However, due to continuous alteration and erosion processes, new soils are formed while old ones are slowly disaggregated by erosion. The notion of inherited and newly formed soils can be illustrated through floodplains submitted to perturbations such as flood events. Plants in particular are very efficient at agglutinating organic and mineral particles and thus increasing topsoil structural stability (Schomburg, Schilling, et al., 2018; Schomburg, Verrecchia, et al., 2018). This is of crucial importance in the case of floodplain restoration projects that aim to rehabilitate water flow regulation, meaning attenuation of runoff and discharge rates, water storage for flow regulation, and mass flow regulation (i.e. erosion protection). For example, Schindler et al. (2016) indicated that renaturation has strong positive impacts on other regulation services such as lateral floodplain reconnection and creation of natural habitats, which is of particular importance in biodiversity conservation.

In fact, earthworms and plants have a great influence on flood mitigation. Soil structure and more precisely

macroporosity play a major role in soil water infiltration and processes related to the control of drainage runoff (Pelíšek, 2018). Earthworms also interact with plant species composition, and certain plant functional groups could significantly alter variations in soil hydraulic properties. According to Fischer et al. (2014), soil infiltration capacity increases with legumes but decreases with grasses, probably due to roots that modify the pore structure. Further, legumes enhance earthworm activity while grasses suppress it. Functional groups of plants may thus affect earthworm and root activities.

The role of plants in soil hydraulic properties is also important for water extraction from deeper layers through roots. Plants adapt to drought by rapidly developing fine roots or by increasing the activity and efficiency of deep roots, which are responsible for water uptake (Teuling et al., 2006). Transpiration is also a key to understand ecosystem functioning and particularly the efficiency of plants to use and store water. Models are usually prevalent (Guderle & Hildebrandt, 2015) with assumptions to determine the sink term for root water uptake in soil water flow models. In this way, standard measurements (e.g. soil water content profiles) are used for the estimation of evapotranspiration and root water uptake. Through transpiration, plants act as a natural regulator of water fluxes between soil and atmosphere, and these fluxes allow as much as 60% of whole land precipitation to return to the atmosphere (Javaux et al., 2013).

4.3.2.3. Tritrophic interactions

Soils provide habitat for thousands of species that regulate pest control and dangerous disease vectors (Dominati et al., 2010). This regulating ES is principally related to soil properties and the biological processes driving inter- and intraspecific interactions (symbiosis, competition). As an example, Blouin et al. (2005) emphasized the importance of belowground interactions in plant ecophysiology. In a controlled experiment, the decrease in rice growth caused by a parasitic nematode was suppressed in the presence of earthworms. Earthworms thus enhanced the tolerance of roots to nematodes, and the expected inhibition of photosynthesis was suppressed. It has also been shown that earthworms are also able to generate hormones and subsequently may render a plant tolerant to parasitic nematodes by inhibiting the gene responsible for the repair of damaged roots, preventing plant death after all leaves have shrivelled (Orgiazzi et al., 2016). More generally, the preservation of existing natural enemies by choosing cultural, mechanical, or selective chemical controls that do not harm beneficial species should be favored (Orgiazzi et al., 2016). With their capacity for creating plant-microbe interactions, plants also present benefits in terms of disease reduction. They may specifically attract microbes for their own benefit as, for example, through the recruitment of different groups of plant-associated microbes that promote plant growth. These microbes then undergo host-specific adaptations, such as highly specialized mutualism leading to a better tolerance to pathogens (Orgiazzi et al., 2016).

4.3.2.4. Pollution control

Soil invertebrates can also be used as indicators of land use, soil fertility, or soil pollution. Their size, limited rapidity in soil displacement, and slow recolonization make them attractive as bioindicators (Paoletti, 1999). Indeed, earthworms are currently considered good environmental indicators or biomarkers of pollution exposure (Pérès et al., 2011).

Earthworms have been applied to the bioremediation of heavy metal pollution. Indeed, some earthworm species are tolerant to heavy metals and can perform their ecological functions and complete their life history in contaminated soil (Mo et al., 2012; Xu et al., 2018). For instance, *Amynthas gracilis* allowed evaluating the bioavailability and ecotoxicity of many soil pollutants (Parelho et al., 2018). Actually, earthworms provide a realistic indication of pollution as they are exposed to soil pollutants in both the soil surface and the deeper topsoil layers through their epi-endogeic activity. This permits an integrated overview of the biological effects of livestock soil pollutants on soil organisms.

When plants perform bioremediation, this cleaning service is called phytoremediation. First, some plants remove pollutants from soil and concentrate them in harvestable part. This phytoremediation is possible because soil organisms increase the heavy metal solubility (Lone et al., 2008). Strong retention is observed in some plants, such as white lupin roots for cadmium pollution, while translocation occurs in wheat (Page et al., 2006). The translocation process may be due to a response of plants that recognize cadmium as a toxic compound. This leads to the activation of defense mechanisms (sequestration in the vacuole or in the cell walls). Plants can then be harvested and materials can be incinerated. Second, phyto-stabilization may be achieved through a suitable zone that plants provide around their roots. In this case, pollutants are stabilized and immobilized by roots that use different mechanisms, such as the production of specific substances, to render heavy metals harmless (Orgiazzi et al., 2016).

4.3.2.5. Climate warming mitigation

Climate change is one of the most important challenges that humans will have to face in the next decades (Orgiazzi et al., 2016). By creating large pores and tunnels, earthworms influence gas permeability and the activity of the microbiota responsible for the natural emission of greenhouse gases (CH_4 and N_2O). Through heterotrophic

respiration, earthworms release CO_2, but reduced-tillage practices support the activities of earthworms and then promote C sequestration and N cycling in soils. Storage of C also increases through the conversion of croplands into permanent pastures and the management of plant diversity. Plants also have an impact on the C cycle by converting CO_2 and light energy into chemical energy (sugars). However, the release of CO_2 into the atmosphere is currently higher than fluxes into C sinks, leading to an unbalanced global C budget. Concerning the N cycle, chemical engineers such as bacteria convert the organic N into mineral forms that may be absorbed by plants. Earthworms also influence the N cycle by their structures particularly rich in nutrients and then become preferred sites for a number of soil processes, such as N fixation (Orgiazzi et al., 2016). Both earthworms and plants are part of complex interactions that lead to the decomposition of organic matter, releasing C and N in the soil. They are consequently crucial to biogeochemical cycles and therefore to the regulation of atmospheric composition and climate.

ESs are needed because they meet a human need. However, this vision remains an anthropocentric concept of ESs, and relatively few studies specify how and what human needs are potentially and actually fulfilled by ESs, particularly by ecosystem engineer services. The contribution of earthworms and plants to soil services is now clearly proven. However, further investigations are needed. For example, Bertrand et al. (2015) noted that the impact of pesticides on earthworms was not completely understood because of lack of field data on the exposure of earthworms to currently used molecules. Additional long-term field studies are essential to understanding the impact of earthworms on crop production (Bertrand et al., 2015). Moreover, major gaps remain in understanding the identification of all the ESs provided by each ecological group of earthworms to other soil biota. Finally, a cost-benefit analysis to assess the monetary values generated by earthworm populations at local or regional scale for economic evaluation should be taken into consideration (Sharma et al., 2017).

4.4. CONCLUSIONS AND FUTURE PROSPECTS

Ecosystem engineers, especially plants and earthworms, are strongly involved in pedogenesis and ecosystem functions. Their bioturbation activities as autogenic and allogenic engineers are at the core of humipedon formation and dynamics, with wide-reaching consequences on provisioning and regulating services at the ecosystem level. Soils as habitats for ecosystem engineers constitute an environment of high spatial and temporal heterogeneity, both in terms of physical properties as well as biological activities. This creates complex interactions, resulting in hotspots and hot moments. The understanding of these temporal and spatial processes is in its infancy. Gaps of knowledge still exist regarding the relationships between soil food webs and engineering processes. In this way, Sanders et al. (2014) underlined that ecosystem engineering species constitute potentially the most important bridges between trophic and nontrophic interactions. Therefore, there is considerable potential for advancing our understanding of engineer and food web dynamics areas via their integration. This approach is crucial to improve our knowledge about soil management in order to better predict the impact of changes in human practices and/or climate warming on ecosystem services.

REFERENCES

Alexandrovskiy, A. L. (2007). Rates of soil-forming processes in three main models of pedogenesis. *Revista Mexicana de Ciencias Geologicas*, *24*(2), 283–292. http://www.scielo.org.mx/scielo.php?script=sci_arttext&pid=S1026-87742007000200014&lng=es&nrm=iso

Amossé, J., Le Bayon, R. C., & Gobat, J.-M. (2015). Are urban soils similar to natural soils of river valleys? *Journal of Soils and Sediments*, *15*(8), 1716–1724. https://doi.org/10.1007/s11368-014-0973-6

Amossé, J., Turberg, P., Kohler-Milleret, R., Gobat, J.-M., & Le Bayon, R. C. (2015). Effects of endogeic earthworms on the soil organic matter dynamics and the soil structure in urban and alluvial soil materials. *Geoderma*, *243–244*, 50–57. https://doi.org/10.1016/j.geoderma.2014.12.007

Angers, D. A., & Caron J. (1998). Plant induced changes in soil structure processes and feedbacks. *Biogeochemistry*, *42*, 55–72. https://doi.org/10.1023/A:1005944025343

Bais, H. P., Weir, T. L., Perry, L. G., Gilroy, S., & Vivanco, J. M. (2006). The role of root exudates in rhizosphere interactions with plants and other organisms. *Annual Review of Plant Biology*, *57*(1), 233–266. https://doi.org/10.1146/annurev.arplant.57.032905.105159

Bardgett, R.D. (2005). *The biology of soil: A community and ecosystem approach*. Oxford and New York: Oxford University Press.

Barois, I., Villemin, G., Lavelle, P., & Toutain, F. (1993). Transformation of soil structure through *Pontoscolex corethrurus* (Oligochaeta) intestinal tract. *Geoderma*, *56*, 57–66. https://doi.org/10.1016/0016-7061(93)90100-Y

Bastardie, F., Capowiez, Y., & Cluzeau, D. (2005). 3D characterisation of earthworm burrow systems in natural soil cores collected from a 12-year-old pasture. *Applied Soil Ecology*, *30*, 34–46. https://doi.org/10.1016/j.apsoil.2005.01.001

Beare, M. H., Coleman, D. C., Crossley, D. A., Hendrix, P. F., & Odum, E. P. (1995). A hierarchical approach to evaluating the significance of soil biodiversity to biogeochemical cycling. *Plant and Soil*, *170*(1): 5–22.

Bengtson, P., Barker, J., & Grayston, S.J. (2012). Evidence of a strong coupling between root exudation, C and N availability, and stimulated SOM decomposition caused by rhizosphere priming effects. *Ecology and Evolution*, *2*, 1843–1852. https://doi.org/10.1002/ece3.311

Berendsen, R. L., Pieterse, C. M. J., & Bakker, P. A. H. M. (2012). The rhizosphere microbiome and plant health. *Trends in Plant Science*, *17*, 478–486. https://doi.org/10.1016/j.tplants.2012.04.001

Berke, S. K., Mahon, A. R., Lima, F. P., Halanych, K. M., Wethey, D. S., & Woodin, S. A. (2010). Range shifts and species diversity in marine ecosystem engineers: Patterns and predictions for European sedimentary habitats: Polychaete range shifts. *Global Ecology and Biogeography*, *19*(2), 223–232. https://doi.org/10.1111/j.1466-8238.2009.00509.x

Bertrand, M., Barot, S., Blouin, M., Whalen, J., de Oliveira, T. & Roger-Estrade, J. (2015). Earthworm services for cropping systems. A review. *Agronomy for Sustainable Development*, *35*(2), 553–567. https://doi.org/10.1007/s13593-014-0269-7

Binet, F., & Le Bayon, R. C. (1998). Space-time dynamics in situ of earthworm casts under temperate cultivated soils. *Soil Biology and Biochemistry*, *31*(1), 85–93. https://doi.org/10.1016/S0038-0717(98)00109-6

Bityutskii, N. P., Maiorov, E. I., & Orlova, N. E. (2012). The priming effects induced by earthworm mucus on mineralization and humification of plant residues. *European Journal of Soil Biology*, *50*, 1–6. https://doi.org/10.1016/j.ejsobi.2011.11.008

Blanchart, E., Albrecht, A., Alegre, J., Duboisset, A., Villenave, C., et al. (1999). Effects of earthworms on soil structure and physical properties. In: P. Lavelle, L. Brussard, & J. Hendrix (Eds.), *Earthworm management in tropical agrogroecosystems* (pp. 149–172). London: CAB International.

Blanchart, E., Bruand, A., & Lavelle, P. (1993). The physical structure of casts of *Millsonia anomala* (Oligochaeta: Megascolecidae) in shrub savanna soil (Côte d'Ivoire). *Geoderma*, *56*, 119–132. https://doi.org/10.1016/0016-7061(93)90104-S

Blanchart, E., Lavelle, P., Braudeau, E., Le Bissonnais, Y., & Valentin, C. (1997). Regulation of soil structure by geophagous earthworm activities in humid savannas of Côte d'Ivoire. *Soil Biology and Biochemistry*, *29*(3–4), 431–439. https://doi.org/10.1016/S0038-0717(96)00042-9

Blankinship, J. C., Fonte, S. J., Six, J., & Schimel, J. P. (2016). Plant versus microbial controls on soil aggregate stability in a seasonally dry ecosystem. *Geoderma*, *272*, 39–50. https://doi.org/10.1016/j.geoderma.2016.03.008

Blouin, M., Hodson, M. E., Delgado, E. A., Baker, G., Brussaard, L., Butt, K. R., et al. (2013). A review of earthworm impact on soil function and ecosystem services: Earthworm impact on ecosystem services. *European Journal of Soil Science*, *64*(2), 161–182. https://doi.org/10.1111/ejss.12025

Blouin, M., Sery, N., Cluzeau, D., Brun, J.-J., & Bédécarrats, A. (2013). Balkanized research in ecological engineering revealed by a bibliometric analysis of earthworms and ecosystem services. *Environmental Management*, *52*(2), 309–320. https://doi.org/10.1007/s00267-013-0079-8

Blouin, M., Zuily-Fodil, Y., Pham-Thi, A.-T., Laffray, D., Reversat, G., Pando, A., et al. (2005). Belowground organism activities affect plant aboveground phenotype, inducing plant tolerance to parasites. *Ecology Letters*, *8*(2), 202–208. https://doi.org/10.1111/j.1461-0248.2004.00711.x

Blum, W., Schad, P., & Nortcliff, S. (2018). *Essentials of soil science: Soil formation, functions,use and classification (World Reference Base)*. Borntrager Science Publishers.

Bodner, G., Leitner, D., & Kaul, H.-P. (2014). Coarse and fine root plants affect pore size distributions differently. *Plant and Soil*, *380*, 133–151. https://doi.org/10.1007/s11104-014-2079-8

Bottinelli, N., Henry-des-Tureaux, T., Hallaire, V., Mathieu, J., Benard, Y., Duc Tran, T., et al. (2010). Earthworms accelerate soil porosity turnover under watering conditions. *Geoderma*, *156*, 43–47. https://doi.org/10.1016/j.geoderma.2010.01.006

Bormann, B. T., Spaltenstein, H., McClellan, M. H., Ugolini, F. Cromack Jr., K. C., & Nay, S. M. (1995). Rapid soil development after wind throw disturbance in Pristine forests. *The Journal of Ecology*, *83*(5), 747. https://doi.org/10.2307/2261411

Bouché, M. B. (1977). Stratégies lombriciennes. In: U. Lohm & T. Person (Eds.), *Soil organisms as components of ecosystems.* Ecological Bulletins no. 25 (pp. 122–132). Stockholm: Swedish Natural Science Research Council.

Bouché, M. B. (1981). Contribution des lombriciens aux migrations d'éléments dans les sols tempérés. *Colloques Internationaux du Centre National de Recherche Scientifique*, *303*, 145–153.

Bowsher, A. W., Evans, S., Tiemann, L. K., & Friesen, M. L. (2018). Effects of soil nitrogen availability on rhizodeposition in plants: A review. *Plant and Soil*, *423*(1), 59–85. https://doi.org/10.1007/s11104-017-3497-1

Briat, J.-F., & Job, D. (2017). *Les sols et la vie souterraine: Des enjeux majeurs en agroécologie*. Quae.

Brown, G. G., Barois, I., & Lavelle, P. (2000). Regulation of soil organic matter dynamics and microbial activity in the drilosphere and the role of interactions with other edaphic functional domains. *European Journal of Soil Biology*, *36*(3–4), 177–198. https://doi.org/10.1016/S1164-5563(00)01062-1

Bruand, A., Cousin, I., Nicoullaud, B., Duval, O., & Begon, J. C. (1996). Backscattered electron scanning images of soil porosity for analysing soil compaction around roots. *Soil Science Society of America Journal*, *60*, 895–901. doi:10.2136/sssaj1996.03615995006000030031x

Bullinger-Weber, G., Guenat, C., Salomé, C., Gobat, J.-M., & Le Bayon, R. C. (2012). Impact of flood deposits on earthworm communities in alder forests from a subalpine floodplain (Kandersteg, Switzerland). *European Journal of Soil Biology*, *49*, 5–11. https://doi.org/10.1016/j.ejsobi.2011.08.001

Bullinger-Weber, G., Le Bayon, R. C., Guenat, C., & Gobat, J.-M. (2007). Influence of some physicochemical and biological parameters on soil structure formation in alluvial soils. *European Journal of Soil Biology*, *43*(1), 57–70. https://doi.org/10.1016/j.ejsobi.2006.05.003

Cameron, E. K., Cahill, J. F., & Bayne, E. M. (2014). Root foraging influences plant growth responses to earthworm foraging. *PLoS One*, *9*, e108873. https://doi.org/10.1371/journal.pone.0108873

Cameron, E. K., Proctor, H. C., & Bayne, E. M. (2013). Effects of an ecosystem engineer on belowground movement of microarthropods. *PLoS ONE*, *8*(4), e62796. https://doi.org/10.1371/journal.pone.0062796

Canti, M. G., & Piearce, T. G. (2003). Morphology and dynamics of calcium carbonate granules produced by different earthworm species: The 7th international symposium on earthworm ecology, Cardiff, Wales, 2002. *Pedobiologia*, *47*(5–6), 511–521. https://doi.org/10.1078/0031-4056-00221

Capowiez, Y., Bottinelli, N., Sammartino, S., Michel, E., & Jouquet, P. (2015). Morphological and functional characterisation of the burrow systems of six earthworm species (Lumbricidae). *Biology and Fertility of Soils*, *51*(7), 869–877. https://doi.org/10.1007/s00374-015-1036-x

Capowiez, Y., Sammartino, S., & Michel, E. (2014). Burrow systems of endogeic earthworms: Effects of earthworm abundance and consequences for soil water infiltration. *Pedobiologia*, *57*(4–6), 303–309. https://doi.org/10.1016/j.pedobi.2014.04.001

Carpenter, D., Hodson, M. E., Eggleton, P., & Kirk, C. (2007). Earthworm induced mineral weathering: Preliminary results. *European Journal of Soil Biology*, *43*, S176–S183. https://doi.org/10.1016/j.ejsobi.2007.08.053

Chapuis-Lardy, L., Le Bayon, R. C., Brossard, M., López-Hernández, D., & Blanchart, E. (2011). Role of soil macrofauna in phosphorus cycling. In E. Bünemann, A. Oberson, & E. Frossard (Eds.), *Phosphorus in Action* (Vol. 26, pp. 199–213). https://doi.org/10.1007/978-3-642-15271-9_8

Churchman, G. J. (2010). The philosophical status of soil science. *Geoderma*, *157*(3–4), 214–221. https://doi.org/10.1016/j.geoderma.2010.04.018

Chauvel, A., Grimaldi, M., Barros, E., Blanchart, E., Desjardins, T., Sarrazin, M., et al. (1999). Pasture damage by an Amazonian earthworm. *Nature*, *398*, 32–33.

Coleman, D. C., Crossley, D. A., & Hendrix, P. F. (2004). *Fundamentals of soil ecology*, 2nd ed. San Diego: Academic Press.

Cortez, J., & Bouché, M. (1987). Composition chimique du mucus cutané de *Allolobophora chaetophora chaetophora* (Oligochaeta: Lumbricidae). *Compte Rendu de l'Académie des Sciences de Paris, Série III*, *305*, 207–210.

Coyle, D. R., Nagendra, U. J., Taylor, M. K., Campbell, J. H., Cunard, C. E., Joslin, A. H., et al. (2017). Soil fauna responses to natural disturbances, invasive species, and global climate change: Current state of the science and a call to action. *Soil Biology and Biochemistry*, *110*, 116–133. https://doi.org/10.1016/j.soilbio.2017.03.008

Cunha, L., Brown, G. G., Stanton, D. W. G., Da Silva, E., Hansel, F. A., Jorge, G., et al. (2016). Soil animals and pedogenesis: The role of earthworms in anthropogenic soils. *Soil Science*, *181*(3/4), 110–125. https://doi.org/10.1097/SS.0000000000000144

Curry, J., & Schmidt, O. (2007). The feeding ecology of earthworms—a review. *Pedobiologia*, *50*, 463–477. http://dx.doi.org/10.1016/j.pedobi.2006.09.001

Cushman, J., Waller, J. C., & Hoak, D. R. (2010). Shrubs as ecosystem engineers in a coastal dune: Influences on plant populations, communities and ecosystems. *Journal of Vegetation Science*, *21*(5), 821–831. https://doi.org/10.1111/j.1654-1103.2010.01196.x

Darwin, C. R. (1881). *The formation of vegetable mould through the action of worms with observations on their habits*. London: Murray.

da Silva, R. T., Fleskens, L., van Delden, H., & van der Ploeg, M. (2018). Incorporating soil ecosystem services into urban planning: Status, challenges and opportunities. *Landscape Ecology*, *33*(7), 1087–1102. https://doi.org/10.1007/s10980-018-0652-x

Decaëns, T. (2000). Degradation dynamics of surface earthworm casts in grasslands of the eastern plains of Colombia. *Biology and Fertiity of Soils*, *32*(2), 149–156. https://doi.org/10.1007/s003740000229

Degens, B. P. (1997). Macro-aggregation of soils by biological bonding and binding mechanisms and the factors affecting these: A review. *Soil Research*, *35*, 431–460. https://doi.org/10.1071/S96016

Dominati, E., Patterson, M., & Mackay, A. (2010). A framework for classifying and quantifying the natural capital and ecosystem services of soils. *Ecological Economics*, *69*(9), 1858–1868. https://doi.org/10.1016/j.ecolecon.2010.05.002

Edwards, C. A. (2004). *Earthworm ecology*, 2nd ed. Boca Raton, FL: CRC Press, St. Lucie Press.

Edwards, C. A., & Bohlen, P. J. (1996). *The biology and ecology of earthworms*. London: Chapman and Hall.

Eisenhauer, N. (2010). The action of an animal ecosystem engineer: Identification of the main mechanisms of earthworm impacts on soil microarthropods. *Pedobiologia*, *53*(6), 343–352. https://doi.org/10.1016/j.pedobi.2010.04.003

Evans A. C. (1948). The identity of earthworms stored by moles. *Proceedings of the Zoological Society of London*, *118* (2), 356–359. https://doi.org/10.1111/j.1096-3642.1948.tb00381.x

FAO (2015). Revised World Soil Charter: 10.

Feeney, D. S., Crawford, J. W., Daniell, T., Hallett, P. D., Nunan, N., Ritz, K., et al. (2006). Three-dimensional microorganization of the soil–root–microbe system. *Microbial Ecology*, *52*(1), 151–158. https://doi.org/10.1007/s00248-006-9062-8

Feller, C., Brown, G. G., Blanchart, E., Deleporte, P., & Chernyanskii, S. S. (2003). Charles Darwin, earthworms and the natural sciences: Various lessons from past to future. *Agriculture, Ecosystems & Environment*, *99*(1–3), 29–49. https://doi.org/10.1016/S0167-8809(03)00143-9

Felten, D., & Emmerling, C. (2009). Earthworm burrowing behaviour in 2D terraria with single- and multi-species assemblages. *Biology and Fertility of Soils*, *45*, 789–797. https://doi.org/10.1007/s00374-009-0393-8

Finzi A., Abramoff, R.Z., Iller, K. S., Brzostek, E. R., Darby, B. A., Kramer, M. A., et al. (2015). Rhizosphere processes are quantitatively important components of terrestrial carbon and nutrient cycles. *Global Change Biology*, *21*, 2082–2094. https://doi.org/10.1111/gcb.12816

Fischer, C., Roscher, C., Jensen, B., Eisenhauer, N., Baade, J., Attinger, S., et al. (2014). How do earthworms, soil texture and plant composition affect infiltration along an experimental plant diversity gradient in grassland? *Plos One*, *9*(6), e98987. https://doi.org/10.1371/journal.pone.0098987

Fonte, S. J., Botero, C., Quintero, D. C., Lavelle, P., & van Kessel, C. (2019). Earthworms regulate plant productivity and the efficacy of soil fertility amendments in acid soils of the Colombian Llanos. *Soil Biology and Biochemistry*, *129*, 136–143. https://doi.org/10.1016/j.soilbio.2018.11.016

Fonte, S. J., Quintero, D. C., Velásquez, E., & Lavelle, P. (2012). Interactive effects of plants and earthworms on the physical

stabilization of soil organic matter in aggregates. *Plant and Soil*, *359*(1–2), 205–214. https://doi.org/10.1007/s11104-012-1199-2

Forey, E., Chauvat, M., Coulibaly, S. F. M., Langlois, E., Barot, S., & Clause, J. (2018). Inoculation of an ecosystem engineer (Earthworm: *Lumbricus terrestris*) during experimental grassland restoration: Consequences for above and below-ground soil compartments. *Applied Soil Ecology*, *125*, 148–155. https://doi.org/10.1016/j.apsoil.2017.12.021

Foster, R. C. (1998). Microenvironments of soil organisms. *Biology and Fertility of Soils*, *6*, 89–203. https://doi.org/10.1007/BF00260816

Frouz, J., Holec, M., & Kalcík, J. (2003). The effect of *Lasius niger* (Hymenoptera, Formicidae) ant nest on selected soil chemical properties. *Pedobiologia*, *47*, 205–212. https://doi.org/10.1016/j.geoderma.2015.10.022https://doi.org/10.1078/0031-4056-00184

Gabet, E. J., Reichman, O. J., & Seabloom, E. W. (2003). The effects of bioturbation on soil processes and sediment transport. *Annual Review of Earth and Planetary Sciences*, *31*(1), 249–273. https://doi.org/10.1146/annurev.earth.31.100901.141314

Ge, F., Shuster, W. D., Edwards, C. A., Parmelee, R. W., & Subler, S. (2001). Water stability of earthworm casts in manure- and inorganic-fertilizer amended agroecosystems influenced by age and depth. *Pedobiologia*, *45*, 12–26. https://doi.org/10.1078/0031-4056-00064

Gianfreda, L. (2015). Enzymes of importance to rhizosphere processes. *Journal of Soil Science and Plant Nutrition*, *15*(2), 283–306. http://dx.doi.org/10.4067/S0718-95162015005000022

Gianinazzi, S., Gollotte, A., Binet, M.-N., van Tuinen, D., Redecker, D., & Wipf, D. (2010). Agroecology: The key role of arbuscular mycorrhizas in ecosystem services. *Mycorrhiza*, *20*(8), 519–530. https://doi.org/10.1007/s00572-010-0333-3

Gilad, E., von Hardenberg, J., Provenzale, A., Shachake, M., & Meron, E. (2007). A mathematical model of plants as ecosystem engineers. *Journal of Theoretical Biology*, *244*, 680–691. https://doi.org/10.1016/j.jtbi.2006.08.006

Gobat, J. M., & Le Bayon, R. C. (2013). Structures des sols et êtres vivants. In *Les sols et leurs structures: Observations à différentes échelles* (pp. 39–62). Paris: QUAE Editions, INRA.

Grigoropoulou, N., & Butt, K. R. (2012). Assessment of burrow re-use by *Lumbricus terrestris* L. through field experimentation. *Zeszyty Naukowe*, *15*, 43–51.

Guderle, M., & Hildebrandt, A. (2015). Using measured soil water contents to estimate evapotranspiration and root water uptake profiles: A comparative study. *Hydrology and Earth System Sciences*, *19*(1), 409–425. https://doi.org/10.5194/hess-19-409-2015

Guéi, A. M., Baidai, Y., Tondoh, J. E., & Huising, J. (2012). Functional attributes: Compacting vs decompacting earthworms and influence on soil structure. *Current Zoology*, *58*(4), 556–565. https://doi.org/10.1093/czoolo/58.4.556

Guggenberger, G., Thomas, R.J., & Zech, W. (1996). Soil organic matter within earthworm casts of an anecicendogeic tropical pasture community, Columbia. *Applied Soil Ecology*, *3*, 263–274. https://doi.org/10.1016/0929-1393(95)00081-X

Gurnell, A., & Petts, G. (2006). Trees as riparian engineers: The Tagliamento river, Italy. *Earth Surface Processes and Landforms*, *31*(12), 1558–1574. https://doi.org/10.1002/esp.1342

Gutiérrez, J. L., & Jones, C. G. (2006). Physical ecosystem engineers as agents of biogeochemical heterogeneity. *BioScience*, *56*, 227–236. https://doi.org/10.1641/0006-3568(2006)056[0227:PEEAAO]2.0.CO;2

Hirth, J. R., McKenzie, B. M., & Tisdall, J. M. (1998). Roots of perennial ryegrass (*Lolium perenne*) influence the burrowing of the endogeic earthworm, *Apporrectodea rosea*. *Soil Biology and Biochemistry*, *14*, 2181–2183. https://doi.org/10.1016/S0038-0717(98)00074-1

Hoang, D. T. T., Razavi, B. S., Kuzyakov, Y., & Blagodatskaya, E. (2016). Earthworm burrows: Kinetics and spatial distribution of enzymes of C-, N- and P- cycles. *Soil Biology and Biochemistry*, *99*, 94–103. https://doi.org/10.1016/j.soilbio.2016.04.021

Hodson, M. E., Black, S., Brinza, L., Carpenter, D., Lambkin, D. C., Mosselmans, J. F. W., et al. (2014). Biology as an agent of chemical and mineralogical change in soil. *Procedia Earth and Planetary Science*, *10*, 114–117. https://doi.org/10.1016/j.proeps.2014.08.039

Horn, R., & Smucker, A. (2005). Structure formation and its consequences for gas and water transport in unsaturated arable and forest soils. *Soil and Tillage Research*, *82*(1), 5–14. https://doi.org/10.1016/j.still.2005.01.002

Huang, X.-F., Chaparro, J. M., Reardon, K., F., Zhang, R., Shen, Q., & Vivanco J. M. (2014). Rhizosphere interactions: Root exudates, microbes, and microbial communities. *Botany*, *92*, 267–275. https://doi.org/10.1139/cjb-2013-0225

Ings, T. C., Montoya, J. M., Bascompte, J., Blüthgen, N., Brown, L., Dormann, C. F., et al. (2009). Review: Ecological networks - beyond food webs. *Journal of Animal Ecology*, *78*(1), 253–269. https://doi.org/10.1111/j.1365-2656.2008.01460.x

Jackson, L. E., Burger, M., & Cavagnaro, T. R. (2008). Roots, nitrogen transformations, and ecosystem services. *Annual Review of Plant Biology*, *59*(1), 341–363. https://doi.org/10.1146/annurev.arplant.59.032607.092932

Javaux, M., Couvreur, V., Vanderborght, J., & Vereecken, H. (2013). Root water uptake: From three-dimensional biophysical processes to macroscopic modeling approaches. *Vadose Zone Journal*, *12*(4). https://doi.org/10.2136/vzj2013.02.0042

Jégou, D., Cluzeau, D., Balesdent, J., & Tréhen, P. (1998). Effects of four ecological categories of earthworms on carbon transfer in soil. *Applied Soil Ecology*, *9*, 249–255. https://doi.org/10.1016/S0929-1393(97)00057-7

Johnson-Maynard, J. L., Graham, R. C., Wu, L., & Shouse, P. J. (2002). Modification of soil structural and hydraulic properties after 50 years of imposed chaparral and pine vegetation. *Geoderma*, *110*, 227–240. https://doi.org/10.1016/S0016-7061(02)00232-X

Johnson-Maynard, J. L., & Strawn, D. G. (2016). Linking physical and biogeochemical properties and processes in the drilosphere. *Soil Science*, *181*, 126–132. doi: 10.1097/SS.0000000000000142

Johnson-Maynard, J. L., Umiker, K. J., & Guy, S. O. (2007). Earthworm dynamics and soil physical properties in the first three years of no-till management. *Soil and Tillage Research*, *94*, 338–345. https://doi.org/10.1016/j.still.2006.08.011

Jones, C. G., Gutiérrez, J. L., Byers, J. E., Crooks, J. A., Lambrinos, J. G., & Talley, T. S. (2010). A framework for understanding physical ecosystem engineering by organisms.

Oikos, *119*(12), 1862–1869. https://doi.org/10.1111/j.1600-0706.2010.18782.x

Jones, C. G, Lawton J. H., & Shachak, M. (1994). Organisms as ecosystem engineers. *Oikos*, *69*, 373–386. doi: 10.2307/3545850.

Jones, C. G., Lawton, J. H., & Shachak, M. (1997). Positive and negative effects of organisms as physical ecosystem engineers. *Ecology*, *78*(7), 1946–1957. https://doi.org/10.1890/0012-9658(1997)078[1946:PANEOO]2.0.CO;2

Jones, D. L., Nguyen, C., & Finlay, R. D. (2009). Carbon flow in the rhizosphere: Carbon trading at the soil-root interface. *Plant and Soil*, *321*, 5–33. https://doi.org/ 10.1007/s11104-009-9925-0

Jouquet, P., Blanchart, E., & Capowiez, Y. (2014). Utilization of earthworms and termites for the restoration ecosystem functioning. *Applied Soil Ecology*, *73*, 34–40. https://doi.org/10.1016/j.apsoil.2013.08.004

Jouquet, P., Chaudhary, E., & Kumar, A. R. V. (2018). Sustainable use of termite activity in agro-ecosystems with reference to earthworms. A review. *Agronomy for Sustainable Development*, *38*(1). https://doi.org/10.1007/s13593-017-0483-1

Kanianska, R., Jadudová, J., Makovníková, J., Kizeková, M. (2016). Assessment of relationships between earthworms and soil abiotic and biotic factors as a tool in sustainable agricultural. *Sustainability*, *8*, 1–14. https://doi.org/10.3390/su8090906

Kim, Y. N., Robinson, B., Lee, K. A., Boyer, S., & Dickinsona, N. (2017). Interactions between earthworm burrowing, growth of a leguminous shrub and nitrogen cycling in a former agricultural soil. *Applied Soil Ecology*, *110*, 79–87. https://doi.org/10.1016/j.apsoil.2016.10.011

Knight, D., Elliott, P. W., Anderson, J. M., & Scholefield, D. (1992). The role of earthworms in managed, permanent pastures in Devon. *Engl. Soil Biology and Biochemistry*, *24*, 1511–1517. https://doi.org/10.1016/0038-0717(92)90142-K

Kooch, Y., Darabi, S. M., & Hosseini, S. M. (2015). Effects of pits and mounds following windthrow events on soil features and greenhouse gas fluxes in a temperate forest. *Pedosphere*, *25*(6), 853–867. https://doi.org/10.1016/S1002-0160(15)30066-7

Kooch, Y., Hosseini, S. M., Samonil, P., & Hojjati, S. M. (2014). The effect of windthrow disturbances on biochemical and chemical soil properties in the northern mountainous forests of Iran. *Catena*, *116*, 142–148. https://doi.org/10.1016/j.catena.2014.01.002

Kooch, Y., Zaccone, C., Lamersdorf, N. P., & Tonon, G. (2014). Pit and mound influence on soil features in an oriental beech (Fagus orientalis Lipsky) forest. *European Journal of Forest Research*, *133*(2), 347–354. https://doi.org/10.1007/s10342-013-0766-2

Kuzyakov, Y., & Blagodatskaya, E. (2015). Microbial hotspots and hot moments in soil: Concept and review. *Soil Biology and Biochemistry*, *83*, 184–199. https://doi.org/10.1016/j.soilbio.2015.01.025

Lambkin, D. C., Gwilliam, K. H., Layton, C., Canti, M. G., Piearce, T. G., & Hodson, M. E. (2011). Production and dissolution rates of earthworm-secreted calcium carbonate. *Pedobiologia*, *54*, S119–S129. https://doi.org/10.1016/j.pedobi.2011.09.003

Landeweert, R., Hoffland, E., Finlay, R. D., Kuyper, T. W., & van Breemen, N. (2001). Linking plants to rocks: Ectomycorrhizal fungi mobilize nutrients from minerals. *Trends in Ecology & Evolution*, *16*(5), 248–254. https://doi.org/10.1016/S0169-5347(01)02122-X

Lavelle, P. (1988). Earthworm activities and the soil system. *Biology and Fertility of Soils*, *6*, 237–251. https://doi.org/10.1007/BF00260820

Lavelle, P., Bignell, D., Lepage, M., Wolters, V., Roger, P., Ineson, P., et al. (1997). Soil function in a changing world: The role of invertebrate ecosystem engineers. *European Journal of Soil Biology (France)*. Retrieved from http://agris.fao.org/agris-search/search.do?recordID=FR1999003405

Lavelle, P., & Spain, A. V. (2001). *Soil ecology*. Dordrecht, The Netherlands: Kluwer Academic Publishers.

Lavelle, P., Spain, A., Blouin, M., Brown, G., Decaëns, T., Grimaldi, M., et al. (2016). Ecosystem engineers in a self-organized soil: A review of concepts and future research questions. *Soil Science*, *181*(3/4), 91–109. https://doi.org/10.1097/SS.0000000000000155

Le Bayon, R. C., & Binet, F. (1999). Rainfall effects on erosion of earthworm casts and phosphorus transfers by water runoff. *Biology and Fertility of Soils*, *30*(1–2), 7–13. https://doi.org/10.1007/s003740050580

Le Bayon, R. C., & Binet, F. (2001). Earthworm surface casts affect soil erosion by runoff water and phosphorus transfer in a temperate maize crop. *Pedobiologia*, *45*(5), 430–442. https://doi.org/10.1078/0031-4056-00097

Le Bayon, R. C., & Binet, F. (2006). Earthworms change the distribution and availability of phosphorous in organic substrates. *Soil Biology and Biochemistry*, *38*(2), 235–246. https://doi.org/10.1016/j.soilbio.2005.05.013

Le Bayon, R. C., Bullinger-Weber, G., Schomburg, A. C., Turberg, P., Schlaepfer, R., & Guenat, C. (2017). Earthworms as ecosystem engineers: A review. In C. G. Horton (Ed.), *Earthworms: Types, roles and research* (pp. 129–178). New York: NOVA Science Publishers.

Le Bayon, R. C., & Milleret, R. (2009). Effects of earthworms on phosphorus dynamics – A review. *Dynamic Soil, Dynamic Plant*, *3*, 21–27.

Le Bayon, R. C., Moreau, S., Gascuel-Odoux, C., & Binet, F. (2002). Annual variations in earthworm surface-casting activity and soil transport by water runoff under a temperate maize agroecosytem. *Geoderma*, *106*(1–2), 121–135. https://doi.org/10.1016/S0016-7061(01)00121-5

Lee, K.E., (1985). *Earthworms: Their ecology and relationships with soil and land use*. Sydney, Australia: Academic Press.

Lehmann, A., Zheng, W., & Rillig, M. C. (2017). Soil biota contributions to soil aggregation. *Nature Ecology & Evolution*, *1*(12), 1828–1835. https://doi.org/10.1038/s41559-017-0344-y

Lehmann, A., Leifheit, E. F., & Rillig, M. C. (2017). Mycorrhizas and soil aggregation. In *Mycorrhizal mediation of soil* (pp. 241–262). Elsevier. Retrieved from https://linkinghub.elsevier.com/retrieve/pii/B9780128043127000140

Lipiec, J., Siczek, A., Sochan, A., & Bieganowski, A. (2016). Effect of sand grain shape on root and shoot growth of wheat seedlings. *Geoderma*, *265*, 1–5. https://doi.org/10.1016/j.geoderma.2015.10.022

Liu, R., Zhu, F., Song, N., Yang, X., & Chai, Y. (2013) Seasonal distribution and diversity of ground arthropods in microhabitats following a shrub plantation age sequence in desertified steppe. *PLoS One*, *8*(10), e77962. https://doi.org/10.1371/journal.pone.0077962

Lone, M.I, He, Z.-L, Stoffella, P.J., Yang, X.-E. (2008). Phytoremediation of heavy metal polluted soils and water: Progresses and perspectives. *Journal of Zhejiang University SCIENCE B*, *9(3),* 210–220. https://link.springer.com/article/10.1631/jzus.B0710633

Lugtenberg, B., & Kamilova, F. (2009). Plant-growth-promoting rhizobacteria. *Annual Review in Microbiology*, *63*, 541–556. https://doi.org/ 10.1146/annurev.micro.62.081307.

Lynch, J. (1990). *The rhizosphere*. London: Wiley.

Marhan, S. & Scheu, S. (2005). The influence of mineral and organic fertilisers on the growth of the endogeic earthworm *Octolasion tyrtaeum* (Savigny). *Pedobiologia*, *49*, 239–249. https://doi.org/10.1016/j.pedobi.2004.11.002

Marinissen, J. C. Y. & Dexter, A. D. (1990). Mechanisms of stabilization of earthworm casts and artificial casts. *Biology and Fertility of Soils*, *9*, 163–167.

McKenzie, B. M., & Dexter, A. R. (1987). Physical properties of casts of the earthworm *Aporrectodea rosea*. *Biology and Fertility of Soils*, *5*, 152–157. https://doi.org/10.1007/BF00257651

MEA (2005). *Ecosystems and Human Well-being: Synthesis*. https://www.millenniumassessment.org/documents/document.356.aspx.pdf

Milcu, A., Schumacher, J., & Scheu, S. (2006). Earthworms (*Lumbricus terrestris*) affect plant seedling recruitment and microhabitat heterogeneity. *Functional Ecology*, *20*, 261–268. https://doi.org/10.1111/j.1365-2435.2006.01098.x

Milleret, R., Le Bayon, R. C., Lamy, F., Gobat, J.-M., & Boivin, P. (2009). Impact of roots, mycorrhizas and earthworms on soil physical properties as assessed by shrinkage analysis. *Journal of Hydrology*, *373*(3–4), 499–507. https://doi.org/10.1016/j.jhydrol.2009.05.013

Milleret, R., Le Bayon, R. C., & Gobat, J.-M. (2009). Root, mycorrhiza and earthworm interactions: Their effects on soil structuring processes, plant and soil nutrient concentration and plant biomass. *Plant and Soil*, *316*(1–2), 1–12. https://doi.org/10.1007/s11104-008-9753-7

Mimmo, Y., Pii, F., Valentinuzzi, S., Astolfi, N., Lehto, B., Robinson, G., et al. (2018). Nutrient availability in the rhizosphere: A review. *Acta horticulturae*, *1217*, 13–28. https://doi.org/10.17660/ActaHortic.2018.1217.2

Mitchell, A. R., Ellsworth, T. R., & Meek, B. D. (1995). Effect of root systems on preferential flow in swelling soil. *Communications in Soil Science and Plant Analysis*, *26*(15–16), 2655–2666. https://doi.org/10.1080/00103629509369475

Mo, X., Qiao, Y., Sun, Z., Sun, X., & Li, Y. (2012). Molecular toxicity of earthworms induced by cadmium contaminated soil and biomarkers screening. *Journal of Environmental Sciences*, *24*(8), 1504–1510. https://doi.org/10.1016/S1001-0742(11)60957-1

Müller-Lemans, H., & van Dorp, F. (1996). Bioturbation as a mechanism for radionuclide transport in soil: Relevance of earthworms. *Journal of Environmental Radioactivity*, *31*(1), 7–20. https://doi.org/10.1016/0265-931X(95)00029-A

Nimmo, J. R. (2004). Porosity and pore size distribution. In D. Hillel (Ed.), *Encyclopedia of Soils in the Environment* (pp. 295–303). London, Elsevier.

Nuutinen, V. (2011). The meek shall inherit the burrow: Feedback in earthworm soil modification. In A. Karaca (Ed.), *Biology of earthworms* (pp. 123–140). Springer, Berlin.

Oades, J. M. (1993). The role of biology in the formation, stabilization and degradation of soil structure. In L. Brussaard & M. J. Kooistra (Eds.), *Soil structure/soil biota interrelationships* (pp. 377–400). Amsterdam: Elsevier. Retrieved from http://www.sciencedirect.com/science/article/pii/B9780444814906500339

Ojha, B., & Devkota, D. (2014). Earthworms: Soil and ecosystem engineers—A review. *World Journal of Agricultural Research*, *2*, 257–260. http://pubs.sciepub.com/wjar/2/6/1/

Orgiazzi, A., Bardgett, R. D., Barrios, E., Behan-Pelletier, V., Briones, M. J. I., Chotte, J.-L., et al. (2016). *Global soil biodiversity atlas*. Luxembourg: European Commission.

Page, V., Le Bayon, R. C. L., & Feller, U. (2006). Partitioning of zinc, cadmium, manganese and cobalt in wheat (*Triticum aestivum*) and lupin (*Lupinus albus*) and further release into the soil. *Environmental and Experimental Botany*, *58*(1–3), 269–278. https://doi.org/10.1016/j.envexpbot.2005.09.005

Paoletti, M. G. (1999). The role of earthworms for assessment of sustainability and as bioindicators. *Agriculture, Ecosystem and Environment*, *74*, 137–155. https://doi.org/10.1016/S0167-8809(99)00034-1

Parelho, C., Rodrigues, A. dos santos, Bernardo, F., do Carmo Barreto, M., Cunha, L., Poeta, P., & Garcia, P. (2018). Biological endpoints in earthworms (*Amynthas gracilis*) as tools for the ecotoxicity assessment of soils from livestock production systems. *Ecological Indicators*, *95*, 984–990. https://doi.org/10.1016/j.ecolind.2017.09.045

Pawlik, Ł., Phillips, J. D., & Šamonil, P. (2016). Roots, rock, and regolith: Biomechanical and biochemical weathering by trees and its impact on hillslopes—A critical literature review. *Earth-Science Reviews*, *159*, 142–159. https://doi.org/10.1016/j.earscirev.2016.06.002

Pelíšek, I. (2018). Investigation of soil water infiltration at a scale of individual earthworm channels. *Soil and Water Research*, *13 (2018)*(No. 1), 1–10. https://doi.org/10.17221/283/2014-SWR

Pérès, G., Bellido, A., Curmi, P., Marmonier, P., & Cluzeau, D. (2010). Relationships between earthworm communities and burrow numbers under different land use systems. *Pedobiologia*, *54*, 37–44. https://doi.org/10.1016/j.pedobi.2010.08.006

Pérès, G., Vandenbulcke, F., Guernion, M., Hedde, M., Beguiristain, T., Douay, F., et al. (2011). Earthworm indicators as tools for soil monitoring, characterization and risk assessment. An example from the national Bioindicator programme (France). *Pedobiologia*, *54*, S77–S87. https://doi.org/10.1016/j.pedobi.2011.09.015

Perreault, J.M., & Whalen, J.K. (2006). Earthworm burrowing in laboratory microcosms as influenced by soil temperature and moisture. *Pedobiologia*, *50*, 397–403.

Pierret, A., Doussan, C., Capowiez, Y., Bastardie, F., & Pagès, L. (2007). Root functional architecture: A framework for

modeling the interplay between roots and soil. *Vadose Zone Journal*, *6*(2), 269–281. https://doi.org/10.2136/vzj2006.0067

Potvin L. R., & Lilleskov, E. A. (2017). Introduced earthworm species exhibited unique patterns of seasonal activity and vertical distribution, and *Lumbricus terrestris* burrows remained usable for at least 7 years in hardwood and pine stands. *Biology and Fertility of Soils*, *53*, 187–198. https://doi.org/10.1007/s00374-016-1173-x

Raaijmakers, J., Paulitz, T., Steinberg, C., Alabouvette, C., & Moënne-Loccoz, Y. (2009). The rhizosphere: A playground and battlefield for soilborne pathogens and beneficial microorganisms. *Plant and Soil*, *321*, 341–361. https://doi.org/10.1007/s11104-008-9568-6

Richter, D. D., Oh, N. H., Fimmen, R. & Jackson, J. (2007). The rhizosphere and soil formation. In: Z. G. Cardon, J. L. Whitbeck (Eds), *The rhizosphere: An ecological perspective* (pp. 179–200). New York: Academic Press.

Rossi, J. P. 2003. The spatiotemporal pattern of a tropical earthworm species assemblage and its relationship with soil structure. *Pedobiologia*, *47*, 497–503. https://doi.org/10.1078/0031-4056-00219

Salmon, S. (2001.) Earthworm excreta (mucus and urine) affect the distribution of springtails in forest soils. *Biology and Fertility of Soils*, *34*, 304–310. https://doi.org/10.1007/s003740100407

Salomé, C., Guenat, C., Bullinger-Weber, G., Gobat, J.-M., & Le Bayon, R. C. (2011). Earthworm communities in alluvial forests: Influence of altitude, vegetation stages and soil parameters. *Pedobiologia*, *54*, S89–S98. https://doi.org/10.1016/j.pedobi.2011.09.012https://doi.org/10.2136/vzj2017.01.0021

Šamonil, P., Daněk, P., Schaetzl, R. J., Vašíčková, I., & Valtera, M. (2015). Soil mixing and genesis as affected by tree uprooting in three temperate forests: Soil mixing and evolution as affected by tree-throw. *European Journal of Soil Science*, *66*(3), 589–603. https://doi.org/10.1111/ejss.12245

Šamonil, P., Král, K., & Hort, L. (2010). The role of tree uprooting in soil formation: A critical literature review. *Geoderma*, *157*(3–4), 65–79. https://doi.org/10.1016/j.geoderma.2010.03.018

Šamonil, P., Tejnecký, V., Borůvka, L., Šebková, B., Janík, D., & Šebek, O. (2010). The role of tree uprooting in Cambisol development. *Geoderma*, *159*(1–2), 83–98. https://doi.org/10.1016/j.geoderma.2010.06.020

Sanders, D., Jones, C.G., Thébault, E., Bouma, T. J., van der Heide, T., van Belzen, J., et al. (2014). Integrating ecosystem engineering and food webs. *Oikos*, *123*, 513–524. https://doi.org/10.1111/j.1600-0706.2013.01011.x

Savin, M. C., Görres, J. H., & Amador, J. A. (2004). Microbial and microfaunal community dynamics in artificial and *Lumbricus terrestris* (L.) burrows. *Soil Science Society of America Journal*, *68*, 116–124. doi:10.2136/sssaj2004.1160

Schaetzl, R. J., Burns, S. F., Small, T. W., & Johnson, D. L. (1990). Tree uprooting: Review of types and patterns of soil disturbance. *Physical Geography*, *11*(3), 277–291. https://doi.org/10.1080/02723646.1990.10642407

Schindler, S., O'Neill, F. H., Biró, M., Damm, C., Gasso, V., Kanka, R., et al. (2016). Multifunctional floodplain management and biodiversity effects: A knowledge synthesis for six European countries. *Biodiversity and Conservation*, *25*(7), 1349–1382. https://doi.org/10.1007/s10531-016-1129-3

Schmidt, M. W. I., Torn, M. S., Abiven, S., Dittmar, T., Guggenberger, G., Janssens, I. A. et al. (2011). Persistence of soil organic matter as an ecosystem property. *Nature*, *478*(7367), 49–56.

Schomburg, A., Schilling, O. S., Guenat, C., Schirmer, M., Le Bayon, R. C., & Brunner, P. (2018). Topsoil structure stability in a restored floodplain: Impacts of fluctuating water levels, soil parameters and ecosystem engineers. *Science of the Total Environment*, *639*, 1610–1622. https://doi.org/10.1016/j.scitotenv.2018.05.120

Schomburg, A., Verrecchia, E. P., Guenat, C., Brunner, P., Sebag, D., & Le Bayon, R. C. (2018). Rock-Eval pyrolysis discriminates soil macro-aggregates formed by plants and earthworms. *Soil Biology and Biochemistry*, *117*, 117–124. https://doi.org/10.1016/j.soilbio.2017.11.010

Schrader, S., & Zhang, H. (1997). Earthworm casting: Stabilization or destabilization of soil structure? *Soil Biology and Biochemistry*, *29*, 469–475. https://doi.org/10.1016/S0038-0717(96)00103-4

Schulmann, O. P., & Tiunov, A. V. (1999). Leaf litter fragmentation by the earthworm *Lumbricus terrestris* L. *Pedobiologia*, *43*, 453–458.

Schulz, S., Brankatschk, R., Dümig, A., Kögel-Knabner, I., Schloter, M., & Zeyer, J. (2013). The role of microorganisms at different stages of ecosystem development for soil formation. *Biogeosciences*, *10*(6), 3983–3996. https://doi.org/10.5194/bg-10-3983-2013

Sharma, D. K., Tomar, S., & Chakraborty, D. (2017). Role of earthworm in improving soil structure and functioning. *Current Science*, *113*(6), 1064–1071.

Shipitalo, M., & Le Bayon, R. C. (2004). Quantifying the effects of earthworms on soil aggregation and porosity. In C. Edwards (Ed.), *Earthworm ecology* (pp. 183–200). https://doi.org/10.1201/9781420039719.pt5

Shipitalo, M. J., & Protz, R. (1988). Factors influencing the dispersibility of clay in worm casts, *Soil Science Society of America Journal*, *52*, 764–769. doi:10.2136/sssaj1988.03615995005200030030x

Shipitalo, M. J., & Protz, R. (1989). Chemistry and micromorphology of aggregation in earthworm casts. *Geoderma*, *45*, 357–374. https://doi.org/10.1016/0016-7061(89)90016-5

Six, J., Bossuyt, H., Degryze, S., & Denef, K. (2004). A history of research on the link between (micro)aggregates, soil biota, and soil organic matter dynamics. *Soil and Tillage Research*, *79*(1), 7–31. https://doi.org/10.1016/j.still.2004.03.008

Six, J., Conant, R. T., Paul, E. A. & Paustian, K. (2002). Stabilization mechanisms of soil organic matter: Implication of C-saturation of soils. *Plant and Soil*, *241*, 155–176. https://doi.org/10.1023/A:1016125726789

Smith, P., Cotrufo, M. F., Rumpel, C., Paustian, K., Kuikman, P. J., Elliott, J. A., et al. (2015). Biogeochemical cycles and biodiversity as key drivers of ecosystem services provided by soils. *Soil*, *1*(2), 665–685. https://doi.org/10.5194/soil-1-665-2015

Stockdill, S. M. J. (1966). The effect of earthworms on pastures. *Proceedings of the New Zealand Ecological Society*, *13*, 68–75.

Suzuki, Y., Matsubara, T., & Hoshino, M. (2003). Breakdown of mineral grains by earthworms and beetle larvae. *Geoderma*, *112*(1), 131–142. https://doi.org/10.1016/S0016-7061(02)00300-2

Taylor, L. L., Leake, J. R., Quirk, J., Hardy, K., Banwart, S. A., & Beerling, D. J. (2009). Biological weathering and the long-term carbon cycle: Integrating mycorrhizal evolution and function into the current paradigm. *Geobiology*, *7*(2), 171–191. https://doi.org/10.1111/j.1472-4669.2009.00194.x

Teuling, A. J., Uijlenhoet, R., Hupet, F., & Troch, P. A. (2006). Impact of plant water uptake strategy on soil moisture and evapotranspiration dynamics during drydown. *Geophysical Research Letters*, *33*(3), 1–5. https://doi.org/10.1029/2005GL025019

Tisdall, J. M., & Oades J. M. (1982). Organic matter and water-stable aggregates in soils. *Journal of Soil Science*, *33*, 141–163. https://doi.org/10.1111/j.1365-2389.1982.tb01755.x

Tiunov, A. V., & Scheu S. (1999). Microbial respiration, biomass, biovolume and nutrient status in burrow walls of *Lumbricus terrestris* L. (Lumbricidae). *Soil Biology and Biochemistry*, *31*, 2039–2048. https://doi.org/10.1016/S0038-0717(99)00127-3

Topoliantz, S., Ponge, J. F., & Viaux, P. (2000). Earthworm and enchytraeid activity under different arable farming systems, as exemplified by biogenic structures. *Plant and Soil*, *225*, 39–51. https://doi.org/10.1023/A:1026537632468

Totsche, K. U., Amelung, W., Gerzabek, M. H., Guggenberger, G., Klumpp, E., Knief, C., et al. (2018). Microaggregates in soils. *Journal of Plant Nutrition and Soil Science*, *181*(1), 104–136. https://doi.org/10.1002/jpln.201600451

Trigo, D., Barois, I., Garvin, M. H., Huerta, E., Irisson, S., & Lavelle, P. (1999). Mutualism between earthworms and soil microflora. *Pedobiologia*, *43*(6), 866–873. https://www.jstor.org/stable/42947357

Uvarov, A. V., Tiunov, A. V., & Scheu, S. (2011). Effects of seasonal and diurnal temperature fluctuations on population dynamics of two epigeic earthworm species in forest soil. *Soil Biology and Biochemistry*, *43*, 559–570. https://doi.org/10.1016/j.soilbio.2010.11.023

Valtera, M., & Schaetzl, R. J. (2017). Pit-mound microrelief in forest soils: Review of implications for water retention and hydrologic modelling. *Forest Ecology and Management*, *393*, 40–51. https://doi.org/10.1016/j.foreco.2017.02.048

van Groenigen, J. W., Lubbers, I. M., Vos, H. M. J., Brown, G. G., De Deyn, G. B., & van Groenigen, K. J. (2014). Earthworms increase plant production: A meta-analysis. *Scientific Reports*, *4*, 6365. https://doi.org/10.1038/srep06365

van Groenigen, J. W., van Groenigen, K. J., Koopmans, G. F., Stokkermans, L., Vosa, H.M.J., & Lubbers, I. M. (2019). How fertile are earthworm casts? A meta-analysis. *Geoderma*, *338*, 525–535. https://doi.org/10.1016/j.geoderma.2018.11.001

Véle, A., Holuša, J., Frouz, J., & Konvička, O. (2011). Local and landscape drivers of ant and carabid beetle communities during spruce forest succession. *European Journal of Soil Biology*, *47*, 349–356. https://doi.org/10.1016/j.ejsobi.2011.09.003

Weil, R. R., & Brady, N. C. (2017). *The nature and properties of soils* (15th ed.). Essex, England: Pearson.

Weisskopf, L., Le Bayon, R. C., Kohler, F., Page, V., Jossi, M., Gobat, J.-M., et al. (2008). Spatio-temporal dynamics of bacterial communities associated with two plant species differing in organic acid secretion: A one-year microcosm study on lupin and wheat. *Soil Biology and Biochemistry*, *40*(7), 1772–1780. https://doi.org/10.1016/j.soilbio.2008.02.018

Whalen, J. K., Sampedro, L., & Waheed, T. (2004). Quantifying surface and subsurface cast production by earthworms under controlled laboratory conditions. *Biology and Fertility of Soils*, *39*, 287–291. https://doi.org/10.1007/s00374-003-0715-1

Wilkinson, M. T., Richards, P. J., & Humphreys, G. S. (2009). Breaking ground: Pedological, geological, and ecological implications of soil bioturbation. *Earth-Science Reviews*, *97*(1–4), 257–272. https://doi.org/10.1016/j.earscirev.2009.09.005

Wilson, G. W. T., Hartnett, D. C. & Rice, C. W. (2006). Mycorrhizal-mediated phosphorus transfer between the tallgrass prairie plants *Sorghastrum nutans* and *Artemisia ludoviciana*. *Functional Ecology*, *20*, 427–435. https://doi.org/10.1111/j.1365-2435.2006.01134.x

Wright, J. P., & Jones, C. G. (2006). The concept of organisms as ecosystem engineers ten years on: Progress, limitations, and challenges. *BioScience*, *56*(3), 203–209. https://doi.org/10.1641/0006-3568(2006)056[0203:TCOOAE]2.0.CO;2

Wu, H., Wang, X., & He, X. (2017). Effects of selected root exudate components on nitrogen removal and development of denitrifying bacteria in constructed wetlands. *Water*, *9*, 430. https://doi.org/10.3390/w9060430

Xu, H. J., Chen, H., Wang, X. L., Zhang, Y. L., Wang, J. J., Li, N. et al. (2018). Earthworms stimulate nitrogen transformation in an acidic soil under different Cd contamination. *Ecotoxicology and Environmental Safety*, *165*, 564–572. https://doi.org/10.1016/j.ecoenv.2018.09.042

Yunusa, I. A. M., & Newton, P. J. (2003). Plants for amelioration of subsoil constraints and hydrological control: The primer-plant concept. *Plant and Soil*, *257*, 261–281. http://www.jstor.org/stable/24124333.

Zanella, A., Ponge, J.-F., Jabiol, B., Sartori, G., Kolb, E., Gobat, J.-M., et al. (2018). Humusica 1, article 4: Terrestrial humus systems and forms—Specific terms and diagnostic horizons. *Applied Soil Ecology*, *122*, 56–74. https://doi.org/10.1016/j.apsoil.2017.07.005

Zangerlé, A., Renard, D., Iriarte, J., Suarez Jimenez, L. E., Adame Montoya, K. L., Juilleret, J., et al. (2016). The Surales, self-organized earth-mound landscapes made by earthworms in a seasonal tropical wetland. *Plos One*, *11*(5), e0154269. https://doi.org/10.1371/journal.pone.0154269

Zhang, D., Chen, Y., Ma, Y., Guo, L., Suna, J., & Tong, J. (2016). Earthworm epidermal mucus: Rheological behavior reveals drag-reducing characteristics in soil. *Soil and Tillage Research*, *158*, 57–66. https://doi.org/10.1016/j.still.2015.12.001

Zorn, M. I., Van Gestel, C. A. M., Morrien, E., Wagenaar, M., & Eijsackers, H. (2008). Flooding responses of three earthworm species, *Allolobophora chlorotica*, *Aporrectodea caliginosa* and *Lumbricus rubellus*, in a laboratory-controlled environment. *Soil Biology and Biochemistry*, *40*, 587–593. https://doi.org/10.1016/j.soilbio.2007.06.028

5

Tephra for the Trees? Geochemical Constraints on Weathering and Tephra Inputs to Soils on New Zealand's North Island

Claire E. Lukens[2] and Kevin P. Norton[1]

ABSTRACT

Weathering turns rock into soil and has profound impacts on soil production and biogeochemical cycling. It is typically quantified in soils using a mass-balance approach and immobile trace element analyses under the assumption that the parent material for soils is primarily the underlying bedrock, with small or negligible amounts of windblown dust. Here we present geochemical data from soils and saprolites that clearly violate these basic assumptions. Our results suggest (1) deep weathering in saprolite, which means that underlying material arrives at the soil-saprolite boundary substantially preweathered, and (2) substantial input of exogenous material to these soils. We use trace element geochemistry to identify the exogenous material as tephra from the Ōruanui eruption of the Taupō Volcanic Center, though no visible tephra layer was apparent in soil pits. We use a simple forward mixing model to determine the relative contributions of local saprolite and tephra to the weathered soil. We find that these soils comprise >40% tephra, and that tephra provides most of the weathering-derived nutrients in soils. Along with soil production rates measured with cosmogenic nuclides, the presence of the 26.5 ka tephra suggests at least 85 cm of recent soil erosion, likely precipitated by deforestation associated with human arrival in the region. At a broader scale, this work shows that weathering and nutrient release in volcanically active regions may be dominated by volcanic inputs rather than underlying bedrock, particularly in areas where deep saprolite weathering is substantial.

5.1. INTRODUCTION

The balance between chemical weathering and physical erosion defines the character of most landscapes, from steep, rocky mountains to rolling hills with rich agricultural histories. Weathering turns rock into soil, setting soil production rates and providing important nutrients to biota (e.g. Drever, 1994; Likens et al., 1967). Over geologic timescales, the weathering of silicate rocks is also a net carbon sink (Berner et al., 1983). This observation has led to widespread recent interest among the geomorphic community to understand spatial patterns in weathering rates and intensity. The result of this ongoing work is a better understanding of how weathering rates are affected by climate (e.g. Dixon et al., 2016; Egli et al., 2003; Kump et al., 2000; Riebe et al., 2004; White & Blum, 1995), mineral supply via tectonic uplift (e.g. Jacobson et al., 2003; Norton & von Blanckenburg, 2010; Riebe et al., 2001; West et al., 2005), underlying parent material (e.g. Hartmann & Moosdorf, 2011; Ibarra et al., 2016; Stallard, 1988; White & Blum, 1995), and topography (e.g. Heimsath et al., 1999; Yoo et al., 2007, 2009).

The magnitude and pace at which these factors affect weathering rates depend heavily on parent material (Brantley, 2008; Chadwick et al., 1999), highlighting the importance of constraining all inputs to the soil system,

[1] *Te Herenga Waka/Victoria University of Wellington, Wellington, New Zealand*

[2] *Department of Life and Environmental Sciences, University of California, Merced, CA, USA*

Hydrogeology, Chemical Weathering, and Soil Formation, Geophysical Monograph 257, First Edition.
Edited by Allen Hunt, Markus Egli, and Boris Faybishenko.

DOI: 10.1002/9781119563952.ch5

including aeolian deposition (e.g. Porder et al., 2007; Ferrier et al., 2011; Arvin et al., 2017). The overall consensus is that for a given parent material, weathering rates scale with increased precipitation and temperature (White & Blum, 1995; Norton et al., 2014), while mineral supply rate can result in either supply limits or kinetic limits on weathering (West et al., 2005; Dixon & von Blanckenburg, 2012; Ferrier & West, 2017). The presence of kinetic limits in particular is important at the global scale, as they imply decreased weathering fluxes in rapidly eroding settings, confounding the potential silicate weathering control on global climate (i.e. Berner et al., 1983).

5.1.1. Conceptual Framework and Previous Work

We employ the commonly used framework of a steady-state weathering profile to quantify weathering using a mass-balance approach (Figure 5.1; e.g. Brimhall & Dietrich, 1987; Anderson et al., 2002; Brantley & White, 2009). In this framework, material from the bottom of the profile moves up towards the surface over time. Soil, which we here define as the mobile regolith layer, develops atop saprolite (defined here as weathered bedrock that maintains its physical structure), which in turn sits atop unweathered rock. The parent material for the saprolite is the underlying bedrock, and the parent material for the soil is the saprolite, plus any windblown particles that are deposited on the surface (e.g. Ferrier et al., 2011; Porder et al., 2007). Mass is lost via physical erosion (E) from the surface and chemical weathering from both the saprolite and soil layers (W_{sap} and W_{soil}, respectively; Figure 5.1). Assuming steady-state thickness of the weathering zone, mass inputs (uplift, U, and dust, d) are equal to outputs via erosion and weathering.

$$U + d = E + W_{sap} + W_{soil} \quad (1)$$

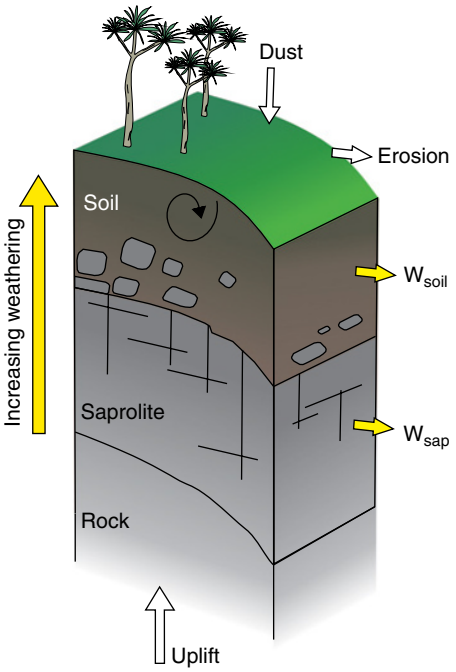

Figure 5.1 Weathering intensity should increase from fresh bedrock towards the surface in a weathered profile. At steady-state thickness, mass inputs from uplift and dust deposition will equal mass outputs via erosion and weathering in saprolite (W_{sap}) and soil (W_{soil}).

Within this geochemical mass-balance approach, immobile elements should be enriched relative to parent material as weathering progresses and weatherable species are removed as solutes (Brimhall & Dietrich, 1987; Chadwick et al., 1999; Riebe et al., 2003). The weathering intensity, as indicated by immobile element profiles (Riebe et al., 2003), should decrease gradually with depth if unmixed, or exhibit a sharp contact at some mixing depth (e.g. Roering et al., 2002). Hillslope diffusion (e.g. by soil creep) should also result in changes in weathering intensity along slopes, corresponding to local slope curvature (Yoo et al., 2007, 2009; Yoo & Mudd, 2008).

Aeolian inputs may fundamentally change the observed relationships between weathering and climate or topography by providing additional parent material for soils. While many weathering studies have assumed neglible input from dust, a number of recent studies recognize the potential consequences of dust inputs to estimates of erosion, weathering, and nutrient fluxes (e.g. Arvin et al., 2017; Ferrier et al., 2011; Porder et al., 2007). In New Zealand, there are multiple sources of dust to consider, including far-traveling Australian dust (Marx et al., 2005), Pleistocene loess deposits (Eden & Hammond, 2003), and volcanic tephra (Cronin et al., 1996; Gehrels et al., 2006; Hopkins & Seward, 2019; Lowe et al., 2008; Wilson, 2001).

Here we present geochemical data from soils and saprolites along two short hillslope transects from New Zealand's Wairarapa region. Along with a simple forward mixing model, these data suggest that the underlying bedrock is moderately weathered before it becomes part of the mobile soil layer, and that substantial tephra inputs contribute to soils. When combined with ^{10}Be-derived soil production rates measured in saprolite, these data allow us to construct a history of deposition and erosion for this landscape over the past 27,000 years, including an estimate of the magnitude of soil stripping associated with human modification of the landscape. Our results have important consequences for understanding deep weathering and solute transport in groundwater, nutrient sources, and tephra inputs to soils in this agricultural region. These observations also reiterate how profoundly long-term landscape histories can affect modern soils; while recent work by Marshall et al. (2015) documented the effects of Pleistocene

climate ("frost for the trees"), we suggest that on New Zealand's north island, nutrient cycling may be significantly influenced by volcanic inputs: tephra for the trees.

5.2. FIELD SITE

The Wairarapa Valley lies at the southern end of New Zealand's North Island (Figure 5.2). The region consists of rolling hills and floodplains and is bounded to the east by the Tararua Mountains, which create a local rain shadow. Mean annual rainfall in the region is ~950 mm, and mean annual temperature is ~13 °C (Masterton Climate Report, NIWA). The field site, Rocky Hill, lies 25 km southeast of Masterton at an elevation of 410 m above sea level. The topography locally enhances precipitation to ~1500 mm per year (Masterson Climate Report, NIWA) with slightly drier summers than winters. Annual temperature at the field site is ~11 °C, with mean summer temperatures of 21 °C and mean winter temperatures of 4 °C. The field site is underlain by the Cretaceous Mangapokia Formation of the Pahaoa Group. The Mangapokia Formation consists primarily of quartzofeldspathic sandstones and mudstones with centimeter to decameter-scale bedding. The bedrock has been extensively fractured (Lee et al., 2002).

Sampling was undertaken on a small, gently curving hillslope to the east of Rocky Hill Road (41.17927°S, 175.79006°E). The hillslope loses 22 m of elevation over its ~40 m length. The hillslope was surveyed using a Trimble GeoHT differential GPS and a 1m DEM was

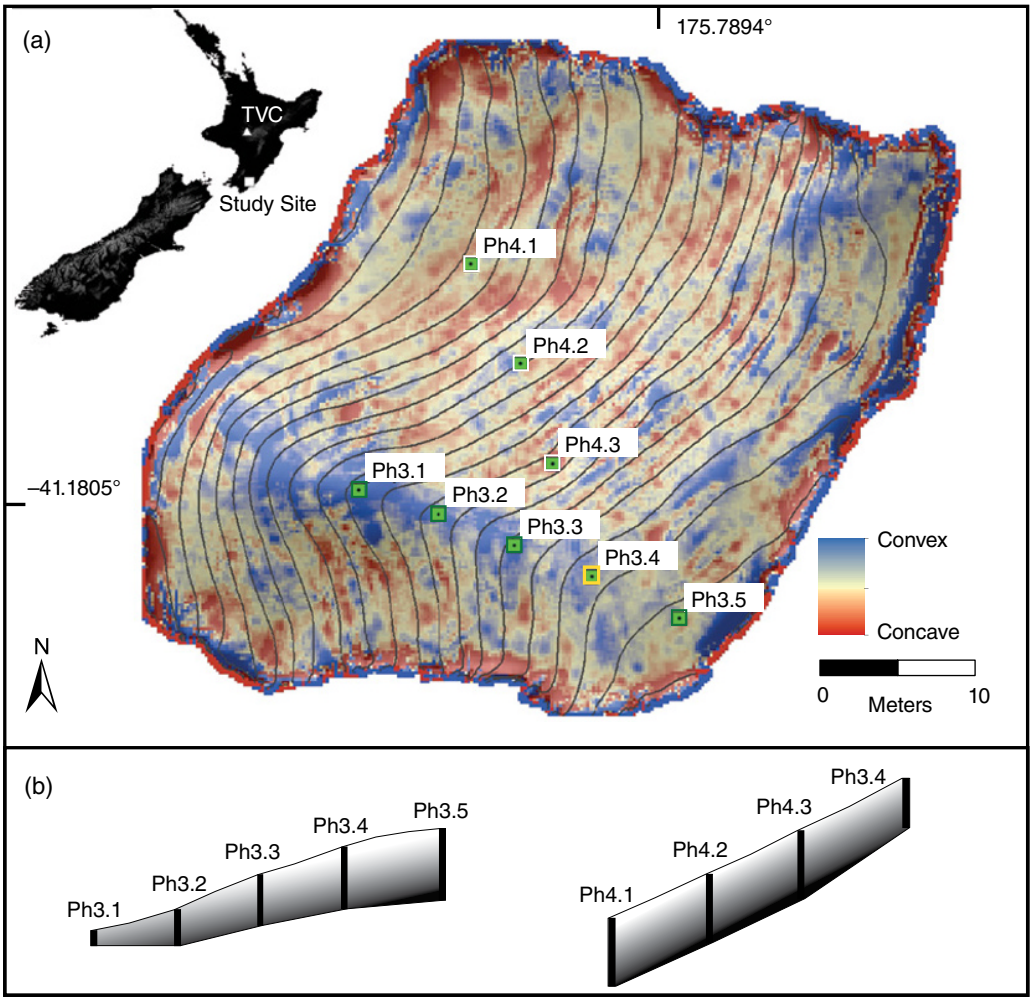

Figure 5.2 Study site at Rocky Hill, in the Wairarapa region of New Zealand. Inset map also shows the location of the Taupō Volcanic Center (TVC). Soils and saprolite were sampled across two transects along a convex nose (pits Ph3.1–3.5) and a planar hillslope (pits Ph3.4, Ph4.1–4.3) (a). Pits in which saprolite was not reached are denoted with white outlines; saprolite was reached in all other pits. The pit from which saprolite was sampled for ^{10}Be-derived soil production rates is shown in yellow. Surface curvature and relative soil pit depths along each transect are shown in (b).

Table 5.1 Cosmogenic nuclides. Brackets denote concentrations.

Sample name	CAMSID	Mass quartz (g)	Mass ^{9}Be carrier (g)	[^{9}Be carrier] (ppm)	Blank-corrected ^{10}Be/^{9}Be (x10^{-14})	[^{10}Be] (at/g, x10^{5})	±	^{10}Be production (at/g/yr)	Depth (cm)
Ph02R	BE45406	12.0933	0.9026	305	1.79396	0.27326	0.01868	3.76	55

produced (Figure 5.2). Five soil pits were dug to saprolite at ~7 m intervals along the crest of the convex hillslope nose (samples Ph3.1–3.5). A second transect of four soil pits (including Ph3.4, where the two transects overlap) was collected at an acute angle to the hillslope crest, into a hollow with roughly planar curvature (samples Ph4.1–4.3). The maximum soil pit depth on the planar transect was 80 cm, and saprolite was not reached in most of these pits (Ph4.1, Ph4.2, and Ph4.3). Data from pit Ph3.4 are plotted as part of the convex transect in the figures that follow. In order to constrain the composition of unweathered bedrock, samples were collected from exposed rock in a road cut next to the sample site and from a rock quarry <300 m from the sampling transects. Saprolite from the bottom of pit Ph3.4 was also collected for ^{10}Be analysis in order to calculate a soil production rate. This sample was 3-4 cm thick and was collected from the soil-saprolite interface. Given the proximity of samples to each other, we take this soil production rate to represent the average soil production for the site.

5.3. METHODS

The local soil production rate was determined using in-situ ^{10}Be in saprolite, sampled from the soil-saprolite interface at a depth of 55 cm. Saprolite was crushed to monomineralic grains, and quartz was isolated using standard magnetic and gravimetric methods. The quartz was then dissolved, spiked with ^{9}Be carrier, and BeO was isolated using standard chemical methods (e.g. Kohl & Nishiizumi, 1992; von Blanckenburg et al., 2004). The ^{10}Be/^{9}Be ratio was measured via accelerator mass spectrometry at Lawrence Livermore National Laboratory. The process blank 18CLB01 (CAMSID BE45408) had a ^{10}Be/^{9}Be ratio of $4.65 \pm 0.58 \times 10^{-15}$ at/g.

Chemical compositions of soil, saprolite, and bedrock samples were determined using a combination of neutron activation analysis and X-ray fluoresence (XRF). Soils were dried, sieved to <2 mm, and soils and saprolites were heat treated at 550 °C to remove organic material. Soils, saprolites, and rocks were powdered and homogenized using an agate or tungsten carbide ring mill. Concentrations of Zr and Ti in soils and saprolites were measured via neutron activation analysis on the OPAL reactor at the Australian Nuclear Science and Technology Organization (ANSTO; Kruger, 1971; Pollard & Heron, 1996). Bedrock samples were analyzed via XRF, using an Olympus Vanta XRF spectrometer.

5.4. RESULTS

5.4.1. Cosmogenic Nuclides and Soil Production Rate

The concentration of ^{10}Be measured in saprolite (Table 5.1) can be used to determine the soil production rate, averaged over the timescale needed to erode roughly 1.4 m of soil or 0.6 m of rock (the attenuation length scale of the dominant production pathway from cosmic radiation; Dunai, 2010; Gosse & Philips, 2001). In active landscapes where this timescale is generally on the order of thousands of years, we can ignore the radioactive decay of ^{10}Be (half-life = 1.387 ± 0.012 Ma) (Chmeleff et al., 2010; Korschinek et al., 2010) and calculate soil production using equation (1) (Heimsath et al., 1997):

$$SPR = \frac{P_d \Lambda}{N \rho} \tag{2}$$

The soil production rate is a function of the ^{10}Be production rate at the top of the saprolite (P_d), the attenuation length of cosmic radiation with depth (Λ, 160 g cm^{-2}), the density of underlying bedrock (ρ), and the measured ^{10}Be concentration (N). Here, P_d is calculated using an exponential decrease in ^{10}Be production with depth through the soil with a density of 1.16 g cm^{-3} (the average density measured in soils). The underlying bedrock density (ρ) is 2.54 g cm^{-3}, based on a compilation of densities from the same lithologic unit measured in the region (Petlab, 2018; Strong et al., 2016). Assuming a steady-state soil thickness through time, we calculate an apparent soil production rate of 86.7 ± 6.0 m My^{-1}.

5.4.2. Bedrock, Saprolite, and Soil Geochemistry

Bedrock provides parent material for saprolite and soils. Concentrations of Zr and Ti measured in bedrock samples average 195 ± 8 ppm and 3186 ± 219 ppm, respectively (Table 5.2; Foley, 1984), consistent with previous measurements from similar Cretaceous

Table 5.2 Bedrock geochemistry.

sample name	Zr (ppm)	± (1σ)	Ti (ppm)	± (1σ)
17CL003RH	213	5	3846	162
17CL004RH	216	5	4086	165
17CL012RH	177	4	2812	150
17CL014RH	161	4	2586	148
17CL015RH	208	5	3283	155
17CL017RH	202	4	2942	151
17CL021RH	189	4	2746	149
mean	*195*	*8*	*3186*	*219*

greywackes around the region (196 ± 3 ppm Zr, 2958 ± 51 ppm Ti; n = 221) (Petlab, 2018).

Concentrations of Zr and Ti in saprolite (Table 5.3) are higher than in the underlying bedrock, consistent with enrichment of immobile elements as solutes are removed by weathering. Weathering intensity in saprolite is calculated as the chemical depletion fraction (CDF; Riebe et al., 2003), which varies from 0 (no weathering) to 1 (complete weathering):

$$CDF = 1 - \frac{C_{i,p}}{C_{i,W}} \quad (3)$$

where $C_{i,p}$ is the concentration of an immobile element (e.g. Ti, Zr) in the parent material (bedrock), and $C_{i,w}$ is the concentration of the same immobile element in the weathered material (saprolite or soil). On average, saprolite CDF calculated with Zr as the immobile element is 0.25 ± 0.06; using Ti as the immobile element, CDF is 0.12 ± 0.09. Though they differ, these mean values are within two standard errors of each other and reflect moderate amounts of weathering in saprolite relative to the underlying parent bedrock.

The observed soil geochemistry is not consistent with spatial patterns shown in previous work (e.g. Yoo et al., 2009), where immobile elements were enriched at sites with higher slope curvature and increasing distance from ridgelines. Here, there is no apparent trend in immobile element concentrations between sample pits, either with local curvature or distance along the slope (Table 5.3). The patterns in measured Zr and Ti concentration with depth are also unexpected. Neither element follows the expected pattern of enrichment from saprolite towards the surface, which would reflect increasing intensity of weathering in material with longer residence time in the soil (gray arrows in Figure 5.3). Measured Zr concentrations are similar in saprolite and soil and are relatively uniform throughout soil profiles. Ti concentrations in soil are depleted relative to saprolite and bedrock, and depletion increases from the soil pit bottom towards the surface. These patterns do not reflect weathering of bedrock below, which should enrich soils in both Zr and Ti. Rather, these observations suggest that the underlying bedrock is not the only parent material for soils; there must also be exogenous (e.g. windblown) inputs contributing mass to the soil.

5.4.3. Possible Dust Inputs

Both Ti and Zr are typically immobile in soils (Brimhall & Dietrich, 1987; Dawson et al., 1991; Harden, 1987; Johnsson et al., 1993; White et al., 2001), so the ratio of these two elements should remain the same in weathered and unweathered material originating from the same parent material. We can use the Ti:Zr ratio in bedrock (16.3) and in possible dust sources to identify the most likely dust source(s) contributing to soils. We expect increasing weathering to produce increasing Ti and Zr concentrations from rock to saprolite to soil, continuing along the same trend as weathering intensity increases (Figure 5.4a; arrow shows expected path of Ti and Zr enrichment). Instead, we observe the expected enrichment from bedrock to saprolite, but soils fall off the expected trend, averaging similar Zr and lower Ti concentrations (Ti:Zr = 12.3) than saprolite and bedrock.

Several possible dust sources may provide additional parent material, which would alter the Ti:Zr ratio in soils. Far-traveling dust from Australia has a high Ti:Zr ratio (33.9) (Marx et al., 2005); mixing of this dust source into soils would tend to pull soil compositions towards higher Ti:Zr ratios, so it seems an unlikely candidate for dust additions to our soils. Loess deposits from the nearby Wairarapa valley have a slightly lower Ti:Zr ratio (11.2) than soils, but Ti and Zr concentrations are both higher in loess than in soils (Eden & Hammond, 2003), so loess is also an unlikely candidate. Recent eruptions from the Taupō Volcanic Center produced significant ash fall and present two options for tephra inputs: the ca. 232 AD Taupō eruption and the 26.5 ka Ōruanui tephra. Both tephras have similar Zr and lower Ti concentrations than bedrock and soils (Froggat, 1982; Petlab, 2018; Sutton et al., 2000; Wilson, 2001, Wilson et al., 2006) and provide likely geochemical candidates for additional parent material to soils in the Wairarapa region (Figure 5.4a). Secondary electron images from a JXA-8230 electron microprobe confirm the presence of rhyolitic volcanic glass in these soils (Figure 5.4 b–e), some of which appear to be highly weathered (Figure 5.4e). Semiquantitative analysis on unpolished surfaces yields major element oxides SiO_2 (65.9%–82.0%), Al_2O_3 (9.6%–16.4%), Na_2O (1.0%–5.8%), K_2O (0.7%–9.5%), and CaO (0.5%–6.0%), which fall within the range of values reported for both Taupō and Ōruanui eruptions (Froggat, 1982; Petlab, 2018; Sutton et al., 2000; Wilson et al., 2006). However, the ca. 232 AD Taupō eruption produced ash fall that was deposited directly east of the

Table 5.3 Saprolite and soil geochemistry measured by neutron activation analysis. Saprolites were sampled from the soil-saprolite interface at the bottom of each soil pit. In pits 4.1-4.3, saprolite was not reached. Brackets denote concentrations. Sample Ph3.1 (italics) is excluded from the analyses that follow as an outlier, based on both geochemical and physical observations.

Saprolites:

Sample pit	depth (cm)	distance from ridge (m)	elevation (m)	density (g cm^{-3})	[Ti] (ppm)	± (1σ)	[Zr] (ppm)	± (1σ)
Ph3.1	15	29.2	408	1.03	4441	213	305	20
Ph3.2	35	22.2	410	1.20	3009	182	226	18
Ph3.3	45	15.3	413	1.39	3126	234	234	16
Ph3.4	55	8.2	416	0.98	3728	268	268	21
Ph3.5	65	0.0	417	1.21	3780	202	262	29
mean					*3617*	*258*	*259*	*14*

Soils - convex transect:

Sample pit	depth (cm)	distance from ridge (m)	elevation (m)	density (g cm^{-3})	[Ti] (ppm)	± (1σ)	[Zr] (ppm)	± (1σ)
Ph3.1	*3*	*29.2*	*408*	*0.77*	*4089*	*208*	*184*	*29*
Ph3.2	5	22.2	410	0.92	3165	188	234	16
Ph3.2	15	22.2	410	1.17	3437	191	282	21
Ph3.2	25	22.2	410	1.14	3744	279	233	17
Ph3.3	5	15.3	413	1.17	2896	160	240	15
Ph3.3	15	15.3	413	1.26	2921	167	242	17
Ph3.3	25	15.3	413	1.25	2785	159	230	15
Ph3.3	35	15.3	413	1.44	2807	175	262	17
Ph3.4	5	8.2	416	0.71	2888	235	235	16
Ph3.4	15	8.2	416	0.98	3324	258	258	17
Ph3.4	25	8.2	416	0.99	3075	305	305	20
Ph3.4	35	8.2	416	1.15	3530	274	274	21
Ph3.4	45	8.2	416	1.11	3567	269	269	16
Ph3.5	5	0.0	417	0.79	2878	162	257	21
Ph3.5	15	0.0	417	0.98	3246	170	258	15
Ph3.5	25	0.0	417	0.78	3540	187	303	21
Ph3.5	35	0.0	417	1.15	3750	184	258	16
Ph3.5	45	0.0	417	1.12	3590	191	302	18
Ph3.5	55	0.0	417	1.23	3710	188	245	19

Soils - planar transect:

Sample pit	depth (cm)	distance from ridge (m)	elevation (m)	density (g cm^{-3})	[Ti] (ppm)	± (1σ)	[Zr] (ppm)	± (1σ)
Ph4.1	5	28.4	401	1.08	2609	166	260	20
Ph4.1	15	28.4	401	1.23	2681	170	304	23
Ph4.1	25	28.4	401	1.31	2882	183	252	19
Ph4.1	35	28.4	401	1.18	2829	180	317	24
Ph4.1	45	28.4	401	1.27	2999	190	282	21
Ph4.1	55	28.4	401	1.30	2721	173	332	25
Ph4.1	65	28.4	401	1.11	3199	284	272	20
Ph4.1	75	28.4	401	1.34	3259	185	306	34
Ph4.2	5	19.0	406	1.16	2911	245	267	20
Ph4.2	15	19.0	406	1.13	3115	154	240	20
Ph4.2	25	19.0	406	1.20	2923	275	250	19
Ph4.2	35	19.0	406	1.35	3492	193	280	20
Ph4.2	45	19.0	406	1.27	3650	197	293	21
Ph4.2	55	19.0	406	1.39	3521	289	301	20
Ph4.2	65	19.0	406	1.11	3708	188	249	18
Ph4.2	75	19.0	406	1.35	3709	192	230	19
Ph4.3	5	10.1	410	1.05	2857	161	240	18
Ph4.3	15	10.1	410	1.05	3456	270	224	18
Ph4.3	25	10.1	410	1.04	3133	177	248	19
Ph4.3	35	10.1	410	1.39	3401	186	257	19
Ph4.3	45	10.1	410	1.31	3584	189	312	25
Ph4.3	55	10.1	410	1.56	3676	337	263	18
Ph4.3	65	10.1	410	1.37	3929	203	234	20
Ph4.3	75	10.1	410	1.35	3992	208	273	21

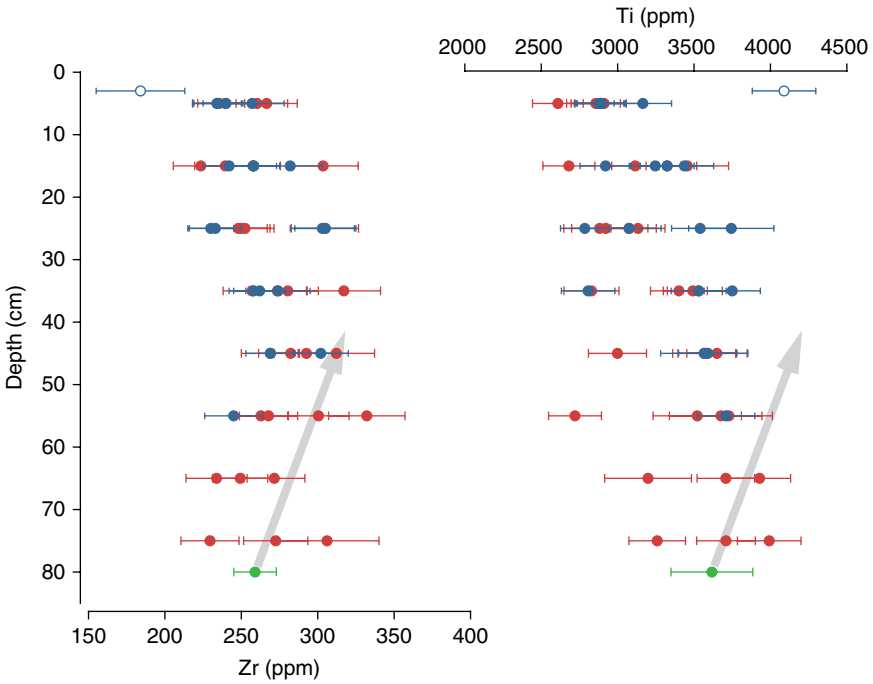

Figure 5.3 Concentrations of Zr (left side) are relatively uniform with depth in pits from both the convex (blue) and planar (red) soil transects and are similar to the average concentration in saprolite (green). Ti concentrations (right side) decrease from the saprolite (green) towards the surface. Neither Zr nor Ti concentrations follow the expected pattern of enrichment from saprolite towards the surface with increasing weathering (gray arrows). In both panels, the open blue circle represents concentrations measured in pit Ph3.1, which is excluded from the analysis that follows as an outlier.

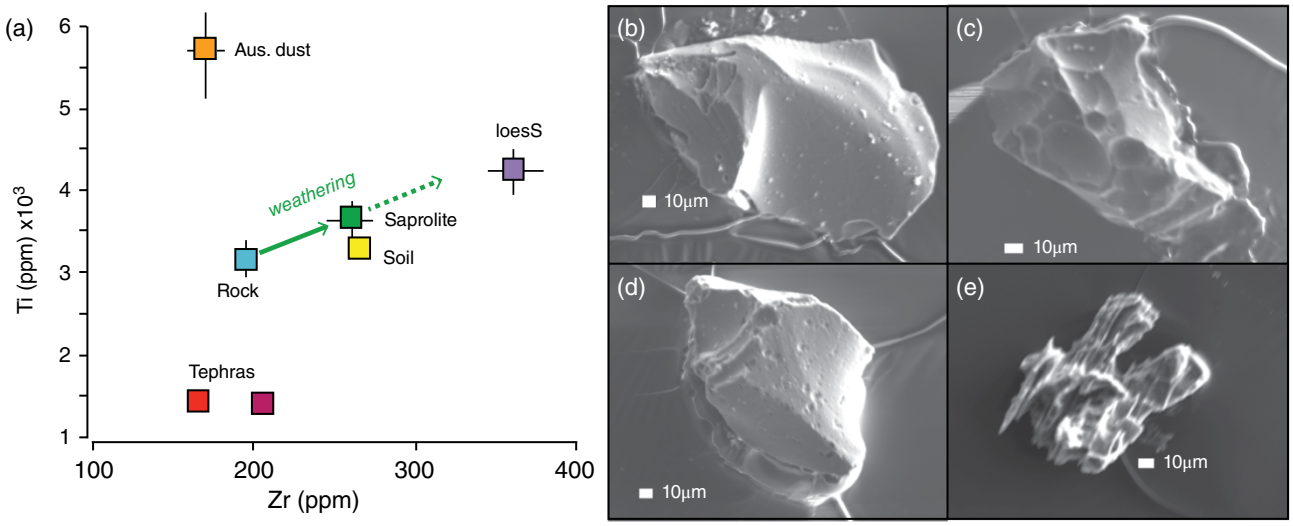

Figure 5.4 In (a), weathering of bedrock should enrich Ti and Zr in saprolite and soil (green arrow); soil composition falls off this expected trend. Based on their Ti and Zr compositions, tephras from the Taupō Volcanic Zone (red and magenta) provide the best candidates for additional inputs to soil, and local loess (violet) and Australian dust (orange) are poor candidates. Errors shown in (a) are one standard error, and where absent are smaller than the markers. Volcanic glass extracted from soils (b–e) is abundant and sometimes appears to be highly weathered (e). Glass is visually distinguished from bedrock-derived grains based on its glassy texture, sharp edges (b–e), conchoidal fracture (b–d), bubbly textures (c), and fresh weathering pits on smooth surfaces (d).

Taupō Volcanic Center and is not known to extend as far south as our field site (Wilson & Walker, 1985). In contrast, the 26.5 ka eruption was much larger, and the Ōruanui tephra is roughly 50 cm thick in ashfall deposits ~40 km northwest of our field site (Wilson et al., 2006). The Ōruanui tephra is thus the most likely source of additional parent material in soils at our field sites.

Using the geochemical composition of bedrock and the Ōruanui tephra as two parent materials, we can calculate the fraction of soils that originate from the tephra (*f_tephra*). Here we follow the approach of Ferrier et al. (2011), who used Ti and Zr concentrations in rock (*r*), soil (*s*), and dust (*d*) to calculate the fraction of dust in soils from Idaho, USA. As Ferrier et al. note, this approach is appropriate for settings in which chemical mass losses to weathering are ongoing during regolith development, rather than assuming negligible mass loss to weathering or requiring direct measurement of dust fluxes as in previous approaches.

$$f\_tephra = \left(\frac{Ti_r}{Ti_s} - \frac{Zr_r}{Zr_s}\right)\left[\frac{Ti_r - Ti_d}{Ti_s} - \frac{Zr_r - Zr_d}{Zr_s}\right]^{-1} \quad (4)$$

Here we have averaged elemental compositions with height above the soil pit bottom across the pits from each transect, and we plot the convex and planar transects separately. In both transects, we calculate *f_tephra* to be at or near 0 in the bottom 15 cm of the soil profile, and ~0.5 for depths >15 cm above the pit bottom (Figure 5.5). This observation, that tephra comprises roughly half the soil, is consistent with a large ashfall volume that is incorporated into a well-mixed soil profile. The near-0 values at the base of each pit also imply that the regolith remains essentially unmixed near the saprolite boundary.

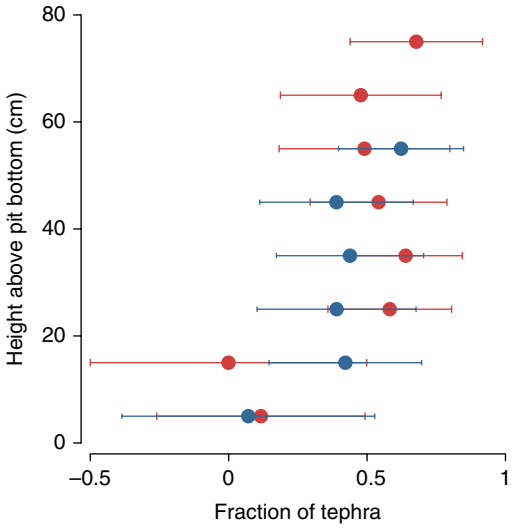

Figure 5.5 The fraction of tephra calculated using equation (4) (Ferrier et al., 2011) in soils from both planar (red) and convex (blue) transects is near zero at the bottom of soil pits. Tephra makes up roughly 50% of the soils >15 cm above pit bottoms, implying a significant volume of tephra input and effective soil mixing to these depths. Note that soil depths from Table 5.3 have been scaled as height above the bottom of the pit.

5.5. FORWARD MODEL AND MODEL RESULTS

The observations in the previous sections constrain the most likely origin of tephra in the Wairarapa soils using geochemistry, and equation (3) allows us to calculate how much tephra is present in soils. In order to understand weathering and nutrient fluxes in these soils, however, we must assess the impact that a weathering tephra may have on the overall weathering profile. To quantify the relative contributions of tephra and bedrock to total weathering in the soil column, we employ a simple forward model.

Our soil model follows the "vertical conveyor belt" framework introduced in Figure 5.1, with the addition of tephra from above that is deposited in a single event. Because of this "bottom-up" framework in which weathering intensity should increase from the bottom of the pit towards the surface, we reference soil depth to the base of the soil pit rather than the surface. The intensity of chemical weathering is quantified by the chemical depletion fraction (CDF, equation [2]) and is defined at the soil-saprolite boundary by the average CDF measured in saprolites (Table 5.3). Inputs to the model are allowed to vary with height above the pit base, and include the CDF of bedrock-derived material, the CDF of tephra, and the fraction of tephra present in the soil (*f_tephra*). The CDF of bedrock-derived material must increase linearly towards the surface, as expected for soils with longer residence time in the soil. The modeled maximum CDF of rock-derived material is allowed to vary between the saprolite value and 1. Based on the fraction of tephra in the soil (*f_tephra*) calculated in the previous section (Figure 5.5), *f_tephra* is assumed to follow a step function with depth. The step change is assigned a height above the pit base of 15 cm, and a value of *f_tehpra* = 0 is assumed for soils below this depth, indicating no soil mixing below that depth. As an independent check against the Ferrier et al. (2011) approach, the modeled value of *f_tephra* is allowed to vary for soils more than 15 cm above the pit base. We assume that all tephra has the same CDF since it was deposited at the same time; this value is allowed to vary between 0 and 1. Varying each of these parameters across the specified ranges, we predict Ti and Zr concentrations in the soil with height above the pit base (Figure 5.6).

We calculate the misfit between predicted and measured concentrations of Ti and Zr, normalized to mean

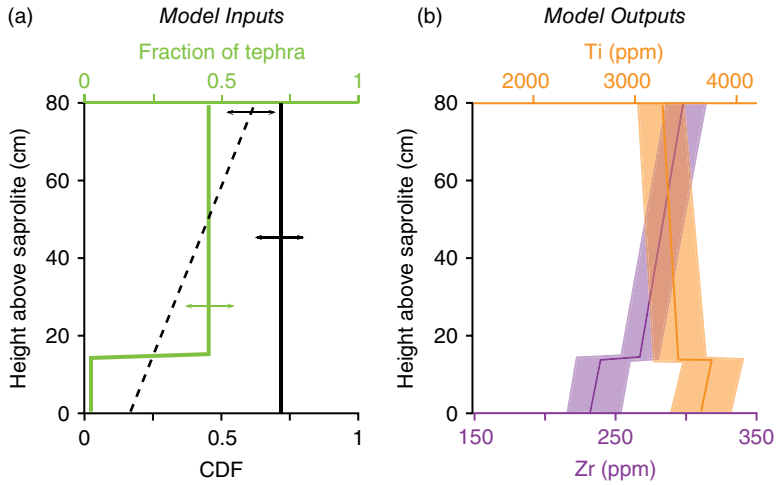

Figure 5.6 Tunable parameters in the mixing model (a) include the chemical depletion fraction (CDF) of tephra (black solid line), the maximum CDF of rock-derived material at the surface (dashed black line), and the fraction of tephra in soils >15 cm from the bottom of the pit (green line). The fraction of tephra below 15 cm is assumed to be 0, and the CDF of rock-derived material at the bottom of the pit is the average saprolite CDF. The model predicts Zr and Ti concentrations through the soil column (b), which can be compared to measured concentrations. Predicted concentrations are here shown as solid lines (Zr in purple, Ti in orange), with 95% confidence intervals (shaded) based on a bootstrapping approach using the uncertainties from bedrock and tephra measurements.

measured concentration for each element across the transect. By normalizing the misfits to Ti and Zr, respectively, we can use both elements to find the best-fit model, giving equal weight to each element. We find the best-fit model by minimizing the total sum of squared errors (SSE) between the modeled and predicted concentrations in both elements. The 95% confidence interval for modeled Ti and Zr concentrations is determined using a bootstrapping approach that incorporates the uncertainties in bedrock and tephra elemental compositions. In this approach, the elemental composition of each parent material is determined randomly from a normal distribution defined by the mean and standard error of Ti and Zr in each material (bedrock, tephra), and the best-fit parameters for weathering and *f_tephra* are employed in the model. The analysis is then repeated 10,000 times. The modeled Ti and Zr concentrations that fall within the 97.5th and 2.5th percentiles at each soil depth are taken to represent the 95% confidence interval (Figure 5.7).

Each transect (convex and planar) is modeled separately, but the best-fit models for each transect agree quite closely. In the best-fit model, the maximum CDF of bedrock-derived material in soils is the same as the CDF of the underlying saprolite; in other words, weathering of rock-derived material in the soil profile is neglible. The best-fit CDF of tephra is 0.45 in the convex transect and 0.47 in the planar transect. The modeled fraction of tephras in soils more than 15 cm above the pit base is 0.47 in both transects, which is consistent with *f_tephra* calculated using Ferrier et al.'s approach (Figure 5.5).

5.6. DISCUSSION

5.6.1. Weathering Trends

Immobile element concentrations from bedrock and saprolite show that the parent rock arrives at the soil/saprolite boundary already moderately weathered. The Cretaceous greywacke that underlays much of New Zealand is dominated by quartz, feldspar, and altered lithic and volcanic fragments (Barnes, 1990). These rocks are also typically highly fractured from intense tectonic activity, which provides pathways for surface water to penetrate deep into bedrock. High rainfall rates and rapid infiltration along fractures may mean that deep saprolite weathering progresses rapidly and leaves relatively few minerals available to weather in soils. In this case, solutes may be leaving the system in deep groundwater, never circulating up into soils.

Our results show no discernable difference in weathering intensity with depth and no difference between pits along the convex and planar transects. This is contrary to expectations from literature (e.g. Dixon et al., 2009; Yoo et al., 2009). This discrepancy from previous work likely arises because of the large fraction of tephra, which was all emplaced at the same time and is well integrated into the soil column. It is also consistent with very little weathering of material incorporated from underlying saprolite, which is already weathered by the time it gets to the soil-saprolite boundary.

The conclusions summarized above are predicated on the immobility of Ti and Zr. While Ti and Zr are

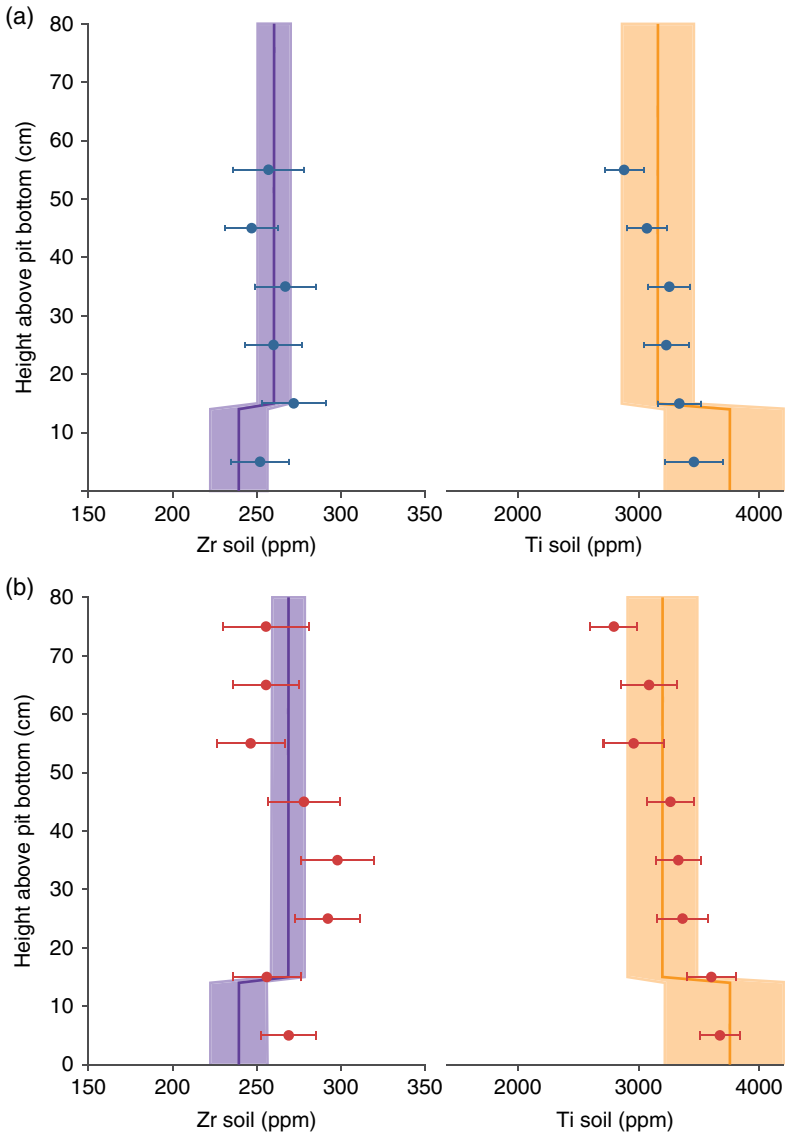

Figure 5.7 Predicted Zr (purple) and Ti (orange) concentrations from best-fit models (solid orange and purple lines) with 95% confidence intervals (shaded areas), plotted with measured trace element concentrations across the convex (blue, panel a) and planar (red, panel b) transects. Measured concentrations are the mean ± standard error of the samples at a given sample depth from each transect.

considered to be highly immobile, there is evidence of Ti mobility in some settings (Gardner, 1980). Observations of Ti mobility are, however, limited to mafic rocks or highly acidic soils (pH < 4), so it seems unlikely that Ti is mobile at our field sites. We have not directly measured pH in our soils, but pH measured in 26 soils in the northern Wairarapa valley range from 4.8 to 7.5, with a mean value of 6.3. Due to similar underlying bedrock, vegetation, and climatic conditions, we expect our soils to have similar pH values. Ti and Zr have also been shown to be immobile in more acidic New Zealand soils (Dawson et al., 1991). If Ti were mobile, the fraction of tephra present in soils would be lower than calculated here. However, rhyolitic glass is certainly present in relatively high abundance in soils (Figure 5.4 b–e), and the low Zr concentrations still suggest very little weathering in the soil profile. Therefore, our main observations and conclusions would remain the same, and we consider them to be robust.

5.6.2. Local History of Tephra Deposition, Soil Mixing, and Deforestation

Based on our observations, the Ōruanui eruption (26.5 ka) is the only likely candidate to provide large amounts of tephra for these soils; a 50 cm ashfall layer from this eruption has been documented 40 km to the northwest of

our site (Wilson, 2001). If these soils are old enough to contain Ōruanui tephra, they must have once been much thicker than they currently are. Using our measured soil production rate for the site and a minimum age of 26.5 ka, the expected steady state soil thickness would be 2.3 m, while the measured soils are only 30–80 cm thick. This implies significant erosion since 26.5 ka, and likely much later, since the tephra is well mixed into the soils. Deforestation coincident with either human arrival (burning) or colonial-era land clearing has caused significant erosion from steep slopes in New Zealand. This pulse of erosion has been observed in lake cores as a sharp increase in charcoal at 750 yrs BP, coincident with increase in sediment accumulation rates and median grain size (McWethy et al., 2010, 2014; Trodahl et al., 2016). Human-induced erosion is also compatible with our data since, if it was quite recent, it will not be reflected in the average long-term soil production rate. In this case, the previous soil thickness would be the dominant influence on the production rate of ^{10}Be at soil-saprolite boundary.

If soil depth has recently changed, we must account for this change when calculating ^{10}Be-derived soil production rates because overlying soil shields the saprolite from cosmic radiation. Using an iterative approach, we can solve for a corrected soil production rate and minimum previous soil depth. For a given hypothetical soil depth, we calculate the ^{10}Be production rate at soil-saprolite boundary and the soil production rate predicted by our measured ^{10}Be concentration. With this new soil production rate, we calculate the thickness of soil generated over 26.5 ka. We then repeat this process with different soil depths until the depth equals the soil thickness generated over 26.5 ka. Since 26.5 ka is a minimum age for these soils, this approach yields a minimum previous soil depth and therefore a maximum soil production rate. The resulting soil production rate, 49 ± 3 m/Myr, is quite slow but is similar to soil production rates measured elsewhere in the region. The modeled soil thickness of 130 cm suggests ~85 cm of soil erosion occurred since human modification of the landscape.

While we have calculated these rates and depths using a "bottom-up" approach, this estimate of soil thickness also agrees with "top-down" models of soil production, wherein soil develops with a downward-advancing weathering front from the surface. Such models depend on water infiltration rates, porosity, and grain size (Egli et al., 2018; Yu et al., 2019). Using a timescale of 26.5 ka as a minimum estimate of the time over which the soil has developed and average values of infiltration, porosity, and grain size from humid sites (1 m/yr, 0.4, and 41 μm, respectively), the percolation model of Yu et al. (2019) predicts a soil production rate of 80 m/Myr and a steady-state soil thickness of 1.0 m. If we include deposition of 50 cm of tephra, the resulting soil production rate (SPR) is about 40 m/Myr and the steady-state soil thickness is ~150 cm (A. Hunt, pers. comm.). While the percolation model–derived SPR and soil thickness are only estimates based on average values, they provide an independent estimate that agrees well with our revised soil thickness and SPR based on ^{10}Be and geochemical observations.

Our data also show that the tephra is well mixed into the soil to within 15 cm of the soil-saprolite boundary. This would have required mixing of soils down to ~1.1 m. Mass movements and colluvial processes, particularly in the absence of vegetation, might have mixed tephra-rich material into soils in localized areas. Bioturbation would provide more spatially uniform mixing (e.g. Roering et al., 2002), though to our knowledge it has not been documented to depths over a meter. Most native New Zealand trees are more shallowly rooted, and there are no burrowing mammals. Kōuka, New Zealand cabbage trees (*Cordyline australis*), however, are deeply-rooted (up to 2 m or more for mature trees; Czernin & Phillips, 2005) and are abundant in native forests across the region, providing a plausible mixing mechanism.

Taken together, these observations allow us to construct a history for Rocky Hill over the last ~27 ka (Figure 5.8). Prior to 26.5 ka, soil developed atop saprolite and accumulated to depths of at least 80 cm. At 26.5 ka, the Ōruanui tephra was deposited to a depth of about 50 cm, burying the landscape. Reforestation by deep-rooted trees and/or shallow landsliding and soil creep mixed the soils to within ~15 cm of the saprolite; and finally, soil stripping coincident with anthropogenic deforestation and burning removed ~85 cm of soil from much of the landscape.

5.6.3. Implications for Deep Weathering and Nutrient Cycling

Our geochemical data suggest that saprolite arrives at the soil-saprolite boundary already moderately weathered, and that little to no weathering of bedrock-derived material occurs in the soil profile. These data have important implications for deep weathering and nutrient cycling in these soils, and by extension to sites underlain by similar bedrock all over New Zealand.

Deep saprolite weathering is likely enabled because of the high rainfall rates and fractured bedrock, which should facilitate high rates of groundwater flow and associated weathering. It is possible that this groundwater flow never recirculates back to the surface, and any rock-derived nutrients are never circulated into soils. Tephra may thus be an important nutrient source, as it provides the bulk of the material that is actually weathering in soils. This is particularly important for this agricultural region given that the bedrock is relatively poor in

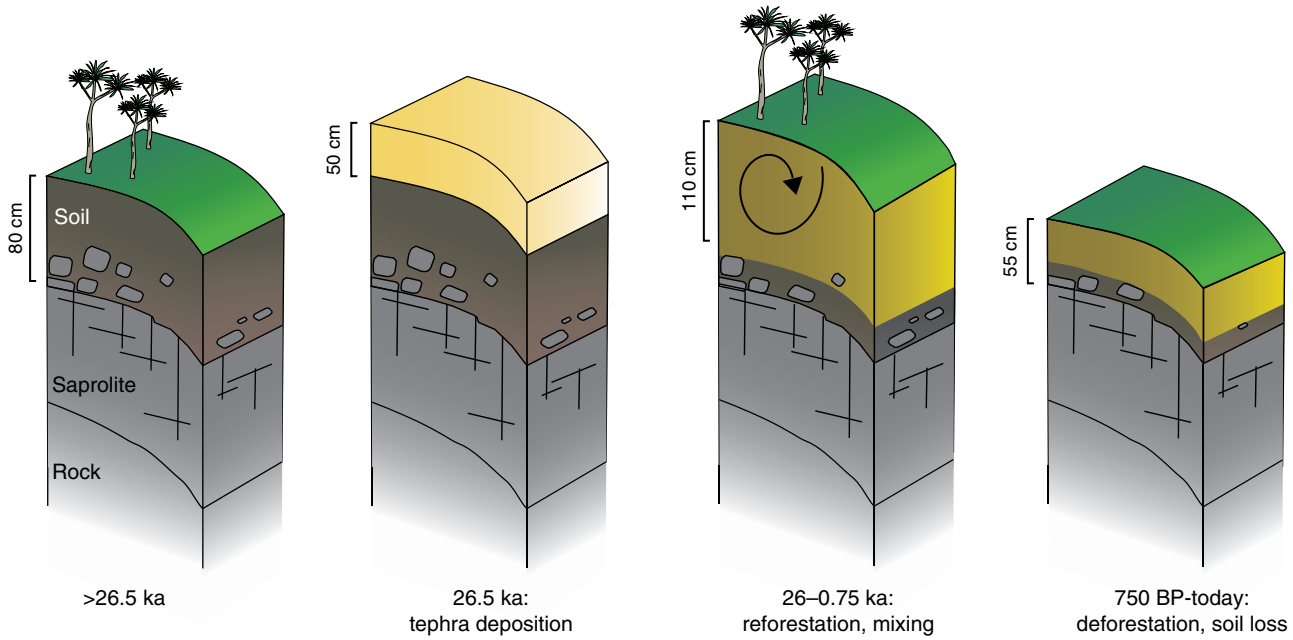

Figure 5.8 Summary of the landscape history of Rocky Hill over the last 27 ka.

rock-derived nutrients like P (average 0.07%; Petlab, 2018). Rhyolitic tephras are also low in most important nutrients that are supplied from rocks (P, Mg, Na, Ca, etc.). However, because weathering of bedrock-derived material in the soil is minimal and rapidly weathering tephras contribute the bulk of the solute flux, even nutrient-poor volcanic glass may be an important source of nutrients for biota.

By removing mass as solutes in groundwater, deep saprolite weathering may be one way to exceed proposed kinetic limits on weathering and soil production (e.g. Dixon & von Blanckenburg, 2012). Kinetic limits to soil production are proposed in settings with rapid erosion rates, where mineral residence times in soils are too short for weathering to keep pace with erosion. If, however, deep weathering in saprolite brings material into the active soil in a preweathered state, weathering in the mobile soil layer need not keep pace with erosion. The soil production rate we measure at Rocky Hill is certainly not fast enough to imply kinetic limitation, but our observation of deep saprolite weathering may provide insight into rapid soil production rates measured elsewhere in New Zealand (i.e. Larsen et al., 2014).

While we argue that the airfall deposits in these Wairarapa soils are dominated by tephra rather than loess, Pleistocene loess deposits are observed in the region. The geochemical data presented here also point to the source of these regional loess deposits. The Ti:Zr ratio of the measured loess deposits follows the expected weathering trend from rock to saprolite (Figure 5.4). This suggests that the loess deposited during glacial-interglacial transitions in the Wairarapa region was originally eroded from bedrock with a similar Ti:Zr ratio as the underlying greywacke at our field site. This same and similar Cretaceous greywacke units make up much of the region, including the nearby Tararua Mountain Range. While we cannot definitively rule out other sources, the composition of loess is more consistent with local origins in the Tararuas rather than far-traveled Australian dust. If loess is indeed dominated by weathered local material rather than exogenous dust, it may not be a significant source of nutrients for biota; this highlights the relative importance of tephras as possible nutrient sources across New Zealand's North Island.

5.7. CONCLUSIONS

Trace element geochemistry and soil production rates from the Waiararapa region on New Zealand's North Island reveal a complex history of weathering and erosion over the last 27 ka. Geochemistry suggests that 47% of the extant soil was deposited as tephra, most likely the Ōruanui tephra erupted from the Taupō Volcanic Center at 26.5 ka. The underlying bedrock is delivered to the saprolite-soil boundary already moderately weathered. This deep weathering of bedrock provides a mechanism to bypass kinetic limits on chemical weathering that should exist in rapidly eroding settings. However, we suggest that the solutes released from this weathering will be flushed out by groundwater, leaving the saprolite relatively

weathered and nutrient-poor. At our field site, further chemical weathering of the bedrock-derived material in soils is negligible, while tephras undergo substantial chemical weathering in the soils. In such cases, weathering inputs to soil from dust (volcanic ash in this case) can supply the majority of rock-derived nutrients to soils.

ACKNOWLEDGMENTS

The authors would like to thank Allen Hunt for excellent editing and two anonymous reviewers for their comments and suggestions. We also thank Gareth Hickey and Gavin Holden for field and lab assistance. Attila Stopic at ANSTO conducted the neutron activation analysis, which was funded by the Australian Institute of Nuclear Science and Engineering. Financial support was also provided by a Rutherford Discovery Fellowship (Te Apārangi Royal Society of NZ) and Victoria University of Wellington.

REFERENCES

Anderson, S. P., Dietrich, W. E., & Brimhall, G. H. (2002). Weathering profiles, mass-balance analysis, and rates of solute loss: Linkages between weathering and erosion in a small, steep catchment. *GSA Bulletin*, *114*, 1143–1158. doi:10.1130/0016-7606(2002)114<1143:WPMBAA>2.0.CO;2

Arvin, L. J., Riebe, C. S., Aciego, S. M., & Blakowski, M. A. (2017). Global patterns of dust and bedrock nutrient supply to montane ecosystems. *Science Advances*, *3*, eaao1588. doi:10.1126/sciadv.aao1588

Barnes, P. M. (1990). Provenance of Cretaceous accretionary wedge sediments: The Mangapokia Formation, Wairarapa, New Zealand. *New Zealand Journal of Geology and Geophysics*, *33*, 125-–35.

Berner, R. A., Lasaga, A. C., & Garrels, R. M. (1983). The carbonate-silicate geochemical cycle and its effect on atmospheric carbon dioxide over the past 100 million years. *American Journal of Science*, *283*, 641–683.

Brantley, S. L. (2008). Kinetics of mineral dissolution. In S. L. Brantley, J. D. Kubicki, & A. F. White (Eds.), *Kinetics of water-rock interaction* (pp. 151–210). New York: Springer New York. doi:10.1007/978-0-387-73563-4_5

Brantley, S. L., & White, A. F. (2009). Approaches to modeling weathered regolith. *Reviews in Mineralogy and Geochemistry*, *70*, 435–484.

Brimhall, G. H., & Dietrich, W. E. (1987). Constitutive mass balance relations between chemical composition, volume, density, porosity, and strain in metasomatic hydrochemical systems: Results on weathering and pedogenesis. *Geochimica et Cosmochimica Acta*, *51*, 567–587, doi:10.1016/0016-7037(87)90070-6

Chadwick, O. A., Derry, L. A., Vitousek, P. M., Huebert, B. J., & Hedin, L. O. (1999). Changing sources of nutrients during four million years of ecosystem development. *Nature*, *397*, 491. doi:10.1038/17276

Chmeleff J., von Blanckenburg F., Kossert K. & Jakob D. (2010). Determination of the ^{10}Be half-life by multicollector ICP-MS and liquid scintillation counting. *Nuclear Instruments and Methods in Physics Research, Section B: Beam Interactions with Materials and Atoms*, *268*(2), 192–199.

Cronin, S. J., Neal, V. E., & Palmer, A. S. (1996). Investigation of an aggrading paleosol developed into andesitic ring-plain deposits: Ruapehu volcano, New Zealand. *Geoderma*, *69*, 119–135.

Czernin, A., & Phillips, C. (2005). Below-ground morphology of Cordyline australis (New Zealand cabbage tree) and its suitability for river bank stabilisation. *New Zealand Journal of Botany*, *43*, 851–864. doi:10.1080/0028825X.2005.9512995

Dawson, B. S. W., Fergusson, J. E., Campbell, A. S., & Cutler, E. J. B. (1991). Depletion of first-row transition metals in a chronosequence of soils in the Reefton area of New Zealand. *Geoderma*, *48*, 271–296. doi:10.1016/0016-7061(91)90048-X

Dixon, J. L., Chadwick, O. A., & Vitousek, P. M. (2016). Climate-driven thresholds for chemical weathering in post-glacial soils of New Zealand. *Journal of Geophysical Research: Earth Surface*, *121*, 1619–1634. doi:10.1002/2016JF003864

Dixon, J. L., Heimsath, A., Kaste, J., & Amundson, R. (2009). Climate-driven processes of hillslope weathering. *Geology*, *37*, 975–978. doi:10.1130/G30045A.1

Dixon, J. L., & von Blanckenburg, F. (2012). Soils as pacemakers and limiters of global silicate weathering. *Comptes Rendus Geoscience*, *344*, 597–609. doi:10.1016/j.crte.2012.10.012

Drever, J. I. (1994). The effect of land plants on weathering rates of silicate minerals. *Geochimica et Cosmochimica Acta*, *58*, 2325–2332. doi:10.1016/0016-7037(94)90013-2

Dunai, T. J. (2010). *Cosmogenic nuclides: Principles, concepts and applications in the Earth surface sciences*. Cambridge University Press.

Eden, D. N., & Hammond, A. P. (2003). Dust accumulation in the New Zealand region since the last glacial maximum. *Quaternary Science Reviews*, *22*, 2037–2052. doi:10.1016/S0277-3791(03)00168-9

Egli, M., Hunt, A., Dahms, D., Raab, G., Derungs, C., Raimondi, S., & Yu, F. (2018). Prediction of soil formation as a function of age using the percolation theory approach. *Frontiers in Environmental Science*. doi:10.3389/fenvs.2018.00108

Egli, M., Mirabella, A., Sartori, G., & Fitze, P. (2003). Weathering rates as a function of climate: Results from a climosequence of the Val Genova (Trentino, Italian Alps). *Geoderma*, *111*, 99–121. doi:10.1016/S0016-7061(02)00256-2

Ferrier, K. L., Kirchner, J. W., & Finkel, R. C. (2011). Estimating millennial-scale rates of dust incorporation into eroding hillslope regolith using cosmogenic nuclides and immobile weathering tracers. *Journal of Geophysical Research*, *116*. doi:10.1029/2011JF001991

Ferrier, K. L., & West, N. (2017). Responses of chemical erosion rates to transient perturbations in physical erosion rates, and implications for relationships between chemical and physical erosion rates in regolith-mantled hillslopes. *Earth and Planetary Science Letters*, *474*, 447–456. doi:10.1016/j.epsl.2017.07.002

Foley, L. A. (1984). *The geology of basement rocks in the south-eastern Tararua Range*, North Island, New Zealand. http://researcharchive.vuw.ac.nz/handle/10063/2289 (accessed April 2019).

Froggatt, P. C. (1982). A study of some aspects of the volcanic history of the Lake Taupo Area, North Island, *New Zealand*. PhD thesis, Victoria University of Wellington.

Gardner, L. R. (1980). Mobilization of Al and Ti during weathering: Isovolumetric geochemical evidence. *Chemical Geology*, *30*, 151–165. doi:10.1016/0009-2541(80)90122-9

Gehrels, M. J., Lowe, D. J., Hazell, Z. J., & Newnham, R. M. (2006). A continuous 5300-yr Holocene cryptotephrostratigraphic record from northern New Zealand and implications for tephrochronology and volcanic hazard assessment. *The Holocene*, *16*, 173–187. doi:10.1191/0959683606hl918rp

Gosse, J. C., & Phillips, F. M. (2001). Terrestrial in situ cosmogenic nuclides: Theory and application. *Quaternary Science Reviews*, *20*, 1475–1560. doi:10.1016/S0277-3791(00)00171-2

Harden, J. W. (1987). Soils developed in granitic alluvium near Merced, California. *US Geol Survey Bull,* # 1590-A.

Hartmann, J., & Moosdorf, N. (2011). Chemical weathering rates of silicate-dominated lithological classes and associated liberation rates of phosphorus on the Japanese Archipelago—Implications for global scale analysis. *Chemical Geology*, *287*, 125–157. doi:10.1016/j.chemgeo.2010.12.004

Heimsath, A. M., Dietrich, W. E., Nishiizumi, K., & Finkel, R. C. (1999). Cosmogenic nuclides, topography, and the spatial variation of soil depth. *Geomorphology*, *27*, 151–172. doi:10.1016/S0169-555X(98)00095-6

Hopkins, J. L., & Seward, D. (2019). Towards robust tephra correlations in early and pre-Quaternary sediments: A case study from North Island, New Zealand. *Quaternary Geochronology*, *50*, 91–108. doi:10.1016/j.quageo.2018.12.001

Ibarra, D. E., Caves, J. K., Moon, S., Thomas, D. L., Hartmann, J., Chamberlain, C. P., & Maher, K. (2016). Differential weathering of basaltic and granitic catchments from concentration–discharge relationships. *Geochimica et Cosmochimica Acta*, *190*, 265–293. doi:10.1016/j.gca.2016.07.006

Jacobson, A. D., Blum, J. D., Chamberlain, C. P., Craw, D., & Koons, P. O. (2003). Climatic and tectonic controls on chemical weathering in the New Zealand Southern Alps. *Geochimica et Cosmochimica Acta*, *67*, 29–46. doi:10.1016/S0016-7037(02)01053-0

Johnsson, M. A., Ellen, S. E., & McKittrick, M. A. (1993). Intensity and duration of chemical weathering: An example from soil clays of the southeastern Koolau Mountains, Oahu, Hawaii. Geological Society of America, Special Paper 284.

Kohl, C. P., & Nishiizumi, K. (1992). Chemical isolation of quartz for measurement of in-situ-produced cosmogenic nuclides. *Geochimica et Cosmochimica Acta*, *56*, 3583–3587. doi:10.1016/0016-7037(92)90401-4

Korschinek G., Bergmaier A., Faestermann T., Gerstmann U. C., Knie K., Rugel G., et al. (2010). A new value for the ^{10}Be half-life by heavy ion elastic recoil detection and liquid scintillation counting. *Nuclear Instruments and Methods in Physics Research Section B: Beam Interactions with Materials and Atoms*, *268*(2), 187–191.

Kruger, P. (1971). *Principles of activation analysis*. New York: Wiley-Interscience.

Kump, L. R., Brantley, S. L., & Arthur, M. A. (2000). Chemical weathering, atmospheric CO2, and climate. *Annual Review of Earth and Planetary Sciences*, *28*, 611–667. doi:10.1146/annurev.earth.28.1.611

Larsen, I. J., Almond, P. C., Eger, A., Stone, J. O., Montgomery, D. R., & Malcolm, B. (2014). Rapid Soil production and weathering in the southern alps, New Zealand. *Science*, *343*, 637–640. doi:10.1126/science.1244908

Lee, J. M., Begg, J. G., & Forsyth, P. J. (2002). *Geology of the Wairarapa area*. Institute of Geological and Nuclear Sciences.

Likens, G. E., Bormann, F. H., Johnson, N. M., & Pierce, R. S. (1967). The Calcium, Magnesium, Potassium, and Sodium Budgets for a Small Forested Ecosystem. *Ecology*, *48*, 772–785, doi:10.2307/1933735.

Lowe, D. J., Shane, P.A.R., Alloway, B. V., & Newnham, R. M. (2008). Fingerprints and age models for widespread New Zealand tephra marker beds erupted since 30,000 years ago: A framework for NZ-INTIMATE. *Quaternary Science Reviews*, *27*, 95–126. doi:10.1016/j.quascirev.2007.01.013

Marshall, J. A., Roering, J. J., Bartlein, P. J., Gavin, D. G., Granger, D. E., Rempel, A. W., et al. (2015). Frost for the trees: Did climate increase erosion in unglaciated landscapes during the late Pleistocene? *Science Advances*, *1*, e1500715. doi:10.1126/sciadv.1500715

Marx, S. K., Kamber, B. S., & McGowan, H. A. (2005). Provenance of long-travelled dust determined with ultra-trace-element composition: A pilot study with samples from New Zealand glaciers. *Earth Surface Processes and Landforms*, *30*, 699–716. doi:10.1002/esp.1169

McWethy, D. B., Whitlock, C., Wilmshurst, J. M., McGlone, M. S., Fromont, M., Li, X., et al. (2010). Rapid landscape transformation in South Island, New Zealand, following initial Polynesian settlement. *Proceedings of the National Academy of Sciences*, *107*, 21343–21348. doi:10.1073/pnas.1011801107

McWethy, D. B., Wilmshurst, J. M., Whitlock, C., Wood, J. R., & McGlone, M. S. (2014). A High-Resolution Chronology of Rapid Forest Transitions following Polynesian Arrival in New Zealand. *PLOS ONE*, *9*, p. e111328, doi:10.1371/journal.pone.0111328.

National Institute of Water and Atmospheric Research (NIWA). Masterton climate report. https://data.niwa.co.nz

Norton, K. P., Molnar, P., & Schlunegger, F. (2014). The role of climate-driven chemical weathering on soil production. *Geomorphology*, *204*, 510–517. doi:10.1016/j.geomorph.2013.08.030

Norton, K. P., & von Blanckenburg, F. (2010). Silicate weathering of soil-mantled slopes in an active Alpine landscape. *Geochimica et Cosmochimica Acta*, *74*, 5243–5258. doi:10.1016/j.gca.2010.06.019

Petlab (2018). New Zealand's national geoanalysis database, http://pet.gns.cri.nz

Pollard, A. M., & Heron, C. (1996). *Archaeological chemistry*. Cambridge, UK: Royal Society of Chemistry.

Porder, S., Hilley, G. E., & Chadwick, O. A. (2007). Chemical weathering, mass loss, and dust inputs across a climate by time matrix in the Hawaiian Islands. *Earth and Planetary Science Letters*, *258*, 414–427. doi:10.1016/j.epsl.2007.03.047

Riebe, C. S., Kirchner, J. W., & Finkel, R. C. (2003). Long-term rates of chemical weathering and physical erosion from cosmogenic nuclides and geochemical mass balance. *Geochimica*

et Cosmochimica Acta, *67*, 4411–4427. doi:10.1016/S0016-7037(03)00382-X

Riebe, C. S., Kirchner, J. W., & Finkel, R. C. (2004). Sharp decrease in long-term chemical weathering rates along an altitudinal transect. *Earth and Planetary Science Letters*, *218*, 421–434. doi:10.1016/S0012-821X(03)00673-3

Riebe, C. S., Kirchner, J. W., Granger, D. E., & Finkel, R. C. (2001). Strong tectonic and weak climatic control of long-term chemical weathering rates. *Geology*, *29*, 511–514. doi:10.1130/0091-7613(2001)029<0511:STAWCC>2.0.CO;2

Roering, J. J., Almond, P., Tonkin, P., & McKean, J. (2002). Soil transport driven by biological processes over millennial time scales. *Geology*, *30*, 1115–1118. doi:10.1130/0091-7613(2002)030<1115:STDBBP>2.0.CO;2

Stallard, R. F. (1988). Weathering and erosion in the humid tropics. In A. Lerman & M. Meybeck (Eds.), *Physical and chemical weathering in geochemical cycles* (NATO ASI Series, pp. 225–246). Dordrecht, The Netherlands: Springer. doi:10.1007/978-94-009-3071-1_11

Strong, D. T., Turnbull, R. E., Haubrock, S., & Mortimer, N. (2016). Petlab: New Zealand's national rock catalogue and geoanalytical database. *New Zealand Journal of Geology and Geophysics*, *59*, 475–481. doi:10.1080/00288306.2016.1157086

Sutton, A. N., Blake, S., Wilson, C.J.N., & Charlier, B.L.A. (2000). Late Quaternary evolution of a hyperactive rhyolite magmatic system: Taupo volcanic centre, New Zealand. *Journal of the Geological Society*, *157*, 537–552. doi:10.1144/jgs.157.3.537

Trodahl, M. I., Rees, A.B.H., Newnham, R. M., & Vandergoes, M. J. (2016). Late Holocene geomorphic history of Lake Wairarapa, North Island, New Zealand. *New Zealand Journal of Geology and Geophysics*, *59*, 330–340. doi:10.1080/00288306.2015.1133663

von Blanckenburg, F. (2004). Cosmogenic nuclide evidence for low weathering and denudation in the wet, tropical highlands of Sri Lanka. *Journal of Geophysical Research*, *109*. doi:10.1029/2003JF000049

West, A. J., Galy, A., & Bickle, M. (2005). Tectonic and climatic controls on silicate weathering. *Earth and Planetary Science Letters*, *235*, 211–228. doi:10.1016/j.epsl.2005.03.020

White, A. F., & Blum, A. E. (1995). Effects of climate on chemical weathering in watersheds. *Geochimica et Cosmochimica Acta*, *59*, 1729–1747. doi:10.1016/0016-7037(95)00078-E

White, A. F., Bullen, T. D., Schulz, M. S., Blum, A. E., Huntington, T. G., & Peters, N. E. (2001). Differential rates of feldspar weathering in granitic regoliths. *Geochimica et Cosmochimica Acta*, *65*, 847–869. doi:10.1016/S0016-7037(00)00577-9

Wilson, C. J. N. (2001). The 26.5ka Oruanui eruption, New Zealand: An introduction and overview. *Journal of Volcanology and Geothermal Research*, *112*, 133–174. doi:10.1016/S0377-0273(01)00239-6

Wilson, C. J. N., Blake, S., Charlier, B. L. A., & Sutton, A. N. (2006). The 26·5 ka Oruanui Eruption, Taupo Volcano, New Zealand: Development, Characteristics and Evacuation of a Large Rhyolitic Magma Body. *Journal of Petrology*, *47*, 35–69, doi:10.1093/petrology/egi066.

Wilson, C. J. N., & Walker, G. P. L. (1985). The Taupo eruption, New Zealand: I. General aspects. *Philosophical Transactions of the Royal Society of London. Series A, Mathematical and Physical Sciences*, *314*, 199–228. doi:10.1098/rsta.1985.0019

Yoo, K., Amundson, R., Heimsath, A. M., Dietrich, W. E., & Brimhall, G. H. (2007). Integration of geochemical mass balance with sediment transport to calculate rates of soil chemical weathering and transport on hillslopes. *Journal of Geophysical Research*, *112*. doi:10.1029/2005JF000402

Yoo, K., & Mudd, S. M. (2008). Toward process-based modeling of geochemical soil formation across diverse landforms: A new mathematical framework. *Geoderma*, *146*, 248–260, doi:10.1016/j.geoderma.2008.05.029

Yoo, K., Mudd, S. M., Sanderman, J., Amundson, R., & Blum, A. (2009). Spatial patterns and controls of soil chemical weathering rates along a transient hillslope. *Earth and Planetary Science Letters*, *288*, 184–193. doi:10.1016/j.epsl.2009.09.021

Yu, F., Hunt, A., Egli, M., & Raab, G. (2019). Comparison and contrast in soil depth evolution for steady state and stochastic erosion processes: Possible implications for landslide prediction. *Geochemistry, Geophysics, Geosystems*, *20(6),* 2886–2906. doi:10.1029/2018GC008125

6

The Origin and Formation of Clay Minerals in Alpine Soils

Markus Egli[1] and Aldo Mirabella[2]

ABSTRACT

Clay minerals are among the most chemically active components and are a bridge between the inorganic and organic parts of a soil. The clay minerals influence pedogenetic processes by interacting with cations and inorganic and organic compounds, influencing the nutrition of the plants and the structure of the soils. Clay minerals are phyllosilicates and can in soils be either inherited from the parent material, neoformed, or transformed from precursor minerals. Relatively shortly after exposure of the parent material to atmospheric conditions, important mineral transformation reactions can occur, even in cold alpine climates. In alpine environments, the soil system reacts in a particularly sensitive way at the beginning of soil formation, i.e. during the first c. 3000 years. With time, the formation and transformation rates, and thus changes, decelerate. Smectitic components, and therefore 2:1 mineral structures, are the weathering steady-state products. Although weathering conditions are particularly intense close to the timberline and on pole-facing sites, 2:1 minerals strongly prevail over kaolinite or gibbsite, which are most often encountered as a weathering steady-state product in tropical regions. Smectitic components enrich under conditions of high percolation rates, cool climates (close to the treeline), high amounts of organic ligands, low erosion, stable conditions, and thus low soil production rates. Smectite formation therefore relates not only to the paradigms of the percolation theory, but the type and presence of vegetation and the production of organic ligands are additional driving factors.

6.1. THE ORIGIN OF CLAYS IN SOILS

6.1.1. Introduction

Soils are complex bodies formed by several constituents, which can be subdivided into two main categories: organic and inorganic. Clay minerals, the most abundant and chemically active part of the surface mineral world from a chemical and biological point of view, are the key to understanding the links between nature (life) and its substrate (Velde & Meunier, 2008). In most cases, clays are a weathering product of the near surface. The formation, transformation, and stability of clays are dependent on the precursor minerals and the surrounding environmental conditions.

Clay minerals in soils usually have a large surface. In addition, clay minerals are often charged electrically (isomorphic cation substitution); they are chemically very active and provide a major driving force for the behavior of many elements and thus pollutants and life-essential nutrients. They respond to changes in vegetation and create the necessary qualities for soil fertility. Soil structure (aggregation and capillary retention of water) is largely dominated by clay mineral interaction with organic matter (Velde & Meunier, 2008). Cation exchange and retention (concerning essential elements for plant growth) are dominated by clay minerals and the organic matter present in the soils. This provides suitable conditions for plant growth. Furthermore, almost 80%–90% of the micro-organisms inhabiting soil are on solid surfaces, particularly on clay minerals. Mechanisms by

[1]*Department of Geography, University of Zürich, Zürich, Switzerland*

[2]*Piazza S. Nicolò 23, 95036 Randazzo, Italy*

Hydrogeology, Chemical Weathering, and Soil Formation, Geophysical Monograph 257, First Edition.
Edited by Allen Hunt, Markus Egli, and Boris Faybishenko.

DOI: 10.1002/9781119563952.ch6

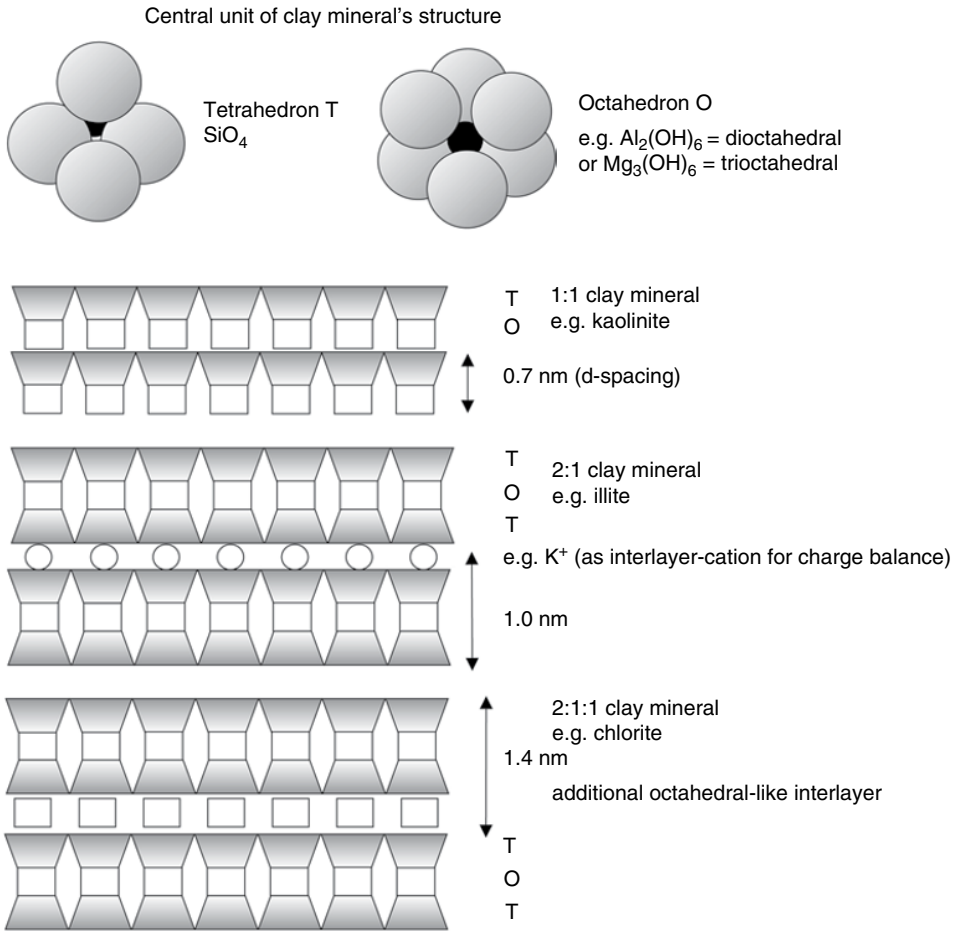

Figure 6.1 Structural elements of clay minerals.

which these microorganisms interact with soil surfaces have been much studied. Some bacterial cells produce extracellular polysaccharides that interact with clay particles, extracellular enzymes may absorb on clay minerals, or DNA may be protected by clays from degradation. On one hand, the adsorption of organic compounds on a clay mineral surface retards their microbial degradation (Nannipieri et al., 2017). On the other hand, the surfaces of clay minerals can themselves catalyze many reactions. Clay minerals and Mn (III and IV) and Fe (III) oxides catalyze electron transfer reactions, such as the oxidation of phenols and polyphenols. Other abiotic reactions catalyzed by soil minerals include deamination, polymerization, polycondensation, and ring cleavage (Nannipieri et al., 2017).

Operationally, clays are defined most commonly as particles having a diameter of <2 μm; consequently, they are minerals having a very small size that are barely visible to the naked eye. Specifically, clay minerals are constituted from hydrated silicates having Al, and to a lesser extent, Mg and Fe. In the clay fraction, clay minerals can be found together with quartz, feldspar, carbonates, oxides, hydroxides, and hydrated oxides of iron, aluminium, manganese, and organic matter. However, with decreasing size, the relative surface area of minerals becomes increasingly important. Clay minerals have more surface area than other minerals of the same grain size, due to their particularity of being sheet shaped.

Clay minerals are phyllosilicates. Their structure is defined by a combination of tetrahedral layers that are composed of SiO_2 and octahedral layers (e.g. Al_2O_3; Figure 6.1). Depending on the sequence of tetrahedral and octahedral layers, 1:1, 2:1, and 2:1:1 clay mineral types are identified.

The origin of clays in soils may be geological (inheritance) or due to weathering (hydrolysis) and transformation of primary minerals. For most clays, stability is in fact only attained at the very surface of the Earth (Velde, 1995). They are hydrated, having interacted with water, and consequently have a physical structure that is different from the pre-existing minerals. In some species of clays, the activity of the surface (surface charge) is increased by an internal surface into which charged ions or molecules can find their way (Velde, 1995).

Until 1929, clay minerals had been considered amorphous, because they were indistinct in optical microscopes. Thanks to the advent of X-ray diffraction and its use in the study of soil clays, it was possible to determine that the clay-sized inorganic material in soils was composed of crystalline components (Cady & Flach, 1997). Ever since, XRD diffraction analysis has been the major tool in the identification of clay minerals and the refinement of their crystal structure, even though other instrumental techniques have also been developed and are used for specific purposes.

Clay minerals and clays are of fundamental importance in the study of weathering and genetic processes that lead to different types of soils, starting from the parent rock. Their peculiarity is due to their important chemical and physical properties. In fact, they are affected by soil formation but also influence nearly all pedogenetic processes by interacting with cations and inorganic and organic compounds; they thus also have an effect on the nutrition of plants and the structure of the soils.

6.1.2. Inheritance, Transformation, and Neoformation

Siliceous rocks are formed beneath the Earth's surface and are unstable when raised to the surface. Soil is a transition phase as the rocks change to more stable chemical states (Bohn et al., 1985). Weathering is the process of this transformation and is a nearly ubiquitous process on the Earth's surface. The processes and rates of alteration of rocks and minerals from their original state to phases that are more stable at the Earth's surface are basic to Earth science research.

Soils form by the weathering of the bedrock (parent material) through physical, chemical, and biological processes. Soils inherit the clays and clay minerals, including primary clay minerals that were liberated during the disintegration of the rock. The primary clay minerals (geological inheritance) in a pedogenic environment are unstable and give rise to the formation of secondary minerals. This is because the rock formation has occurred under much higher temperature and pressure conditions than those found at the soil surface.

In turn, over geological time, clays may undergo distinct transformations, e.g. those caused by erosion, sedimentation, deep burial, or hydrothermal processes. Different natural environments of clay formation and transformation exist (Wilson, 1994). Following wind and water erosion, the weathered rock material and soils can be transported from where they were formed and deposited in a sedimentary environment. Following their burial, these sediments can undergo further deep burial, where they are subjected to medium pressures and temperatures and endure chemical and biological transformations; thus, this is a diagenetic process. When the altered material interacts with water at conditions below the earth surface, clay minerals can form under the influence of hydrothermal action. Upon burial and heating, dioctahedral smectite, for example, reacts in the diagenetic environment to yield mixed-layered illite-smectite and finally illite (Eberl, 1984). If the sediments undergo a deep burial, in which they can also encounter igneous rocks, the process of alteration is much stronger and the sedimentary rocks are subject to metamorphic alterations or even can melt to produce igneous rocks. When these rocks rise to the surface, they enter again into the described cycle of transformations.

As previously mentioned, primary minerals inherited in the soil by the parent material undergo physical, chemical, and biological alteration and change their mineralogical characteristics. As an example, (newly formed) kaolinites in soils are often highly disordered and many of the peaks in their XRD patterns are poorly resolved; that means that the peaks are broader and their intensities lower when compared with kaolinites of an unaltered rock (Churchman & Lowe, 2012). As regards secondary illites in soils, there is little doubt that they derive from the transformation of primary micas. In younger less-weathered soils in warm-arid environments, micas are found in the clay fraction and derive from the fragmentation of primary micas by physical weathering processes (Fanning et al., 1989). Early on, Kapoor (1972) recognized that the crystal structures of clay minerals determine their weathering and alteration behavior: e.g. dioctahedral mica species are more resistant to weathering than trioctahedral species. For example, when di- and trioctahedral micas are the principal minerals in the C horizon of Podzols, the latter is degraded to various types of clays depending upon the degree of weathering, while muscovite remains practically unaffected.

The mineralogy of clays neoformed in the weathering environment is a function of solution chemistry, with the most dilute solutions favoring the formation of the least soluble clays (Eberl, 1984). Chemical weathering and (clay) mineral neoformation or transformation determines the evolution trajectory of soils. The velocity and direction of change is fundamentally dependent on the composition of the parent material in which the soils develop. Any changes in the soils must, therefore, be seen in the context of the parent material composition.

6.2. ENVIRONMENTAL CONDITIONS AND CLAY FORMATION

6.2.1. Introduction

The formation, transformation, and stability of clays are dependent on the precursor minerals and, particularly, the surrounding environmental conditions. Soil sequences may give insight into the influence of a state

factor on the weathering rates. According to Jenny (1941), soils are understood to develop under the influence of the following state factors: parent material, climate, topography, biological activity, and time. In order to be quantitatively useful, Jenny (1941) suggested treating the state factors as independent variables, in the sense that field sites exist where the factors can be considered to vary independently (Dahms et al., 2012). The ways in which a factor is considered to be independent are (1) the range of variability of the factor is quite small and (2) variation in the factor is large but has only a negligible effect on the property studied.

In this chapter we summarize results performed in the European Alps, where the effect of some state factors on the general trait of mineral weathering and clay minerals formation and transformation was drawn. An overview of the considered sites is given in Figure 6.2. We focus on the state factors time, climate (and topography), and parent material. Organisms are implicitly also included in the factor climate as they notably change, e.g. with altitude or aspect (Gómez-Brandón et al., 2017). Theoretical and experimental studies of chemical weathering indicate that the rate at which chemical weathering, and thus mineral formation and transformation (in other words, the rate at which reaction products may be removed from the weathering front) occurs is very often limited by solute transport (Egli et al., 2018; Hunt & Ghanbarian, 2016; Yu & Hunt, 2017). The contact time of soil water with mineral surfaces and the percolation rate of water through the soil is decisive for mineral reactions and chemical weathering.

6.2.2. Time (Chronosequences)

The time over which natural chemical weathering, mineral formation, and transformation occur (White & Hochella, 1992) can usually not be reproduced in experimental studies (White & Brantley, 2003). Chronosequences are useful for estimating field weathering rates (element depletion rates, mineral transformation rates, etc.; e.g. Föllmi et al., 2009; Mavris et al., 2011; etc.) and tracing mineral reactions and transformations. A sequence of soils formed on progressively older landscapes is considered a chronosequence, and the quantitative variability of a characteristic along these landscapes is a chronofunction (Birkeland, 1999; Dahms et al., 2012; Mahaney et al., 2011). Soil chronosequences can provide information about weathering regimes and soil morphogenesis (Mahaney et al., 2011) and have greatly advanced our understanding of short- to long-term landscape processes (Walker et al., 2010; Dahms et al., 2012).

Egli et al. (2001) and Egli, Mirabella & Fitze (2003) noted that the most distinct changes in soil clay mineralogy of soils in the European Alps on granitic or gneiss host material occur within the first 1000–3000 years of soil development. Trioctahedral phyllosilicates are especially strongly weathered over a time span of about 11,000 years. Smectite and regularly interstratified dioctahedral

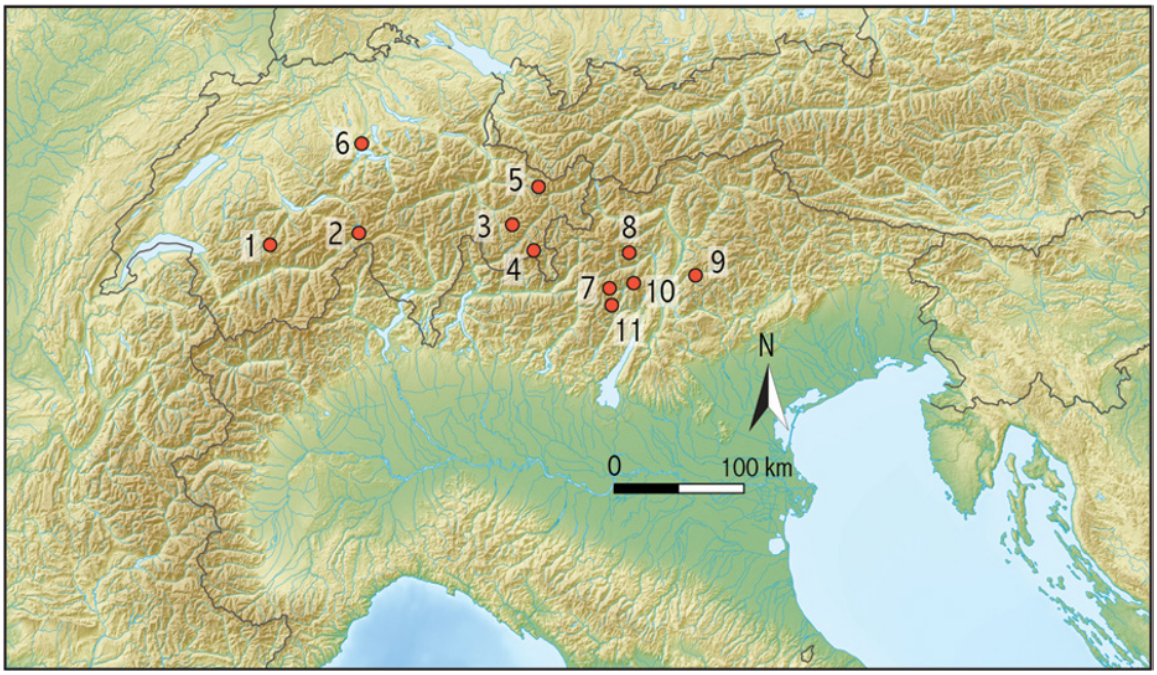

Figure 6.2 Alpine investigation areas with data used. 1 = Schmadri, 2 = Gletsch, 3 = Val Mulix, 4 = Morteratsch, 5 = Vereina, 6 = Meggerwald, 7 = Val Genova, 7 = Val di Rabbi, 9 = Val di Fiemme, 10 = Val di Fumo, 11 = Val Breguzzo.

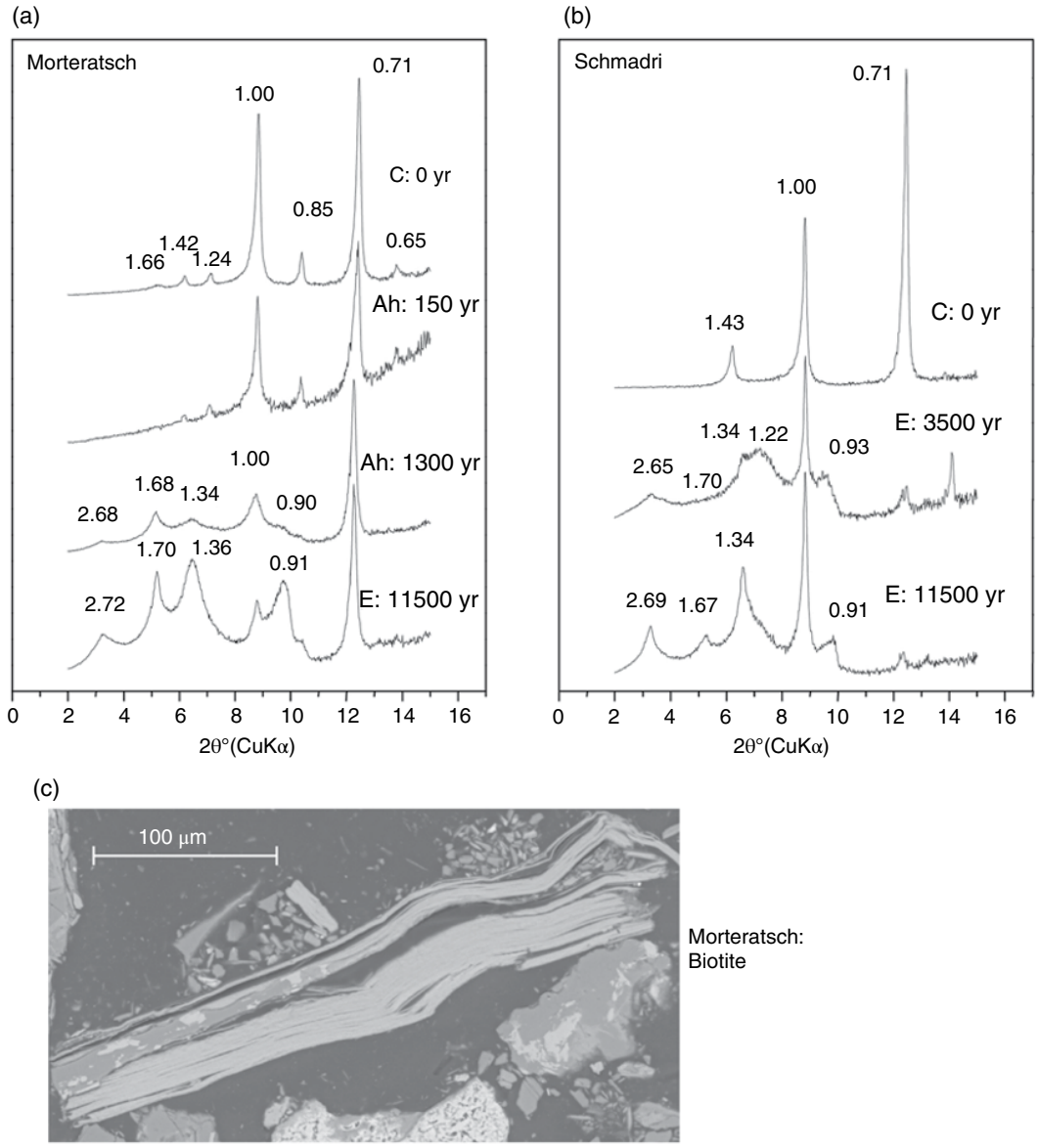

Figure 6.3 X-ray diffractograms of ethylene glycol solvated clay samples from the surface horizons of soils having different ages and SEM image from different areas (modified from Egli et al., 2003a): (a) Morteratsch and (b) Schmadri. (c) Delamination (start of weathering) of a biotite crystallite (modified from Mavris et al., 2012).

mica/smectite can usually be found in the most weathered horizons (Figure 6.3). The origin of smectite is traced back to both chlorite and trioctahedral mica, which supports the notion that smectite is the steady-state product of chlorite alteration, while regularly interstratified mica/smectite (or even smectite) are the steady-state products of mica weathering in strongly leached and acidified horizons (Figure 6.3; Egli et al., 2001; Egli, Mirabella, & Fitze, 2003). The pedogenetic smectites from an E or Bs horizons of alpine Podzols often include several populations with various interlayer charges. This heterogeneity seems to be related to the nature of the precursor minerals. The easily weatherable chlorite transforms via intermediate weathering products such as HIV (hydroxy-interlayered vermiculite) or HIS (hydroxy-interlayered smectite) into smectite (cf. Egli et al., 2001).

Trioctahedral mica also transforms easily into smectite. This process is accompanied by a concomitant decrease of trioctahedral and a corresponding increase of dioctahedral minerals in the clay fraction. The first stage of weathering of mica leads to a regularly interstratified mica-vermiculite (hydrobiotite) that is often present in the Bhs horizon of Podzols (cf. Egli et al., 2001). Similarly, mica-HIS is an intermediate weathering product

(Figure 6.3). Further weathering usually leads to a regularly or irregularly interstratified mica-smectite mineral that can often be found in the E horizon of Podzols. Thus, extensive mineral weathering results in significant losses of chlorite and mica and the corresponding formation of smectite or interlayered smectite products.

Mavris et al. (2011) were able to identify rapid changes in the clay mineralogical composition at the very early stages of soil formation in a glacier forefield. These soils all had ages of less than 150 years. Smectite was found to be actively formed from the beginning of soil evolution. However, some smectite (low charge) and vermiculite (high charge) were already present in the parent material. Different sources apparently contributed to the formation of smectite, such as biotite, hornblende, and plagioclase. Furthermore, irregularly and regularly interstratified clay minerals (mica-HIV or mica-vermiculite) formed immediately after the start of the moraine's exposure to weathering. As a consequence of these transformations, (1) the layer charge distributions changed over time with the formation of some new low- and high-charged phases, and (2) dioctahedral species increased at the expense of trioctahedral ones.

Both chemical and physical transformations, namely, elemental depletion of K versus Fe, and increased delamination over time, confirm biotite weathering in these glacier forefield sediments (Figure 6.3). Biotite typically expands with time, delaminates, and contributes to an increase in porosity of the weathered rock (Caner, 2011; Graham et al., 2010; Mavris et al., 2012; Meunier et al., 2007). The opening of fissures in mineral grains and the increase in porosity ultimately give rise to accelerated alteration rates (Figure 6.3).

Several studies confirm that the formation rates of clay minerals are highest in young soils (Egli et al. 2001, 2003a; Föllmi et al., 2009; Mavris et al., 2011, 2012). These rates steadily decrease with increasing soil age (Egli et al., 2002). It seems to be a common feature in Alpine soils that smectitic components are a steady-state product of mineral weathering and transformation. Consequently, the amount of smectite or smectitic compounds is indicative of the age of soils in these alpine environments.

An important issue, however, that emerges with soil chronosequences is the following: is the assumption of continuous soil development justified? Changes in soil-forming factors may be continuous or abrupt, e.g. by natural erosion, catastrophic natural events (landslide) and by influence of humans (land-usage change, intensification of agriculture). In a coevolutional model, soil formation is regarded to be discontinuous over time and conceptualized by "progressive" or "regressive" process groups (Johnson & Watson-Steger 1987; Sommer et al., 2008). By necessity, the assumption then is that the environmental conditions did not change over the considered period and that soil evolution has been progressive and constant. However, changing environmental conditions and soil-landscape development itself can lead to an acceleration, deceleration, or reversal of process rates, e.g. coevolution (Phillips, 2015). For instance, in sensitive Alpine environmental areas, a recent acceleration of (geomorphic) processes is measured or postulated, particularly in the permafrost zone where melting subsurface ice leads to increased slope activities (Zollinger et al., 2017). In this light, the way clay minerals react to fast-changing or repeatedly changing environmental conditions remains a topic that merits further investigation. The main weathering trajectories are, however, known (see Figure 6.4).

6.2.3. Climate and Vegetation (Climosequences)

In the Alps, as in most alpine regions, mean annual temperature decreases and annual precipitation increases with increasing altitude (Figure 6.5). Along such a sequence, vegetation also changes, usually from deciduous forest to mixed forests to coniferous forests. The timberline in the mid to southeastern part of the Alps varies between about 1800 m a.s.l. and 2300 m a.s.l. Above the treeline, dwarf shrubs and alpine meadows follow.

Climate in general and hydrologic conditions are expected to affect soil erosion and accumulation rates, chemical weathering, and biological processes. Investigation of elevational gradients of soils from moderate to high alpine climate zones (climosequences) often shows that element denudation is greatest in subalpine forests near timberline (Egli, Mirabella, Sartori, et al., 2003). Weathering rates decrease with both higher and lower altitudes. Similar to the weathering rates, the highest smectite contents (the steady-state product of weathering in Alpine soils) in the clay fraction were measured at sites near the timberline (Figure 6.5). Figure 6.6 shows that the smectite content does not have a linear relationship to either mean annual temperature or annual precipitation. Higher precipitation rates, incomplete organic matter decomposition (Ascher et al., 2012; Bardelli et al., 2017; Egli et al., 2006, 2016), and the production of chelating compounds in the soil are believed to promote the production of smectites. Together with the high production of chelating compounds and the relatively high soil percolation rates, ideal conditions for intense weathering and clay mineral transformation are found close to the timberline (Figure 6.7). As an intermediate product of intense weathering, HIS is often found. The more chelating components present in the soil solution, the more readily HIS transforms into smectite.

In a study carried out in an altitudinal sequence of five podzolic soils in Italian Alpine regions, Mirabella and

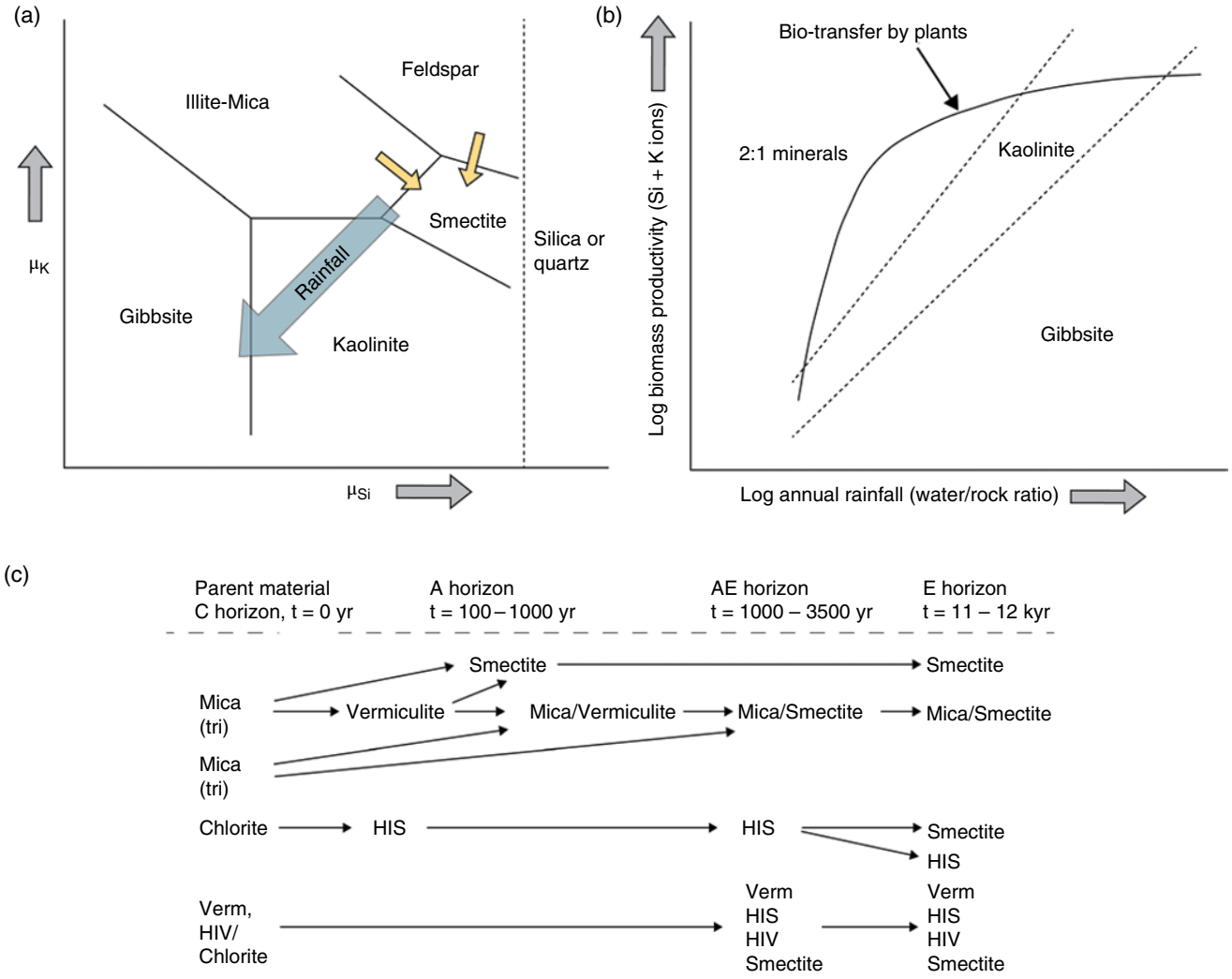

Figure 6.4 (a) μSi–μK diagram showing the normal water-rock interaction path of chemical change. Loss of potassium (i.e. lowering of the chemical potential) and decrease in silica (lower chemical potential of Si) change the clay mineralogy from 2:1 minerals, illite-mica and smectites to kaolinite and eventually gibbsite (according to Velde & Meunier, 2008). (b) Schematic diagram representing the effect of rainfall on plant activity (biomass) and thus translocation within the soil profile of alkalis and silica. Depending on the amount of rainfall and plant productivity, either 2:1 clay minerals or kaolinite and gibbsite prevail (scheme according to Velde & Meunier, 2008). (c) Weathering and transformation trajectories observed in Alpine soils. Steady state product of weathering in Alpine soils remain in the fields of 2:1 clay minerals (see [a] and [b]).

Egli (2003) found that smectites formed in the surface horizons either from chlorite (through the removal of hydroxy interlayers) or from mica. Mica weathers in a first step to regularly or irregularly interstratified clay minerals. One important finding was that the intermediate products of chlorite weathering, found in the intermediate Bhs and Bs horizons, were HISs. This means that the reduction of charge of chlorite occurred before the removal of the hydroxy interlayer by chelating organic acids (Figure 6.4).

The effect of precipitation on weathering rates and mineral transformation seems to be greater at higher temperatures and thus lower altitudes. In moderate to subalpine climate zones, changes in precipitation are more relevant for weathering and mineral transformation. A change in water availability has a greater effect than at high altitudes where water availability is less limiting. At very low mean annual temperatures, however, changes in temperature seem to account more for changes in weathering rates and mineral transformations.

One of the major factors in alteration (water/rock interaction) is that of rainfall and hence the ionic concentrations in solutions in alteration profiles. The lower the rainfall and evapotranspiration, the more influence a

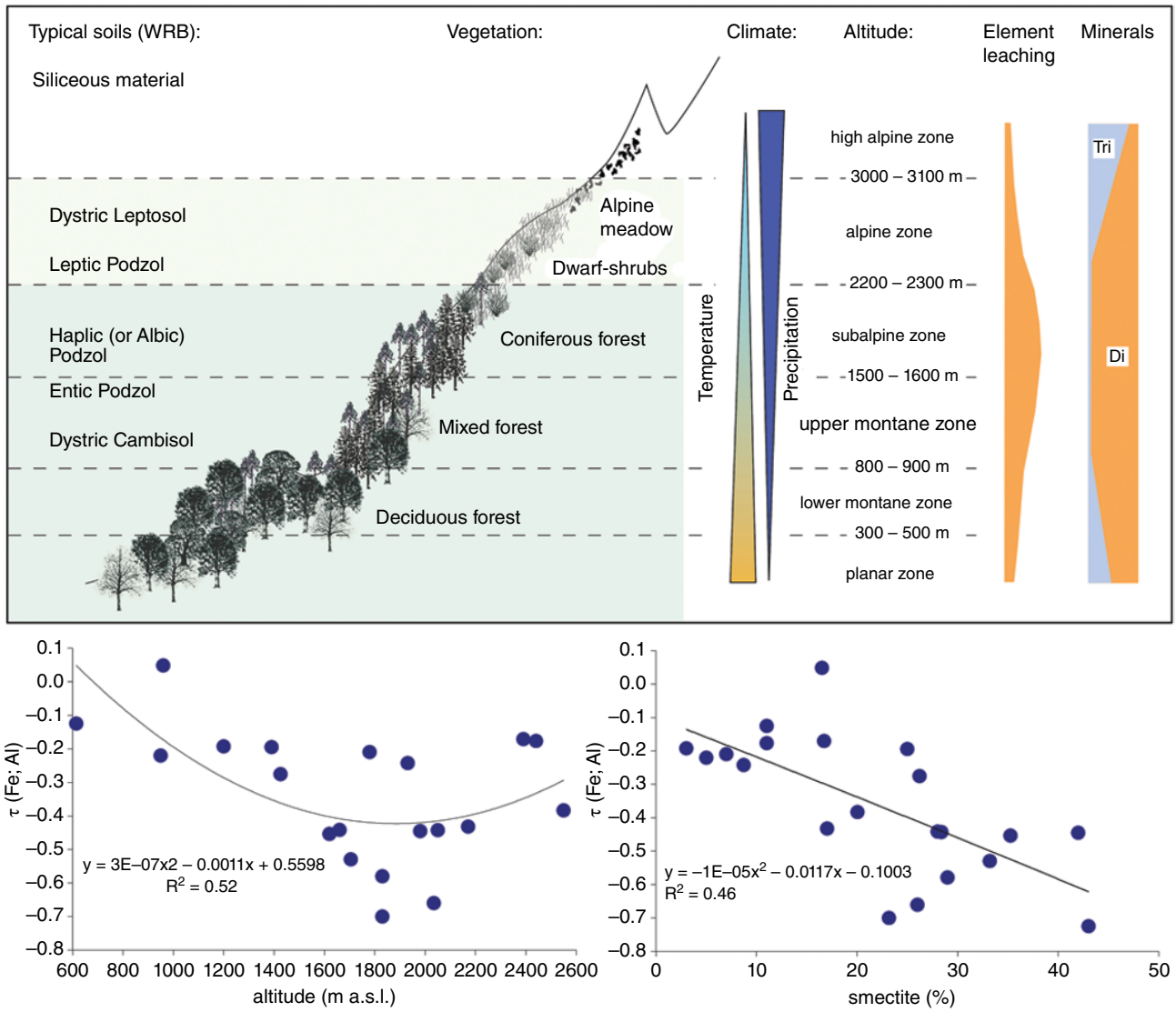

Figure 6.5 Altitudinal sequence with soils, vegetation, climate, and elemental leaching. $\tau_{j,w}$ = open-system mass transport function (relative losses of Fe and Al) with: $\tau_{j,w} = \left(\frac{C_{j,w}C_{i,p}}{C_{i,w}C_{j,p}}\right) - 1$; where $C_{j,p}$ (g/t) = the concentration of element j in the unweathered parent material and $C_{j,w}$ (g/t) = the concentration of element j in the weathered product. $\tau_{j,w}$ is plotted as a function of altitude and smectite content.

rock and its chemistry will have on the clays formed (Velde & Meunier, 2008). Although tropical plants (rainforests) are among the most effective Si recyclers (Street-Perrot & Barker, 2008), the stronger loss over time of silica relative to aluminium (and iron) marks one important difference between the alteration of soils developing in temperate/alpine and humid tropical climates, respectively, and it has strong implications on the overall chemistry of clay minerals. In addition, tropical soils are often depleted in basic cations (e.g. K). As a result, humid tropical soils do not have high smectite contents (Velde & Meunier, 2008), as the main constituent of clays in humid tropical soils is kaolinite (Figure 6.4). Particularly in such environments, high rainfall rates promote kaolinite formation at the expense of 2:1 clay minerals. Vegetation, which is strongly dependent on the climate, can counteract such a process. In tropical environments, the incredibly high biomass uptakes these nutrients almost as quickly as they are released, whereas the high rates of precipitation flush them out of the profile. Plants are often associated with fertile silica- and potassium-rich clay minerals such as smectite and illite. Most plants contain silica in the form of phytoliths (Farmer et al., 2005). After decomposition of the plant material, the soil is

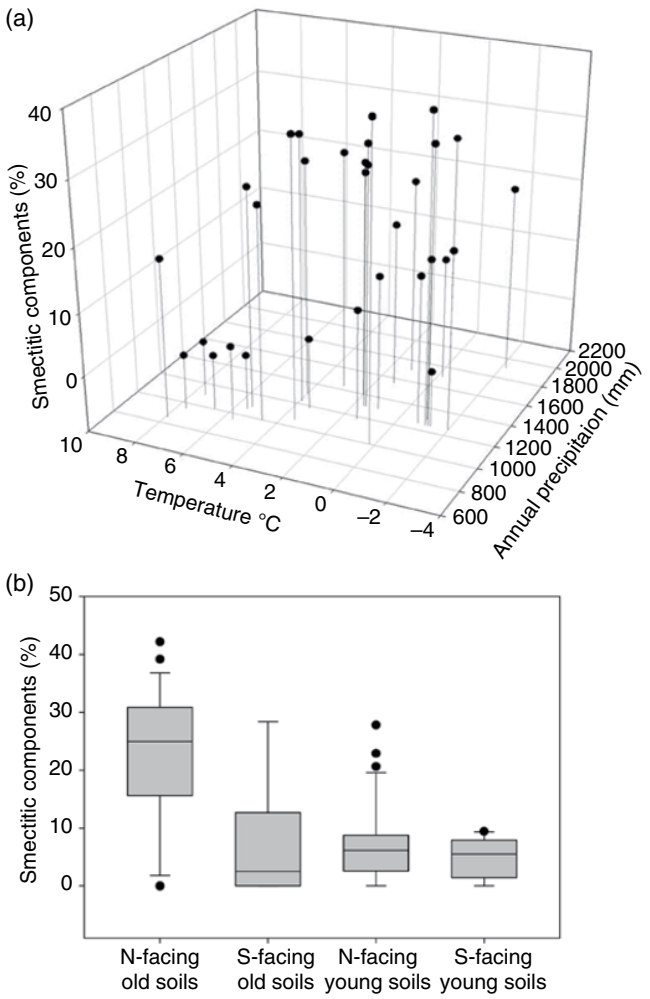

Figure 6.6 Content of smectitic minerals as function of climate (amount of precipitation and mean annual temperature) for a) old soils (age > 3000 yr) and b) as a function of slope aspect for old and young soils.

enriched with these very active forms of silica. In addition, the plants contain a significant amount of K, which is thus also enriched in the surface horizon of the soil. Furthermore, plants can translocate chemical elements from the alterite (saprock) zone to the surface. As a consequence of this element translocation, 2:1 type clay minerals are maintained (Velde & Meunier, 2008). With increasing precipitation, biomass production usually also increases, although this relationship is not linear and a saturation value is reached. However, biomass is not only controlled by climate but also by other environmental factors. An increased productivity increases the K and Si content in the upper portions of the soil and favors the formation or stabilization of 2:1 compared to 1:1 clay minerals. Although elemental leaching is pronounced in Alpine soils, vegetation and the presence of a relatively high proportion of Si favor the formation of 2:1 clay minerals, and the whole process towards a distinct formation of kaolinite or gibbsite is hindered (Figure 6.4).

The data regarding modern ongoing climate change clearly show that temperatures are increasing. In Middle Europe, annual precipitation remains mostly unaffected or has decreased slightly (IPCC, 2014). The increase in temperature will result in a shift of coniferous forests towards higher altitudes and will lead to enhanced weathering rates in regions that are presently near or above the timberline (subalpine and alpine climates). The migration of the timberline towards higher altitudes is, however, rather slow and it may take decades to centuries before changes are observable (Dial et al., 2016; Wildi & Schütz, 2000). At lower altitudes it has to be expected that water availability will become scarcer and that consequently the bedrock or parent material and its chemistry will have a more dominant role in the future formation of clay minerals.

6.2.4. Substratum (Lithosequences)

Parent material lithology determines the physical and mineralogical nature of a soil. The mineralogy governs ecological soil properties, such as nutrient supply and retention, and water movement (Chadwick & Graham, 2000). Igneous rocks contain a suite of minerals that weather to provide a broad mix of nutrients with a broad mix of secondary weathering products. In contrast, limestone is nearly pure calcite that releases Ca and H_2CO_3 when it reacts with water. Soils forming on limestone-rich parent materials have inherited their colloidal fraction from weathering of impurities in the rock or from aeolian addition. Several studies have been carried out on the formation of clay minerals in Podzols that derived from different substrata, such as granite (Righi et al., 1999), rhyolite porphyry (Egli et al., 2004), granodiorite, slate, and tonalite till (Mirabella et al., 2002), tephra (Shoji et al., 1993; Ugolini et al., 1991), and sandstone drift (Carnicelli et al., 1997). Expandable minerals form from the weathering of either mica or chlorite via the intermediate stage of hydroxy-interlayered minerals and the subsequent removal of the hydroxide polymers (Carnicelli et al., 1997; Righi et al., 1993; Righi & Meunier, 1991). Depending on the parent material, these processes can be more or less advanced. Egli et al. (2004) found that the development of clay minerals with smaller layer charges was more advanced in Podzols on rhyolitic porphyry material, where smectite was detected also in the Bhs and Bs horizons. In soils on tonalitic or granodioritic parent material, smectite was identified only in the surface horizon.

As shown by Mirabella et al. (2002), a different siliceous lithology of the parent material ultimately leads to differences in the clay mineral assemblages in the

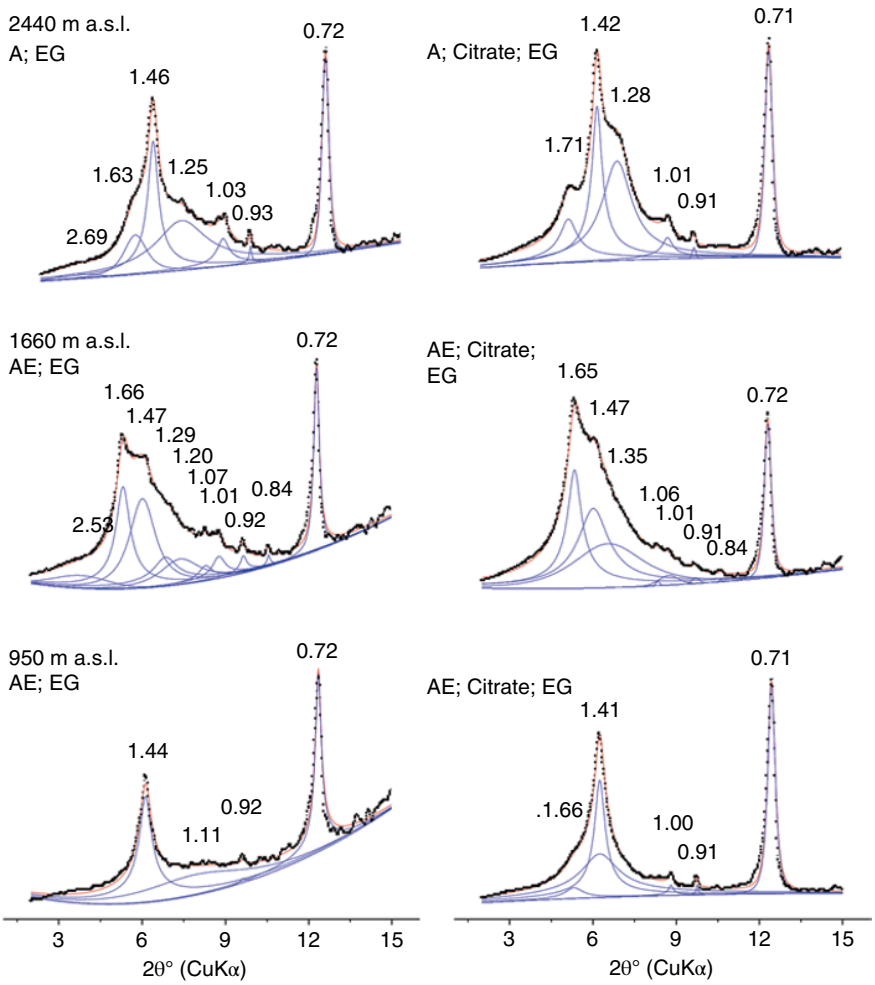

Figure 6.7 XRD patterns of ethylene glycol (EG)-solvated soil clays from the surface soil horizons before and after a Na-citrate extraction (data from Mirabella & Egli, 2003). The *d*-spacings are given in nm. The Na-citrate procedure extracts hydroxy-Al (or Fe) contaminants from the interlayers of 2:1 clay minerals and enables the detection of HIS (hydroxy-interlayered smectites; with a typical peak around 1.6–1.7 nm). The diffractograms are given as a function of altitude and thus climate.

weathered soil, although the other state factors are similar. As other studies have shown, smectite can be formed from both mica and chlorite (Carnicelli et al., 1997; Righi et al., 1999). If mica has a predominant dioctahedral structure, then smectite formation is retarded and another mineral source is needed to enable higher amounts of smectite to be formed (and detected). Mirabella et al. (2002) compared soils that developed on three different geological substrates: granodiorite, tonalite, and slate. Due to the persistence of mica in the surface horizons of soils and the disappearance of chlorite, smectitic components found in these upper horizons derive from the weathering of chlorite. The formation of smectite in the E horizon during pedogenesis is essentially dependent on the presence of chlorite in the parent material. Soils on granodiorite and on tonalite showed a pronounced transformation of trioctahedral into dioctahedral minerals, leading to the formation of expandable minerals in the surface horizons. In the soil on slate glacial till, where smectitic or vermiculitic components in the surface horizon were absent, this transformation was either not discernible or much less so. As a consequence, dioctahedral species strongly increased and trioctahedral species decreased during pedogenesis in soils developed on granodiorite; this trend was much less discernible in soils developed on slate (Figure 6.8).

Not only mineralogical but also slight physical differences can alter the weathering trajectories (Egli et al., 2002). Two soils (Meggerwald), a Haplic Podzol and a Dystric Cambisol, developed from postglacial (granitic) till but even with the same climate, vegetation, and topography showed some particular differences in their clay

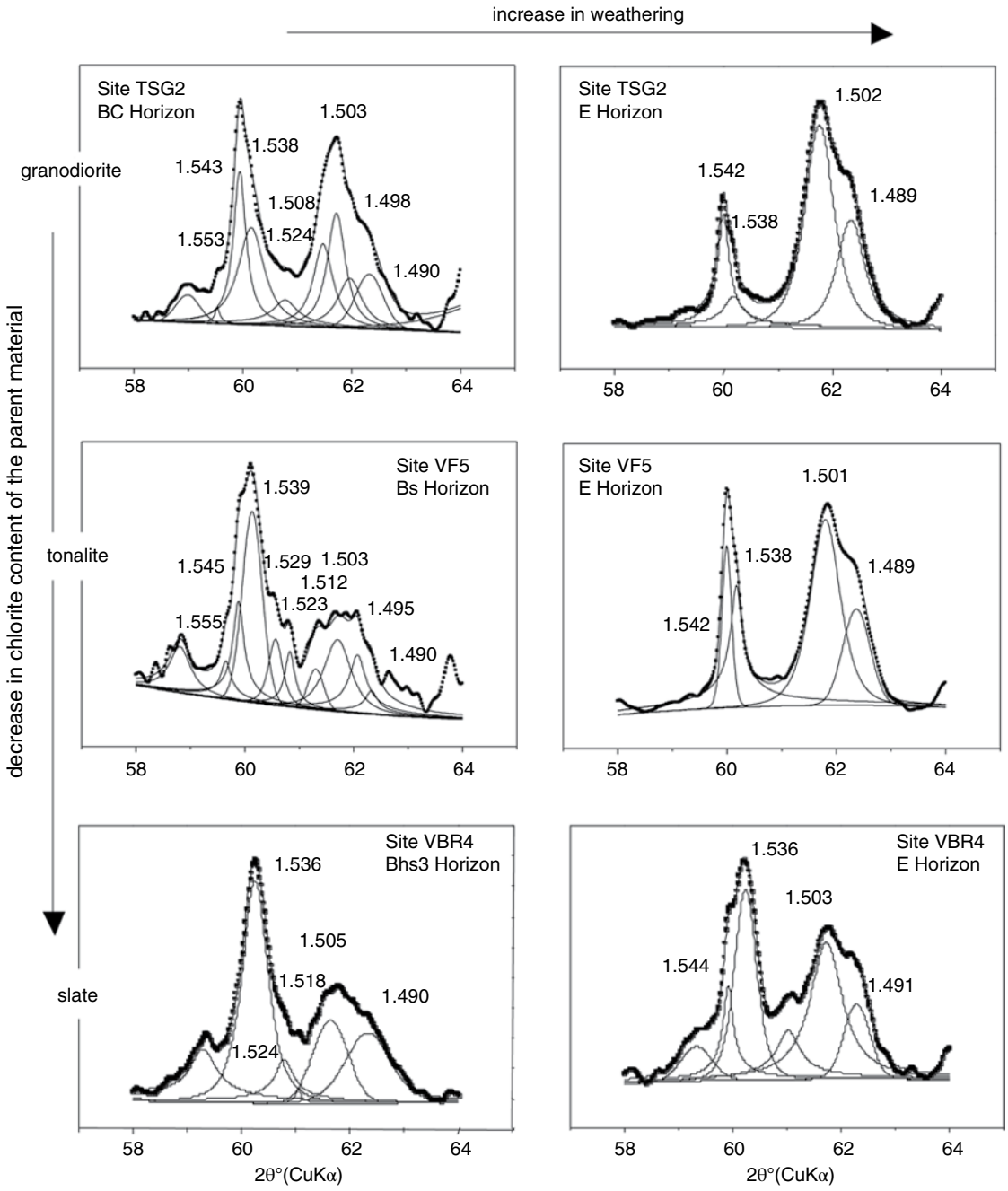

Figure 6.8 XRD-diffractograms of the *d*(060) peak region separating trioctahedral from dioctahedral mineral species. The *d*-spacings are given in Å. The d(060) is plotted with increasing weathering conditions and as function of the parent material (granodiorite of the Val Genova valley [TSG], tonalite of the Val di Fumo [VF], and slate of the Val Breguzzo [VBR]). (*Source:* Mirabella et al., 2002.)

mineral assemblages. The E horizon of the Podzol contained distinctly more smectite, characterized by a montmorillonite-beidellite-mixed phase. The neoformation of smectite can be traced back to the weathering of mica and chlorite. The Podzol had less HIS in the surface horizons than the Cambisol. The physical structure of the soil material seemed to be the most important factor for the different soil evolution. The higher abundance of coarse pores in the Podzol gave rise to a faster percolation of the soil water and, consequently, to a faster acidification and intense leaching of organic compounds, Fe, Al, and nutrients.

These few examples demonstrate that mineral weathering, clay mineral formation, and transformation

are strongly governed by the minerals present in the parent material, their structure, and soil physical properties that finally determine the type and intensity of interactions of water with mineral surfaces. The mineralogy determines the precipitation and dissolution reactions as well as the solid-solution interface. The solid-solution interface itself regulates adsorption and desorption of chemical constituents such as H^+, OH^-, metal ions, and organic and inorganic ligands (Stumm & Morgan, 1996). Only minor variations in the mineralogical composition of the silicatic parent material and/or additions of aeolian materials can lead to distinct differences in the development trajectories over time.

The formation of smectite-like compounds in the E-horizon during pedogenesis often requires a minimal amount of chlorite or trioctahedral mica. If nearly no other 2:1 mineral components are present in the parent material, then a micaceous (muscovite-like) mineral component becomes the dominant steady-state product of clay mineral weathering on siliceous parent material.

An important point that should be stressed is that the soil structure and therefore the soil physical characteristics can be very different from one horizon to another. Thus, water circulation in soils may vary greatly with time and space. Structural aspects and particle size of soils or the corresponding parent material are decisive parameters for the circulation of water and, therefore, the control of mineral reactions. The effect of physical properties of a specific parent material on soil evolution and weathering or mineral transformation processes is a rather rarely investigated topic and needs more attention in the future (see below).

Righi and Meunier (1995) argued that after a sufficient time, the mineralogical composition of soils depends more on climatic conditions than on the chemical composition of the parent rock. This might be true for timescales >1, 000,000 years; however, the rock composition is a determinative parameter for soil and clay chemistry in the "early" stages of weathering, whatever the climate may be (Egli, Mirabella, & Fitze, 2003).

6.2.5. Water Percolation and Erosion

Landscape and soils may respond noticeably and differentially to climate change as they integrate all ecological and historical factors. Hence, climate is an exclusive controlling factor of the transition from periods of geomorphodynamic activity to periods of stability (Günster & Skowronek, 2001). Atmospheric and soil-temperature variations influence the rate of reactions such as mineral weathering and biological breakdown of organic matter. Thermal conditions and solar radiation distinctly influence soil moisture and water percolation in a soil. The amount of precipitation, thermal conditions, and solar radiation not only influence soil biology (Ascher et al., 2012) and organic matter decay processes (Bardelli et al., 2017) but also the hydrological cycle, chemical weathering rates, and mineral formation and transformation (Egli et al., 2011).

A further driving factor in chemical weathering and mineral transformation is surface erosion. Up to a certain threshold value, increasing erosion causes increasing chemical weathering rates (Dixon & von Blanckenburg, 2012).

The degree of chemical weathering in soils usually increases from south- to north-facing sites in the European Alps due to distinct thermal and hydrological differences (Figure 6.6). North-facing sites are characterized by lower temperatures, lower evapotranspiration, and consequently by higher near-surface humidity (water content). Although precipitation in Alpine regions is mostly abundant, the availability and flux of water through the soil is the prime factor in weathering intensity. This understanding derives from the percolation theory, that both vegetation growth and soil formation processes are proportional to the water fluxes remaining after direct evaporation processes are excluded, including interception (Hunt et al., 2015). Soil production, in the sense of pedogenesis, is closely related to chemical weathering. If predictions for the rates of soil formation and weathering, at both regional and global scales, can be made accurately, then future climate change effects on Alpine systems can be assessed more reliably. Hunt & Ghanbarian (2016) recently proposed upper bounds for three processes described by scaling relationships: soil depths, natural vegetation, and crop heights, each as a power of time. The bounds are related to maximum water flow rates. The general scaling relationship can be represented as

$$x = x_0 \left(\frac{t}{t_0} \right)^P , \tag{1}$$

with the primary distinction in the three cases being the value of the exponent P. The variable x represents, for both natural vegetation and intensively managed crops, the height or root radial extent, and for soils, the depth. The variable t represents the time since germination for plant growth; for soil depth, it is the time since exposure at the surface. The spatial scale x_0 relates to a grain or pore (or plant xylem) diameter, and x_0/t_0 is the water flow rate, v_0, underlying the particular process.

Limitations to silicate weathering generally include two different processes: *transport limitation* and *kinetic limitation*. The supply of water, acids and (organic) ligands relative to the supply of silicate minerals is large in *transport*-limited weathering regimes (West et al., 2005).

Usually, old and flat topographies belong in this category. Where *kinetic* limitation is the main control on chemical weathering, silicate weathering ω depends on the kinetic rate of mineral dissolution W, the supply of material (e.g. by erosion or deposition) e, and the time t available for reaction (West et al., 2005):

$$\omega = W \cdot e \cdot t \tag{2}$$

where the value W depends on environmental conditions such as temperature and runoff (or precipitation).

It has been shown that, under the assumption that chemical weathering is limited by solute transport (and thus water flow into the soil), the process of soil production may be predictable (Yu & Hunt, 2017). Such predictions are successful when applying percolation theory for solute transport in porous media. The percolation theory can be used when the medium is highly disordered and chemical weathering in situ is transport limited (Hunt et al., 2015; Yu & Hunt, 2017). Variations of soil depth and vegetation characteristics with topography appear to be better understood when effects on the aspect dependence of erosion rates and soil production from water supply and energy balance are considered. Soil depth integrates soil production and denudation. Denudation (D) is the sum of erosion (E) and chemical leaching (W): $D = W + E$.

Temporal differentiation of equation (1) for the soil depth (x) generates the soil production (R) function:

$$\begin{aligned}\frac{dx}{dt} = R - E(t) &= \frac{1}{1.87}\frac{x_0}{t_0}\left(\frac{t}{t_0}\right)^{-0.87} - E(t) \\ &= \frac{1}{1.87}\frac{I(t)}{\phi}\left(\frac{x}{x_0}\right)^{-0.87} - E(t)\end{aligned} \tag{3}$$

with $I(t)/\phi$ as the net infiltration rate that varies, as does E, over time. From this equation it is evident that solute transport through soil (and erosion) limits the formation of soils. Solute transport limitations reflect the necessity for flowing water to bring reagents, chiefly CO_2, to, and remove reaction products from, the reaction zone (the bottom soil boundary), preventing equilibration. Soil depth therefore implicitly reflects hill-slope activities in terms of erosional and biological processes.

The data used for modeling are publicly available in the repository PANGAEA Data Archiving & Publication (https://doi.org/10.1594/PANGAEA.899503; Hunt & Egli, 2019). The model (equation [3]) slightly overestimates soil depth over time and thus soil production (Figure 6.9). Although the model reduces chemical weathering in soils to a few physical parameters such as infiltration rate, particle size, erosion and surface age, it captures the general trend and variability. Egli et al. (2018) concluded that this model may overestimate soil production in young soils because these soils also exhibit a strong kinetic limitation. The degree of weathering represented by the amount of smectitic components in the soils is also dependent on physical processes (Figure 6.9). Surface erosion notably influences the content of smectites: a high erosion rate gives rise to a low smectite content. This demonstrates that smectite is formed and accumulated on older and rather stable surfaces exhibiting a low erosion but a high infiltration rate. In Alpine areas, this situation is usually found at sites having a high vegetation cover and a higher production of soil organic matter. The production of organic complexing molecules is necessary for smectites to be formed from precursor minerals. Egli et al. (2007) demonstrated that at south-facing sites, the podzolization process (i.e. strong leaching of Fe, Al, and organic compounds) was less pronounced because of a lower water flux through the soil and less complexing organic molecules that would remove the interlayer polymers to produce smectites. Besides the eluviation process, clay minerals underwent a process of ionic substitutions in the octahedral sheet that led to the reduction of the layer charge. This process was again most obvious in the north-facing sites that are subjected to stronger weathering conditions.

Concepts like site capacity, sustainability, and vulnerability of soils are clearly linked to the mineralogy of the soil parent material and dissolution rate of minerals within the soil profile (Olsson & Melkerud, 2000). Transformation of rock minerals into clays occurs because of chemical reactions between the minerals and water that comes from rainfall. Therefore, the amount of rainfall and its distribution over the year determine the type of weathering and the type of soil that is formed (Righi & Meunier, 1995). Temperature influences the kinetics of chemical reactions (White & Brantley, 2003). This usually means that the reactions occur more quickly when the temperatures are higher. The interrelationship between mineral dissolution or transformation and precipitation and temperature is, however, not so simple. Weathering by complexing organic acids (which are dependent on climatic, biotic, and physico-chemical factors) are hypothesized to be a major active process in topsoils (Brahy et al., 2000) in the transformation of hydroxy-interlayered 2:1 clay minerals into vermiculite or smectite by the removal of their Al-interlayers.

6.3. CONCLUSION

Clay minerals in soils exhibit large differences across alpine landscapes. The precursor minerals in parent and deposited aeolian materials determine the start and to a certain extent the weathering trajectory over time. The

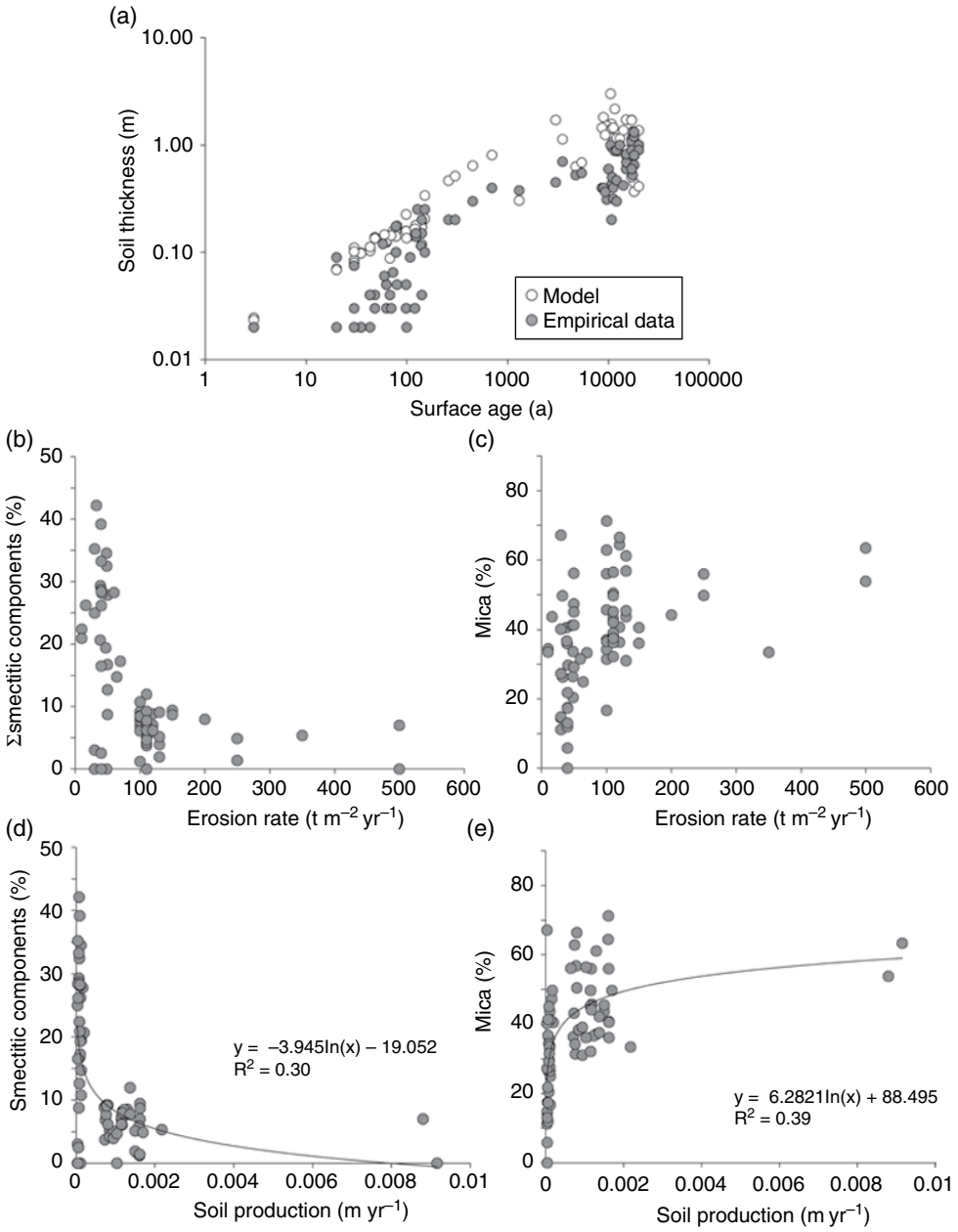

Figure 6.9 Relating principles of the percolation theory with (a) soil thickness and time of formation, (b) smectite content and soil erosion rates, (c) mica content and soil erosion rates, (d) smectite content and soil production rates, and (e) mica content and soil production rates. Under stable conditions (low erosion and low soil production rates), a high smectite content is found.

age-related evolution of soils and clay minerals appears to be predictable by infiltration and erosion rates using a theoretical approach based on the fractal dimensionality of the percolation backbone for vertical flow (percolation theory). Solute transport, rather than kinetic limitation, seems dominant over a large range of soil evolution. On stable sites with low erosion, a favorable mineral composition (chlorite or trioctahedral mica), relatively old soils, and relatively low soil production rates, smectitic components are a steady-state product of mineral weathering. However, smectitic components are particularly enriched when high amounts of organic ligands are present in the percolating water. Smectite formation can, therefore, not only be explained by the percolation theory. The mineralogical composition of the parent material, the type and presence of vegetation, and the production of organic ligands distinctly codetermine chemical weathering and mineral reactions.

ACKNOWLEDGEMENTS

We thank Dennis Dahms and Eleonora Bonifacio for their constructive suggestions on an earlier version of the manuscript.

REFERENCES

Ascher, J., Sartori, G., Graefe, U., Thornton, B., Ceccherini, M. T., Pietramellara, G., & Egli, M. (2012). Are humus forms, mesofauna and microflora in subalpine forest soils sensitive to thermal conditions? *Biology and Fertility of Soils*, *48*, 709–725. doi: 10.1007/s00374-012-0670-9

Bardelli, T., Gómez-Brandón, M., Ascher-Jenull, J., Fornasier, F., Arfaioli, P., Francioli, D., et al. (2017). Effects of slope exposure on soil physico-chemical and microbiological properties along an altitudinal climosequence in the Italian Alps. *Science of the Total Environment*, *575*, 1041–1055. https://doi.org/10.1016/j.scitotenv.2016.09.176

Birkeland, P. W. (1999). *Soils and geomorphology*, 3rd ed. New York: Oxford University Press.

Bohn, H. L., McNeal, B. L., & O'Connor, G. (1985). *Soil chemistry*. New York: Wiley-Interscience.

Brahy, V. Titeux, H., & Delvaux, B. (2000). Incipient podzolization and weathering caused by complexation in a forest Cambisol on loess as revealed by a soil solution study. *European Journal of Soil Science*, *51*, 475–484. doi: 10.1046/j.1365-2389.2000.00324.x

Cady, J. G., & Flach, K.W. (1997). History of soil mineralogy in the United States Department of Agriculture. *Advances in GeoEcology*, *29*, 211–240.

Caner, L. (2011). *Phyllosilicates des sols: de l'altération à la quantification*. Habilitation, University of Poitiers, France.

Carnicelli, S., Mirabella, A., Cecchini, G., & Sanesi, G. (1997). Weathering of chlorite to a low-charge expandable mineral in a Spodosol on the Apennine mountains, Italy. *Clays and Clay Minerals*, *45*, 28–41. doi: 10.1346/CCMN.1997.0450104

Chadwick, O. A., & Graham, R. C. (2000). Pedogenic processes. In M. E. Sumner (Ed.), *Handbook of soil science* (pp. E41–75). Boca Raton, FL: CRC Press.

Churchman, G. J., & Lowe, D. J. (2012). Alteration, formation, and occurrence of minerals in soils. In P. M. Huang, Y. Li, & M. E. Summer (Eds.), *Handbook of soil science*, 2nd ed. (vol. 1, pp 20.1–20.72). Boca Raton, FL: CRC Press.

Dahms, D. Favilli, F., Krebs, R., & Egli, M. (2012). Soil weathering and accumulation rates of oxalate-extractable phases from alpine chronosequences of up to 1 Ma in age. *Geomorphology*, *151–152*, 99–113. https://doi.org/10.1016/j.geomorph.2012.01.021

Dial R. J., Smeltz, T. S., Sullivan, P. F., Rinas, C. L., Timm, K., Geck, J. E., et al. (2016). Shrubline but not treeline advance matches climate velocity in montane ecosystems of south-central Alaska. *Global Change Biology*, *22*, 1841–1856, doi: 10.1111/gcb.13207

Dixon, J. L., & von Blanckenburg, F. (2012). Soils as pacemakers and limiters of global silicate weathering. *Comptes Rendus Geoscience*, *344*, 596–609. https://doi.org/10.1016/j.crte.2012.10.012

Eberl, D. D. (1984). Clay mineral formation and transformation in rocks and soils. In D. D. Eberl, V. C. Farmer, & R. M. Barrer (Eds.), *Clay minerals: Their structure, behaviour and use*. Philosophical Transactions of the Royal Society of London. Series A, Mathematical and Physical Sciences, vol. 311, no. 1517, pp. 241–257.

Egli, M., Hafner, S., Derungs, C., Ascher-Jenull, J., Camin, F., Sartori, et al. (2016). Decomposition and stabilisation of Norway spruce needle-derived material in Alpine soils using a ^{13}C-labelling approach in the field. *Biogeochemistry*, *13*, 321–338. https://doi.org/10.1007/s10533-016-0281-x

Egli, M., Hunt, A., Dahms, D., Raab, G., Derungs, C., Raimondi, S., & Fang, Y. (2018). Prediction of soil formation as a function of age using the percolation theory approach. *Frontiers in Environmental Science*, *6*, 108. doi: 10.3389/fenvs.2018.00108

Egli, M., Mirabella, A., & Fitze, P. (2001). Clay mineral formation in soils of two different chronosequences in the Swiss Alps. *Geoderma*, *104*, 145–175. https://doi.org/10.1016/S0016-7061(01)00079-9

Egli, M., Mirabella, A., & Fitze, P. (2003). Formation rates of smectites derived from two Holocene chronosequences in the Swiss Alps. *Geoderma*, *117*, 81–98. https://doi.org/10.1016/S0016-7061(03)00136-8

Egli, M., Mirabella, A., Mancabelli, A., & Sartori, G. (2004). Weathering of soils in Alpine areas as influenced by climate and parent material. *Clays and Clay Minerals*, *52*, 287–303. https://doi.org/10.1346/CCMN.2004.0520304

Egli, M., Mirabella, A., Sartori, G., & Fitze, P. (2003). Weathering rates as a function of climate: Results from a climosequence of the Val Genova (Trentino, Italian Alps). *Geoderma*, *111*, 99–121. https://doi.org/10.1016/S0016-7061(02)00256-2

Egli, M., Mirabella, A., Sartori. G., Giaccai, D., Zanelli, R., & Plötze, M. (2007). Effect of slope aspect on transformation of clay minerals in Alpine soils. *Clay Minerals*, *42*, 375–401. https://doi.org/10.1180/claymin.2007.042.3.09

Egli, M., Mirabella, A., Sartori, G. Zanelli, R., & Bischof, S. (2006). Effect of north and south exposition on weathering and clay mineral formation in Alpine soils. *Catena*, *67*, 155–174. doi: 10.1016/j.catena.2006.02.010

Egli, M., Wernli, M., Burga, C., Kneisel, C., Mavris, C., Valboa, G., et al. (2011). Fast but spatially scattered smectite-formation in the proglacial area Morteratsch: An evaluation using GIS. *Geoderma*, *164*, 11–21. https://doi.org/10.1016/j.geoderma.2011.05.001

Egli, M., Zanelli, R., Kahr, G., Mirabella, A., & Fitze, P. (2002). Soil evolution and development of the clay mineral assemblage of a Podzol and Cambisol in "Meggerwald" (Switzerland). *Clay Minerals*, *37*, 351–366. https://doi.org/10.1180/0009855023720039

Fanning, D. S., Rabenhorst, M. C., Burch, S. N., Islam, K. R., & Tangren, S. A. (1989). Sulfides and sulfates. In J. B. Dixson & D. G. Schulze (Eds.), *Soil mineralogy with environmental applications* (pp. 229–260). Madison, Winsconsin: Soil Science Society of America.

Farmer, V., Delbos, E., & Miller, J. (2005). The role of phytolith formation and dissolution in controlling concentrations of silica in soil solutions and streams. *Geoderma*, *127*, 71–79. https://doi.org/10.1016/j.geoderma.2004.11.014

Föllmi, K. B., Arn, K., Hosein, R., Adatte, T., & Steinmann, P. (2009). Biogeochemical weathering in sedimentary chronosequences of the Rhône and Oberaar Glaciers (Swiss Alps): Rates and mechanisms of biotite weathering. *Geoderma*, *151*, 270–281. https://doi.org/10.1016/j.geoderma.2009.04.012

Gómez-Brandón, M., Ascher-Jenull, J., Bardelli, T., Fornasier, F., Sartori, G., Pietramellara, G., et al. (2017). Ground cover and slope exposure effects on micro- and mesobiota in forest soils. *Ecologial Indicators*, *80*, 174–185. https://dx.doi.org/10.1016/j.ecolind.2017.05.032

Graham, R.C., Rossi, A.M., & Hubbert, K.R. (2010). Rock to regolith conversion: Producing hospitable substrates for terrestrial ecosystems. *GSA Today*, *20*, 4–9. doi: 10.1130/GSAT57A.1

Günster, N., & Skowronek, A. (2001). Sediment-soil sequences in the Granada Basin as evidence for long- and short-term climatic changes during the Pliocene and Quaternary in the Western Mediterranean. *Quaternary International*, *78*, 17–32. https://doi.org/10.1016/S1040-6182(00)00112-9

Hunt, A. G., & Egli, M. (2019). Characteristics of the alpine sites and related climate and erosion input data used for modelling. *PANGAEA*, https://doi.org/10.1594/PANGAEA.899503

Hunt, A. G., & Ghanbarian, B. (2016). Percolation theory for solute transport in porous media: Geochemistry, geomorphology, and carbon cycling. *Water Resources Research*. doi: 10.1002/2016WR019289

Hunt, A. G., Ghanbarian-Alavijeh, B., Skinner, T. E., & Ewing, R. P. (2015). Scaling of geochemical reaction rates via advective solute transport. *Chaos*. doi: 10.163/1.4913257

IPCC (2014). *Climate Change 2014: Synthesis Report*. Contribution of Working Groups I, II and III to the Fifth Assessment Report of the Intergovernmental Panel on Climate Change [Core Writing Team, R. K. Pachauri and L. A. Meyer (Eds.)]. Geneva, Switzerland: IPCC.

Jenny, H. (1941). *Factors of soil formation*. New York: McGraw-Hill.

Johnson, D. L., & Watson-Stegner, D. (1987). Evolution model of pedogenesis. *Soil Science*, *143*, 349–366. doi: 10.1097/00010694-198705000-00005

Kapoor, B. S. (1972). Weathering of micaceous minerals. *Norsk Geologisk Tidsskrift*, *52*, 451–452.

Mahaney, W. C., Hancock, R.G.V., & Melville, H. (2011). Late glacial retreat and Neoglacial advance in the Zillertal Alps, Austria. *Geomorphology*, *130*, 312–326. https://doi.org/10.1016/j.geomorph.2011.04.013

Mavris, C., Götze, J., Plötze, M. W., & Egli, M. (2012). Weathering and mineralogical evolution in a high Alpine soil chronosequence: A combined approach using SEM-EDX, cathodoluminescence and Nomarski DIC microscopy. *Sedimentary Geology*, *280*, 108–118. https://doi.org/10.1016/j.sedgeo.2012.04.008

Mavris, C., Plötze, M., Mirabella, A., Giaccai, D., Valboa, G., & Egli, M. (2011). Clay mineral evolution along a soil chronosequence in an Alpine proglacial area. *Geoderma*, *165*, 106–117. https://doi.org/10.1016/j.geoderma.2011.07.010

Meunier, A., Sardini, P., Robinet, J. C., & Prêt, D. (2007). The Petrography of weathering processes. Facts and outlooks. *Clay Minerals*, *42*, 415–435. doi: 10.1180/claymin.2007.042.4.01

Mirabella, A., & Egli, M., 2003. Structural transformations of clay minerals in soils of a climosequence in an Italian Alpine environment. *Clays and Clay Minerals*, *51*, 264–278. doi: 10.1346/CCMN.2003.0510303

Mirabella, A., Egli, M., Carnicelli, S., & Sartori, G. (2002). Influence of parent material on clay minerals in podzols of Trentino – Italy. *Clay Minerals*, *37*, 699–707. https://doi.org/10.1180/0009855023740071

Nannipieri, P., Ascher, J., Ceccherini, L., Landi, G., Pietramellara, G., & Renella, G. (2017). Microbial diversity and soil functions. *European Journal of Soil Science*, *68*, 1–26.

Olsson, M. T., & Melkerud, P.-A. (2000). Weathering in three podzolized pedons on glacial deposits in northern Sweden and central Finland. *Geoderma*, *94*, 149–161. https://doi.org/10.1016/S0016-7061(99)00081-6

Phillips, D. J. (2015). The robustness of chronosequences. *Ecological Modelling*, *298*, 16–23. doi: 10.1016/j.ecolmodel.2013.12.018.

Righi, D., Huber, K., & Keller, C. (1999). Clay formation and podzol development from postglacial moraines in Switzerland. *Clay Minerals*, *34*, 319–332. doi: https://doi.org/10.1180/000985599546253

Righi, D., & Meunier, A. (1991). Characterization and genetic interpretation of clays in an acid brown soil (Dystrochrept) developed in a granitic saprolite. *Clays and Clay Minerals*, *39*, 519–530. doi: 10.1346/CCMN.1991.0390507

Righi, D., & Meunier, A. (1995). Origin of clays by rock weathering and soil formation. In B. Velde (Ed.), *Origin and mineralogy of clays* (pp. 43–161). Berlin: Springer-Verlag.

Righi, D., Petit, S., & Boucher, A. (1993). Characterization of hydroxy-interlayered vermiculite and illite/smectite interstratified minerals from the weathering of chlorite in a Cryorthod. *Clays and Clay Minerals*, *41*, 484–495. doi: 10.1346/CCMN.1993.0410409

Shoji, S., Dahlgren, R., & Nanzyo, M. (1993). Classification of volcanic ash soils. In S. Shoji, M. Nanzyo, & R. Dahlgren (Eds.), *Volcanic ash soils - genesis, properties and utilization* (Developments in Soil Science, vol. 21, pp. 73–100). Amsterdam: Elsevier.

Sommer, M., Gerke, H. H., & Deumlich, D. (2008). Modelling soil landscape genesis - A "time split" approach for hummocky agricultural landscapes. *Geoderma*, *145*, 480–493. doi: 10.1016/j.geoderma.2008.01.012

Street-Perrot, F. A., & Barker, P. A. (2008). Biogenic silica: A neglected component of the coupled global continental biogeochemical cycles of carbon and silicon. *Earth Surface Processes and Landforms*, *33*, 1436–1457. https://doi.org/10.1002/esp.1712

Stumm, W., & Morgan, J. J. (1996). *Aquatic chemistry: Chemical equilibria and rates in natural waters*, 3rd ed. New York: John Wiley & Sons.

Ugolini, F. C., Dahlgren, R., LaManna, J., Nuhn, W., & Zachara, J. (1991). Mineralogy and weathering processes in Recent and Holocene tephra deposits of the Pacific Northwest, USA. *Geoderma*, *51*, 277–299. https://doi.org/10.1016/0016-7061(91)90074-4

Velde, B. (1995). Geology of clays. In B. Velde (Ed.), *Origin and mineralogy of clays* (pp. 1–7). Berlin: Springer-Verlag.

Velde, B., & Meunier, A. (2008). *The origin of clay minerals in soils and weathered rocks*. Berlin: Springer-Verlag.

Walker, L. R., Wardle, D. A., Bardgett, R. D., & Clarkson, B. D. (2010). The use of chronosequences in studies of ecological succession and soil development. *Journal of Ecology*, *98*, 725–736. https://doi.org/10.1111/j.1365-2745.2010.01664.x

West, A. J., Galy, A., & Bickle, M. (2005). Tectonic and climatic controls on silicate weathering. *Earth and Planetary Science Letters*, *235*, 211–228. https://doi.org/10.1016/j.epsl.2005.03.020

White A. F., & Brantley, S. L. (2003). The effect of time on the weathering rates of silicate minerals. Why do weathering rates differ in the lab and in the field? *Chemical Geology*, *202*, 479–506. https://doi.org/10.1016/j.chemgeo.2003.03.001

White, A. F., & Hochella Jr., M. F. (1992). Surface chemistry associated with the cooling and subaerial weathering of resent basalt flows. *Geochimica et Cosmochimica Acta*, *56*, 3711 –3721.

Wildi, O., & Schütz, M. (2000). Reconstruction of a 405 year recovery process from pasture to forest. *Community Ecology*, *1*, 25–32. https://doi.org/10.1556/ComEc.1.2000.1.5

Wilson, M. J. (1994). *Clay mineralogy: Spectroscopic and chemical determinative methods*. London: Chapman & Hall.

Yu, F., & Hunt, A. G. (2017). Predicting soil formation on the basis of transport-limited chemical weathering. *Geomorphology*, *301*, 21–27. https://doi.org/10.1016/j.geomorph.2017.10.027

Zollinger, B., Alewell, C., Kneisel, C., Brandova, D., Petrillo, M., Plötze, M., et al. (2017). Soil formation and weathering in a permafrost environment of the Swiss Alps: A multi-parameter and a non-steady-state approach. *Earth Surface Processes and Landforms*, *42*, 814–835. doi: 10.1002/esp.4040

Part IV
Application of Chemical Weathering/Soil Formation in Other Disciplines

7

Weathering Rinds as Tools for Constraining Reaction Kinetics and Duration of Weathering at the Clast-Scale

Peter B. Sak[1,2]

ABSTRACT

The weathering of rock fragments at or near Earth's surface results in the *in situ* conversion of unweathered core material to weathering rind. In field settings, rind thicknesses have been used to constrain the relative ages of surficial deposits. The progressive conversion of core to rind material is marked by abrupt changes in physical and chemical properties. In clasts with low-porosity parent material, the reaction front between the reactive core material and the depleted rind is a narrow (<1000 μm wide) feature. Detailed investigations of chrono- and climosequences suggest that parent material composition, ambient climatic conditions (mean annual temperature and precipitation), and curvature of the core-rind boundary exert first-order controls on weathering rind thickness. Uranium-series disequilibria dating can reliably quantify rates of weathering rind formation and the duration of weathering. Rind formation is modeled as a diffusion-limited process. The straightforward weathering rind system has proven a well-constrained intermediate between laboratory and landscape weathering systems.

7.1. INTRODUCTION

Weathering includes a complex suite of chemical, physical, and biological processes that transform rock to regolith (the altered material coating the unaltered bedrock), thus re-equilibrating high-temperature, high-pressure mineral assemblages to earth surface conditions (Amundson, 2004; Anderson et al., 2004). These processes span the grain (millimeter), clast (centimeter), pedon (meter), landscape (kilometer), and global (thousands of kilometers) scales (Brantley et al., 2007). For example, in the laboratory, primary minerals dissolve to form secondary minerals that precipitate at the bottom of a flask or coat grains in a column: this is the regolith in a laboratory dissolution experiment. Similarly, as a clast dissolves, a weathering rind forms and grows in thickness around a central core. At the landscape scale, weathered material accumulates at the top of a pedon developing on the protolith. At each scale, weathering of parent material produces solutes and regolith material, and resulting changes in either water or solid chemistry can be used to estimate weathering rate.

Rock fragments in the near-surface environment weather to produce porous and friable alteration rinds. Although the friable nature of the weathering rind presents challenges for sampling, it also makes weathering rinds superb chronometers of landscape stability, as rind thickness increases with weathering duration. However, disaggregation of the weathering rind resets the clock when the weathered clast is remobilized and comes to rest. Weathering is presumed to commence at the time of deposition (rind thickness = 0) (Cernohouz & Solc, 1966; Colman & Pierce, 1981; Knuepfer, 1988). Weathering rinds provide valuable information about the duration of weathering, long-term reaction kinetics, and sensitivity of weathering rates to variability in ambient climatic

[1]*Department of Earth Sciences, Dickinson College, Carlisle, PA, USA*

[2]*Earth and Environmental Systems Institute and Dept. of Geosciences, Pennsylvania State University, University Park, PA, USA*

Hydrogeology, Chemical Weathering, and Soil Formation, Geophysical Monograph 257, First Edition.
Edited by Allen Hunt, Markus Egli, and Boris Faybishenko.

DOI: 10.1002/9781119563952.ch7

conditions. They are readily distinguished from both unweathered parent core material and surrounding regolith (Figures 7.1 and 7.2) on the basis of color, composition, texture, and porosity. Compared to unweathered core, weathering rinds are enriched in relatively immobile elements (e.g. Ti, Fe, Th, and Al) and depleted in more soluble mobile elements (e.g. Mg, Ca, Na, and K) (e.g. Cernohouz & Solc, 1966; Colman, 1982a, 1982b). Studies of weathering rinds developed on clasts in periglacial environments from Iceland (Etienne, 2002) and the Sierra Nevada (Gordon & Dorn, 2005) have documented *in situ* spalling of outer portions of the weathering rind. The potential for disaggregation of the outer weathering rind highlights that the measured weathering rind thickness should be considered as minimum thicknesses. Notable excepts are instances where depositional ornamentation such as glacial striations recognized along the outer surfaces of rinds developed on weathering clasts within glacial moraine deposits (Colman & Pierce, 1981). Such exquisite preservation indicates that in some situations rind formation is the chemical weathering end-member of field weathering in the absence of physical erosion.

Figure 7.1 Soil profile developed in a weathering volcanic debris deposit in Guadeloupe. Note the presence of weathering clasts that are distinguished by color.

This review highlights advances in chemical weathering near Earth's surface by focusing on three illustrative examples of *in situ* development of weathering rinds on clasts from Costa Rica, central Japan, and the Lesser Antilles. Weathering rinds can be used to investigate near-surface weathering processes and rates in well-constrained field settings. Here, weathering rinds and the unweathered core materials are distinguished from rock coating such as Mn enrichments typical of desert varnish (e.g. Dorn, 1998), Si glaze (Dixon et al., 2002), or other coatings that can accrete or precipitate on exposed surfaces (Dorn et al., 2017). Weathering rinds result from the *in situ* incongruent dissolution of core material, whereas rock coatings are not genetically related to the materials they mantle. The relationship between rinds and the parent materials facilitate the use of mass balance calculations and balancing of chemical reactions describing the transformation of core to rind material.

7.2. WEATHERING RINDS AS TOOLS FOR CALIBRATED AGE DATING

It has been widely recognized in chronosequences that the pedogenic maturity (soil structure and texture, horizonation, and clay film abundance) of the host deposit and thickness of weathering rinds increase with the duration of weathering, making weathering rinds a valuable tool for constraining landscape age (e.g. Carroll, 1974; Colman & Pierce, 1981; Oguchi & Matsukura, 1999; Sak et al., 2004; Yoshida et al., 2011). Field measurements of

(a)

(b)

Figure 7.2 (a) and (b) Close-up images of weathering clasts within a volcanic debris deposit. The weathering rind is distinguished from the surrounding matrix by color and texture.

rind thickness have been employed in a range of settings to determine the relative degree of weathering of the host deposit (e.g. Anderson & Anderson, 1981; Cernohouz & Solc, 1966; Chinn, 1981; Colman & Pierce, 1981; Knuepfer, 1988; Meyer & Leidecker, 1999; White et al., 1996) (Figure 7.3).

Historically, weathering rind thickness has been used in conjunction with other relative dating methods, including soil profile development (e.g. Knuepfer et al., 1988; Mills & Allison, 1995), clast shape analysis (e.g. Cernohouz & Solc, 1966; Kirkbride & Bell, 2010; Powers, 1953), and lichenometry (Locke et al., 1979) to yield calibrated age estimates of geomorphic surfaces (Colman et al., 1987). Calibrated ages facilitate correlations of moraine deposits (e.g. Anderson & Anderson, 1981; Carroll, 1974; Colman & Pierce, 1981; Gellatly, 1984; Graham et al., 2010; McSaveney, 1992; Rossi & Graham, 2010), alluvial fans and terraces (e.g. Fisher et al., 1998; Knuepfer, 1988; Ricker et al., 1993; Sak et al., 2009; Yoshida et al., 2011), periglacial features (e.g. Birkeland, 1974; Cook-Talbot, 1991; Kellerer-Pirklbauer et al., 2008; Laustela et al., 2003), and archeological features (e.g. Curran et al., 2002; Sheppard & Pavlish, 1992). Weathering rinds have also proven effective tools for constraining the rates of tectonic processes such as faulting or uplift (e.g. Fisher et al., 1998; Knuepfer, 1988; McCalpin & Khromovskikh, 1995; Morriss & Wegmann, 2017; Ricker et al., 1993; Sak et al., 2009) and stream incision (Pazzaglia & Brandon, 2001; Pazzaglia et al., 1998).

Where independent absolute age constraints of the host deposits are available (i.e. from radiocarbon dating of organic debris, cosmogenic dating, tephra chronologies, optically stimulated luminescence, etc.) empirical best-fit models (Table 7.1) have been developed that relate rind thickness to the duration of weathering for clasts of similar composition (e.g. Colman, 1986; Colman &

Figure 7.3 Map illustrating the geographic extent of a representative sampling of weathering rind studies.

Table 7.1 Empirical models for rind development as a function of time.

Relationship	Equation	Parent Material	Study Area	Reference
Logarithmic	$r_r = 4.64 \times \log(1 + 1 \times 10^{-5}\ t)$	Basalt	Bohemia	Cernohouz and Sole (1966)
Logarithmic	$r_r = \log(0.73 + 3.8 \times 10^{-5}\ t)$	Basalt	W. Yellowstone,	Colman and Pierce (1981)
	$r_r = \log(0.73 + 8 \times 10^{-5}\ t)$	Basalt	MT	
	$r_r = \log(0.73 + 3 \times 10^{-4}\ t)$	Basalt	Yakima, WA	
	$r_r = \log(0.73 + 7 \times 10^{-5}\ t)$	Basalt	McCall, ID	
	$r_r = \log(0.73 + 5.8 \times 10^{-5}\ t)$	Andesite	Puget Lowland, WA	
	$r_r = \log(0.73 + 8.2 \times 10^{-5}\ t)$	Andesite	Truckee, CA	
	$r_r = \log(0.73 + 1.7 \times 10^{-4}\ t)$	Andesite	Lassen CA	
			Rainier, WA	
Power Law	$r_r = 0.00373(t^{0.806})$	Sandstone	New Zealand	Chinn (1981)
Power Law	$r_r = 1.03 \times 10^{-3}(t^{0.75})$	Sandstone	New Zealand	Knuepfer (1988)
	$r_r = 9.89 \times 10^{-4}\ (t^{0.86})$			
Relaxation Law	$r_r = 8.7(1\text{-}e^{-\text{«}^{10530}})$	Sandstone	New Zealand	Whitehouse et al. (1986)
Diffusion Limited	$r_r = x't^{0.5}$	Submarine Basalt	Hawaii	Moore (1966)

Measured rind thickness (r_r)
Age of deposit (t)
x' = constant

Pierce, 1981; Knuepfer, 1994). Empirical models suggest that rates of increasing rind thickness may be expressed by a power law (Chinn, 1981; Knuepfer, 1988), a relaxation law (Whitehouse et al., 1986), or a logarithmic law (Cernohouz & Solc, 1966; Colman & Pierce, 1992). Although none of these early studies based their modeling on physico-chemical models of weathering, empirical models based on rind thickness have been used to estimate age of landforms in temperate climates such as the western United States (i.e. Colman & Pierce, 1981; Meyer & Leidecker, 1999; Porter, 1975), New Zealand (i.e. Chinn, 1981; Gellatly, 1984; Ricker et al., 1993), Japan (Oguchi & Matsukura, 1999; Yoshida et al., 2011), and Bohemia (Cernohouz & Solc, 1966) or arctic and alpine climates (e.g. Anderson & Anderson, 1981; Burke & Birkeland, 1979; Carroll, 1974; McCarroll, 1991a; Shiraiwa & Watanabe, 1991; Lilliesköld & Sundqvist, 1994), where rind thickness is small relative to clast size.

These early empirical models lacked a physical basis and were not thought to predict accurate ages for deposits characterized by thick weathering rinds, such as those found in tropical climates (Knuepfer, 1994). In tropical climates, surface and near-surface weathering rates are more rapid than in temperate climates (e.g. Strakhov, 1967; White, 1995; White & Blum, 1995), resulting in accelerated rates of both pedogenesis and rind formation. Accelerated rind formation translates into greater temporal sampling resolution relative to those developed in high latitudes (e.g. Dixon et al., 2002; Hausrath et al., 2008; Salvatore et al., 2013) or under temperate or alpine climate regimes (e.g. Colman & Pierce, 1981; Oguchi et al., 2004). Detailed field and laboratory investigations of weathered basaltic and andesitic composition clasts from Costa Rica, central Japan, and Guadeloupe (Figure 7.3) are used to constrain relationships between chemical and mechanical transformations across the abrupt core-rind boundary of low porosity clasts. The transition from core to rind material is marked by an abrupt change in color, compressive strength, elemental abundances, and porosity. The three study areas are introduced below.

7.3. CASE STUDIES

Where different aged deposits (i.e. a chronosequence) contain weathering rinds developed under similar climatic conditions in clasts of similar composition, such as uplifted alluvial fans (e.g. Oguchi, 2004; Oguchi & Matsukura, 1999) and terraces (Navarre-Sitchler et al., 2009, 2011; Sak et al., 2004; Yoshida et al., 2011) or glacial moraines (e.g. Colman, 1986; Colman & Pierce, 1981) it is possible to assess the influence of time on weathering rind development. Elsewhere, climosequences have been used to evaluate the role of climatic variability on weathering rind formation (Engel et al., 2016; Ma et al., 2019; Porter, 1975; Sak et al., 2018).

7.3.1. The Costa Rican Chronosequence

Weathered basaltic andesite and andesite clasts were collected from the lower reaches (<200 m elevation) of a flight of three Quaternary alluvial fill terraces preserved along the central Pacific coast of Costa Rica (Navarre-Sitchler et al., 2009, 2011; Sak et al., 2004) to elucidate the influence of time on weathering rind formation. The central Pacific coast of Costa Rica is characterized by a humid tropical climate with a mean annual temperature (MAT) of 27.3°C and a mean annual precipitation (MAP) of 3085 mm yr^{-1}, resulting in rapid rind advance rates. Mean monthly temperatures vary by <2 °C throughout the year, while monthly mean precipitation is highly variable, ranging from a maximum of 570 mm in October to a minimum of <30 mm in March (Instituto Meteorologico Nacional de Costa Rica, 1992, unpublished data). Pedogenic maturity and weathering rind thickness in the three Quaternary alluvial fill terraces (designated as Qt1, Qt2, and Qt3) increased with increasing elevation. These terraces define a chronosequence where the relative deposition sequence and weathering age are Qt1 > Qt2 > Qt3. The mean thickness of the weathering rinds ranges from 13 ± 1 to 69 ± 6 mm from the lowest (Qt3) to highest (Qt1) terrace in the chronosequence (Table 7.2). The depositional ages of the terraces were initially constrained using geomorphic arguments, where Sak et al. (2004) linked the formation of alluvial fill terraces near sea level to eustatic highstands. This geomorphic model is calibrated by a maximum age constraint for Qt1 provided by a dated subjacent pyroclastic flow (Marshall et al., 2003) and a minimum age based on radiocarbon dead woody debris in Qt2. Subsequent optically stimulated luminescence (OSL) dating of quartz grains from the matrix of Qt3 provide additional age constraint (Navarre-Sitchler et al., 2011).

Field measurements of weathering clasts throughout the Costa Rican chronosequence highlight the relationship between both intrinsic and extrinsic variables and measured weathering rind thickness. Additionally, high-resolution investigations of incipient weathering across the core-rind boundary of weathering clasts constrain chemical and physical transformations accompanying *in situ* conversion of core to rind material. These observations underpin a physico-chemical model of weathering rind formation that is applicable even for thick weathering rinds.

7.3.2. Nasuno-ga-hara Chronosequence, Central Japan

The Nasuno-ga-hara chronosequence consists of four alluvial fan deposits developed in a temperate climate with a MAT of ~11 °C and a MAP of 1300 mm yr^{-1}. The

Table 7.2 Pedogenic properties and isotopic age constraints of Costa Rican chronosequence alluvial terraces.

Terrace Number	Radiometric age	Maximum height above base level (m)	Maximum B horizon thickness (cm)	Matrix Color	Texture[1]	Structure[2]	Consistency[3]	Clay Films[4]	Rind Thickness[5] (cm)
Qt 1	>46.0 ka (Beta-79380)[†¥] <352 ka (Ar/Ar)[¨]	150·	540+·	2.5YR/10R·	c·	abk·	s,p·	4p·	6.9 ± 0.6
Qt 2	>40.3 ka[¥] (Beta-146591)	185	350+	2.5 YR – 5YR	c, cl	c,sbk	s,p	2–3,pf	2.9 ± 0.1
Qt 3	~55 ka[††]	42	200	10YR 4/4	sicl	m,abk	s,sp	2,pf	1.3 ± 0.1

[1]c = clay, si = silt, s = sand, l = loam.
[2]m = medium, c = coarse, sbk = subangular blocky, abk = angular blocky.
[3]s = sticky, p = plastic, sp = slightly plastic.
[4]2 = common, 3 = many, 4 = continuous; pf = on ped faces.
[5]Uncertainty reported as standard error.
[¥]Radiocarbon ages determined by Beta Analytical, Inc. (Maimi, FL).
[†]Data from Fisher et al. (1998).
[·]Data from Marshall (2000).
[¨]Data from Marshall et al. (2003).
[††] OSL dating of terrace matrix material (Navarre-Sitchler et al., 2011).

deposits are dated at 20, 130, 290, and 660 ka using tephra stratigraphy, with the age of the surfaces and extent of weathering (rind thickness and pedogenesis) increasing with elevation above the modern river (Oguchi & Matsukura, 1999). Clasts collected from the modern floodplain lack weathering rinds, whereas clasts in the abandoned terraces show a consistent pattern of increasing weathering rind thickness with age (Oguchi & Matsukura, 1999). Chemical and mineralogic composition are constrained by X-ray fluorescence and X-ray diffraction (XRD) analyses, respectively. Bulk chemical and mineralogic composition covary with changes in physical (color and porosity) and mechanical (hardness) properties as a function of position away from the core-rind boundary within individual clasts and among weathering clasts from different terrace deposits.

7.3.3. Basse-Terre Island, Guadeloupe

Basse-Terre is a small (~850 km^2) volcanic island in the Guadeloupe archipelago of the Lesser Antilles volcanic arc where the MAT is consistently near 25 °C, at sea level. The island is composed of andesitic flows that decrease in age from north to south, parallel to the topographic divide (Samper et al., 2007). The topographic divide imparts a pronounced east to west orographic precipitation gradient. The MAP decreases from >6500 mm yr^{-1} east of the topographic divide to <200 mm yr^{-1} west of the divide. This configuration results in a setting where areas of similar bedrock age and MAT, but differing MAP, can be directly compared.

Weathering clasts collected from a narrow elevation band (50 to 300 m) have proven instrumental for (1) quantifying the relationship between clast shape and weathering rind advance rate (Engel et al., 2016; Lebedeva et al., 2015; Ma et al., 2012; Sak et al., 2010), (2) establishing U-series isotopes as a dependable tool for constraining the rates and durations of weathering at the clast scale, even in deposits of indeterminate age (Engel et al., 2016; Ma et al., 2012, 2019), (3) shedding insights into communication between the weathering rind and the host regolith (Sak et al., 2018), and (4) constraining discrepancies in chemical weathering rates measured at different spatial scales in field settings (Engel et al., 2016; Ma et al., 2019; Sak et al., 2018).

7.4. VARIABLES INFLUENCING WEATHERING RIND THICKNESS

Clasts collected from chronosequences are instrumental in isolating factors (separate from time) that result in variable weathering rind thickness. As weathering clasts are removed from the outcrop, the friable weathering rind material frequently disaggregates, leaving the rind-matrix boundary in the exposure (e.g. Navarre-Sitchler et al., 2011; Oguchi & Matsukura, 1999; Sak et al., 2004, 2010). The total weathering rind thickness equals the sum of the rind remaining in the outcrop and the portion adhering to the extracted clast. In the Costa Rican chronosequence, weathering rinds developed on clasts of a variety of compositions (claystones, mudstones, volcaniclastics, lithic sandstones, and basaltic compositions) are present within each terrace unit. Within a single exposure, the thickness, color, and nature of weathering rinds vary as a function of the parent material. Most notably, in clasts with porous core materials, the core-rind boundary

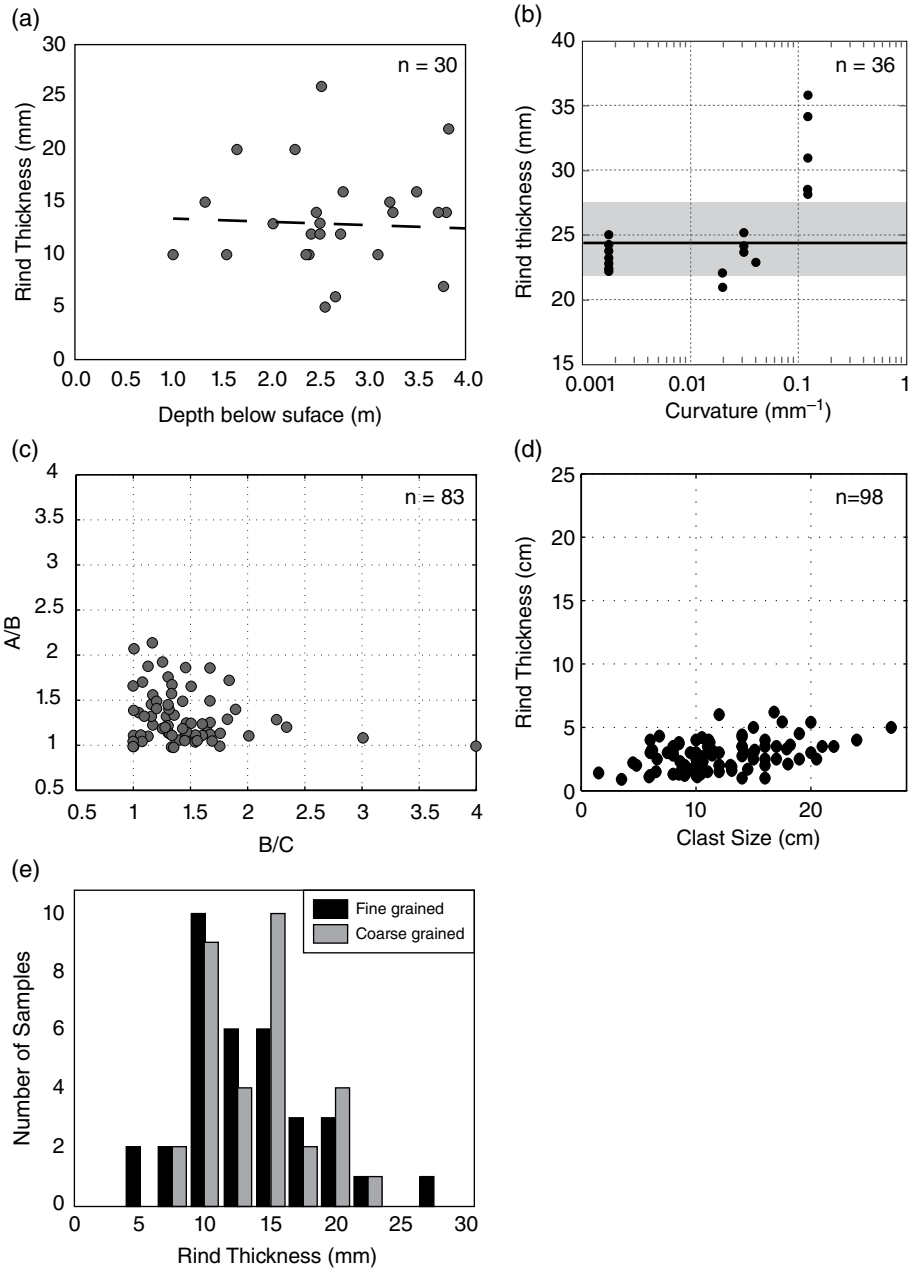

Figure 7.4 **(a)** Rind thickness on basaltic andesite clasts as a function of burial depth from a single exposure of terrace Qt3 of the Costa Rica chronosequence. Linear fit of the data has an R^2 value of 0.003, indicating depth of burial explains little of the variations in rind thickness (modified after Navarre-Sitchler et al., 2011). **(b)** Rind thickness as function of curvature of the visually defined core-rind boundary. Rind thickness and curvature measurement were collected at 10° increments around the clast. Note that for low curvature ($<3.1 \times 10^{-2}$ mm^{-1}), rind thickness is within 1σ (gray horizontal bar) of the mean (horizontal black line), but for high curvature segments (≥ 0.12 mm^{-1}) all rind thickness values are >1σ larger than the mean (modified after Sak et al., 2010). **(c)** Axial ratios of clasts (oblate ellipsoids) from deposits of terrace Qt2. The horizontal axis is the ratio of the intermediate (B) to short (C) axes and the vertical axis is the ratio of the long (A) to intermediate (B) axes (from Sak et al., 2004). **(d)** Measured rind thickness as a function of clast radius (measured along the intermediate (B) axis) for clasts from multiple exposures terrace Qt2. Rind thickness is independent of clast size. (modified after Sak et al., 2004). **(e)** Histograms of weathering rind thickness on clasts from the Qt3 terrace a function of grain size of the unweathered core material. Fine-grained basalts (grain diameter <~500 μm) have a mean of 12.5 ± 0.8 mm. Coarse-grained basalts have a mean of 13.7 ± 0.9 mm (from Navarre-Sitchler et al., 2011).

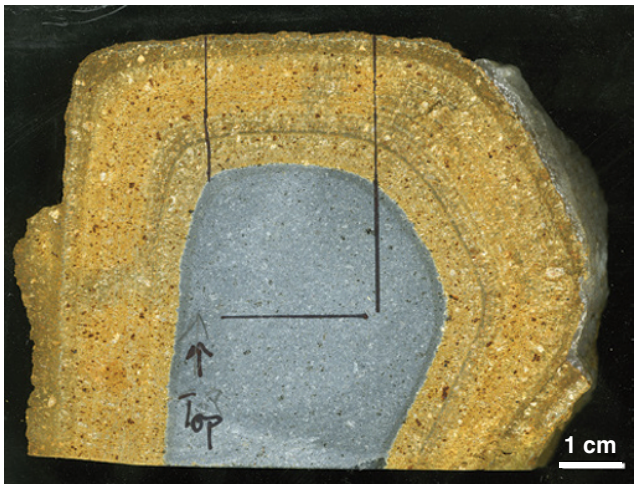

Figure 7.5 Weathering reactions at the clast scale occur at the core-rind interface.

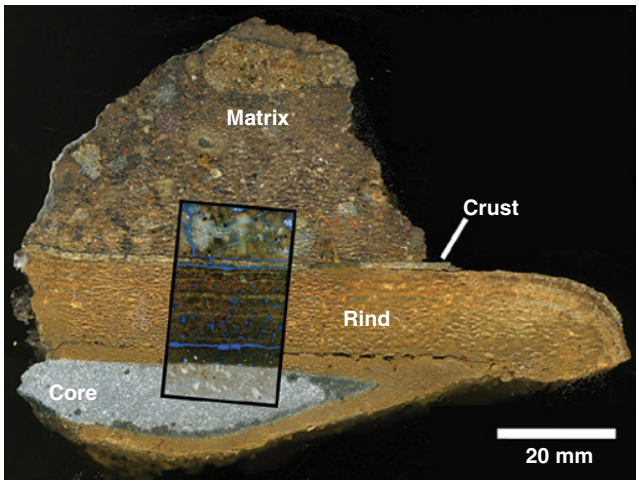

Figure 7.6 Cut slab of an oriented sampled clast spanning from the unweathered core across the weathering rind and into the surrounding matrix material. Black box denotes the extent of a petrographic thin section. Within the thin section, blue shows the extent of porosity.

is diffuse, whereas clasts with nonporous cores such as basaltic andesite compositions are characterized by an abrupt boundary that separates unweathered rock from weathered rind material (Anderson et al., 2004; Sak et al., 2004). Within a single exposure, clasts with basaltic andesite cores are characterized by thinner weathering rinds than rinds developed on clasts with different core compositions (Navarre-Sitchler et al., 2011; Sak et al., 2004). Variability in rind thickness between Qt3 exposures <1 km apart are statistically insignificant with mean values of 11.4 ± 5 mm and 14.2 ± 5 mm, respectively (Navarre-Sitchler et al., 2011). The thickness of weathering rinds developed on clasts with low-porosity basaltic andesite and andesitic cores are used to evaluate variability in weathering rind thickness as a function of the five field parameters: (1) exposure age, (2) depth of clast burial, (3) clast shape, (4) clast size, and (5) grain size of the parent material.

To determine if weathering rind formation rates vary as a function of clast burial depth, Navarre-Sitchler et al. (2011) measured weathering rind thicknesses and burial depth (0–4 m) on 30 basaltic andesite clasts from a single Qt3 exposure. No correlation between weathering rind thickness and depth of burial was reported (Navarre-Sitchler et al., 2011) (Figure 7.4a). This finding is consistent with results reported for weathering rinds on sandstone clasts in the >20 m thick Upper Terrace of the Fukui chronosequence (central Japan), where rind thickness does not vary with burial depth (Yoshida et al., 2011). Similarly, Porter (1975) reports no statistical difference between rind thicknesses measured on basaltic clasts at the surface or within the B horizon of a terrace along the eastern flanks of the Cascade Mountains (Porter, 1975).

In Guadeloupe, detailed investigations of several clasts were used to quantify the relationship between rind thickness and curvature of the core-rind boundary (Engel et al., 2016; Lebedeva et al., 2015; Ma et al., 2012; Sak et al., 2010). It has been widely reported that weathering of clasts in the near-surface environment blunts the corners of clasts (e.g. Cernohouz & Solc, 1966; Chinn, 1981; Kirkbride, 2005; Kirkbride & Bell, 2010). This often results in core-rind boundaries that are more rounded than the corresponding rind-matrix boundary in nonspherical clasts (Figure 7.2 a and b). In one field study, Sak et al. (2010) extracted an oriented clast from the clayey matrix of a volcaniclastic debris flow (Figure 7.1). As the sample was removed from the outcrop, a narrow (<0.5 cm thick) portion of the outer rind remained in the outcrop. Back in the laboratory, the wrapped clast was impregnated in molten paraffin to preserve the structural integrity of the remaining rind. The wax impregnated clast was sectioned along the vertical axis (Figure 7.5). After sectioning, curvature of the visually defined core-rind boundary was quantified and the thickness of the weathering rind from the core-rind boundary to a prominent continuous dark horizon in the weathering rind were measured normal to the core-rind boundary at 10° increments using a digital caliber. Measured rind thickness varies from 20.6 to 35.8 mm with a mean of 24.4 ± 3.1 mm (1σ) and is nearly twice as thick across portions of the clast characterized by high curvature (Figure 7.4b).

Clast size and shape are quantified by measuring the lengths of three mutually perpendicular axes. In general, andesitic clasts from the Qt2 terrace of the Costa Rican chronosequence are oblate ellipsoids with low aspect

ratios (Figure 7.4c). Clast shape does not vary systematically among sampled exposures. The relationship between clast size (defined as the length of the intermediate axis of the clast) and weathering rind thickness was established using a dataset consisting of 98 clasts from Qt3 of the Costa Rican chronosequence. Here rind thickness is independent of clast size (Figure 7.4d). The one notable exception are ghost clasts, where the entire clast has been converted to rind material. An increase in the size of ghost clasts is recognized within Qt1 and Qt2 deposits, and ghost clasts are not recognized in Qt3 or in modern floodplain deposits (Sak et al., 2004).

Textural variations in cores of clasts from the Costa Rican chronosequnece do not result in significant variations in mean rind thickness. Rind thicknesses were measured on 67 clasts from Qt3 and designated as coarse or fine grained based upon a 500 μm diameter threshold. Although the coarse-grained clasts have slightly thicker mean weathering rind thickness (13.7 ± 0.9 mm) compared to fine-grained clasts (12.5 ± 0.8 mm), the difference is not statistically significant (Navarre-Sitchler et al., 2011) (Figure 7.4e).

7.5. THE CORE-RIND BOUNDARY AND INCIPIENT CHEMICAL WEATHERING

Rind disaggregation biases most laboratory-based investigations by focusing on the incipient stages of chemical weathering marked by *in situ* conversion of core to rind material. In one notable exception, the rind-matrix boundary was preserved around a sampled clast from Guadeloupe (Figure 7.6) (Sak et al., 2018). The abrupt rind-matrix boundary is marked by textural and color differences that are readily identifiable in the field (Figures 7.1, 7.2, and 7.6). Transformations at the core-rind boundary provide insights into rates of chemical weathering and the initiation step. Color, elemental concentration, and porosity are characterized by relatively constant values in the core and rind, whereas the transition zone between the two reveals variations as a function of position. This transition zone defines the "reaction front" or zone across which a reaction occurs. The width and position of the reaction front depend on the variable defining the front. Profiles spanning the core-rind boundary have been collected on clasts from the Costa Rica (Navarre-Sitchler et al., 2009, 2011; Sak et al., 2004), Nasuno-ga-hara (Oguchi, 2001, 2004), and Fukui (Yoshida et al., 2011) chronosequences. These samples provide observations of the geometry of the reaction front and its position through time (the weathering advance rate) as well as the reproducibility of the reaction front geometry within deposits characterized by a constant weathering duration. U-series dated samples from Guadeloupe (Engel, 2016; Ma et al., 2012, 2019; Sak et al., 2018) constrain a similar time series for evaluating the reaction front geometry and position as a function of time in samples collected from undated Quaternary deposits.

7.6. CHEMICAL AND MINERALOGIC PROPERTIES

7.6.1. Compositional Variability

Spatial variations in bulk elemental concentrations across a single clast can be determined through chemical analysis. Bulk samples may be obtained by drilling cores along a linear transect and noting position relative to the visually defined core-rind boundary (e.g. Oguchi, 2001; Oguchi & Matsukura, 1999; Sak et al., 2004, 2018). Higher spatial resolution can be achieved by analyzing polished thin sections using electron microprobe (e.g. Dorn, 1995; Navarre-Sitchler et al., 2011; Sak et al., 2010), backscatter electron images and X-ray net intensity map (Navarre-Sitchler et al., 2009, 2011; Sak et al., 2010, 2018), or laser ablation ion coupled plasma mass spectrometer (LA-ICP-MS) (Ma et al., 2019).

Chemical data were obtained across the core-rind interface of multiple andesitic clasts from Costa Rica (Navarre-Sitchler et al., 2011; Sak et al., 2004) and Guadeloupe (Engel, 2016; Ma et al., 2012, 2019; Sak et al., 2010, 2018). Sak et al. (2004) characterized bulk chemical changes by analyzing nine samples collected along a ~30 mm linear profile oriented perpendicular to the core-rind boundary (Figure 7.7a). Sample powders were digested and analyzed using X-ray fluorescence and inductively coupled plasma mass spectrophotometry (ICP-MS) for major (Si, Al, Ca, Mg, Na, K, Fe, Mn, Ti, P) and some trace (Cr, Sr, Y, Zr and Ba) elements. Weathering rinds enveloping basaltic composition cores are characterized by increasing concentrations in Al_2O_3, Fe_2O_3, and TiO_2 and decreasing concentrations of CaO, K_2O, MgO, MnO, Na_2O, and SiO_2 relative to the cores. Spatially, compositional changes occur over a narrow zone coincident with a visually defined core-rind boundary. Across this boundary, the sum totals for all analyzed elements reported as oxides decrease from 85% to 95% in the core to <50% in the rind (Sak et al., 2010, 2018; Navarre-Sitchler et al., 2011), where they were attributed to the presence of hydrated phases within the rind.

7.6.2. Mineralogic Gradients and Weathering Reactions

Mineralogic variability of core material is determined from the bulk chemical composition using a CIPW norm because point counting of the fine-grained groundmass is impossible. The most common minerals identified in the core by XRD and optical microscopy are plagioclase and augite. For example, in a clast from Guadeloupe, the normalized modal abundances based on a CIPW norm are 34% anorthite, 25% albite, 16% quartz, 7% hypersthene, 6%

hematite, and <4% orthoclase, diopside, ilmenite, magnetite, and apatite (Sak et al., 2010). It is likely that the two pyroxene phases represent a single phase from the solid solution series. Feldspar, pyroxene, Fe oxide, magnetite, ilmenite, and apatite were all observed in the rock; quartz was not. The calculated quartz fraction is likely representative of Si-rich glass, as quartz is not observed and is not expected to form in this type of volcanic system. If the volume fractions are recalculated assuming a glass + groundmass phase with a composition similar to that of a well-studied calc-alkaline arc system, the modal abundances of the core are 53% groundmass + glass, 26% plagioclase, 9% pyroxene, 9% porosity, and <2% ilmenite, rutile, and apatite, consistent with point counting (Sak et al., 2010).

Similar calculations can be completed in the rind, acknowledging that the weathering rind is composed mainly of secondary minerals. Consequently, the modal abundances are constrained using the modified normative scheme described by Sak et al. (2004). The calculated model composition of the rind material of the same clast is 66% allophane + kaolinite, 16% iron oxyhyroxides, 10% gibbsite, 4% ilmenite, 1% pyroxene, 1% apatite, <1% albite, and <1% groundmass + glass.

Based on these model concentrations, the following balanced weathering reactions are hypothesized for this system. Equation 1a describes the reaction for plagioclase dissolution:

$$\mathrm{Na_{0.3}Ca_{0.7}Al_{1.7}Si_{2.3}O_{8(s)} + 6.3H_2O_{(l)} + 1.7H^+_{(aq)} \rightarrow 0.3Na^+_{(aq)} + 0.7Ca2^+_{(aq)} + 2.3H_4SiO_{4(aq)} + 1.7Al(OH)3_{(s)}.} \quad (1a)$$

Equation 1b describes the reaction for augite dissolution:

$$\mathrm{Ca_{0.8}Mg_{0.8}Fe(II)_{0.2}\,Fe(III)_{0.1}\,Al_{0.3}Si_{1.8}O_{6(s)} + 0.05O_{2(g)} + 1.85H_2O_{(l)} + 3.2H^+_{(aq)} \rightarrow 0.3FeOOH_{(s)} + 0.15Al_2Si_2O_5(OH)_{4(s)} + 1.5H_4SiO_{4(aq)} + 0.8Ca^{2+}_{(aq)} + 0.8Mg^{2+}_{(aq)}.} \quad (1b)$$

Equations 1c and 1d express the reactions for glass and kaolinite dissolution, respectively:

$$\mathrm{Ca_{0.03}Na_{0.09}K_{0.03}Fe_{0.02}Al_{0.18}SiO_{2.38(s)} + 2.16H_2O_{(l)} + 0.22H^+_{(aq)} \rightarrow 0.09Na^+_{(aq)} + 0.03Ca^{2+}_{(aq)} + 0.03K^+_{(aq)} + 0.02Fe^{2+}_{(aq)} + 0.18Al(OH)_{3(s)} + H_4SiO_{4(aq)}.} \quad (1c)$$

$$\mathrm{0.5Al_2Si_2O_5(OH)_{4(s)} + 2.5H_2O_{(l)} \rightarrow Al(OH)_{3(s)} + H_4SiO_{4(aq)}.} \quad (1d)$$

Based on these reactions, changes in chemical concentrations across the core-rind boundary can be interpreted as the following: Na is a proxy for plagioclase dissolution, equation 1a; Mg loss indicates pyroxene dissolution, equation 1b; and K loss represents dissolution of the glass + groundmass phase, equation 1c.

7.6.3. Open System Mass-Balance Calculations

Mass-balance calculations across the core-rind boundary can be used to quantify volumetric strain, relative cation mobility, and elemental loss associated with rind development. Weathering clasts are useful model systems for applying mass-balance calculations to quantify the extent of open-system mass transport because the weathering rind forms in a homogenous parent material of uniform age (Brimhall & Dietrich, 1987), and weatherable elements can be ratioed against an inert component present in both the core and weathering rind. Since weathering rinds envelop a single clast of known composition (i.e. the parent material is well constrained), clasts are well suited for this type of analysis.

Weathering in field systems can be accompanied by changes in the volume of solid material. These volumetric changes, associated with the conversion of core to rind material, are quantified as strain, $\varepsilon_{i,w}$, defined as the ratio of the change in volume that occurs during weathering divided by the initial volume. When an immobile element, i, is present in the system, strain $\varepsilon_{i,w}$ can be calculated (Brimhall & Dietrich, 1987) as

$$\varepsilon_{i,w} = \left(\frac{\rho_p c_{i,p}}{\rho_w c_{i,w}}\right) - 1. \quad (2)$$

Here ρ_p is the dry bulk density of the core (g cm^{-3}), ρ_w is the dry bulk density of the weathering rind, and c is the concentration (mol kg^{-1}) of an element assumed to be immobile (subscript i) in the core (p) or weathering rind (w). Positive strain represents dilation, negative strain represents collapse, and $\varepsilon_{i,w} = 0$ represents isovolumetric weathering.

In different lithologies, different elements are immobile because of differences in mineralogy. For basaltic andesite and andesite clasts from both Costa Rica and Guadeloupe, Ti is assumed to be immobile (i.e. i = Ti). The assumption of Ti immobility is consistent with previously published field studies documenting that Ti is often immobile, even in tropical settings at depths where organic acid concentrations are minimal (i.e. Barshad, 1964; Buss et al., 2008, 2010; C. E. Marshall, 1977; Milnes & Fitzpatrick, 1989; Sak et al., 2004, 2010; White, 1995). Similarly, results of column experimental studies (i.e. Neaman et al., 2005) indicate Ti is highly immobile relative to other elements, even in the presence of organic ligands.

The extent of loss (or gain) of an element j from the rind is quantified using the open system elemental mass

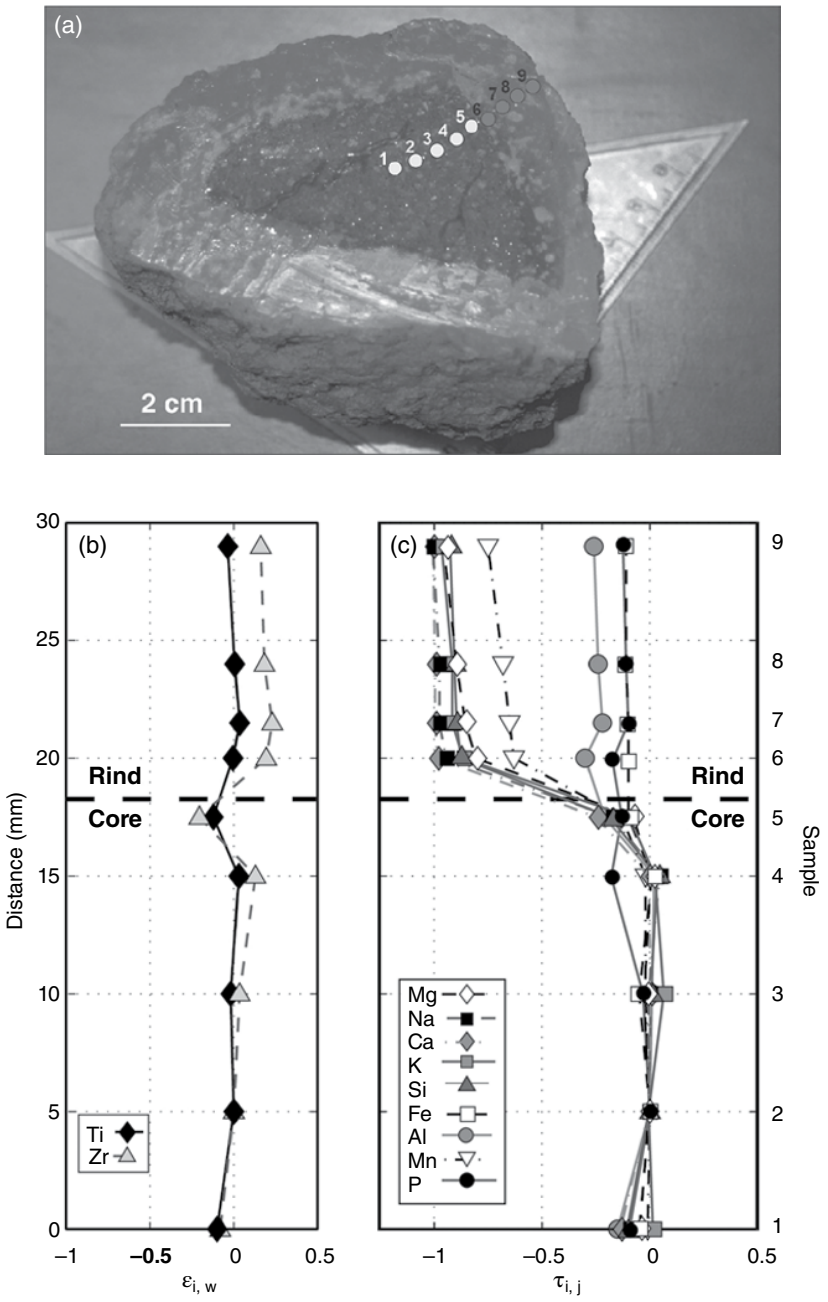

Figure 7.7 **(a)** Section of a weathering clast, the Qt2 unit of the Costa Rica chronosequence. The numbered dots show locations of bulk samples along the ~30 mm transect spanning the core-rind boundary. **(b and c)** Volumetric strain $\varepsilon_{l,w}$ and elemental mass transfer $\tau_{l,j}$ calculated using equations 2 and 3. Data are plotted as a function of distance increasing from the coreward end of the transect. The $\varepsilon_{l,w} < 0$ in sample 5 is consistent with a 0.3 g cm^{-3} density decrease within 2 mm of the visually defined core-rind boundary. The $\tau_{l,j}$ calculations assume constant core and rind densities except for sample 5, where density is set to 2.5 g cm^{-3}, based upon the density decrease inferred in **(b)**. Negative values of $\tau_{l,j}$ imply loss of the element j (–1 represents 100% loss) in the rind relative to the parent material. Reported values of $\tau_{l,j} < 0$ within the core may reflect localized compositional variability or analytical errors. Horizontal dashed line documents the core-rind boundary (modified after Sak et al., 2004).

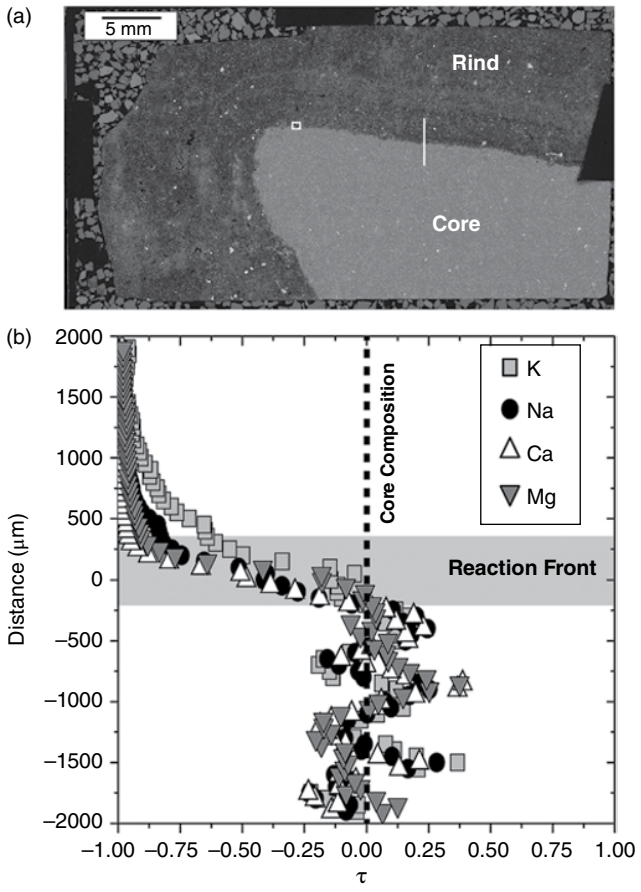

Figure 7.8 **(a)** SEM backscatter image of a thin section spanning the core-rind boundary of a clast from the Qt3 unit of Costa Rica chronosequence. The white box shows the location of Figure 7.10; white line shows the location of the 4 mm EMP transect shown in (b). **(b)** Elemental mass transfer $\tau_{i,j}$ calculated using equation 3 plotted as a function of position relative to the core-rind boundary at 0. Negative values of $\tau_{i,j}$ imply loss of the element *j* (–1 represents 100% loss) in the rind relative to the core. Reported values of $\tau_{i,j} \neq 0$ within the core may reflect localized compositional variability due to phenocrysts or analytical error. Gray horizontal bar denotes reaction front width.

transfer coefficient, $\tau_{i,j}$ (Brimhall et al., 1991; Brimhall & Dietrich, 1987). The loss or gain of a mobile element *j* relative to Ti is calculated as follows (Anderson et al., 2002; Brimhall & Dietrich, 1987):

$$\tau_{i,j} = \frac{C_{j,w}}{C_{j,p}} \frac{C_{i,p}}{C_{i,w}} - 1. \quad (3)$$

When $\tau_{i,j} = 0$, neither depletion nor enrichment has occurred for *j* with respect to Ti in the parent; when $\tau_{i,j} < 0$ or > 0, there is elemental loss or gain, respectively. Furthermore, when $\tau_{i,j} = -1$, 100% of element *j* has been loss relative to Ti in the parent material.

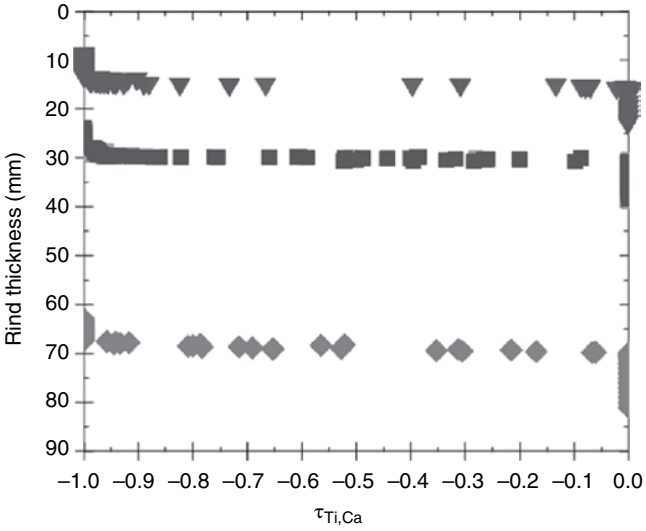

Figure 7.9 Elemental mass transfer $\tau_{Ti,Ca}$ values for Costa Rica basalts calculated using equation 3 and plotted as a function of distance from outer edge of the weathering rind. Weathering rind thickness increases in clasts from Qt3 (triangles) to Qt2 (squares) to Qt1 (diamonds). The distance over which $\tau_{Ti,Ca}$ decrease from 0 (core composition) to –1 (complete depletion) defines the reaction front thickness. Independent of the weathering rind thickness, the Ca reaction front is ~1 mm thick (modified after Navarre-Sitchler et al., 2011).

Plots of elemental mass transfer as a function of position are shown in Figures 7.7c and 7.8 for clasts from the Costa Rican chronosequence. Independent of deposit age, rind thickness, and the type of samples (bulk versus probe) used to constrain the elemental concentrations, the resultant profiles share several features in common. Most notably, in each of the analyzed clasts the outermost rind was completely depleted in Na, K, Ca, Mg, and Si ($\tau_{Ti,j} = -1$ at the outer surface). In other words, the elemental depletion profiles were completely developed (Brantley & White, 2009). The Fe mass transfer ($\tau_{Ti,Fe}$) profile is characterized by values ranging from –0.11 to >1.0, indicative of incomplete depletion or enrichment across the weathering rind. Within the unweathered core material, mass transfer coefficients of highly mobile elements such as Na are variable (ranged by >0.5) when constrained by EMP data (Figure 7.8) (Navarre-Sitchler et al., 2011) and display limited variability (<0.15) when constrained by the drilled powders (Figure 7.7c) (Sak et al., 2004). Variability in the EMP-derived profiles is attributed to heterogeneity of the core material (phenocrysts versus groundmass) at scales larger than the 50 μm spot size. While the larger sample volumes represented by the individual bulk samples (0.08 to 0.12 cm^3) are more effective at homogenizing the parent materials, the coarse sample size is ill suited for the dense sampling

necessary to characterize compositional variability across reaction front.

Elemental reaction fronts coincide with the visually defined core-rind boundary. Within the Costa Rica chronosequence, the Ca reaction front defined using EMP high-resolution data is consistently ~1 mm thick in clasts from Qt1, Qt2, and Qt3, although rind thickness increases with terrace age (Figure 7.9) (Navarre-Sitcher et al., 2011). As the narrow reaction front migrates into the unweathering core, depleted rind material is left in the wake. Elemental loss from the core to the rind of clasts from Costa Rica and Guadeloupe varies in the order Ca ≈Na > K ≈Mg > Si > Al > Fe ≈P ≫Ti. This pattern of elemental loss is consistent with the relative reactivity of phases from plagioclase ≈ pyroxene ≈ glass > apatite > ilmenite.

7.7. PHYSICAL AND MECHANICAL PROPERTIES ACROSS THE CORE-RIND BOUNDARY

7.7.1. Quantifying Changes in Color

Few studies have endeavored to quantify color changes across the core-rind boundary beyond noting Munsell color notation for the core and rind. In a novel study of the Nasuno-ga-hara chronosequence, color changes were quantified both among the deposits and as a function of distance from the visually defined core-rind boundary (Oguchi, 2001; Oguchi & Matsukura, 1999). Chromatic analysis uses spectral data measured with a visual microspectrometer to quantify color using three components: L*, a*, and b* for lightness, red-green chroma, and yellow-blue chroma, respectively. Weathering rinds in the older terraces are characterized by a narrow, Ca-depleted band of the white- to brown-colored rind (similar to the weathering rinds developed on clasts in the 20 ka deposit) near the core-rind boundary. This white band is mantled by a brittle brown weathering rind at increasing distance away from the core rind in the weathering rind, characterized by higher $FeO + Fe_2O_3$ content and lower alkali/alkaline earth metal content (Oguchi, 2001). Color and compositional changes reflect changes in the predominant mechanisms of weathering rind formation; the brown band results from oxidation and leaching, whereas the inner white band is interpreted to reflect leaching (Oguchi, 2001).

7.7.2. Hardness Measurements

Direct measurement of the interrelated mechanical properties of hardness (compressive strength), bulk density, and porosity have proven useful for determining the relative extent of weathering. For example, measurements of compressive strength obtained using a Schmidt hammer (e.g. Kellerer-Pirklbauer et al., 2008; Matthews & Shakesby, 1984; McCarroll, 1991b; Winkler, 2005) provide a quantitative value for the extent of weathering of individual clasts, though the target area is large relative to the weathering rind thickness. Although this method shows that compressive strength decreases with increasing rind thickness and allows correlations among isolated exposures, it is not amenable to resolving spatial trends across a single clast or relating changes in hardness to chemical or physical transformations at the core-rind boundary. In contrast, microhardness measurements have the advantage of quantifying hardness changes across a single clast. For example, Oguchi and Matsukura (1999) present high-resolution microhardness measurements along linear transects oriented perpendicular to the core-rind boundary on 5–10 mm thick test samples from five terraces of the Nasuno-ga-hara chronosequence. Hardness was quantified as Vickers hardness numbers (VHN) at 0.2 to 0.5 mm intervals using a Vickers' microhardness tester. Hardness values group into three domains, a ~1000–2000 μm thick reaction front separating core values (VHN ≈ 500 g/μm^2) from weathering rind values (VHN of 10 to 80 g/μm^2) (Oguchi & Matsukura, 1999). Interestingly, hardness values for the core and rind materials are constant, independent of the host deposit age, and reaction front thickness varies more among similar aged samples than across the chronosequence.

7.7.3. Porosity Development

The conversion of basaltic andesite and andesitic composition core to rind material is accompanied by an abrupt increase in porosity. Several common features are recognized independent of the method used to quantify

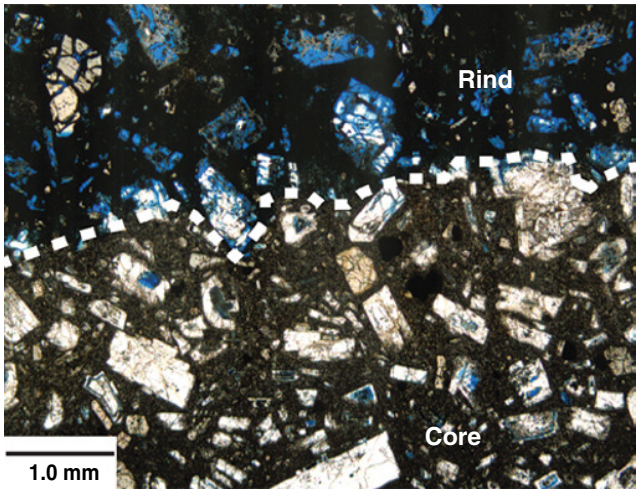

Figure 7.10 Representative photomicrograph across the core-rind boundary of the clast shown in Figure 7.5. The core-rind boundary corresponds with the abrupt increase in porosity evidenced by the abundance of blue epoxy–filled voids.

porosity. Porosity values in the cores of these clasts are consistently low (<5%) and show little variability. Porosity in the weathering rind is typically high (>30%), and the narrow (<1500 μm) porosity reaction front coincides with the visually defined core-rind boundary. Porosity in weathering clasts has been constrained over a range of scales using a variety of methods. Mass-balance calculations and total weight percent of EMP analyses have been used to estimate the magnitude and distribution of porosity (i.e. Sak et al., 2004, 2010, 2018). Porosity can be measured using water saturation (Sak et al., 2010; Yoshida et al., 2011), mercury porosimetry (Oguchi & Matsukura, 1999), analysis of electron and optical microscopy images (Lebdeva et al., 2015; Navarre-Sitchler et al., 2009; Sak et al., 2010, 2018), X-ray computed tomography (Navarre-Sitchler et al., 2009), or neutron scattering (Navarre-Sitchler et al., 2013, 2015).

In the absence of direct measurements, porosity can be inferred by combining strain values ($\varepsilon_{Ti,w}$) calculated using equation 2 with petrographic observations. For example, along a transect across a clast from the Costa Rica chronosequence, $\varepsilon_{Ti,w}$ is consistently close to 0, indicating isovolumentric weathering and Ti immobility. In this sample, core and rind densities of 2.8 and 1.4 g cm^{-3}, respectively, were constrained by standard immersion techniques (Sak et al., 2004). Strain calculations indicate that porosity in the weathering rind approaches 50% and that the transition from low porosity basaltic andesite in the core to porous weathering rind material is abrupt and occurs across a narrow (≤2.5 mm) reaction front coincident with the visually defined core-rind boundary (Sak et al., 2004) (Figure 7.7b). The presence of undistorted ghosts of plagioclase phenocrysts in the weathering rind is consistent with this finding. A negative strain excursion ($\varepsilon_{Ti,w}$ = –0.12) was calculated for powders from a drill hole located <2 mm coreward from the visually defined core-rind boundary (Sak et al., 2004). Assuming $\varepsilon_{Ti,w}$ = 0 for this sample, like the other eight samples, would require a 0.3 g cm^{-3} decrease in density <2 mm coreward of the core-rind boundary. This decrease in density corresponds to an increase in core porosity from the <1% elsewhere in the core to 10% approaching the core-rind boundary (Sak et al., 2004).

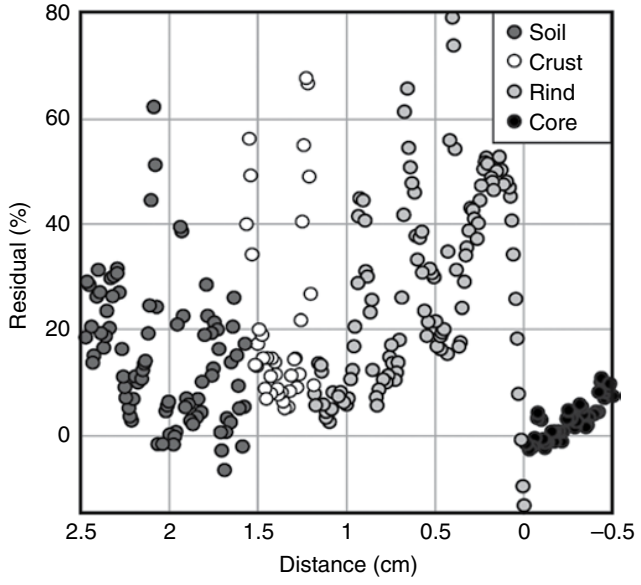

Figure 7.11 Residual values plotted as a function of distance from the visually defined core rind boundary of the clast shown in Figure 7.6. Negative residual values are attributed to variability in porosity and averaged loss on ignition values. The abrupt increase in percent residual defines a 900 μm wide reaction from coincident with the visually defined core-rind boundary. The two spikes in porosity at greater distance from the core-rind boundary are located along the margins of the crust (modified after Sak et al., 2018).

Bulk porosity at the mm scale can be quantified using image analysis of a high-resolution photomosaic of the entire thin section. High-resolution photomosaics are created by stitching together 285 individual photomicrographics collected at 5x magnification using a petrographic microscope. The photomosaic is analyzed using a script that isolates the RGB color spectra range corresponding to the blue epoxy visible in the thin section filling pore spaces (Figures 7.6 and 7.10). This methodology quantifies the amount of porosity and maps the spatial distribution of the pores. Similarly, at higher resolution, backscattered electron scanning electron microscope (SEM) images can be used to quantify and map the distribution of porosity (Dorn, 1995). Porosity profiles (plots of porosity as a function of distance from the core-rind boundary) can be produced by summing total number of pore-pixels in each column of the photomosaic (e.g. Lebedeva et al., 2015).

Higher-resolution porosity estimates are calculated as the difference between the ICP-AES (inductively coupled plasma–atomic emission spectrometer) loss on ignition and the porous-hydrated fraction (PHF) for core and rind materials, where the PHF is defined as the difference between 100 and the sum total for all elements analyzed by electron microprobe (EMP) (Sak et al., 2010; 2018). Porosity values measured using the PHF method are significantly larger than measurements from image analysis, suggesting either that the majority of the porosity is smaller than the macropores visible in photomicrographs, or that much of the porosity was not impregnated by the stained blue epoxy (Figure 7.11).

Total pore volume and bulk density can be directly measured simultaneously using mercury intrusion porosimetery. Here porosity of a given sample is calculated as

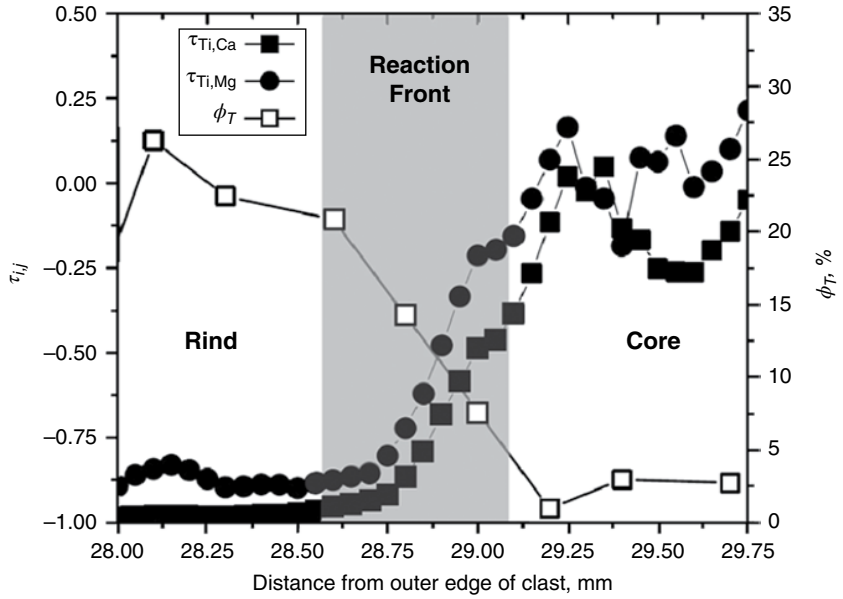

Figure 7.12 Plot of elemental mass transfer $\tau_{i,j}$ for Ca and Mg and total porosity ϕ_T plotted as a function of distance from the outer edge of a Qt2 clast from the Costa Rica chronosequence. Across the reaction front (gray bar), $\tau_{i,j}$ values for Ca and Mg decrease, consistent with plagioclase and augite weathering. There is a corresponding increase in total porosity across the reaction front associated with weathering (modified after Navarre-Sitchler et al., 2009).

the product of the total pore volume and bulk density. In weathered clasts from the Nasuno-ga-hara chronosequence, Oguchi and Matsukura (1999) quantified the volumes of pores with diameters between 3 nm and 33 μm, revealing a correlation with rind color. The brown portion of the weathering rind has higher porosity than the white rind band. Comparisons between analyzed samples indicate a positive correlation between the measured porosity and weathering rind advance rate. These observations led Oguchi (2004) to emphasize the importance of the porosity of the core material when using weathering rind thickness as a chronometer.

Neutron scattering intensity contains information about pore sizes and geometries, which change in the narrow core-rind boundary zone. Core pores are small (typically <100 nm) and are concentrated along boundaries and at grain triple junctions (Navarre-Sitchler et al., 2013). Pores within the unweathered core generally lack connectivity, and nanopores are an important conduit for connecting networks of pores. As primary minerals weather, pores increase in size and intragrain porosity develops (Navarre-Sitchler et al., 2013; 2015). The growth of pores associated with weathering rind development in the Costa Rican chronosequence has been analyzed at higher resolution using X-ray computed tomography (Navarre-Sitchler et al., 2009) and neutron scattering (Navarre-Sitchler et al., 2013). Porosity increased from ~3% in the core to >30% away from the core-rind boundary across the weathering rind. (Navarre-Sitchler et al., 2013).

The effective porosity is a measure of the porosity within a pore network and increases once the total porosity exceeds 9% (Navarre-Sitchler et al., 2009). Significantly, tracer and numerical simulations highlight that increases in total and effective porosity promote solute transport through weathering rind materials, dissolution of primary minerals at the core-rind boundary, and *in situ* conversion of core to rind material (Figure 7.12) (Navarre-Sitchler et al., 2009). This is visualized in SEM-EDS images that document changes in chemistry and mineralogy at the core-rind boundary. In clasts from both Guadeloupe (Figure 7.13) and Costa Rica (Figure 7.14), phenocrysts are dominantly unaltered in the core but partially to completely altered in the rind. The interiors of the porous plagioclase ghosts contain a framework of an Al-rich, Si-, Fe-, Ca-, and Na-deficient solid, consistent with weathering reaction 1a, where plagioclase weathers to gibbsite. Altered pyroxene phenocrysts contain Fe- and Al-interiors, consistent with pyroxene alteration to Fe-oxyhdroxide and gibbsite (Figures 7.13 and 7.14).

7.8. DIFFUSION MODEL OF WEATHERING RIND DEVELOPMENT

Early pyroxene oxidation without observable pore formation followed by significant pore formation due to plagioclase dissolution is observed in weathered clasts from Costa Rica (Figure 7.14) (Hausrath et al., 2008;

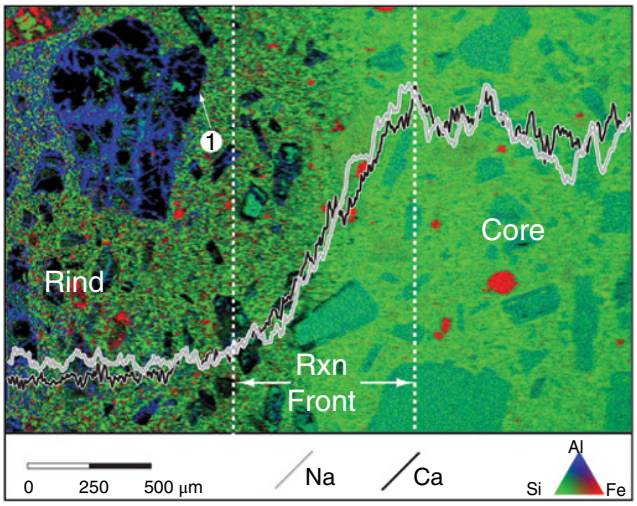

Figure 7.13 EDS SEM map of the core-rind boundary of the clast shown in Figure 7.5. The image is colored for the relative elemental concentrations: green is Si, blue is Al, and red is Fe (see scale in lower corner of image). Superimposed on the image are concentrations for Na (gray) and Ca (black) plotted as a function of position across the field of view. These spectra represent summations of Na and Ca intensities across the entire 2000 µm field of view along a horizontal profile across the image. The Na and Ca spectra track together, as expected if these elements are found in the same dissolving phase, e.g. plagioclase. Here the plagioclase reaction front is 700 µm wide. Point 1 highlights a plagioclase phenocryst ghost within the rind that contains secondary Al precipitation. The Al precipitation is likely gibbsite, recognized in XRD spectra of the rind materials. Some secondary porosity (black) is imaged within phenocrysts coreward of the labeled reaction front.

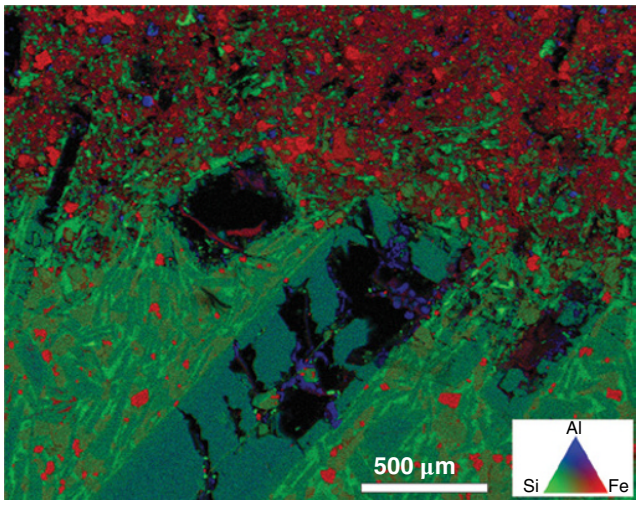

Figure 7.14 EDS image of a plagioclase phenocryst dissolving at the core-rind boundary of a clast collected from Qt2 of the Costa Rican chronosequence. Extent of the image is shown in Figure 7.8a. The plagioclase crystal is dissolving in the center forming secondary porosity (balck). The andesitic matrix consists mainly of small plagioclase grains (green-blue color), augite (greenish-red), and ilmenite (red). The blue phase precipitated in the crystal interior contains Al but not Si, consistent with gibbsite, which was also detected in XRD of rind materials (Navarre-Sitchler et al., 2011). Here plagioclase appears to weather directly to gibbsite with no other clay phase intermediate like kaolinite (modified after Navarre-Sitchler et al., 2011).

Navarre-Sitchler et al., 2009) and Guadeloupe (Figure 7.13) (Engel, 2016; Sak et al., 2010, 2018). Furthermore, the creation of porosity within plagioclase and pyroxene and precipitation of secondary phases due to this reaction occurred where the reaction fronts for plagioclase and pyroxene were coincident (Figures 7.13 and 7.14). For two minerals to dissolve at the same rate and same location (coincident reaction fronts), the reactions are most likely controlled by transport rather than interfacial reaction. Largely for that reason, it was concluded that weathering of clasts was transport limited and that the transport mechanism was diffusion of reactants or products into or out of the core. While advective transport is likely to be important within the outermost sections of the high-porosity rind or within the soil matrix, the low porosity of the cores and innermost rind materials precludes fast rates of advective transport. Alteration of pyroxene is recognized at greater distances coreward of the core-rind boundary, characterized by oxidation of iron around the pyroxene crystals with no visible porosity development. The dissolution of plagioclase phenocrysts begins closer to the visually defined core-rind boundary than pyroxene oxidation. Significantly, at the scale of observation of optical microscopy, plagioclase is the first phase to alter and produce measurable porosity.

For one-dimensional diffusion limited weathering rind formation, the reaction front thickness (h) represents a balance between the product of the porosity (ϕ) and diffusivity (D) divided by the product of the rate constant for solubilization of a given element (k) and the mineral-water interfacial area (A) (Lichtner, 1988):

$$h = \left(\frac{\varphi D}{kA} \right)^{\frac{1}{2}}. \quad (4)$$

This relationship is only strictly true for weathering of a single-component, single-phase system. Although this equation will not strictly apply to the multicomponent, multiphase weathering rind system, it is nonetheless expected that the reaction front thickness may vary inversely with the rate constant, as suggested by equation 4 (Navarre-Sitchler et al., 2009).

Exploring the effect of curvature on the rind thickness and dissolution rate requires a slightly more complex model. The sensitivity of weathering advance rates to curvature of the core-rind boundary has been observed in the field (e.g. Chinn, 1981; Sak et al., 2010) and is well supported by modeling results (Lebedeva et al., 2015). For a curvilinear weathering front with a constant curvature $K < 0$, constant diffusivity, and constant porosity, the normal component of the weathering advance rate can be calculated using an advection-like term, where the advection velocity (v) can be expressed as (Lebedeva et al., 2015)

$$v = D\varphi[K]. \tag{5}$$

At points along the core-rind boundary with $K < 0$, rind thickness is directly proportional to the absolute value of the curvature. The reaction front thickness also decreases with K, consistent with field observations (Engel et al., 2016; Sak et al., 2010). The positive correlation between the weathering advance rate (ω_n) and curvature of the weathering interface is shown by

$$\omega_n = \omega_o - \left(\frac{D\varphi\left(C^e - C^R\right)}{Q^0} \right) K. \tag{6}$$

Here, ω_o is the advance rate of planar weathering front; C^e and C^R are the equilibrium solute concentration and the solute concentration at the interface during dissolution, respectively; and Q^0 is the concentration of reactive minerals in the core.

7.9. QUANTIFYING THE DURATION OF WEATHERING

Uranium-series isotopes (e.g. ^{238}U, ^{234}U, ^{230}Th, and ^{232}Th) provide a means to quantify rates and duration of weathering (e.g. Bourdon et al., 2009; Dequincey et al., 2002; DePaolo et al., 2006; Dosseto, Bourdon, et al., 2008; Dosseto, Turner, et al., 2008; Krishnaswami et al., 2004; Ma et al., 2010; 2012; Maher et al., 2004; Pelt et al., 2008; Sarin et al., 1990; also reviews by Chabaux et al., 2003; 2008). Fractionation of radionuclides of U, Th, and Ra occurs on various time scales that depend upon the decay half-lives and geochemical properties (e.g. Bourdon et al., 2003; Ivanovich & Harmon, 1992). These radionuclides have long been used as a geochronologic tool for processes such as magmatic differentiation or carbonate deposition (reviews by Condomines et al., 2003; Edwards et al., 2003). With recent improvements in our understanding of their behaviors during low-temperature water-rock interaction, U-series isotopes have emerged as a reliable chronometer to directly constrain the rates and duration of chemical weathering (e.g. reviews by Chabaux et al., 2003; 2008).

Rind formation processes modify U-series activity ratios such that the ^{238}U-^{234}U-^{230}Th disequilibria can be used to measure the rind formation ages and weathering rates (Pelt et al., 2008; Ma et al., 2012). Thorium phases are typically insoluble, so Th is generally immobile and particle reactive during water-rock interactions (Chabaux et al., 2003), especially in tropical climates (Pelt et al., 2008; Ma et al., 2012). In contrast, U is mobile during water-rock interactions in oxidizing conditions (Chabaux et al., 2003). Both leaching processes and U addition during chemical weathering modify the (^{234}U/^{238}U) activity ratios in the rind. Calculated (^{234}U/^{238}U) values are >1 in rind samples and are consistent with two important processes of chemical leaching that generates (^{234}U/^{238}U) ratios <1 in the solid weathering products and the continuous addition of U as a precipitate or sorbate from soil pore waters with (^{234}U/^{238}U) ratios >1, which leads to excess ^{234}U and ^{238}U in rind materials. Over time, the excess ^{234}U (half-life, $T_{1/2}$ = 244 kyr) decays to ^{230}Th ($T_{1/2}$ = 75 kyr). Radioactive production of ^{230}Th and Th immobility account for the observed continuous increase in the (^{230}Th/^{232}Th) activity ratio across the weathering rind, away from the core-rind boundary. An open-system U-series mass balance model accounting for continuous leaching and addition of U-series isotopes during rind development (Dequincey et al., 2002; Ma et al., 2012), and changes in the U-series isotopes with time in the rind, can be modeled by a system of equations (Engel, 2016; Ma et al., 2012; Sak et al., 2018).

The simplicity of weathering rind systems (i.e. protolith and regolith are collected and analyzed together in the same sample) has led to several studies that demonstrate the applicability of U-series isotopes to quantify the regolith formation processes related to the creation and development of porosity in a low-porosity rock (e.g. Emmanel & Berkowitz, 2007; Navarre-Sitchler et al., 2009). Specifically, rind formation rates have been quantified on clasts from Costa Rica (Pelt et al., 2008) and Guadeloupe (Engel et al., 2016; Ma et al., 2012, 2019; Sak et al., 2018). Pelt et al. (2008) were the first to use U-series isotopes to measure the rind formation rate on a basaltic andesite clast from the Costa Rica chronosequence (Figure 7.7a). As anticipated, the duration of weathering increases with distance across the weathering rind, away from the core-rind boundary, and these ages calculated using U-series are consistent with the independent (optically stimulated luminescence and radiocarbon) age constraints for the host terrace deposits (Table 7.2).

Weathering rind advance rates have been determined using U-series isotope disequilibrium on multiple transects across individual clasts, highlighting the

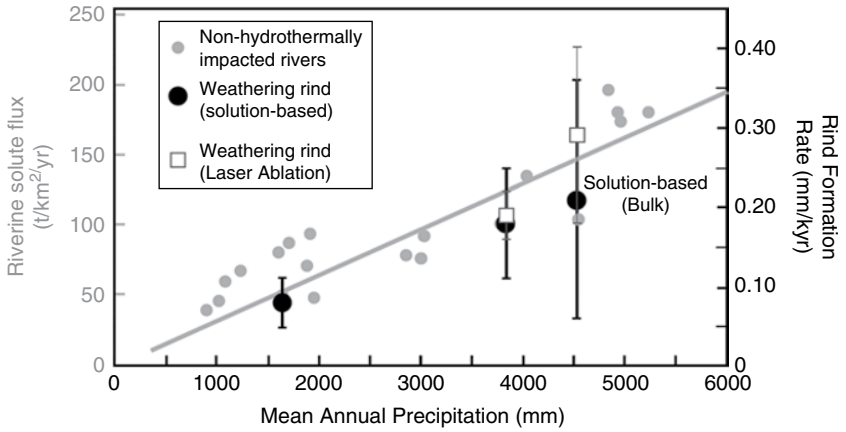

Figure 7.15 Rind formation rates and riverine solute fluxes from Guadeloupe plotted as a function of watershed mean annual precipitation. Rind formation rates calculated using LA MC-ICPMS are plotted as white squares (Ma et al., 2019), and solution MC-ICPMS are shown as black circles (Engel et al., 2016; Ma et al., 2012; Sak et al., 2018) for the same clasts. Riverine fluxes for major rivers not impacted by hydrothermal activities are shown as gray circles that define a linear relationship (gray line) (Gaillardet et al., 2011). Rind advance rates determined for low-curvature segments of the core-rind boundary define a linear relationship with a similar slope to the watershed scale flux rates.

relationship between the rind advance rate and curvature of the core-rind boundary. These transects corroborate the assumption that continuous prominent horizons within a weathering rind are the same age despite being located at different distances from the core-rind boundary (Sak et al., 2010). Calculated rind advance rates in individual clasts increase with increasing curvature of the core-rind boundary (Engel et al., 2016; Ma et al. 2012). Taken together, these results demonstrate the utility of U-series dating as a reliable means of quantifying variability in weathering rates in individual clasts. The ability to quantify the duration of weathering using U-series dating makes it possible to compare rind formation rates from clasts in undated deposits. These data also highlight the importance of comparing rind advance rates across segments of the core-rind boundary that are characterized by similar curvature, as calculated rind advance rates can vary by as much as a factor of 1.3 in a single clast.

More recently, Ma et al. (2019) demonstrated that LA-MC-ICPMS and LA-Q-ICPMS can be used for the rapid and reliable *in situ* measurement of U-series isotope compositions and elemental distributions that are consistent with measurements obtained using conventional analyses (Ma et al., 2010; Sak et al., 2018). The high resolution *in situ* analyses obtained using laser suggest that the spatial variability in U precipitation in the weathering rind correlates with variations in porosity (Ma et al., 2019). This level of detail was inaccessible when analyzing bulk samples. The denser sample resolution and small sample area results in these robust data sets are well-suited for distinguishing between linear and power law rind thickness-age relationships across the reaction front and potentially identifying *in situ* erosion within the weathering rind (e.g. Etienne, 2002; Gordon & Dorn, 2005). The larger data sets are also amenable to statistical treatments.

7.10. WEATHERING ADVANCE RATES ACROSS PRECIPITATION GRADIENTS

The importance of variability in precipitation on rind formation rates was originally highlighted by Porter (1975) along the Bullfrog Terrace climosequence in the Yakima Valley of Washington State. Here the thicknesses of rinds developed on basaltic composition clasts collected from the Bullfrog Terrace varied as a function of MAP (77 to 23 cm), although the MAT remained relatively constant (7.9 to 8.3 °C). Measured weathering rind thicknesses in the climosequence increased linearly from 0.3 mm to 0.78 mm with increasing precipitation at a rate of 1.0×10^{-3} $mm_{rind\ thickness}$ mm_{rain}^{-1}.

Comparisons between calculated weathering rind advance rates across low curvature segments of the core-rind boundary of clasts weathering under similar MAT (25 °C) and variable MAP (1800 to 4500 mm yr^{-1}) in Guadeloupe highlight the relationship between MAP and rind advance rates (Engel et al., 2016; Ma et al., 2012, 2019; Sak et al., 2018). Here, the rind advance rates for two basins characterized by the greatest MAP (4500 and 3400 mm yr^{-1}) are 0.21 ± 0.15 mm kyr^{-1} (Sak et al., 2018) and 0.18 mm kyr^{-1} (Ma et al., 2012), respectively. Both of these rind advance rates are ~60%

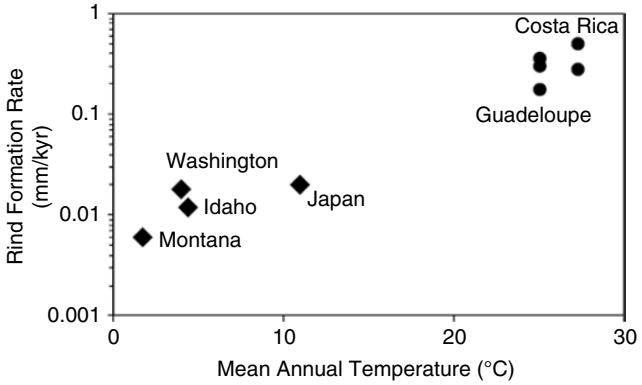

Figure 7.16 Rind formation rates for andesitic and basaltic composition clasts plotted as function of mean annual temperature. Diamonds = data sets constrained by mean rind thickness and calibrated dating of the host deposit. Circles = data sets constrained by U-series dating. Rind formation rates compiled from Porter (1975), Colman and Pierce (1981), Oguchi (2004), Ma et al. (2012), Engel et al. (2016), and Sak et al. (2018).

faster than the 0.08 mm kyr^{-1} drier (MAP = 1800 mm yr^{-1}) watershed (Engel et al., 2016), independently demonstrating the control of precipitation on weathering rates over a duration of the dated weathering rinds (Figure 7.15).

Gaillardet et al. (2011) calculated a similar trend among the same three catchments using chemical weathering derived from solute chemistry. The weathering rate constrained by the solute chemistry is ~50% slower in the driest watershed than in the other two basins. This is significant because the formation rates at the clast scale are constrained using the chemistry of the rind materials and represent rates integrated over the ~75 ka history of the weathering rind. Catchment scale weathering rates, however, are derived from riverine fluxes and reflect short-term chemical weathering rates. Although the absolute magnitudes of precipitation have likely fluctuated over the 75 kyr interval recorded by the weathering clasts, the persistence of spatially consistent weathering rates when comparing solute- and residuum-derived rates suggests a long-lived precipitation gradient across the island of Basse-Terre in Guadeloupe (Figure 7.15).

Weathering rates calculated along transects spanning low-curvature segments of the core-rind boundary of clasts from the Guadeloupe chronosequnece are ~2000 times slower than the catchment scale weather rates for these same host catchments (Figure 7.15). This discrepancy in weathering rates was anticipated and has been attributed to differences in how surface areas are measured using different "rulers" at different scales of observation (e.g. Navarre-Sitchler & Brantley, 2007; Pope et al., 1995).

Rind formation rates also correlate with variations in MAT. Rind advance rates on clasts with low-porosity andesitic and basaltic andesite composition cores are compiled from the literature. Data on weathering rinds derived from studies in the western United States (Colman & Pierce, 1981; Porter, 1975) and Japan (Oguchi, 2001) are calibrated ages based upon mean rind thickness values. In contrast, reported rind formation rates from Costa Rica and Guadeloupe are constrained by U-series dating (Engel et al., 2016; Ma et al., 2010; Pelt et al., 2008; Sak et al., 2018). Rind formation rates are more rapid in deposits weathering at a higher MAT (Figure 7.16).

7.11. SUMMARY POINTS

The *in situ* development of weathering rinds on clasts weathering in the near surface environment provide a well-constrained system for investigating the incipient stages of chemical weathering in the absence of physical weathering. The progressive increase in rind thickness has made weathering rinds an effective tool for determining relative ages of surficial deposits. The nature and rates of weathering rinds observed in field settings are sensitive to clast composition, porosity of the parent material, clast shape, and climatic conditions.

Clast-scale weathering is a well-constrained intermediate between laboratory- and landscape-scale investigations of chemical weathering. Detailed investigations spanning the visually defined core-rind boundary of clasts with low-porosity core material reveal that conversion of reactive core material to depleted rind material occurs across a narrow reaction front. Reactions fronts defined by variations in color, composition, porosity, and mechanical properties occur at the same locations. The collocation of the reaction fronts suggests rind formation is transport limited. X-ray mapping across the core-rind boundary reveal the *in situ* dissolution of plagioclase and pyroxene phenocrysts, resulting in increases in porosity.

Uranium-series disequilibria in the rind are significant and are the result of mobility characteristics of U-series isotopes during weathering, including leaching and isotope fractionation by circulating pore fluids. Uranium-series disequilibria are linked to the rind formation processes porosity formation and precipitation of Fe-Al oxides initiating at the core-rind boundary. As such, the U-series constrain weathering rind ages, which increase with distance away from the core-rind boundary. Age constraints obtained using U-series dating techniques shed insights into reaction kinetics at the weathering interface and expand the use of weathering rinds to date previously undated geomorphic surfaces, facilitating comparisons between deposits weathering under different climatic conditions. Rates of rind formation increase

with increasing mean annual temperature and mean annual precipitation.

ACKNOWLEDGMENTS

Costa Rica research was funded partially by the National Science Foundation grant CHE-0431328 for the Center for Environmental Kinetics Analysis at Pennsylvania State, Department of Energy grant DE-FG02-05ER15675, and National Aeronautics and Space Administration grant NNG05GN72G. National Science Foundation grant EAR 1251969 supported research in Guadeloupe. Insightful and fruitful collaborations and discussions with S. Brantley, J. Gaillardet, L. Ma, and A. Navarre-Sitchler have helped to shape and broaden my understanding of weathering clasts. Constructive reviews by A. Curley, two anonymous reviewers, and Editor Allen Hunt greatly improved this manuscript.

REFERENCES

Amundson, R. (2004). Soil formation. In H. D. Holland & K. K. Turekian (Eds.), *Treatise on Geochemistry* (pp. 1–35). Amsterdam: Elsevier Press.

Anderson, L. W., & Anderson, D. S. (1981). Weathering rinds on quartz arenite clasts as a relative-age indicator and the glacial chronology of Mount Timpanogos, Wasatch Range, Utah. *Arctic and Alpine Research*, *13*, 25–31.

Anderson, S. P., Blum, J., Brantley, S. L., Chadwick, O., Chorover, J., Derry, L. A., et al. (2004). Proposed initiative would study Earth's weathering engine. *EOS Transactions*, *85*(28), 265–269.

Anderson, S. P., Dietrich, W. E., & Brimhall, G. H. (2002). Weathering profiles, mass-balance analysis, and rates of solute loss: Linkages between weathering and erosion in a small, steep catchment. *Geol. Soc. Am. Bull.*, *114*, 1143–1158.

Barshad, I. (1964). Chemistry of soil development. In F. E. Bear (Ed.), *Chemistry of the soil* (pp. 1–70). New York: Reinhold Publishing.

Birkeland, P. W. (1974). Use of relative age dating methods in a stratigraphic study of rock glacier deposits, Mt. Sopris, Colorado. *Artic and Alpine Research*, *5*, 401–416.

Bourdon, B., Bureau, S., Andersen, M. B., Pili, E., & Hubert, A. (2009). Weathering rates from top to bottom in a carbonate environment. *Chemical Geology*, *258*, 275–287.

Bourdon, B., Henderson, G. M., Lundstrom, C. C., & Turner, S. P. (2003). Uranium-series geochemistry, *Mineralogical Society of America Reviews in Mineralogy and Geochemistry 52*, 656.

Brantley, S. L., Godhaber, M. B., & Ragnarsdottir, K. V. (2007). Crossing disciplines and scales to understand the critical zone. *Elements*, *3*, 370–314.

Brantley, S. L., & White, A. F. (2009). Approaches to modeling weathering regolith. In E. H. Oelkers & J. Schott (Eds.), *Thermodynamics and kinetics of water-rock interaction*, Reviews of Mineralogy and Geochemistry (vol. *70*, pp. 435–484).

Brimhall, G. H., Chadwick, O. A., Lewis, C. J., Compston, W., Williams, I. S., Danti, K. J., et al. (1991). Deformational mass transport and invasive processes in soil evolution. *Science*, *255*, 695–702.

Brimhall, G. H., & Dietrich, W. E. (1987). Constitutive mass balance relations between chemical composition, volume, density, porosity, and strain in metasomatic hydrochemical systems: Results on weathering and pedogenesis. *Geochim. Cosmochim. Acta*, *51*, 567–587.

Burke, R. M., & Birkeland, P. W. (1979). Reevaluation of multiparameter relative dating techniques and their application to the glacial sequence along the eastern escarpment of the Sierra Nevada, California. *Quaternary Research*, *11*, 21–51.

Buss, H. L., Sak, P. B., Webb, S. M., & Brantley, S. L. (2008). Weathering of the Rio Blanco quartz diorite, Luquillo Mountains, Puerto Rico: Coupling oxidation, dissolution and fracturing. *Geochim. Cosmochim. Acta*, *72*, 4488–4507.

Buss, H. L., White, A. F., Dessert, C., Gaillardet, J., Blum, A. E., & Sak, P. B. (2010). Depth profiles in a tropical, volcanic critical zone observatory: Basse-Terre, Guadeloupe. In I. S. Torres-Alvarado & P. Birkle (Eds.), *Proc. of the 13th Intl. Symp. on Water–Rock Interaction*.

Carroll, T. (1974). Relative age dating techniques and Quaternary chronology, Arikaree Cirque, Colorado. *Geology*, *2*, 321–325.

Cernohouz, J., & Solc, I. (1966). Use of sandstone wanes and weathered basaltic crust in absolute chronology. *Nature*, *212*, 806–807.

Chabaux, F., Bourdon, B., & Riotte, J. (2008). U-series geochemistry in weathering profiles, river waters and lakes. *Radioactivity in the Environment*, *13*, 49–104.

Chabaux, F., Riotte, J., & Dequincey., O. (2003). U-Th-Ra fractionation during weathering and river transport. *Reviews in Mineralogy and Geochemistry*, *52*, 533–576.

Chinn, T.J.H. (1981). Use of rock weathering-rind thickness for Holocene absolute age-dating in New Zealand. *Arctic Alpine Res.*, *13*, 33–45.

Colman, S. M. (1982a). Chemical weathering of basalts and basaltic andesites: Evidence from weathering rinds. Geological Survey Professional Paper 1246. Washington, DC: U.S. Govt Printing Office.

Colman S. M. (1982b). Clay mineralogy of weathering rinds and possible implications concerning the sources of clay minerals in soil. *Geology*, *10*, 370–375.

Colman S. M. (1986). Levels of time information in weathering measurements, with examples from weathering rinds on volcanic clasts in the western United States. In S. M. Colman & D. P. Dethier (Eds.), *Rates of chemical weathering of rocks and minerals* (pp. 379–393), San Diego: Academic Press.

Colman, S. M., & Pierce, K. L. (1981). Weathering rinds on andesitic and basaltic stones as a Quaternary age indicator. Geological Survey Professional Paper 1210. Washington, DC: U.S. Govt Printing Office.

Colman, S. M., & Pierce, K. L. (1992). Varied records of early Wisconsinan alpine glaciation in the western United States derived from weathering-rind thicknesses. In P. U. Clark & P. D. Lea (Eds.), *The last interglacial-glacial transition in North*

America (vol. *270*, pp. 269–278). Geological Society of America.

Colman, S., Pierce, K., & Birkeland, P. (1987). Suggested terminology for quaternary dating methods. *Quaternary Research*, *28*(2), 314–319.

Condomines, M., Gauthier, P.–J., & Sigmarsson, O. (2003). Timescales of magma chamber processes and dating of young volcanic rocks. *Reviews in Mineralogy and Geochemistry*, *52*, 125–174.

Cook-Talbot, J. D. (1991). Sorted circles, relative-age dating and paleoenvironmental reconstruction in an alpine periglacial environment, eastern Jotunheimen, Norway: Lichenometric and weathering-based approaches. *The Holocene*, *1*, 128–141.

Curran, J., Smith, B., & Warke, P. (2002). Weathering of igneous rocks during shallow burial in an upland peat environment: Observations from the Bronze Age Copney Stone Circle Complex, Northern Ireland. *Catena*, *49*, 139–155.

DePaolo, D. J., Maher, K., Christensen, J. N., & McManus, J. (2006). Sediment transport time measured with U-series isotopes: Results from ODP North Atlantic drift site 984. *Earth and Planetary Science Letters*, *248*, 394–410.

Dequincey, O., Chabaux, F., Clauer, N., Sigmarsson, O., Liewig, N., & Leprun J.-C. (2002). Chemical mobilizations in laterites: Evidence from trace elements and 238U-234U-230Th disequilibria. *Geochim Cosmochim Acta*, *66*, 1197–1210.

Dorn, R. I. (1995). Digital processing of back-scatter electron imagery: A microscopic approach to quantifying chemical weathering. *Geological Society of America Bulletin*, *107*, 725–741.

Dosseto, A., Bourdon, B., & Turner, S. P. (2008). Uranium-series isotopes in river materials: Insights into the timescales of erosion and sediment transport. *Earth and Planetary Science Letters*, *265*, 1–17.

Dosseto, A., Turner, S. P., & Chappell, J. (2008). The evolution of weathering profiles through time: New insights from uranium-series isotopes. *Earth and Planetary Science Letters*, *274*, 359–371.

Dixon, J. C., Thorn, C. E., Darmody, R. G., & Campbell, S. W. (2002). Weathering rinds and rock coatings from an Artic alpine environment, northern Scandinavia. *GSA Bulletin*, *114*, 226–238.

Dorn, R. I. (1995). Digital processing of back-scatter electron imagery: A microscopic approach to quantifying chemical weathering. *Geological Society of America Bulletin*, *107*, 725–741.

Dorn, R. I. (1998). *Rock coatings*, vol. *6*. Amsterdam: Elsevier.

Dorn, R. I., Mahaney, W. C., and Krinsley, D. H. (2017). Case hardening: Turning weathering rinds into protective shells. *Elements*, *13*, 165–169.

Edwards, R. L., Gallup, C. D., & Cheng, H. (2003). Uranium-series dating of marine and lacustrine carbonates. *Reviews in Mineralogy and Geochemistry*, *52*, 363–405.

Emmanuel, S., & Berkowitz, B. (2007). Effects of pore-size controlled solubility on reactive transport in heterogeneous rock. *Geophysical Research Letters*, *34*. doi:10.1029/2006GL028962

Engel, J. M., Ma, L., Sak, P. B., Gaillardet, J., Minghua, R., Engle, M. A., & Brantley, S. L. (2016). Quantifying chemical weathering rates along a precipitation gradient on Basse-Terre Island, French Guadeloupe: New insights from U-series isotopes in weathering rinds: *Geochemica et Cosmochemica Acta*, *195*, 26–67.

Etienne, S. (2002). The role of biological weathering in periglacial areas: A study of weathering rinds in southern Iceland. *Geomorphology*, *47*, 75–86.

Fisher, D. M., Gardner, T. W., Marshall, J. S., Sak, P. B., & Protti, M. (1998). The effect of subducting seafloor roughness on forearc kinematics, Pacific coast, Costa Rica. *Geology*, *26*, 467–470.

Gaillardet, J., Rad, S., Rive, K., Louvat, P., Gorge, C., Allegre, C. J., & Lajeunesse, E. (2011). Orography-driven chemical denudation in the Lesser Antilles: Evidence for a new feedback mechanism stabilizing atmospheric CO2. *Am. J. Sci.*, *311*, 851–894.

Gellatly A. M. (1984). The use of rock weathering-rind thickness to redate moraines in Mount Cook National Park, New Zealand. *Alpine and Arctic Research*, *16*(2), 225–232.

Gordon, S. J., & Dorn, R. I. (2005). *In situ* weathering rind erosion. *Geomorphology*, *67*, 97–113.

Graham, R. C., Rossi, A. M., & Hubbert, K. R. (2010). Rock to regolith conversion: Producing hospitable substrates for terrestrial ecosystems. *GSA Today*, *20*, 4–9.

Hausrath, E. M., Navarre-Sitchler, A., Sak, P. B., Steefel, C. I., & Brantley, S. L. (2008). Basalt weathering rates on Earth and the duration of liquid water on the plains of Gusev Crater, Mars. *Geology*, *36*, 67–70.

Ivanovich, M., & Harmon, R. S. (1992). *Uranium-series disequilibrium: Applications to Earth, marine, and environmental sciences*. Oxford: Clarendon Press.

Kellerer-Pirklbauer, A., Wangensteen, B., Farbrot, H., & Etzelmüller (2008). Relative surface age-dating of rock glacier systems near Hólar in Hjaltadalur, northern Iceland. *Journal of Quaternary Science*, *32*, 137–151.

Kirkbride, M. P. (2005). Boulder edge-roundness as an indicator of relative age: A Lochnagar case study. *Scott. Geog. J.*, *121*, 219–236.

Kirkbride, M. P., & Bell, C. M. (2010). Edge-roundness of boulders of Torridonian Sandstone (Northwest Scotland): Applications for relative dating and implications for warm and cold climate weathering rates. *Boreas*, *39*, 187–198.

Knuepfer, P.L.K. (1988). Estimating ages of late Quaternary stream terraces from analysis of weathering rinds and soils. *Geol. Soc. Amer. Bull.*, *100*, 1224–1236.

Knuepfer, P.L.K. (1994). Use of rock weathering rinds in dating geomorphic surfaces. In C. Beck (Ed.), *Dating in exposed and surface contexts* (pp. 15–28), University of New Mexico Press.

Krishnaswami, S., Williams, G. A., Graustein, W. C., & Turekian, K. K. (2004). The effect of weathering regime on uranium decay series and osmium in two soil profiles. *Geochemical Journal*, *38*, 651–660.

Laustela, M., Egli, M., Frauenfelder, R., Kääb, A., Maisch, M., & Haeberli, W. (2003). Weathering rind measurements and relative age dating of rockglacier surfaces in crystalline regions of the Eastern Swiss Alps. In P. M. Springman & L. U. Arenson (Eds.), *Proceedings of the Eighth International Conference on Permafrost* (vol. *1*, pp. 627–632). BalkemaL Lisse.

Lebedeva, M. I., Sak, P. B., Ma, L., & Brantley, S. L. (2015). Using a mathematical model of a weathering clast to explore

the effects of curvature on weathering. *Chemical Geology*, *404*, 88–99.

Lichtner, P. (1988). The quasi-stationary state approximation to coupled mass transport and fluid–rock interaction in a porous medium. *Geochim. Cosmochim. Acta*, *52*, 143–165.

Lilliesköld, M., & Sundqvist, B. (1994). Weathering of surface clasts as an indicator of the relative age glacial deposits on Jameson Land, *East Greenland. Boreas*, *23*, 473–478.

Locke, W. W. III, Andrews J. T., & Webber, P. J. (1979). A manual for lichenometry. *British Geomorphological Research Group Bulletin*, *26*.

Ma, L., Chabaux, F., Pelt, E. Blaes, E., Jin, Lixin, Brantley, & S. L. (2010). *Regolith production rates calculated with uranium-series isotopes at Susquehanna/Shale Hills Critical Zone Observatory. Earth Planet. Sci. Lett.*, *297*, 211–225.

Ma, L., Chabaux, F., Pelt, E., Mranet, M., Sak, P. B, Gaillardet, J., et al. (2012). The effect of curvature on weathering rind formation: Evidence from Uranium-series isotopes in basaltic andesite weathering clasts in Guadeloupe. *Geochemica et Cosmochemica Acta*, *80*, 92–107.

Ma, L., Dosseto, A., Gaillardet, J., Sak, P. B., & Brantley S. L. (2019). Quantifying weathering rind formation rates by *in situ* measurements of U-series isotopes with laser ablation and inductively coupled plasma-mass spectrometry. *Geochemica et Cosmochemica Acta*, *247*, 1–26.

Maher, K., DePaolo, D. J., & Lin, J. C. F. (2004). Rates of silicate dissolution in deep-sea sediment: *In situ* measurement using U-234/U-238 of pore fluids. *Geochimica et Cosmochimica Acta*, *68*, 4629–4648.

Marshall, C. E. (1977). *Physical chemistry and mineralogy of soils*, vol. *II*. Wiley and Sons.

Marshall, J. S. (2000). Active tectonics and quaternary landscape evolution across the western Panama block, Costa Rica, Central America [Ph.D. thesis]. Pennsylvania State University, 304 p.

Marshall, J. S., Idleman, B. D., Gardner, T. W., & Fisher, D. M. (2003). Landscape evolution within a retreating volcanic arc, Costa Rica, Central America. *Geology*, *31*, 419–422.

Matthews, J. A., & Shakesby, R. A. (1984). The status of the 'Little Ice Age' in southern Norway: A relative age-dating of Neoglacial moraines with Schmidt hammer and lichenometry. *Boreas*, *13*, 333–346.

McCalpin, J. P., & Khromovskikh, V. S. (1995). Holocene paleoseismicity of the Tunka fault, Baikal rift, Russia. *Tectonics*, *14*, 594–605.

McCarroll, D. (1991a). The age and origin of Neoglacial moraines in Jotunheimen, southern Norway: New evidence from weathering-based data. *Boreas*, *20*, 283–295.

McCarroll, D. (1991b). The Schmidt hammer, weathering and rock surface roughness. *Earth Surface Processes and Landforms*, *16*, 477–480.

McSaveney, M. J. (1992). *A* manual of weathering-rind data for sandstone clasts of the Torlesse Supergroup. Lower Hutt, New Zealand, Institute of Geological and Nuclear Sciences Report 92/4.

Meyer, G. A., & Leidecker, M. E. (1999). Fluvial terraces along the Middle Fork Salmon River, Idaho, and their relationship to glaciation, landslide dams, and incision rates: A preliminary analysis and rive-mile guide. In S. S. Hughes & G. D. Thackray (Eds.), *Guidebook to the geology of eastern Idaho* (pp. 219–235). Idaho Museum of Natural History.

Mills, H. H., & Allison, J. B. (1995). Weathering and soil development on fan surfaces as a function of height above modern drainageways, Roan Mountain, North Carolina. *Geomorphology*, *14*, 1–17.

Milnes, A. R., Fitzpatrick, R. W. (1989). Titanium and zirconium minerals. In J. B. Dixon & S. B. Weed (Eds.), *Minerals and soil environments* (book series no. 1, pp. 1131–1205). Soil Science Society of America.

Morriss, M. C., & Wegmann, K. W. (2017). Geomorphology of the Burnt River, eastern Oregon, USA: Topographic adjustments to tectonic and dynamic deformation. *Geomorphology*, *278*, 43–59.

Navarre-Sichler A., & Brantley, S. L. (2007). Basalt weathering across scales. *Earth and Planetary Science Letters*, *261*, 321–334.

Navarre-Sitchler, A., Brantley, S. L, & Rother, G. (2015). How porosity increases during incipient weathering of crystalline silicate rocks. *Reviews in Mineralogy and Geochemistry*, *80*, 331–354.

Navarre-Sitchler, A. K., Cole, D., Rother, G., Jin, L., Buss, H. L., & Brantley, S. L. (2013). Porosity and surface area evolution during weathering of two igneous rocks. *Geochim Cosmochim Acta*, *109*, 400–413.

Navarre-Sitchler, A., Steefel, C., Sak, P. B., & Brantley, S. L. (2011). A reactive-transport model for weathering rind formation on basalt. *Geochim. Cosmochim. Acta*, *75*, 7644–7667.

Navarre-Sitchler, A., Steefel, C. I., Yang, L., Tomutsa, L., & Brantley, S. L. (2009). Evolution of porosity and diffusivity associated with chemical weathering of a basalt clast. *Journal of Geophysical Research*, *114*, F02016. doi:10.1029/2008JF001060

Neaman, A., Chorover, J., & Brantley, S. L. (2005). Implications of the evolution of organic acid moieties for basalt weathering over geological time. *American Journal of Science*, *305*, 147–185.

Oguchi, C. T. (2001). Formation of weathering rinds on andesite. *Earth Surface Processes and Landforms*, *26*, 847–857.

Oguchi C. T. (2004). A porosity-related duffusion model of weathering rind development. *Catena*, *58*, 65–75.

Oguchi C. T., & Matsukura Y. (1999). Effect of porosity on the increase in weathering-rind thicknesses of basaltic andesite gravel. *Engineering Geology*, *55*, 77–89.

Pazzaglia, F. J., & Brandon M. T. (2001). A fluvial record of long-term steady-state uplift and erosion across the Cascadia forearc high, western Washington State. *American Journal of Science*, *301*, 385–431.

Pazzaglia, F., Gardner, T., & Merritts, D. (1998). Bedrock fluvial incision and longitudinal profile development over geologic time scales determined by fluvial terraces. In E. Wohl & K. Tinkler (Eds.), *Rivers over rock: Fluvial processes in bedrock channels* (vol. *106*, pp. 207–236). American Geophysical Union.

Pelt, E., Chabaux, F., Innocent, C., Navarre-Sitchler, A., Sak, P. B., & Brantley, S. L. (2008). Uranium-thorium chronometry of weathering rinds: Rock alteration rate and paleoisotopic

record of weathering fluids. *Earth Planet. Sci. Lett.*, *276*, 65–75.3.

Pope, G. A., Dorn, R. I., & Dixon, J. C. (1995). A new conceptual model for understanding geographical variations in weathering. *Annals of American Geographers*, *88*, 38–64.

Porter, S. C. (1975). Weathering rinds as a relative-age criterion: Application to subdivision of glacial deposits in the Cascade Range. *Geology*, *3*, 101–104.

Powers, M. C. (1953). A new roundness scale for sedimentary particles. *J. of Sed. Petrology*, *23*, 117–119.

Ricker, K. E., Chinn, T. J., & McSaveney, M. J. (1993). A late Quaternary moraine sequence dated by rock weathering rinds, Craigieburn Range, New Zealand. *Canadian Journal of Earth Science*, *30*, 1861–1869.

Rossi, A. M., & Graham, R. C. (2010). Weathering and porosity formation in subsoil granitic clasts, Bishop Creek Moraines, California. *Soil Sci. Soc. Am. J.*, *74*, 172–185.

Sak, P. B., Fisher, D. M., Gardner, T. W., Marshall, J. S., & LaFemina, P. C. (2009). Rough crust subduction, forearc kinematics, and Quaternary uplift rates, Costa Rican segment of the Middle American Trench. *Geological Society of America Bulletin*, *121*, 992–1012.

Sak, P. B., Fisher, D. M., Gardner, T. W., Murphy, K., & Brantley, S. L. (2004). Rates of weathering rind formation on Costa Rican basalt. *Geochim. Cosmochim. Acta*, *68*, 1453–1472.

Sak, P. B., Murphy, M., Ma, L., Gaillardet, J., Herndon, E. M., Brantley, S. L., & Daniel, C. (2018). From unweathered core to regolith: Rates and trends of *in situ* chemical weathering on a tropical volcanic island (Basse Terre Island, French Guadeloupe). *Chemical Geology*, *498*, 17–30.

Sak, P. B., Navarre-Sitchler, A., Miller, C. E., Daniel, C. C., Gaillardet, J., Buss, H. L., et al. (2010). Controls on rind thickness on basaltic andesite clasts weathering in Guadeloupe. *Chem. Geol.*, *276*, 129–143.

Salvatore, M. R., Mustard, J. F., Head, J. W., Cooper, R. F., Marchant, D. R., & Wyatt, M. B. (2013). Development of alteration rinds by oxidative weathering processes in Beacon Valley, Antarctica, and implications for Mars. *Geochim. Cosmochim. Acta*, *115*, 137–161.

Samper, A., Quidelleur, X., Lahitte, P., Mollex, D. (2007). Timing of effusive volcanism and collapse events within an oceanic arc island: Basse-Terre, Guadeloupe Archipelago (Lesser Antilles arc). *Earth Planet. Sci. Lett.*, *258*, 175–191.

Sarin, M. M., Krishnaswami, S., Somayajulu, B. L. K., & Moore, W. S. (1990). Chemistry of uranium, thorium, and radium isotopes in the Ganga-Brahmaputra river system – weathering processes and fluxes to the Bay of Bengal. *Geochimica et Cosmochimica Acta*, *54*, 1387–1396.

Sheppard, P. J., & Pavlish, L. A. (1992). Weathering of archaeological cherts: A case study from the Solomon Islands. *Geoarchaeology*, *7*, 41–53.

Shiraiwa, T., & Watanabe, T. (1991). Late Quaternary glacial fluctuations in the Langtang Valley, Nepal Himalaya, reconstructed by relative dating methods. *Artic and Alpine Research*, *23*, 404–416.

Strakhov, N. M. (1967). *Principles of lithogenesis*. Oliver and Boyd.

White, A. F. (1995). Chemical weathering rates of silicate minerals in soils. In A. F. White & S. L. Brantley (Eds.), *Chemical weathering rates of silicate minerals* (vol. *31*, pp. 407–461), Mineralogical Society of America.

White, A. F., & Blum, A. E. (1995). Effects of climate on chemical weathering in watersheds. *Geochim. Cosmochim. Acta*, *59*, 1729–1747.

White, A. F., Blum, A. E., Schultz, M. S., Bullen, T. D., Harden, J. W., & Peterson, M. L. (1996). Chemical weathering rates of a soil chronosequence on granitic alluvium: I. Quantification of mineralogical and surface area changes and calculation of primary silicate reactions. *Geochim. Cosmochim. Acta*, *60*, 2533–2550.

Whitehouse, I. E., McSaveney, M. J., Knuepfer, P.L.K., & Chinn, T.J.H. (1986). Growth of weathering rinds on Torlesse Sandstone, Southern Alps, New Zealand. In *Rates of chemical weathering of rocks and minerals* (pp. 419–435). San Diego: Academic Press.

Winkler, S., 2005, The Schmidt hammer as a relative-age dating technique: Potential and limitations of its application on Holocene moraines in Mt Cook National Park, Southern Alps, New Zealand. *New Zealand Journal of Geology and Geophysics*, *48*(1), 105–116.

Yoshida, H., Metcalfe, R., Nishimoto, S., Yamamoto, H., & Katsuta, N. (2011). Weathering rind formation in buried terrace cobbles during periods of up to 300 ka. *Appl. Geochem.*, *26*, 1706–1721.

8

Unraveling Loess Records of Climate Change from the Chinese Loess Plateau Using Process-Based Models

Peter A. Finke[1], Keerthika Nirmani Ranathunga Arachchige[1], Ann Verdoodt[1], Yanyan Yu[3], and Qiuzhen Yin[2]

ABSTRACT

Loess deposits often contain paleosols that are documenting phases of soil formation associated with interglacials or interstadials. Linkage of the paleosols to paleoclimates is not straightforward when paleoclimates are represented by dynamic (simulated) variables and paleosols by static (measured) soil parameters. We therefore propose to combine a dynamic soil model with a climate model. We define the required processes in such soil model and the output variables that would allow usage of the soil-climate model combination to be used for (past and future) climate change studies. Issues to be considered are the time- and spatial scale of the soil and the climate model. For predictive (global change) studies, the usage of (soil) model outputs to quantify the evolution of the soil natural capital and of ecosystem services must be considered. We give examples for the Chinese Loess Plateau of the evaluation of paleoclimate-paleosol linkages and of simulated soil natural capital and soil ecosystem services with the LOVECLIM-earth system model linked to the SoilGen soil evolution model and conclude that such model combination is an important step forward.

8.1. INTRODUCTION

Loess is a sediment of mostly silt-sized (2–50 μm) mineral fragments deposited as aeolian dust. It covers a substantial part (10%) of the world's land area and may reach thicknesses of tens to hundreds of meters. For loess to accumulate over time, there must be a source area (with a dry climate), sufficient wind energy to transport the dust, and a suitable accumulation area (Pye, 1995). Such circumstances occur predominantly nearby polar deserts under the influence of katabatic winds associated with large glaciers, in semiarid climates with nearby deserts and seasonally prevailing winds and in areas where braided river systems formed by meltwater fall dry during part of the year. Therefore, loess deposits can be linked to past glaciations or are associated with periglacial circumstances or semiarid climates. Most loess is found in the temperate zones. Under favorable climate, soil formation processes may outpace loess deposition or erosion and then soils may develop. If such soils are preserved (i.e. they are not eroded but are instead buried under new sediments), they form a document of the circumstances under which they formed (e.g. Sun et al., 2006). The best preserved of such geo-archives are found on the Chinese Loess Plateau (CLP), where the soils represent a period of several millions of years (An et al., 1991; Guo et al., 2002), but also in Europe (e.g., Marković et al., 2009) and the Americas (e.g., Bader et al., 2016; Schellenberger et al., 2006), loess

[1]*Department of Soil Management, Ghent University, Ghent, Belgium*

[2]*Earth and Life Institute, Georges Lemaitre Center for Earth and Climate Research, Université Catholique de Louvain, Louvain-la-Neuve, Belgium*

[3]*Institute of Geology and Geophysics, Chinese Academy of Sciences, Beijing, China*

Hydrogeology, Chemical Weathering, and Soil Formation, Geophysical Monograph 257, First Edition.
Edited by Allen Hunt, Markus Egli, and Boris Faybishenko.

DOI: 10.1002/9781119563952.ch8

geo-archives have been documented. Schaetzl et al. (2018) provide a comprehensive overview.

Substantial research has been done on the question how to relate paleosols to the paleoclimate in which they were formed. Paleoclimate reconstructions are either based on the evaluation of local proxies or on simulations by climate models, while paleosol research is almost entirely based on the analysis of field data, by field observations, and a variety of geochemical, physical, and biological laboratory analyses. After constraining the period of deposition of the loess sediment, soil properties can be measured and correlated to climate signals. Rough dating has been done by identifying paleomagnetic reversals (Rutter et al., 1990). More precise dating is done by luminescence analysis, ^{14}C, but also examples of U-series dating exist (Rowe & Maher, 2000). The most successful soil properties that were related to climate signals are quartz grain size and magnetic susceptibility (Bradley, 2013). Quartz grain sizes were related to the transport distance from the source and to wind velocity (Fang et al., 1999; Feng & Wang, 2006) for the CLP. In some cases, coarser grain sizes have been associated with colder periods. Magnetic susceptibility relates to the presence of pedogenic Fe, which is a proxy for the intensity of weathering and soil formation (e.g. Balsam et al., 2011). Higher magnetic susceptibility has been associated with greater summer monsoon strength (i.e. more rainfall) in China, although at rainfall amounts below 200 mm/year the relation disappears because pedogenesis is then limited (Balsam et al., 2011).

Relating paleoclimates to paleosols is not straightforward for the following reasons:

1. While paleoclimates can be characterized by climatic variables produced by paleoclimate model results (Yin & Berger, 2012), soil properties integrate the full period of soil formation (Johnson et al., 1990) obtained from the loess. Thus, climate dynamics are not easily captured from soil properties.

2. Additionally, the period of soil formation may or may not equal the paleoclimatic period studied, for instance, the paleoclimate during an interglacial period does not necessarily explain effects of leaching during later periods that may overprint the paleosol (Johnson et al., 1990).

3. Moreover, soil formation is not only controlled by climate (including temperature and precipitation) but also by dust accumulation rates, erosion rates, vegetation, and the duration that soil takes to form (Schaetzl et al., 2018).

This makes the interpretation of the climate signal of the loess and therefore the loess-climate model comparison complicated. To solve this problem, a soil formation model that allows to dynamically simulate soil properties must be used to distinguish the relative role of different soil-forming factors and to fill the gap between climate model and loess observation. Such soil-climate model combination allows not only the more precise reconstruction of paleosol-paleoclimate linkages but is also essential to dynamically project future soil development under global change. The central focus of this chapter, applied to loess soils, is therefore the development of global change-sensitive dynamic models of soil evolution. In the next sections, we will elaborate on the requirements of these models and provide examples of soil-climate model studies for illustration.

8.2. GLOBAL-CHANGE RESPONSIVE MODELS OF SOIL FORMATION

If soil evolution models are to be useful for both reconstruction of soil development under paleoclimate change and projection of future soil development under global change, they must meet certain demands. Both purposes imply that certain soil variables must be dynamically simulated by the model and that the model must be responsive to external forcings related to climate and land use change. Below, we discuss these issues.

8.2.1. Reconstruction of the Formation of Paleosols: Key Soil Model Output Variables

Previous research on paleosols in loess has identified paleosols based on observable characteristics, such as color, and measured characteristics. The most important of these are (1) the depth distribution of clay content as a proxy for migration of clay minerals (Han et al., 1998); (2) the clay mineralogy as an indicator of new formation of silicate minerals (Zheng et al., 1994); (3) mineralogy in general as an indicator of loss of primary minerals by weathering processes (Eden et al., 1994); (4) the presence of pedogenic iron minerals (Jeong et al., 2011) as a proxy for weathering and soil formation with effects on soil color and magnetic susceptibility (Shi et al., 2010); (5) the depth distribution of less soluble salts such as gypsum (Jeong et al., 2011), and more importantly calcite (Feng et al., 2004) as a proxy for the leaching regime. Soil properties (1) to (4) have in common that they do not change rapidly and likely change little after burial of the paleosol by new loess. This is not always true for properties in group (5). Additionally, thermoluminescence measurements and data on decay of isotopes are useful for dating and identifying transport, weathering, and mixing processes in paleosols. A soil formation model that can reproduce these soil properties is the most useful for paleosol-paleoclimate linkage studies, because the measured paleosol properties can be confronted by simulations for calibration and subsequent accuracy evaluation. Soil organic carbon is not of relevance for confrontations to measurements because of its decay after paleosol formation, but as the presence of soil organic carbon influences the hydraulic properties of soils, and thus leaching, its correct assessment is still

needed. Stable isotopes such as ^{26}Mg (Huang et al., 2013) and cosmogenic nuclides such as ^{10}Be would, if simulated, contribute to model calibration and accuracy assessment as well, but these are seldomly measured in paleosols.

8.2.2. Prediction of Future Soil Development: Key Soil Model Output Variables and Processes

While paleosols comprise the response to climate-related factors, future soil development is strongly under human influence, either intentional or unintentional. We therefore take an anthropocentric approach to define key soil variables for soil modeling. This approach puts the use potential of (future) soils central, by (1) regarding soil as a natural capital, consisting of stocks that can contribute to the performance of soils but at the same time must not be depleted, and (2) regarding soil performance itself via the concept of soil ecosystem services (Dominati et al., 2010).

8.2.2.1. Soil as a natural capital

The soil natural capital consists of inherent stocks that relate to the naturally developed properties that are slow to change, and manageable properties via human land use practices. These stocks change by degradation processes (such as erosion and compaction) and supporting processes (soil formation and managed change in the nutrient and water cycle). Two stocks of importance to land use and that are partly manageable, partly inherited from soil formation, are

a. Soil organic carbon (SOC; Mg/ha)

b. Available nutrients such as expressed by the total reserve of exchangeable bases (TREB; $kmol_+$/ha), which is part of the cation exchange capacity determined by SOC, clay content, and clay mineralogy.

The size of these stocks, combined with that of available soil moisture, directly relates to biomass productivity, and therefore we consider these key soil variables for soil modeling. Relevant processes to be considered are the supporting processes of soil formation as in the paleosols, land use management via tillage and fertilization, and the degradation processes erosion and compaction.

8.2.2.2. Soil as an ecosystem service

Ecosystem services are usually (Dominati et al., 2010) subdivided into cultural services (recreation, heritage conservation), regulating services (flooding mitigation, filtering, C-storage) and provisioning services (mainly biomass production for food, wood, and fiber). Two examples of ecosystem services are

a. Water yield (mm/ha) being the difference of annual precipitation and actual evapotranspiration integrated over the rooted zone over an area.

b. C-sequestration capacity (Mg/ha), being the capacity of the soil to sequester additional C above the amount already present.

Table 8.1 Key processes and model outputs of soil evolution models for paleosol and future soil studies. TREB = total reserve of exchangeable bases, WY = water yield, SOC = soil organic carbon.

Purpose of (Loess) Soil Evolution Model	Relevant Process	Key Soil Model Output Variables
Paleosol studies	Solute flow	Salts (gypsum, calcite)
	particle transport	Clay
	New formation	Clay minerals
		Pedogenic (Fe-) oxides
	Weathering	(Primary) minerals
Future soil studies	Soil formation	(All stocks)
	Element cycles	TREB
	Solute flow	WY
	Water flow	
	C-sequestration	SOC
	Tillage	
	Compaction	Bulk density
	Bioturbation	
	Fertilization	TREB
	Erosion	Texture, SOC

Until now, expert judgments are used to assess soil ecosystem service performance (e.g. Gonzalez-Redin et al., 2016), but it is possible to identify key soil processes that must be part of a soil model to allow for process-based assessments: water flow, solute flow, C-sequestration, and plant-soil element cycles (Vereecken et al., 2016).

Table 8.1 summarizes key soil model output variables that would serve the purpose of paleosol studies and future soil studies.

8.2.3. Model Responsiveness to Factors of Global Change

Process models for paleosol evolution as well as for projections need to be responsive to forcing factors related to global change. In soil science, these factors have long been known as the *factors of soil formation* (climate, organisms, relief, parent material, and time; Jenny, 1941). The factors can easily be translated to boundary inputs for a soil model when their change over time is quantified (e.g. the climate change or the change in land management) or when the initial situation is known (e.g. the parent material properties of loess). Table 8.2 (based on Opolot et al., 2015) summarizes how soil-forming factors relate to boundary inputs for global change-responsive soil models. These forcings influence soil processes that themselves affect soil variables. When running a soil model, the forcings at the model boundary must be quantified in the form of time series (e.g. of temperature, precipitation, vegetation type). Basically, there

Table 8.2 Forcing (or soil forming) factors, associated soil model boundary inputs and processes, and affected soil variables. Factors and processes that respond to global change are indicated in Italics. Based on Opolot et al., 2015.

Factor	Boundary Inputs (forcing)	Process	Affected Soil Variables (depth dependent)
Climate	*Temperature*	*Heat flow*	Temperature regime
	Atmospheric deposition	*Solute flow*	Solute composition
	Precipitation, evaporation	*Water flow*	Moisture regime
Organisms (incl. men)	*(Regulated) vegetation*	*Water flow*	
	(Regulated) biomass production	*C-cycle*	C-status, hydraulic properties
		Nutrient cycles	Solute composition
	Fertilization	*Solute transport*	
	Tree fall, faunal activity	*Bioturbation*	Solid phase composition (texture, C, minerals), hydraulic properties
	Tillage	*Turbation*	
Relief	*Truncation*	*Erosion*	
	Burial	*Deposition*	
	Exposition (local radiation, *precipitation*)	*Water flow*	Moisture regime
Parent material	Initial mineralogy	*Chemical weathering*	Mineralogical composition
	Initial texture	*Physical weathering*	Texture, hydraulic properties
		Particle transport	
	Initial chemical composition	*Chemical Solution/ adsorption/precipitation*	Chemical composition of solution, adsorption complex, precipitates
Time	*Variation in boundary conditions*	*Process dynamics*	Regime dynamics

are three options: (1) defining artificial time series, (2) creating time series via independent proxy-based reconstructions, and (3) deriving the time series by using the output of other models, such as climate and vegetation models. Option (1) has the complication that the definition must include the temporal covariation between forcings, which is not easily realized. Option (2) can be applied onto paleosols if proxy data with sufficient temporal resolution are available. Finke and Hutson (2008) give an example for Holocene loess soils in Europe, where pollen data were used for vegetation reconstruction as well as to modulate temperature and precipitation anomalies over the Holocene. These kinds of reconstructions presumably reproduce covariations between boundary inputs of the soil model, as they are based on the same proxies. Option (3) was followed by Finke et al. (2017) for loess paleosols in China and will be described in a following section. This option is the most suitable for projective soil model studies due to the obvious lack of proxy-based inputs for future studies. Generating boundary inputs by a mechanistic model include covariations between (e.g.) temperature and evaporation because of the (physical) relations between these variables inside this model.

While the above text defines global-change-responsive soil models to some degree in terms of inputs and outputs, little has yet been said on the processes inside these models. Minasny et al. (2015) report on a literature scan of soil models and counted what general soil forming processes are represented in these models, using the process descriptions of Bockheim and Gennadiyev (2000). They concluded that process coverage is still limited (Figure 8.1), although for (nonsaline and nonaquic) loess soils, most soil forming processes are covered by at least some models.

We refer to Vereecken et al. (2016), who discuss recent and foreseen developments in soil models and their components. Although the processes that should be represented are named in Table 8.2, many alternative process descriptions and implementations can be envisaged, and no systematic comparisons are documented for global-change-responsive soil models.

One important aspect for soil model studies covering a large temporal extent is that many soil properties should be considered as variables rather than static parameters. For instance, the relations between pressure head, water content, and hydraulic conductivity (h-θ-K) cannot be considered constant over longer time periods, as these relations are affected by changing SOC, biological processes (bioturbation), particle transport (clay migration), and land management (tillage). The consideration that most soil properties are variables at longer timescales introduces several possible feedbacks in a soil model that would otherwise have been neglected.

8.3. SOILGEN-LOVECLIM: A SUITABLE COMBINATION FOR GLOBAL CHANGE STUDIES IN LOESS SOILS

Above, we formulated what are key input (Table 8.2) and output (Table 8.1) variables of soil models used for global change studies, and we indicated some essential

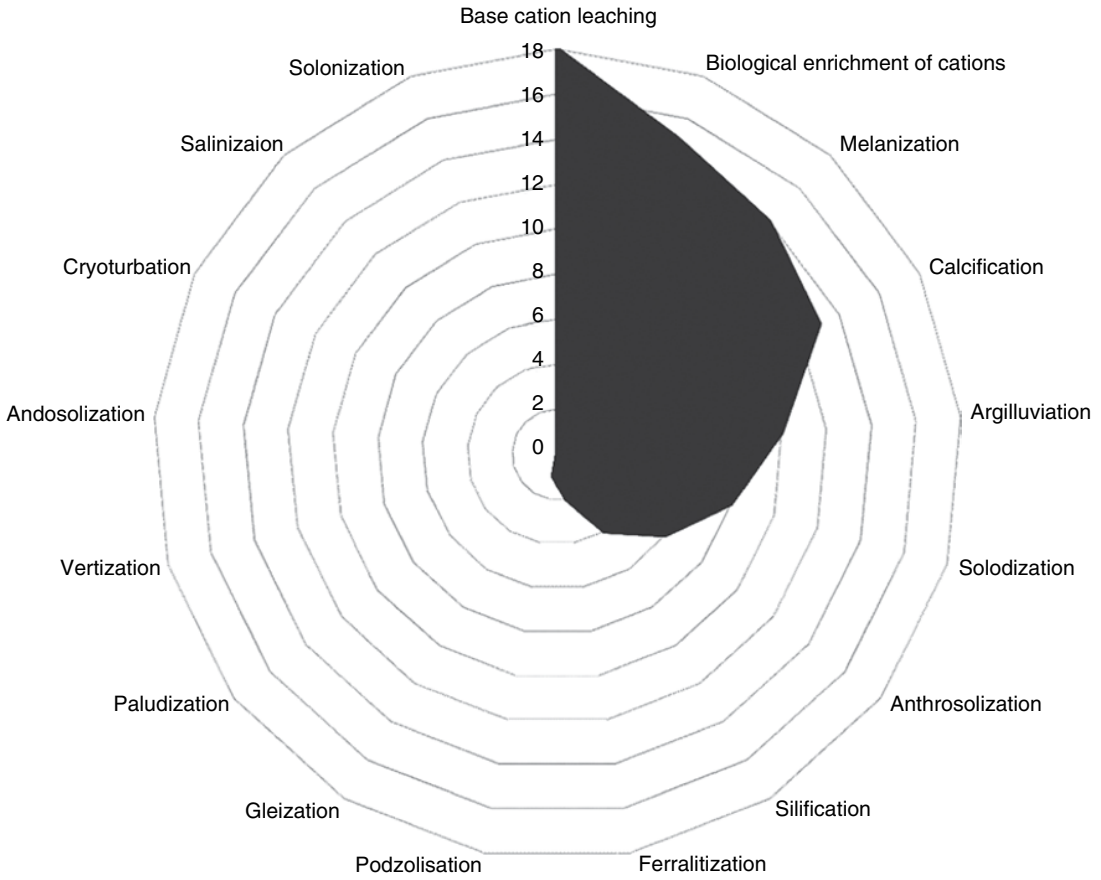

Figure 8.1 Counted coverage of soil-forming processes (terminology of Bockheim & Gennadiyev, 2000) in 19 soil model case studies (updated after Minasny et al., 2015).

processes that should be represented in such models (Table 8.2, Figure 8.1). Also, we concluded that generating boundary time-series inputs for the soil model by a climate-vegetation model will honor covariations between these inputs. Next, we focus on a combination of two models, the Earth system model LOVECLIM and the soil formation model SoilGen, and a study of the CLP to unravel differences in paleosols corresponding to Marine Isotope Stage (MIS) 5e and MIS 13. Below, we will briefly discuss the models, how they are connected to satisfy data needs, and the purpose and results of the case study.

8.3.1. LOVECLIM

LOVECLIM is a three-dimensional Earth system model of intermediate complexity (Goosse et al., 2010). It includes five components of the climate system: atmosphere, ocean-sea ice, land surface-vegetation, ice sheets, and carbon cycle. In the climate simulations of MIS 13 and MIS 5e, modules for atmosphere (ECBilt), ocean-sea ice (CLIO), and the terrestrial biosphere (VECODE) are interactively coupled, whereas ice sheet (AGISM) and carbon cycle (LOCH) modules are switched off. ECBilt is a quasi-geostrophic atmospheric model with three vertical levels and a horizontal resolution of 5.6°x5.6° and 4-hour time steps. CLIO is an ocean general circulation model coupled to a comprehensive thermodynamic-dynamic sea-ice model. It has 20 vertical levels in the ocean and a horizontal resolution of 3°x3° with 1-day timesteps. VECODE is a model of vegetation dynamics computing the evolution of the vegetation cover described as a fractional distribution of desert, tree, and grassland at the same resolution as that of ECBilt and with 1-year time steps. See Figure 8.2 for a graphical representation of spatial and temporal scales.

Numerous climate proxy records show that not only the intensity but also the duration of the interglacials vary in time. LOVECLIM has been used to simulate the climates of all the interglacials of the last 800 ka (Yin & Berger, 2012, 2015). Time-dependent insolation (incoming solar radiation) and greenhouse gases concentration (here including CO_2, CH_4, and N_2O) were used to drive LOVECLIM, as described in Yin and Berger (2015), which uses a 10 times acceleration technique that is not included in this study. Due to the uncertainties in ice sheet reconstruction during the interglacials, especially

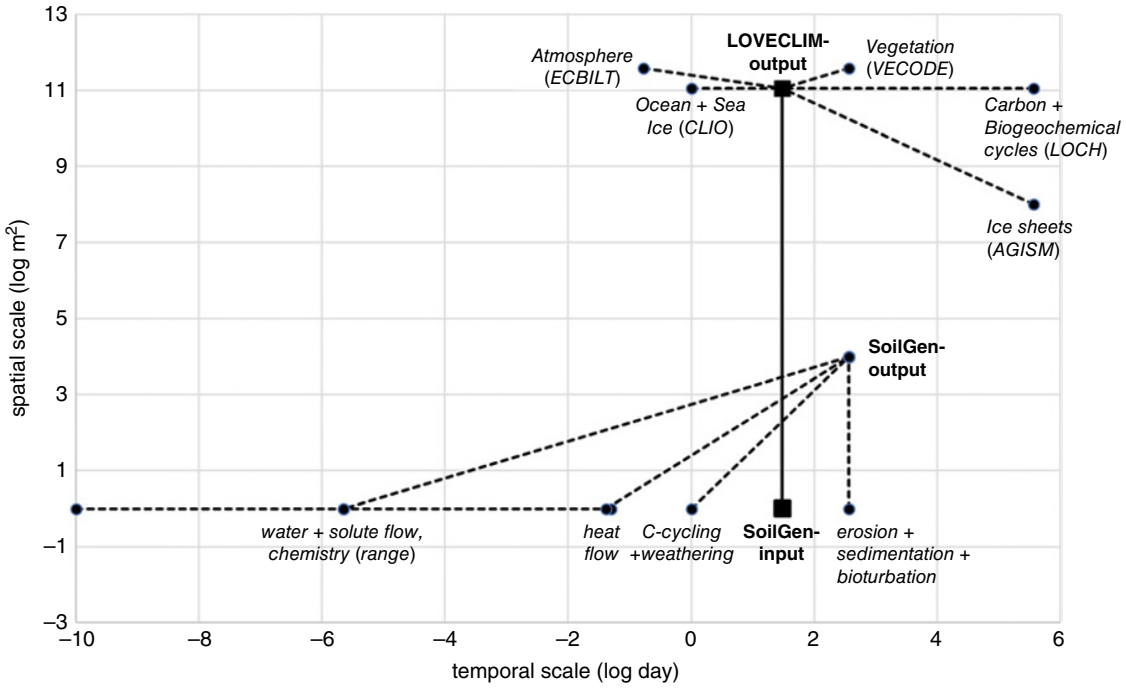

Figure 8.2 Spatial and temporal scales of model components (italic text, dotted lines) and necessary scale transfer between LOVECLIM-output and SoilGen-input (bold text, solid line).

the older one MIS 13, the variation of ice sheets is not considered, and they are fixed to present condition.

Monthly mean temperature, precipitation, and evaporation are produced by LOVECLIM. Like most of the climate models, bias exists in the LOVECLIM simulation in particular when regional features are considered. To reduce the bias, we have corrected the simulated climate fields with the differences between observed and simulated present-day values.

8.3.2. SoilGen

SoilGen (Finke, 2012; Finke & Hutson, 2008) simulates the change in soil properties as a function of initial material properties and external drivers such as climate, vegetation and faunal activity, relief, and deposition or erosion processes. The model operates at a typical spatial scale of 1 m^2, considers periods of millenniums, but takes time steps that vary per process. The smallest time steps occur under extreme hydrological conditions and may be less than a second, the largest time steps are 1 year for slow processes such as bioturbation and erosion/sedimentation events (Figure 8.2). The flow of water, heat, gas, and solutes is simulated by numerical solutions to partial differential equations (Richards' equation, heat flow equation, gas diffusion equation, solute advection/dispersion equation). Hereto soil profiles are discretized in 5-cm compartments. The essential relationship between pressure head, water content, and hydraulic conductivity is dynamically parameterized using a prediction function (Wösten et al., 1999) that is based on the texture, organic matter content, and bulk density. These are dynamically simulated:

- The fate of organic carbon is simulated according to the concepts of the RothC26.3 model (Yu et al., 2013).
- The simulated physical (Finke, 2012) weathering of minerals changes the texture of the soil. Clay migration is simulated (Finke, 2012), as well as the effect of bioturbation on vertical distribution of all soil components (Finke & Hutson, 2008).
- The bulk density varies because of changing mass of the solid components in a soil compartment. The current model version assumes that soil volume in each compartment is constant.

Additionally, chemical (Opolot & Finke, 2015) weathering as well as organic matter decomposition release ions in the soil solution. These ions are distributed over precipitated, solution, and exchange phases using a Gapon exchange mechanism and chemical equilibriums. The model can simulate the effect of human actions such as plowing, cropping schemes, and fertilizing and can also accommodate the removal of top layers by erosion or addition by sedimentation (such as dust addition).

Yearly model outputs are in most cases expressed in mass units per hectare per compartment. After a sensitivity analysis, Keyvanshokouhi et al. (2016) concluded that SoilGen is suitable for the analysis of global change scenarios.

8.3.3. Satisfying Data Needs Across Scales

The data needs of SoilGen follow the boundary inputs specified in Table 8.2.

• The parent material properties (texture, bulk density, calcite and gypsum as minerals reacting sensitive to climate change, 17 additional aluminum- or silicate minerals) of sediment present at the start of the interglacial and of the dust deposited during the interglacial can be derived from the loess above and below the paleosol. In the Supplementary Information of Finke et al., 2017 we list the literature from which these data were taken. In general, for the simulations we took for each site the same composition of parent material and of aeolian dust for both MIS5e and MIS 13 for the aluminum- and silicate minerals. Texture, calcite content and gypsum content however may be different between parent material and dust, according to available data (Table 8.3).

• Dust deposition rhythms over MIS 5e and MIS 13 were derived from Guo et al. (2009) at Xifeng and Changwu and scaled to site-specific dust deposition rates using spatially distributed total dust addition data (Lu & Sun, 2000).

• Other time-variant inputs (temperature, precipitation, evaporation and vegetation) were derived from LOVECLIM after correcting for bias, but this is not a straightforward conversion because the spatial unit sizes ("scale") of LOVECLIM-modules are unequal to those of SoilGen. This is illustrated in Figure 8.2. Consequently, spatial downscaling from the LOVECLIM-cells of 5.6°x5.6° to the SoilGen-cells of 1x1 m^2 was needed to be able to represent the effect of climate gradients inside the CLP. Detailed maps of today's mean annual temperature (Liao, 2007), mean annual precipitation (Hu, 2007) and aridity (Feng et al., 2004) were used for downscaling (Bierkens et al., 2000) using either a difference (temperature) or a ratio (precipitation and evaporation) correction. The vegetation type is calculated as a (yearly) probability distribution for different vegetation types within a LOVECLIM cell and is downscaled to high spatial detail using the aridity map (Feng et al., 2004). We refer to Finke et al., 2017 for details.

8.3.4. Case Study: Comparison of Paleosols from MIS 5e and MIS 13

The combination LOVECLIM-SoilGen was recently (Finke et al., 2017) applied to tackle a paradox between observed paleosols of MIS 5e and MIS 13 and the simulated paleoclimates for these interglacials. Whereas the paleosol from MIS 13 is the strongest developed middle Pleistocene soil in the Eurasian loess belt (Guo et al., 1998; Marković et al., 2009), and the paleosol from MIS 5e is less developed, climate model studies (Karami et al., 2014; Muri et al., 2013; Yin et al., 2009) suggest the opposite in terms of the intensity of the East Asian summer monsoon. The climate models indicate a stronger monsoon over the CLP in MIS 5e, with higher temperatures and precipitation. Since soil formation is additionally controlled by factors like vegetation, dust deposition, and duration of the interglacial, which may have counteracting effects on soil formation (Johnson et al., 1990), soil modeling forced by all these factors was done to find explanations for the above paradox.

The simulation period of each interglacial was determined by using the marine oxygen isotope records (to define the glacial and interglacial stages) and covers at least 22 ka (to include the climate response to a large range of insolation covering a full precession cycle). The transient simulation by LOVECLIM for MIS 13 then covered 30 ka (one and a half precession cycles) from 511 to 481 ka BP, and it covered 22 ka (one precession cycle) from 133 to 111 ka BP for MIS 5e. The same was done by Yin and Berger (2015). The same periods were simulated with SoilGen, using the (downscaled) monthly outputs for precipitation, evaporation, and temperature and the yearly output for vegetation type as input. Parent materials for MIS 5e and MIS 13 were the same for each site. Results (Table 8.4) show that the vertical distributions of some simulated soil properties differed significantly (at 95% two-sided) between MIS 5e and MIS 13, even though the parent materials were equal. A paired *t*-test (at the same depths, over the upper 150 cm of paleosol) of simulated calcite, clay, and anorthite content (in kg m^{-2}) was done for eight loess sections on a climate gradient, whereby each site is represented by the percentage of the CLP that currently has a lower aridity than that site:

• Calcite contents differed, but except for Jingyuan, these differences were not significant.

• Clay content was significantly higher in MIS 5e paleosols for all plots, indicating that more clay was leached in MIS 13 paleosols.

• Anorthite content was significantly higher in MIS 5e paleosols, indicating that more anorthite was weathered in MIS 13 paleosols.

Furthermore, Finke et al. (2017) graphically showed that the field-observed difference in the expression of the paleosols (by depth distributions of clay, calcite, pH, anorthite, and chloride) of MIS 13 and MIS 5e was confirmed by the simulations, and they showed how these expressions evolved over time. Figure 8.3 gives an example for the Weinan site. Clay migration and weathering of the mineral anorthite were much stronger for the MIS 13 paleosol. Also, decalcification and formation of calcic horizons was stronger (deeper) in the MIS 13 soil, chloride concentrations in the soil solution were lower, and soil pH was lower. This led to the conclusion that leaching in MIS 13 was stronger than in MIS 5e,

Table 8.3 Mineralogical composition and texture of parent material and deposited aeolian dust during MIS 5e and MIS 13 used for input to the SoilGen model. Data taken from various sources mentioned in Finke et al., 2017 (Supplementary Information).

Site	Object	Clay	Silt	Sand	Calcite	Gypsum	Albite	K-Feldspar	Muscovite	Quartz	Chlorite	Anorthite	Kaolinite	Montmorillonite	Hornblende
		Mass %													
Wugong	Parent material	23.0	67.0	10.0	10.70	0.13	5.19	3.12	22.84	33.96	12.59	2.23	5.77	2.23	1.23
	Dust	32.0	61.0	7.0	10.70	0.13	5.19	3.12	22.84	33.96	12.59	2.23	5.77	2.23	1.23
Chang'an	Parent material	37.2	62.5	0.3	8.00	0.15	5.35	3.21	23.53	34.99	12.97	2.29	5.94	2.30	1.27
	Dust	27.3	72.5	0.2	8.00	0.15	5.35	3.21	23.53	34.99	12.97	2.29	5.94	2.30	1.27
Weinan	Parent material	27.0	69.0	4.0	16.00	0.15	8.08	4.86	13.28	30.61	1.74	3.46	2.93	17.01	1.85
	Dust	28.0	70.0	2.0	16.00	0.15	8.08	4.86	13.28	30.61	1.74	3.46	2.93	17.01	1.85
Luochuan	Parent material	14.0	74.0	12.0	13.00	0.15	5.30	3.19	23.88	32.42	8.14	2.27	5.76	4.69	1.20
	Dust	17.0	79.0	4.0	13.00	0.15	5.30	3.19	23.88	32.42	8.14	2.27	5.76	4.69	1.20
Changwu	Parent material	13.0	80.0	7.0	9.00	0.15	5.29	3.18	23.28	34.60	12.83	2.27	5.88	2.27	1.25
	Dust	13.0	60.0	27.0	9.00	0.15	5.29	3.18	23.28	34.60	12.83	2.27	5.88	2.27	1.25
Xifeng	Parent material	25.0	53.4	21.6	12.00	0.15	5.12	3.07	22.51	33.46	12.40	2.19	5.68	2.20	1.21
	Dust	25.0	53.4	21.6	12.00	0.15	5.12	3.07	22.51	33.46	12.40	2.19	5.68	2.20	1.21
Pengyang	Parent material	0.5	86.5	13.0	15.00	0.15	4.94	2.97	21.74	32.32	11.98	2.12	5.49	2.12	1.17
	Dust	0.5	86.5	13.0	15.00	0.15	4.94	2.97	21.74	32.32	11.98	2.12	5.49	2.12	1.17
Jingyuan	Parent material	12.0	73.0	15.0	11.00	0.15	5.17	3.11	22.76	33.84	12.55	2.22	5.75	2.22	1.23
	Dust	12.0	73.0	15.0	14.00	0.15	5.00	3.00	21.99	32.70	12.12	2.14	5.55	2.15	1.18

Table 8.4 Results of paired *t*-test on difference between MIS 13 and MIS 5e of means for eight loess sections on the Chinese Loess Plateau (CLP) representing an aridity gradient. H_0: no difference between means. Pairs are equal depth intervals of simulated mass, over the upper 150 cm of paleosol.

Site	Aridity Percentile Over CLP		Calcite Content		Clay Content		Anorthite Content	
			Mean Difference (kg $CaCO_3$ m^{-2})	$P(H_0)$	Mean Difference (kg clay m^{-2})	$P(H_0)$	Mean Difference (kg $CaAl_2Si_2O_8$ m^{-2})	$P(H_0)$
Wugong	Wet→Dry	0.127	−0.716	0.346	−2.139	0.002	−0.462	<0.001
Chang'an		0.185	−0.416	0.586	−1.249	0.080	−0.494	<0.001
Weinan		0.241	0.649	0.419	−1.417	0.013	−0.505	0.004
Luochuan		0.349	−0.066	0.948	−1.226	<0.001	−0.608	<0.001
Changwu		0.430	0.378	0.639	−0.691	0.001	−0.389	<0.001
Xifeng		0.676	0.468	0.474	−1.132	0.001	−0.078	<0.001
Pengyang		0.761	−2.238	0.012	−0.035	0.039	−0.038	<0.001
Jingyuan		0.869	6.193	0.000	−0.413	0.000	−0.452	<0.001

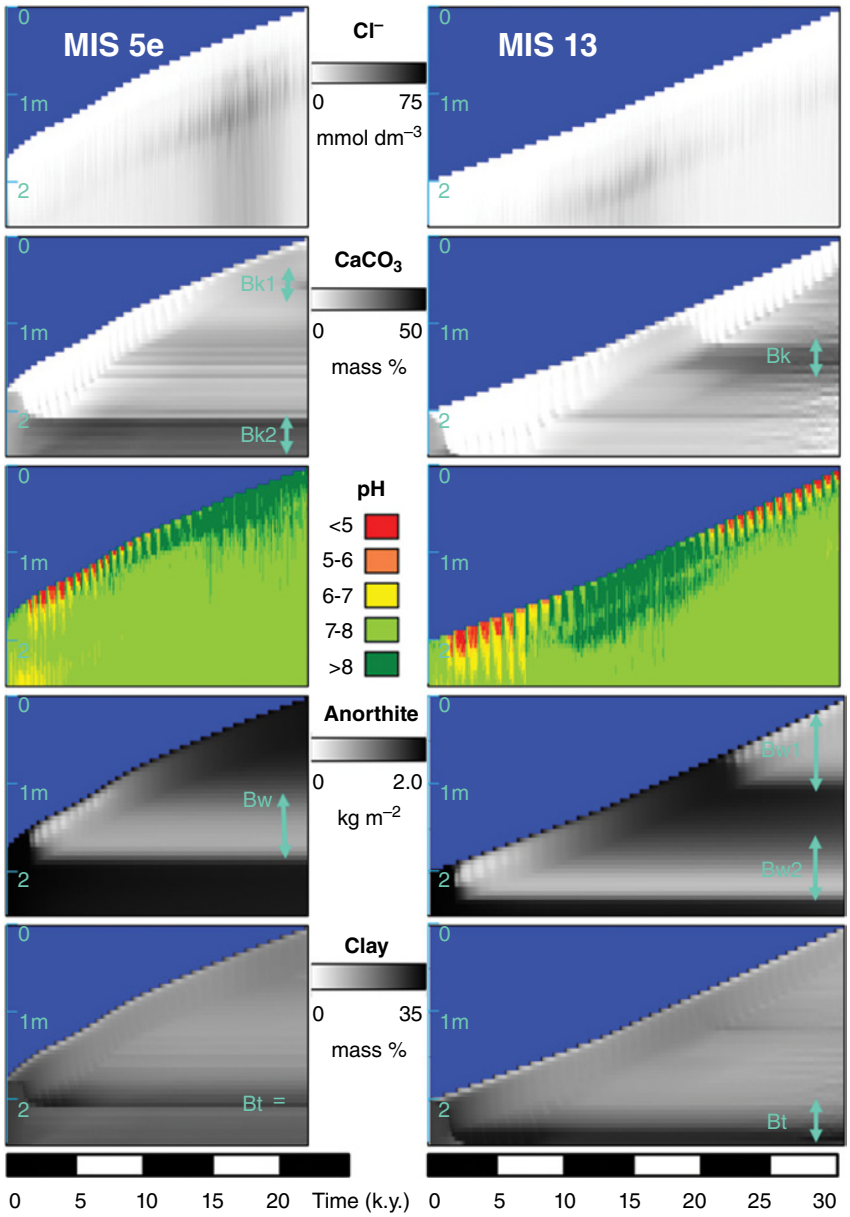

Figure 8.3 Simulated evolution of soil properties over time (abscissa) and depth (ordinate) for MIS 5e (22 ka, left graphs) and MIS 13 (30 ka, right graphs) at Weinan. All graphs are scaled to a maximal soil depth of 2.5 m. Blue = air; gray shade or other colors indicate value of soil properties. From top to bottom: chloride, calcite, pH, anorthite and clay content. Soil horizons are also indicated.

notwithstanding the higher precipitation during MIS 5e. Leaching is a resultant of the precipitation surplus, and the higher temperatures during MIS 5e caused higher evaporation that more than compensated the higher precipitation. A count of the number of months with a precipitation surplus (mostly occurring during the summer monsoon) yielded a systematically higher number of such months, even when for both interglacials only the first (simulated) 22 ka were considered (see Finke et al., 2017, Figure 4 therein).

Thus, the above-mentioned paradox was solved by simulation modeling, which illustrates its additional value. Additionally, it was concluded that the differences between MIS 5e and MIS 13 soils decrease under increasing aridity.

8.3.5. Case Study: Evolution of the Natural Capital and Ecosystem Services During MIS 5e

Soil variables simulated by the LOVECLIM-SoilGen combination can be converted to new variables that describe soil stocks or soil performance. As an example, we calculated two stocks and two ecosystem services using the simulation of MIS 5e at the Luochuan site in the CLP. As mentioned above, soil stocks contribute to the potential performance of soils in relation to land use (including natural vegetations), while ecosystem services describe soil performance itself for a chosen function. Both natural capital and ecosystem services are defined from an anthropocentric perspective, and therefore application of these concepts to MIS 5e is somewhat artificial and is meant for illustration only. Application in a Holocene or Anthropocene context is no doubt more useful but does require a profound understanding and precise reconstruction of the land use history and associated land management, and it also requires model calibration. This is beyond the scope of this study.

The stocks that were calculated (for each simulation year) are the following:

• Soil organic carbon: $SOC\left(Mg/ha\right)=\sum_{c=1}^{6}\left(SOC_c\right)$, where SOC_c = simulated mass of soil organic carbon (Mg/ha) per depth compartment (5 cm), summed over the upper 30 cm. SOC is an important indicator for soil fertility and erodibility.

• Total reserve of exchangeable bases: $\mathrm{TREB}\left(\frac{kmol_+}{ha}\right)=\sum_{c=1}^{6}\left(XCa_c+XMg_c+XK_c+XNa_c\right)\times \rho_c \times 0.5$, where XCa, XMg, XK, and XNa are exchangeable basic cations ($mmol_+$/kg soil) and ρ = bulk density (kg/dm^3), per depth compartment and summed over the upper 30 cm, and 0.5 is for conversion to $kmol_+$/ha. TREB is an indicator of chemical soil fertility.

Two simulated ecosystem services that were calculated for each simulation year are the following:

• C-sequestration capacity: $CSC\ (Mg/ha) = \left(0.5 \times \sum_{c=1}^{6}\left(Csat_c \times \rho_c\right)\right) - SOC$, where *Csat* (g/kg) is the soil organic carbon saturation level, estimated by 4.09 + X * 0.37 (Hassink, 1997), with X = the (simulated) mass fraction of soil particles smaller than 20 μm. ρ = bulk density (kg/dm^3), 0.5 is for conversion to Mg/ha, and *SOC* (*Mg/ha*) is the soil organic carbon content in that year. All these are summarized over the upper 30 cm of soil. CSC quantifies the capacity of the soil to sequester organic carbon.

• Water yield: $WY\left(mm/ha\right)=P-\sum_{t=0}^{365}\sum_{c=1}^{20}Ea_{tc}$, where P is the annual precipitation (mm/ha, output from LOVECLIM corrected for interception evaporation by the vegetation and downscaled to the simulation location) and Ea_{tc} is the actual evapotranspiration (simulated root water uptake plus surface evaporation, mm/ha), which is summed over the rooted compartments (top 100 cm, 5 cm compartments) over the year. Water yield expresses the amount of water produced at a site after correction for water usage by plant uptake, surface evaporation, and interception evaporation. At the level of a catchment, the water yield is the amount of water that leaves the catchment via water streams and subsurface drainage and indicates how much water is available besides for biomass production.

Results of the calculations over MIS 5e are in Figure 8.4. The sawtooth pattern in parts a, b, and d of Figure 8.4 is because dust deposition was modeled as an episodic process, i.e. when cumulative dust addition reached 50 mm, a new soil compartment was added.

Simulated SOC over the top 30 cm (Figure 8.4a) temporarily decreases after a dust input pulse, then stabilizes to a level corresponding to climate and vegetation. The increase between 15,000 and 18,000 after the start of the precession cycle (SPC, equivalent to 133 ka BP) is due to dominance of steppe vegetations in this period (Figure 8.5a) and slower decomposition of soil organic matter due to lower temperature (Figure 8.5b) and soil moisture content.

The simulated ecosystem service CSC (Figure 8.4b) does not show the inverse pattern, as might be expected. The reason for this is that the organic carbon saturation (Csat) level of the 30 cm topsoil decreases because (1) fine material is lost by clay migration, and (2) the bulk density of the topsoil layers decreases for the same reason. These fluctuations of SOC and Csat largely compensate each other.

The simulated ecosystem service water yield (Figure 8.4c) mostly reflects the interannual variability of the precipitation (Figure 8.5c) and can take both positive and negative values. This variability strongly decreased

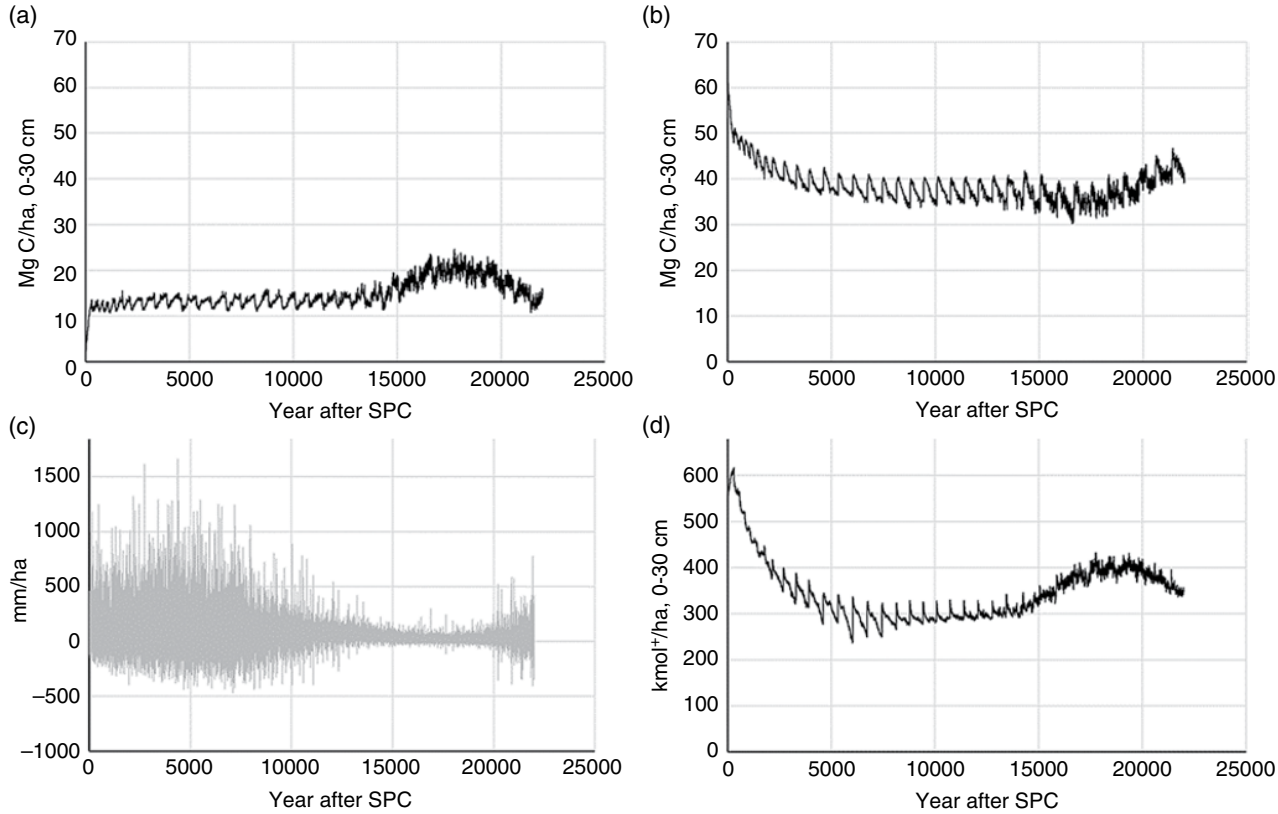

Figure 8.4 Simulated soil natural capital and Ecosystem Services over MIS 5e for Luochuan. SPC = start precession cycle (133 ka BP). (a) Soil organic carbon. (b) C-sequestration capacity. (c) Water yield. (d) Total reserve of exchangeable bases.

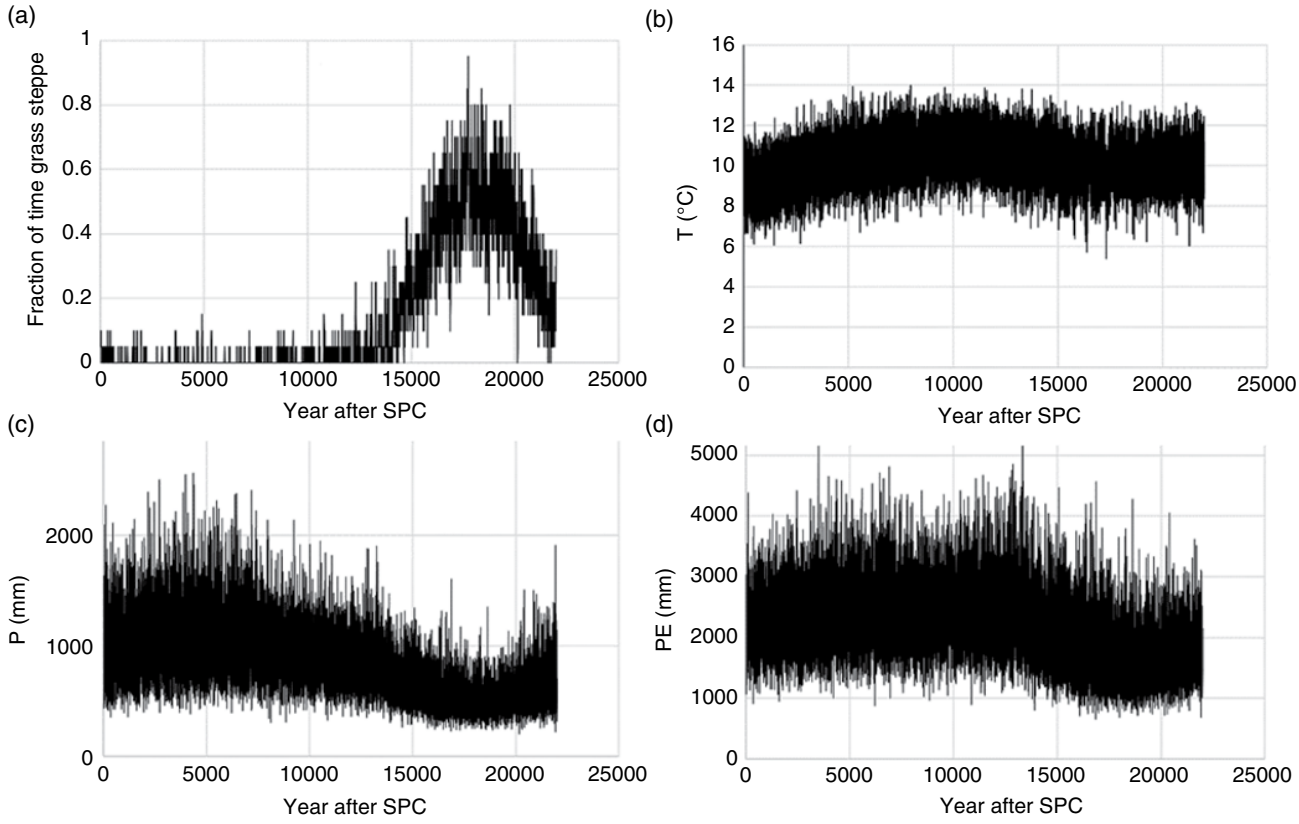

Figure 8.5 Simulated climate and vegetation over MIS 5e by LOVECLIM, downscaled to Luochuan. SPC = start precession cycle (133 ka BP). (a) Fraction of the time with grass steppe vegetation (20-year moving average). (b) Average annual temperature. (c) Annual precipitation. (d) Annual potential evapotranspiration.

12,000 years after SPC, while that of the potential evapotranspiration (Figure 8.5d) remains similar.

The simulated TREB (Figure 8.4d) decreases the first 5,000 years after SPC, which is related to the leaching of basic cations and clay from the topsoil. The increase at 15,000 years after SPC is related to a lower precipitation (less leaching) in combination with ongoing dust deposition bringing in new basic cations and clay.

These calculations show that it is possible to obtain meaningful expressions of stocks representing the soil natural capital, and of ecosystem services that soil can deliver. When applied in a context of future climate and land use, combined climate-vegetation-soil models can provide a powerful alternative to current expert-based assessments.

8.4. ACHIEVEMENTS AND CHALLENGES

The examples for loess soils and sediments from the Chinese Loess Plateau given in this chapter of combined climate-vegetation-soil modeling show the benefits of such an approach:

- It allows a dynamic comparison of climate and soil variables instead of the traditional (and arduous) comparison of climate variables and (static) soil properties. As a consequence, it becomes possible to identify causes for observed soil phenomena.
- It allows future work combining measured soil and proxy data and simulations to constrain, calibrate, and improve simulation results.
- It allows detaching oneself from the traditional expert assessments of future soil behavior under global change.

Several challenges remain:

- Though process coverage of the soil model may be sufficient for loess sediments, this coverage must be extended and tested for other combinations of climate, land use, and parent materials.
- Scale transfer between the soil model and the climate model complicates considering feedbacks between the two. For instance, feedbacks between the C-cycles in the atmospheric compartment and the soil compartment are yet not easily accounted for.
- The disadvantage of using a 1-D soil model is that erosion and sedimentation processes are inputs, and regional mass balances (e.g. of sequestered carbon) are not easily made.

REFERENCES

An, Z. S., Liu, T. S., Lu, Y. C., Porter, S. C., Kukla, G., Wu, X. H., & Hua, Y.M. (1991). The long-term palaeomonsoon variation recorded by the loess-palaeosol sequence in central China. *Quaternary International*, *7–8*, 91–95.

Bader, N. E., Spencer, P. K., Bailey, A. S., Gastineau, K. M., Tinkler, E. R., Pluhar, C. J., & Bjornstad, B. N. (2016). A loess record of pre-Late Wisconsin glacial outburst flooding, Pleistocene paleoenvironment, and Irvingtonian fauna from the Rulo site, southeastern Washington, USA. *Palaeogeography Palaeoclimatology Palaeoecology*, *462*, 57–69. https://doi.org/10.1016/j.palaeo.2016.08.042

Balsam, W. L., Ellwood, B. B., Ji, J., Williams, R. R., Long, X., & Hassani, A. E. (2011). Magnetic susceptibility as a proxy for rainfall: Worldwide data from tropical and temperate climate. *Quaternary Science Reviews*, *30*, 2732–2744.

Bierkens, M.F.P., Finke, P. A., & de Willigen, P. (2000). *Upscaling and downscaling methods for environmental research*. Dordrecht: Kluwer Academic Publishers.

Bockheim, J. G., & Gennadiyev, A. N. (2000). The role of soil-forming processes in the definition of taxa in Soil Taxonomy and the World Soil Reference Base. *Geoderma*, *95*, 53–72.

Bradley, R. S. (2013). *Paleoclimatology: Reconstructing climates of the quaternary*. San Diego: Academic Press.

Dominati, E. J., Patterson, M. G., & Mackay, A. D. (2010). A framework for classifying and quantifying the natural capital and ecosystem services of soils. *Ecological Economics*, *69*, 1858–1868.

Eden, D. M., Qizhong, W., Hunt, J. L., & Whitton, J. S., 1994. Mineralogical and geochemical trends across the Loess Plateau, North China. *Catena*, *21*, 73–90.

Fang, X.-M., Li, J-J., & Van der Voo, R. (1999). Rock magnetic and grain size evidence for intensified Asian atmospheric circulation since 800,000 years B.P. related to Tibetan uplift. *Earth and Planetary Science Letters*, *165*, 129–144.

Feng, Z-D., & Wang, H. B. (2006). Geographic variations in particle size distribution of the last interglacial pedocomplex S1 across the Chinese Loess Plateau: Their chronological and pedogenetic implications. *Catena*, *65*, 315–328.

Feng, Z.-D., Wang, H. B., Olson, C., Pope, G. A., Chen, F. H., Zhang, J. W., & An, C. B. (2004). Chronological discord between the last interglacial paleosol (S1) and its parent material in the Chinese Loess Plateau. *Quaternary International*, *117*, 17–26.

Finke, P. A. (2012). Modeling the genesis of Luvisols as a function of topographic position in loess parent material. *Quaternary International*, *265*, 3–17.

Finke, P. A., & Hutson, J. (2008). Modelling soil genesis in calcareous löss. *Geoderma*, *145*, 462–479. https://dx.doi.org/10.1016/j.geoderma.2008.01.017

Finke, P. A., Yin, Q., Bernardini, N. J., & Yu, Y. Y. (2017). Climate-soil model reveals causes of differences between MIS 5e and MIS 13 paleosols. *Geology*, *46*(2), 99–102. https://doi.org/10.1130/G39301.1

Gonzalez-Redin, J. Luque, S., Poggio, L. Smith, R., & Gimona, A. (2016). Spatial Bayesian belief networks as a planning decision tool for mapping ecosystem services trade-offs on forested landscapes. *Environmental Research*, *144*, 15–26. https://doi.org/10.1016/j.envres.2015.11.009

Goosse, H., Brovkin, V., Fichefet, T., Haarsma, R., Huybrechts, P., Jongma J., et al. (2010). Description of the Earth system model of intermediate complexity LOVECLIM version 1.2. *Geoscientific Model Development*, *3*, 603–633.

Guo, Z. T., Berger, A., Yin, Q. Z., & Qin, L. (2009). Strong asymmetry of hemispheric climates during MIS 13 inferred from correlating China loess and Antarctica ice records. *Climate of the Past*, *5*, 21–31.

Guo, Z. T., Liu, T. S., Fedoroff, N., Wei, L. Y., Ding, Z. L., Wu, N. Q., et al. (1998). Climate extremes in Loess of China coupled with the strength of deep water formation in the North Atlantic. *Global Planet. Change*, *18*(3–4), 113–128. https://doi.org/10.1016/S0921-8181(98)00010-1.

Guo, Z. T., Ruddiman, W. F., Hao, Q. Z., Wu, H. B., Qiao, Y. S., Zhu, R. X., et al. (2002). Onset of Asian desertification by 22 Myr ago inferred from loess deposits in China. *Nature*, *416*, 159–163.

Han, J., Fyfe, W.S., & Longstaffe, F.J. (1998). Climatic implications of the S5 Paleosol complex on the southernmost Chinese Loess Plateau. *Quaternary Research*, *50*, 21–33.

Hassink, J. (1997). The capacity of soils to preserve organic C and N by their association with clay and silt particles. *Plant and Soil*, *191*(1), 77–87. https://doi.org/10.1023/A:1004213929699

Huang, K. J., Teng, F. Z., Elsenouy, A., Li, W. J., & Bao, Z. Y. (2013). Magnesium isotopic variations in loess: Origins and implications. *Earth and Planetary Science Letters*, *374*, 60–70. https://doi.org/10.1016/j.epsl.2013.05.010

Jenny, H. (1941). *Factors of soil formation: A system of quantitative pedology*. New York: Dover.

Jeong, G. Y., Hillier, S., & Kemp, R. A. (2011). Changes in mineralogy of loess–paleosol sections across the Chinese Loess Plateau. *Quaternary Research*, *75*, 245–255.

Johnson, D. L., Keller, E. A., & Rockwells, T. K. (1990). Dynamic pedogenesis: New views on some key soil concepts and a model for interpreting Quaternary soils. *Quaternary Research*, *33*, 306–319. https://doi.org/10.1016/0033-5894(90)90058-S

Karami, M. P., Herold, N., Berger, A., Yin, Q. Z., & Muri H. (2014). State of the tropical Pacific Ocean and its enhanced impact on precipitation over East Asia during Marine Isotopic Stage 13. *Climate Dynamics*. https://doi.org/10.1007/s00382-014-2227-0

Keyvanshokouhi, S., Cornu, S., Samouëlian, A., & Finke, P. (2016). Evaluating SoilGen2 as a tool for projecting soil evolution induced by global change. *Science of the Total Environment*, *571*, 110–123.

Lu, H. & Sun, D. (2000). Pathways of dust input to the Chinese Loess plateau during the last glacial and interglacial periods. *Catena*, *40*, 251–261.

Marković, S. B., Hambach, U., Catto, N., Jovanović, M., Buggle, B., Machalett, B., et al. (2009). The middle and late Pleistocene loess–palaeosol sequences at Batajnica, Vojvodina Serbia. *Quaternary International*, *198*, 255–266. https://doi.org/10.1016/j.quaint.2008.12.004

Minasny, B., Finke, P., Stockmann, U., Vanwalleghem, T., & McBratney, A. (2015). Resolving the integral connection between pedogenesis and landscape evolution. *Earth-Science Reviews*, *150*, 102–120. http://dx.doi.org/10.1016/j.earscirev.2015.07.004

Muri H., Berger A., Yin Q. Z., Karami M., & Barriat P. (2013). The climate of the MIS-13 interglacial according to HadCM3. *Journal of Climate*, *26*, 9696–9712.

Opolot, E., & Finke, P. A. (2015). Evaluating sensitivity of silicate mineral dissolution rates to physical weathering using a soil evolution model (SoilGen2.25). *Biogeosciences*, *12*, 6791–6808.

Opolot, E., Yu, Y. Y., & Finke, P. A. (2015). Modeling soil genesis at pedon and landscape scales: Achievements and problems. *Quaternary International*, *376*, 34–46. http://dx.doi.org/10.1016/j.quaint.2014.02.017

Pye, K. (1995). The nature, origin and accumulation of loess. *Quaternary Science Reviews*, *14*, 653–667. https://doi.org/10.1016/0277-3791(95)00047-x

Rowe, P. J., & Maher, B. A. (2000). 'Cold' stage formation of calcrete nodules in the Chinese Loess Plateau: Evidence from U-series dating and stable isotope analysis. *Palaeogeography Palaeoclimatology Palaeoecology*, *157*(1–2), 109–125. https://doi.org/10.1016/S0031-0182(99)00157-1

Rutter, N. Zhongli, D., Evans, M. E., & Yuchun, W. (1990). Magnetostratigraphy of the Baoji loess-paleosol section in the north-central China Loess Plateau. *Quaternary International*, *7–8*, 97–102.

Schaetzl, R. K., Bettis III, E. A., Crouvic, O., Fitzsimmons, K. E., Grimleye, D. A., Hambach, U. (2018). Approaches and challenges to the study of loess: Introduction to the LoessFest special issue. *Quaternary Research*, *89*, 563–618. https://doi.org/10.1017/qua.2018.15.

Schellenberger, A, & Veit, H. (2006). Pedostratigraphy and pedological and geochemical characterization of Las Carreras loess-paleosol sequence, Valle de Tafi, NW-Argentina. *Quaternary Science Reviews*, *25*(7–8), 811–831. https://doi.org/10.1016/j.quascirev.2005.07.011

Shi P., Yang, T., Xu, A., & Tian, Q. (2010). Magnetic susceptibility variations and influence factors at Jingyuan loess section, northwestern China. *Marine Geology & Quaternary Geology*, *30*(4), 193–200 (in Chinese, with English abstract).

Sun, Y., Chen, J., Clemens, S. C., Liu, Q., Ji, J., & Tada, R. (2006). East Asian monsoon variability over the last seven glacial cycles recorded by a loess sequence from the northwestern Chinese Loess Plateau. *Geochemistry, Geophysics, Geosystems*, *7*, Q12Q02. https://doi.org/10.1029/2006GC001287

Vereecken, H., Schnepf, A., Hopmans, J. W., Javaux, M., Or, D., & Roose T., et al. (2016). Modeling soil processes: Review, key challenges, and new perspectives. *Vadose Zone Journal*, *15*(5). http://dx.doi.org/10.2136/vzj2015.09.0131

Wösten, J.H.M., Lilly, A., Nemes, A. & Le Bas, C. (1999). Development and use of a database of hydraulic properties of European soils. *Geoderma*, *90*, 169–185.

Yin Q. Z., & Berger, A. (2012). Individual contribution of insolation and CO2 to the interglacial climates of the past 800,000 years. *Climate Dynamics*, *38*, 709–724. http://doi.org/10.1007/s00382-011-1013-5

Yin, Q. Z., & Berger, A. (2015). Interglacial analogues of the Holocene and its natural near future. *Quaternary Science Reviews*, *120*, 28–46.

Yin, Q. Z., Berger, A., & Crucifix, M. (2009). Individual and combined effects of ice sheets and precession on MIS-13 climate. *Climate of the Past*, *5*, 229–243.

Yu, Y. Y., Finke, P. A, Guo, Z. T, & Wu, H. B. (2013). Sensitivity analysis and calibration of a soil carbon model (SoilGen2) in two contrasting loess forest soils. *Geoscientific Model Development*, *6*, 29–44.

Zheng, H., Theng, B.K.G., & Whitton, J. S. (1994). Mineral composition of loess-paleosol in the Loess Plateau of China and its environmental implications. *Geochimica*, *23*, 113–123 [in Chinese, with English abstract].

9

Relations Between Soil Development and Landslides

Arnaud J.A.M. Temme

ABSTRACT

Soils and landslides are intimately related, particularly for shallow landslides that occur in soil or weathered bedrock. Although landslides can occur in practically all soil types, maps of soil types and soil properties are often and successfully used as copredictors in statistically based landslide susceptibility modeling. This chapter explores which soil properties affect the landsliding process and how and where such properties develop. Higher soil clay percentage generally increases landslide susceptibility, whereas higher bulk density and soil organic matter content negatively affect susceptibility. The other way around, landslides dramatically and suddenly affect soils. Stoniness and organic matter percentage are most strongly affected, by means of mixing of the landslide deposit. Smeared, low-permeability clay layers are created along the sliding surface and can continue to form under appropriate hydrological conditions. In some cases, these low-shear strength layers increase the likelihood of continuation or recurrence of landsliding activity. The mutual effects create soil-landslide feedbacks, which can be positive or negative. Negative feedbacks exist, for instance, where landslides completely evacuate thin soils from a slope and where recurrence of landslides requires renewed weathering of bedrock. Positive feedbacks exist especially where landslides locally change soil properties such that sliding becomes more likely, such as through the creation of thin, weakly permeable clay layers. Positive feedbacks have been shown to be quantifiable at the regional scale. Knowledge of the history of landsliding and its impact on soil development can substantially improve performance of susceptibility mapping efforts.

9.1. INTRODUCTION

Soil development and landslides are an odd pair: soil development is typically slow, requiring centuries for substantial progress, whereas landslides are usually fast, happening in minutes or hours. Nonetheless, both are closely related. On one hand, landslides are more likely to happen when and where soils are susceptible. On the other hand, soils are obviously affected, or even erased and newly formed, by landsliding. This chapter covers the various relations between soil development and landslides, with a focus on shallow landslides, which are most strongly related to soils. The chapter takes a systems perspective, discussing different kinds of relations between soil development and landslides in the following sections, from large scales to small scales (Figure 9.1). First, we will discuss the properties that make soils susceptible to landsliding, and the soil development that leads to these properties, at the catchment and regional scale levels. At the scale of individual landslides, we will discuss the impacts that landslides have on soils. Finally, we will discuss the intimate soil-landslide relations that give rise to landslide path-dependency at catchment scales: the notion that landslides are partly determined by local landslide history.

Department of Geography and Geospatial Sciences, Kansas State University, Manhattan, Kansas, USA

Hydrogeology, Chemical Weathering, and Soil Formation, Geophysical Monograph 257, First Edition.
Edited by Allen Hunt, Markus Egli, and Boris Faybishenko.

DOI: 10.1002/9781119563952.ch9

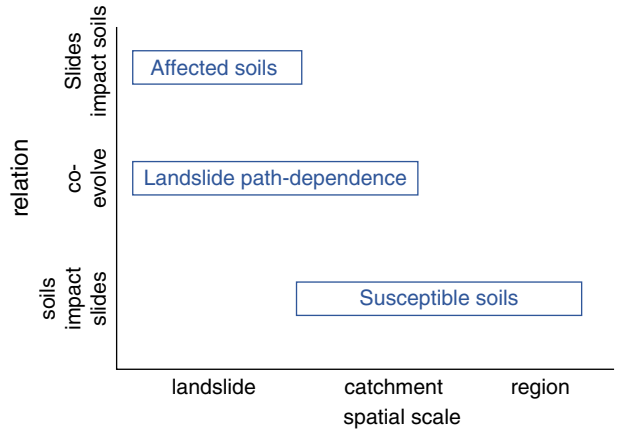

Figure 9.1 Topics covered in this chapter with the range of spatial scales, and the range of soil-landslide relations.

9.2. HOW SOILS INCREASE SUSCEPTIBILITY TO LANDSLIDES

Detached objects fall off a slope when the gravitational force acting on the material exceeds the frictional force holding the material in place. Shallow landslides, where the sliding material is initially attached to the slope as soil or weathered bedrock (regolith), happen when gravitational shear stresses exceed the shear strength of the slope material. The question thus becomes which properties of soils affect shear strength and shear stress.

Soil plays a role in determining both the size of the gravitational stress and the magnitude of the shear strength. A crucial soil property is its ability to increase the magnitude of the gravitational force by taking up water and releasing it slowly. A soil's clay content is central to this ability. Soils with clay (including loam, silt loam, clay loam, and clay textures) can contain up to 40% water by volume (e.g. Wösten et al., 1999). About half of this water is almost permanently bound to the soil. The other half can vary and thus increase or decrease the gravitational force. This means that, assuming bulk density of the dry soil of 1600 kg/m3, clayey soils can increase their mass and their gravitational stress by about 15% upon wetting (e.g. Birle et al., 2008). The corresponding number for sand is only about 7%.

Shear strength also varies with soil properties, and clay again plays an important role. The Mohr-Coulomb equation states that soil shear strength τ (Nm^{-2}) is determined by soil cohesion c (Nm^{-2}) and the angle of shear resistance (also called internal friction) Φ (°):

$$\tau = c + \sigma \tan \phi,$$

where σ is the applied normal stress (Nm^{-2}). This equation is valid for situations where pore fluid pressures that occur during soil shearing can be ignored, and it states that shear strength has a static component; the soil cohesion, as well as a component that increases with stress as a function of shear resistance.

Soil cohesion is the resistance of particles within soil to displacement, and in the context of bodies of soil on hillslopes, is larger in soils with dry clay and roots that hold the soil together. It is also increased through cementation, for instance with clay or iron- and aluminum oxides and hydroxides. The angle of shear resistance is a positive function of soil bulk density and a negative function of soil moisture (Zhang et al., 2001). Wetting of soil substantially decreases its cohesion and internal friction angle and thus soil shear strength (Yalcin, 2007), so that clayey soils that get wetter experience both increased gravitational stress and reduced shear strength. Soil organic matter, when it has the effect of strengthening soil aggregates, increases shear strength (e.g. Ekwue, 1990).

Permeability in clayey soils often decreases with depth, and bulk density typically increases with depth, which can lead to a clear transition from wet, low-shear strength soil to dry, strong layers below (Simon et al., 1990; van Breemen & Buurman, 2003). This transition can be at the Bt horizon for clayey soils that have experienced clay translocation, or at the boundary to more massive, less structured C- or R horizons in some other soils (Duzgoren-Aydin & Aydin, 2006; Gerke & Hierold, 2012; Kitutu et al., 2009; Knapen et al., 2006). In this way, soil development can influence the position of the sliding surface of landslides over long timescales (Iverson, 2000). Over shorter timescales, a strong increase of landsliding has been observed during recent warm summers in melting permafrost soils (Lewkowicz & Way, 2019). In these cases, the frozen subsoil serves as the sliding surface. The melting ice in the topsoil was already present in the soil and hence does not increase gravitational stress but decreases shear strength.

9.3. SOIL DEVELOPMENT

Ultimately, all soils and soil types are potentially vulnerable to landslides, and globally, the regions where soils are susceptible to landsliding are not determined only by soil properties. The steepness of slopes, the state of vegetation, and the geology of a region are usually more important than soil properties, especially for deep-seated landslides. Therefore, global landslide susceptibility models and maps do not always take soil properties into account: Y. Hong and Adler (2007) included soil type and soil texture as predictors, whereas the global landslide susceptibility mapping approach of Stanley and Kirschbaum (2017) includes slope steepness, the presence of faults, geology, and the presence of road networks, but not soil properties. At spatial scales less than a continent, landslide susceptibility models more commonly include

soil-related properties (Reichenbach et al., 2018). Version 2 of the European landslide susceptibility map (Wilde et al., 2018), for instance, included a lithological dataset from the International Hydrogeological Map of Europe as predictor, and version 1 (Günther et al., 2014) included a soil parent material dataset as predictor. The landslide susceptibility map of Africa (Broeckx et al., 2018) includes eight lithological classes that relate to soil parent material. The 1982 compilation of landslide susceptibility for the United States (Radbruch-Hall et al., 1982) was created by expert judgment based on a geological map, but the 2011 United States prototype landslide hazard map defined susceptible zones using merely geomorphometric variables (Godt et al., 2011).

For smaller countries and regions within them, more detailed landslide inventories and more detailed soil maps are available. The soil maps at these scales often provide more detail than geological maps by including the effect of other soil-forming factors such as relief and (micro-) climate (Wielemaker et al., 2001). Hence, soil types and properties are common predictors in modern susceptibility mapping studies at these scales (e.g. Broeckx et al., 2019; Chawla et al., 2019; H. Hong et al., 2019; Kaur et al., 2019; Moayedi et al., 2019; Mondal & Mandal, 2019; Nsengiyumva et al., 2019).

Many empirical findings confirm that prelandslide soil development can make soils more susceptible to landsliding. For instance, Kitutu et al. (2009) found that soil texture, particularly the depth profile of clay content, determined the likelihood of landsliding in a region in Uganda. Soils developing by in situ weathering of basaltic rock into a state susceptible to landsliding in Cameroon were found to increase the content of 2:1 clay minerals (low-shear strength smectites) and 1:1 clay minerals (e.g. kaolinite), and to develop textural heterogeneity along the profile due to redistribution of minerals (Che et al., 2012). Azañón et al. (2010) similarly found that smectite layers within Flysch deposits in Spain increased susceptibility to landslides, and Duzgoren-Aydin and Aydin (2006) highlighted the importance of the development of thin, weakly permeable low-shear strength zones in soil profiles developed on felsic igneous rocks. Parry et al. (2000) linked millimeter-thickness layers of kaolinite clays in saprolite from mixed rhyolitic and granitic rocks in Hong Kong to the occurrence of local landslides. Finally, Shuzui (2001) confirmed that smectites are present along slip surfaces of recurring landslides, and crucially that these continue to form after initial sliding due to favorable groundwater chemistry and the tuffaceous lithology in his study area in Japan.

Slopes that face in different directions can experience different rates of weathering due to different precipitation and evaporation rates (e.g. Deepthy & Balakrishnan, 2005; Rech et al., 2001). This effect can create differences between wet, weathered, clay-rich soils that are susceptible to landsliding, and dry, unweathered, coarse soils that are less susceptible. Different rates and processes of landsliding between differently exposed slopes are indeed commonly found, e.g. by Beaty (1956) in California, by Churchill (1982) in South Dakota, and by Aniya (1985) in Japan. The differential soil weathering on different slope aspects due to microclimatic differences is one of the reasons for the widespread use and success of slope aspect in statistical landslide susceptibility models, although the microclimatic differences themselves are also a reason. Similar reasoning explains the success of slope curvature in susceptibility models (e.g. Claessens et al., 2007): on convex slopes that steepen downslope, infiltration and gravity act differently than on concave slopes that flatten downslope.

Postvolcanic landscapes such as on Hawaii illustrate the impact of landscape-scale variation in soil development on landslides in another way. After fluvial incision of V-shaped valleys and the corresponding creation of steep slopes, chemical weathering and soil development on the volcanic rock produces deep and clayey soil that subsequently becomes susceptible for landsliding. The slope retreat due to landsliding exposes new bedrock that is weathered and itself becomes susceptible to sliding (Scott & Street, 1976). This long-term process is controlled by the speed of weathering and soil development and leads to the formation of wide, U-shaped valleys over Ma-timescales.

One particular landslide-related soil development deserves extra attention: the formation of quick clay. Quick clays are formed when rainwater leaches original Na-dominated marine pore water out of unconsolidated glaciomarine clay deposits. Such deposits are mainly found in areas that experienced deposition of fine marine sediment when they were isostatically depressed during the last glaciation. These marine deposits were exposed to the air and to rain after they were isostatically uplifted when the ice receded about 15 ka ago. As a result, they are mainly found in regions close to former icecaps, including in Alaska, East Canada, Scandinavia, and Russia.

Quick clay is susceptible to landsliding because it experiences a 30-fold or greater loss in shear strength when remolded, for instance through seismic activity (He et al., 2014). This loss in shear strength and the release of pore water associated with the collapse of the sensitive unconsolidated clay structure can lead to very large retrogressive landslides, where initial sliding undermines slopes that subsequently slide (L'Heureux, 2011). Quick-clay landslides have famously caused very large losses. The most damaging historical slide occurred in 1893 near Verdal in Norway. It involved about 60 million m^3 of soil material, killed 116 people, and destroyed 105 farms (Solberg et al., 2012). In 1971, a quick-clay (locally called

Leda clay) slide in Saint-Jean-Vianney in Canada killed 31 people (Tavenas et al., 1971) and led to the abandonment of nearby Lemieux after it, too, was found to be situated on quick-clay deposits. A landslide in quick clay indeed occurred in Lemieux, in 1993 (Evans & Brooks, 1994).

9.4. HOW LANDSLIDES AFFECT SOIL DEVELOPMENT

In turn, landslides strongly and immediately affect soil properties. To discuss these changes, it is useful to distinguish between the unaffected (prelandslide or nearby) soils, the soils developing in the depletion zones that experienced landslide erosion, and the disturbed, transported soils in landslide accumulation zones.

Studying a chronosequence of soils developing at the transition between depletion and accumulation zones of landslides of different age on Mount Elgon in Uganda, and making a comparison with nearby unaffected soils, Van Eynde et al. (2017) established that the process of landsliding increased stoniness and decreased organic carbon content of soils. Both effects are consistent with mixing of surface and subsurface horizons during landsliding, as well as with a loss of well-developed, organic-rich soils to the accumulation zone. Soil organic carbon content reached prelandslide levels about six decades after landslide events. Studying a 20-year chronosequence of soils developing on landslides in Ecuador, Wilcke et al. (2003) found that landslides removed organic O-horizons and that these horizons did not re-establish within 20 years. Lower soil organic carbon contents in the landslide depletion zone were also observed by Błońska et al. (2018) who studied soil patterns in a landslide in Poland. They also found larger spatial diversity of soil physical, chemical, and biological properties in the depletion and accumulation zones.

Mirus et al. (2017) compared unaffected, forest-covered clayey soils developed in glacial deposits in Washington State to soils on a nearby slope where a landslide had disturbed vegetation and moved soil but not evacuated it from the slope. The slide-affected soils were found to have less root reinforcement, less developed soil structure, and fewer macropores. Correspondingly, matrix porosity and hydraulic conductivity were lower as well, and the transported soils saturated earlier and retained positive pore pressures longer than unaffected soils. As a result of these findings, it was argued that landslide-caused, dominantly hydraulic soil changes had raised the susceptibility for remobilization of the transported soils, despite the reduction in slope steepness due to sliding (Mirus et al., 2017). In terms of the effect on future landslide susceptibility, Mirus' observations confirmed computer simulations by Basile et al. (2003), who evaluated the impact of a pedological discontinuity created by a 1998 landslide in Italy on soil water storage. This storage was increased by more than 30% relative to the same soil without the discontinuity.

9.5. SOIL-LANDSLIDE FEEDBACKS AND LANDSLIDE PATH-DEPENDENCE

The impact of landslides on soil development, and the effect that soil properties have on landslide susceptibility, make up a soil-landslide system with a feedback loop (Figure 9.2). Depending on the impact of landsliding on soil properties and the role of soil properties in determining susceptibility, the feedback can be positive or negative. The best-known example of a negative feedback loop involves geomorphology, not soils, and involves the lowering of slopes by landsliding, leading to less susceptibility for future slides. The lower susceptibility would persist until slopes steepen again, for instance through fluvial incision. An example of a negative feedback loop involving soils is the complete removal of thin soils by landsliding, and the resulting local lowering of susceptibility for future landslides until weathering has produced new soil. This feedback loop seems to fit environments

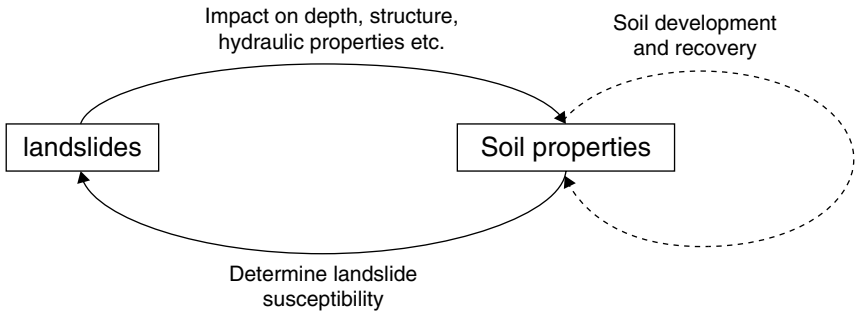

Figure 9.2 Soil-landslide feedback loop.

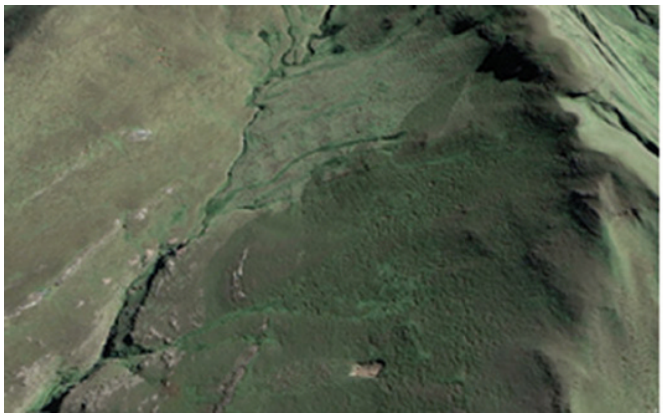


Figure 9.3 Left: landslides in the basaltic rocks of the South African Drakensberg (29.4064 S – 29.504 E). Right: two landslides in marls near Perugia, Italy. (Courtesy of Arnaud Temme.)

with thin soils over steep, resistant bedrock such as in the South African Drakensberg (Singh et al., 2008) (Figure 9.3).

An example of a positive feedback loop would be the formation of a weakly permeable soil layer along a sliding surface and the resulting increase in likelihood of water saturation and thus landsliding over such a layer (e.g. Duzgoren-Aydin & Aydin, 2006; Parry et al., 2000), until and unless the sliding surface is removed, for instance by roots burrowing through it. This feedback loop seems to fit environments with soils that have experienced clay illuviation and frequent shallow landsliding (Figure 9.3).

Samia et al. (2017a, 2017b) studied the soil-landslide feedback loop using a 17-time slice multitemporal landslide inventory for the Collazone study area near Perugia in Italy. Landslides in the region are generally shallow and do not evacuate slid material from slopes. The inventory spanned the period 1939–2014. From visual inspection of landslide polygons, the area seemed to feature an unusual amount of overlapping landsliding, more than would be expected if landslides occurred randomly (Samia et al., 2017b). Slides overlapping earlier slides were found to be significantly larger and rounder than other slides. GIS analysis further indicated that polygons overlapped more if they were from time slices that are temporally closer to each other (Samia et al., 2017a). In later work using Ripley's (1976) K-factor to quantify the unknown landslide-on-landslide effect, Samia et al. (2019) determined that landslides increased the likelihood for further landslides over spatial scales of about 60 m, and over temporal scales of about 17 years. The maximum increase in likelihood was 40%, at very short space and time scales. Although no mechanism for the landslide-on-landslide effect was established, preliminary field observations point to the creation of thin, weakly permeable clay layers by first landslides that would impact wetness of soils in the accumulation zone, and which in turn would lead to increased susceptibility for sliding (Figure 9.4). The impact of such thin layers had already been established, e.g. by Shuzui (2001).

Accounting for the landslide-on-landslide feedback led to substantial improvements in a landslide susceptibility model for the study area. Values for the area under curve (AUC) of the Receiver Operator Characteristic (Swets, 1988) improved from 0.70 for a traditional logistic regression-based susceptibility model with 14 geomorphometric explanatory variables, to 0.76 for a model that additionally included two variables reflecting the local landslide history. A third model that used only the two variables reflecting local landslide history had an AUC of 0.72 (Samia et al., 2018). These findings establish that landslide-on-landslide effects are substantial in the Collazone study area and presumably in others where landslides create smooth, weakly permeable sliding surfaces and do not evacuate slid material from slopes. The findings may lead to a different approach to susceptibility mapping, where landslide susceptibility maps change over time as the impacts of recent landslides weaken and background levels of susceptibility return (Figure 9.5).

9.6. CONCLUSIONS

Over time, soils can develop properties that are associated with increased landslide susceptibility, even though topography and climate differences are often the main drivers of landsliding patterns. The weathering of bedrock into clay and the subsequent translocation of clays into subsurface horizons are the main causes of increases in the risk of landsliding. This has been clearly documented in case studies and is reflected in finer-resolution landslide susceptibility maps and models. The development of quick clays is an extreme example of hydrology-driven soil development leading to increased risk.

Figure 9.4 Left: looking vertically down at a landslide scarp in the Collazone study area, Italy, showing how the slid material in the top of the image has smoothed underlying, uneroded material into a thin clayey layer. Landsliding here happened in different phases over a few days, and as a result the earliest exposed smooth layer to the right has already cracked when drying out in the air. The most recently exposed smooth layer left of the hammer is still smooth, as unexposed layers probably are as well. Right: Zoomed in to the recently exposed smooth layer, showing smooth, parallel clay minerals. (Courtesy of Arnaud Temme.)

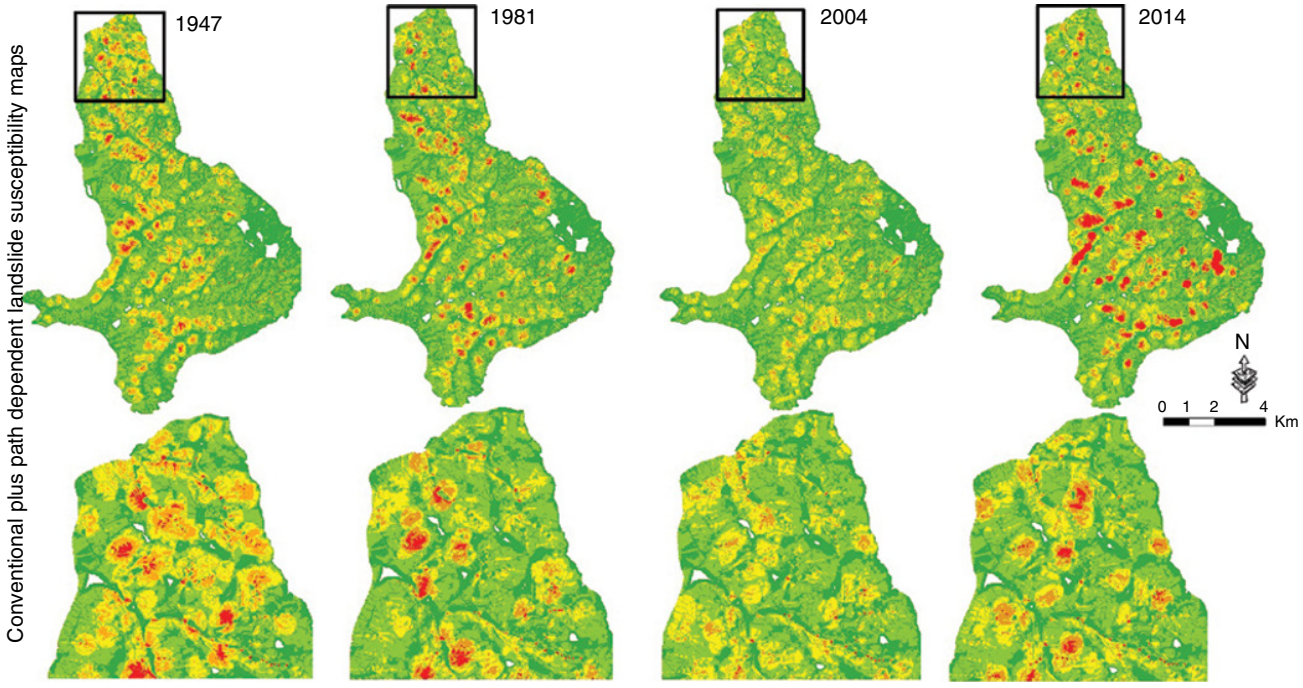

Figure 9.5 An example of landslide susceptibility maps for the Collazone region. The susceptibility for landsliding is a function of static geomorphometric variables and two dynamic variables that reflect the local landslide history. Over time, susceptibility in each location can increase from, and decrease to, a background level as landslides happen and their effects on local soils disappear. Image adapted from Samia et al. (2019).

Landslides greatly affect soils as well, and not only through their complete removal. In many cases where landslides are not evacuated from the hillslope, both the landslide deposit and its contact with the underlying soils are changed. Decreased porosity, decreased structure, and increased rate of saturation have been described for the landslide deposit, and decreased permeability has been described for the contact with the underlying soil. Individually and together, these landslide impacts lead to increased susceptibility for subsequent slides.

Given their mutual effects, soils and landslides form a system with feedbacks. Where soils are completely evacuated from a subsequently soil-less slope, these feedbacks are negative. Where soils are affected as described in the previous paragraph, and increase susceptibility for future slides, these feedbacks are positive. Understanding these positive feedbacks particularly, appears to hold promise for improved landslide susceptibility maps and models.

REFERENCES

Aniya, M. (1985). Landslide-susceptibility mapping in the Amahata River Basin, Japan. *Ann. Assoc. Am. Geogr.*, *75*, 102–114. https://doi.org/10.1111/j.1467-8306.1985.tb00061.x

Azañón, J. M., Azor, A., Yesares, J., Tsige, M., Mateos, R. M., Nieto, F., et al. (2010). Regional-scale high-plasticity clay-bearing formation as controlling factor on landslides in Southeast Spain. *Geomorphology*, *120*, 26–37. https://doi.org/10.1016/J.GEOMORPH.2009.09.012

Basile, A., Mele, G., &Terribile, F. (2003). Soil hydraulic behaviour of a selected benchmark soil involved in the landslide of Sarno 1998. *Geoderma*, *117*, 331–346. https://doi.org/10.1016/S0016-7061(03)00132-0

Beaty, C.H. (1956). Landslides and slope exposure. *J. Geol.*, *64*, 70–74.

Birle, E., Heyer, D., & Vogt, N. (2008). Influence of the initial water content and dry density on the soil–water retention curve and the shrinkage behavior of a compacted clay. *Acta Geotech.*, *3*, 191–200. https://doi.org/10.1007/s11440-008-0059-y

Błońska, E., Lasota, J., Piaszczyk, W., Wiecheć, M., & Klamerus-Iwan, A. (2018). The effect of landslide on soil organic carbon stock and biochemical properties of soil. *J. Soils Sediments*, *18*, 2727–2737. https://doi.org/10.1007/s11368-017-1775-4

Broeckx, J., Maertens, M., Isabirye, M., Vanmaercke, M., Namazzi, B., Deckers, J., et al. (2019). Landslide susceptibility and mobilization rates in the Mount Elgon region, Uganda. *Landslides*, *16*, 571–584. https://doi.org/10.1007/s10346-018-1085-y

Broeckx, J., Vanmaercke, M., Duchateau, R., & Poesen, J. (2018). A data-based landslide susceptibility map of Africa. *Earth-Science Rev.*, *185*, 102–121. https://doi.org/10.1016/J.EARSCIREV.2018.05.002

Chawla, A., Pasupuleti, S., Chawla, S., Rao, A.C.S., Sarkar, K., & Dwivedi, R. (2019). Landslide susceptibility zonation mapping: A case study from Darjeeling District, eastern Himalayas, India. *J. Indian Soc. Remote Sens.*, *47*, 497–511. https://doi.org/10.1007/s12524-018-0916-6

Che, V. B., Fontijn, K., Ernst, G.G.J., Kervyn, M., Elburg, M., Van Ranst, E., & Suh, C. E. (2012). Evaluating the degree of weathering in landslide-prone soils in the humid tropics: The case of Limbe, SW Cameroon. *Geoderma*, *170*, 378–389. https://doi.org/10.1016/J.GEODERMA.2011.10.013

Churchill, R. R. (1982). Aspect-induced differences in hillslope processes. *Earth Surf. Process. Landforms*, *7*, 171–182. https://doi.org/10.1002/esp.3290070209

Claessens, L., Knapen, A., Kitutu, M. G., Poesen, J., & Deckers, J. A. (2007). Modelling landslide hazard, soil redistribution and sediment yield of landslides on the Ugandan footslopes of Mount Elgon. *Geomorphology*, *90*, 23–35.

Deepthy, R., & Balakrishnan, S. (2005). Climatic control on clay mineral formation: Evidence from weathering profiles developed on either side of the Western Ghats. *J. Earth Syst. Sci.*, *114*, 545–556. https://doi.org/10.1007/BF02702030

Duzgoren-Aydin, N. S., & Aydin, A. (2006). Chemical and mineralogical heterogeneities of weathered igneous profiles: Implications for landslide investigations. *Nat. Hazards Earth Syst. Sci.*, *6*, 315–322. https://doi.org/10.5194/nhess-6-315-2006

Ekwue, E. I. (1990). Organic-matter effects on soil strength properties. *Soil Tillage Res.*, *16*, 289–297. https://doi.org/10.1016/0167-1987(90)90102-J

Evans, S. G., & Brooks, G. R. (1994). An earthflow in sensitive Champlain Sea sediments at Lemieux, Ontario, June 20, 1993, and its impact on the South Nation River. *Can. Geotech. J.*, *31*, 384–394. https://doi.org/10.1139/t94-046

Gerke, H. H., & Hierold, W. (2012). Vertical bulk density distribution in C-horizons from marley till as indicator for erosion history in a hummocky post-glacial soil landscape. *Soil Tillage Res.*, *125*, 116–122. https://doi.org/10.1016/j.still.2012.06.005

Godt, J. W., Coe, J. A., Baum, R. L., Highland, L. M., Keaton, J. R., & Roth, R. J. (2011). Prototype landslide hazard maps of the conterminous United States. *Proceedings of the 11th International/2nd North American Symposium on Landslides*, p. 6.

Günther, A., Van Den Eeckhaut, M., Malet, J.-P., Reichenbach, P., & Hervás, J. (2014). Climate-physiographically differentiated Pan-European landslide susceptibility assessment using spatial multi-criteria evaluation and transnational landslide information. *Geomorphology*, *224*, 69–85. https://doi.org/10.1016/J.GEOMORPH.2014.07.011

He, P., Ohtsubo, M., Abe, H., Higashi, T., & Kanayama, M. (2014). Quick clay development and cation composition of pore water in marine sediments from the Ariake Bay Area, Japan. *Int. J. Geosci.*, *05*, 595–606. https://doi.org/10.4236/ijg.2014.56054

Hong, H., Shahabi, H., Shirzadi, A., Chen, W., Chapi, K., Ahmad, B. B., et al. (2019). Landslide susceptibility assessment at the Wuning area, China: A comparison between multi-criteria decision making, bivariate statistical and machine learning methods. *Nat. Hazards*, *96*, 173–212. https://doi.org/10.1007/s11069-018-3536-0

Hong, Y., & Adler, R. F. (2007). Towards an early-warning system for global landslides triggered by rainfall and

earthquake. *Int. J. Remote Sens.*, *28*, 3713–3719. https://doi.org/10.1080/01431160701311242

Iverson, R. M. (2000). Landslide triggering by rain infiltration. *Water Resour. Res.*, *36*, 1897–1910. https://doi.org/10.1029/2000WR900090

Kaur, H., Gupta, S., Parkash, S., Thapa, R., Gupta, A., & Khanal, G. C. (2019). Evaluation of landslide susceptibility in a hill city of Sikkim Himalaya with the perspective of hybrid modelling techniques. *Ann. GIS*, *25*, 113–132. https://doi.org/10.1080/19475683.2019.1575906

Kitutu, M. G., Muwanga, A., Poesen, J., & Deckers, J. A. (2009). Influence of soil properties on landslide occurrences in Bududa district, Eastern Uganda. *African Journal of Agricultural Research*, *4*, 611–620.

Knapen, A., Kitutu, M. G., Poesen, J., Breugelmans, W., Deckers, J., & Muwanga, A. (2006). Landslides in a densely populated county at the footslopes of Mount Elgon (Uganda): Characteristics and causal factors. *Geomorphology*, *73*, 149–165. https://doi.org/10.1016/j.geomorph.2005.07.004

Lewkowicz, A. G., & Way, R. G. (2019). Extremes of summer climate trigger thousands of thermokarst landslides in a High Arctic environment. *Nat. Commun.*, *10*, 1329. https://doi.org/10.1038/s41467-019-09314-7

L'Heureux, J. S. (2011). A study of the retrogressive behaviour and mobility of Norwegian quick clay landslides. *Proceedings of the 11th International/2nd North American Symposium on Landslides*. Banff, p. 8.

Mirus, B. B., Smith, J. B., & Baum, R. L. (2017). Hydrologic impacts of landslide disturbances: Implications for remobilization and hazard persistence. *Water Resour. Res.*, *53*, 8250–8265. https://doi.org/10.1002/2017WR020842

Moayedi, H., Mehrabi, M., Mosallanezhad, M., Rashid, A.S.A., & Pradhan, B. (2019). Modification of landslide susceptibility mapping using optimized PSO-ANN technique. *Eng. Comput.*, *35*, 967–984. https://doi.org/10.1007/s00366-018-0644-0

Mondal, S., & Mandal, S. (2019). Landslide susceptibility mapping of Darjeeling Himalaya, India using index of entropy (IOE) model. *Appl. Geomatics*, *11*, 129–146. https://doi.org/10.1007/s12518-018-0248-9

Nsengiyumva, J. B., Luo, G., Amanambu, A. C., Mind'je, R., Habiyaremye, G., Karamage, F., et al. (2019). Comparing probabilistic and statistical methods in landslide susceptibility modeling in Rwanda/Centre-Eastern Africa. *Sci. Total Environ.*, *659*, 1457–1472. https://doi.org/10.1016/j.scitotenv.2018.12.248

Parry, S., Campbell, S.D.G., & Churchman, G. J. (2000). Kaolin-rich zones in Hong Kong saprolites: Their interpretation and engineering significance. *ISRM* International Symposium, 19–24 November, Melbourne, Australia.

Radbruch-Hall, D.H., Colton, R. B., Davies, W. E., Lucchitta, I., Skipp, B. A., & Varnes, D. J. (1982). Landslide overview map of the conterminous United States. Washington, DC: U.S. Govt. Printing Office.

Rech, J. A., Reeves, R. W., & Hendricks, D. M. (2001). The influence of slope aspect on soil weathering processes in the Springerville volcanic field, Arizona. *Catena*, *43*, 49–62. https://doi.org/10.1016/S0341-8162(00)00118-1

Reichenbach, P., Rossi, M., Malamud, B. D., Mihir, M., & Guzzetti, F. (2018). A review of statistically-based landslide susceptibility models. *Earth-Science Rev.*, *180*, 60–91. https://doi.org/10.1016/J.EARSCIREV.2018.03.001

Ripley, B. D. (1976). The second-order analysis of stationary point processes. *J. Appl. Probab.*, *13*, 255–266. https://doi.org/10.2307/3212829

Samia, J., Temme, A., Bregt, A., Wallinga, J., Guzzetti, F., & Ardizzone, F. (2019). Dynamic path dependent landslide susceptibility modelling. *Nat. Hazards Earth Syst. Sci. Discuss.* *1*–20. https://doi.org/10.5194/nhess-2019-125

Samia, J., Temme, A., Bregt, A., Wallinga, J., Guzzetti, F., Ardizzone, F., & Rossi, M. (2017a). Characterization and quantification of path dependency in landslide susceptibility. *Geomorphology*, *292*, 16–24. https://doi.org/10.1016/j.geomorph.2017.04.039

Samia, J., Temme, A., Bregt, A., Wallinga, J., Guzzetti, F., Ardizzone, F., & Rossi, M. (2017b). Do landslides follow landslides? Insights in path dependency from a multi-temporal landslide inventory. *Landslides*, *14*. https://doi.org/10.1007/s10346-016-0739-x

Samia, J., Temme, A., Bregt, A., Wallinga, J., Stuiver, J., Guzzetti, F., et al. (2018). Implementing landslide path dependency in landslide susceptibility modelling. *Landslides*, *15*, 2129–2144. https://doi.org/10.1007/s10346-018-1024-y

Scott, G., & Street, J. (1976). The role of chemical weathering in the formation of Hawaiian amphitheatre-headed valleys.

Shuzui, H. (2001. Process of slip-surface development and formation of slip-surface clay in landslides in Tertiary volcanic rocks, Japan. *Eng. Geol.*, *61*, 199–220. https://doi.org/10.1016/S0013-7952(01)00025-4

Simon, A., Larsen, M. C., & Hupp, C. R. (1990). The role of soil processes in determining mechanisms of slope failure and hillslope development in a humid-tropical forest eastern Puerto Rico. *Geomorphology*, *3*, 263–286. https://doi.org/10.1016/0169-555X(90)90007-D

Singh, R. G., Botha, G. A., Richards, N. P., & McCarthy, T. S. (20080. Holocene landslides in KwaZulu-Natal, South Africa. *South African J. Geol.*, *111*, 39–52. https://doi.org/10.2113/gssajg.111.1.39

Solberg, I.-L., Hansen, L., Rønning, J. S., Haugen, E. D., Dalsegg, E., & Tønnesen, J. F. (2012). Combined geophysical and geotechnical approach to ground investigations and hazard zonation of a quick clay area, mid Norway. *Bull. Eng. Geol. Environ.*, *71*, 119–133. https://doi.org/10.1007/s10064-011-0363-x

Stanley, T., & Kirschbaum, D. B. (2017). A heuristic approach to global landslide susceptibility mapping. *Nat. Hazards*, *87*, 145–164. https://doi.org/10.1007/s11069-017-2757-y

Swets, J. A. (1988). Measuring the accuracy of diagnostic systems. *Science*, *240*(4857), 1285–1293.

Tavenas, F., Chagnon, J.-Y., & La Rochelle, P. (1971). The Saint-Jean-Vianney landslide: Observations and eyewitnesses accounts. *Can. Geotech. J.*, *8*, 463–478. https://doi.org/10.1139/t71-048

van Breemen, N., & Buurman, P. (2003). *Soil formation*. Springer Netherlands.

Van Eynde, E., Dondeyne, S., Isabirye, M., Deckers, J., & Poesen, J. (2017). Impact of landslides on soil characteristics:

Implications for estimating their age. *Catena*, *157*, 173–179. https://doi.org/10.1016/J.CATENA.2017.05.003

Wielemaker, W. G., de Bruin, S., Epema, G. F., & Veldkamp, A. (2001). Significance and application of the multi-hierarchical landsystem in soil mapping. *Catena*, *43*, 15–34.

Wilcke, W., Valladarez, H., Stoyan, R., Yasin, S., Valarezo, C., & Zech, W. (2003). Soil properties on a chronosequence of landslides in montane rain forest, Ecuador. *Catena*, *53*, 79–95. https://doi.org/10.1016/S0341-8162(02)00196-0

Wilde, M., Günther, A., Reichenbach, P., Malet, J.-P., & Hervás, J. (2018). Pan-European landslide susceptibility mapping: ELSUS Version 2. *J. Maps*, *14*, 97–104. https://doi.org/10.1080/17445647.2018.1432511

Wösten, J.H.M., Lilly, A., Nemes, A., & Le Bas, C. (1999). Development and use of a database of hydraulic properties of European soils. *Geoderma*, *90*, 169–185.

Yalcin, A. (2007). The effects of clay on landslides: A case study. *Appl. Clay Sci.*, *38*, 77–85. https://doi.org/10.1016/J.CLAY.2007.01.007

Zhang, B., Zhao, Q., Horn, R., & Baumgartl, T. (2001). Shear strength of surface soil as affected by soil bulk density and soil water content. *Soil Tillage Res.*, *59*, 97–106. https://doi.org/10.1016/S0167-1987(01)00163-5

10A

Soils in Agricultural Engineering: Effect of Land-Use Management Systems on Mechanical Soil Processes

Rainer F. Horn

ABSTRACT

Soil is the most critical life-supporting component of the biosphere. It provides numerous ecosystem services such as habitat for biodiversity, source of water and nutrients, and media for producing food, feed, fiber, and energy. However, soil is prone to intense and irreversible changes when subjected to some non-site-adjusted land management and improper use of machinery and farming techniques. With the world population increasing, there is an urgent need for a more reliable dataset of soil properties and functions. Credible datasets are needed to develop reliable models for diverse uses. The mechanical strength defines the actual in situ soil rigidity boundary. It distinguishes between the recompression stress and the virgin compression stress range, where plastic deformation including irreversible changes of properties and functions occurs. However, each stress applied to the soil by wheel traffic and trampling is transmitted three-dimensionally, and it causes irreversible soil deformation if the precompression stress is exceeded. The deformation processes during stress application are more pronounced with the increase in the shear component of the total stress and may even result in a complete liquefaction if soil water cannot be drained off adequately. The ratio of the actual soil strength and the transmitted stresses at various depths due to the three-dimensional stress transmission defines the soil resilience. Values >1.2 classify soils and soil horizons as completely resilient, while those <0.8 are indicative of the nonresilient conditions. Changes in the hydraulic or pneumatic functions primarily occur in the nonresilient range. It is equivalent to the virgin compression stress range and is linked to numerous processes via an alteration in accessibility and availability of pore or particle surfaces. Predominant among processes affected by this range include intense changes of redox reactions and the biological activity (respiration) in soils that also affect the carbon sequestration potential and the global carbon cycle. Thus, there exists a strong need for a more precise definition and understanding of site-specific functionality differences, which may exclude or concentrate on certain land use or management to optimize agronomic yield, soil protection, and a sustainable land use management under the conditions of simultaneous occurrence of a limited site-specific resilience.

10A.1. INTRODUCTION

Properties of agricultural and forestry soils, substrate for horticulture and landscape, are the basis not only for producing food, filtering, and buffering of clean potable water and sufficient groundwater recharge but are also the basis of raw material, biological diversity, and archive of human and planetary history. Depending on mechanical, hydrological, and physico-chemical properties, soil can be a source or sink for atmospheric carbon dioxide and other greenhouse gases. This process of soil carbon dynamics is described in chapter 10B. The objective of chapter 10A is to deliberate the effects of land-use and management on engineering properties and mechanical processes. However, soil as a three-phase system has only a finite resilience, and exceeding these boundary conditions can lead to soil degradation, which can be mostly irreversible.

Institute for Plant Nutrition and Soil Science, Christian Albrechts University, Kiel, Germany

Hydrogeology, Chemical Weathering, and Soil Formation, Geophysical Monograph 257, First Edition.
Edited by Allen Hunt, Markus Egli, and Boris Faybishenko.

DOI: 10.1002/9781119563952.ch10a

The European Soil Framework Directive (2006) stated that soil compaction, along with erosion by water and wind, is one of the main physical processes with severe threats of soil degradation. It is estimated that 32% of the subsoils in Europe are highly degraded and 18% are moderately vulnerable to compaction. The main reasons for such intense increase in compacted agricultural or forested soils are the ever-increasing weight of the machines and the increased frequency of wheeling under unfavorable soil conditions (Riggert et al., 2016). Shear- and vibration-induced soil deformation enhances the degradation of soil properties, especially if the soil water content is high and the internal soil strength low. The same is true for animal trampling in combination with overgrazing of moist to wet pastures, which subsequently causes denser (i.e. reduced proportion of coarse pores with smaller continuity) but still structured soil horizons and will eventually lead to a compacted platy structure. Combination of a high water content and shearing by trampling leads to complete muddy homogeneous (puddled) soil with no structure (Krümmelbein et al., 2013).

Soil compaction and especially subsoil compaction is one of the ten major threats of soil degradation globally (Bridges & Oldeman, 1999). The reduction of pore space and especially of macropores, along with the conversion of three-dimensionally uniform pore systems to completely horizontal anisotropic conditions in platy structured soil horizons by compaction, has severe consequences for hydraulic, gas, and heat transport processes as well as for nutrient storage and uptake by plants, all of which results in compaction. Soil compaction is also responsible for accelerated erosion by water. Wind-induced mass transport is enhanced due to a more intense drying of the topsoil and the inhibited capillary rise from the subsoil to the topsoil.

Soil compaction commonly refers to an increase in soil mass per unit volume. However, such a definition does not permit direct prediction of any changes in physical, chemical, or biological properties and functions. For example, if a shear-induced rearrangement of particles occurs during wheeling, trampling, or tillage, even a less dense configuration of soil particles per volume can weaken soil structure, decrease pore continuity, and reduce gaseous exchange, among other outcomes (Horn, 1976; Kühner, 1997; Mordhorst et al., 2014). How far these connectivity and tortuosity effects can be quantified are still debatable. Ghanbarian et al. (2013) developed a model to quantify the water fluxes within soil samples which show mechanically induced changes of pore continuity or tortuosity. Changes in soil strength by compaction and shearing can be detected in the deeper subsoil if the stress distribution exceeds the internal soil strength, and it will lead to a further change of pore functions until a new equilibrium is reached. Thus, the most severe and mostly permanent degradation of soil functions occurs due to deformation in subsoil horizons with no chance of natural soil loosening or of maintaining soil functionality, i.e. below the plow pan. These soil compartments are the major problems, because pore functions are not renewable for decades to centuries. Keller et al. (2019) reported that yield of wheat has stagnated in northern Europe since 1990, despite the fact that many yield-supporting factors (i.e. fertilizer, seed quality, increased CO_2 concentration of the atmosphere, higher temperature) should theoretically all enhance crop growth. However, depth of root penetration is retarded and restricted to the topsoil, leading to increased risks of drought. Thus, a separation between the intensely rooted but dry topsoil from the moist subsoil due to the highly compacted plow pan layer results in a shallow physiological soil functionality.

The most likely reason for such growth alterations is the increased average mass of the agricultural machines during the last four decades, which has reached more than 40 Mg. Such a high mass, in combination with the higher frequency of wheeling, leads to a deeper propagation of stress beyond the plow depth (Duttmann et al., 2014; Hartge & Horn, 2016; Horn, 2015; Horn et al., 2017). However, this problem is not just confined to cropland or forest land but is also prevalent in rangelands and grassland. Thus, it is important to analyze static (i.e. divergent component = compaction) and shearing processes, because both components affect not only the total pore volume and its functions but also the connectivity, pore continuity, and soil strength, as well as an altered resilience with respect to the consequences of soil deformation for functions and site properties. (Hartge & Horn, 2016; Horn et al., 2019; Keller et al., 2019). Soil as a three-phase system is highly susceptible to such soil deformation because of the combined effects of limited mechanical rigidity and the stress and shear-induced mobilization of particles or aggregates, of gas and pore water. Inhibited drainage of excess soil water during the stress and shear application can exacerbate degradation because of anaerobiosis. Occurrence of positive pore water pressure can lead to kneading (i.e. puddling) during shearing, and these processes may either aggravate compaction and/or lead to liquefaction. The latter coincides with a complete loss of mechanical and also hydraulic soil strength and a complete disturbance of all functions, including the physicochemical processes and biological composition. These processes can be easily documented if, e.g. wheeling or plowing is done under unfavorable soil conditions. Zhai and Horn (2018, 2019) documented a severe change in gaseous and water fluxes during static and even more pronounced cyclic (i.e. partly shearing) loading, including the formation of positive pore water pressure. Further, pure static and cyclic loading effects at a given stress level can lead to different changes in soil

properties and functions. The effect of stress-induced alterations of pore water pressure also underlines the importance of pore connectivity for strength and stress transmission effects, because it may either result in a complete deterioration of former soil properties and functions. In addition, a weakening or incompressible soil water may cause a kind of aquaplaning in the soil. Thus, wheeling throughout the growing season but also during harvesting or tillage operations, as well as animal grazing and trampling, alter numerous physical or physicochemical properties as soon as the actual stresses applied to the soil exceed the internal soil strength. It is, therefore, necessary to quantify the rigidity of soils (its strength) by the precompression stress. Thus, a site-specific adequate machinery and moisture dependent work plan needs to be developed to sustain soil properties (Berisso et al., 2012; Hartge & Horn, 2016; Holthusen et al., 2018; Horn, 1985; Horn et al., 2014, 2019; Keller et al., 2007, 2013, 2019; Krümmelbein, 2007; Richards & Peth, 2006).

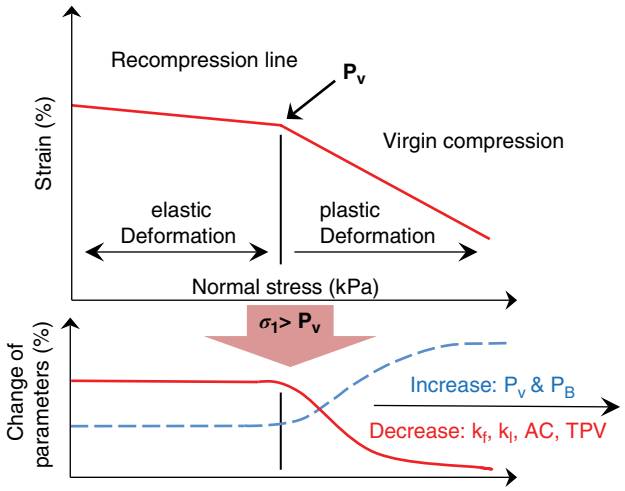

Figure 10A.1 Mechanical processes in soils. Consequences of stress strain and the definition of the precompression stress Pv, as well as changes in soil properties with increasing stress.

10A.2. MECHANICAL PROCESSES IN SOILS

The question as to whether a mechanical (static or dynamic) stress leads to additional soil deformation and also to degradation can be answered using the mechanical strength of the individual horizons in conjunction with the respective load-dependent pressure propagation.

Before discussing the consequences of stress strain and shear processes in more detail, as well as factors influencing compaction, one needs to differentiate between several terms used to define compressive properties. These definitions have been taken from Fredlund and Rahardjo (1993), Hartge and Horn (2016), Parry (2004) and McCarthy (2007).

10A.2.1. Mechanical Stresses

Horn and Peth (2011) defined stress as force per unit area within a solid body. Stress can be induced by external or internal forces on a body that, if the body is nonrigid, leads to a change in its volume and/or shape expressed as deformations or strains. The mechanical behavior of a soil can, therefore, be characterized by its stress-strain relationships. Strength typically refers to the maximum amount of stress a solid material can withstand before it fails. Thus, exceeding soil strength results in failure or yield. It is well known that all soils are preloaded either by hydraulic, chemical, biological, or mechanical processes in the past, while gravity would result in normal or virgin compacted soils (Hartge & Horn, 2016). The consequences of stress application are strain processes primarily in the virgin compression load range with plastic deformation, while soils, which had been prestressed in the past by natural, biological, geological, or anthropogenic processes to a certain extent, are rigid and show primarily elastic deformation within the formerly applied stresses (Figure 10A.1).

Thus, stresses in the recompression stress range do not lead to further changes in soil functions but exhibit a dominant elastic behavior which results in permanent structure-dependent soil functions (with a reversible deformation) if the actually applied stresses do not exceed the precompression stress value. The precompression stress can, therefore, be defined as the process memory of the soil, which can be quantified by physical values. Stresses higher than the precompression stress value result in a further plastic (irreversible) deformation (Horn, 1981; Horn et al., 1995; Horn & Peth, 2011). The latter is caused in the virgin compaction range, e.g. by higher bulk densities or reduced permeability. The precompression stress values differ within a soil profile and are sensitive enough also to quantify the consequences of aggregate formation, actual water status (Horn, 1981, Horn & Dexter, 1989), soil management (Lebert, 1989; Riggert, 2015; Semmel, 1993; Wiermann, 1998; Zink, 2009; among others), geological origin (Horn, 1985), climate (Krümmelbein, 2007), or biology (Kühner, 1997).

In general, soils or soil horizons are the more stable under the following conditions:

- the coarser and the rougher the texture with the same bulk density,
- the stronger the aggregation with comparable texture (e.g. single-grain < coherent < prismatic < polyhedral < subangular blocky),
- the more intense the precompression (e.g. plow pan horizons [App] with platy structure),

• the higher the organic matter content or the higher the fraction of unsaturated fatty acids and lipids with a comparable content of organic matter (refer to chapter 10B),
• the more wetting inhibited the grain contact points at the same matrix potential,
• the drier, i.e. the more negative the matric potential or the pore water pressure,
• the higher the remaining hydraulic conductivity and therefore the faster the expelled soil water can be drained away,
• the higher the valence of the exchangeable ions (monovalent < divalent < trivalent),
• the higher the salt concentration in the soil solution,
• the lower the swelling capacity of the clay minerals.

As a very important but mostly ignored property affects the pore water the strength changes during stress strain processes. Within the recompression stress range, initial negative pore water pressure (i.e. matric or water potential) can either remain constant or it can result in a more intense drying due to the process of water redistribution in newly formed finer pores from originally air-filled macropores. However, soil structure collapses within the virgin compression range due to stress application, and the pore water pressure changes to either more negative if initially still air-filled pores were available, or to even positive values in case of a 2- phase system (water/solid) including a feedback mechanism between stress and strain. Most relevant at this stage are hydraulic flux processes, which are required to drain off the excess soil water (Figure 10A.2). However, the absolute changes in pore water pressure depend on aggregate type and the applied stress. Based on in situ measurements and corresponding analyses of changes in pore water pressure in structured unsaturated soils during loading, it became obvious that the stronger the aggregation the less pronounced are the pore water pressure changes, and the latter can be detected only at higher applied stresses (Nissen, 1999)

10A.2.2. Time-Dependent Strain Processes

Each stress application, especially in the virgin compression stress range, results in time-dependent changes of the strains (i.e. in the solid, liquid, gaseous phase). Three consecutive processes can be distinguished in the time-strain settlement process. The first settlement fraction is defined as immediate settlement and comprises at most the soil volume that is filled with air. Because the gas conductivity in soils is high, the strains transmitted through the gaseous phase can dissipate immediately and result in a corresponding volume decrease. In contrast, the strains that are transmitted through the liquid phase, depending on the hydraulic conductivity and the building-up of hydraulic gradients, can be expressed as pore water pressures and can, therefore, be measured over a longer period. Because of this, the soil-stabilizing water menisci forces are now transformed into destabilizing convex meniscus forms (Hartge & Horn, 2016). In this phase, the soil matrix loses its inherent strength, and the effective strain is largely relieved. Strains can also reduce the diameter of the pores through stress induced strain of air-filled pores, and therefore contribute to a redistribution of water in the pores. A further decrease in the negative pore water pressure (= matric potential) can be measured during this process (Figure 10A.2). The finer pores are filled again due to settlement only when the load-dependent inherent strength has been reached, and water saturation or even positive pore water pressure is finally reached. Under sustained stress (e.g. in conjunction with soil mechanical

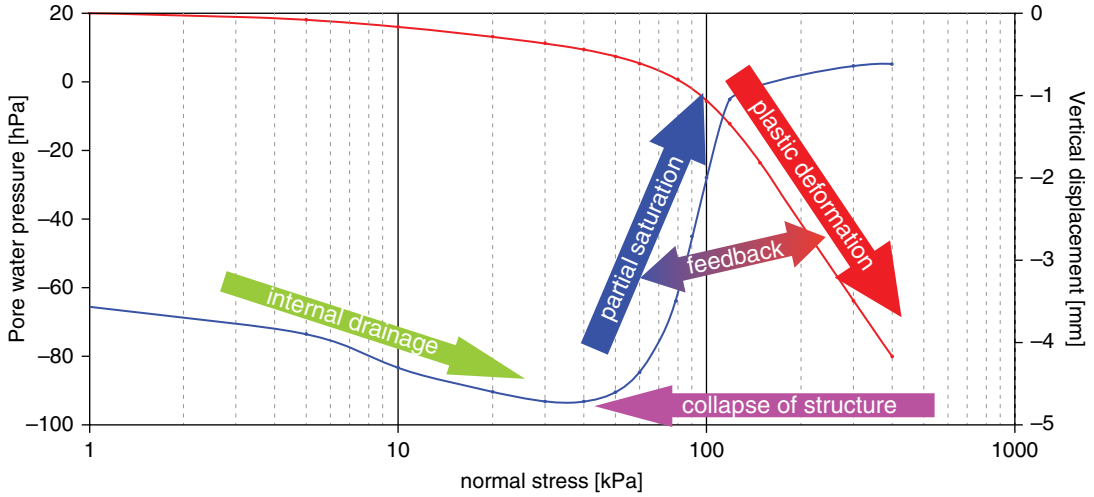

Figure 10A.2 Interaction of stress strain and pore water pressure changes (taken from Horn and Peth 2011).

foundation measures, especially in clayey soils), the secondary settlement must also be considered, which is caused by particle alignment and can lead to long-term creeping movement and therefore to fissuring.

10A.2.3. Stress Distribution in Soils

Stresses applied at the soil surface or during plowing at a defined depth are always transmitted three-dimensionally and result in changes of the three-phase soil systems. Stresses, defined as applied mass per contact area, alter physical, chemical, and biological properties of the soil (e.g. water infiltration, root penetration, etc.) if the internal mechanical strength is exceeded. Stress propagation theories are rather old and have been often modified and adapted to in situ situations. The fundamental theory of Boussinesq (1885) is only valid for completely elastic material, while Fröhlich (1934) and Soehne (1958) included elasto-plastic properties through the introduction of concentration factor values (υ_k). More comprehensive descriptions of these models are given by Koolen and Kuipers (1983), Bailey et al. (1986), Johnson and Bailey (1990), and Bailey et al. (1992). Horn et al. (1989) introduced precompression stress (P_v) dependent values for the concentration factor, which are smaller in the recompression stress range, while they increase in the virgin compression stress range. The latter can be explained by the plastic deformation behavior, which causes a deeper stress transmission closer to the perpendicular line. The stress compensation with depth requires a greater and deeper soil volume for a constant contact area pressure and when both contact area and machine mass are correspondingly increased (Figure 10A.3).

With further consideration of stress propagation, enormous variations are observed due to shear and lateral stresses, which differ depending on the machine configuration (e.g. tire or belt, high slip effects, counterweights for a more effective thrust; Figure 10A.4). Further, the "strain prehistory" is reflected by corresponding different values for the concentration factors. The concentration factors are much smaller in more strongly aggregated and/or drier, and therefore, more stable horizons, and likewise in mechanically precompacted soils. These parameters indicate more horizontally aligned lines of equal pressure or more densely concentrated equi-potentials under the load surface. In contrast, in less aggregated, moister, or more loosely packed soils, the soil pressures are transmitted deeper into the profile but are also propagated more narrowly, concentrated around the load surface, which results in greater values for the concentration factors. Depending on the soil development and land use, the stress propagation varies extensively so that horizon-, matric potential-, structure-, load surface-, and load-dependent values for the concentration factors must be used. However, if the acting pressure exceeds the inherent strength (e.g. of the existing plow pan), and if, due to the mechanical or hydraulic prehistory, there is a less stable horizon underneath that cannot compensate the remaining pressures, the plow pan ruptures and the total soil volume is further compacted to greater depths. In doing so, the higher the shearing component, the more pronounced and also the more sustained the soil deformation. In addition, there is a lateral bulging of the soil surface in the area surrounding the load surface (wheel rut, footsteps), whereby the shape and extent can be described

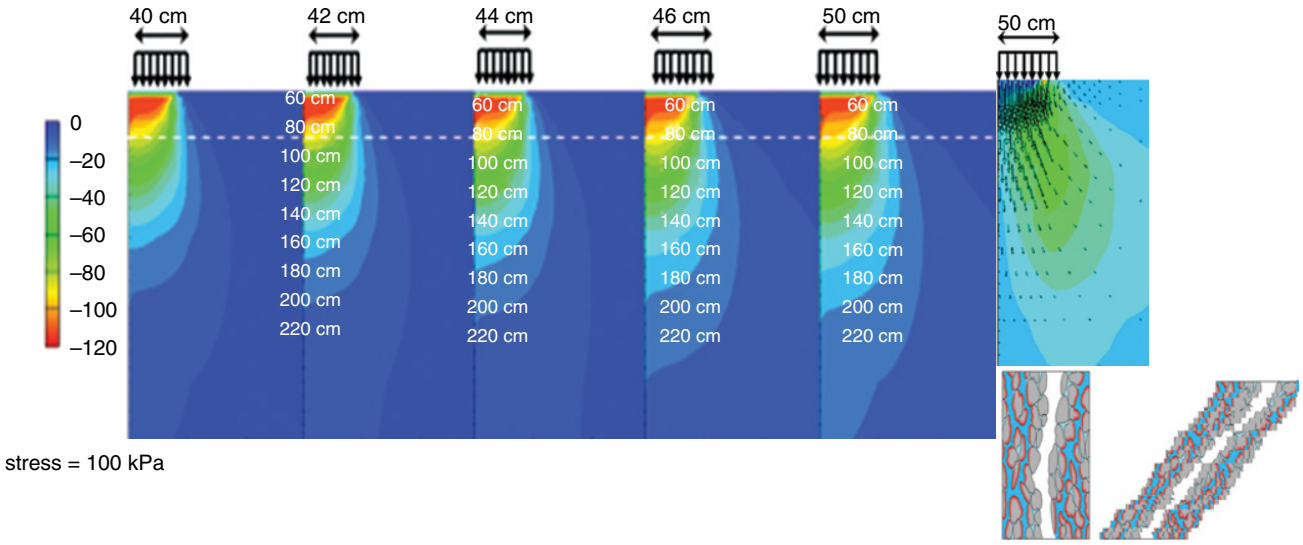

Figure 10A.3 Stress distribution in soils as a function of increasing contact area at a given mechanical stress (mass/area) as well as shear induced formation of strain vectors and changes in pore continuity.

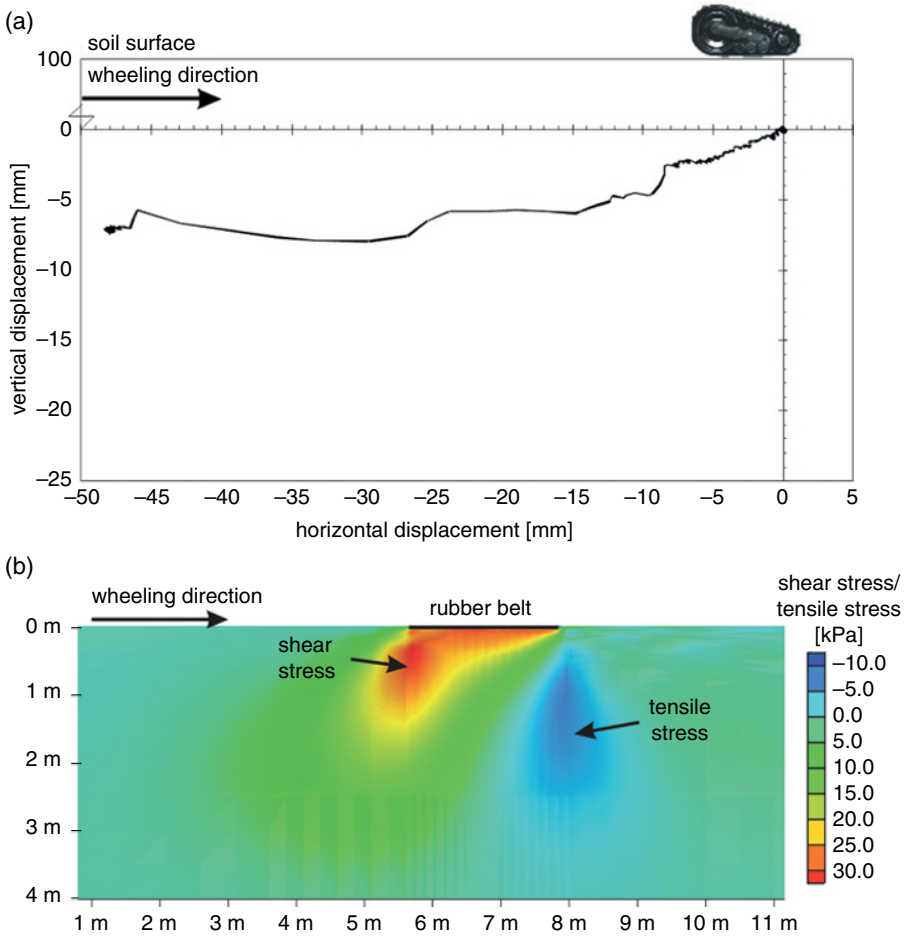

Figure 10A.4 (a) Effect of shear deformation due to wheeling (rubber belt) on stress and strain. (Source: Horn et al., 2003.) (b) Differentiation between shear and tensile stress during wheeling with a rubber belt system. (Source: Richards & Peth, 2006.)

using the Rankine Prandtl failure theory (Fredlund & Rahardjo, 1993). The pattern of the flow lines, which are always perpendicular to the equipotential lines, depends on the soil development and land use. Beyond the boundary state, there is a complete soil failure, which results in a landslide.

10A.2.4. Definition of Site-Specific Soil Management

The quantification of a resilient or sustainable soil management requires the combination of quantified mechanical processes and the internal soil strength as well as the analyses of internal soil processes at the transition between the elastic and plastic soil deformation. These analyses need to include the kind of stress application together with the actual hydraulic properties and functions, as they may decrease the internal rigidity due to kneading, puddling, or aquaplaning and may result in an intense soil strength loss and irreversible soil deformation.

As long as the internal soil strength exceeds the applied stress, no changes in soil functions are expected and the soil properties remain constant. The light traffic system can be defined as green, and the corresponding machinery can be applied without any problems for future land use (Riggert et al. 2019). If however, the applied stresses already exceed the internal soil strength, it is pertinent to consider the initial changes in soil properties, which can be also detected by a slight rutting. The sensitivity of the side increases and requires a careful consideration of further management decisions.

If in this plastic deformation range shearing and in combination with high soil water content are detected, it is pertinent to define such a situation with the given machinery as extremely dangerous, since not only the soil properties and functions will be heavily changed, but the whole soil profile down to deeper depth will be destroyed irreversibly. Thus, such machines as the rubber belt version should be classified as extremely negative and be avoided to maintain sustainable or resilient soil properties (Figure 10A.5).

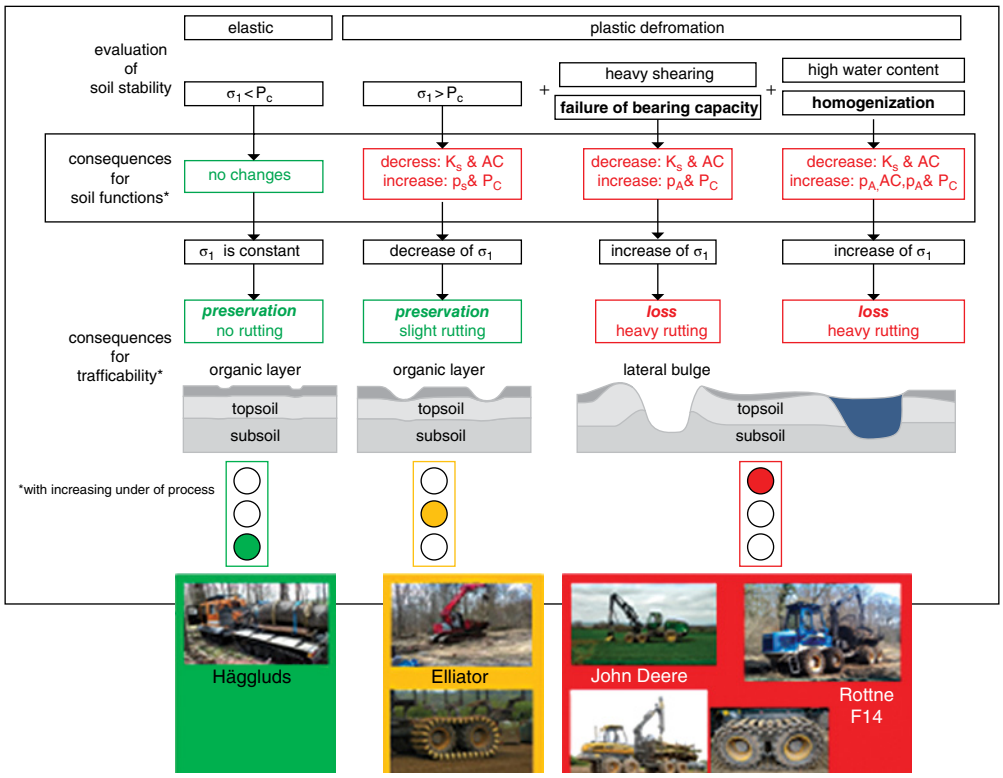

Figure 10A.5 Analyses of site-specific soil strength and stress-induced changes in soil properties and definition of corresponding machinery (acceptable or not acceptable). (Modified from Riggert, 2015, and Riggert et al., 2019.)

10A.3. EFFECT OF STRESS APPLICATION ON CHANGES IN ECOLOGICAL SOIL FUNCTIONS

The structure-dependent formation of interaggregate pore systems always affects pore continuity and directions and alters the values of the corresponding three-dimensional flux tensors of water, gas, heat, and ions (Figure 10A.6). As soon as the external stress applied exceeds the internal soil strength, changes in soil properties and functions (e.g. structure deterioration, water storage and fluxes, plant growth restrictions, erosion, or land sliding) and yield uncertainty are obvious.

10A.3.1. Capacity or Intensity Parameters

The soil science literature (e.g. Brady & Weil, 2008; Huang et al., 2012; Blume et al., 2016) defines the capacity parameters such as cation exchange capacity, air capacity, or plant-available water capacity related to plant growth, yield, or environmental processes. This approach is certainly less straightforward than the intensity parameters, which are only valid in the rigidity ranges (Horn & Kutilek, 2009). However, such an approach and the link to mechanical or hydraulic stresses among others improve the reliability of predictions for all kinds of hydraulic, mechanical, chemical, or even climatic soil interaction processes. Changes in soil functions (e.g. hydraulic conductivity, air permeability, redox potential, and cation exchange capacity process) must be related to parameters like precompression stress, aggregate strength, cohesion, and angle of internal friction. These strength parameters are appropriate to document the transition from elastic to plastic (irreversible) changes in soil functions.

A quick approach to quantify stress-induced changes in soil properties and consequences for ecological processes is the description of the rooting pattern, as it shows the effects of structure formation on plant growth, altered or even prevented accessibility of nutrients, water, air, and the anchorage of the plant (Figure 10A.6).

It is obvious that deep rooting in soils is mostly prevented through a platy structure (e.g. under conventional tillage or intensely trampled conditions) and can be even further reduced if more stress is applied (Figure 10A.7). Conservation tillage or natural conditions with stronger aggregates and less dense conditions at the same time result in an even and deeper rooting, which guarantees a better plant growth with increased accessible particle or pore surfaces. The process of carbon sequestration in soils for combatting climate change effects is also linked with the accessibility and availability of particle or pore surfaces (see chapter 10B). However, exceeding the internal soil strength (i.e. the precompression stress) results in a reduced rooting depth and intensity and less positive effects.

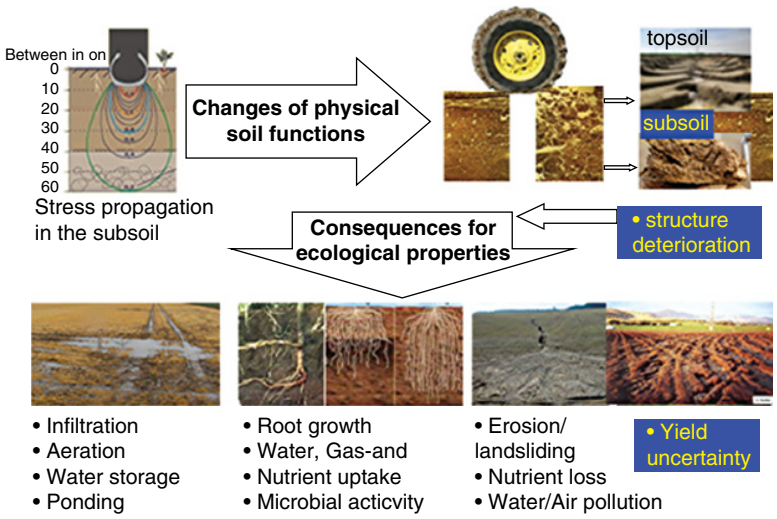

Figure 10A.6 Consequences of mechanical stress application on changes of ecological properties and functions. (Adapted from Horn, 2011.)

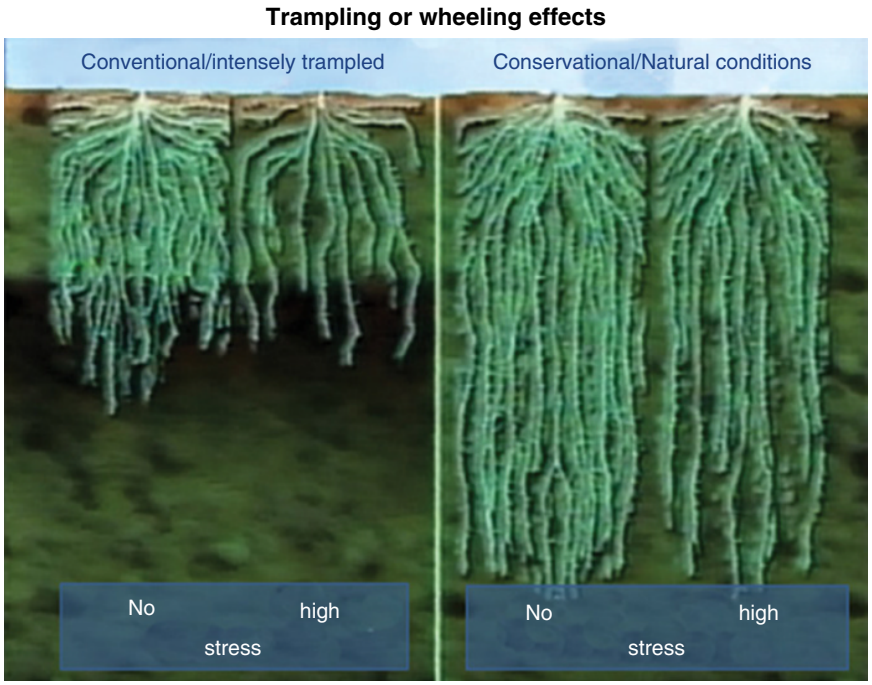

Figure 10A.7 Root growth and depth in soils: effects on availability and accessibility. (Slightly modified from Horn, 2011.)

Furthermore, intensity parameters are mostly vectors and sensitive markers for soil properties changes in directions and time. Thus, pedogenic, geogenic, or anthropogenic processes and their effects on flux processes or interrelated changes in biological, physical, and chemical functions, including filtering and buffering, soil water erosion, or even the gas emission, are direction dependent. They differ in quantity and quality at any given structure conditions and can only be quantified and extrapolated within the rigidity range of the pore system. Furthermore, the actually existing properties are a result of former management reference points for additional changes when exceeding the rigidity of pore functions.

10A.3.2. Interaction Between Mechanical and Hydraulic Properties

Soil deformation due to applied mechanical stresses alters both pore volume and size distribution (Horn &

Peth, 2011; Krümmelbein, 2007; Zhao et al., 2010), as well as pore connectivity, with major impacts on water and air conductivity (Figure 10A.8).

Reszkowska et al. (2011) proved that, depending on the trampling intensity, not only a drastic and mostly irreversible reduction of the hydraulic conductivity occurred, especially in the topsoil, but the direction-dependent changes in the fluxes would serve as indicators for the preservation of soil sustainability.

Within the recompression stress range, the pore size distribution and the hydraulic conductivity both remain constant, as proven by uncounted measurements summed up in DVWK (1995,1997) directives. The virgin compression load range, however, decreases the total pore volume, air capacity, and the saturated hydraulic conductivity even if the plant-available water capacity partially increases at low-stress application. In total, the pore system, as well as its functions, are unstable and react flexibly in this stress range (Figure 10A.9).

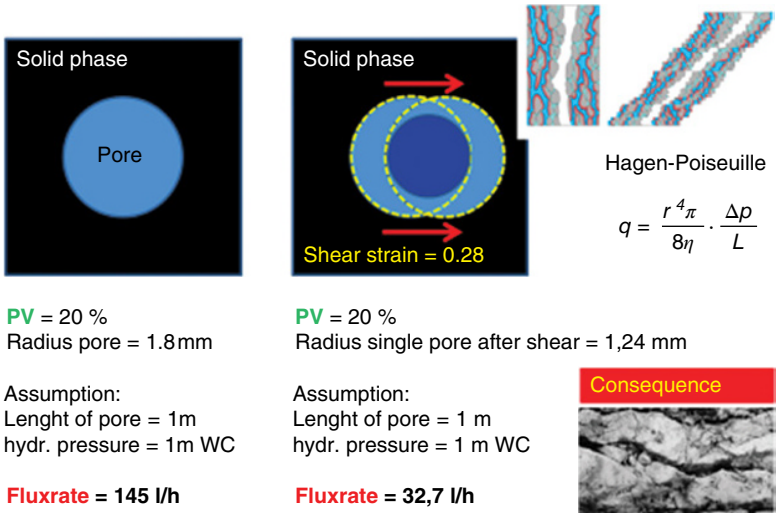

Figure 10A.8 Effect of shear deformation on pore space dynamics and water flux. (Modified from Horn & Peth, 2011)

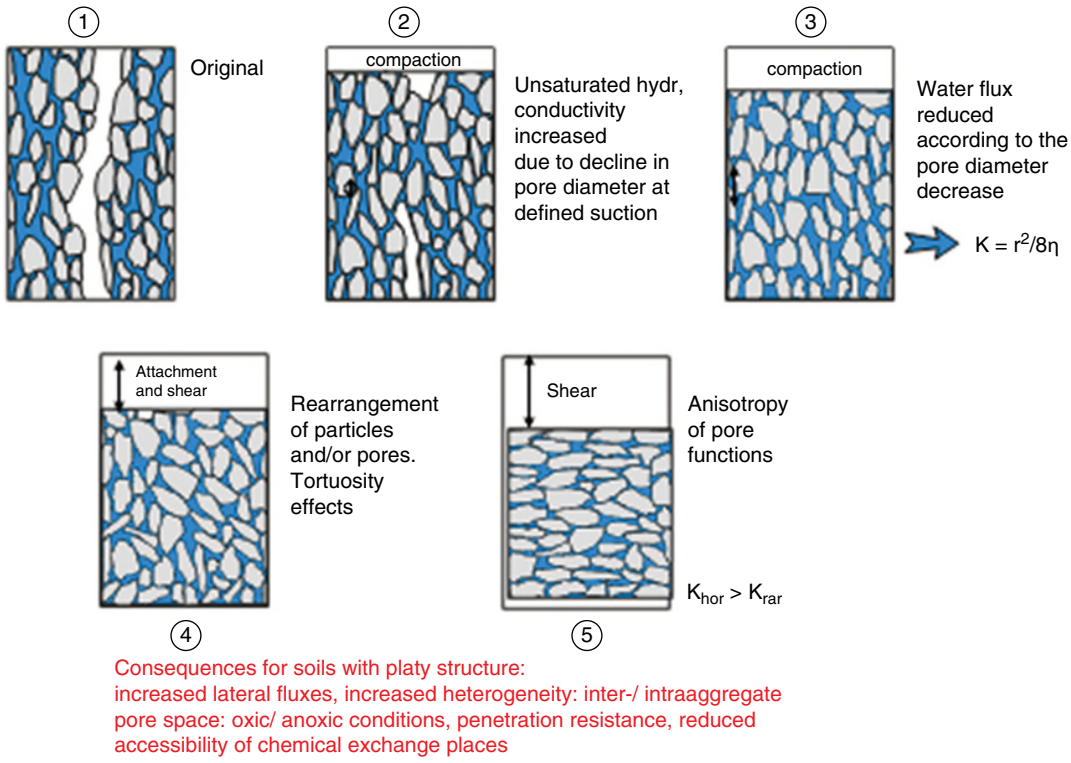

Figure 10A.9 Stress and strain effects on hydraulic properties (Adapted from Horn, 2011.)

10A.3.3. Coupling of Physical, Chemical, and Biological Processes

Soil structural properties and functions are interlinked with mechanical stresses (Figure 10A.10) and result in a continuous cycling with even less-favorable site conditions due to pore water problems weakening in combination with particle rearrangement processes.

The intensity of these interactions also depends on the microbial activity, and if soil is stressed mechanically, it depends on changes in the sink or source of CO_2 or CH_4 flux under stress (Figure 10A.11). As long as the internal soil strength is not exceeded, the stress-induced decline in redox potential regains the former values after the stress is released. If the internal soil stress exceeds the rigidity of the soil structure, it results in a continuous and permanent decrease of the redox potential values. The strong interactions between stress application and changes in biological activity can also be derived from the changes in CO_2 emission and even in the formation and release of methane because of complete anoxic conditions in soils (Haas et al., 2016; Horn, 1985). Exceeding the precompression stress also separates microbial species from their origins, which again underlines the necessity to quantify and to separate the internal strength and related permanent properties from unpredictable soil properties and behavior in the virgin compression load range.

The gaseous exchange with the atmosphere, the aeration of the rhizosphere, and the composition of the microorganisms (oxic/anoxic) can also be discussed in the same context (Horn & Smucker, 2005; Krümmelbein et al., 2013; Uteau et al., 2015). Dörner and Horn (2006) and Hass et al. (2016) documented the increasing effect of stress and shear caused by horizontal anisotropy on the hydraulic and air permeability, which coincides with a retarded gaseous exchange and an increased proportion of e.g. CO_2 or even CH_4 in soil pores (refer to chapter 10B) and which hinders the normal growth of the microbial population (Figure 10A.11). If the internal soil strength is exceeded, the microbial composition and activity are converted to anoxia and result in the emission of CH_4. Additionally, an aggregate dependent carbon sequestration is enhanced and depends on its previous soil management or history (Wiesmeier et al., 2012). Thus, the rigidity quantified as precompression stress separates the beneficial storage and increased accessibility from the nonrigid conditions and a complete alteration of the physicochemical properties and processes and affects not only the internal soil processes but the atmospheric composition as well (refer to chapter 10B).

Figure 10A.12 underlines the multidisciplinary effects of soil deformation on site properties.

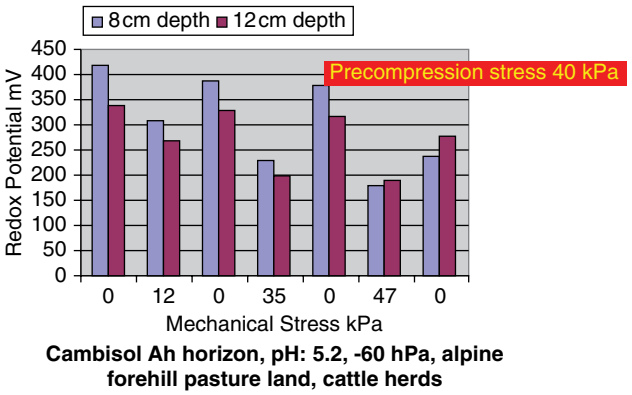

Figure 10A.11 Redox potential values as function of applied mechanical stress. (Data from Horn, 1985.)

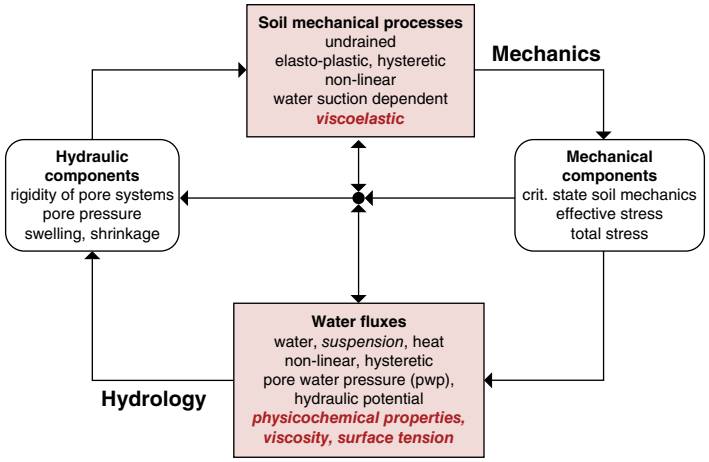

Figure 10A.10 Coupled mechanical and hydraulic properties and processes (Modified from Richards et al., 1997.)

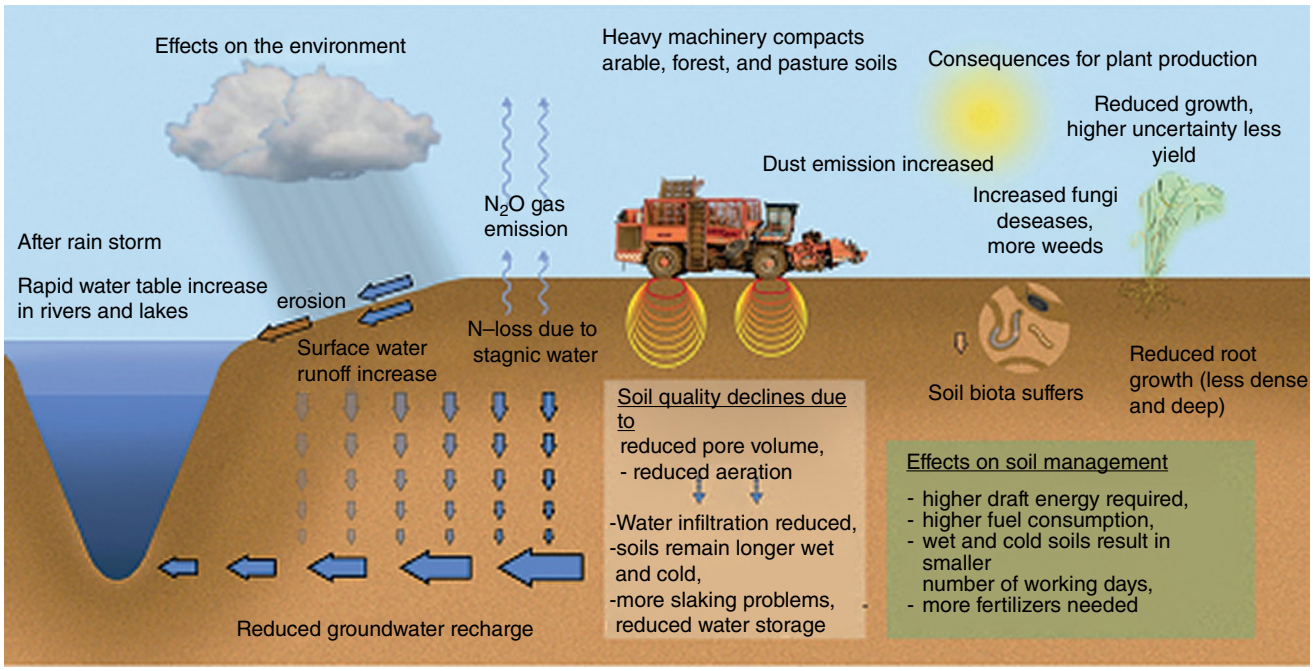

Figure 10A.12 Multidisciplinary effects of soil deformation on soil properties. (Translated and modified from van der Ploeg et al., 2006.)

10A.4. CONCLUSIONS

1. Soil structure formation results in increased mechanical strength, which can be quantified both by the precompression stress or the parameters of the Mohr-Coulomb failure line. The higher the internal soil strength the more pronounced is the rigidity of the pore system and the more elastic the reaction of soils within the recompression load range.

2. The elasticity is replaced by plastic irreversible soil deformation within the virgin compression load range and causes additional changes in soil functions.

3. Physical, chemical, and biological properties show an identical pattern with mostly constant values within the recompression load range and alterations beyond the precompression stress value. Thus, within the recompression load range, soils behave primarily elastically, while in the virgin compression load range (beyond the precompression stress), soils react with a plastic deformation and a corresponding intense change in physical, chemical, and biological properties and functions.

4. All corresponding modeling attempts are therefore limited to this recompression stress range, where the rigidity assumption still holds true. As long as the soil structure remains rigid, all soil functions remain and can guarantee corresponding ecological functions and even maintain an extended biodiversity.

5. The main parameters and functions of the hydraulic, gas, or heat flux under given potential gradients must be added by the rigidity information in order to obtain in future work also a more complete insight in the effect of land-use management systems on coupled hydraulic mechanical soil processes defining the climate-food-energy-water nexus.

REFERENCES

Bailey, A. C., Johnson, C. E., & Schafer R. L. (1986). A model for agricultural soil compaction. *J. Agric. Eng. Res.*, *33*, 257–262.

Bailey, A. C., Raper, R. L., Johnson, C. E., & Burt, E. C. (1992). An integrated approach to soil compaction modelling. *Proc. Int. Agric. Eng. Conf*. Uppsala, Sweden.

Berisso, F. E., Schjønning, P., Keller, T., Lamandé, M., Etana, A., de Jonge, L. W., et al. (2012). Persistent effects of subsoil compaction on pore size distribution and gas transport in a loamy soil. *Soil Tillage Res.*, *122*, 42–51.

Blume, H.-P., Brümmer, G.W., Fleige, H., Horn, R., Kandeler, E., Kögel-Knabner, I., et al. (2016). *Scheffer/Schachtschabel soil science*. Springer.

Boussinesq, I. (1885). *Applications des potentiels à l'étude de l'équilibre et du mouvement des solides élastiques*. Paris: Gauthier-Villars.

Brady, N. C., & Weil, R. R. (2008). *The nature and properties of soils*, International Edition. Pearson.

Bridges, E. M., & Oldeman, L. R. (1999). Global assessment of human-induced soil degradation. *Arid Soil Research and Rehabilitation*, *13*, 319–325.

Dörner J., & Horn, R. (2006). Anisotropy of pore functions in structured stagnic luvisols in the weichselian moraine region

in Northern Germany. *J. Plant Nutrition and Soil Science*, *169*, 213–220.

Duttmann, R., Schwanebeck, M., Nolde, M., & Horn, R. (2014). Predicting soil compaction risks related to field traffic during silage maize harvest. *Soil Science Soc. Amer. J.*, *78*(2), 408–421.

DVWK (1995). *Soil strength in structured unsaturated soils. Part I: precompression stress*. (in German, with English summary and captures) Merkblätter 234, Wirtschafts- and Verlagsges. Bonn: Gas and Wasser.

DVWK (1997). Soil strength in structured unsaturated soils. Part II: physical soil properties (in German, with English summary and captures) Merkblätter 235, Wirtschafts- and Verlagsges. Gas and Wasser, Bonn

Fredlund, D. G., & Rahardjo, H. (1993). *Soil mechanics for unsaturated soils*. New York: John Wiley and Sons.

Fröhlich, O. K. (1934). *Druckverteilung im Baugrund*. New York: Springer.

Ghanbarian, B., Hunt, A. G., Sahimi, M., Ewing, R., Skinner, T. (2013). Percolation theory generates a physically based description of tortuosity in saturated and unsaturated porous media. *Soil Sci. Soc. Am. J.*, *77*, 1920–1929.

Haas, C., Holthusen, D., Mordhorst, A., Lipiec, J., & Horn, R. (2016). Elastic and plastic soil deformation and its influence on emission of greenhouse gases *Int. Agrophys.*, *30*, 173–184.

Hartge, K. H., & Horn, R. (2016). *Essential soil physics*. Schweizerbart Science Publ. ISBN: 978-3-510-65339-3.

Holthusen, D., Brandt, A., Reichert, J., Horn, R. (2018). Soil porosity, permeability and static and dynamic strength parameters under native forest/grassland compared to no-tillage cropping. *Soil and Tillage Res*., 113–124.

Horn, R. (1976). Mechanical strength changes due to aggregate formation of a mesocoic clay. (in German) PHD Thesis TU Hannover.

Horn, R. (1981). Effect of soil aggregation on the mechanical soil strength and its consequences on physical properties. (in German) Schriftenreihe des FB 14 TU Berlin, H.10, 200S. ISBN 379830792 X.

Horn, R. (1985). Effect of animal trampling on physical properties in alpine regions. *Z.f. Kulturtechnik u.Flurbereinigung*, *26*, 42–51.

Horn, R. (2011). Management effects on soil properties and functions. In Glinski, Horabik, & Lipiec (Eds.), *Encyclopedia of agrophysics* (pp. 447–455). Dordrecht: Springer Verlag, ISBN: 978-90-481-3584-4.

Horn R. (2015). Soil compaction and consequences of soil deformation on changes in soil functions. In S. Nortcliff (Ed.), *Task force: Soil matters—Solutions under foot* (pp. 28–33). Catena Publ. Geoecology Essays. ISBN: 978-3-923381-63-0

Horn, R., Baumgartl, T., Gräsle, W., & Richards, B. G. (1995). Stress induced changes of hydraulic properties in soils. In E. E. Alonso & P. Delage, *Proc. 1st. Int. Conference on Unsaturated Soils, Paris* (pp. 123–128). Balkema Verlag ISBN: 9054105844.

Horn, R., & Dexter, A. R. (1989). Dynamics of soil aggregation in an irrigated desert loess. *Soil and Tillage Research.*, *13*, 253–266.

Horn, R., Fleige, H., Zimmermann, I., & Peng, X. (2017). Soil physical compaction and erosion as a threat to food production and human health. In B. R. Singh, M. J. McLaughlin, & E. C. Brevik (Eds.), *The nexus of soils, plants, animals and human health* (pp. 42–49). Schweizerbart, ISBN: 978-3-510-65417-8.

Horn, R., Holthusen, D., Dörner, J., Mordhorst, A., & Fleige, H. (2019). Research innovations in soil physics: What do we need to know to head for a sustainable environment. *Soil Tillage Research*, *195*, 1–25.

Horn, R., & Kutilek M. (2009). The intensity-capacity concept: How far is it possible to predict intensity values with capacity parameters. *Soil and Tillage Res.*, *103*, 1–3.

Horn, R., Lebert, M., & Burger, N. (1989). Prediction of the mechanical strength of arable soils based on laboratory and in situ measurements. (in German, with English summary and captures). Abschlußbericht Bayer. StMLU Bewilligungs-Nr. 6333-972-57238, 178 S.

Horn, R., Peng, X., Fleige, H., & Dörner, J. (2014). Pore rigidity in structured soils—only a theoretical boundary condition for hydraulic properties? *Soil Science and Plant Nutrition*, *60*, 3–14.

Horn, R., & Peth, S. (2011). Mechanics of unsaturated soils for agricultural applications. In P. M. Huang, Y. Li, & M. Sumner (Eds.), *Handbook of soil sciences* (2nd ed., chap. 3, pp. 1–30). Taylor and Francis, ISBN: 978-1-4398-0305-93-14.

Horn, R., & Smucker, A. (2005). Structure formation and its consequences for gas and water transport in unsaturated arable and forest soils. *Soil and Tillage Res.*, *82*, 5–14.

Huang, P. M., Li, Y., & Sumner, M. (2012). *Handbook of soil sciences*, 2nd ed. CRC Press, ISBN: 978-1-4398-0307

Johnson, C. E., & Bailey A. C. (1990). A shearing strain model for cylindrical stress states. *Proc. ASAE.*, *90*, 1085.

Keller, T., Arvidsson, J., & Dexter, A. R. (2007). Soil structures produced by tillage as affected by soil water content and the physical quality of soil. *Soil and Tillage Res.*, *92*, 45–52.

Keller, T., Lamandé, M., Peth, S., Berli, M., Delenne, J. Y., Baumgarten, W., et al. (2013). An interdisciplinary approach towards improved understanding of soil deformation during compaction. *Soil Tillage Res.*, *128*, 61–80.

Keller, T., Sandin, M., Colombi, T., Horn, R., & Or, D. (2019). Historical evolution of soil stress levels and consequences for soil functioning. *Soil & Tillage Research*, *194*.

Koolen, A. J., & Kuipers, H. (1983). *Agricultural soil mechanics*. Berlin: Springer.

Krümmelbein, J. (2007). Influence of various grazing intensities on soil stability and water balance of a steppe soil in Inner Mongolia, P.R. China Vol 74. Schriftenreihe Inst. Pflanzenen., Bodenkunde, CAU Kiel, ISBN: 0933-680X

Krümmelbein, J., Horn, R., Pagliai, M. (2013). *Soil degradation. Advances in Geoecology*, vol. *42*. Catena Verlag ISBN: 978-3-923381-59-3

Kühner, S. (1997). Simultane Messung von Spannungen und Boden bewegungen bei statischen und dynamischen Belastungen zur Abschätzung der dadurch induzierten Bodenbeanspruchung Band 39; Schriftenreihe des Instituts für Pflanzenernährung und Bodenkunde, CAU Kiel ISSN:0933-680X

Lebert, M. (1989). Beurteilung und Vorhersage der mechanischen Belastbarkeit von Ackerböden. Bayreuther Bodenkundliche Berichte, 12.

McCarthy, D. F. (2007). *Essentials of soil mechanics and foundations*. New York: Prentice Hall.

Mordhorst, A., Peth, S., Horn, R. (2014). Influence of mechanical loading on static and dynamic CO2 efflux on differently textured and managed Luvisols. *Geoderma*, *219–220*, 1–13.

Nissen, B. (1999). Vorhersage der mechanischen Belastbarkeit von repräsentativen Ackerböden in der Bundesrepublik Deutschland: bodenphysikalischer Ansatz. PhD Thesis. Schriftenreihe des Instituts für Pflanzenernährung und Bodenkunde 50. Christian-Albrechts-University zu Kiel, 159p.

Parry, R.H.G. (2004). *Mohr circles, stress paths and geotechnics*. London: Spon Press.

Reszkowska, A., Krümmelbein, J., Gan, L., Peth, S., & Horn, R. (2011). Influence of grazing on soil water and gas fluxes of two Inner Mongolian steppe ecosystems. *Soil Till. Res.*, *111*, 180–189.

Richards, B. G., Baumgartl, T., Horn, R., & Gräsle, W. (1997). Modelling soil strength and soil compressibility of arable soils by FEM (finite element model). *International Agrophysics*, *11*, 68–79.

Richards, B. G., & Peth, S. (2006). Modeling soil behavior with particular reference to soil science. *Proceedings of ISTRO*, 17, *1–15* (ISBN 3-9811134-0-3)

Riggert, R. (2015). Spannungseinträge unter Holzerntemaschinen und Auswirkungen auf bodenphysikalische Parameter Band 107 Schriftenreihe des Instituts für Pflanzenernährung und Bodenkunde, CAU Kiel ISSN: 0933-680X

Riggert, R., Fleige, H., Horn, R. (2019). An assessment scheme for soil degradation caused by forestry machinery on skid trails in Germany. *Soil Sci. Soc. Am. J.* doi:10.2136/sssaj(2018.07.0255

Riggert, R., Fleige, F., Kietz, B., Gaertig, T., & Horn, R. (2016). Stress distribution under forestry machinery and consequences for soil stability. *Soil Science Society of America Journal*, *80*(1), 38–47.

Semmel, H. (1993). Auswirkungen kontrollierter Bodenbelastug auf das Druckfortpflanzungsverhalten physikalisch mechanischer Kenngrößen von Ackerböden Band 26; Schriftenreihe des Instituts für Pflanzenernährung und Bodenkunde, CAU Kiel ISSN: 0933-680X

Soehne, W. (1958). Fundamentals of pressure distribution and soil compaction under tractor tires. *Agric. Eng.*, *39*, 276–290.

Uteau, Puschmann, D., Pagenkemper, S., Peth, S., & Horn, R. (2015). Oxygen and redox potential gradients in the rhizosphere of alfalfa grown on a loamy soil.*J. Plant Nutrition Soil Science*, *178*, 278–289.

van der Ploeg, R. R., Ehlers, W., & Horn, R. (2006). Schwerlast auf dem Acker. *Spektrum der Wissenschaft.* 80–88

Wiermann, C. (1998). Auswirkungen differenzierter Bodenbearbeitungen auf die Bodenstabilität und das Regenerationsvermögen lößbürtiger Ackerstandorte Nr. 45; Schriftenreihe des Instituts für Pflanzenernährung und Bodenkunde, CAU Kiel ISSN: 0933-680X

Wiesmeier, M., Steffens, M., Mueller, C. W., Kolbl, A., Reszkowska, A., Peth, S., et al. (2012). Aggregate stability and physical protection of soil organic carbon in semi-arid steppe soils. *European Journal of Soil Science*, *63*, 22–31.

Zhao, Y., Peth, S., Horn, R., Krümmelbein, J., Ketzer, B., Gao, Y. Z., et al. (2010). Modeling grazing effects on coupled water and heat fluxes in Inner Mongolia grassland. *Soil Tillage and Research*, *109*, 75–86.

Zhai, X., & Horn, R. (2018). Effect of static and cyclic loading including spatial variation caused by vertical holes on changes in soil aeration. *Soil and Tillage Research*, *177*, 61–68.

Zhai X., & Horn, R. (2019). Dynamics of pore functions and gas transport parameters in artificially ameliorated soils due to static and cyclic loading. *Geoderma*, *337*, 300–310.

Zink, A. (2009). Bodenstabilität und Auswirkungen dynamischer Lasteinträge auf physikalische Eigenschaften von Ackerböden unter konservierender und konventioneller Bodenbearbeitung Band 84; Schriftenreihe des Instituts für Pflanzenernährung und Bodenkunde, CAU Kiel ISSN: 0933-680X

10B

Soil Strength and Carbon Sequestration

Rattan Lal

ABSTRACT

Sequestration of carbon in soil, both soil organic carbon (SOC) and soil inorganic carbon (SIC), is strongly determined by management-induced differences in soil physical, mechanical, strength, and hydrological properties. These properties affect SOC sequestration through creation of either a positive or negative soil/ecosystem carbon budget. A positive SOC budget positively affects agronomic productivity and above and below ground biomass, and thus, is a sink for atmospheric carbon dioxide (CO_2) and methane (CH_4). On the contrary, adverse changes in soil mechanical properties make soil a source of greenhouse gases GHGs, and this also has a negative impact on productivity.

10B.1. INTRODUCTION

Soil strength, total porosity, pore continuity and size distribution, air porosity, and plant available water storage also impact plant growth, root development and depth distribution, total biomass production, and the type and amount of soil carbon (C) sequestration. Therefore, the objective of management of soil mechanical properties is to make soil a sink of atmospheric CO_2.

10B.2. PROCESSES OF SOIL CARBON SEQUESTRATION

Soil C sequestration refers to the transfer of atmospheric CO_2 into soil C pools of a long mean residence time through biotic and abiotic processes. There are two types of soil C sequestration: soil organic C (SOC) and soil inorganic C (SIC), and there can be an interconnectivity among them through microbial processes (Figure 10B.1; Lal, 2004, 2010). The rate of SOC sequestration depends on soil properties, including the formation of stable microaggregates (<200 μm). Even the labile SOC, encapsulated within stable microaggregates, is physically protected against microbial processes and has a long mean residence time.

There are several mechanisms of protection of SOC against the microbial processes (Figure 10B.2). Physical mechanisms limit the access of SOC either through encapsulation within stable aggregates or transfer of SOC deep into the subsoil through biotic (earthworms, termites, deep root systems) and abiotic (leaching of dissolved organic carbon) processes. Examples of chemical mechanisms consist of interaction with metallic cations (e.g. Fe, Al, Mn) and absorption of organic substances on clay particles because of the charge properties, etc. Biological mechanisms include productions of recalcitrant compounds (e.g. Suberin) and other substances that do not readily decompose.

Ecological mechanisms originate through interactions between the pedosphere, biosphere, hydrosphere, and the anthropogenic activities. The latter involve targeted interventions that enhance both the above-ground and below-ground biodiversity, enhance soil quality (physical, chemical, and biological), and increase biomass production.

10B.3. SEQUESTRATION OF SOIL INORGANIC CARBON

Dryland ecoregions, covering as much as 45% of Earth's ice-free land (Lal et al., 2000), contain a large amount of SIC. The land area under dry land may

Carbon Management and Sequestration Center, The Ohio State University, Columbus, Ohio, USA

Hydrogeology, Chemical Weathering, and Soil Formation, Geophysical Monograph 257, First Edition.
Edited by Allen Hunt, Markus Egli, and Boris Faybishenko.

DOI: 10.1002/9781119563952.ch10b

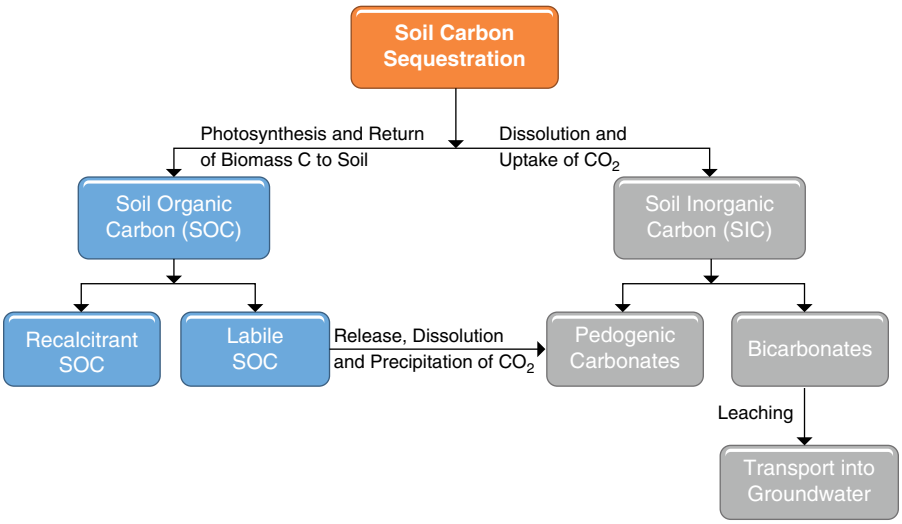

Figure 10B.1 Types of soil carbon sequestration.

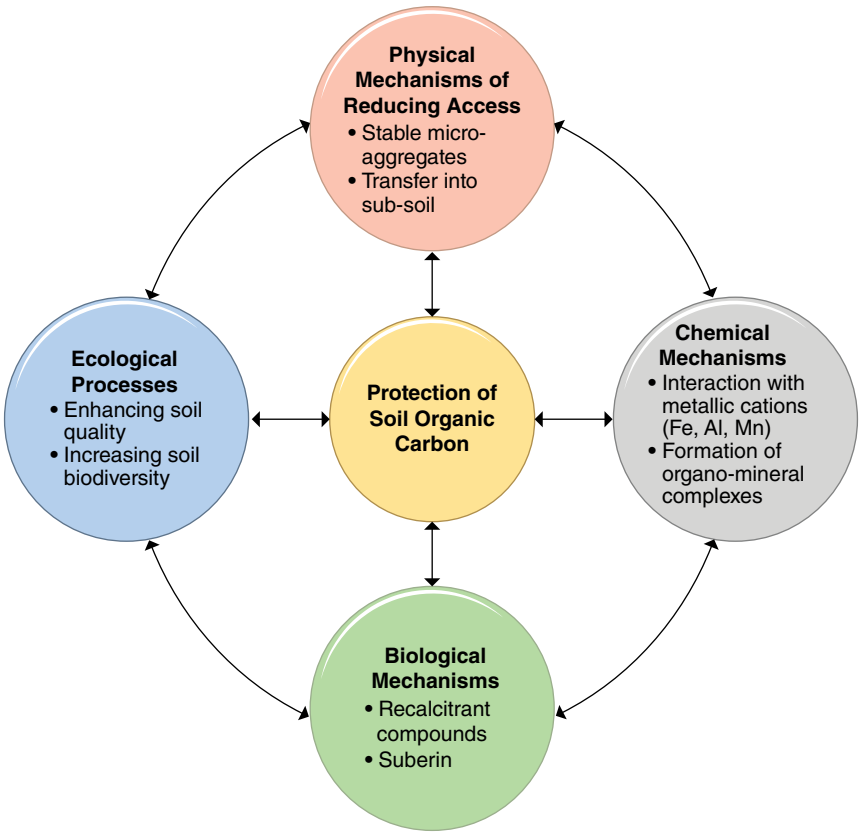

Figure 10B.2 Mechanisms of protection of soil organic carbon against microbial processes. (Drawn from concepts outlined in Lal, 2018.)

increase to as much as 50% of the Earth's total area by the year 2100 (Lal, 2019). Similar to the effects of SOC, the SIC pool is also a source of numerous ecosystem services (Groshans et al., 2018). The SIC occurs in soil in three forms: (1) gas, (2) dissolved CO_2 in the form of dilute carbonic acid (H_2CO_3) and bicarbonate (HCO_3^-), and (3) solid form as carbonate (CO_3^{2-}) in aqueous and solid phase ($CaCO_3$, $MgCO_3$) (Groshans et al., 2018). Predominance of any specific form of SIC may depend on soil strength properties, especially soil wetness,

aeration, anaerobiosis, etc. In addition to lithogenic (primary) carbonates derived from the weathering of parent rock, soils of arid regions also contain pedogenic or secondary carbonates. The latter are formed authigenically in soil under alkaline arid conditions (Lal, 2019; Monger et al., 2015) and when cations (Ca, Mg) are brought in from outside the system.

10B.4. RESTORING SOIL PROPERTIES THROUGH ECO-EFFECTIVE MANAGEMENT

Eco-intensification of agro-ecosystems involves conversion to a restorative land use and adoption of innovative agricultural practices that enhance productivity while reducing the environmental footprint (Lal, 2019). There is also a distinction between eco-efficient and eco-effective agricultural practices (Czyzéwski et al., 2018). Eco-efficiency implies the efficiency with which the ecological resources are used in an agro-ecosystem. Eco-effectiveness refers to the environmental effect or footprint of a system (Czyzéwski et al., 2018). Whereas these two concepts are not mutually exclusive, the strategy is to reconcile the need for meeting demands of the growing and increasingly affluent human population with the necessity of restoring the environment. It is important that eco-effectiveness not be short-changed by eco-efficiency. Thus, appropriate land-use and farming systems must satisfy both criteria.

10B.5. TECHNICAL AND ACTUAL RATE OF SOIL CARBON SEQUESTRATION

The potential rate of SOC sequestration depends on the magnitude of the historic loss, type and severity of soil degradation, texture and minerology, depth of soil solum, landscape position and aspect, and climate (precipitation, evaporation, temperature, water and energy balance, biome/eco-region). In general, the rate of SOC sequestration is higher in (1) cooler and wetter climates compared with warmer and drier climates, (2) fine-textured and 2:1 expanding type minerals compared with course-textured and 1:1 lattice clays, (3) concave landscape facing poleward compared with convex shape facing toward the equator, (4) systems that maintain a continuous ground cover and return the biomass to the soil compared with those that disturb the soil and harvest the biomass, (5) complex farming systems with a cover crop during the off-season compared with mono-culture and less diverse systems, and (6) systems based on integration of crops with trees and livestock compared with those involving only the seasonal crops. In general, the rate of SOC sequestration ranges from 1 Mg C/ha· y for the ideal situation vs <0.1 Mg C/ha· y for traditional systems (which can be improved, Lal et al., 2000). Similarly, the rates of SIC sequestration via the formation of pedogenic carbonates and leaching of bicarbonates may also range from 1 Mg C/ha·y to 0.005 Mg C/ha·y (Lal et al., 2000).

Examples of eco-effective land use and cropping system include those that conserve soil and water and minimize risks of soil erosion, create a positive soil/ecosystem C budget through regular and substantial input of biomass-C, adopt systems of integrated nutrient management and ensure balanced application of plant nutrients, convert from plow-based to no-till systems of seedbed preparation in conjunction with the retention of crop residue mulch and elimination of infield biomass burning, and minimize wheeling and the use of heavy vehicular traffic, especially when soil is wet, to avoid kneading.

Sustainable management of SOC content, maintaining it at about 2% in the top 0–30 cm layer, enhances and restores soil engineering/strength properties, accentuates formation of stable aggregates, improves porosity (macropores) and continuity of pores, enhances gaseous exchange or aeration, and reduces gaseous emissions through methanogenesis (CH_4) and nitrification/denitrification (N_2O). Restoring SOC content to above the threshold level (~2% in the root zone) sets in motion the restorative processes with an upward spiral. Improvement in soil strength and engineering properties has a positive impact on plant growth, animal health, human well-being, and the environment.

10B.6. SUSTAINABLE DEVELOPMENT GOALS OF THE UNITED NATIONS

Soil quality, as impacted by engineering and mechanical properties along with the management of SOC and SIC pools, also impacts the Sustainable Development Goals (SDGs) or the Agenda 2030 of the U.N. (Lal et al., 2018). Sustainable management of soil quality is specifically pertinent to advancing SDG #2 (Zero Hunger), SDG 6 (Clean Water and Sanitation), SDG #13 (Climate Action) and SDG #15 (Life on Land).

10B.7. CONCLUSIONS

1. Soil mechanical and engineering properties also affect soil C pool and its dynamics. Total soil C pool consists of SOC and SIC components, and both are interlinked. The SOC pool is larger in soils of the humid and subhumid regions, and SIC is more predominant in those of arid and semiarid climates.

2. Sequestration of atmospheric CO_2 in soil C pool with mean residence time has strong impact on ecosystem services, including moderation of the global carbon cycle and the attendant impact on the greenhouse impact or global warming. The maintenance of SOC to above the threshold level of ~2.0% in the root zone is critical to advancing the SDGs of the U.N.

REFERENCES

Czyzyewski, B., Matuszczak, A., Burja, C., & Muntean, A. (2018). Eco-efficiency vs. eco-effectiveness in the sustainable development of agriculture: A comparative analysis in EU regions. *Proc. of the 2018 VIII International Scientific Conference Determinants of Regional Development #1, Piela, 12–13 April 2018*, pp. 56–64.

Groshans, G. R., Mikhailova, E. A., Post, C. J., & Schlautman, M. A. (2018). Accounting for soil inorganic carbon in the ecosystem services framework for United Nations Sustainable Development Goals. *Geoderma*, *324*, 37–46.

Lal, R. (2004). Soil carbon sequestration impacts on global climate change and food security. *Science*, *304*, 1623–1627. www.sciencemag.org/cgi/content/full/305/5690/1567DCI

Lal, R. (2010). Managing soils and ecosystems for mitigating anthropogenic carbon emissions and advancing global food security. *BioScience*, *60*(9), 708–721.

Lal, R. (2018). Digging deeper: A wholistic perspective of factors affecting SOC sequestration. *Global Change Biology*, 24(8). doi: 10.1111/gcb.14054

Lal, R. (2019). Eco-intensification through soil carbon sequestration: Harnessing ecosystem services and advancing sustainable development goals. *Journal of Soil and Water Conservation*, *74*(3), 55A–61A.

Lal, R., Horn, R., & Kosaki T. (Eds.) (2018). *Soil and the sustainable development goals*. Stuttgart: Catena-Schweizerbart.

Lal, R., Kimble, J. M., & Stewart, B. A. (Eds.) (2000). *Global climate change and pedogenic carbonates*. Boca Raton, FL: Lewis/CRC Press.

Monger, C. H., Kraimer, R. A., Khresat, S., Cole, D. R., Wang, X., & Wong, J. (2015). Sequestration of inorganic carbon in soil and ground water. *Geology*, *43*, 375–378.

Part V
Integrated Studies of Soils

11

Chemical Weathering in the McMurdo Dry Valleys, Antarctica

W. Berry Lyons[1], Deborah L. Leslie[2], and Michael N. Gooseff[3]

ABSTRACT

While chemical weathering has not always been considered an active process in the McMurdo Dry Valleys (MDV), Antarctica, long-term geochemical and hydrological investigations have provided an overall better understanding of chemical weathering in this polar desert environment. Liquid water on the landscape is limited to stream channels as well as shallow subsurface melt features, as there is no overland flow. Stream total suspended sediment loads are low, with the sources of sediment from stream channels, aeolian input, and/or from the surfaces of glaciers. MDV soils contain high concentrations of soluble salts with little clay material, but since absent of water, these soils are a minimal location of chemical weathering. Hyporheic zones exchange water during streamflow, and these areas control the stream geochemistry over various temporal scales. Hyporheic zones promote rapid aluminosilicate weathering by moving dilute glacial meltwater into intimate contact with sediment surfaces. Rapid weathering of the aluminosilicates in the streambed and hyporheic zones is the most plausible explanation for chemostasis observed in these streams, indicating that little to no catchment processes are necessary to explain the observed chemostasis in the MDV. Shallow subsurface waters with distinct geochemical signatures have much higher dissolved Si concentrations than the stream waters and indicate that they are responsible for enhanced aluminosilicate weathering in this polar desert environment. The dissolution of $CaCO_3$ is also a major process in the hyporheic zones as generally the streams are unsaturated with respect to calcite. Cation-exchange reactions are also important in the evolution from Na-Cl brines to Ca-Cl brines within the soil column, while authigenic $CaCO_3$ can both dissolve and precipitate depending on the condition of the system. Recently, stream channel landscapes are changing due to the melting of buried ice, creating thermokarst and water track features, resulting in a sediment and solute influx to the stream.

11.1. INTRODUCTION

If one were to pick up a classical geomorphology textbook, especially ones published prior to 20 years ago, most might have a plot of temperature vs. precipitation with the description of the types of weathering for the various climatic categories. Notably, under polar environments, those that are very cold and dry, there would be no mention of chemical weathering being an active process. However, this orthodoxy has changed over the past two decades. This change has come in part to our overall better understanding of glacial and subglacial landscapes (Anderson, 2007; Deuerling et al., 2018; Tranter, 2003; Wadham et al., 2010), the recognition that chemical weathering in Arctic regions underlain by permafrost is seasonal, but extensive (Keller et al., 2007; Tank et al., 2012), and that quantitative chemical weathering models based on temperature as a driver grossly underpredict dissolved chemical fluxes (Hartmann et al., 2014).

[1]*School of Earth Sciences and Byrd Polar & Climate Research Center, The Ohio State University, Columbus, OH, USA*

[2]*Department of Earth Sciences, University of Memphis, Memphis, TN, USA*

[3]*Hydrology, Water Resources and Environmental Fluid Mechanics, Environmental Engineering, University of Colorado Boulder, CO, USA*

Hydrogeology, Chemical Weathering, and Soil Formation, Geophysical Monograph 257, First Edition.
Edited by Allen Hunt, Markus Egli, and Boris Faybishenko.

DOI: 10.1002/9781119563952.ch11

Although much work on this topic has been done recently in both the northern and southern polar regions, due to logistical and other constraints, the amount of work pales in contrast to what is known about chemical weathering in both temperate and tropical landscapes. In addition, some of the Earth's polar regions are undergoing some of the most rapid change observed on the planet, and the loss of the cryosphere and hence the conversion of ice, snow, and ground ice to liquid water will have important impacts in enhancing chemical weathering in these environments in the near future. In this chapter, we review and synthesize information generated from long-term geochemical and hydrological investigations in the McMurdo Dry Valleys region in Antarctica at ~78° S over ~25 yrs. This represents the most continuous and comprehensive data set on chemical weathering in the Antarctic.

This chapter focuses on chemical weathering. This polar desert landscape has been considered fairly stable for a long time (Summerfield et al., 1999). We have, however, observed thermal erosion of beds and banks of streams, especially those overlain by buried ice, undergoing permafrost degradation, causing significant downcutting with sediment remobilization over the past decade (Gooseff et al., 2016; Levy et al., 2018; Sudman et al., 2017). Erosion rates greater than 5 cm/yr have been determined through comparative LIDAR measurements in mainstem streams (Levy et al., 2018). These values are very much larger than those determined in exposed bedrock in the region using cosmogenic isotopes, where denudation rates have been estimated at between 0.1 and 1.0 m/Myr (Bruno et al., 1997; Ivy-Ochs et al., 1995; Nishizumi et al., 1991; Summerfield et al., 1999). However, these physical processes are fairly recent, and so our focus here is on the more extensive body of knowledge on chemical weathering in the streams of this region.

11.2. STUDY AREA

The McMurdo Dry Valleys (MDV) are the largest ice-free area in Antarctica (Levy, 2013) and have been a major site of scientific research since the 1960s. Since 1993, Taylor Valley (TV), a low-elevation east-west trending feature, has been the primary focus of the McMurdo Dry Valleys Long-Term Ecological Research (MCM-LTER) program, where long-term environmental monitoring and experiments have taken place (Figure 11.1). These scientific activities include climatological, hydrological, ecological, and geochemical measurements involving the glaciers, soils, streams, and lakes in the valleys (see http://mcm.lternet.edu/ for more information).

The MDV are climatologically classified as polar deserts, with TV having a mean annual temperature of –18 °C, and annual water equivalent precipitation of <5 cm (Doran et al., 2002; Fountain et al., 2010). Ephemeral glacial meltwater streams flow through fixed channels during the austral summer for 4–12 weeks (McKnight et al., 1999; Wlostowski et al., 2016). The glaciers are cold-based, and the meltwater generated from them is generated at and flows along their surfaces, as they are frozen to the underlying substrate (Fountain et al., 1999). All but two of the streams in TV flow into closed-basin lakes, and the majority of these streams are gaged prior

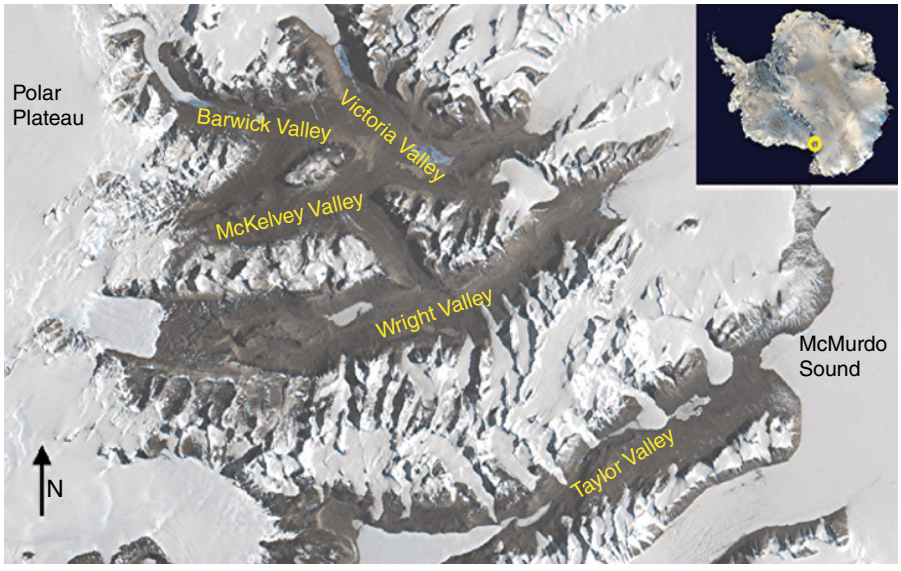

Figure 11.1 The McMurdo Dry Valleys (MDV), Antarctica.

to entering the lakes. There is no overland flow, and much of the snow that does occur within the valley is rapidly sublimated.

The lower elevation soils in TV were deposited from glacier advances and retreats of both the East and West Antarctic Ice Sheets, depending on the location within the valley, over the past ~130,000 years, while higher elevation surfaces could be as much as 2 million years old (Hall & Denton, 2000). The mineralogy, organic carbon concentration and source, and soil geochemistry, especially the soluble salt content and composition, are dependent on their elevation and age (Bockheim, 1997; Burkins et al., 2000; Toner et al., 2013). The lower elevation surfaces have been exposed to water over the past 300,000 years at a minimum as the present-day lakes have waxed and waned as the climate varied (Hendy, 2000). Deposition of organic matter and sediments from the lakes can still be observed in the lower elevation soils. The higher elevation soils with wetting due to snow and ice melt have accumulated high concentrations of soluble soils through atmospheric deposition of aerosols (Bockheim, 1997). These higher elevation surfaces have remained exposed for millions of years. These ultraxerous soils have been described as a sandy-skeletal textural class and are strongly oxidized (Bockheim, 1997). The active layer above the permafrost averages ~50 cm depth, and Bockheim (1997) has termed this "dry" permafrost due to the fact that although frozen, there is insufficient water for cementation.

Prior to 2005, it was thought that the only liquid water from cryospheric melt was generated by glacier melting and the hydrologic connectivity from the glaciers to the stream channels (Figure 11.2) to the lakes and/or ocean (Lyons et al., 1999). Subsurface melt features termed "seep," and later referred to as "water tracks" were described by MCM-LTER workers in the mid-2000s (Harris et al., 2007; Lyons et al., 2005). These features were thought to be derived from either permafrost and/or buried ice and/or snowpack melt (Harris et al., 2007). Recent high-resolution LIDAR studies have clearly demonstrated a large number of buried ice bodies in the lower elevations/valley floors of MDV (Levy et al., 2018). As the climate warms, these newly discovered features may become important new sources of water for driving weathering reactions (Fountain et al., 2014).

11.3. FLUVIAL EROSION/DENUDATION

Little work has been done examining suspended sediment transport in the streams of the MDV, and what has been done has not been done in a systematic manner (Lyons et al., 2016). As there is no overland flow or subglacial discharge, the source of suspended materials in these streams originates from the stream channels themselves, aeolian input, and/or from the surfaces of the glaciers. Given these potential sources, it is expected that the total suspended sediment loads of these streams should be low. What little work has been done suggests that in low-gradient streams this is the case. Low-gradient streams in the Fryxell basin have measured total suspended sediment values between 0.6 and 18 mg/L, with a mean loss on ignition of 38% (Lyons et al., 2016).

11.4. SOILS

As noted above, the soils in MDV have very low moisture content with a mean value of ~1% in the top 3 cm that can reach ~10% at the base of the active layer in coastal regions (Campbell et al., 1998). These authors estimated that >95% of the soil surfaces in the coastal regions of the MDV are not moistened by liquid water except through the potential of melting snow, which in

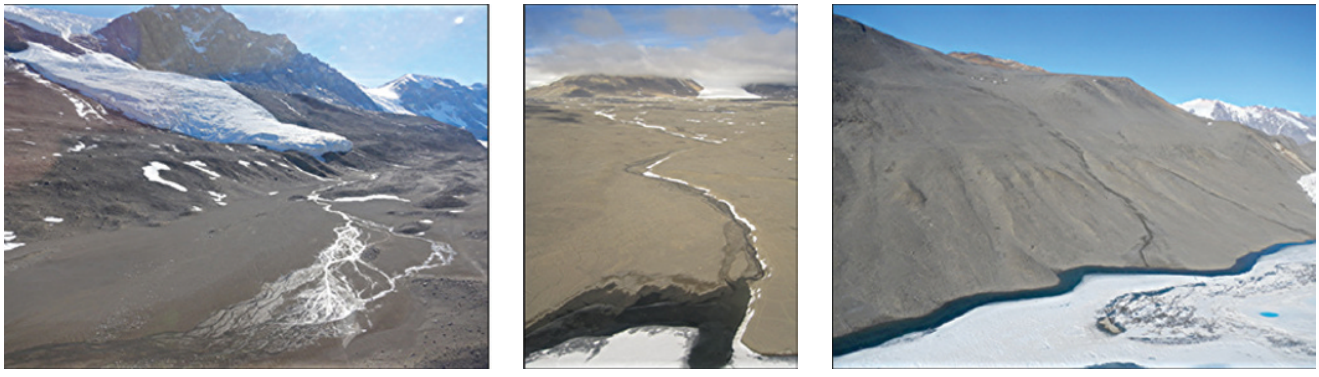

Figure 11.2 Streams (a) Priscu Stream, emerging from melt of the LaCroix Glacier. (b) Delta Stream, originating at the Howard Glaicer in the background, and water tracks in the McMurdo Dry Valleys. (c) Along the south shore of Lake Hoare.

turn may only last a few hours. The mineralogy of the soils reflects the glacial history of the valleys and contains materials from all the local rock types: the early Paleozoic Cambrian and Precambrian metamorphic basement rocks, the Jurassic Ferrar Dolerite, the Devonian-Jurassic aged Beacon supergroup sedimentary rocks, and the late Miocene to present McMurdo volcanics. These volcanic rocks are much more abundant in the eastern part of TV than in the western portion (Hall & Denton, 2000).

Due to the lack of water, there is minimal chemical weathering in these soils (Campbell et al., 1998). There are a number of lines of evidence for this conclusion. Away from the few wetted zones, these soils contain high concentrations of very soluble salts, with values as high as >2 g/cm^2 in the upper 70 cm of soil where surface ages are 250,000 years, with even greater amounts in soils that are older surfaces (Bockheim, 1997). These salts include a wide range of minerals but are dominated by halite, gypsum, mirabilite, and nitrate salts that vary systematically as one moves away from the ocean and with elevation (Bisson et al., 2015; Bockheim, 1997; Keys & Williams, 1981). Given the solubility of these salts, especially the high solubility of the nitrate salts, it is clear that these soils experience little interaction with liquid water (Lyons et al., 2017).

In addition, there exists very little clay-sized material in these soils, and what does exist is mainly unweathered or very slightly weathered feldspar and mica (Campbell et al., 1999). Smectite clays have been reported in low abundance in some samples and are thought to be due to the weathering on Mg-rich minerals within the dolerite (Campbell et al., 1999; Conca & Wright, 1987; Green et al., 1988); however, Bockheim (1997) has observed only a slight broadening in the 10 angstrom mica peak, suggesting only slight alterations of the mica present. There is some oxidation of ferrous iron–bearing minerals as seen in their change in coloring, but Bochkeim (1997) has argued that the soils are dominated by physical weathering processes.

11.5. SHALLOW GROUNDWATER SEEPS AND WATER TRACKS

Liquid water outside of the ephemeral stream channels has been recognized in the MDV. MCM-LTER scientists described what they termed "subsurface ice melt seeps" in the mid-2000s (Harris et al., 2007; Lyons et al., 2005). The geochemistry of these waters was very different than the glacier meltwaters contributing to streamflow. Notable differences were elevated total dissolved soils (TDS), higher NO_3 concentrations, and generally more enriched water stable isotope signatures. These water sources were attributed to buried ice, perennial snow patches, and/or shallow groundwaters derived from permafrost thaw (Harris et al., 2007). These isotopic data suggested that some evaporation of the water had taken place, and the high TDS indicated either evapoconcentration and/or the dissolution of ions from older, salt-rich soils.

"Water tracks" are defined as zones of high soil moisture flowing downslope above the permanent ice table in the MDV (Levy et al., 2011). Like the seeps, they have high TDS, but the water tracks can exceed the seeps' TDS values by 1–2 orders of magnitude (Levy et al., 2011, 2012). They also have enriched water isotope values that suggest a mixture of recent snow and melted permafrost (Levy et al., 2011), and because of this have been linked to the previously mentioned soil water brines (Toner & Sletten, 2013). These features have water saturated thicknesses greater than the depth to the permanent ice cemented soil. This leads to water discharge onto the surface, making some seeps the result of water tracks (Levy et al., 2011). In these brackish to hypersaline waters, there is no consistent relationship between Ca and HCO_3, suggesting that these fluids are not actively involved in carbonate weathering.

11.6. STREAMS

As noted above, streamflow is primarily generated by glacier ice melt, which depends on the surface energy balance. Streams generally begin flowing in early December and cease flow in mid to late February. Short streams (~1 km) tend to have more consistent flow and low electrical conductivity, compared to long streams (>5 km) (Singley et al., 2017; Wlostowski et al., 2016). Streams in the MDV are connected to hyporheic zones along their lengths. These hyporheic zones are locations of rapid exchange of stream water during streamflow. However, at the beginning of the flow season, they are unsaturated and their pores represent a significant reservoir that must be filled before flow can persist downstream. Thus, in low flow years, longer streams are intermittent throughout the season. Because of the continuous sunlight during the austral summer flow season, daily stream hydrographs often have a distinct cycle of low flows through the morning and high flows in the evening. Streams can warm to 15 °C on warm, sunny afternoons (Cozzetto et al., 2006). Streambeds thaw to approximately 50–75 cm (which is more than the soil thaw depth in the MDV), providing the volume for hyporheic zones to occupy.

The cross-sectional areas of the hyporheic zones of streams in the Fryxell basin of TV range from 0.01 to 4.9 m^2, and residence times of water in them can be up to 1550 hrs (Gooseff et al., 2003, 2004; Koch et al., 2011; McKnight et al., 2004; Runkel et al., 1998). Thus, it is thought that long contact times, along with the

interaction of fresh mineral surfaces produced via freeze-thaw action, enhanced the chemical weathering rates in these environments, with modeled rates normalized to mineral surface area rivaling rates determined for plagioclase in temperate climates (Maurice, 2009). The thawing and refreezing of the hyporheic zones could occur on a regular basis, and during the freezing process, not only can minerals be broken and etched to produce fresh surfaces for subsequent weathering, but simple salts can be precipitated to be solubilized as the porewater thaws. This dynamic probably plays a significant role in controlling stream geochemistry over temporal scales, from daily to annual.

In general, the streams are unsaturated with respect to calcite, indicating that the dissolution of $CaCO_3$ is a major process, especially in the younger landscapes (Lyons et al., 2013) (Figure 11.3). This is supported by the fact that the stream waters are enriched in Ca to Mg compared to rivers and streams globally (Welch et al., 2010). The $^{87}Sr/^{86}Sr$ data also reflects a less radiogenic value, comparable to the local pedogenic carbonate found in soils (Lyons et al., 2020). This hypothesis is also substantiated by comparing alkalinity generated by aluminosilicate weathering to total alkalinity using the model of Hodson et al., (2000), where only between 4% and 21% of the total alkalinity found in the MDV streams apparently is generated through silicate weathering (Table 11.1). Having said this, aluminosilicate weathering is significant and can be demonstrated to be taking place in the hyporheic zones of these streams (Figure 11.4). Using small, plastic piezometers placed perpendicular to the stream flow, hyporheic zone samples were obtained at one location in Von Guerard Stream and analyzed for H_4SiO_4;

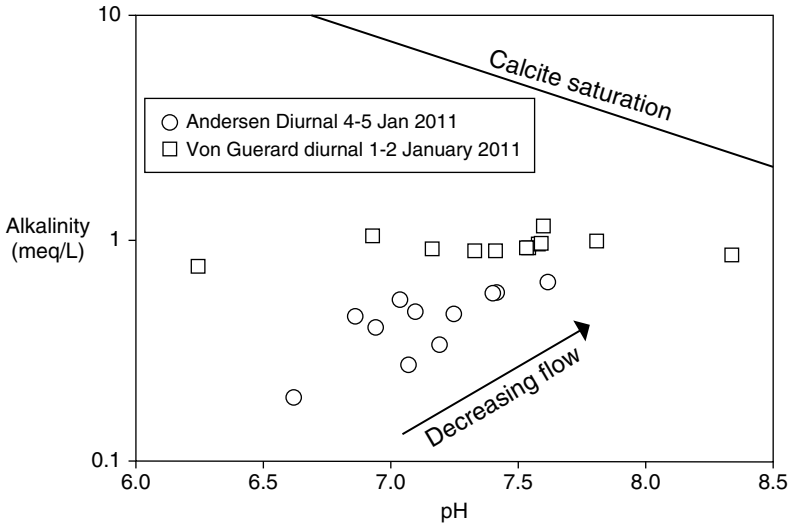

Figure 11.3 Alkalinity and pH in two MDV streams over a daily hydrograph.

Table 11.1 Mean values of titration alkalinity and H_4SiO_4 for McMurdo Dry Valley streams and calculated alkalinity due to aluminosilicate weathering.

	Stream	Alk (meq/L)	Si (mM)	Alk_{Si}^* (mM)	$\frac{Alk_{Si}}{Alk_T}$ %
Taylor Valley	Commonwealth	0.255	0.016	0.025	10
	McKnight	0.877	0.050	0.079	9
	Von Guerard	1.243	0.087	0.138	11
	Green	0.308	0.025	0.040	13
	Canada	0.200	0.025	0.040	20
	Andersen	0.403	0.018	0.028	7
	Priscu	0.956	0.043	0.068	7
Other	Miers	0.820	0.019	0.030	4
	Garwood	1.050	0.040	0.063	6
	Onyx	0.341	0.046	0.073	21

*Calculated from the technique of Hodson et al. (2000).

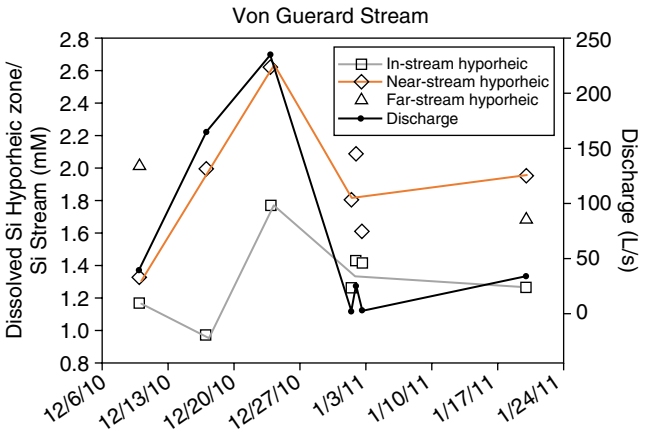

Figure 11.4 Dissolved Si in Von Guerard hyporheic zone relative to streamwater Si concentrations.

these values were then "normalized" to H_4SiO_4 in the stream water collected at the same time. The highest normalized values are observed during the highest flow sampled (Figure 11.4).

11.7. WEATHERING PROCESSES

11.7.1. Other Soil Processes/Cation Exchange and Authigenic $CaCo_3$ Production-Dissolution

Toner and Sletten (2013) have demonstrated that soil waters in TV evolve from Na-Cl brines to Ca-Cl ones at shallow depths within the soil column. This transformation is brought about through cation exchange reactions that involve the uptake of Na, derived through marine aerosol input, onto soil surfaces, liberating Ca and Mg from the soils. $CaCO_3$ dissolution also plays a role in controlling soil water interactions, which also contributes to high Ca values in these waters (Toner et al., 2013). Modeling indicates that after cation exchange is taken into account, upon freezing, Ca can be removed from these soil waters through calcite and gypsum precipitation (Toner & Sletten, 2013). Pedogenic carbonate in the form of calcite exists in soils throughout the MDV, averaging about 1.1% in the lowest elevation soils, 2.0% in the youngest soils, and in general, lower concentrations with depth and distance from the ocean (Foley et al., 2006). Stable O and C isotopic signatures of this pedogenic carbonate strongly indicate that the major source of carbon is atmospheric CO_2 and that it is formed by rapid evaporation of thin water films that become supersaturated with respect to calcite (Lyons et al., in press). The former observation is not surprising given the very low organic carbon concentrations in these soils (Burkins et al., 2000). The rates of pedogenic carbonate production are low (Foley et al., 2006) and may suggest the dynamic nature of $CaCO_3$ in these soils, where it can be both produced and removed, depending on the physiochemical state of the soil. Ca isotope measurements in the ephemeral streams in the MDV also suggest dynamic behavior of $CaCO_3$ in these systems in that in some locations (or perhaps even at the same location, but at difference times), calcite can be precipitated and at others it can be dissolved (Lyons et al., 2016).

11.7.2. Aluminosilicate Weathering by Shallow Groundwaters

Previously unpublished H_4SiO_4 data from six of the seep waters collected by Harris et al. (2007) range between 72 and 175 μM with a mean of 117 μM. Eighty-six water track samples collected during the 2014–2015 austral summer had H_4SiO_4 concentrations of 1–670 μM with a mean of 180 μM (J. S. Levy and others, unpublished data); if the two highest sample values (657,670) are removed, the mean value for this large data set reduces to 168 μM. Clearly these waters originating from the shallow subsurface have much higher dissolved Si concentrations than the stream waters in TV (Welch et al., 2010), indicating that they are responsible for enhanced aluminosilicate weathering in this polar desert environment. Higher rock/water ratios and/or the highly saline nature of these waters may be responsible for the high H_4SiO_4 values observed.

11.7.3. Weathering in Streambeds

The hyporheic zones, through which stream water exchanges throughout the flow season, promote rapid weathering by moving dilute glacial meltwater into intimate contact with sediment surfaces that are relatively "fresh" geologically speaking and ready to react. These surprisingly high weathering rates were originally identified from analyses of dissolved Si concentrations and an assessment of the "watershed" that could contribute to these dissolved loads (Lyons et al., 1997, 1998). Nezat et al. (2001) calculated approximate watershed areas for MDV streams, estimating the watershed dimensions to be the length of the stream with a fixed width of 4 m. Synoptic sampling along MDV streams revealed that concentrations of most major ions increased in the downstream direction (Gooseff et al., 2002). These patterns, when simulated with a reactive transport model, can account for dissolution of streambed sediments, indicating some of the highest weathering rates in the world (Gooseff et al., 2002).

Recently, Wlostowski et al. (2018) have also identified the MDV streams as chemostatic: that is, for changes in stream discharge over several orders of magnitude, stream dissolved ion concentrations change very little

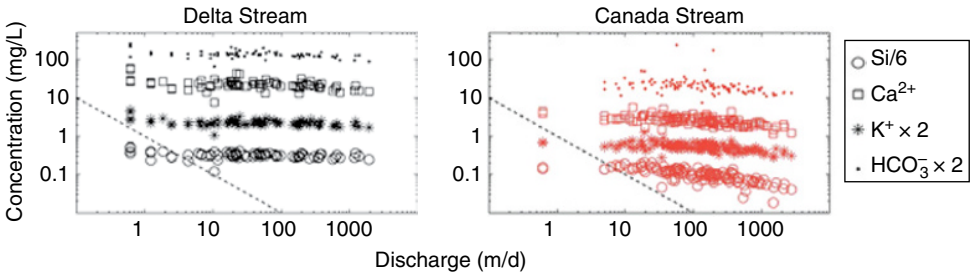

Figure 11.5 Chemostasis of silica, calcium, potassium, and bicarbonate in Delta Stream, a long stream (7.5 km), and Canada Stream, a short stream (0.7 km). Dashed line is the 1:1 line of perfect dilution in these log-log plots. (*Source:* Wlostowski et al., 2018.)

(Figure 11.5). This phenomenon is observed in many temperate streams around the world (Godsey et al., 2009). The challenge to understanding weathering solute dynamics in temperate streams is that their catchments are relatively large in volume (i.e. soil depths to bedrock may be tens of meters, and catchments are areas generally bounded by topology) and can therefore store a lot of old water in their aquifers. So chemostasis in temperate streams may be due to changes in the water source to streams with more older, high-concentration water contributing at high-flow conditions. As we described above, the watershed volumes of the MDV streams are quite small, and there is little capacity to hold extensive reservoirs of water. Thus, rapid weathering of the silicates in the streambed is the most plausible explanation for chemostasis in these streams. Wlostowski et al. (2018) use a fairly simple reactive transport model to simulate solute concentrations over several orders of magnitude of streamflow.

11.8. IMPLICATIONS OF MELTING BURIED ICE

Stream channel landscapes are changing due to the melting of buried ice (Fountain et al., 2014; Gooseff et al., 2016). Stream bank and bed erosion occurred in Crescent Stream, Taylor Valley, in January 2012 (Figure 11.6). A thermokarst tunnel (~20 km long) transferred water downstream with significant bank erosion along 3 km of the stream. This sediment influx increased the dissolution of Na, Cl, and NO_3 when comparing the inflow to the outflow. If increases in solar radiation occur, these areas would be prone to thaw and be major sources of solutes to the stream water.

11.9. CONCLUSIONS

Over 20 years of research in the MDV demonstrate that chemical weathering is surprisingly high in this dry, cold landscape. From a thermodynamic perspective, the low temperatures would be expected to retard weathering rates. Similarly, the cold conditions, which do not allow

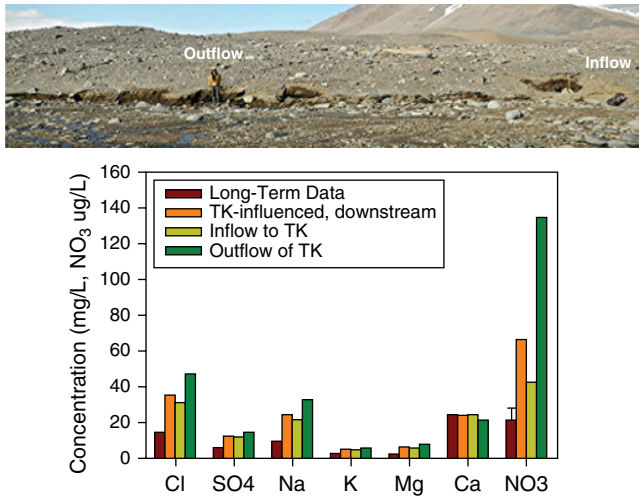

Figure 11.6 Stream channel erosion on Crescent Stream. Solute concentrations are compared to MCM-LTER long-term data (www.mcmlter.org), downstream thermokarst influence, thermokarst inflow, and thermokarst outflow.

for any rain events and no overland flow (excepting water tracks), would also potentially inhibit weathering rates. However, the MDVs have several locations where enhanced liquid water occurs (seeps, water tracks, and streams) and rapid silicate weathering of relatively unweathered minerals takes place. Even with small water volumes and holding capacity, rapid silicate weathering is the most plausible explanation supporting chemostasis observed in the stream water chemistry, which is a similar observation in many temperate streams around the world.

With changing austral summer climate conditions, either increased solar radiation or warming temperatures or both will increase glacier and buried ice melt and permafrost thaw. In addition, a longer duration of the melt could also occur. Much "potential" liquid water exists in the system, but it is currently sequestered as ice. Temperature variations as small as ~0 °C can have profound impacts on liquid water production in the MDV

(Doran et al., 2002). Although chemical weathering rates may change little with a small temperature increase in these systems, it is hypothesized that with increased flow, the hyporheic zones of the fixed stream channels will increase in size, thereby enhancing the production of soluble weathering by-products, as minerals previously not in contact with liquid water will interact during increased water flows. In addition, near-surface permafrost thaw will increase "water tracks" that will in turn solubilize salts from previously dry soils. Clearly, a warming climate will enhance both weathering and soil development in this currently very arid and waterless environment. Ongoing monitoring will be needed in order to assess the impact of climate change and variability on both the terrestrial and fluvial components of this unusual landscape.

ACKNOWLEDGMENTS

This work was supported by NSF grants OPP-ANT- OPP 1637708, 1115245, 0423595, 9810219, and 921177. We are grateful to the many researchers, staff, and students for collecting and analyzing these data. We are especially thankful to Dr R.S Harmon, the University of Colorado's Stream Team led by Dr D.M McKnight. The MCM-LTER long-term data repository is available at http://mcm.lternet.edu/.

REFERENCES

Anderson, S. P. (2007). Biogeochemistry of glacial landscape systems. *Annu. Rev. Earth Planet. Sci.*, *35*, 375–399.

Bisson, K. M., Welch, K. A., Welch, S. A., Sheets, J. M., Lyons, W. B., Levy, J. S., & Fountain, A. G. (2015). Patterns and processes of salt efflorescences in the McMurdo region, Antarctica. *Arctic, Antarctic, and Alpine Research*, *47*(3), 407–425. DOI: 10.1657/AAAR0014-024

Bockheim, J. G. (1997). Properties and classification of Cold Desert soils from Antarctica. *Soil Sceince Society of America Journal*, *61*, 224–231.

Bruno, L. A., Baur, H., Graf, T., Schluchter, C., Signer, P., & Wieler, R. (1997). Dating of Sirius Group tillites in the Antarctic Dry Valleys with cosmogenic 3 He and 21 Ne. *Earth and Planetary Science Letters*, *147*(1), 37–54.

Burkins, M. B., Virginia, R. A., Chamberlain, C. P., & H, W. D. (2000). Origin and distribution of soil organic matter in Taylor Valley, Antarctica. *Ecology*, *81*(9), 2377–2391.

Campbell, I. B., Claridge, G.G.C., Campbell, D. I., & Balks, M. R. (1998). The soil environment of the McMurdo Dry Valleys, Antarctica. In J.C. Priscu (Ed.), *Ecosystem dynamics in a polar desert: The McMurdo Dry Valleys, Antarctica* (vol. *72*, pp. 297–322). Washington, DC: American Geophysical Union Antarctic Research Series.

Conca, J., & Wright, J. (1987). The aqueous chemistry of weathering solutions in dolerite of the Allan Hills, Victoria Land, Antarctica. *Antarctic Journal of the U.S.*, *22*, 42–44.

Cozzetto, K., McKnight, D. M., Nylen, T., & Fountain, A. G. (2006). Experimental investigations into processes controlling stream and hyporheic temperatures, Fryxell Basin, Antarctica. *Advances in Water Resources*, *29*, 130–153. http://dx.doi.org/10.1016/j.advwatres.2005.04.012

Deuerling, K. M., Martin, J. B., Martin, E. E., & Scribner, C. A. (2018). Hydrologic exchange and chemical weathering in a proglacial watershed near Kangerlussuaq, west Greenland. *Journal of Hydrology*, *556*, 220–232. https://doi.org/10.1016/j.jhydrol.2017.11.002

Doran, P. T., McKay, C. P., Clow, G. D., Dana, G. L., Fountain, A. G., Nylen, T., & Lyons, W. B. (2002). Valley floor climate observations from the McMurdo dry valleys, Antarctica, 1986–2000. *Journal of Geophysical Research: Atmospheres*, *107*, 1–12. https://doi.org/10.1029/2001JD002045

Foley, K. W., Lyons, B., Barrett, J. E., & Virginia, R. A. (2006). Pedogenic carbonate distribution within glacial till in Taylor Valley, Southern Victoria Land, Antarctica. In A. M. Alonso-Zarza & L. H. Tanner, *Paleoenvironmental record and applications of calcretes and palustrine carbonates* (pp. 89–103). Geological Society of America. doi:10.1130/2006.2416(06)

Fountain, A. G., Levy, J. S., Gooseff, M. N., & Van Horn, D. J. (2014). The McMurdo Dry Valleys: A landscape on the threshold of change. *Geomorphology*, *225*, 25–35.

Fountain, A. G., McKnight, D. M., Lyons, W. B., Burkins, M. B., Dana, G. L., Doran, P. T., et al. (1999). Physical controls on the Taylor Valley ecosystem. *BioScience*, *49*(12), 961–971. https://doi.org/10.2307/1313730

Fountain, A. G., Nylen, T. H., Monaghan, A., Basagic, H. J., & Bromwich, D. (2010). Snow in the McMurdo Dry Valleys, Antarctica. *International Journal of Climatology*, *30*(5), 633–642. https://doi.org/10.1002/joc.1933

Godsey, S. E., Kirchner, J. W., & Clow, D. W. (2009). Concentration–discharge relationships reflect chemostatic characteristics of US catchments. *Hydrological Processes*, *1864*(May), 1844–1864. https://doi.org/10.1002/hyp

Gooseff, M. N., McKnight, D. M., Lyons, W. B., & Blum, A. E. (2002). Weathering reactions and hyporheic exchange controls on stream water chemistry in a glacial meltwater stream in the McMurdo Dry Valleys. *Water Resources Research*, *38*(12), WR000834.

Gooseff, M. N., McKnight, D. M., Runkel, R. L., & Duff, J. H. (2004). Denitrification and hydrologic transient storage in a glacial meltwater stream, McMurdo Dry Valleys, Antarctica. *Limnology and Oceanography*, *49*(5), 1884–1895.

Gooseff, M. N., McKnight, D. M., Runkel, R. L., & Vaughn, B. H. (2003). Determining long time-scale hyporheic zone flow paths in Antarctic streams. *Hydrological Processes*, *17*(9), 1691–1710.

Gooseff, M. N., Van Horn, D., Sudman, Z., McKnight, D. M., Welch, K. A., & Lyons, W. B. (2016). Stream biogeochemical and suspended sediment responses to permafrost degradation in stream banks in Taylor Valley, *Antarctica. Biogeosciences*, *13*(6), 1723–1732. https://doi.org/10.5194/bg-13-1723-2016

Green, W. J., Angle, M. P., & Chave, K. E. (1988). The geochemistry of Antarctic streams and their role in the evolution of four lakes of the McMurdo Dry Valleys. *Geochimica et Cosmochimica Acta*, *52*, 1265–1274.

Hall, B. L., & Denton, G. H. (2000). Radiocarbon chronology of Ross Sea drift, eastern Taylor Valley, Antarctica: Evidence for a grounded ice sheet in the Ross Sea at the last glacial maximum. *Geografiska Annaler*, *82A*, 305–336.

Harris, K. J., Carey, A. E., Lyons, W. B., Welch, K. A., & Fountain, A. G. (2007). Solute and isotope geochemistry of subsurface ice melt seeps in Taylor Valley, Antarctica. *Geological Society of America Bulletin*, *119*(5), 548–555. http://dx.doi.org/10.1130%252FB25913.1

Hartmann, J., Moosdorf, N., Lauerwald, R., Hinderer, M., & West, J. (2014). Global chemical weathering and associated P-release: The role of lithology, temperature and soil properties. *Chemical Geology*, *363*, 145–163. https://doi.org/10.1016/j.chemgeo.2013.10.025

Hendy, C. H. (2000). Late Quaternary lakes in the McMurdo Sound regions of Antarctica. *Geografiska Annaler*, *82*(2–3), 411–432. https://doi.org/10.1111/j.0435-3676.2000.00131.x

Hodson, A, Tranter, M., & Vatne, G. (2000). Contemporary rates of chemical denudation and atmospheric CO_2 sequestration in glacier basins: An Arctic perspective. *Earth Surface Processes and Landforms*, *25*(13), 1447–1471.

Ivy-Ochs, S., Schlüchter, C., Kubik, P. W., Dittrich-Hannen, B., & Beer, J. (1995). Minimum ^{10}Be exposure ages of early Pliocene for the Table Mountain plateau and the Sirius Group at Mount Fleming, Dry Valleys, Antarctica. *Geology*, *23*(11), 1007–1010. doi: https://doi.org/10.1130/0091-7613(1995)023<1007:MBEAOE>2.3.CO;2

Keller, K., Blum, J. D., & Kling, G. W. (2007). Geochemistry of soils and streams on surfaces of varying ages in arctic Alaska. *Arctic, Antarctic, and Alpine Research*, *39*(1), 84–98. DOI: 10.1657/1523-0430(2007)39[84:GOSASO]2.0.CO;2

Keys, J. R., & Williams, K. (1981). Origin of crystalline, cold desert salts in the McMurdo region, Antarctica. *Geochimica et Cosmochimica Acta*, *45*, 2299–2309.

Koch, J. C., McKnight, D. M., & Neupauer, R. M. (2011). Simulating unsteady flow, anabranching, and hyporheic dynamics in a glacial meltwater stream using a coupled surface water routing and groundwater flow model. *Water Resources Research*, *47*, W05530. doi:10.1029/2010WR009508

Levy, J. (2013). How big are the McMurdo Dry Valleys? Estimating ice-free area using Landsat image data. *Antarctic Science*, *25*(1), 119–120. doi:10.1017/S0954102012000727

Levy, J. S., Fountain, A. G., Dickson, J. L., Head, J. W., Okal, M., Marchant, D. R., & Watters, J. (2013). Accelerated thermokarst formation in the McMurdo Dry Valleys, Antarctica. *Scientific Reports*, *3*, 2269. http://dx.doi.org/10.1038/srep02269

Levy, J. S., Fountain, A. G., Gooseff, M. N., Welch, K. A., & Lyons, W. B. (2011). Water tracks and permafrost in Taylor Valley, Antarctica: Extensive and shallow groundwater connectivity in a cold desert ecosystem. *Geological Society of America Bulletin*, *123*, 2295–2311.

Levy, J. S., Fountain, A. G., Obryk, M. K., Telling, J., Glennie, C., Pettersson, R., et al. (2018). Geomorphology Decadal topographic change in the McMurdo Dry Valleys of Antarctica: Thermokarst subsidence, glacier thinning, and transfer of water storage from the cryosphere to the hydrosphere. *Geomorphology*, *323*, 80–97. https://doi.org/10.1016/j.geomorph.2018.09.012

Levy, J. S., Fountain, A. G., Welch, K. A., & Lyons, W. B. (2012). Hypersaline "wet patches" in Taylor Valley, *Antarctica. Geophysical Research Letters*, *39*, L05402, doi:10.1029/2012GL050898.

Lyons, W. B., Bullen, T., & Welch, K. A. (2017) Ca isotopic geochemistry of an Antarctic aquatic system. *Geophysical Research Letters*, *44*, 882–891.

Lyons, W. B., Deuerling, K., Welch, K. A., Welch, S. A., Michalski, G., Walters, W. W., et al. (2016). The soil geochemistry in the Beardmore Glacier region, Antarctica: Implications for terrestrial ecosystem history. *Scientific Reports*, *6*, 26189. https://doi.org/10.1038/srep26189

Lyons, B., Foley, K., Carey, A., Diaz, M., Bowen, G., & Cerling, T. (2020). The isotopic geochemistry of CaCO3 encrustations in Taylor Valley, Antarctica: Implications for their origin. *Acta Geographic Slovenica*, *60*(2). doi:https://doi.org/10.2986/AGS.7233.

Lyons, W. B., Frape S. K, & Welch, K. A. (1999). History of McMurdo Dry Valley lakes, Antarctica, from stable chlorine isotope data. *Geology*, *27*(6), 527–530. https://doi.org/10.1130/0091-7613(1999)027<0527:HOMDVL>2.3.CO;2

Lyons,W.B., Leslie,D.L., Newmann,K., Harmon,R., Welch,K.A., Bisson,K.,et al.(2013). The carbon stable isotope biogeochemistry of streams, *Taylor Valley, Antartica, Applied Geochemistry*, 32, 26–36. https://doi.org/10.1016/j.apgeochem.201.

Lyons, W. B., Welch, K. A., Carey, A. E., Doran, P. T., Wall, D. H., Virginia, R. A., et al. (2005). Groundwater seeps in Taylor Valley Antarctica: An example of a subsurface melt event. *Annals of Glaciology*, *40*, 200–206.

Lyons, W. B., Welch, K. A., Neumann, K., Toxey, J. K., McArthur, R., Williams, C., et al. (1998). Geochemical linkages among glaciers, streams, and lakes within the Taylor Valley, Antarctica. In J. C. Priscu (Ed.), *Ecosystem dynamics in a polar desert: The McMurdo Dry Valleys, Antarctica* (vol. *73*). Washington, DC: American Geophysical Union.

Lyons, W. B., Welch, K. A., Nezat, C. A., Crick, K., Toxey, J. K., Mastrine, J. A., & McKnight, D. M. (1997). Chemical weathering rates and reactions in the Lake Fryxell Basin, Taylor Valley: Comparison to temperate river basins. In W. B. Lyons, C. Howard-Williams, & I. Hawes (Eds.), *Ecosystem processes in Antarctic ice-free landscapes* (pp. 147–154). Balkema Press.

Maurice, P. A. (2009). *Environmental surfaces and interfaces from the nanoscale to the global scale: A textbook*. John Wiley & Sons.

McKnight, D. M., Niyogi, D. K., Alger, A. S., Bomblies, A., Conovitz, P. A., & Tate, C. M. (1999). Dry valley streams in Antarctica: Ecosystems waiting for water. *BioScience*, *49*(12), 985–995.

McKnight, D. M., Runkel, R. L., Tate, C. M., Duff, J. H., & Moorhead, D. (2004). Inorganic N and P dynamics of Antarctic glacial meltwater streams as controlled by hyporheic exchange and benthic autotrophic communities. *Journal of the North American Benthological Society*, *23*(2), 171–188.

Nezat, C. A., Lyons, W. B., & Welch, K. A. (2001). Chemical weathering in streams of a polar desert (Taylor Valley, Antarctica). *Geological Society of America Bulletin*, *113*(11), 1401–1408.

Nishiizumi, K., Kohl, C. P., Arnold, J. R., Klein, J., Fink, D., & Middleton, J. L. (1991). Cosmic ray produced ^{10}Be and ^{26}Al in Antarctic rocks: Exposure and erosion history. *Earth Planet. Sci. Lett.*, *104*, 440–454.

Runkel, R. L., McKnight, D. M., & Andrews, E. D. (1998). Analysis of transient storage subject to unsteady flow: Diel flow variation in an Antarctic stream. *Journal of the North American Benthological Society*, *17*, 143–154.

Singley, J. G., Wlostowski, A. N., Bergstrom, A. J., Sokol, E. R., Torrens, C. L., Jaros, C., et al. (2017). Characterizing hyporheic exchange processes using high-frequency electrical conductivity-discharge relationships on subhourly to interannual timescales. *Water Resources Research*, *53*(5), 4124–4141. https://doi.org/10.1002/2016WR019739

Sudman, Z., Gooseff, M. N., Fountain, A. G., Levy, J. S., Obryk, M. K., & Van Horn, D. (2017). Impacts of permafrost degradation on a stream in Taylor Valley, Antarctica. *Geomorphology*, *285*, 205–213. https://doi.org/10.1016/j.geomorph.2017.02.009

Summerfield, M. A., Stuart, F. M., Cockburn, H.A.P., Sugden, D. E., Denton, G. H., Dunai, T., & Marchant, D. R. (1999). Long-term rates of denudation in the Dry Valleys, Transantarctic Mountains, southern Victoria Land, Antarctica based on in-situ-produced cosmogenic. *Geomorphology*, *27*, 113–129. doi: 10.1016/S0169-555X(98)00093-2

Tank, S. E., Raymond, P. A., Striegl, R. G., McClelland, J. W., Holmes, R. M., Fiske, G. J., & Peterson, B. J. (2012), A land-to-ocean perspective on the magnitude, source and implication of DIC flux from major Arctic rivers to the Arctic Ocean. *Global Biogeochem. Cycles*, *26*, GB4018. doi:10.1029/2011GB004192

Toner, J. D., & Sletten, R. S. (2013). The formation of Ca-Cl-rich groundwaters in the Dry Valleys of Antarctica: Field measurements and modeling of reactive transport. *Geochemica et Chosmochimica Acta*, *110*, 84–105.

Toner, J. D., Sletten, R. S., & Prentice, M. L. (2013). Soluble salt accumulations in Taylor Valley, Antarctica: Implications for paleolakes and Ross Sea Ice Sheet dynamics, *J. Geophys. Res. Earth Surf.*, *118*, 198–215. doi:10.1029/2012JF002467

Tranter, M. (2003) Geochemical weathering in glacial and proglacial environments. In J. I. Drever (Ed.), *Treatise on geochemistry* (vol. *5*, pp. 189–205). Elsevier. DOI: 10.1016/B0-08-043751-6/05078-7

Wadham, J. L., Tranter, M., Skidmore, M., Hodson, A. J., Priscu, J., Lyons, W. B., et al. (2010). Biogeochemical weathering under ice: Size matters. *Global Biogeochem. Cycles*, *24*, GB3025. doi:10.1029/2009GB003688

Welch, K. A., Lyons, W. B., Whisner, C., Garnder, C. B., Gooseff, M. N., McKnight, D. M., & Priscu, J. C. (2010). Spatial variations in the geochemistry of glacial meltwater streams in the Taylor Valley, Antarctica. *Antarctic Science*, *22*, 662–672.

Wlostowski, A. N., Gooseff, M. N., McKnight, D. M., Jaros, C., & Lyons, W. B. (2016). Patterns of hydrologic connectivity in the McMurdo Dry Valleys, Antarctica: A synthesis of 20 years of hydrologic data. *Hydrological Processes*, *30*(17), 2958–2975. https://doi.org/10.1002/hyp.10818

Wlostowski, A. N., Gooseff, M. N., McKnight, D. M., & Lyons, W. B. (2018). Transit times and rapid chemical equilibrium explain chemostasis in glacial meltwater streams in the McMurdo Dry Valleys, Antarctica. *Geophysical Research Letters*, *45*, 13322–13331. https://doi.org/10.1029/2018GL080369

12

Carbon and Nutrient Fluxes Within Southeastern Piedmont Critical Zones

Todd C. Rasmussen, Maryam Foroughi, and Daniel Markewitz

ABSTRACT

The critical zone encompasses terrestrial and aquatic systems that extend from local (soil pedon) to continental (watershed) scales, with heterogeneous fate and transport processes across these systems and scales. We present an exploratory analysis of carbon and nutrient fluxes on a Southeastern US landscape: from forest soils, subsurface transport to rivers and streams, and then to and within lakes. Data from field studies in the warm-humid Southeastern Piedmont (Calhoun Critical Zone Observatory, Lake Lanier) are used to develop a conceptual model of interactions between carbon, nitrogen, phosphorus, organic matter, clays, and iron within the critical zone, which is useful for long-term soil, watershed, and lake management. We see modest, positive relationships between iron, carbon, and nutrients at pedon scales along a hillslope that extends to streams and lakes. While this association is phenomenological, and thus variable, it can be ascribed to fundamental chemical and physical processes. Sorption of phosphorus and ammonium to colloidal iron, organic matter, and clay allows the subsurface migration of each to lotic aquatic systems (first- to fifth-order streams), where they are transported into lentic environments (lakes, wetlands, estuaries). A better understanding of these processes can lead to improved management and control of phytoplankton and eutrophication in these systems.

12.1. INTRODUCTION

Forests once dominated southeastern landscapes in the United States, from fire-dominated longleaf-pine and wiregrass communities on the Coastal Plain to mixed hardwood-conifer communities on the Piedmont and Appalachian Highlands (Whitney, 1994). Soils with high organic matter were abundant in the Piedmont, with topsoil being described by early settlers as dark and rich. This changed with the deforestation and onset of large-scale agriculture, which reached a peak between 1860 and 1920 (Trimble, 1972).

Warnell School of Forestry and Natural Resources, University of Georgia, Athens, GA, USA

Widespread soil loss due to land-disturbing activities slowed dramatically during the 1920s and 30s, primarily due to agricultural pests (e.g., boll weevils) and market forces (i.e., the Great Depression). Reforestation since then has increased forest cover, resulting in declining soil losses and increasing soil organic matter accumulation (Lamon et al., 2007; Richter & Markewitz, 2001). In addition, the construction of reservoirs for hydropower, flood-control, recreation, navigation, and water supply has provided lentic conditions for sediment and nutrient accumulation.

Yet modern agricultural and municipal development continue to affect southeastern soils and aquatic habitats, especially organic matter and nutrient cycling. Wastewater treatment plants discharge point-sources of carbon and nutrients, while row-crop agriculture and land-application of poultry manure on pasturelands contribute to

Hydrogeology, Chemical Weathering, and Soil Formation, Geophysical Monograph 257, First Edition.
Edited by Allen Hunt, Markus Egli, and Boris Faybishenko.

DOI: 10.1002/9781119563952.ch12

nonpoint sources of carbon and nutrients to rivers, streams, and reservoirs.

The combination of point and nonpoint inputs adversely affects aquatic ecosystems due to eutrophication, as well as municipal drinking-water treatment costs. For example, Lake Lanier is a large reservoir used by the Atlanta Metropolitan Area in North Georgia that is used for recreation and drinking water. Occasional nutrient-driven algae blooms lead to aquatic impairment and increased municipal drinking water treatment costs.

We place these environmental-management challenges in the context of the critical zone, which incorporates environmental processes that extend from pedon (local) to landscape (watershed) scales (White et al., 2015). Understanding how these processes respond to point and nonpoint carbon and nutrient loadings is central for promoting environmental sustainability by increasing system resiliency and reducing vulnerability to degradation.

This study summarizes components of our current understanding relating to processes and factors that account for carbon and nutrient mobility within soils, streams, and lakes. Many southeastern soils have deep subsoils that are enriched in iron and clay minerals, both of which affect carbon and nutrient transport within soils, as well as within rivers and lakes (West et al., 2017). Colloidal iron and clays react with organic matter, dissolved nitrogen, and phosphorus to form complexes that can either promote retention or support transport. We use this understanding to present a conceptual model that can be used for further research and management of environmental systems within the southeastern Piedmont.

12.1.1. Geographic Setting

The southeastern Piedmont is a rapidly developing region that occupies the landscape between the Appalachian highlands and the southeastern Coastal Plain (Figure 12.1). The region has developed substantially since the Second World War after emerging from destitute poverty following the collapse of the Cotton Era that extended from 1840 to 1930. Unlike today, where modern commerce and agriculture supports unprecedented growth, the Cotton Era was a period when soils were managed unsustainably, leading to erosion and loss of productivity (Trimble, 1972). This legacy endures through depleted topsoil, gullies, aggraded stream channels, and loss of reservoir storage due to sediment entrainment (Jackson et al., 2005). In addition to physical alteration of the landscape, the soils have been depleted of carbon and nitrogen, and in some cases contain enriched phosphorous and calcium due to agricultural inputs that have been slow to recover to their natural conditions (Foroughi, 2019).

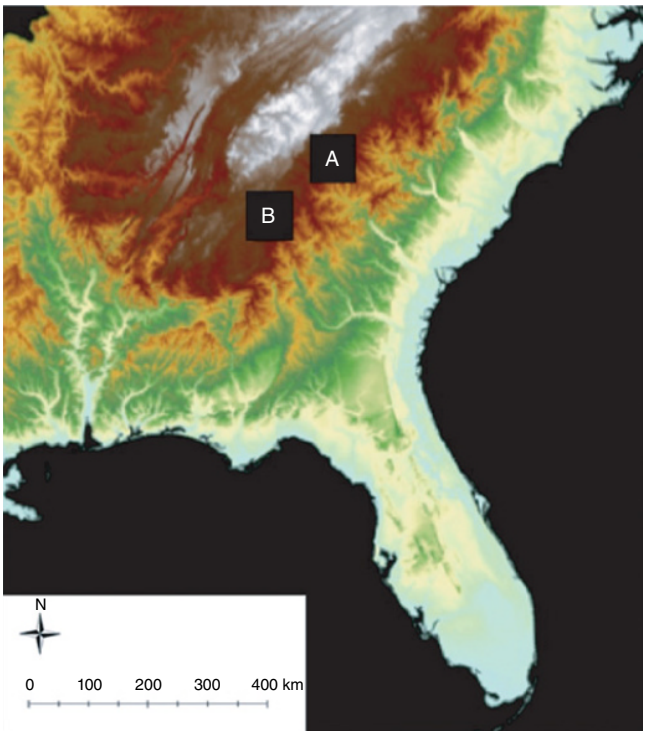

Figure 12.1 Shaded relief map of the Southeastern United States showing the Calhoun Experimental Forest (A) and Lake Lanier (B).

The Calhoun Critical Zone Observatory (Calhoun CZO), which incorporates the Calhoun Experimental Forest, is located in the Piedmont region of South Carolina (Figure 12.1, "A") in the US Department of Agriculture (USDA) Forest Service's Sumter National Forest. The mean annual temperature and precipitation of the Calhoun CZO are approximately 17 °C and 1260 mm, respectively. Elevations range from 120 to 180 m amsl. Upland soils are typically acidic, highly weathered Ultisols, while floodplain soils are Entisols (Richter et al., 2015). The Calhoun CZO area has a history of severe surface erosion (~17 cm during the Cotton Era) from cotton, corn, wheat, and other crops that were cultivated from 1800 until agricultural lands were abandoned in the early 20th century (Hayes et al., 2014; Richter & Markewitz, 2001). The legacy effect of agriculture and its replacement by forested ecosystems is currently being investigated at this site (Richter et al, 2015).

Lake Lanier (managed by the US Army Corps of Engineers) is 240 km west of the Calhoun CZO on the same landscape position within the southeastern Piedmont (Figure 12.1, "B"). Lake Lanier is one of many reservoirs, both small and large, that have been constructed in the last 70 years for hydropower, navigation, water supply, recreation, and flood control. Lake Lanier

experiences hypereutrophic conditions in the upper sections and mesotrophic conditions near the dam. Mean residence times in the reservoir approach 500 days, and the water column is vertically stratified from May through December (Zeng & Rasmussen, 2005). Two fourth-order streams, the Chattahoochee and Chestatee Rivers, and numerous smaller tributaries feed the reservoir from watersheds that drain from the adjacent Piedmont and Blue Ridge physiographic provinces. In addition, the effects of legacy and modern agriculture, along with rapidly growing populations, is the focus of ongoing studies at this site (Zeng & Rasmussen, 2005; Zeng et al., 2006).

Lake water quality concerns include both point and nonpoint sources of pollution. Nonpoint sources are ubiquitous, including eight landfills, numerous onsite septic disposal systems, nearby land application of dairy and poultry wastes, and stormwater runoff from agricultural and rapidly expanding urban sources. Point sources include 13 municipal wastewater treatment plants and 33 private and industrial facilities (Hatcher, 1994, 1998).

12.1.2. Conceptual Model Definition

Figures 12.2 and 12.3 present our proposed conceptual model of carbon and nutrient fluxes within southeastern Piedmont critical zones. While precipitation drives the hydrologic cycle, carbon and nutrient fluxes are primarily driven by landscape sources and sinks. The redistribution of soil carbon and nutrients is controlled by evaporation and plant water uptake that supports nutrient uptake and productivity, and by downslope losses to aquatic systems via surface and subsurface pathways. The historical alteration of the southeastern Piedmont landscape resulted in soils depleted in carbon and nutrients (although see P and Ca caveats above), with concomitant accumulation in floodplains as well as in stream and lake sediments.

Our model assumes that carbon (C) is found in soil and dissolved organic matter, standing biomass, and in inorganic forms, including dissolved carbonates (e.g., carbon dioxide, carbonic acid, bicarbonate, carbonate) or minerals (e.g., calcium carbonate, siderite). The relative

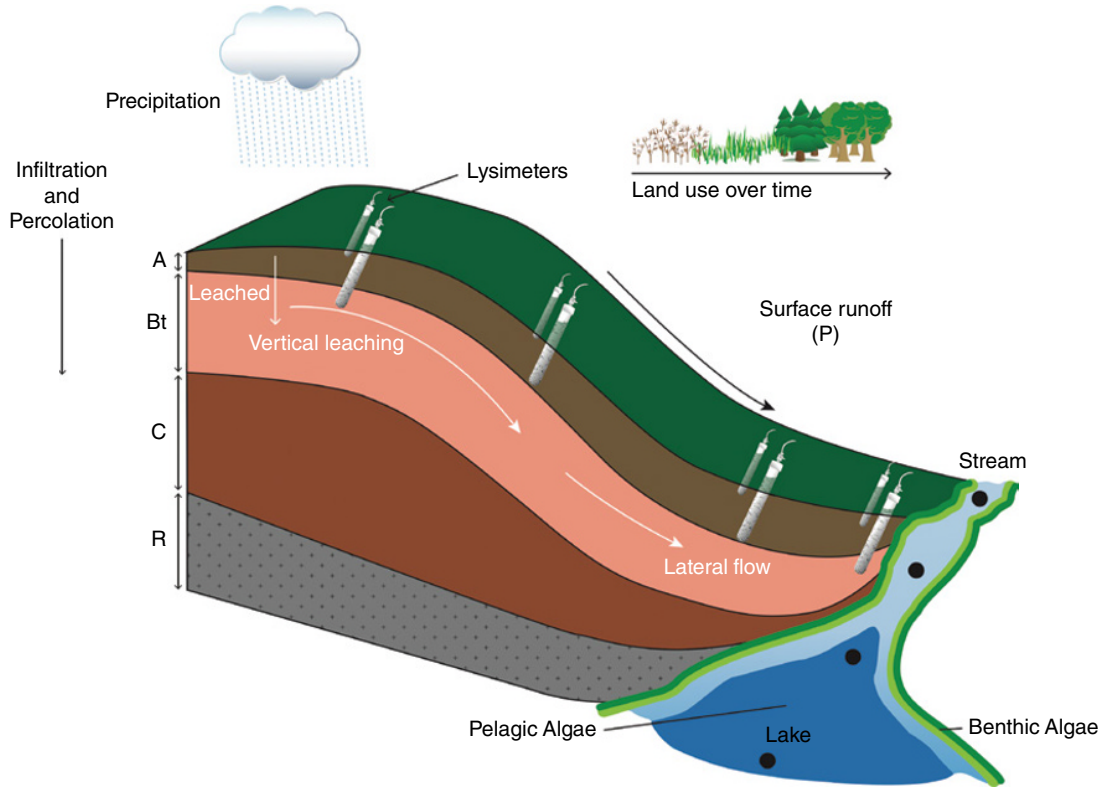

Figure 12.2 Conceptual landscape model of carbon and nutrient flux processes at hillslope, stream, and lake scales. Hillslope processes include surface runoff (overland flow), infiltration and percolation, vertical leaching, and lateral flow. Channel and lake processes include benthic and pelagic transport of inorganic (dissolved and suspended sediment) and organic (algae) carbon and nutrients. Land use changed from row-crop agriculture, to abandoned fields, to forests (upper inset). A, Bt, C, and R refers to soil master horizons. Black dots in stream and lake refer to sampling locations.

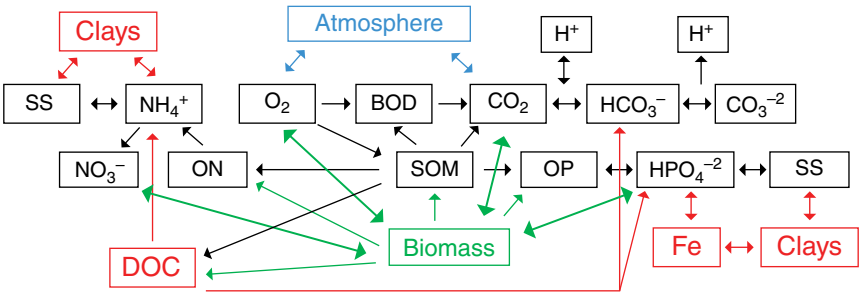

Figure 12.3 Conceptual model of carbon and nutrient cycling in Lake Lanier, a Southeastern Piedmont impoundment. Green indicates biomass components, while red highlights the processes that are the focus of this investigation. SS = suspended solids, DOC = dissolved organic carbon, ON = organic nitrogen, OP = organic phosphorus, SOM = soil/sediment organic matter. BOD = biochemical oxygen demand.

abundance of inorganic C is determined, in large part, by soil or water acidity (i.e. pH), while the abundance of organic C reflects the balance of photosynthesis and decomposition at the large scale and local physiochemical conditions that alter the decomposition rates (e.g. O_2 content, abundance of mineral sorbents, microbial activity) (Schmidt et al., 2011). Nutrients are also found in organic and inorganic forms: as either ammonium/ammonia (pH dependent), nitrate, nitrite, or N_2 gas (redox dependent) for nitrogen, or as the multiple forms of H_3PO_4 that are also pH dependent. Ammonium, in particular, is strongly sorbed to clay mineral surfaces (Kleber et al., 2007).

Alfred Redfield first reported in 1934 (Redfield, 1934) a remarkable consistency in nitrate and phosphate data from various ocean waters at a molar ratio of 20:1 that was later refined to 16:1, and expanded to include C to define the well-known molar Redfield ratio of C:N:P in marine systems, 106:16:1. In aquatic systems at circum-neutral pH, the Redfield equation can be written as (Hatcher, 1998)

$$106\,HCO_3^- + 16\,NO_3^- + HPO_4^{-2} + 16\,H_2O + 124\,H^+ + \text{energy} \Rightarrow (CH_2O)_{106}(NH_3)_{16}(H_3PO_4) + 138\,O_2. \quad (1)$$

Nitrates are commonly found where sufficient oxidation is present (e.g. wastewater treatment plants) and are less likely to sorb to clays. Phosphorus is strongly bound to positively charged iron (oxyhydr)oxides, but only for specific pH (<8.5) and redox (DO > 1 mg/L) conditions. Phosphate is released as the hydroxide ion becomes more abundant at increasing pH. Also, iron bound to clays can be transported by colloid-assisted transport.

This conceptual model posits that (1) pH and redox are the master parameters that control the fate and transport of carbon and nutrients, and that (2) colloidal organic matter, clay minerals, and iron (oxyhydr)oxides facilitate transport by mobilizing otherwise insoluble forms of carbon and nutrients. In addition, temperature is an important cofactor by driving phytoplankton growth and decomposition (Zeng et al., 2006).

Clay-sized (<2 μm) and colloidal (<450 nm) particles consist of organic matter, clay minerals, and iron (oxyhydr)oxides. Because of their small size, they are able to move through pores without adsorption under specific conditions of pH and Eh. Clay minerals have a permanent negative charge due to isomorphic substitution of less-positive atoms for more-positive atoms within the mineral lattice (e.g. Al^{+3} substitution for Si^{+4}), so that nutrient cations (ammonium) can become electrostatically bound to clay mineral surfaces.

Other clay-sized particles (iron, manganese, organic matter) have pH-dependent surface charges, with low pH inducing a net-positive charge and high pH inducing a net-negative charge. Thus, nutrient cations (ammonium) are bound at high pH while nutrient anions (nitrate, phosphate) are bound at low pH. The zero-point of charge characterizes the pH at which electro-neutrality occurs.

Redox also affects nutrient transport, in that reducing conditions favor ammonium and denitrification (N_2 formation), while oxidizing conditions favor nitrate forms. Redox also affects iron minerals, in that ferric (Fe^{+3}) iron (oxides such as hematite and oxyhydroxides such as Goethite) are more stable under oxidizing conditions, while ferrous (Fe^{+2}) iron is more soluble under reducing conditions. Southeastern Piedmont lakes (including Lake Lanier) have higher temperatures, oxygen concentrations, and pH within the photic zone, and lower values below the thermocline (Zeng et al., 2006). These conditions support reduced forms of iron, manganese, and nitrogen at depth, and oxidized forms near the surface.

Here, we present data to evaluate this conceptual model of landscape fluxes. We start with a pedon-hillslope-stream model developed at the Calhoun CZO, which is then linked to a stream-lake model developed for Lake

Lanier. We then expand that model to soil solutions, low-order streams, and higher-order rivers. Our goal is to develop an integrated landscape-scale model that couples disparate spatial and temporal scales, and that accounts for the hydrologic, chemical, and physical processes that influence carbon and nutrient fluxes.

We hypothesize that soil solutions collected in shallow (15 cm) lysimeters have higher phosphorus (P) and dissolved organic carbon (DOC) and lower iron (Fe) than in deeper (30 cm) lysimeters due to higher soil organic matter and dissolved organics displacing P without need for Fe reduction and release. At the 60 cm depth we expect little P or Fe as these are clay- and oxygen-rich environments. On hillslope transects, we expect higher P on ridgetops due to a history of P fertilization but not higher Fe. We also expect higher Fe-associated P lower on the hillslope and along streambanks due to lower redox conditions.

We also expect low Fe- and DOC-associated P in low-order streams due to limited dissolved and suspended sediments, but greater Fe- and DOC-associated P in higher-order streams (Enoree and Tyger Rivers in the Calhoun CZO) due to their elevated sediment concentrations. These dissolved and suspended sediments travel through these lotic systems and then enter lentic systems (lakes), where they trigger phytoplankton blooms within the photic zone during the growing season.

12.2. METHODS

12.2.1. Calhoun CZO

Soil-water samples were collected from four different hillslope positions (ridge, mid-slope, toe-slope, and streambank) from two depths (15 cm and 60 cm) using ceramic-cup lysimeters that were installed following Artiola et al. (2004). Two landscape types were sampled, watersheds influenced by historical agriculture and reference sites on forested hillslopes lacking historical agriculture. Three hillslopes in each landscape type were sampled in each hillslope location, except that the reference hillslopes only had lysimeters in two of the streambank locations. Instream water samples were also collected from all former agricultural watersheds, but only one reference hillslope composed enough of the watershed to be representative. Figure 12.4 provides a map of the watershed and sampling locations.

Water samples were collected from lysimeters every 10–20 days between Jan 2017 and Dec 2018 for former agricultural lands, while solutions on reference sites were collected between May 2017 and Dec 2018. Surface water was collected monthly from former agricultural and reference streams between July 2014 and July 2017. An additional 13 stream locations of varying stream order and mixed land use were also sampled during this time, for a total of 17 different streams. Samples were kept on ice and transferred to the laboratory after collection.

Unfiltered lysimeter and stream samples were used to measure the specific conductance (Rhoades et al., 1996), pH (Page, 1982), and alkalinity to an endpoint pH of 4.2 titrated with 0.01 N HCl (Jenkins, 1982) on an auto-titrator (Mettler-Toledo, Columbus, OH). Thereafter, soil solution and stream samples were filtered within 24 hrs of collection using a 0.40 μm polycarbonate filter and stored cold. Samples were measured for DOC and total dissolved nitrogen (Shimadzu TOC-TN analyzer; Shimadzu Corp., Kyoto, Japan), anions (Cl, SO_4, NO_2, NO_3, PO_4) and cations (Na, K, Mg, Ca) (Dionex ICS-2100 Ion Chromatograph), and Fe, Al, and Mn (Perkin Elmer Inductively Coupled Plasma-MS model Elan DRCII). Soil-solution samples were digested using a persulfate oxidation reagent (Koroleff, 1983) to measure total phosphorus (reported as PO_4). Total and inorganic phosphate were analyzed using a Spectronic Genesys 2 spectrophotometer using the molybdate blue chemistry (Murphy & Riley, 1962).

12.2.2. Lake Lanier

Field and laboratory data were collected from the mouths of 10 tributaries to Lake Lanier and at 17 locations within Lake Lanier at multiple depths over a one-year period (Figure 12.5). Field data included water temperature, specific conductance, pH, and oxygen concentrations. Laboratory analyses included total solids (dissolved, suspended), carbon (total, dissolved organic, inorganic), nitrogen (total, Kjeldahl, ammonium, nitrite plus nitrate), phosphorus (total, dissolved), chlorophyll a, alkalinity, sulfur (dissolved sulfide, sulfate), iron (total, dissolved), and manganese (total, dissolved), where dissolved fractions are those that pass through a 0.45 μm filter. A summary of data collection and analysis are provided in Zeng and Rasmussen (2005) and Zeng et al. (2006). Mass concentration ratios are calculated as the ratio between observed concentrations (e.g., mg-P/L / mg-Fe/L = mg-P/mg-Fe) and then converted to mg/kg.

12.3. RESULTS

12.3.1. Calhoun CZO

Soil solution concentrations of total dissolved phosphorus has a poor, but positive, relationship with total Fe and DOC at two different soil depths (Figure 12.6), which is consistent with dependent and independent transport along hillslopes. Note that the inorganic P fraction of total P increases moving downslope, especially in the former agricultural sites and might reflect this downslope

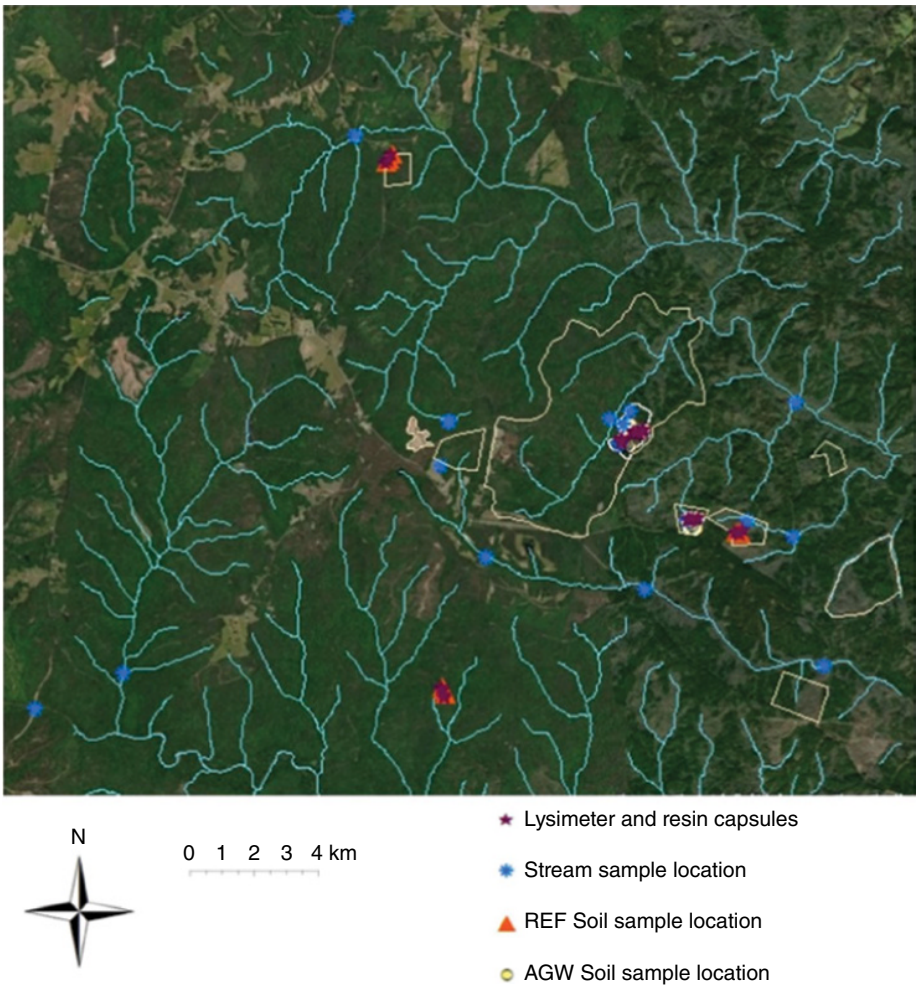

Figure 12.4 Calhoun Critical Zone Observatory location, watersheds, and sample locations.

P movement (Table 12.1). While former agricultural ridge sites have a history of P fertilization, mobilized P concentrations were lower than at other former agricultural landscape positions.

Mean total dissolved phosphorus on reference sites at 15 cm (0.55 μM) was greater than on historical agricultural sites (0.48 μM). Yet the dissolved inorganic forms of phosphorus were not substantially different at the same depth (0.34 and 0.30 μM, respectively). At 60 cm, mean dissolved total and inorganic phosphorus on reference sites (0.64 and 0.41 μM, respectively) were greater than on the agricultural sites (0.2 and 0.1 μM; Table 12.1). This was unexpected due to historical fertilization of agricultural sites but may be due to the absence of fertilization in the 70 years since agricultural lands were abandoned. We also expected greater organic P cycling on reference sites due to more roots and lower losses of organic matter in these less disturbed locations

In general, total dissolved phosphorus concentrations in soil solutions increase downslope on reference sites (i.e., from ridgetops to streambanks), with greater differences on streambank sites relative to ridgetop, mid-slope, and toe-slope at 60 cm. On formerly agricultural watersheds, approximately 43%–51% of total dissolved phosphorus was inorganic, with the remaining percentage (49%–57%) present as dissolved organic phosphorus across the different hillslope positions at 15 and 60 cm (Table 12.1). On reference sites, the dissolved organic form was variable but exceeded 60% at the toe-slopes at 15 cm and at ridgetops for 60 cm (Table 12.1).

DOC is consistently higher at 15 cm than 30 cm on all reference and former agricultural sites except for former agricultural streambank sites (Table 12.2). This can be explained by subsurface decay processes along downward flowpaths, with an exception made for legacy organic sediments that may have been buried near former agricultural streambanks during the Cotton Era.

Total phosphorus is weakly related to both total Fe and DOC at all stream sites (Figure 12.7); high-elevation (low-order) streams tended to exhibit better relationships

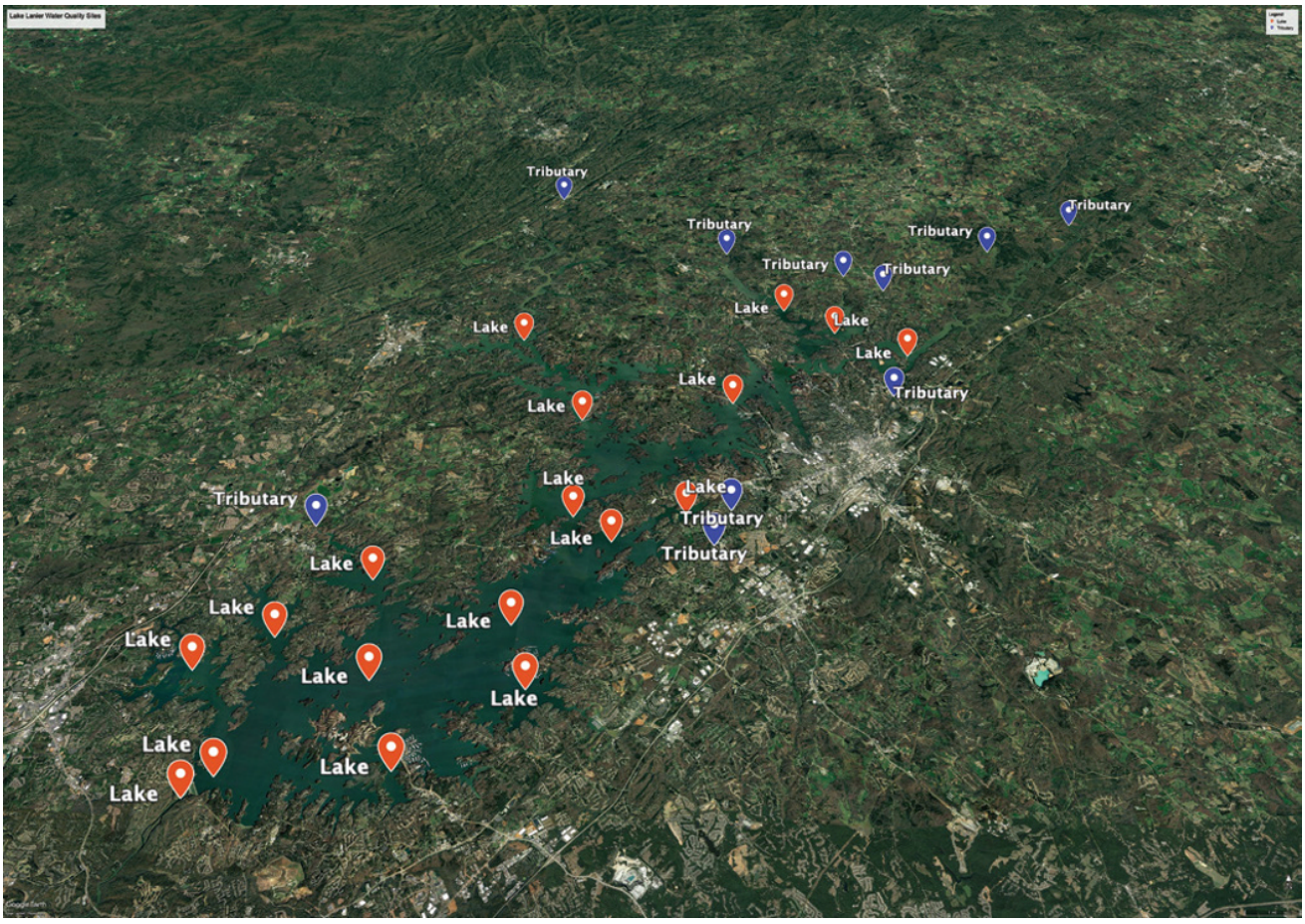

Figure 12.5 Lake (orange) and tributary (blue) sampling locations for Lake Lanier in the southeastern Piedmont near Atlanta, Georgia. (Modified from Zeng et al., 2006.)

between dissolved inorganic phosphorus and dissolved iron (Table 12.3). All streams showed similar inorganic phosphorus concentrations (0.69 to 076 μM) that were lower than large rivers (1.79 μM).

12.3.2. Lake Lanier

Table 12.4 summarizes water-quality parameters for both tributary and lake samples. Note that dissolved inorganic carbon dominates the total carbon pool, nitrite plus nitrate dominate the total nitrogen pool, and dissolved inorganic phosphorus is a small fraction of the total phosphorus pool for both tributary and lake samples.

Figure 12.8 shows that nutrients (total phosphorus, Kjeldahl nitrogen) in lake tributaries are strongly related to total suspended solids, unfiltered (total) iron, and filtered (dissolved) organic carbon. Note that some samples display high P and N nutrients in the absence of suspended solids and iron, which is consistent with our knowledge that wastewater treatment plants release clearer water with elevated nutrients and dissolved organic carbon (Zeng & Rasmussen, 2005). This might also explain the deviations from a linear slope for DOC, especially for phosphorus. Yet interactions with sediments and iron, as well as pH and redox conditions, might also account for this behavior (Zeng et al., 2006).

Figure 12.9 shows how lake nutrients (total phosphorus, Kjeldahl nitrogen) are positively related to total suspended solids, total iron, and DOC. While trends are consistent with tributary data, they show poorer relationships. Table 12.5 compares mass-concentration ratios for both lake and tributary data. Note the similarity between lake and tributary samples for total phosphorus and both total suspended solids and total iron; while Total Kjeldahl N in lake samples tend to have higher values than tributary samples. Also note that ratios with DOC are lower in lake samples than tributaries for both phosphorus and nitrogen.

These trends suggest that nutrients, carbon, and iron are moving together, which can be explained by colloid-facilitated transport (Frimmel et al., 2007). If colloidal

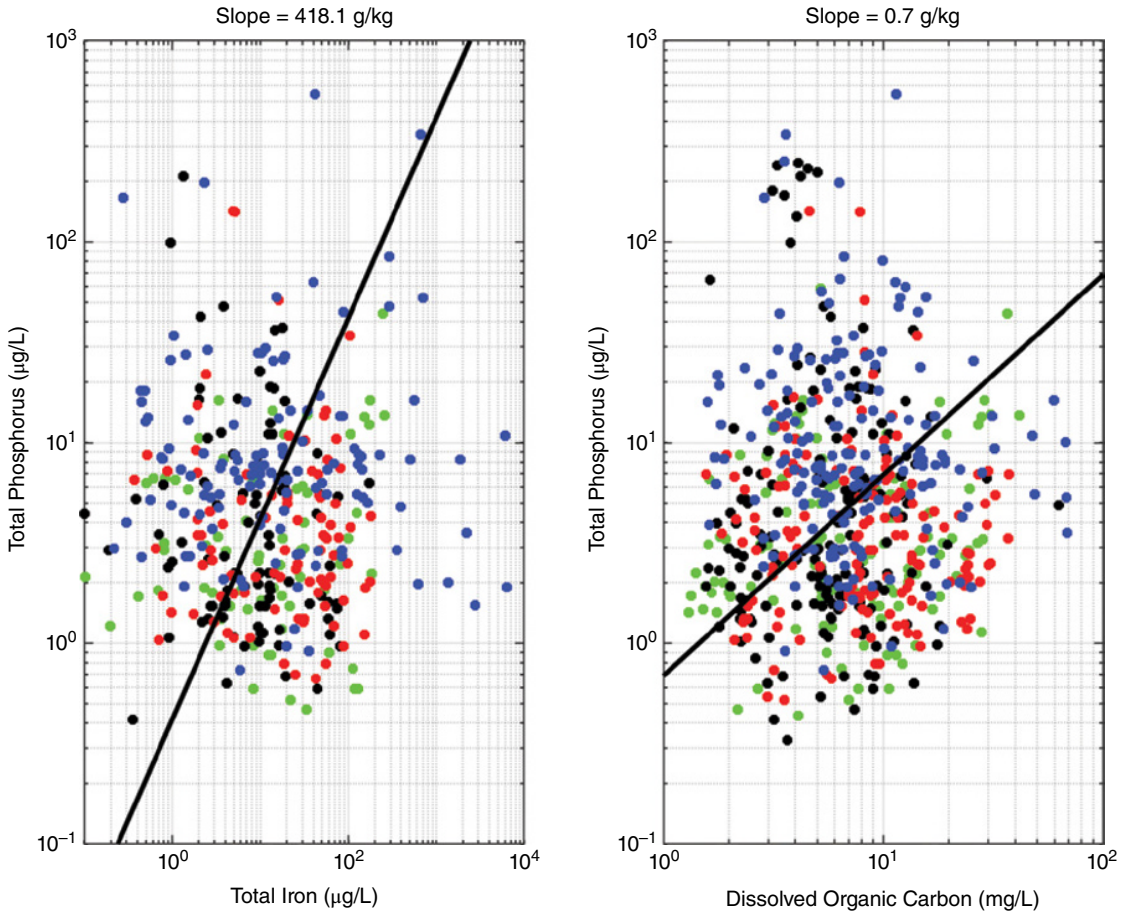

Figure 12.6 Calhoun CZO total phosphorus relationships with total dissolved iron and dissolved organic carbon collected from ceramic-cup lysimeters at two soil depths (15 and 60 cm) across four hillslope positions. Also shown is best-fit linear relationship with slope above each figure. Green indicates ridgetop positions, black indicates mid-slope, red indicates toe-slope, and blue indicates streambanks.

Table 12.1 Calhoun CZO total and inorganic phosphorous concentrations in soil solutions collected from ceramic-cup lysimeters across land uses with historical agricultural use (AGW) and with no historical agricultural use (REF) on four hillslope positions from Jan 2017 to Dec 2018.

		Total P (µM)				Inorganic P (µM)				Fraction Inorganic P	
		15 cm		60 cm		15 cm		60 cm		15 cm	60 cm
Site	Position	Mean	SE	Mean	SE	Mean	SE	Mean	SE	Mean	Mean
AGW	Ridgetop	0.09	0.01	0.10	0.01	0.05	0.01	0.06	0.01	56%	60%
AGW	Mid-slope	0.83	0.25	0.20	0.09	0.69	0.21	0.16	0.08	83%	80%
AGW	Toe-slope	0.11	0.02	0.14	0.03	0.08	0.01	0.05	0.01	73%	36%
AGW	Streambank	0.41	0.15	0.27	0.05	0.39	0.27	0.11	0.01	95%	41%
REF	Ridgetop	0.61	0.16	0.37	0.15	0.12	0.04	0.13	0.07	20%	35%
REF	Mid-slope	0.52	0.07	0.25	0.06	0.32	0.09	0.11	0.02	62%	44%
REF	Toe-slope	0.59	0.27	0.16	0.02	0.46	0.25	0.08	0.01	78%	50%
REF	Streambank	0.60	0.12	1.47	0.47	0.26	0.06	0.82	0.27	43%	56%

Table 12.2 Calhoun CZO dissolved organic carbon in soil solutions collected from ceramic-cup lysimeters across two land uses with historical agricultural use (AGW) and with no historical agricultural use (REF) on four hillslope positions from Jan. 2017 to Dec. 2018.

		Dissolved Organic Carbon (mg/L)			
		15 cm		60 cm	
Site	Hillslope Position	Mean	SE	Mean	SE
AGW	Ridgetop	9.84	1.01	7.71	0.78
AGW	Mid-slope	7.73	0.85	7.49	0.60
AGW	Toe-slope	17.6	1.28	7.98	0.59
AGW	Streambank	10.7	1.96	15.1	1.73
REF	Ridgetop	26.6	3.45	4.15	0.47
REF	Mid-slope	6.07	0.50	3.17	0.32
REF	Toe-slope	6.31	0.47	3.17	0.29
REF	Streambank	8.72	0.70	4.31	0.38

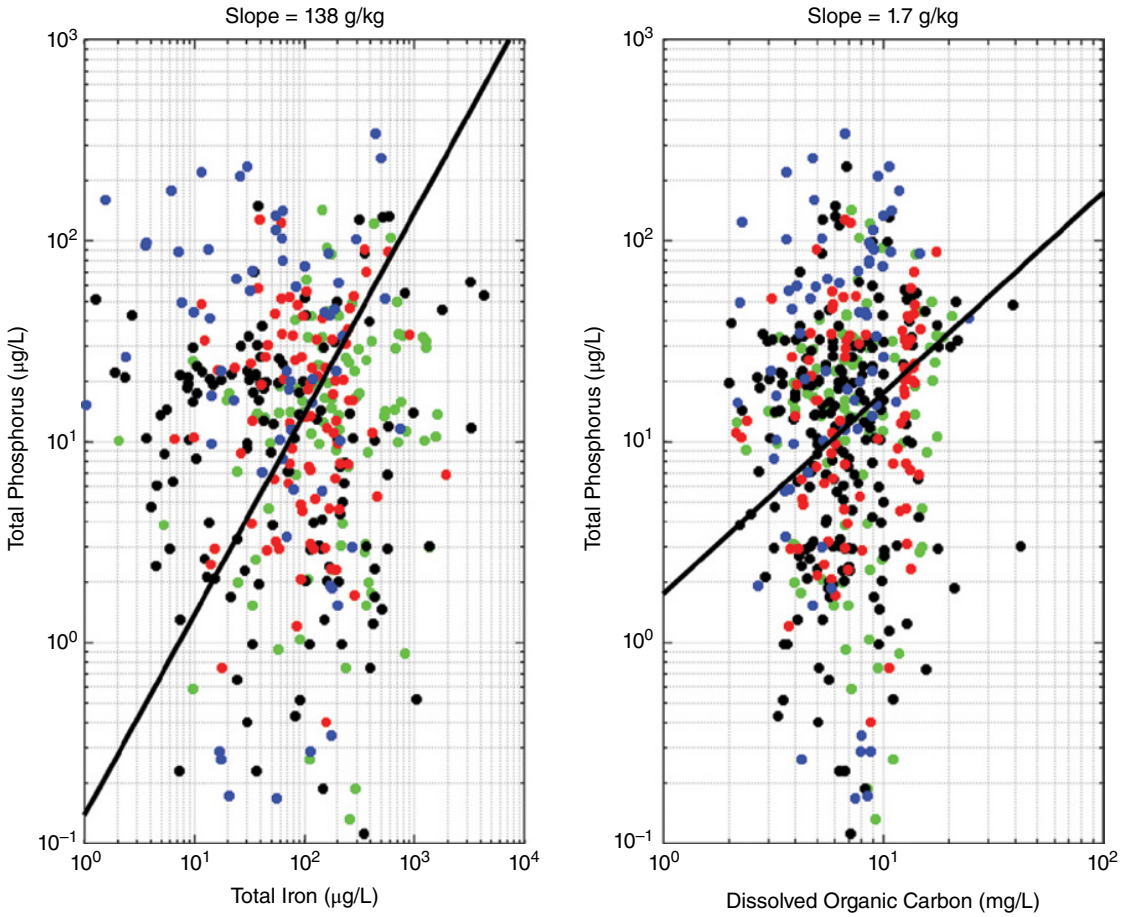

Figure 12.7 Calhoun CZO total phosphorus and nitrogen relationships with total dissolved iron and dissolved organic carbon collected from 17 different streams between July 2014 and July 2018. Also shown is best-fit linear relationship with slope above each figure. Green indicates higher elevation streams (three sites), black indicates mid-elevation streams (five sites), red indicates lower elevation streams (three sites), and blue indicates larger rivers (two sites).

Table 12.3 Calhoun CZO stream inorganic phosphorous concentrations collected between July 2014 and July 2017. Elevations refer to upper, middle, and lower landscape positions of low-order streams while large rivers (Tyger and Enoree) are receiving bodies for these and other streams.

			Inorganic Phosphorus (µM)	
Stream Type	# Streams	# Samples	Mean	Std Dev
High elevation	3	94	0.69	0.08
Mid elevation	5	201	0.76	0.11
Low elevation	3	100	0.73	0.08
Large river	2	68	1.79	0.27

Table 12.4 Lake Lanier water-quality data for 10 tributaries and 18 lake sites.

		Tributary				Lake			
Parameter		Mean	Min	Max	Count	Mean	Min	Max	Count
Alkalinity	mg/L	**19.7**	1.0	230	215	**10.8**	1.0	24	485
Total suspended solids	mg/L	**61.8**	0.50	1,450	215	**4.15**	0.50	72.0	488
Total dissolved solids	mg/L	**69.7**	12.0	488	215	**25.7**	2.00	202	486
Chlorophyll a	µg/L	—	—	—	0	**2.39**	0.10	42.0	1,133
Total inorganic carbon	mM	**477**	390	607	11	**421**	15.8	2,986	486
Total organic carbon	mM	**276**	15.8	1,813	183	**149**	15.8	413	445
Dissolved organic carbon	mM	**201**	15.8	897	183	**124**	15.8	226	443
Total nitrogen	µM	**185**	20.0	1,167	215	**43.3**	0.357	346	1,129
Kjeldahl nitrogen	µM	**40.1**	1.43	614	212	**19.5**	1.428	150	1,087
Nitrite plus nitrate	µM	**146**	2.14	1,078	215	**24.6**	0.357	264	1,127
Ammonium	µM	**7.04**	0.36	213	212	**5.17**	0.357	106	1,090
Total phosphorus	µM	**5.78**	0.06	123	215	**0.40**	0.065	4.04	1,023
Inorganic phosphorus	µM	**1.34**	0.05	50.7	214	**0.08**	0.032	1.61	1,022
Sulfate	µM	**439**	31	2,932	15	**71.0**	15.6	374	595
Total dissolved sulfide	µM	—	—	—	0	**13.2**	1.56	4,991	486
Total iron	µM	**49.8**	0.045	1,005	214	**7.33**	0.045	201	477
Dissolved iron	µM	—	—	—	0	**2.50**	0.045	99.2	474
Total manganese	µM	**2.05**	0.018	55.5	214	**1.71**	0.018	94.5	474
Dissolved manganese	µM	—	—	—	0	**1.09**	0.018	17.1	470

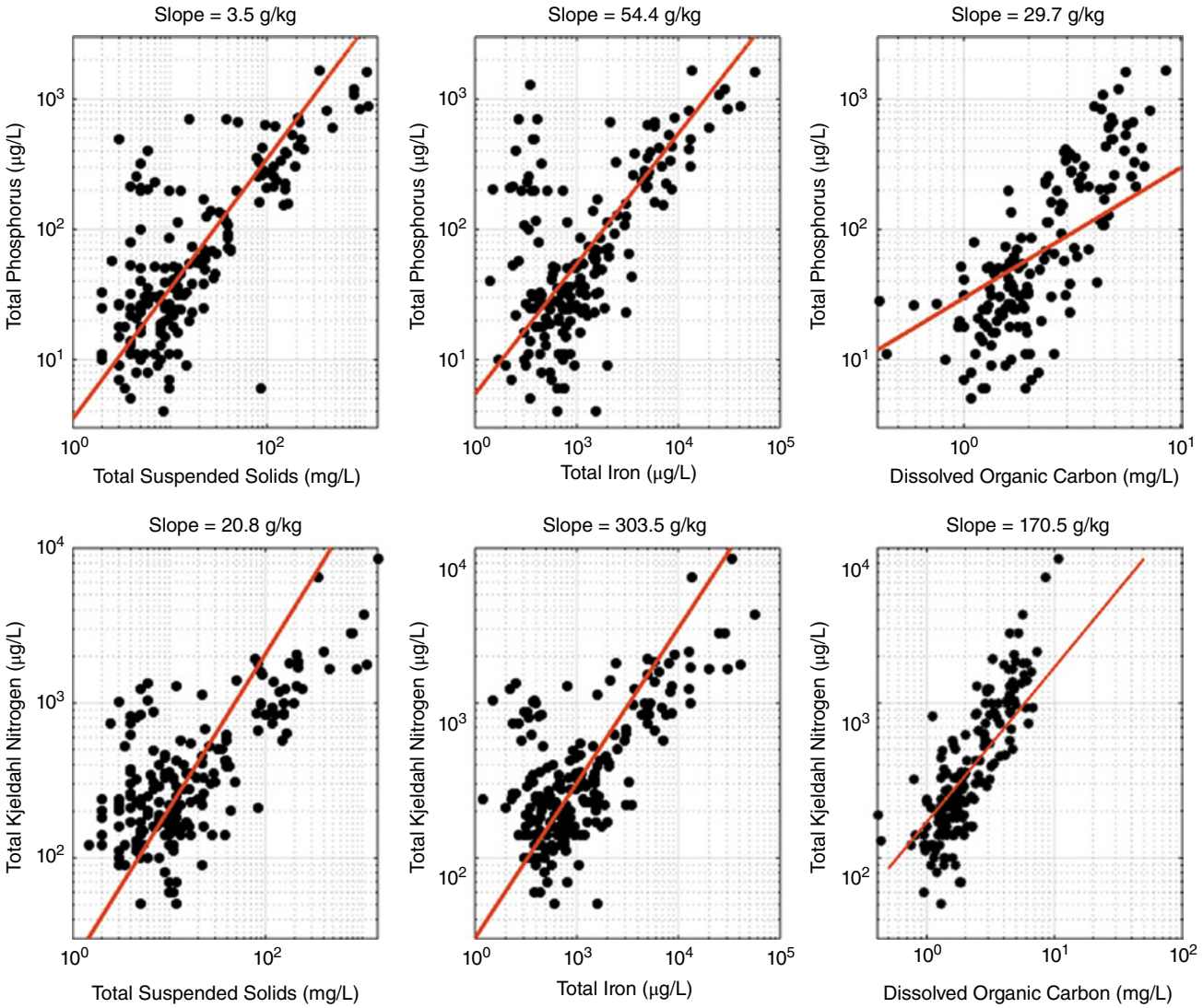

Figure 12.8 Lake Lanier tributary relationships between nutrients (total phosphorus, top; total Kjeldahl nitrogen, bottom) and total suspended solids (left), total iron (center), and dissolved organic carbon (right). Also shown is best-fit linear relationship with slope above each figure.

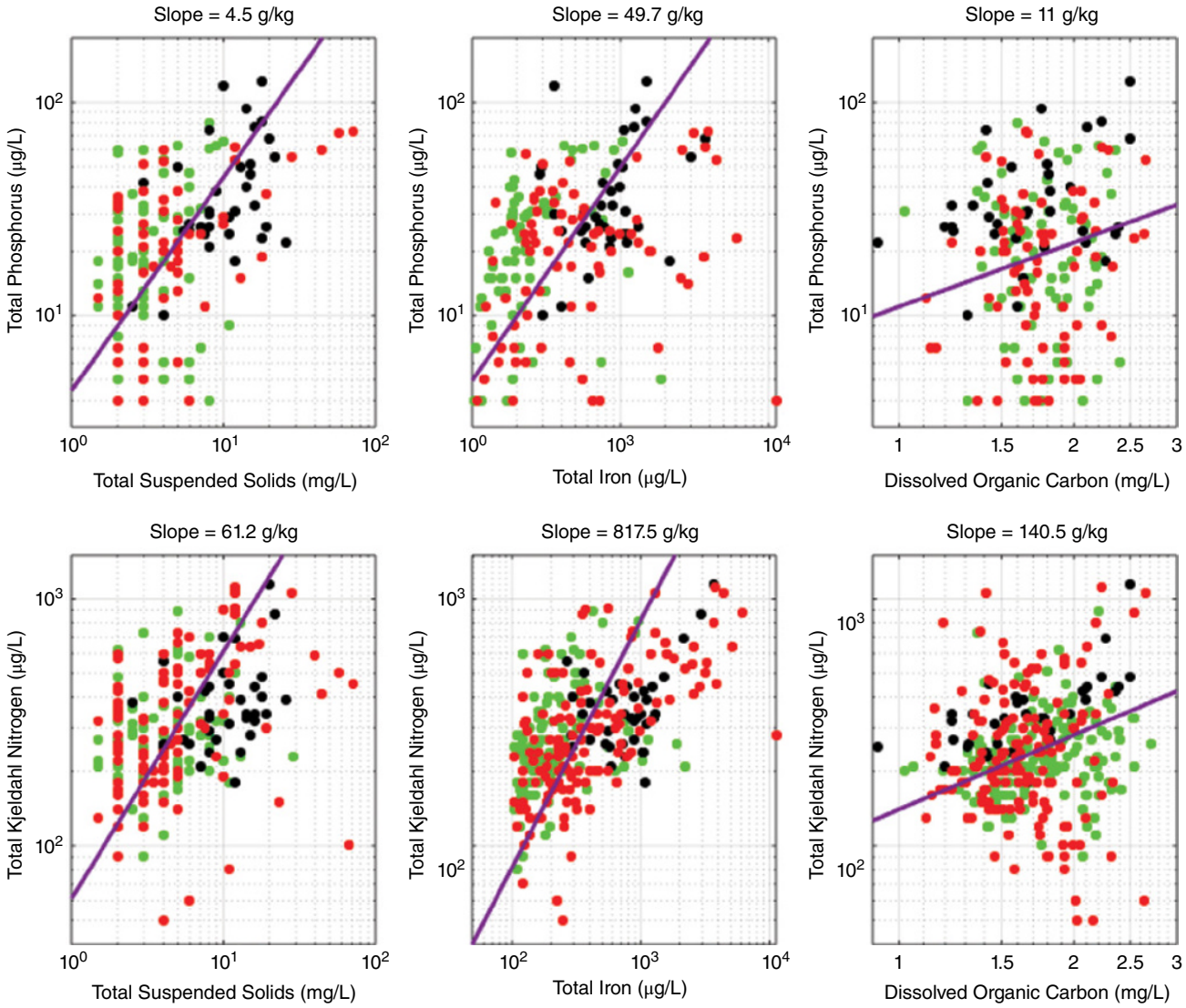

Figure 12.9 Lake Lanier within-lake relationships between nutrients (total phosphorus, top; total Kjeldahl nitrogen, bottom) and total suspended solids (left), total iron (center), and dissolved organic carbon (right). Also shown is best-fit linear relationship with slope above each figure. Green indicates surface samples (<3 m), black indicates mid-depth (3–10 m), and red indicates profundal samples (>10 m).

Table 12.5 Lake Lanier and tributary mass ratios (g/kg) between selected nutrients (total phosphorus, total Kjeldahl nitrogen) and selected water-quality parameters (total suspended solids, total iron, dissolved organic carbon). Mass ratios are calculated as the ratio between observed concentrations (e.g. µg-P/L / µg-Fe/L = µg-P/µg-Fe) and then converted to g/kg.

	Total Phosphorus		Total Kjeldahl Nitrogen	
Parameter	Tributary	Lake	Tributary	Lake
Total suspended solids	3.50	4.50	20.8	61.2
Total iron	54.4	49.7	304	818
Dissolved organic carbon	29.7	11.0	171	141

clays and organic matter are small enough to pass through regolith pores, then nutrients sorbed to these materials would also be mobile in groundwater. Once in aquatic environments, biogeochemical processes would provide the opportunity for release and phytoplankton uptake of these nutrients from these colloidal materials.

Sampling depth (shown using colors in Figure 12.9) does not appear to affect the relationship between total phosphorus and total Kjeldahl nitrogen with total suspended solids. For total iron, however, surface samples (green symbols) tend to lie above the lines, while mid-depth (black) and the deeper, profundal (red) samples are evenly divided. This can be attributed to higher pH within the photic zone that provides the opportunity for phytoplankton uptake (Zeng et al., 2006). For dissolved organic carbon, mid-depth samples lie above the trend line for both total phosphorus and total Kjeldahl concentrations. Again, lower pH relative to surface waters may be responsible for this enrichment (Zeng et al., 2006).

12.4. CONCLUSIONS

This study presents field and laboratory data on nutrient, carbon, and iron concentrations within southeastern Piedmont critical zones. Data were collected from two sites: the Calhoun Critical Zone Observatory, South Carolina, augmented with data collected from tributaries to, and sites within, Lake Lanier, Georgia. These data are used to develop a conceptual model of physico-chemical mechanisms for carbon and nutrient transport in the critical zone, which is key to the sustainable management of these systems.

A key component of our conceptual model is the linkage between dissolved (including colloidal) clay and iron, carbon, and nutrients. As pedons export carbon and nutrients to hillslopes, soil and other subsurface processes allow these mobile materials to reach headwater streams. The relationship between these materials persist within low- and mid-order streams, enriching downstream water bodies. While within-lake nutrient cycling alters these relationships, they are still important processes that help us understand carbon and nutrient fluxes.

REFERENCES

Artiola, J., Pepper, I., & Brusseau, M. (2004). *Environmental monitoring and characterization*. Burlington, MA: Elsevier Academic Press.

Foroughi, M. (2019). *Soil phosphorus biogeochemistry in the Calhoun Critical Zone Observatory, South Carolina: Effects of land use, topography, and time*. PhD Dissertation, University of Georgia, Athens.

Frimmel, F. H., von der Kammer, F., Flemming, H. C. (2007). *Colloidal transport in porous media*. Springer. ISBN 978-3-540-71338-8.

Hatcher, K. J. (1994). *Diagnostic/ feasibility study of Lake Sidney Lanier, Georgia.* Project completion report. University of Georgia, Athens GA.

Hatcher, K. J. (1998). *Diagnostic/ feasibility study of Lake Sidney Lanier, Georgia.* Project completion report. University of Georgia, Athens GA.

Hayes, D. C., Stout, S. L., Crawford, R. F., & Hoover, A. P. (2014). *USDA Forest Service experimental forests and ranges: Research for the long-term*. Springer.

Jackson, C. R., Martin, J. K., Leigh, D. S., West, L. T. (2005). A Southeastern Piedmont watershed sediment budget: Evidence for a multi-millennial agricultural legacy, *Journal of Soil and Water Conservation*, *60*(6), 298–310.

Jenkins, S., Connors, J. J., & Jenkins, D. (Eds.) (1981). *Standard methods for the examination of water and wastewater*, 15th ed. Washington, DC: American Public Health Association.

Kleber M., Sollins, P., & Sutton, R. (2007). A conceptual model of organo-mineral interactions in soils: Self-assembly of organic molecular fragments into zonal structures on mineral surfaces. *Biogeochemistry*, *85*, 9–24.

Koroleff, F. (1983). Simultaneous oxidation of nitrogen and phosphorus compounds by persulfate. In K. Grasshoff, K. Kremling, & M. Ehrhardt (Eds.), *Methods of seawater analysis* (2nd ed., pp. 205–206). Weinheim/Deerfield Beach, FL: Verlag Chemie.

Lamon, E. C., Qian, S. S., & Richter, D. D. (2007). Temporal changes in the Yadkin River flow versus suspended sediment concentration relationship, *Journal of the American Water Resources Association*, *40*(5), 1219–1229. https://doi.org/10.1111/j.1752-1688.2004.tb01581.x

Murphy J, & Riley, J. P. (1962). A modified single solution method for the determination of phosphate in natural waters. *Analytica Chimica Acta*, *27*, 31–36.

Page, A. L. (1982). *Methods of soil analysis. Part 2: Chemical and microbiological properties*. American Society of Agronomy, Soil Science Society of America.

Redfield, A. C. (1934). On the proportions of organic derivations in sea water and their relation to the composition of plankton, In R. J. Daniel (Ed.), *James Johnstone Memorial Volume* (pp. 177–192). University Press of Liverpool.

Rhoades J., Sparks, D., Page, A., Helmke, P., Loeppert, R., Soltanpour, P., et al. (1996). Salinity: Electrical conductivity and total dissolved solids. In *Methods of Soil Analysis.Part 3: Chemical Methods* (pp. 417–435).

Richter, D. D., Bacon, A. R., Billings, S. A., Binkley, D., Buford, M., Callaham, M., et al. (2015). Evolution of soil, ecosystem, and critical zone research at the USDA FS Calhoun Experimental Forest. In D. C. Hayes, S. L. Stout, R. H. Crawford, & A. P. Hoover (Eds.), *USDA Forest Service Experimental Forests and Ranges* (pp. 405–433). Springer.

Richter, D. D., & Markewitz, D. (2001). *Understanding soil change: Soil sustainability over millennia, centuries, and decades*. Cambridge, UK: Cambridge University Press.

Schmidt, M. W. I., Torn, M. S., Abiven, S., Dittmar, T., Guggenberger, G., Janssens, I. A., et al. (2011). Persistence of

soil organic matter as an ecosystem property. *Nature*, *478*(7367), 49–56.

Trimble, S. W. (1972). *Man-induced soil erosion on the southern Piedmont, 1700–1970*. Ankeny IA: Soil and Water Conservation Society.

West, L. T., Shaw, J. N., & Mersiovsky, E. P. (2017). Soils of the Southeastern USA: LRRs O, P, and T. In L. West, M. Singer, & A. Hartemink (Eds.), *The soils of the USA.* World Soils Book Series. Springer.

Whitney, G. G. (1994). *From coastal wilderness to fruited plain: A history of environmental change in temperate North America from 1500 to the present*. New York: Cambridge Univ Press.

White, T., Brantley, S., Banwart, S., Chorover, J., Dietrich, W., Derry, L., et al. (2015). The role of Critical Zone Observatories in critical zone science. *Developments in Earth Surface Processes*, *19*, 15–78.

Zeng, X., Rasmussen, T. C., Beck, M. B., Parker, A. K., & Lin, Z. L. (2006). A biogeochemical model for metabolism and nutrient cycling in a Southeastern Piedmont impoundment, *Environmental Modelling & Software*, *21*(8), 1073–1095.

Zeng, X., & Rasmussen, T. C. (2005). Multivariate statistical characterization of water quality in Lake Lanier, Georgia, USA. *J Environmental Quality*, *34*, 1980–1991.

13

Is This Steady State? Weathering and Critical Zone Architecture in Gordon Gulch, Colorado Front Range

Suzanne P. Anderson[1], Patrick J. Kelly[2*], Noah Hoffman[2], Katherine Barnhart[3], Kevin Befus[4], and William Ouimet[5]

ABSTRACT

Landscapes are often assumed to be in steady state, yet it is unclear how steady state persists when climate has varied during landscape evolution. The architecture of the critical zone, including topography and the character of regolith, reflects the combined influences of weathering and denudation processes integrated over time. We synthesize observations in an unglaciated but periglacially influenced semiarid catchment in the Boulder Creek Critical Zone Observatory to elucidate the processes that shape the critical zone in a landscape interpreted as in steady state. Weathering in the bedrock extends to an average of ~12 m depth, and based on denudation rates of 3.1 cm/kyr represents exposure to >350 kyr of weathering. The strong contrast in solar radiation on N-facing and S-facing hillslopes imposes differing environmental conditions. Aspect differences affect weathered rock, which reaches greater depth and is mechanically weaker under N-facing slopes than S-facing slopes, but not mobile regolith, which is thin (~0.4 m) and relatively uniform across aspects. Patterns in chemical alteration are difficult to quantify given the heterogeneity of the biotite gneiss bedrock (i.e. noise is high) and the minor degree of weathering (i.e. signal is low). Mobile regolith is more homogeneous in mineralogy than is the weathered rock, showing the effect of transport processes in mixing particles released from the banded bedrock. Long-term cosmogenic radionuclide-based erosion rates and mobile regolith residence times show no slope aspect-controlled differences in transport and erosion. Together these observations suggest that mechanical processes dominate in bedrock weathering and in mobile regolith production in this setting. Moreover, the presence of mobile regolith shows that weathering does not limit denudation; instead, the critical zone architecture represents the state of weathering achievable given the overall mass loss imposed by the fluvial system.

[1]*Institute of Arctic and Alpine Research and Department of Geological Sciences, University of Colorado, Boulder, Colorado, USA*

[2]*INSTAAR and Dept. of Geography, University of Colorado, Boulder, Colorado, USA*

[3]*Cooperative Institute for Research in Environmental Sciences, University of Colorado, Boulder, Colorado, USA*

[4]*Department of Civil and Architectural Engineering, University of Wyoming, Laramie, Wyoming, USA*

[5]*Department of Geography and Center for Integrative Geosciences, University of Connecticut, Storrs, Connecticut, USA*

**Now at: US EPA Pacific Southwest, Region 9, San Francisco, California, USA*

13.1. INTRODUCTION

Critical zone architecture comprises the shape and characteristics of the surface environment, where meteoric waters attack and alter bedrock, gravitationally driven processes strip away weathered and mobilized material, and biotic agents aid and abet these processes. We use the term *critical zone architecture* to encompass soil, mobile regolith, saprolite, and weathered rock: all the materials altered and affected by proximity to the ground surface. Climate and tectonic processes energize the weathering and erosion processes that produce critical zone architecture, as these control important

Hydrogeology, Chemical Weathering, and Soil Formation, Geophysical Monograph 257, First Edition.
Edited by Allen Hunt, Markus Egli, and Boris Faybishenko.

DOI: 10.1002/9781119563952.ch13

conditions such as water phase and flux, thermal state, biotic communities, and river base level. The time over which critical zone architecture develops depends upon its thickness and the rates of the processes responsible for its evolution. Commonly, this implicates long timescales, such that for instance, a modern-day critical zone profile has evolved longer under the influence of Pleistocene glacial climate than Holocene climate (e.g. Marshall et al., 2015). Tectonic imprints may be even longer lived, for example in building deep-rooted mountain ranges whose relief persists postorogeny due to isostasy (Molnar & England, 1990; Tucker & van der Beek, 2013) or by emplacing fracture systems in the deep rock (Molnar et al., 2007). Imbalances between weathering and erosion over time will either enhance or contract the weathered profile. Periods of imbalance produce the range of deep to minimal weathering profiles seen globally, although in general the thickness of the weathering zone falls within narrow limits (West, 2012). Commonly, landscapes are assumed to be in steady state or dynamic equilibrium (Hack, 1960), meaning that ground surface and the weathering front both lower at the same rate (Pavich, 1986). In this contribution, we compile numerous lines of evidence, from both published and previously unpublished work, to describe critical zone architecture and discuss steady state in an upland, bedrock-dominated site. In this setting, a cool dry climate might be expected to minimize weathering processes, and a lack of erosional perturbations due to glaciation or tectonics leads to an expectation of a steady state between denudation and weathering. In eroding uplands of this sort, rock can be thought of as transiting upward toward the surface over time as erosion lowers the surface. Uplands of this sort contrast with depositional basins, where sedimentation results in burial and long-term downward movement of rock. The study site features pole-facing and equator-facing hillslopes (in this case N-facing and S-facing, respectively) that prompt consideration of the effects of radiation on processes that shape the critical zone.

If we think of the critical zone in upland, denudational areas as a coherent boundary layer, in which rock is altered (weathered) due to its proximity to the Earth's surface, then we can ask how the character of this boundary layer is affected by weathering processes and erosion or denudation processes (Figure 13.1). *Weathering* here is taken as the suite of chemical (including biogeochemical) and mechanical processes that both advance weathering fronts into fresh rock and that alter rock within the critical zone. *Denudation* is mass loss from the critical zone and, in its most general sense, includes net mass removal by both physical transport and solute flux. In most settings, physical processes accomplish more denudation than chemical processes (Summerfield & Hulton, 1994), and hence physical transport processes rather than solute fluxes control denudation. Because physical denudation commonly substantially exceeds chemical denudation, denudation is often conflated with erosion. *Erosion* is lowering of the ground surface (or exhumation, in the sense of Molnar & England, 1990) due to sediment transport. For any particular vertical column through the critical zone, erosion reflects greater sediment flux out of than into the column over a period of time. This situation highlights the importance of mobile regolith, the layer of weathered material that has been released from bedrock and mobilized, as this is the material that participates in hillslope transport processes. Most soil horizons (other than Cr or R horizons; Soil Survey Staff, 2014) form within mobile regolith, prompting our use of the term *soil* as shorthand for mobile regolith. Thus, we identify two important fundamental layers of weathered material within the critical zone, bounded by three interfaces (e.g. R. S. Anderson et al., 2013). These are mobile regolith, which is bounded by the ground surface and the weathered rock surface, and weathered rock, which extends from the weathered rock surface down to fresh rock (Figure 13.1).

While weathering processes advance the weathering front into fresh rock and denudation processes tend to thin the weathered rock zone, feedbacks between these processes confound simple generalizations about weathering and erosion. Weathering process rates tend to slow as the thickness of the weathered zone increases (e.g. Chinn, 1981), limited by diffusion and porosity development (Fletcher et al., 2006; Navarre-Sitchler et al., 2011). Chemical weathering rates also decline as mineral surfaces age (White & Brantley, 2003). Thus, erosion can be viewed as enhancing weathering rates by limiting the thickness of the weathered zone, which in turn effectively introduces fresh rock into the weathering zone (S. P. Anderson et al., 2007). The hillslope sediment flux processes responsible for erosion are limited by production of mobile regolith (R. S. Anderson & Humphrey, 1989). The rate of mobile regolith production (release of rock from the top of the weathered rock layer into the mobile regolith layer) is likely to depend on the strength of the weathered rock from which it is produced, and hence to depend on the degree of weathering (e.g. R. S. Anderson et al., 2013; Dixon et al., 2009). The notion that soil thickness affects the rate of mobile regolith production is long established (Gilbert, 1877), with a general consensus that deeper soil impedes the production of new mobile regolith at its base (Humphreys & Wilkinson, 2007). It is therefore relevant to ask how these complementary and competing processes interact to shape the critical zone.

When studying weathering process rates in the critical zone, it is common to assume that the landscape is in steady state (Dixon & Riebe, 2014; Gilbert, 1909; Pavich,

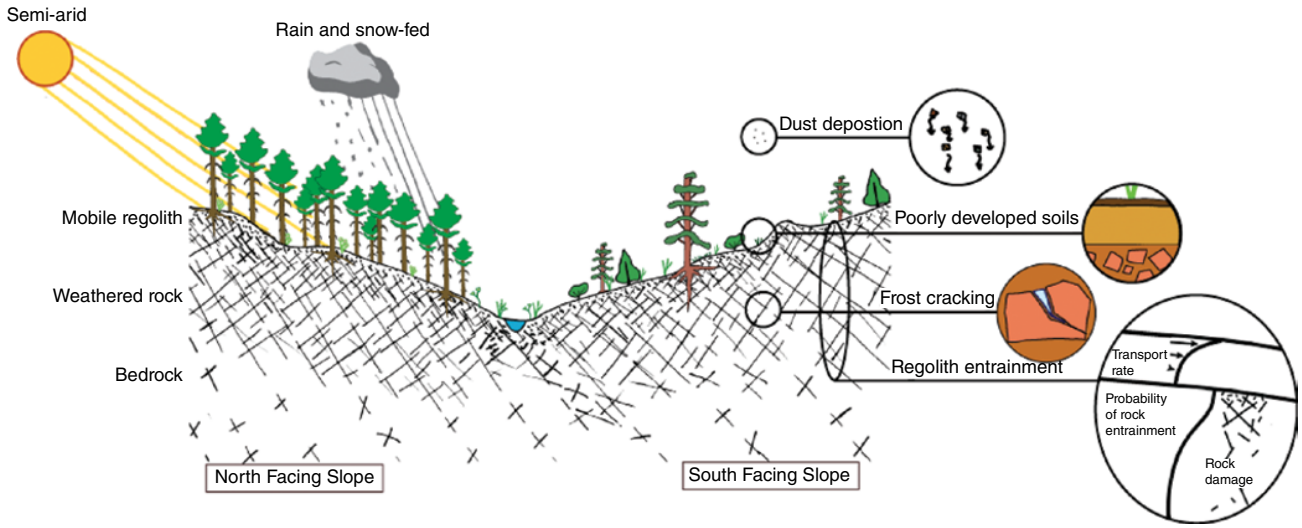

Figure 13.1 Critical zone architecture reflects the integrated effects of weathering and denudation processes over time. In general, two weathered layers, mobile regolith and weathered rock, overlie fresh bedrock. Denudation includes all forms of mass loss, most prominently that produced by physical transport. Weathering includes both chemical and physical processes that alter rocks and minerals. Commonly, the physical transport rate is a non-linear function of depth within mobile regolith. Material enters this mobile layer through a variety of processes whose effects are lumped into the soil production rate. Rock chemical and mechanical weathering processes together advance a weathering front into fresh rock. The rate of weathering most likely decreases with depth in the rock. The figure shows a schematic of modern Gordon Gulch vegetation differences across aspects.

1986), meaning that weathering fronts and landscape lowering occur at equivalent rates. This simplifying assumption allows use of one denudation rate to describe rates of lowering of all interfaces. It does raise a question, however: how is the deepest weathering front, namely the interface between weathered and fresh rock, connected to lowering of the surface? We return to this in the discussion.

We synthesize observations on critical zone architecture from Gordon Gulch, a study site within the Boulder Creek Critical Zone Observatory in the Colorado Front Range. The location is unglaciated, but given its proximity to Pleistocene glaciers, experienced periglacial climate through much of the time over which the present critical zone architecture developed. Due to the east-west orientation of the channel system, hillslopes in Gordon Gulch are largely north- or south-facing, which prompts consideration of the impacts of the substantial differences in the energy balance on weathering and denudation processes. We combine published seismic refraction profiles and cosmogenic radionuclide data with previously unpublished soil profile and rock strength data to build insight into weathering, denudation, and steady state.

13.2. STUDY LOCATION

Gordon Gulch is a 2.6 km^2 headwater in Boulder Creek, one of the eastward draining rivers in the Front Range (Figure 13.2). To understand the erosional history of Gordon Gulch, we need to review briefly the geologic history of the region. One of the ranges uplifted during the Laramide orogeny (75–35 Ma, Bird, 1998), the Front Range rises ~2400 m above the western edge of the grasslands of the Great Plains. The Front Range physiography, in common with other Laramide ranges, features an abrupt topographic rise at the boundary between soft sedimentary rocks of the Plains and hard basement rock of the range, a broad high-elevation, low-relief central region, and a narrow glaciated summit spine (R. S. Anderson et al., 2006). Since the end of Laramide thrusting and associated uplift at about 40 Ma, the range has primarily experienced erosion, credited with forming the low-relief surface on which Gordon Gulch sits. From the Pliocene to present, erosion of both the range and the Plains have enhanced relief and produced the present Front Range physiography (Tucker & van der Beek, 2013). More efficient exhumation of the easily eroded sedimentary rocks underlying the Plains produced the abrupt topographic front to the range and drove incision of bedrock canyons into the low-relief surface, like Boulder canyon in Boulder Creek watershed (Figure 13.2). Quaternary glaciation shaped the cirques cut into the summit spine (R. S. Anderson et al., 2006).

Within the Front Range, erosional perturbations are thought to have broadly affected critical zone architecture in several key locations. First, in the alpine headwaters of Boulder Creek, Quaternary glaciation eroded through

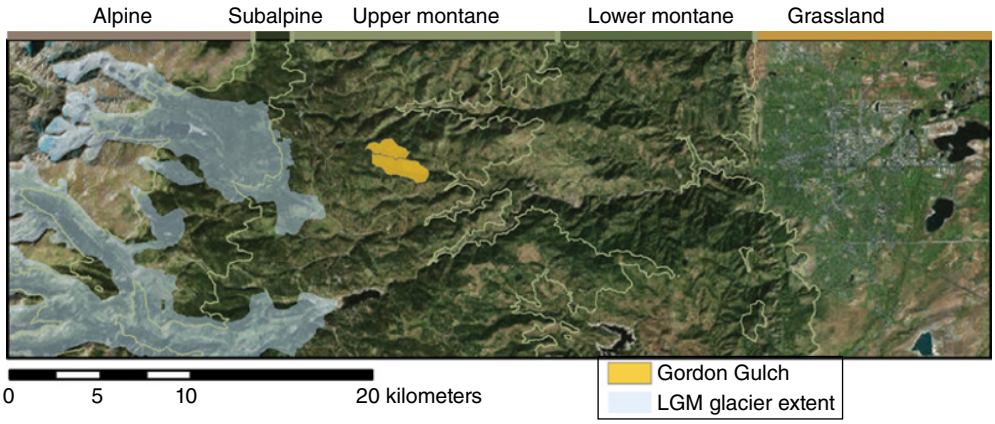

Figure 13.2 Swath map of the east side of the Colorado Front Range in vicinity of Boulder Creek. Study site Gordon Gulch is a small headwater located on the broad low-relief shoulder of the Range. The extent of Pleistocene glaciers is taken from Madole (1969) and Madole et al. (1998). Major vegetation zones (Marr, 1961) across the >2500 m relief from the Plains to alpine peaks are labeled across the top of the map, and approximate boundaries are delineated. Gordon Gulch lies within the Upper Montane vegetation zone, which occupies the broad low-relief area from ~2400–2800 m. (Courtesy of Suzanne P. Anderson.)

weathered rock in U-shaped alpine valleys (Dühnforth & Anderson, 2011), truncating the weathered zone. Second, a headward-propagating knickzone in Boulder Creek produced the bedrock-dominated walls of Boulder Canyon (S. P. Anderson, Anderson, et al., 2012; Shobe et al., 2016). Gordon Gulch (2440–2730 m) lies on the low-relief high-elevation surface into which Boulder Canyon is cut, and is not directly affected by the erosional effects of glaciers. Gordon Gulch is only about 5 km east of the terminal moraines of the glaciers that sourced from Green Lakes Valley (Madole et al., 1998), a proximity that suggests that periglacial processes would have been active during Quaternary glaciations.

The bedrock geology of the Front Range is dominated by Precambrian-age biotite gneiss intruded by Precambrian granites (Gable, 1980a, 1996). Within Gordon Gulch, the rock is dominantly cordierite-bearing garnet sillimanite-biotite gneiss, with minor intrusions of Boulder Creek granodiorite and Silver Plume quartz monzonite (Gable, 1980b). The gneiss foliation planes strike WNW, with northward dips of 44°–68°. The metamorphic rocks have undergone retrograde metamorphism and have also been affected by hydrothermal alteration associated with intrusions during the Laramide.

13.2.1. Gordon Gulch

Gordon Gulch comprises two east-west oriented basins, connected by a channel that jogs south between the upper and lower basins (Figure 13.3). The upper basin has lower relief (~120 m) and shallower slopes (~13°) than the lower basin (~290 m and ~20°, respectively). Apart from the steep reach in which the channel cuts south, the catchment is dominated by N- and S-facing hillslopes. The hillslopes appear pimpled in high-resolution maps (Figure 13.3), owing to bedrock tors with dimensions from one to tens of meters.

13.2.2. Climate and Vegetation

At present, Gordon Gulch has a mean annual precipitation of about 520 mm and a mean annual temperature of 5 °C, based on a 30-year record from National Atmospheric Deposition Program collection station NADP CO94, located 2 km south of Gordon Gulch. In recent years (2010–2014), annual precipitation ranged from 533 to 839 mm, of which 37%–60% (mean 49%) fell as snow. Precipitation shows a pronounced seasonal peak in spring (May), a secondary peak in summer, and a minimum in winter (Dec–Jan; Barry, 1973; Hansen et al., 1978). Under present climate, snow tends to persist on N-facing slopes but is more likely to melt completely between storms on S-facing slopes, especially on exposed slopes in the lower basin. Soil temperatures are lower on N-facing slopes, and freezing (sub-0°C) conditions are more likely to occur more deeply (>25 cm) and for longer on N-facing slopes.

Modern climate conditions result in soil moisture on N-facing slopes being low and steady during winter and consistently wet during spring snowmelt and precipitation. On S-facing slopes, soil moisture is much more variable, with wetting associated with multiple winter and spring snowmelt events, and summer rains. Groundwater wells in the upper basin show that recharge most commonly occurs in spring on both slope aspects but can also occur in large summer or fall storms.

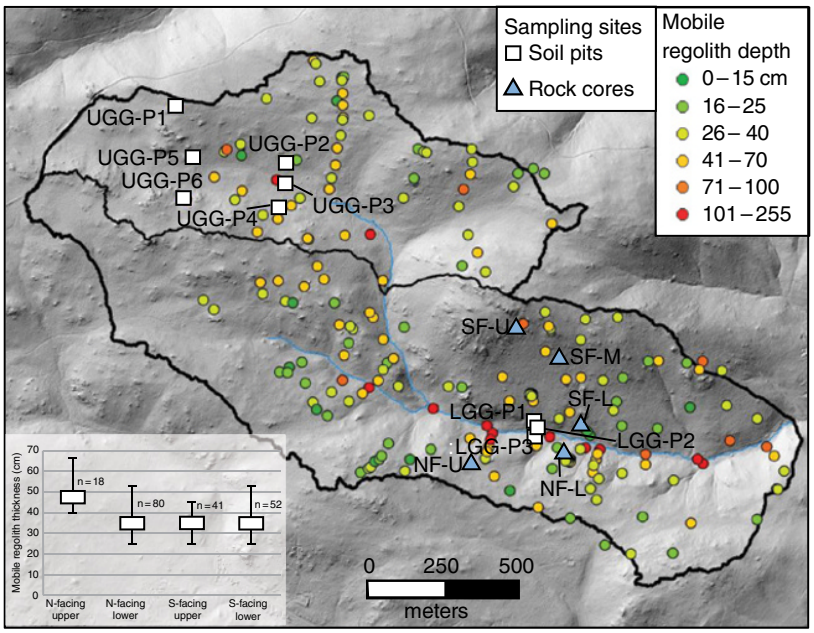

Figure 13.3 Shaded relief DEM of Gordon Gulch, showing the smaller upper basin and larger lower basin, linked by a generally east-flowing stream. Colored circles keyed to mobile regolith depth, determined from soil pits (modified from Shea et al., 2012). Statistics of the mobile regolith data are summarized in inset box plot. Soil pit and rock core sampling sites discussed in the text are labeled. DEM based on S. P. Anderson, Qinghua, et al. (2012).

Gordon Gulch is within the upper montane forest vegetation zone of Marr, 1961. On S-facing slopes, an open ponderosa pine (*Pinus ponderosa*) woodland with grass, herb, and shrub understory dominates, while N-facing slopes support a dense lodgepole pine (*Pinus contorta*) forest with little understory (Peet, 1981). According to Marr (1961), the lodgepole pine stands in the upper montane forest are a successional ecosystem and will eventually be replaced by Douglas fir (*Pseudotsuga menziesii*) and ponderosa pine stands. Holocene pollen records from the Snowy Range in southern Wyoming (Minckley et al., 2012), however, suggest that frequent perturbations (i.e. fire and changes in effective moisture regime) prevent Rocky Mountain ecosystems from reaching compositional equilibrium with the climate.

Late Quaternary climate and vegetation are relevant for the time span represented by the weathered profile in Gordon Gulch. As noted above, its close proximity (~5 km) to the terminal moraines of the Green Lakes Valley glacier suggests that Gordon Gulch experienced periglacial conditions during glacial climates. Based on 1-D and 2-D numerical models of the Green Lakes Valley glacier maximum extent and early Holocene retreat, Dühnforth and Anderson (2011) inferred Last Glacial Maximum temperatures that were 4.5–6 °C cooler than present, and with little or no change in precipitation.

The closest pollen record is from glacial Lake Devlin (Madole, 1986), a formerly ice-dammed lake located 7.2 km west of Gordon Gulch at 2953 m elevation (>200 m above Gordon Gulch). The Lake Devlin record indicates that the site was above the tree line during Last Glacial Maximum time; Legg and Baker (1980) interpreted the dominance of *Artemisia* and nonarboreal pollen as evidence of sagebrush steppe vegetation in an alpine tundra environment. *Picea*/*Pinus* (spruce/pine) pollen ratios suggest that the Last Glacial Maximum tree line was about 500 m lower than at present (Legg & Baker, 1980). This record is in agreement with pollen records from the region, which record lowered tree line in the Late Pleistocene, followed by a rise in tree line above the present level in early Holocene and a decline to present tree line levels in late Holocene time (Brunelle, et al., 2005; Mensing et al., 2011; Minckley et al., 2012; Vierling, 1998). Given the present tree line elevation of about 3350 m, the analysis of Legg and Baker (1980) suggests that Gordon Gulch would have been about 100 m below tree line during glacial times, but the uncertainties on this estimate are large.

Legg and Baker (1980) use local climate station records with their pollen analysis to estimate a Pinedale (Last Glacial Maximum) climate with summer temperatures about 5 °C cooler and mean annual precipitation about

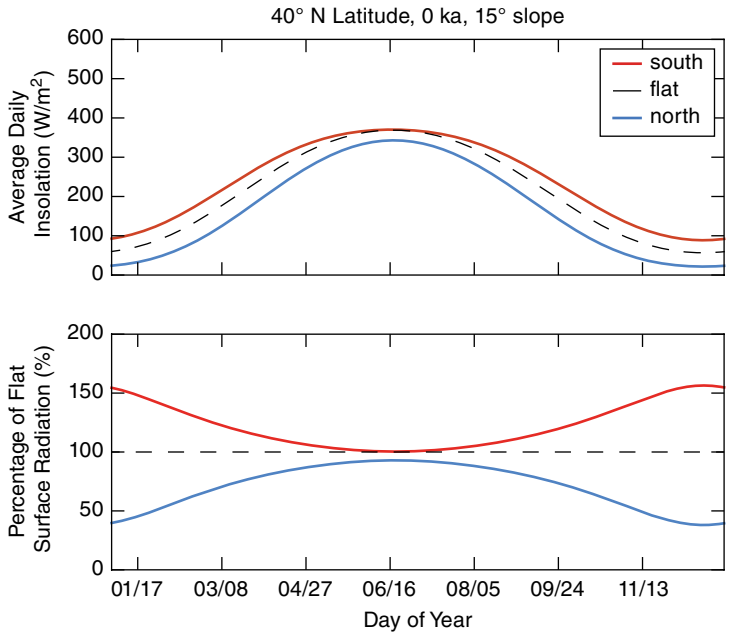

Figure 13.4 Top: Variation over a year of the average daily shortwave insolation for a flat surface (black, dashed), a N-facing surface (blue), and a S-facing surface (red) at the latitude of Gordon Gulch (40° N). The sloped surfaces have a 15° inclination. Bottom: Variations in average daily shortwave insolation shown as a percentage of the radiation on a flat surface. The differential between slope aspects is greatest during winter and least at midsummer.

150 mm higher than present. Given the agreement of the pollen analysis and glacial reconstruction (Dühnforth & Anderson, 2011), it is likely that Gordon Gulch temperatures were similarly depressed during glacial intervals and would have crossed into a temperature regime in which thin permafrost may have existed (i.e. mean annual temperature of –1 to 0.5 °C).

13.2.3. Solar Radiation

The east-west orientation of Gordon Gulch means that hillslope aspects are dominantly either pole facing (N-facing) or equator facing (S-facing). The resulting contrasts in incoming direct shortwave solar radiation affect soil temperature, snow melt, soil moisture, and vegetation. There are secondary energy balance effects in the downward longwave radiation and surface temperature due to shading. Here, however, we focus on the direct shortwave radiation term of the energy balance, which is the larger component on cloud-free days common in this region.

The total annual direct shortwave radiation to a horizontal surface on the Earth decreases with latitude in a predictable way. Relative to flat surfaces, pole-facing slopes will intercept less direct radiation, while equator-facing slopes will intercept a greater amount (Garnier & Ohmura, 1968). The slope aspect differential varies with season, from a maximum at the winter solstice when the solar elevation angle is low, to a minimum at summer solstice when the solar elevation angle is high. Figure 13.4 illustrates the differences in shortwave radiation over the course of a year at the latitude of Gordon Gulch (40° N) for surfaces sloping 15° poleward or equatorward and for a flat surface. The 15° slope angle was chosen for this calculation as it is typical of hillslopes over much of Gordon Gulch. At midwinter, the S-facing slope receives over 50% more, whereas the N-facing slope receives less than 50% of the radiation incident on a flat surface.

We have used a high-resolution digital elevation model (DEM) of the topography to calculate the incident shortwave solar radiation across Gordon Gulch and integrated over a year. Calculation of incident radiation followed Garnier and Ohmura (1968) and Hock (1999). The resulting map (Figure 13.5) shows that, due to topographic aspect alone, S-facing slopes receive 2–3 times more shortwave solar radiation annually than N-facing slopes. These radiation and consequent soil moisture differences, as well as fire disturbance, affect modern vegetation (Peet, 1981). The resulting differences in modern vegetation across aspects would amplify the topographic radiation contrast, as N-facing slopes are shaded by the closed-canopy lodgepole forest, while the open ponderosa woodland on S-facing slopes provides less shading.

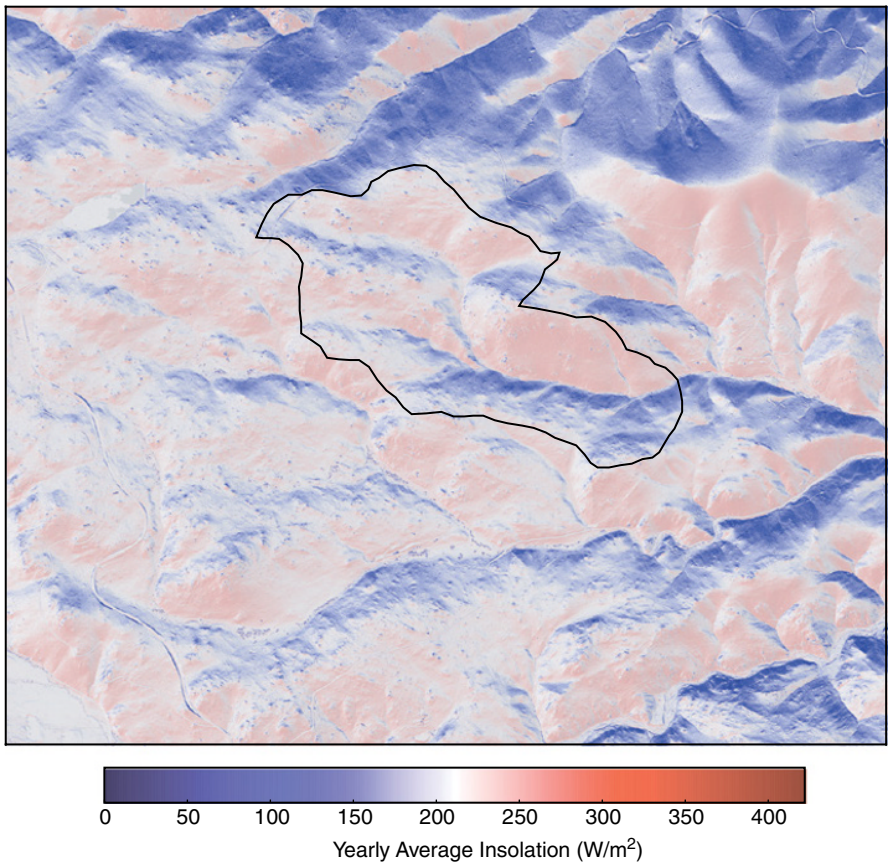

Figure 13.5 Modeled solar radiation integrated over each day of the year to yield the average annual insolation distributed across the landscape for Gordon Gulch (black outline) and surrounding terrain. S-facing slopes receive as much as three times more radiation over the course of a year than do N-facing slopes.

13.3. CRITICAL ZONE ARCHITECTURE

We now describe the critical zone architecture in Gordon Gulch, beginning with the overall thickness of the weathered zone and distribution of mobile regolith. The methods and results of analysis of geochemical and mechanical characteristics of the mobile regolith and near-surface weathered rock are described. Our description of the critical zone concludes with a brief review of the rates of denudation and mobile regolith production in Gordon Gulch.

13.3.1. Weathered Profile Thickness

A first-order descriptor of critical zone architecture is the thickness of the weathered profile. This is also the most difficult characteristic to measure, as exposures, such as boreholes, cores, or cuts into the subsurface, are rare and provide a limited view of subsurface variability. Geophysical imaging techniques provide spatial information, although resolution of critical zone features is challenging due to lateral (as opposed to vertical) structures (Parsekian et al., 2015) and small velocity contrasts between weathered rock, saprolite, and mobile regolith (Befus et al., 2011).

An extensive survey of groundwater well drillers' logs found a mean depth to fresh rock of 7.7 m in the region around Gordon Gulch (Dethier & Lazarus, 2006). The clearest picture of the depth of the weathered profile comes from shallow seismic refraction profiles along lines in Gordon Gulch totaling 4.4 km in length collected by Befus et al. (2011). Along these catchment traverses, the average depth to a high P-wave velocity (V_p) of 3.5 km/s (associated with unweathered crystalline bedrock; Befus et al., 2011) is 11.7 ± 3.1 m. The thickness of low and intermediate velocity materials representative of saprolite and weathered rock is greater under N-facing slopes than S-facing slopes throughout the catchment (Figure 13.6). In the upper basin, P-wave velocities <3.5 km/s (i.e. weathered rock) extend to depths of >10 m under

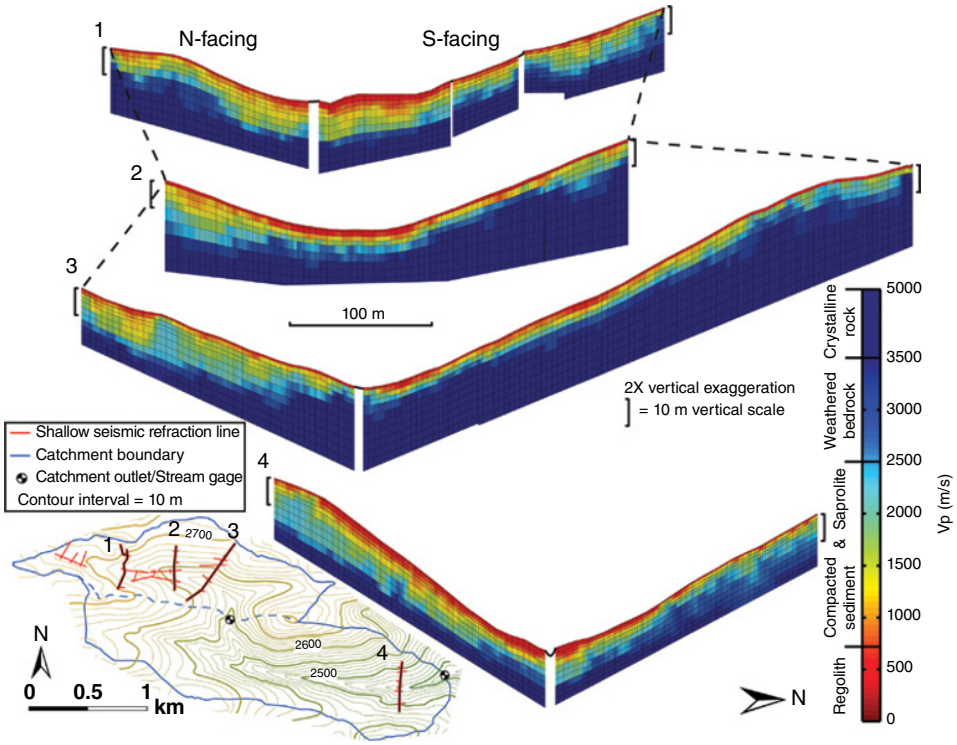

Figure 13.6 Seismic refraction profiles in Gordon Gulch. The four longest seismic refraction survey lines crossing Gordon Gulch are shown. Seismic velocities (V_p) greater than 3.5 km/s are considered unweathered rock. Note 10 m vertical scale bars shown adjacent to each cross-section, and the 2x vertical exaggeration. Mobile regolith is not resolved in the seismic refraction surveys. Inset shows where the lines are located within Gordon Gulch. (Source: Befus et al., 2011.)

N-facing slopes but only 5–7 m under valley bottom and S-facing slopes (Befus et al., 2011). In the lower basin, weathered rock reaches 15 m thickness under N-facing slopes and 5–10 m thickness under S-facing slopes. Individual seismic lines show what Befus et al. (2011) called "domes" of high velocity (unweathered rock) rising within a few meters of the surface in places on both slope aspects (Figure 13.6); these features emphasize the need for full hillslope length on seismic survey lines to judge the mean depth across slope aspects.

The observations of Befus et al. (2011) are consistent with seismic refraction surveys conducted in Gordon Gulch by St. Clair et al. (2015). That work addressed the influence of topographic stress under differing regional stress regimes on critical zone architecture. Their model calculations show that topographic perturbations to weak regional compressive stress regimes of the Colorado Front Range should produce surface parallel patterns of bedrock fracturing. For this reason, St. Clair et al. emphasized the relatively shallow (<20 m) and surface-parallel pattern of the weathered rock zone from ridge crest to valley floor in Gordon Gulch. St. Clair et al. contrast the pattern at Gordon Gulch with that found under strong regional compression, exemplified by a site in the Calhoun Critical Zone Observatory in South Carolina. In contrast to Gordon Gulch, Calhoun displays a "bowtie" pattern (St. Clair et al., 2015) of deep weathering (low seismic refraction velocities) under ridges compared to valleys; weathering under ridges reaches depths of the same order as the topographic relief, while weathering depths under channels are comparatively shallow. In Gordon Gulch, the thickness of the weathered profile (overall from 2 to 21 m; Befus et al., 2011), is much less than the relief between ridge top and valley floor, which ranges from 70 to >200 m in parts of Gordon Gulch. In comparison to Calhoun, the weathered zone is indeed largely a surface-parallel feature in Gordon Gulch.

Foliation of the gneiss bedrock may affect critical zone architecture in Gordon Gulch. While the hillslopes are shallower than the 44°–68° N dip of the foliation, the N-facing slopes subtend a smaller angle with the foliation, while the S-facing slopes more distinctly cut across the foliation. This structural feature may explain why tors (bedrock outcrops) are more common on the S-facing than N-facing slopes (Shea, 2013; Trotta, 2010).

In summary, seismic refraction surveys (Befus et al., 2011; St. Clair et al., 2015) show that weathered rock within Gordon Gulch extends to depths of 2–21 m, generally paralleling the surface topography. In detail, the thickness of the weathered zone tends to be greater under N-facing slopes than S-facing slopes, and domes of less weathered rock near the surface disrupt the general surface parallel pattern of weathered rock.

13.3.2. Mobile Regolith

Both geophysical methods and shallow excavations have been used to assess the depth of mobile regolith in Gordon Gulch. An electrical resistivity tomography (ERT) survey reported that "stratified slope deposits" averaged 3.0 ± 2.2 m thickness in Gordon Gulch (Leopold et al., 2013), a finding in stark contrast with measurements from hundreds of manually excavated soil pits across the catchment that yield mean mobile regolith thicknesses of substantially less than 1 m (Diek et al., 2014; Shea, 2013; Shea et al., 2012). The discrepancy between the ERT and soil pit observations seems to lie in the reliance by Leopold et al. (2013) in equating electrical resistivity values measured under unreported moisture conditions in small exposures of subsurface materials throughout the Front Range with the specific resistivity values generated by inversion of ERT survey lines in Gordon Gulch. We are more confident in the hand-dug soil pit observations of the depth of mobile regolith, and attribute the "stratified slope deposit" mapping unit of Leopold et al. (2013) to a combination of mobile regolith and saprolite.

Mobile regolith thickness does display variability within the catchment (Figure 13.3). Although not specifically identified in Figure 13.3, bedrock tors with no mobile regolith cover are estimated to account for ~10% of the catchment area. Between these tors, the mobile regolith thickness averages 38.7 ± 17.6 cm (n = 191) (Shea, 2013). In a few restricted locations, primarily near the base of N-facing slopes, mobile regolith reaches as much as 2 m (mean of 113.6 ± 36.2 cm, n = 7). These thickened toe slope deposits appear to be stagnated periglacial slope deposits on the basis of their high stone content at depth and significant meteoric ^{10}Be accumulations (Foster et al., 2015). Narrow mapped alluvial terraces in the lower basin, which display interlayering of sand, gravels, and fine-grained sediment, are also sites of deep mobile regolith accumulation (Shea, 2013). These appear to form the base level for the periglacial slope deposits. Finally, small alluvial fans are found in the lower basin, with deep accumulations of massive to weakly stratified sediment. Charcoal fragments in one such deposit in the lower basin yielded ^{14}C dates of 5,150–9,876 yr BP, indicating more than 2 m of sediment deposition on this fan in the Holocene (Shea, 2013).

13.3.3. Methods of Determining Material Characteristics of the Critical Zone

Soil and weathered rock geochemistry and mechanical properties have not been previously published. In this subsection we describe methods of sample collection and analysis before presenting the results in the following subsection.

13.3.3.1. Sample collection

Soil and saprolite samples were collected from nine soil pits dug by hand to depths that ranged from 30 to 180 cm along N–S transects, two in the upper basin and one in the lower basin (Figure 13.3). Seven pits on hillslopes were dug to refusal or to a depth at which continued progress through saprolite was very slow. The two valley bottom excavations reached the greatest depths (160 and 180 cm) but did not reach bedrock. Soil samples were collected from upslope working faces of soil pits, either in ~15 cm increments with a slide-hammer piston corer or as grab samples. The weathered bedrock encountered at the base of the mobile regolith was gneiss, generally with clearly visible foliation and layering. Additional samples were collected from the same pits for microbial community analysis (Eilers et al., 2012) and for leaching water-soluble organic matter (Gabor et al., 2014).

Rock was sampled by drilling at paired sites on tors (outcrops) and adjacent mobile-regolith mantled bedrock. Cores were drilled with a backpack portable drill fitted with a water-cooled diamond bit 36 mm interior diameter core barrel (Shaw Tools). Boreholes were drilled to depths of 1 to 1.66 m, producing cores of 0.32–1.18 m in length (mean core recovery of 63%). Cores were drilled at five locations in the lower basin, three on the S-facing slope and two on the N-facing slope (Figure 13.3). At each site, two cores were obtained, one from a tor (outcrop) and one from the weathered bedrock underneath mobile regolith (drilling began in the bottom of an excavation) a few meters from the tor borehole. The cores from mobile-regolith mantled bedrock are weathered sufficiently to be considered saprolite (isovolumetrically weathered rock) and will be designated "saprolite cores" to distinguish them from saprolite collected manually from the nine soil pits described above.

An effort was made to select these rock drilling sites within the bodies of relatively homogeneous Boulder Creek granodiorite, rather than in the metamorphic rock that dominates Gordon Gulch. The igneous rock is more homogeneous than the gneiss and simplifies interpretation of depth trends within the rock. The cores spanned the entire granite composition range and probably included some large-scale granitic zones within the metamorphic unit (Kelly, 2012).

Soil, saprolite, and rock samples were oven dried at 90 °C. Soil pit samples were weighed, then disaggregated and dry

sieved to separate out the <2 mm size fraction, which was analyzed; saprolite samples were crushed and analyzed in bulk. Bulk density was determined from the slide-hammer piston core samples, assuming no compaction during collection. Rock cores were subjected to mechanical testing (described below) before being powdered in a ring mill for mineralogical and geochemical analysis. Bulk density of rock core segments was determined by coating weighed samples in wax, reweighing, and measuring the water displaced by the coated samples.

13.3.3.2. Geochemistry

Mineralogy of the samples was determined by quantitative X-ray diffraction (XRD) (Srodon et al., 2001) at the U.S. Geological Survey laboratory in Boulder, Colorado. One gram of sample was mixed with 0.25 g of corundum standard. The sample was then mixed with 4 mL of methanol and ground in a McCrone micronizing mill and dried at 85 °C overnight. Once dried, the sample was sieved through a 250-micron sieve and packed in a random mount. XRD patterns were obtained on a Siemens D-500 X-ray diffractometer with a 1° slit by scanning for peaks between 5° and 65° using a 0.02° increment. Mineral concentrations were determined using the Rock Jock program (Eberl, 2003), which fits the sample spectra as the sum of the spectra from measured mineral standards. The proportion of each standard required to give the best fit is the integrated intensity of that particular mineral.

XRD is generally not considered a powerful technique for characterizing amorphous phases such as organic matter and glass. The ability to approximate roughly organic content from XRD is important, however, since an accurate fit to the XRD patterns requires standards that will accurately account for the XRD intensity of all the major phases present, including abundant amorphous phases. Good correlations have been found between organic carbon determined by XRD using RockJock and independent carbon analyses of soils (A. Blum, personal communication, 2008). Many of the soil surface samples contained high organic content, and the organic matter was modeled in RockJock using a Florida peat standard, which has been shown to correlate well with organic matter content determined with loss on ignition. All mineral abundances have been corrected for organic matter content based on the XRD analysis.

Elemental analysis was done by X-ray fluorescence (XRF) at the U.S. Geological Survey laboratory in Boulder, Colorado. A 1.5 g aliquot of powdered sample was placed in a ceramic crucible and placed in a furnace at 550 °C for 1 hour, then weighed. Samples were then fired at 925 °C for 25 minutes to burn off hydroxyl water and weighed again. Loss on ignition was determined as the total weight loss during both the 550 °C and 925 °C burns. Fused glass beads were prepared from the fired samples in a 1:10 mixture with anhydrous lithium tetraborate flux, following U.S.G.S. guidelines (Taggart et al., 1987, p E10), as detailed in Kelly (2012). The spectral detector on the XRF spectrometer used a count protocol of 5 seconds for major elements and 20 seconds for trace elements.

13.3.3.3. Rock quality

Rock drilling rates and solid core recovery varied between coring sites. Weathering grades varied not only between sites but often at submeter scale within the same outcrop. These differences were quantified by keeping track of the length of core segments recovered and total core obtained over the length of a borehole.

13.3.3.4. Rock strength

The tensile strength of core samples was evaluated using the widely accepted engineering method known as the Brazilian tensile test (or splitting test). The literature suggests that laboratory tensile stresses accurately simulate in situ stresses exerted by drivers such as tree roots (Aydin & Basu, 2005). Details of sample preparation and testing are found in Kelly (2012). In brief, core sections were visually screened to select specimens representative of the dominant lithology. Pegmatitic veins and areas of obvious mica aggregation were excluded where possible. Following ASTM D 3967-95a (ASTM, 1995), samples were cut with a water-lubricated diamond saw to a thickness-diameter ratio (t/D) of 0.5, using care to make cuts parallel to each other and perpendicular to the longitudinal axis of the core. Sample thickness and diameter were measured with digital calipers to determine t/D.

The Brazilian tensile test is conducted by loading a cylindrical core section between two steel platens. The load frame then compresses the sample along the cylinder's longitudinal axis, creating a line load. Force increases until the sample splits diametrically; failure force is reached within 1 to 10 minutes of test initiation. The splitting tensile strength is computed as

$$\sigma = \frac{2P}{\pi t D},$$

where σ is the splitting tensile strength (MPa), P is the maximum applied load indicated by the testing machine (N), t is the thickness of the specimen (mm), and D is the diameter of the specimen (mm). Tests were conducted on an MTS Systems Corporation hydraulic load frame at a displacement rate of 5.08×10^{-6} m/s. Loads were measured and recorded every 0.1 seconds. Resolution for all tests was approximately 1.48 N.

13.3.4. Critical Zone Geochemistry

Two features stand out in the mineralogy of samples collected from the soil pits (Figure 13.7). First, as a whole, the mineralogy is much more variable in saprolite than in the mobile regolith. Within the saprolite, quartz,

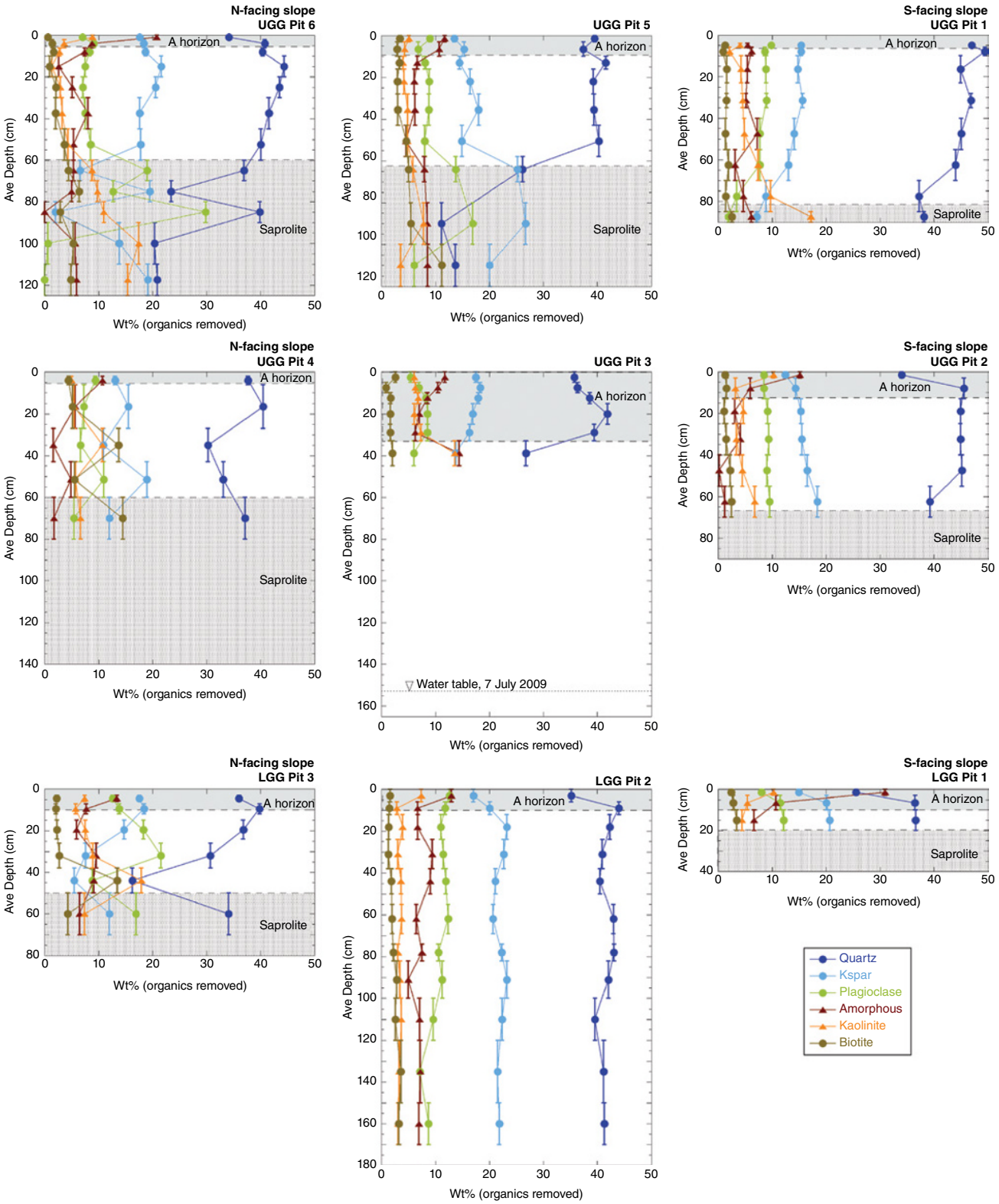

Figure 13.7 Mineralogy of soil pits in Gordon Gulch. Error bars show vertical extent of each sample. Gray shading at the top of each plot shows depth of the A-horizon identified in the field by dark color. Gray shading at the bottom of each plot shows saprolite. Each plot shows the vertical extent of the excavation; in some cases, samples were not analyzed through entire profile. Plots are arrayed left to right from N-facing to S-facing slope, and from the highest transect at the top of the figure to the lowest transect at the bottom of the figure. Pit locations shown in Figure 13.3.

Table 13.1 Summary of mineralogy from soil pits, cores from tors, and from mobile regolith mantled saprolite compared with averaged compositions from regional bedrock.

	Gordon Gulch				Regional Bedrock	
	Mobile Regolith (from pits) (wt%)	Saprolite (from pits) (wt%)	Saprolite (from cores) (wt%)	Rock (tor cores) (wt%)	Biotite Gneiss[a] (vol%)[b]	Boulder Creek Granodiorite[c] (vol%)[b]
Quartz	39.3 ± 5.8	27.4 ± 10.3	37.8 ± 12.1	30.4 ± 7.5	39.7	25.0
K-feldspar	16.9 ± 3.8	14.9 ± 7.9	29.1 ± 18.3	28.6 ± 21.7	8.8	10.0
Plagioclase	9.4 ± 2.9	11.2 ± 9.3	15.3 ± 11.6	31.2 ± 19.9	10.5	42.0
Sillimanite	4.8 ± 2.0	8.1 ± 4.8	4.8 ± 11.1	0.1 ± 0.4	8.6	
Amorphous silica[d]	7.8 ± 4.8	5.6 ± 2.7	—	—		
Total nonclays	*82.4 ± 7.4*	*71.1 ± 7.5*	*89.9 ± 10.3*	*91.6 ± 5.0*		
Illite (1M & 2M)	7.4 ± 3.2	6.9 ± 4.2	1.2 ± 1.6	0.3 ± 0.5		
Biotite + Phlogopite	4.7 ± 3.0	12.0 ± 5.4	6.8 ± 10.0	6.3 ± 4.8	21.7	16.0
Kaolinite	5.6 ± 3.0	10.1 ± 4.7	1.2 ± 0.9	0.9 ± 0.7		
Total clays	*17.6 ± 7.4*	*28.9 ± 7.5*	*10.1 ± 10.3*	*8.4 ± 5.0*		
Number of samples	55	11	25	43		

[a] Average modes for garnet-sillimanite-biotite gneiss north of the Idaho Springs-Ralston shear zone from Table 28 in Gable (1996).
[b] Gable (1980a) reports modal mineralogy in volume %; given the similarity in density of the silicate minerals considered here, there is little difference between volume and weight %.
[c] Summary values for Boulder Creek granodiorite in metasedimentary rocks, from Table 5 in Gable (1980a).
[d] Amorphous silica is fitted to the White River tephra in RockJock and represents noncrystalline Si/Al material.

plagioclase, K-feldspar, and biotite contents vary considerably from one sample to the next, reflecting the compositional layering in the gneiss bedrock. In contrast, mobile regolith samples vary within a narrow range in most pits. UGG Pit 4, which displayed greater variability in mobile regolith mineralogy than other pits, was noted in the field for containing abundant (~30%) rock fragments throughout. A simple way to quantify the difference in variability between the mobile regolith and the saprolite is to compare the standard deviations for the mean values (Table 13.1). Pit saprolite samples display a much greater standard deviation around the mean values than do the mobile regolith samples.

The second feature is that regolith contains weatherable primary minerals, including plagioclase, K-feldspar, and biotite, in quantities that are not readily distinguishable from the saprolite samples at the base of the soil pits (Figure 13.7). Clay minerals are also present throughout the profiles, with no obvious layer of accumulation. Descriptions of the gneiss bedrock of the Front Range (Gable, 1996) note the presence of kaolinite, illite, and muscovite-sericite in the rock, all of which may have formed in part during hydrothermal alteration associated with Laramide intrusions. In our soil pit samples, kaolinite in mobile regolith and saprolite occurs in both a poorly crystalline phase and a crystalline phase (halloysite) typical of incipient weathering. We also find illite in both the mobile regolith and saprolite. Thus, much of the clay found in the mobile regolith is probably not an in situ weathering product.

The presence of biotite throughout the rock, saprolite, and mobile regolith is notable. Weathering of biotite to hydrobiotite was found to be responsible for a high degree of rock disintegration (grussification) in Boulder Creek granodiorite at a site a few kilometers east of Gordon Gulch (Isherwood & Street, 1976). No significant chemical alteration accompanied the disintegration, and in fact biotite was present even in the grus. Biotite hydration is accompanied by a large volume increase (Buss et al., 2008), and this physical transformation sends microfractures through the surrounding mineral grains in the rock (Isherwood & Street, 1976).

The drilled rock cores provide an opportunity to inspect at bedrock mineralogy at greater depths. The mineralogy of these cores is summarized in Table 13.1, for both the cores from tors and for the cores obtained from mobile-regolith mantled rock. The latter are weathered enough to be considered saprolite. The cores contain less clay than the mobile regolith and saprolite collected from pits, and consequently contain greater fractions of quartz, K-feldspar, and plagioclase.

Elemental analysis from XRF shows differentiation between soil pit mobile regolith and saprolite and the drilled cores (Figure 13.8). The loss on ignition (LOI) data, which measures a combination of organic matter and hydroxyl water, clearly segregates bedrock, saprolite,

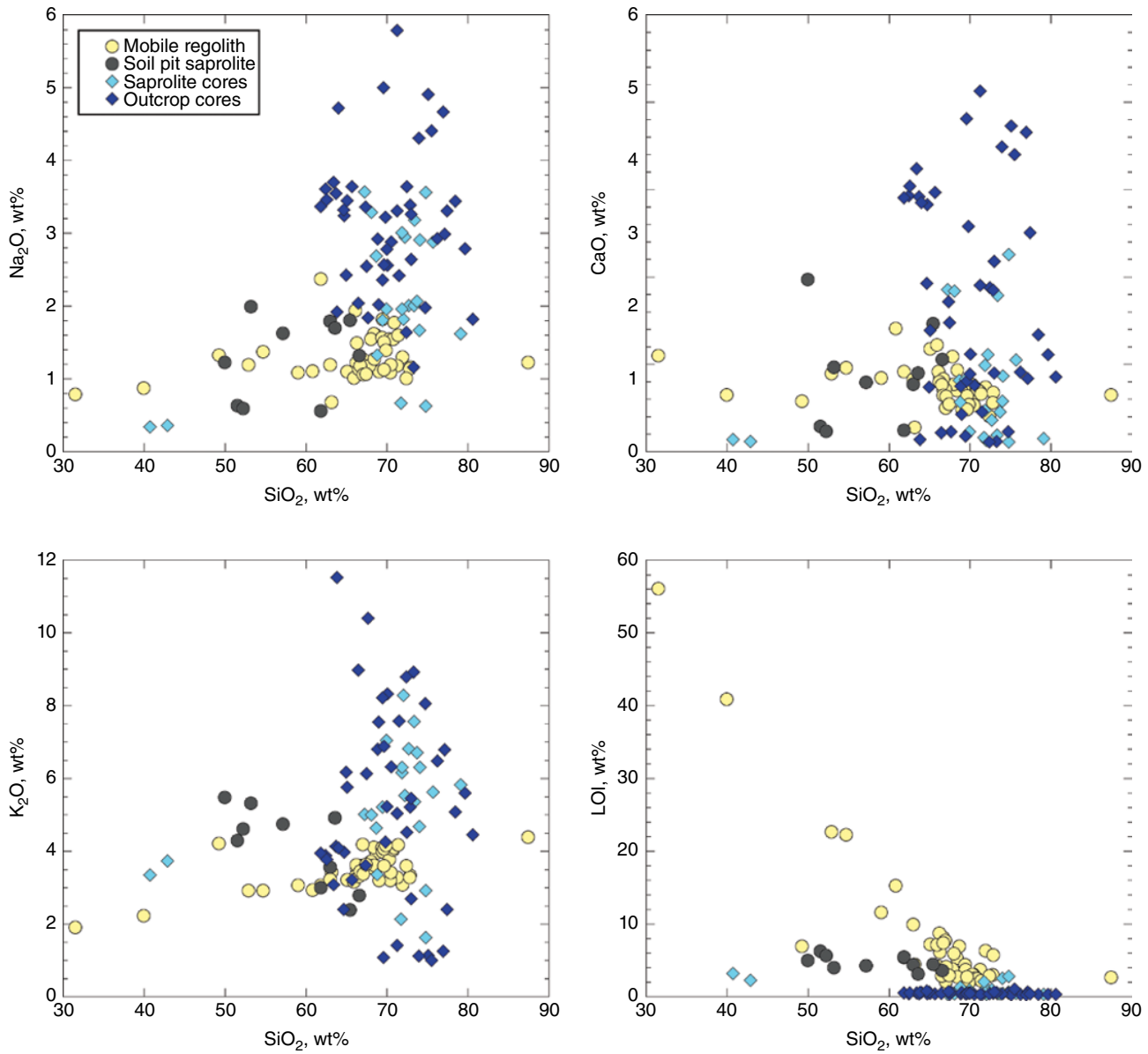

Figure 13.8 Elemental analyses from X-ray fluorescence for samples from soil pits (mobile regolith and saprolite) and from drilled cores. The saprolite core samples come from mobile regolith mantled bedrock, while outcrop cores samples are drilled on tors. LOI is loss on ignition, from burning samples at 925 °C.

and mobile regolith samples. Outcrop cores have the lowest LOI at 0.5 ± 0.2 wt%, followed by saprolite cores (1.1 ± 0.8 wt%) and soil pit saprolite (4.6 ± 1.0 wt%), and the highest LOI is found in mobile regolith (7.8 ± 10.0 wt%). These data clearly show an accumulation of organic matter from rock to saprolite to mobile regolith.

Alkali metals (sodium and potassium) as well as calcium are more abundant in the drilled core samples than in the soil pit samples (Figure 13.8). Although there is considerable overlap in the abundance of these cations in the core samples, the highest concentrations are found in outcrop cores. The pattern suggests that cations are progressively lost as rock weathers to form saprolite and ultimately mobile regolith. However, we must address the fact that core drilling targeted intrusive granodiorites, while our soil pits are on the dominant gneiss bedrock that dominates Gordon Gulch. The Boulder Creek granodiorite is much richer in plagioclase and lower in quartz than the biotite gneiss (Table 13.1; Gable, 1980a, 1996). Higher silica and cations in the core samples than

in the soil pit mobile regolith and saprolite (Figure 13.8) are therefore likely to reflect differences in parent bedrock compositions rather than being caused by weathering.

Against the heterogeneous nature of the bedrock geochemistry, it is difficult to identify a clear weathering signal. Statistically, we see more kaolinite in the soil pit saprolite than in mobile regolith (Table 13.1). However, the vertical distribution of kaolinite in the soil pit saprolite seems to reflect layering in the gneiss rather than weathering accumulation. Nor is there an obvious kaolinite accumulation bulge within the mobile regolith (Figure 13.7). Dethier et al. (2012) used a grain size definition of clay rather than mineralogy to quantify clay amounts in Gordon Gulch mobile regolith. They found an average of 4 ± 2 wt% clay in 13 soil profiles in Gordon Gulch (computed from their supplementary data), an amount significantly less than the clay mineral contents reported here (Table 13.1). In common with our observations (Figure 13.7), Dethier et al. (2012) note that horizon boundaries are indistinct in Gordon Gulch hillslope soils, and B-horizon accumulations of clay are lacking. A further complication to identifying a weathering signal is that eolian dust deposition is likely to influence soils in this area (Muhs & Benedict, 2006), although late Quaternary dust deposition rates in the region seem to be low (Ouimet et al., 2015). Ambiguity on clay sources in soils in the Colorado Front Range has been noted by other authors. Low clay formation rates, parent rock clay, and possible eolian contributions confound the interpretation of clays in soils developed on gneissic tills (Birkeland et al., 1987) and soils developed on Boulder Creek granodiorite (Dethier & Bove, 2011).

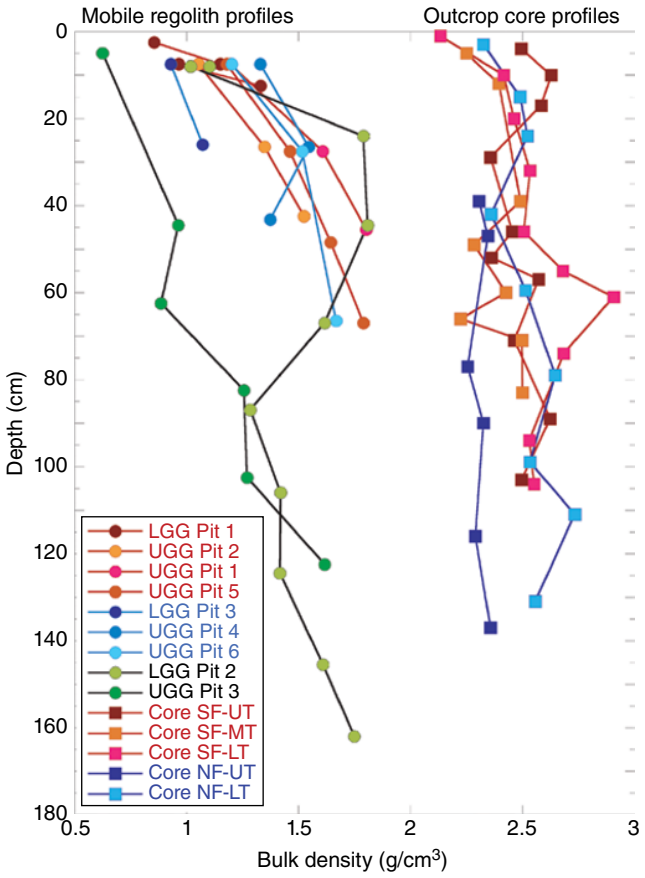

Figure 13.9 Bulk density of mobile regolith from soil pits and of bedrock from outcrop cores (locations shown in Figure 13.3). Red-hued symbols used for profiles on S-facing slopes, blue-hued symbols for profiles on N-facing slopes, and green-hued symbols used for two soil pits in valley bottom locations.

13.3.5. Mechanical Properties of the Critical Zone

The bulk density of outcrop core samples is greater than for mobile regolith samples (Figure 13.9). The bulk density of outcrop core samples shows little variation with depth, centered around a bulk density of 2.5 g/cm^3. Mobile regolith samples increased in bulk density with depth, from surface values around 1.0 g/cm^3 to values ~1.6 g/cm^3 at depth. Difficulty using the slide hammer piston corer in saprolite precluded saprolite bulk density measurements in the soil pits. These values imply, assuming that both rock and mobile regolith are composed of mineral grains of density 2.65 g/cm^3, that the rock has a porosity of ~5%, while mobile regolith has a porosity of ~40%.

An observation from the soil pits was that saprolite at the pit base seemed weaker and easier to excavate with hand tools on N-facing slopes than on S-facing slopes. Our excavations extended 40–80 cm into saprolite on N-facing slopes, but only 10–20 cm into saprolite on S-facing slopes (Figure 13.7). This qualitative observation inspired our coring and tensile strength testing of rock outcrops and rock at the base of mobile regolith.

A summary of drill core recovery and core segment lengths is presented in Table 13.2. The backpack coring system did a poor job of recovering rock, resulting in an overall core recovery of 63% in the 10 boreholes. Core recovery was greater in outcrop sites (41%–88%) than in mobile-regolith mantled sites (27%–81%). Among the outcrop sites, core recovery was greater on S-facing sites (87%) than N-facing sites (63%), but there was no aspect difference among the saprolite cores. In addition, core segments recovered were slightly longer and more variable in length in S-facing slope cores than N-facing slope cores at both outcrop and saprolite sites. Overall, the recovery and core segment length data suggest that outcrops are stronger than mobile-regolith mantled rock, and hint at rock on S-facing slopes being stronger than N-facing slopes. The low core recovery implies that sampling is skewed toward stronger materials, as material

Table 13.2 Summary of core recovery and tensile failure stress from drilling sites.

	Outcrop Cores							Saprolite Cores						
	NF-LT	NF-UT	All N-Facing Outcrop	SF-LT	SF-MT	SF-UT	All S-Facing Outcrop	NF-LP	NF-UP	All N-Facing Saprolite	SF-LP	SF-MP	SF-UP	All S-Facing Saprolite
Mobile regolith cover depth (cm)	0	0	**0**	0	0	0	**0**	95	57	**76 (mean)**	70	86	104	**87 (mean)**
Borehole depth (cm)	138	137	**275**	118	99	121	**338**	166	105	**271**	105	120	104	**329**
Core recovery (cm)	118	56	**174**	100	86	106	**292**	94	42	**136**	43	32	84	**159**
Core recovery (%)	85	41	**63**	86	87	88	**87**	57	40	**51**	41	27	81	**49**
Number of core segments			**33**				**41**			**22**				**30**
Mean segment length ± variance (cm)			**5.89 ± 9.39**				**7.75 ± 21.67**			**5.77 ± 3.83**				**6.27 ± 16.13**
Mean failure stress ± variance (MPa)			**2.14 ± 0.98**				**2.95 ± 1.29**			**1.95 ± 0.46**				**1.55 ± 0.45**

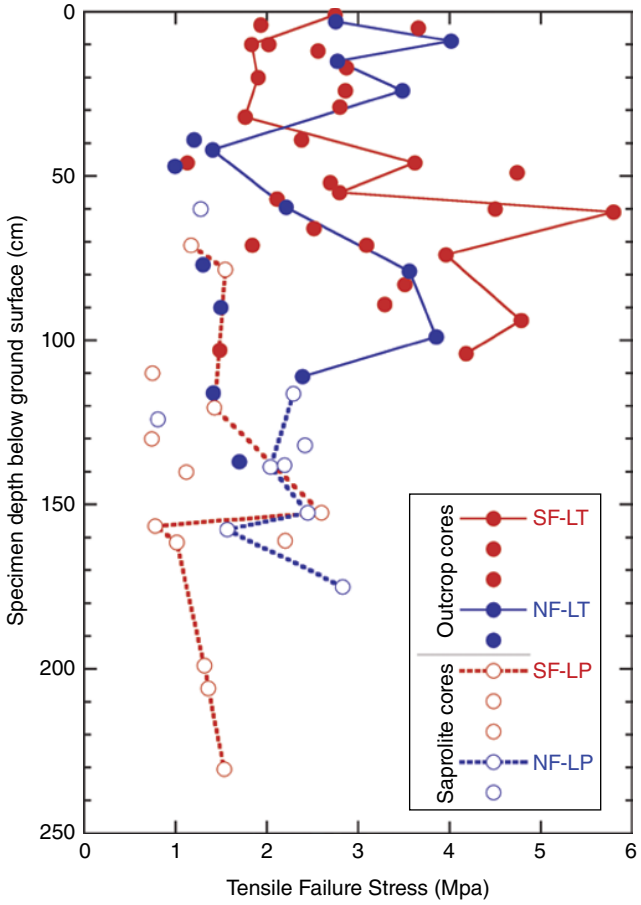

Figure 13.10 Brazilian tensile test results in outcrop and saprolite (mobile-regolith mantled) cores. Outcrop cores are shown with filled points, while saprolite cores are shown with open points. Profiles on S-facing slopes are red, and profiles on N-facing slopes are blue. For simplicity, points are connected for only one profile per aspect and site type.

between segments either was too fractured or too weak to survive the coring process.

Brazilian tensile test results from all core samples are shown in Figure 13.10. The tensile failure strength ranged from less than 1 to nearly 6 MPa. These values fall well within the range of tensile failure stresses reported for Malanjkhand granite (1.0–16.1 MPa; Gupta & Rao, 2000) and Kowloon granite (1–10 MPa; Aydin & Basu, 2005), both of which are medium-grained plutons of relatively homogeneous biotite monzonite composition. However, the strongest Gordon Gulch samples are 4–9 MPa lower than the maximum values measured elsewhere, which suggests that even the freshest outcrop samples in Gordon Gulch have undergone weathering-induced mechanical strength reduction. In this regard, it is worth noting that none of the Gordon Gulch cores reach depths where fresh rock was observed in the seismic refraction surveys (Figure 13.6).

Tensile failure strength was greater in outcrop cores (2.14 ± 0.98 MPa and 2.95 ± 1.29 MPa in N-facing and S-facing site cores, respectively) than in saprolite cores (1.95 ± 0.46 MPa and 1.55 ± 0.45 MPa in N-facing and S-facing sites, respectively) (Table 13.2). There is a great deal of scatter in tensile failure strength profiles (Figure 13.10), but there is a slight tendency for the tensile failure strength to trend to greater values with increasing depth below the surface in both the outcrop and saprolite cores.

13.3.6. Residence Time in the Critical Zone

Foster et al. (2015) used in situ and meteoric cosmogenic radionuclides (CRNs) to quantify the production rates and residence time of mobile regolith in Gordon Gulch. From in situ ^{10}Be they found that the mobile regolith production rate is 3.1 cm/kyr. The meteoric ^{10}Be inventories yield mobile regolith residence times of 10–20 kyr, except in a deep profile on a N-facing slope toe slope in the lower basin, where residence time likely exceeds 40 kyr. They found no difference in denudation or mobile regolith residence time across slope aspects. Foster et al. conclude from comparison of in situ and meteoric ^{10}Be data that steady, uniform lowering of the landscape has occurred across most landscape positions. The exception to the assumption of steady state is in the thick toe-slope deposits found at the base of the N-facing slopes in the lower basin (Figure 13.3), where mobile regolith residence times exceed the prediction from steady-state lowering. Although Foster et al. did not collect CRN data in the upper basin, presumably the valley bottom accumulation of sediment in the upper basin (Figure 13.3) also violates the steady-state assumption.

From the mobile regolith production rate and the assumption of steady-state weathering, we can estimate the residence time for material in the weathered profiles in Gordon Gulch. The seismic refraction surveys yield an average depth to fresh rock (>3.5 km/s p-wave velocity) of 11.7 ± 3.1 m across Gordon Gulch. This implies a residence of rock within the weathered zones of 380 ± 10 kyr. Most of this time is spent in the weathered rock and saprolite, and less than 10% is spent in the mobile regolith.

13.4. DISCUSSION

Gordon Gulch displays critical zone architecture that comprises thin mobile regolith with protruding tors, over a broadly surface-parallel zone of weathered rock. The depth to fresh rock (V_p > 3.5 km/s) is greater on N-facing hillslopes (>10 m) than on S-facing hillslopes (5–7 m), although there is variation in weathered zone thickness on both aspects. Mobile regolith thickens into a broad

valley bottom fill in the upper basin, and thickened toe-slope deposits are found on N-facing slopes in the lower basin. Narrow fluvial terraces, to which the toe-slope deposits grade, line the channel in the lower basin. Chemical alteration of the weathered rock and mobile regolith is difficult to quantify, given the heterogeneity of the predominantly gneiss bedrock. Primary weatherable minerals are present in near fresh rock abundances in both saprolite and mobile regolith; the slight alteration of biotite present in the rock is a process recognized as driving significant physical disintegration of rock in this setting (Isherwood & Street, 1976). Clay minerals are present in both saprolite and mobile regolith and do not show horizons of accumulation. Pedogenic iron (characterized with citrate-buffered dithionate extractable iron, Fe_d) does not show B-horizon enrichment in Gordon Gulch soils (Dethier et al., 2012), although there is an increase in pedogenic iron with soil age in the region (Birkeland et al., 1987; Dethier et al., 2012). Combining the CRN-based denudation rates (Foster et al., 2015) with the seismic refraction based depth-to-fresh rock (Befus et al., 2011) reveals that rock spends several hundred thousand years (i.e. three full glacial-interglacial cycles) in the near-surface weathered zone, and a few tens of thousands of years in transport on the hillslopes in the mobile regolith layer. The hillslope residence time results agree with the interpretation from pedogenic iron accumulation (Dethier et al., 2012). The CRN data support an interpretation of steady-state denudation of the landscape in all locations other than the toe slopes, and probably the valley bottom of the upper basin. If correct, these observations imply that the critical zone architecture documented here is neither transient nor in an incipient stage of development.

Taken together, these observations reveal a system that produces significant physical alteration of rock but accomplishes little chemical alteration. The presence of mobile regolith, reduced seismic velocities, and reduced tensile strength of weathered rock are all manifestations of weathering processes. These alterations can be accomplished by physical weathering processes (S. P. Anderson, 2019), such as frost cracking, biomechanical processes, and thermal or hydration expansion, possibly modulated by topographic and regional stress (St. Clair et al., 2015). The surprise is that breakdown of rock by these mechanical processes does not lead to more chemical weathering over the residence time of material in the critical zone of this landscape.

13.4.1. Is This Steady State?

Although we lean on an assumption of steady state, CRN-based determinations of denudation rate and mobile regolith production rate (e.g. Foster et al., 2015) do not directly measure the advance rate of the weathered rock/fresh rock interface. The production of in situ ^{10}Be falls off exponentially with depth over a length-scale of about 0.7 m in rock. Foster et al.'s (2015) samples were collected in soil pits that accessed only the top of the weathered rock. Nor does meteoric ^{10}Be, which accumulates in mobile regolith and to some extent in saprolite, provide insight into the dynamics of the deep weathering front. Instead, agreement between surface lowering rate and mobile regolith production rates from both in situ and meteoric ^{10}Be are taken as evidence for steadiness of all three interfaces (surface, mobile regolith/weathered rock, and weathered rock/fresh rock). Is this a fair assumption? It seems most likely that steadiness in the upper weathering interface does go hand-in-hand with steadiness in the lower weathering interface. If the deep weathering front (weathered/fresh rock) advanced more slowly than the mobile regolith/weathered rock interface, the weathered rock zone would ultimately thin to zero. On the other hand, if the deep weathering front advanced more rapidly, we would expect the weathered zone to be thicker than the ~10 m present in Gordon Gulch given the 40 Myr of evolution since the Laramide orogeny. Variations in weathering interface advance rates cannot be ruled out, although Occam's razor implies that these are unlikely (e.g. Willenbring & Jerolmack, 2016).

The long-term steady-state denudation rate from CRNs of 3.1 cm/kyr can be translated into a mass loss rate of 820 kg/ha/yr. Modern dissolved fluxes from the upper basin of Gordon Gulch measured for water years 2011 and 2012 (Mills, 2016) show that modern solute exports are ~10 kg/ha/yr, which is less than 2% of the long-term CRN-based denudation rate (Table 13.3). Mills et al. (2017) quantify an additional loss of predominantly SiO_2 in the form of colloidal material in the stream, but this adds only about 30% to the total dissolved flux. Although the particular years that Mills (2016) monitored were low runoff years, the deviation from modern norms is insufficient to explain the gap between CRN-based total denudation and solute fluxes. Analyses of past climates for the region highlight differences in temperature over changes in precipitation (e.g. Legg & Baker, 1980; Dühnforth & Anderson, 2011). Although cooler conditions may have reduced evapotranspiration, and hence might have enhanced runoff and dissolved fluxes, the likely increase in the depth and duration of frozen ground would likely have limited chemical weathering processes. In sum, chemical fluxes are responsible for little of the overall development of the critical zone.

We have recently explored the role of climate (i.e. precipitation) on the development of critical zone architecture by modeling the long-term evolution of hydrologic flow paths, chemical weathering, and physical denudation under wetter and drier conditions (R. S. Anderson et al.,

Table 13.3 Comparison of modern dissolved fluxes and long-term CRN-based total denudation rates for Gordon Gulch.

Modern Solute Flux Data[a]							CRN-Based	Diss./Total
Year[b]	Ca (kg/ha/yr)	Mg (kg/ha/yr)	Na (kg/ha/yr)	K (kg/ha/yr)	SiO_2 (kg/ha/yr)	Total Dissolved Flux (kg/ha/yr)	Total Denudation[c] (kg/ha/yr)	Denudation (%)
2011	2.0	1.3	1.7	0.6	8.3	14	820	1.7
2012	1.2	1.0	1.1	0.4	6.2	10	820	1.2

[a] Dissolved flux data from Mills (2016) for 0.95 km^2 upper basin of Gordon Gulch.
[b] Data is for water year (Oct 1–Sep 30).
[c] Long-term total denudation based on in situ cosmogenic ^{10}Be from Foster et al. (2015)

2019). The model compared a deeply weathered, wet system (modeled after landscapes of the SE United States studied by the Calhoun Critical Zone Observatory) and a shallowly weathered, dry system (modeled after Gordon Gulch). At the low effective precipitation (precipitation minus evapotranspiration) rates representative of Gordon Gulch, the plagioclase chemical weathering front (the reaction considered in this model) remained shallow and surface parallel once steady state was established (in less than 50 kyr), even as the hillslopes and channel continued to erode. R. S. Anderson RS et al. suggest that shallow, surface-parallel weathering is to be expected for cases in which the ratio of weathering front advance rate to total denudation rate, w_f/e, is low (less than 1). The research we have presented herein sheds light on how such a system works. Mechanical alteration processes proceed with sufficient vigor to produce mobile regolith. At the same time, physical transport of the mobile regolith is inefficient enough that the hillslopes remain in the geomorphic transported-limited regime in which denudation is limited by transport process rates rather than mobile regolith production rates. All the while, both in the weathered rock zone and the mobile regolith layer, lack of water limits chemical reaction progress.

Mobile regolith thickness and geochemistry do not vary across the slope aspects (Figure 13.7), despite the large differences in shortwave solar radiation (Figure 13.5). The time rock spends in the weathered zone is overwhelmingly spent in the weathered rock layer, rather than in the mobile regolith (a roughly 90%-10% split). The thermal influence of solar radiation falls off rapidly with depth and is insignificant below about 2 m. Instead, it is likely that the influence of radiation on water flux is most critical. While modern water flow paths differ across the aspects (Hinckley et al., 2014), under the glacial climates that dominate the >350 kyr residence time of material in the weathered zone, aspect differences in water flux may have been smaller.

We have argued in the past that periglacial processes of frost cracking and frost creep can explain the aspect differences in weathered profile depths in Gordon Gulch (R. S. Anderson et al., 2013). The thermal state required to drive frost cracking is strongly modulated by surface energy balance, and during glacial climates is likely to have been active at depths required to produce the weathered rock in Gordon Gulch. Given the much greater direct shortwave radiation on S-facing slopes than on N-facing slopes in Gordon Gulch (Figure 13.5), this mechanism remains a likely candidate to produce the broad-scale features of critical zone architecture that have developed in the last few hundred thousand years. The other likely process to produce the weakened, yet minimally chemically altered weathered rock zone in Gordon Gulch is biotite hydration. Unlike frost cracking, biotite hydration could operate during interglacial climates. Biomechanical processes associated with tree roots seem unlikely to be important in weathering rock in this setting, given the lowered tree line during the dominant glacial climate. Hence, biotite hydration and frost cracking complement each other in maintaining continuous weathering in the bedrock through changing climate cycles.

Over the Holocene, however, frost processes have probably declined in their influence and other drivers are coming into the fore. The Holocene represents most of the 10–20 kyr residence time of material in the mobile regolith. The aspect differences in forest structure and associated root architectures, for instance, are likely to be important and may affect water fluxes (Adams et al., 2014). Water delivery into the subsurface depends strongly on aspect (Hinckley et al., 2014; Langston et al., 2015), particularly in the present conditions of thin, ephemeral snow with contrasting snow persistence across slope aspects. Nonetheless, these differences have been insufficient to produce obvious differences in mobile regolith geochemistry across slope aspects, again implying that water limitation keeps geochemical modification of near-surface materials low.

Finally, it is worth addressing the question of steady state in Gordon Gulch over its recent history and looking forward in time. The thickened periglacial slope deposits on N-facing toe slopes in the lower basin and the sediment fill in the valley floor of the upper basin both speak to reduced sediment mobility and export over Holocene

time. Dethier et al. (2012) suggest that spatial variations in pedogenic iron accumulation-based residence times within Gordon Gulch reflect the episodic nature of sediment movement over tens of thousands of years. If steady state holds, the long-term CRN-based denudation rate of 3.1 cm/kyr must be matched by sediment transport rates out of the basin (given the very small denudation contribution by dissolved fluxes). Sediment fluxes have not been monitored in Gordon Gulch because the channel is very small (peak flows are ~150–180 L/s, and much of the year flow is less than 30 L/s) and water flows are generally visibly free of sediment above colloidal size. From these qualitative observations, we infer that the annual sediment flux is much less than that needed to maintain steady state. While episodic events undoubtedly play an outsized role in exporting sediment from the basin, the presence of the small Holocene terraces in the lower basin suggest that sediment is accumulating. It is likely that true steady state applies only when the system is averaged over glacial-interglacial climate swings, which serve to alternately enhance and hinder sediment transport efficiency.

13.5. SUMMARY

The critical zone in Gordon Gulch has developed over more than 350 kyr, producing an architecture with minimal chemical alteration, but comprising mobile regolith punctuated by tors over a roughly surface-parallel weathered rock zone. Mobile regolith geochemistry and thickness do not vary across N- and S-facing slope aspects, despite a two- to threefold difference in shortwave radiation. The weathered rock zone, however, is thicker and is perhaps mechanically weaker on N-facing slopes than S-facing slopes. Mechanical breakdown by frost cracking most likely controls these differences. In the semiarid modern climate and the colder glacial climates that dominate the past, low water flux and low temperatures have limited the chemical evolution of the system. This critical zone architecture is in steady state with the long-term climate, averaged over glacial-interglacial cycles, and incision of the river system.

ACKNOWLEDGMENTS

We thank the BcCZO team members who have been involved in generating the data presented here. In particular, we thank Alex Blum, Rachel Gabor, Katie Eilers, Zan Frederick, Andy Sufulko, Joel Jones, Ben Hoffman, Jeana Lee, Rory Cowie, Nate Rock, and Wendy Roth. We thank R. S. Anderson, Allen Hunt, and two anonymous reviewers for comments on the manuscript. This work was supported by grants to the Boulder Creek CZO (NSF 0724960 and 1331828) and an Earth Sciences postdoctoral fellowship to KRB (NSF 1725774).

REFERENCES

Adams, H. R., Barnard, H. R., & Loomis, A. K. (2014). Topography alters tree growth-climate relationships in a semi-arid forested catchment. *Ecosphere*, *4*, art148. doi:10.1890/ES14-00296.1

Anderson, R. S., Anderson, S. P., & Tucker, G. E. (2013). Rock damage and regolith transport by frost: An example of climate modulation of critical zone geomorphology. *Earth Surface Processes and Landforms*, *38*, 299–316. doi:10.1002/esp.3330

Anderson, R. S., & Humphrey, N. F. (1989). Interaction of weathering and transport processes in the evolution of arid landscapes. In Cross, T. (Ed.), *Quantitative dynamic stratigraphy* (pp. 349–361). Englewood Cliff, NJ: Prentice-Hall.

Anderson, R. S., Rajaram, H., & Anderson, S. P. (2019). Climate driven co-evolution of weathering profiles and hillslope topography generates dramatic differences in critical zone architecture. *Hydrological Processes*, *33*(1), 4–19. doi:10.1002/hyp.13307

Anderson, R. S., Riihimaki, C. A., Safran, E. B., & MacGregor, K. R. (2006). Facing reality: Late Cenozoic evolution of smooth peaks, glacially ornamented valleys, and deep river gorges of Colorado's Front Range. *Geological Society of America Special Papers*, *398*, 397–418.

Anderson, S. P. (2019). Breaking it down: Mechanical processes in the weathering engine. *Elements*, *15*, 247–252. doi: 10.2138/gselements.15.4.247

Anderson, S. P., Anderson, R. S., & Tucker, G. E. (2012). Landscape scale linkages in critical zone evolution. *Comptes rendus – Geoscience*, *344*, 586–596. doi:10.1016/j.crte.2012.10.008

Anderson, S. P., Qinghua, G., & Parrish, E. G. (2012). *Snow-on and snow-off Lidar point cloud data and digital elevation models for study of the topography, snow, ecosystems and environmental change at Boulder Creek Critical Zone Observatory*, INSTAAR, University of Colorado at Boulder, digital media. doi: 10.5069/G93R0QR0

Anderson, S. P., von Blanckenburg, F., & White, A. F. (2007). Physical and chemical controls on the critical zone. *Elements*, *3*, 315–319.

ASTM (1995). ASTM D3967-95a, Standard method for splitting tensile strength of intact rock core specimens, ASTM International, West Conshohocken, PA. doi: 10.1520/D3967-95A

Aydin, A., & Basu, A. (2005). The use of Brazilian test as a quantitative measure of rock weathering. *Rock Mechanics & Rock Engineering*, *39*(1), 77–85.

Barry, R. G. (1973). A climatological transect on the east slope of the Front Range, Colorado. *Arctic and Alpine Research*, *5*(2), 89–110.

Befus, K.M., Sheehan, A.F., Leopold, M., Anderson, S.P. and Anderson, R.S. (2011). Seismic constraints on critical zone architecture, Boulder Creek watershed, Front Range, Colorado. *Vadose Zone Journal 10*, 915–927. doi: 10.2136/vzj2010.0108

Bird, P. (1998). Kinematic history of the Laramide orogeny in latitudes 35°–49°N, western United States. *Tectonics*, *17*(5), 780–801.

Birkeland, P. W., Burke, R. M., & Shroba, R. R. (1987). Holocene alpine soils in gneissic cirque deposits, Colorado Front Range. *US Geological Survey Bulletin*, 1590-E.

Brunelle, A., Whitlock, C., Bartlein, P., & Kipfmueller, K. (2005). Holocene fire and vegetation along environmental gradients in the Northern Rocky Mountains. *Quaternary Science Reviews*, *24*, 2281–2300. doi: 10.1016/j.quascirev.2004.11.010

Buss, H. L., Sak, P. B., Webb, S. M., & Brantley, S. L. (2008). Weathering of the Rio Blanco quartz diorite, Luquillo Mountains, Puerto Rico: Coupling oxidation, dissolution, and fracturing. *Geochemica et Cosmochimca Acta*, *72*, 4488–4507. doi: 10.1016/j.gca.2008.06.020

Chinn, T.J.H. (1981). Use of rock weathering-rind thickness for Holocene absolute age-dating in New Zealand. *Arctic and Alpine Research*, *13*(1), 33–45.

Dethier, D. P., Birkeland, P. W., & McCarthy, J. A. (2012) Using the accumulation of CBD-extractable iron and clay content to estimate soil age on stable surfaces and nearby slopes, Front Range, Colorado. *Geomorphology*, *173–174*, 17–29. doi:10.1016/j.geomorph.2012.05.022

Dethier, D. P., & Bove, D. J. (2011). Mineralogic and geochemical changes from alteration of granitic rocks, Boulder Creek catchment, Colorado. *Vadose Zone Journal*, *10*, 858–865. doi: 10.2136/vzj2010.0106

Dethier, D., & Lazarus, E. (2006). Geomorphic inferences from regolith thickness, chemical denudation and CRN erosion rates near the glacial limit, Boulder Creek catchment and vicinity, Colorado. *Geomorphology*, *75*, 384–399. doi:10.1016/j.geomorph.2005.07.029

Diek, S., Temme, A.J.A.M., & Teuling, A. J. (2014). The effect of spatial soil variability on the hydrology of a semi-arid Rocky Mountains catchment. *Geoderma*, *235–236*, 113–126. doi: 10.1016/j.geoderma.2014.06.028

Dixon, J. L., Heimsath, A. M., & Amundson, R. (2009). The critical role of climate and saprolite weathering in landscape evolution. *Earth Surface Processes and Landforms*, *34*, 1507–1521. doi: 10.1002/esp.1836

Dixon, J. L., & Riebe, C. S. (2014). Tracing and pacing soil across slopes. *Elements*, *10*, 363–368. doi: 10.2113/gselements.10.5.363

Dühnforth, M., & Anderson, R. S. (2011). Reconstructing the glacial history of Green Lakes valley, North Boulder Creek, Colorado Front Range. *Arctic, Antarctic, and Alpine Research*, *43*(4), 527–542. doi: 10.1657/1938-4246-43.4.527

Eberl, D. D. (2003). User's guide to RockJock: A program for determining quantitative mineralogy from powder X-ray diffraction data (Open-File Report 03-78). Boulder, CO: U.S. Geological Survey.

Eilers, K. G., Debenport, S., Anderson, S. P., & Fierer N. (2012). Digging deeper to find unique microbial communities: the strong effect of depth on the structure of bacterial and archaeal communities. *Soil Biology & Biochemistry*, *50*, 58–65. doi:10.1016/j.soilbio.2012.03.011

Fletcher, R. C., Buss, H. L., & Brantley, S. L. (2006). A spheroidal weathering model coupling porewater chemistry to soil thicknesses during steady-state denudation. *Earth and Planetary Science Letters*, *244*, 444–457. doi: 10.1016/j.epsl.2006.01.055

Foster, M. A., Anderson, R. S., Wyshnytzky, C. E., Ouimet, W. B., & Dethier, D. P (2015). Hillslope-lowering rates and mobile-regolith residence times from *in situ* and meteoric ^{10}Be analysis: Boulder Creek Critical Zone Observatory, Colorado. *Geological Society of America Bulletin*, *125*(5–6). 862–878. doi 10.1130/B31115.1

Gable, D. J. (1980a). The Boulder Creek batholith, Front Range, Colorado. *United States Geological Survey Professional Paper*, *1101*.

Gable, D. J. (1980b). Geologic map of the Gold Hill quadrangle, Boulder County, Colorado. *United States Geological Survey Map* GQ-1525, 1:24,000.

Gable, D. J. (1996). Mineralogy, geochemistry, metamorphism, and provenance of the early Proterozoic metamorphic rocks of the central Front Range, *Colorado. United States Geological Survey Open-File Report*, 96–522.

Gabor, R. S., Eilers, K. G., McKnight, D. M., Fierer, N., & Anderson, S. P. (2014). From the litter layer to the saprolite: Chemical changes in water-soluble soil organic matter and their correlation to microbial community composition. *Soil Biology & Biochemistry*, *68*, 166–176. doi: 10.1016/j.soilbio.2013.09.029

Garnier, B. J., & Ohmura, A. (1968). A method of calculating the direct shortwave radiation income of slopes. *Journal of Applied Meteorology*, *7*, 796–800.

Gilbert, G. K. (1877). *Report on the geology of the Henry Mountains*. U.S. Geographical and Geological Survey of the Rocky Mountain Region. Washington, DC: U.S. Government Printing Office.

Gilbert, G. K. (1909). The convexity of hilltops. *Journal of Geology*, *17*, 344–350.

Gupta, A. S., & Rao, K. S. (2000). Weathering effects on the strength and deformation behaviour of crystalline rocks under uniaxial compression state. *Engineering Geology*, *56*, 257–274.

Hack, J. T. (1960). Interpretation of erosional topography in humid temperate regions. *American Journal of Science*, *258-A*, 80–97.

Hansen, W. R., Chronic, J., & Matelock, J. (1978). Climatography of the Front Range urban corridor and vicinity, Colorado. *U.S. Geological Survey Professional Paper*, *1019*.

Hinckley, E.-L., Ebel, B. A., Barnes, R. T., Anderson, R. S., Williams, M. W., & Anderson, S. P. (2014). Aspect control of water movement on hillslopes near the rain-snow transition of the Colorado Front Range, U.S.A. *Hydrological Processes*, *28*, 74–85. doi:10.1002/hyp.9549

Hock, R. (1999). A distributed temperature-index ice-and snowmelt model including potential direct solar radiation. *Journal of Glaciology*, *45*(149), 101–111.

Humphreys, G. S., & Wilkinson, M. T. (2007). The soil production function: A brief history and its rediscovery. *Geoderma*, *139*, 73–78.

Isherwood, D., & Street, A. (1976). Biotite-induced grussification of the Boulder Creek Granodiorite, Boulder County, Colorado. *Geological Society of America Bulletin*, *87*, 366–370.

Kelly, P. J. (2012). *Subsurface evolution: Characterizing the physical and geochemical changes in weathered bedrock of lower Gordon Gulch, Boulder Creek Critical Zone Observatory*. MA thesis, University of Colorado, Boulder.

Langston, A., Tucker, G. E., Anderson, R. S., & Anderson, S. P. (2015). Evidence for climatic and hillslope-aspect controls on vadose zone moisture and saprolite weathering. *Earth Surface Processes and Landforms*, *40*, 1254–1269. doi:10.1002/esp.3718

Legg, T. E., & Baker, R. G. (1980). Palynology of Pinedale sediments, Devlins Park, Boulder County, Colorado. *Arctic and Alpine Research*, *12*(3), 319–333.

Leopold, M., Völkel, J., Huber, J., & Dethier, D. (2013). Subsurface architecture of the Boulder Creek Critical Zone Observatory from electrical resistivity tomography. *Earth Surface Processes and Landforms*, *38*, 1417–1431. doi:10.1002/esp.3420

Madole, R. F. (1969). Pinedale and Bull Lake glaciation in upper St. Vrain drainage basin, Boulder County, Colorado. *Arctic and Alpine Research*, *1*(4), 279–287.

Madole, R. F. (1986). Lake Devlin and Pinedale Glacial history, Front Range, Colorado. *Quaternary Research*, *25*, 43–54.

Madole, R. F., VanSistine, D. P., & Michael, J. A. (1998). Pleistocene glaciation in the upper Platte River drainage basin, *Colorado. US Geological Survey Geologic Investigations Series*, *I-2644*.

Marr, J. W. (1961). Ecosystems of the east slope of the Front Range in Colorado. *Series in Biology*, Paper 21. http://scholar.colorado.edu/sbio/21

Marshall, J. A., Roering, J. J., Bartlein, P. J., Gavin, D. G., Granger, D. E., Rempel, A. W., et al. (2015). Frost for the trees: Did climate increase erosion in unglaciated landscapes during the late Pleistocene? *Science Advances*, *1*(10), e1500715. doi:10.1126/sciadv.1500715

Mensing, S., Korfmacher, J., Minckley, T., & Musselman, R. (2011). A 15,000 year record of vegetation and climate change from a treeline lake in the Rocky Mountains, Wyoming, USA. *The Holocene*, *22*(7), 739–748. doi: 10.1177/0959683611430339

Mills, T. J. (2016). *Water chemistry under a changing hydrologic regime: Investigations into the interplay between hydrology and water-quality in arid and semi-arid watersheds in Colorado, USA*. Ph.D. dissertation, Dept. of Geography, University of Colorado, Boulder.

Mills, T. J., Anderson, S. P., Bern, C., Aguirre, A., & Derry, L. A. (2017). Colloid mobilization and seasonal variability in a semi-arid, headwater stream. *Journal of Environmental Quality*, *46*(1), 88–95. doi:10.2134/jeq2016.07.0268

Minckley, T. A., Shriver, R. K., & Shuman, B. (2012). Resilience and regime change in a southern Rocky Mountain ecosystem during the past 17,000 years. *Ecological Monographs*, *82*(1), 49–68.

Molnar, P. H., Anderson, R. S., & Anderson, S. P. (2007). Tectonics, fracturing of rock, and erosion. *Journal of Geophysical Research-Earth Surface*, *112*, F03014. doi:10.1029/2005JF000433

Molnar, P. H., & England, P. (1990). Late Cenozoic uplift of mountain ranges and global climate change: Chicken or egg? *Nature*, *346*, 29–34.

Muhs, D. R., & Benedict, J. B. (2006). Eolian additions to Late Quaternary alpine soils, Indian Peaks Wilderness Area, Colorado Front Range. *Arctic, Antarctic, and Alpine Research*, *38*(1), 120–130.

Navarre-Sitchler, A., Steefel, C. I., Sak, P. B., & Brantley, S. L. (2011). A reactive-transport model for weathering rind formation on basalt. *Geochemica et Cosmochimica Acta*, *75*, 7644–7667.

Ouimet, W., Dethier, D., Bierman, P., Wyshnytzky, C., Shea, N., & Rood, D. H. (2015). Spatial and temporal variations in meteoric 10Be inventories and long-term deposition rates, Colorado Front Range. *Quaternary Science Reviews*, *109*, 1–12. doi: 10.1016/j.quascirev.2014.11.003

Parsekian, A. D., Singha, K., Minsley, B. J., Holbrook, W. S., & Slater, L. (2015). Multiscale geophysical imaging of the critical zone. *Reviews of Geophysics*, *53*, 1–26. doi:10.1002/2014RG000465

Pavich, M. (1986). Processes and rates of saprolite production and erosion on a foliated granitic rock of the Virginia Piedmont. In S. M. Colman & D. P. Dethier, *Rates of chemical weathering of rocks and minerals* (pp. 551–590). Orlando, FL: Academic Press.

Peet, R. K. (1981). Forest vegetation of the Colorado Front Range: Composition and dynamics. *Vegetatio*, *45*(1), 3–75.

Shea, N. (2013). *Spatial patterns of mobile regolith thickness and meteoric* ^{10}Be in Gordon Gulch, Front Range, CO, M.S. thesis, Storrs, University of Connecticut.

Shea, N., Ouimet, W., Dethier, D., Bierman, P., & Rood, D. (2012). Spatial patterns of mobile regolith thickness and meteoric 10Be in the Boulder Creek Critical Zone Observatory, Front Range, Colorado, *Eos Transactions AGU*, *93*(52), Fall Meeting Suppl., Abstract EP41D–0835.

Shobe, C. M., Tucker, G. E., & Anderson, R. S. (2016). Hillslope-derived blocks retard river incision. *Geophysical Research Letters*, *43*. doi: 10.1002/2016GL069262

Soil Survey Staff (2014). *Keys to soil taxonomy*, 12th ed. U.S. Department of Agriculture, Natural Resources Conservation Service, 360 pp.

Srodon, J., Drits, V. A., McCarty, D. K., Hsieh, J. C. C., & Eberl, D. D. (2001). Quantitative mineral analysis by powder X-ray diffraction from random preparations. *Clays and Clay Minerals*, *49*, 514–528.

St. Clair, J., Moon, S., Holbrook, W. S., Perron, J. T., Riebe, C. S., Martel, S. J., et al. (2015). Geophysical imaging reveals topographic stress control of bedrock weathering. *Science*, *350*, 534–538. doi: 10.1126/science.aad2210

Summerfield, M. A., & Hulton, N. J. (1994). Natural controls of fluvial denudation rates in major world drainage basins. *Journal of Geophysical Research*, *99*(B7), 13871–13883.

Taggart, J. E., Jr, Lindsay, J. R., Scott, B. A., Vivit, D. V., Bartel, A. J., & Stewart, K. C. (1987). Analysis of geological materials by wavelength-dispersive X-ray fluorescence spectrometry. In P. H. Baedecker (Ed.), *Methods for geochemical analysis.* U. S. Geological Survey Bulletin 1770, E1–E19.

Trotta, J. R. (2010). *The distribution of tors in Gordon Gulch, Front Range, Colorado*. Senior honors thesis, Geosciences, Williams College, 68 pp.

Tucker, G. E., & van der Beek, P. (2013). A model for post-orogenic development of a mountain range and its foreland. *Basin Research*, *24*, 241–259. doi:10.1111/j.1365-2117.2012.00559.x

West, A. J. (2012). Thickness of the chemical weathering zone and implications for erosional and climatic drivers of weathering and for carbon-cycle feedbacks. *Geology*, *40*(9). 811–814. doi:10.1130/G33041.1

White, A. F., & Brantley, S. L. (2003). The effect of time on the weathering of silicate minerals: Why do weathering rates differ in the laboratory and field? *Chemical Geology*, *202*, 479–506.

Willenbring, J. K., & Jerolmack, D. J. (2016). The null hypothesis: Globally steady rates of erosion, weathering fluxes and shelf sediment accumulation during Late Cenozoic mountain uplift and glaciation. *Terra Nova*, *28*, 11–18. doi: 10.1111/ter.12185

Vierling, L. A. (1998). Palynological evidence for late- and post-glacial environmental change in central Colorado. *Quaternary Research*, *49*, 222–232.

14

Where Are We and Where Are We Going? Pedogenesis Through Chemical Weathering, Hydrologic Fluxes, and Bioturbation

Allen Hunt[1,2], Markus Egli[3], and Boris Faybishenko[4]

ABSTRACT

A review of the status of fundamental research into soil genesis and development is given, together with a discussion of the outstanding problems from various perspectives, such as the geological, hydrological, and soil ecological points of view. The urgency of understanding what soil is, how it forms and evolves, relates fundamentally to its connection with the cycling of water and those elements of deep significance to biology, e.g. carbon, nitrogen, and phosphorus, as well as to the uptake and fate of the (mostly) solar energy input. The coupling is inherent in the close relationships between soil genesis and the formative process of chemical weathering, together with its abiotic drawdown of atmospheric carbon, as well as the relationship between soil evolution and the biological processes that change the soil. Each of these phases links soils to the atmospheric carbon composition and the Earth's climate system. More recently, the link between soil formation and Earth's water cycle has become clearer with the recognition that field weathering rates are more likely flux-limited (water, organic acids, and reaction products) than kinetics-limited. While a link between water and CO_2 drawdown appears explicit in the photosynthetic reaction, the relationship between plant productivity and transpiration fundamentally links water and cycling of elements such as carbon, nitrogen, and phosphorus. The summary is intended to place the works of the present book into the context of present research efforts and future goals.

14.1. WHAT AND WHERE IS SOIL PHYSICALLY, HYDROLOGICALLY, CHEMICALLY, BIOLOGICALLY, CONCEPTUALLY, AND SCIENTIFICALLY?

The need to understand soil genesis and evolution has never been higher. The soil is a center of the cycling of carbon, nitrogen, and water, and the foundation of the critical zone (CZ), (NRC, 2001), which stretches from the bedrock to the treetops. In the soil, vegetation, microbes, and atmospheric water combine to transform bedrock from its original state into a medium that forms the basis of agriculture, foundations for our buildings, and the habitat for evolution.

Just coming up with a definition of a soil as an object, and a field of study, is not trivial. The chapter by Huggett (this volume) details the development of the modern concept of soil as an independent entity or system, starting with Hilgard (1860). Notably, Darwin (1881) referred to soil as "vegetable mould." Early definitions were closely related to the worth of soil as a basis for agriculture (a medium for plant growth; Lyon & Buckman, 1922), and addressed its natural formation in the absence of human influence (Joffe, 1936). More in line with geomorphological applications, some viewed the soil as a mantle of loose and weathered rock (Hilgard, 1906; Coffey, 1912). Vernadsky (1926) developed the concept of the biosphere,

[1] *Department of Earth & Environmental Sciences, Wright State University, Dayton, Ohio, USA*

[2] *Department of Physics, Wright State University, Dayton, Ohio, USA*

[3] *Department of Geography, University of Zürich, Zürich, Switzerland*

[4] *Earth and Environmental Sciences Area, E. O. Lawrence Berkeley Laboratory, Berkeley, California, USA*

Hydrogeology, Chemical Weathering, and Soil Formation, Geophysical Monograph 257, First Edition.
Edited by Allen Hunt, Markus Egli, and Boris Faybishenko.

DOI: 10.1002/9781119563952.ch14

of which soil is a component with ecological functions responsible for biodiversity, productivity, etc. (Bockheim et al., 2005). In the agricultural context, the zonation of the top few meters of the Earth's surface was accorded prime position and relevance. However, from what is now known as the O (organic) horizon to successive incorporations of the A (topsoil) and B (subsoil) horizons into the solum, and more recently the C horizon (variously parent material, or chemically weathered bedrock) as well (Richter & Yaalon, 2012), the concept of soil has been changing to become more compatible with an understanding of its position in Earth science between the bedrock and the atmosphere at the crown of the rock cycle. Further, although from the outset it has been the rule to regard soil formation in a context of "unchanging" conditions, such as the Holocene, it is now clear that soils may preserve a record of many changes in climate and, e.g., human influences, thus deserving the designation polygenetic (Richter & Yaalon, 2012). Over a similar time period, recognition of the importance of the suite of climatic and land-use changes imposed by human civilization has led to the suggestion that the present is no longer the Holocene, but the Anthropocene (Crutzen, 2002; Crutzen & Stoermer, 2000). These changes in our understanding of the role, position, and evolution of soil have challenged historical attributes of the study of soils as well as soil science within science itself. The soil is now seen as the "most complicated biomaterial on the planet" (Young & Crawford 2004, p. 1634), or "the crucible of life, a self-regulating, biophysical factory, acting like a composite living entity" (Hillel, 2005).

In the process of defining a soil at the interface of several complicated, interacting systems, it became necessary to define a soil not on the basis of the history of its constituents, which may move into and out of the soil, but on its position, both topographical and sequential, in the process of soil formation and erosion. In this context, the entire soil catena of a slope, located between a water channel and a ridge, is included, as is what is located between the parent material and the atmosphere, excluding to varying degrees purely organic material, such as plants or leaf litter. Most simply put, soil is the layer at the solid Earth surface, which is derived from, and distinct from, its source material, sediment, rock, or plant matter, through a wealth of chemical, biological, and physical processes, and what is not yet displaced from its catena by fluvial processes, which effectively convert the soil to sediment. The relative simplicity of this characterization of soil, like simplifications in its description or processes, hides further complexity.

From our perspective atop the soil, we are at that level where the input hydrologic flux, precipitation, is divided into four principle components: infiltration, surface runoff, transpiration, and evaporation. The topic "chemical weathering" provides the link, as it were, between "hydrogeology" and "soil formation." Chemical weathering increases surface area, porosity, and the concentration of mineral nutrients needed for plants to grow, apparently simultaneously a precondition for growth and a result of that plant growth. As chemical weathering in the field is mostly limited by the flow of water into the soil (Maher, 2010), so is the rate of soil formation limited principally by chemical weathering (Burke et al., 2006, 2009; Dixon et al., 2009, 2012; Egli et al., 2014; Hunt & Ghanbarian, 2016; Yu & Hunt, 2017a, 2017b). Indeed, the chapter of Lyons et al. (this volume) on chemical weathering in the Antarctic's McMurdo dry valleys demonstrates the clear link to water, with weathering resulting almost exclusively from melting of subsurface ice and in the hyporheic zone of meltwater streams. However, see also the chapter by Anderson et al. (this volume; note that Anderson and Anderson, 2010, helped bring chemical processes, such as weathering, to the forefront of landscape evolution), who argue that at Gordon Gulch such chemical processes may only be limiting to the weathering of bedrock, not to the actual development of the regolith, which in steady state is controlled by surface physical processes.

The complex interplay of weathering and biota in the critical zone poses challenges for advancing research on how Earth's surface evolves in response to environmental factors (Brantley et al., 2011). In the context of hydrogeology, it is important to emphasize that soil formation and erosion processes are directly tied to two of the pathways of water encountering the surface of the Earth: surface runoff and infiltration.

To stimulate future research, we hypothesize that weathering, erosion, soil formation, and biogeochemical cycling are essentially limited by water fluxes.

14.1.1. Soil Formation, Erosion, and Burial

• Physical erosion is proportional to precipitation and thus, presumably, surface run-off (Reiners et al., 2003), while soil deepening, mineral transformation (see chapter by Egli and Mirabella, this volume), and chemical erosion processes are proportional to infiltration (run-in?).

• Soil formation joins fundamentally with the carbon cycle, as the two principle terrestrial means to draw carbon down from the atmosphere are in plant growth through photosynthesis, with an instantaneous rate proportional to a local water flux, and chemical weathering of silicate minerals in rocks, with a rate proportional to infiltration.

Formation, transport, and burial of sediment are the surface expression of the rock cycle. The burial of carbonate minerals as products of chemical weathering of silicate minerals represents by far the dominant sequestration of atmospheric carbon, with its relevance to

global temperature regulation (Berner, 1992). In the process, carbon passes through the soil in inorganic forms, such as bicarbonate, while water is buried together with the sediments, connecting to the deep-water cycle.

14.1.2. Biological Processes

Many biological processes in soil formation depend on chemical weathering for the resulting increase in mineral surface area, together with the release of mineral nutrients, such as potassium, phosphorus (Hartmann et al., 2014), and iron. Conversely, the chemical weathering process is often directly mediated by microbes. Soil fertility correlates strongly with the fixing of (predominantly) atmospheric nitrogen through interactions of soil microorganisms with plants.

- The productivity of plants is expressed in their ability to draw down carbon from the atmosphere, which is then released into the soil through metabolic activity. This productivity appears to be most strongly controlled by the water and essential nutrients drawn from the soil.
- The chemical weathering reaction itself is mostly a complex biogeochemical process that depends on the CO_2 and organic acids released by the plants within their ecosystems. The tendency for soil nitrogen and carbon components, and therefore cycles, to be linked, but that of phosphorus to vary more independently (Tian et al., 2010), as expressed in the terrestrial Redfield ratio (Redfield, 1958), is thus broadly understandable in the context of the more important influence of parent materials relative to the atmosphere in phosphorus, although the relative immobility of phosphorus is also important.

An increased understanding of the details of these interactions, including the multiple possible combinations of fungal synergisms and root types (Brantley et al., 2017a), is required for future progress in this field. Plants, their roots and associated microorganisms, and earthworms are the main soil engineers. Through their physical activities (e.g. tree uprooting) and soil aggregation they act as catalyst and provide, transform, and translocate organic matter and nutrients throughout the soil profile (as shown by Le Bayon et al., this volume).

14.2. SOIL-FORMING FACTORS AND SOIL PRODUCTION; CONNECTIONS WITH GEOMORPHOLOGY AND HYDROLOGY

Let's return to the question of what soil is, since this is currently a topic of relevance in both CZ science and geomorphology. Jenny (1941) quotes Ramann (1911; 1928): "The soil is the upper weathering layer of the solid earth crust," then continues with the inevitable criticism, "Joffe (1936), a representative of the Russian school, objects to Ramann's formulation on the grounds that it does not distinguish between soil and loose rock material." Jenny adds that, although there will probably never be agreement between all soil scientists as to what soil is, the one characteristic that all soils appear to share is anisotropy, which at its best developed, can be classed as horizonation, while conceding that even that classification can be arbitrary. Jenny continues with the observation that the distinction between freshly fallen leaves or living grass to plant matter sufficiently decayed to be considered part of the O (organic) horizon, is artificial, as is the distinction between the lowest soil layer and parent material. Overall, he summarizes, "In the opinion of the author, the distinction between soil and environment is arbitrary; it exists only in our minds, not in nature." "Fortunately, there is no urgent need for universal agreement." These questions reappear in Cline (1961) and in Richter and Yaalon (2012), but with increasing urgency for their resolution.

Richter and Yaalon (2012) in "The Changing Model of Soil, Revisited" and Richter and Markewitz (1995) in "How Deep Is Soil?" address points made in an essay by Cline (1961). First, they propose, echoing Ramann (1911; 1928), that "the lower boundary of the soil is much deeper than the solum historically confined to O to B horizons," extending the bottom of the soil to the bottom of the C layer. Lukens and Norton's results (this volume) suggest deep weathering boundary as the bottom of the soil, meaning that the material arriving at the soil-saprolite boundary already may be substantially preweathered. This mechanism has an important impact on weathering and nutrient release. The basis for this argument is that the important effects of biogeochemical weathering throughout the column are accorded their proper due, while lending support to Cline's argument that a more holistic view of soil, divorced from its agricultural background, is achieved. Second, Richter and Markewitz (1995) state, "Cline was most impressed with how geomorphology was enriching pedology, and with the increasingly sophisticated view of soil time and of the dynamic processes of soil formation." Particularly when soil production is that process which provides the strongest limitation on the delivery of sediments from their sources on the continents and islands to their sinks in lakes and oceans, this measure of the effectiveness of the erosion process is crucial to understand. However, it is important to keep in mind that, although Gilbert (1877) made one of the first references to soil production, this reference was largely forgotten until the 1960s (Humphreys & Wilkinson, 2007), finally coming into its own starting in the 1990s (Heimsath et al., 1997). Yet, Gilbert wrote rather presciently, "Solution and frost, the chief agents of rock decay, are both retarded by the excessive accumulation of disintegrated rock. Solution gradually decreases as the zone of its activity descends and the circulation on which it depends becomes more sluggish."

In actuality, it is more often true that infiltration, as a fraction of precipitation, is higher where soil is deeper, but more likely because soil depth increases with the infiltration rate (Hunt & Ghanbarian, 2016). However, solution transport does become more sluggish with increasing time or distance (e.g., Berkowitz & Scher, 1995; Cortis & Berkowitz, 2004).

Notwithstanding, for over a century, soil formation has been addressed as a process that depends on a range of external factors (i.e. climate, organisms, relief, parent material, and time, in the line of Dokuchaev [1880/1948, translated from earlier Russian] and Jenny [1941]). As formulated by Jenny,

$$S = f\left(cl,o,r,p,t\right) \tag{1}$$

for the soil depth (or other soil property), S, as a function f of cl (climate), o (organisms), r (relief), p (parent material), and t (time). Note that the functional form of S is not, in general, given, as the equation is more intended to focus one's attention on the most important factors controlling the depth or properties of the soil. The suite of properties described by equation (1) gives the state of the soil.

If the dependence on time of individual soil variables is more naturally described in terms of discrete variability, such as associated with fairly abrupt climate change, then it may be advantageous to think of soil production in terms of an amalgamation of discrete paleoprocesses with a variety of imprints on the soil (Richter & Yaalon, 2012), leading to the term *polygenetic paleosol*. The soil functional properties are often products and witnesses of Quaternary events, natural and human induced, that occurred in the landscape. Many soils started to form under conditions that were different from the current ones (Costantini, 2018). Relict paleosoils remain at the surface and continue to develop.

The posited functional relationship, equation (1), appears to place the formation or evolution of soil on a sound footing, but in actuality, without a specific functional form, its main value is its delivery of a historically connected and familiar formulation. The typical means to investigate equation (1) is to correlate statistically various of the input factors with the output factor, S. As an example, Jenny (1941) investigated California soils in distinct biomes, such as grasslands, and correlated the dependence of the C:N ratio with precipitation, P. He found that, within a specific biome, the C:N ratio slightly decreases with increasing P, but considering all biomes simultaneously led to a significant increase in C:N with P. A soil catena is believed to eliminate climatic and parent material influences from soil variability and isolate relief as a variable (Bockheim et al., 2005). Chronosequences isolate the time variable, etc. (Jenny, 1941). This process lends scientific sophistication to a formulation that is not directly linked by mathematics to a specific process, or combination of processes, and may, moreover, hide synergisms and nonlinearities, such as threshold processes.

Consider, however, the perceived role of the soil catena in the isolation of topographic variables. According to the geomorphological perspective, this must be done by comparison between catenas, rather than within one catena (Heimsath et al., 1999), since surface translocation of soil is, under steady-state conditions, considered to be governed by the diffusion equation, a consequence of transport linear in the surface gradient and the equation of continuity. The diffusion equation thus constrains surface soil transport to be equal along the catena. Nevertheless, this approach does not yet take into account coupled effects of the variation of soil production with depth as well as infiltration (Yu et al., 2017), weakening the conclusion.

Since the advent of the 21st century, it has become increasingly evident that soil production and chemical weathering (Burke et al., 2006, 2009; Dixon et al., 2009, 2012; Egli et al., 2014; Hunt & Ghanbarian, 2016; Yu & Hunt, 2017a, 2017b) as well as denudation rates (Figure 4, DiBiasi et al., 2012) are proportional to each other.

How can these results be understood? In theoretical treatments of surface reactions in porous media, the proportionality of both soil formation rates and chemical weathering rates to flow velocity arises whenever the progress of the weathering reactions is limited by the ability of flowing water to transport product solutes from the reaction front. This question is addressed using what is called the Damköhler number, Da_I (Salehikhoo et al., 2013), a ratio between solute advection time and a reaction time. The latter time scale is calculated assuming complete mixing (Yu & Hunt, 2017c). $Da_I << 1$ signifies that reaction kinetics limit (dominate), whereas $Da_I >> 1$ indicates that solute transport dominates (but see Bandopadhyay et al., 2017, or Reeves & Rothman, 2014, who calculate Da_I using a ratio of diffusion to reaction times, implying that the form of transport limiting reactions is molecular diffusion). The calculation depends sensitively on both the reaction kinetics and the fluid flow rates, but Da_I tends to increase in time (Gilbert, 1877; Cortis & Berkowitz, 2004) because the solution efficiency (velocity) diminishes over time when solute transport is non-Fickian, nowadays considered the rule, rather than the anomaly (Cushman & O'Malley, 2015). While a trend towards increasing relevance of transport with increasing time is likely universal, a crossover at about $Da_I = 1$ can apparently occur on time scales of roughly a day and length scales of a fraction of a millimeter (Maher, 2010) up to hundreds of years (and length scales of centimeters, Egli et al., 2018). Assuming that the entirety of such

variability has not been plumbed, such time and length spans may sometimes be much larger, i.e. millennia.

Rates of physical erosion and chemical weathering are often positively correlated across diverse landscapes (Dixon et al., 2012, Dixon & von Blanckenburg, 2012). This positive relationship exists up to a certain threshold where a limit of weathering rate is reached. Soil production rates cannot be infinitely high. It is, however, still questionable where this speed limit is: some authors set it at about 320–450 t km^{-2} yr^{-1} and others at 800–2000 t km^{-2} yr^{-1} (Egli et al., 2014). However, in the New Zealand Alps, with precipitation rates 10 m yr^{-1}, Larsen et al. (2014) have measured soil production rates as high as 4000 t km^{-2} yr^{-1}, a result that has been shown consistent with a linear dependence of soil production rates on precipitation over almost 4 orders of magnitude of precipitation (Hunt & Ghanbarian, 2016), from the driest place on Earth (the Atacama Desert) to among the wettest (New Zealand Alps). Other authors, e.g. West et al. (2005), noted that silicate weathering is, in principle, limited by two processes: solute transport and reaction kinetics. The supply of water, acids, and (organic) ligands relative to the supply of silicate minerals is large in transport-limited weathering regimes that are mostly found on relatively old and flat surfaces. Areas having a high erosion rate, a high uplift rate, or young surfaces also have a high supply of fresh minerals. Under such circumstances, the main control on chemical weathering depends particularly on the kinetic rate of mineral dissolution and time available for reaction. Thus, erosion rates may be so high that the associated soil production rate based on the calculation of transport-limitations may exceed the rate of reaction of a fresh mineral surface. On a soil evolutional time-axis, Egli et al. (2018) showed that the limitations on mineral weathering imposed by reaction kinetics can affect the system until 100–200 yr of soil evolution, a result generally in accord with Damköhler number calculations of Yu and Hunt (2017b). Thereafter, solute transport seems dominant. Within regolith, faster erosion rates and shallower thicknesses mean minerals move rapidly through the weathering zone, leading to shorter residence time and hence a lower degree of weathering. For example, Ferrier and Kirchner (2008) predicted that weathering rates approach zero when denudation exceeds roughly half of the maximum soil production rate.

Both laboratory experiments (short duration, simplification) and field observations have shortcomings (lack of control of variables, changing climatic conditions, etc.). Despite the limitations associated with using either approach, it has become increasingly evident that weathering rates strongly depend on the rate at which fluid flows through the medium, be it soil (Maher, 2010) or an experimental column (Salehikhoo et al., 2013) (Figure 14.1). Here an approximately linear dependence of reaction rate on flow is demonstrated over 7 orders of magnitude of flow rate.

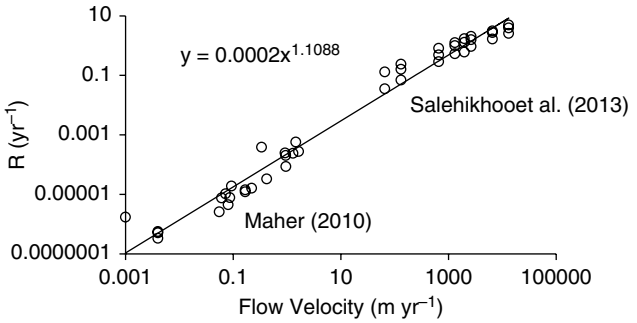

Figure 14.1 The dependence of weathering rate reactions on flow velocity in field measurements and lab experiments. Field results for silicate minerals are due to Maher (2010) and cover typical vertical flow rates of about 3 cm to about 2 m per year, though a few are for flow rates in the millimeters per year. Lab results on $MgCO_3$ were obtained by Salehikhoo et al. (2013) and span flow rates from about 30 m to 14,000 m per year. Cumulatively, the results demonstrate a 7 order-of-magnitude increase in reaction rate over 7 orders of magnitude change in flow rate.

Note that, for the proportionality to flow rate to continue to such high flow rates as used in lab experiments, however, the parent materials must have a high intrinsic reaction rate; the source material for the Salehikhoo et al. (2013) experiments was $MgCO_3$, with dissolution rates orders of magnitude higher than for typical silicate minerals.

Thus, for purposes of prediction of weathering rates, a critical input is the fluid flow rate, a quantity which, in the field, is a hydrologic variable. Therefore, proportionality of weathering rates to flow rates puts soil formation squarely in the domain of hydrologic sciences, in view of the need to determine the partitioning of water at the terrestrial surface, and into soil physics as well, as a result of the relevance of the flow and transport properties of the medium. However, although the chemistry is explicitly omitted from Figure 14.1, for more slowly reacting species, the dependence of R on flow rate becomes horizontal at lower velocities (Maher, 2010), commensurate with a cross-over to $Da_I < 1$ (Yu & Hunt, 2017b). Since employment (with success) of this sort of reductionism is counter to current trends in ecohydrology and biogeochemistry, there is a need to provide additional context for how it may work.

Specific interpretations of limitations to weathering in the field ascribe varying relevance to the roles of biota, chemistry, and physics. The possible array of processes that could be thus described is immense. Therefore, take a single example, the effects of bedrock fracturing on weathering rates. Such a topic may bring in a variety of

variables. It is clear that fracturing of bedrock promotes fluid infiltration into newly exposed rock surfaces, enhancing infiltration compared with overland flow, and thus soil formation over soil erosion. But what controls the fracturing process? Is it principally a result of freezing (physics), tree roots (biota), or chemical weathering (chemistry)? Established means of thinking favor the first two, but it has been shown that tree roots are not really capable of prying apart rock (except for relatively weak sandstone; Brantley, 2017a, and references therein), while mineral volume changes due to chemical weathering are quite capable, under sub-critical conditions, of extending fractures (Eppes & Keanini, 2017). In that case, chemical weathering is the process limiting the effectiveness of fracturing and thus soil formation. But chemical weathering is mostly controlled by water fluxes (Maher, 2010), and thus the physics of flow and transport (within the discipline of hydrology, or soil physics). Sak (this volume) nicely presents that rock weathering and the formation of weathering rinds on the surface of such rocks is governed by the rocks' composition and ambient climatic (and thus also hydrologic) conditions.

A problem often emphasized is the need to develop theory and descriptive expressions that cross scales in time and space (Brantley, 2007). When water tends to follow paths of least resistance, the same physical basis for employing percolation theory may be invoked at all scales (Hunt & Ewing, 2016) and results for vegetation growth and soil formation over immense time scales are generated from the percolation optimal paths exponent and the fractal dimensionality of the percolation backbone, respectively (Hunt, 2017). A scaling plot (Figure 14.2) of water, earth, and biota that describes the cumulative effect of flow rates and time on soil formation and vegetation growth, demonstrates the increasing separation of time scales for, e.g., vegetation growth and soil formation, with increasing length scale, even though at scales of a few pores, these two time scales are approximately the same (and equal to the ratio of a pore size to a water flow rate), since transpiration is typically only a factor of 2 higher than infiltration. Understanding this profound separation of time scales is key to understanding the relative roles of chemistry and biology in soil development and, as it turns out, in the global carbon and water cycles.

Identifying the great slowing of chemical weathering processes relative to, e.g., biological processes with increasing length scale, lends additional theoretical

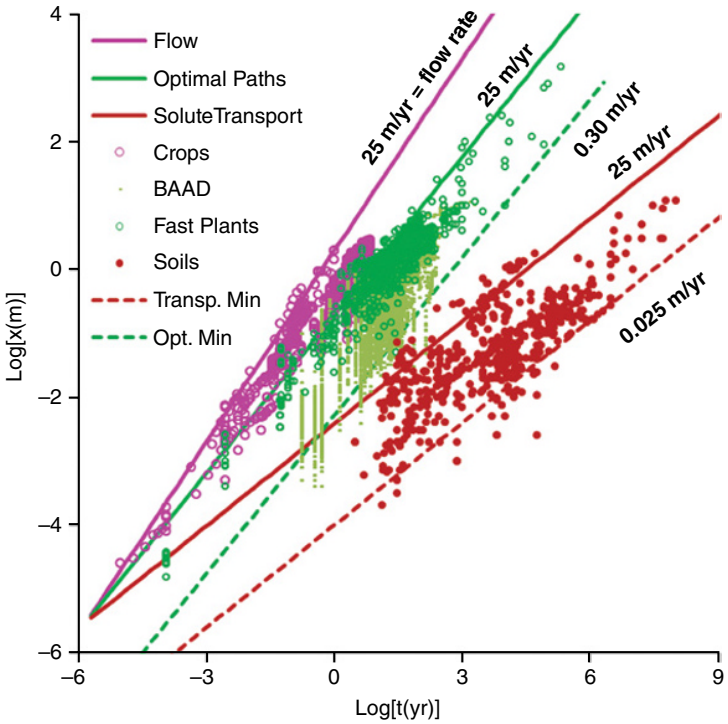

Figure 14.2 Scaling diagram of relationships limiting the growth of fertilized crops (linear in time equal to the flow rate), natural vegetation (optimal paths exponent of percolation theory and the same flow rate), and soil formation (backbone fractal dimensionality and the same flow rate). Note that the lower flow rate limit for soil formation, 2.5 cm yr^{-1}, is a bound for most of the data of Maher (2010), while the upper limit, 25 m yr^{-1}, is the quotient of the world's maximum precipitation divided by a typical porosity. The lower limit in space is 30 μm, while the shortest time scale is determined by the ratio of this length scale to the flow rate. Data sources are given in Hunt (2017); BAAD = Biometric and Allometric Database (Falster et al., 2015). (Source: Hunt, 2017).

justification to the conclusion from field work that chemical weathering is the fundamental limiting process in soil formation. The conclusion from field studies derives from the close correspondence of soil production and chemical weathering rates over long time scales. Moreover, it has been possible to use analytical formulations of the time-dependence of chemical weathering to generate an actual functional form for the soil formation function of Jenny and Dokuchaev (Yu et al., 2017).

Even though the study of chemical weathering may provide a basis to define not only the depth of the soil but also the vertical distribution of various mineralogical or chemical species, it has its own limitations. Effects of bioturbation may decouple variables that describe vertical soil structure from soil depth, necessitating additional generalization of the Dokuchaev perspective. As discussed by Johnson and Schaetzl (2015), such a revision in fundamental thinking would be a return to the concepts of Darwin (1881). Although not a primary subject of this summary, it is interesting to note that the processes that lead to vertical sorting of particles include burrowing by animals at least from the size of worms up to the size of rodents.

14.3. HUMAN IMPACTS AND RELEVANCE TO HUMAN SOCIETY

Land-use change, including the development of agriculture and the subsequent translocation of the majority of the human population to cities, has had profound impacts on soil characteristics and soil erosion, and through these, soil production (inferred from DiBiase et al., 2012). Richter and Yaalon (2012) give, as one of three fundamental changes in understanding of soils that motivate a rethinking of the discipline, the global transformation of soils from a "natural to a human-natural body." Forman and Stinchcomb (2015) include both the critical zone (including its geologic history) and human impacts on surface processes as among their six grand challenges for Quaternary geology. Forman and Stinchcomb (2015) quote Steffen et al. (2015) to imply that "human activities continue to affect earth surface processes with non-analog responses compared to Holocene landscape dynamics." Thus, the present time is described as the Anthropocene, in view of massive geochemical, biological, and geomorphic changes at the Earth's surface, and their expression in sediment yield and composition. While the onset of the Anthropocene may be defined in terms of stratigraphy, geochemistry, geomorphology, or other ways (see, e.g., Edgeworth et al., 2015), it is noteworthy that the boundary as expressed in the human impacts on the soil itself has been termed the Golden Spike (Certini & Scalenghe, 2011). Here, investigations into human impacts on soils are concentrated in the chapter of Horn and Lal (this volume) on compaction of agricultural soil due to inappropriate uses of heavy machinery; these effects include permanent changes in the stress structure of the soil, reduced air and water flow, and their impacts on agriculture as well as how to diagnose the resilience of soil ecosystems to such treatment.

The impact of humans on the soil is so large, it can no longer be neglected in any comprehensive theory of soil. The "Jinji unconformity" divides human and natural deposits (which may straddle the soil) and provides understanding of pollutant migration zones, weakness, and fracturing, as well as soil liquefaction (Edgeworth et al., 2015). Instead of emphasizing a role of human beings separate from nature, however, it may be more constructive to seek a higher order unity of principles (Haff, 2014a) that describes both human and natural processes. Some parallels include the following: The principle of superposition works in archaeology as in geology; newer cities are invariably constructed on top of older ones, and different technologies, e.g. stone, iron, and bronze, are found in superposed layers (Harris, 1979, 2014). Even subsequent reorganization of the subsurface by human activities is a form of bioturbation in soils or sediments and can invalidate superposition (Harris, 2014) in the same way as activities of other animals. Storm water removal systems can be considered artificial karst in their function and may have analogues to real karst in their architecture (Garcia-Fresca, 2007), though not in composition or rate of formation. In spite of the parallels between human and non-human natural activities, Haff (2014b) is able to list six principles that distinguish the so-called "technosphere," an additional realm of the Earth that is an analogue to Vernadsky's (1926) biosphere.

Practical problems with a need for timely solution include not just the loss of soil itself (Blanco & Lal, 2010; Montgomery, 2007) but the loss of soil carbon (Lal, 2004) as well as the loss of biodiversity in agricultural soils (e.g. Wilcove et al., 2013). Related problems that are only slightly further afield include the loss of land surface to productivity (through conversion of solar energy to sugar) by the replacement of permeable with impermeable surfaces, with resulting increases in sensible heat fluxes and runoff (Taha, 1997). Basic concepts are needed to guide research, whereas specific proposals are needed to lead engineering. Can the changes in energy and water partitioning be represented (Faybishenko, 2010) within traditional Budyko (1958, 1974) strategies, or do they represent fundamental deviations from theoretical guiding concepts, such as optimization of work (see Hunt, this volume)? Can we reverse the loss of carbon in soils? An important such strategy has been promoted by Taylor et al. (2016), who proposed the use of crushed basalt in agriculture, both as a means to

increase the fertility of the soil, and for its role in drawdown of atmospheric carbon.

14.4. WHERE IS SOIL AS A DISCIPLINE?

Within the evolution of the geosciences is the continued gradual movement to change its character from observational to predictive. A predictive science, by definition, must develop hypotheses, which can guide the use of mathematics to make verifiable quantitative predictions. The model or hypotheses live or die from the success or failure of these predictions. An observational science tells a story. Both sides are, of course, still represented in professional organizations such as the American Geophysical Union, as indeed both connotations are found in the term *geophysics* itself. Beyond this distinction lies a question of the applicability of models, as pointed out by Cline (1961) and reiterated by Richter and Yaalon (2012). Cline (1961) said,

> Within the framework of its accumulated knowledge, every science develops a mental image of the thing with which it is concerned. This model of a science is the organized aggregate of accumulated facts, and laws and *theories based on those facts*: it is a mental picture of that which is known viewed in organized perspective through verified quantitative relationships, which we call laws, *with varying degrees of distortion by virtue of theories* that attempt to explain the observed relationships. The picture is *not the same to all who work in the science*, for it is composed of knowledge and the extensions of theory from knowledge into the unknown, and different men know, or think they know, different things. The picture is sharply in focus in those parts for which quantitative relationships have been defined; it becomes progressively more blurred as one approaches the limits of quantitative data and *progressively more distorted with increasing dependence on theory*.

We have added italics to portions of this statement that emphasize Cline's fundamental distrust of what he calls theory. Thus, Cline apparently suggests that a theoretical underpinning of a quantitative relationship would make it less reliable. In physics and chemistry, such is certainly not the case; rather, it is the lack of a theoretical explanation that should trigger suspicions.

Richter and Yaalon (2012) go on to state that Thomas Kuhn's (1962) concept of "paradigm," published in *The Structure of Scientific Revolutions*, was analogous to Cline's mental image. Kuhn suggested that science advanced through periods of utilization of recognized methods and organization of research, together with its results (that fill in the holes in the field), which build a paradigm, to discovering anomalies incompatible with that paradigm. Upon recognition of the difficulties, the cognizant scientific community reaches a crisis, which is followed by the overthrow of the existing paradigm in a kind of revolution. Such an occurrence has come in time to be known as a paradigm shift. The physics-centricity of this picture is allegedly at odds with how other sciences change, notably biology, as Ian Hacking noted in his introductory essay to the 2012 republication of Kuhn's 1962 book. Hacking points to the immense social differences between physics and biology, as well as the loss of pre-eminence suffered by physics since 1962, at the height of the Cold War. However, soil physics, on which much of the primary analysis for flow and solute transport and diffusion is built, might be considered a branch of physics (Hunt et al., 2013). As such, the Kuhn picture may yet take precedence.

In the language of Kuhn, we should become alert when a number of problems that could be related become evident, particularly if they are repeatable and significant enough to be important. These results, inexplicable within the existing paradigm, are what Kuhn calls "anomalies."

Such anomalies have been accumulating within the discipline of soil physics since Fatt (1956a, 1956b, 1956c), together with the occasional clear criticism (Scheidegger, 1959; Berkowtiz & Scher, 1995; Cushman & O'Malley, 2015) of the existing mathematical structure and its basis in a flawed mental picture. Fatt (1956a, 1956b, 1956c) pointed out that only network models could represent truthfully real porous media, while Scheidegger (1959) reported that the Advection-Dispersion Equation (ADE), the use of which was justified in the conventional "bundle of capillary tubes" picture, was not accurate. This criticism of the ADE has been continued by Berkowitz and Scher (1995), Berkowitz et al. (2002), and Benson et al. (2000a, 2000b), among others. The bundle of capillary tubes model attributes longitudinal dispersion in solute transport to the particular distribution of pore sizes relevant for each medium (in contrast to non-Gaussian transport models; Hunt & Ghanbarian, 2016), while it admits of no transverse dispersion (perpendicular to the flow direction) at all. Yu and Hunt (2017a, 2017b, 2017c) argue that impacts from reliance on the ADE are felt in the theory of solute transport through chemical weathering to soil formation. Thus, a related question, as to whether the traditional hierarchical view of soil science, with physics at the base moving up through chemistry to biology, is a valid and useful picture, may depend on whether the physical basis is flawed or not. Accordingly, the tendency of practitioners of soil science to move away from this hierarchical view towards a paradigm that considers biological matters as unconnected with physics (consider the refusal of USDA to support fundamental soil physics for the past decade), may be more a result of an unacknowledged problem.

This reasoning leads to the following important questions:

• To what extent is the conventional understanding of chemical weathering based on soil physics?

• To what extent might soil physics be in need of a paradigm shift?

• Is soil physics part of soil science or part of physics (Hunt et al., 2013)?

As a consequence, we have to ask: Do anomalies in soil science exist?

We provide an incomplete list of what turns out mostly to be related unsolved questions, or anomalies. These questions should also relate, if feasible, to some of the chapters received. Other chapters will address other unsolved problems which, however, relate more clearly to how complete our understanding is of the range of possible influences on soil formation and evolution which have not yet been incorporated fully in a single model.

1. Why does the Advection-Dispersion Equation underestimate solute arrivals at both short times (early breakthroughs) and at long times (providing the explanation for the difficulty of environmental clean-up; Cortis & Berkowitz, 2004)?

2. Why does mass conservation require scale-independent flow velocities of water under saturated conditions, but not of solute?

3. Why do field measurements of the dispersivity increase almost linearly with spatial scale (Gelhar et al., 1992; Hunt et al., 2011)?

4. Why are chemical weathering rates in the field up to 6 orders of magnitude slower than in the lab? And why does this decline not depend on mineralogy (at least for plagioclase, K-feldspar, biotite, and hornblende; White & Brantley, 2003)? According to, e.g., Hunt and Ghanbarian (2016), the distinction is between predominantly kinetic-limited reactions in the lab and the dominance of transport limitations in the field.

5. Under which conditions is mineral weathering purely related to water percolation? When is the production of organic ligands or acids the driving factor of mineral weathering and transformation? When do we have consequently a purely kinetic limitation or a kinetic control of weathering? Does weathering of different minerals depend differently on these driving factors?

6. Why do chemical reaction rates, including weathering, (appear to) decay according to a power law in time, both in laboratory experiments (Liu et al., 2008, 2009; Peng et al., 2012; Zhong et al., 2005) and the field (White & Brantley, 2003; Maher, 2010)? (It should be noted that power laws may not always be easily distinguished from exponential functions, a theme to which we return). And why are they proportional to the rate at which water flows through the medium?

7. Why do chemical weathering rates appear to decay as a different power of soil depth than they do of soil age (Hunt & Ghanbarian, 2016)?

8. Either a power law or an exponential soil production function predicts a maximum soil production rate under thin or infinitely thin soils, as well as an inverse relationship between soil thickness and soil production. The exponential form is almost universally applied. Why would soil production rates decay exponentially in depth (Heimsath et al., 1997), particularly if chemical weathering decays according to a power law (White & Brantley, 2003)?

9. Within the general exponential form of a soil production function, an alternative that has been predicted (Gilbert, 1877) and sometimes observed (Heimsath et al., 2011; Dixon & von Blanckenburg, 2012) is "humped" in form. In this case, soil is produced fastest under a critical soil thickness, and soils thinner than the critical thickness are unstable, leading to the exposure of bedrock. Can a humped soil production function exist also in the general power-law formulation? The answer is yes. If the hydraulic conductivity limiting the flow rate is that of the soil, and chemical weathering induces fracturing of the bedrock (with hydraulic conductivity no less than the soil), the relevant flow velocity will be closely related to precipitation, but if soil is very thin with little or no vegetation, then chemical weathering may be unable to produce significant fracturing and the relevant water flow velocity will be reduced by the ratio contrasting soil and bedrock hydraulic conductivities. A model of such simplicity nevertheless reproduces a humped soil production function.

10. How can one reconcile the great depth of weathered bedrock (saprolite [Richter & Yaalon, 2012], laterite, and bauxite [Yu & Hunt, 2017, and references therein]) with exponential models of soil production (Heimsath et al., 1997) that use an explicit length scale of about 0.5 m, preventing deepening of soils significantly past 1 m?

11. Why do the soil production and erosion rates in any given region tend so often to be the same (DiBiase et al., 2012)? Often criticized, the assumption of steady-state landscapes thus appears very often to hold. Soil formation rates (and also erosion rates) strongly depend on the time factor (in conditions with enough precipitation; see Egli et al., 2014). One might ask: Why are soil formation rates (of soils having the same age) worldwide in a similar range when water is not the limiting factor?

12. Given that soil production rates vary over about 4 orders of magnitude (Hunt & Ghanbarian, 2016), depending primarily on rainfall and relief, why does the solum have such a robust tendency to be about 1 m deep in temperate to boreal climates (Yu et al., 2017), with the topsoil and the typical rooting depth about one third of that (Gentine et al., 2012; although a more comprehensive statement is that virtually all roots are confined to a depth of about 2 m; Fan et al., 2017)?

13. Why is the total evapotranspiration so often just under two thirds of the precipitation (Lvovitch, 1973; Schlesinger & Jasechko, 2014; Williams et al., 2012)?

14. Can the theory of nonlinear dynamics and chaos be applied to predict processes taking place in the rhizosphere (Faybishenko & Molz, 2013)?

It is not simply the number of such anomalies that have been accumulating, but the time span, over which they have become noticeable, that appears to reveal a problem in soil physics. Given that such a crisis has been developing in soil physics since 1955 without general acknowledgment, it is not clear whether Hacking (2012) may not actually be right, in which case soil physics should be considered as a field unrelated to physics. If this "crisis" were not particularly relevant to the subject of the current book, it could be omitted here as well.

Point 14 suggests that traditional soil physics may not lack merely the unifying concepts from applying percolation theory to network models but an important component from nonlinear dynamics as well, particularly as it affects our understanding of explicit interactions in the biosphere. Here it should also be noted that still a third facet of the relatively new science of complexity is addressed in publications of Lin (e.g. Lin, 2010), who cites physicist Prigogine (Prigogine, 1980; Nicolis & Prigogine, 1989) to support the statement, "The irreversible dual-partitioning of pedogenesis, … indicates that soils generally evolve towards increased ordering." In this article, Lin (2010) addresses the concept of preferential flow which, however, viewed from the perspective of percolation theory, is simply the "critical path." Further discussion of the potential advantages of applying any particular one, or all of these methods from complexity simultaneously, is beyond the present scope.

14.5. RESEARCH DIRECTIONS, NETWORKS, AND FOUNDATIONAL SUPPORT: CURRENT AND FUTURE

The production of soil *by definition* brings in, in the vertical direction, the processes of dissolved CO_2–induced chemical weathering and thus water flow, with CO_2 contents enriched by decaying plant material and metabolism of a range of organisms. Recognition of the close relationship with plant processes and their dependence on climate has helped the community and the National Science Foundation organize a network of critical zone observatories to collect data on the primary vertical processes involved in soil formation. Three such integrative studies and their conclusions as of this time are reported here (Anderson et al., Lyons et al., Rasmussen et al., this volume). However, the story of how the CZO network came about, including persistence and collaboration across continents and disciplines, is best told in Brantley et al. (2017b), as the proliferation of organizations and agencies is vast.

Understanding the transport of soil downslope, essential to generate a landscape understanding of soil genesis and depth, brings in the horizontal directions and thus, directly, the field of geomorphology (Gilbert, 1877; Heimsath et al., 1999; Humphreys & Wilkinson, 2007; Forman and Stinchcomb, 2015). At this point, the functional form of such transport is still uncertain, as well as its dependence on biological inputs such as tree roots, tree-throw, burrowing rodents, etc. Soil mass transport along slopes depends on several factors and occurs by gradual mechanisms such as soil creep as well as threshold (and sporadic) processes, such as landsliding. One factor of critical influence in landsliding, along with slope angle and slope shape, is the soil depth. Understanding soil depth development on steep topography is fundamental for understanding and predicting the occurrence of landsliding at threshold landscapes (Yu et al., 2019). Soils and landslides are intimately related. The weathering of bedrock into clay and the subsequent translocation of clays into subsurface horizons are the main causes of increases in the risk of landsliding (Temme, this volume). Given their mutual effects, soils and landslides form a system with feedbacks.

The dependence of soil formation on chemistry, more pronounced when reaction kinetics limits the weathering reaction (high flow rates, slowly weathering minerals), and more likely at shorter time scales (Yu & Hunt, 2017b; Egli et al., 2018), emphasizes distinctions between parent materials, rather than similarities in other soil formation factors, such as climate or relief.

The actual geochemistry is highly dependent on the symbiotic relationships between plants and fungi and microbial communities, as well as on substrate and climate. The details of these interactions are underrepresented here, both in the volume generally, and in this summary.

Hydrology, by assessing critical fluxes for both the formation of soil and its removal, unifies the fields of soil science and geomorphology, including (2D) basin architecture. This relationship provided crucial motivation to establish CUAHSI (Consortium of Universities for the Advancement of Hydrologic Science), as well as a foundation for the NRC publication "Opportunities in the Hydrologic Sciences" (NRC, 1991), which underlies the establishment of the Hydrologic Sciences Program at the USA NSF. This thematic integration with soil science occurs over increasing time scales, first geomorphology, then hydrology, and finally, tectonics, biological evolution, and atmospheric changes.

In this volume, we have attempted to address a range of such questions and, here, to draw additional attention to

one possible way forward that is, perhaps, based on a stronger foundation for soil physics.

14.6. WAYS FORWARD

The fundamental question to be answered is this:

How does bedrock, as well as such unconsolidated media as landslide deposits, glacial moraines, and alluvium, become soils, of which type and what depth, with which mineralogical transformations and physical reorientations/reorganizations, associated with which ecosystems and climates? There is no one answer nor a single course of action that results.

In considering the future of research into chemical weathering and soil formation, it is helpful to see where we are and where we have come from. From Cline (1961): "At a given time, our concepts are consequences of the knowledge we have gained, which in turn depends substantially on the techniques at our disposal. Yet those concepts govern to a major degree our approach to the solution of current problems, and thus, they control developments of the immediate future." Thus, different researchers, with their different disciplinary histories, will see different challenges, goals, and envisioned means of solution. Past thinking, with its influence on curriculum, experimental techniques, data collected, instrumentation, and archival development, has a continued influence on the present to challenge paradigm shifts. Even when a paradigm shift may be sought, a substantial divide exists across disciplines and within disciplines, between seeking solutions with a degree of universality, and those which seek to define the variability.

First, let us consider the long-standing question of whether soil should refer to the solum (A and B horizons) or also what Richter and Yaalon (2012) call the C horizon. Since this corresponds to highly weathered "saprolites" of the southeastern US, perhaps the "laterites" and "bauxites" described by other authors as due to deep tropical weathering should be incorporated as well. Yu and Hunt (2017a) already extended the percolation theory prediction of weathering depths as a function of time to deep (mostly) tropical weathering expressed as laterite or bauxite. The fundamental percolation scaling function applied was $x = x_0 (t/t_0)^{1/Db}$ (also in Figure 14.2) with exponent $D_b = 1.87$ equal to the backbone fractal dimensionality (Hunt & Ghanbarian, 2016), x_0 the fundamental length scale, or typical grain size, and t_0 the (hydrologic) mean flow rate. In Yu and Hunt (2017a), typical values of particle diameters $x_0 = 30$ μm and flow rates x_0/t_0 of 0.5 m/yr were chosen as parameters, and the prediction was compared with data from Wright (1994), Cooper (1936), Hill et al. (2000), Taylor et al. (1992), Boulange and Carvalho (1989), Freyssinet and Farah (1997), Pavich (1986), Bestland et al. (1996), and Migon and Lidmar-Bergstro (2002). Since Richter and Yaalon (2012) explicitly mention the "saprolites" of the Atlantic piedmont, we now include together with those of Yu and Hunt (2017a), in Figure 14.3 four examples of these (Price et al., 2005; Cleaves et al., 1974, Pavitch et al., 1989; Pavitch, 1986), as well as a new example from central Europe (Felix-Henningsen, 2018). As is evident, a single reasonable prediction suffices to capture the chief variability, linking time scales of up to 150 Myr with pore-scale quantities. The same equation, but with parameter values appropriate for each particular soil, generates measured soil depths across a wide range of conditions (Yu & Hunt, 2017a, 2017b, 2017c; Egli et al., 2018).

Note that, in $x = x_0(t/t_0)^{1/Db}$, the soil-forming factors are represented (Yu et al., 2017) as follows: time (t) is explicit, x_0 defines the grain size of the parent porous medium (p). The flow velocity is determined by the interaction of the biota with the climate (cl and o) (Budyko, 1958, 1974) and substrate (p, depending on where the limiting hydraulic conductivity is found). Topography (r) enters when effects of erosion are considered. Implicit is that the form of the relationship is determined by transport limitations on chemical weathering (involves cl and o), while use of the transport limitation as a general result is restricted to cases for which $Da_I > 1$.

This result is the basis for answers to most of the 13 questions in section 14.4.

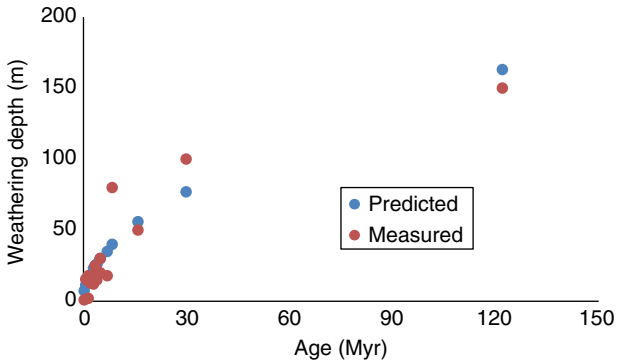

Figure 14.3 Extension of depth predictions for soils to chemical weathering at great ages for what are called "laterites," "bauxites," or "saprolites." Typical flow rates (roughly in the middle of Maher's 2010 data) of about 0.5 m yr^{-1} are assumed, along with a typical soil particle in the middle of the silt, about 30 μm and a typical porosity of 0.4. The initial predictions were tabulated in Yu and Hunt (2017b) for the data of Wright (1994), Cooper (1936), Hill et al. (2000), Taylor et al. (1992), Boulange and Carvalho (1989), Freyssinet and Farah (1997), Pavich (1986), Bestland et al. (1996), and Migon et al. (2002). New data for this synthesis include Price et al. (2005), Cleaves et al. (1974), Pavitch et al. (1989), Pavitch (1986), and Felix-Henningsen (2018). Note that these data follow the same trend as the data in the middle of the soil depths collected in Figure 14.2.

Continuing, we give some other perspectives on the study of soil evolution and chemical weathering.

First, consider geomorphology. Here soil production is inextricably linked with soil transport in shaping the landscape. The form of the soil production function, whether only decreasing with depth or humped (Gilbert, 1887; Heimsath et al., 2009), may determine the stability of soils against erosion down to bedrock. Variation in soil production rates with landscape curvature may be a consequence of the relevance of the model of soil surface transport as diffusive (Heimsath et al., 1999), rather than having anything to do with a spatially variable soil production function (Yu & Hunt, 2017c). An entire range of biologic processes related to plant (Amundson et al., 2015) and animal behavior emerges for study. These authors examined climatic influences on soil production using a ratio of mean annual precipitation (MAP) to mean annual temperature (MAT). Hunt and Ghanbarian (2016), however, found that soil production rates correlated more strongly (less scatter) to estimates of an infiltration rate using the difference between precipitation and evapotranspiration.

From the perspective of geology (e.g. Driese et al., this volume), it is essential to understand the coevolution of soil, plants, and the composition of the atmosphere through geologic time expressed in, e.g., rates of soil development and the suite of soil types found. Accordingly, these authors argue for the inclusion of a deep-time component in the Earth observatories devoted to the critical zone. Because the surface of the Earth is where humans are found, it is doubly important to trace the development of ecosystems and soil formation over geologic time and how biota adapts to and influences the evolution of the atmosphere and the terrestrial surface. The potential variety of such systems, including the soil microbiology, presents already a daunting task of classification, and even more so when the influence of extinction-triggering events, tectonic and climatic changes, and anthropogenic influences are considered. Yet, if circular inferences are avoided, the history of the Earth can, through analysis of the increasing complexity of the soil ecosystem and its geochemistry over time, reveal the impacts of various soil-forming factors individually. Such an analysis must be based on accurate forward modeling. In contrast to Amundson et al. (2015), who try to correlate the change in maximum soil production rates with the ratio of MAP/MAT, Driese et al. (this volume) extract separately MAP estimates for paleosols based on the CIA-K (chemical index of alteration less potash) geochemical proxy of Sheldon et al. (2002) and MAT estimates based on an Na/K salinization model (Driese et al., 2018; Liivamägi et al., 2014).

From the perspective of physics, what is sought are the (quasi-)universal laws or processes governing the evolution of a geophysical system. The understanding of the history of the Earth requires the best understanding of the physical processes and physical laws that underlie the evolution of the Earth, its chemistry, and its biota. In the context of the present volume, an important part of the conventional physical understanding may be flawed. For our hydrologic science, we usually rely on laws that express local conservation of mass, charge, elemental composition, momentum, energy, etc. These laws are expressed as (partial) differential equations. In these formulations, scale effects on solute transport are essentially inexplicable; they are mysteries to be explained by non-Euclidean media, for which our imagination is the only bound. In this framework, the putative link between non-Gaussian (non-Fickian) solute transport and chemical weathering went undiscovered (note that Reeves and Rothman, 2014, attribute the link between fluid flow rates and time dependences to diffusion). In order to address these problems efficiently, it is important to abandon the continuum models of porous media and turn to network models. Then, nearly all the puzzles posed in section 14.4 appear to trace back to the single conceptual model failure of representing porous media as a bundle of capillary tubes and the mathematical inadequacy of the Advection-Dispersion Equation. The solution lies not in particular models of the medium but in the tendency for water flow through disordered media to be dominated by paths of least resistance, together with the topological description of these paths from percolation theory (Hunt & Sahimi, 2017). A particular challenge in the context of soil modeling and weathering is the consideration of a dynamic comparison of climate and soil variables instead of the traditional (and arduous) comparison of climate and (static) soil properties (Finke et al., this volume).

What about the hydrological perspective? Consider water partitioning at the Earth's surface. Since evapotranspiration (ET) removes water from being used for soil formation, while encouraging plant growth, which provides an essential contribution (CO_2) to soil formation from plant metabolism, this quantity is of interest. Arguably, the variability of ecosystems and climate, substrate and relief, should produce huge variation in the water balance. Yet there seems to be a rather high degree of consistency in the fraction of precipitation returned to the atmosphere, ET, when considered as a function of aridity index (Budyko, 1958, 1974). Moreover, for landscapes neither strongly energy limited nor water limited, there is a rather universal tendency for ET to be close to the global average, just under two thirds of precipitation (Lvovitch, 1975; Williams et al., 2012; Schlesinger & Jasechko, 2015). Hunt (this volume) shows that the tendency to constrain ET may be related to an optimization of ecosystem productivity under the constraints of

optimal horizontal water (and thus nutrient) flow paths for transpiration within the root zone, and optimal (random) solute transport paths in the vertical direction. The latter defines the soil depth as well, meaning that net primary productivity is not just a passive response to the partitioning of surface water but the primary driver of it. This result makes explicit a comment from the National Research Council (1991), "The more we learn about our desiccated, and apparently barren, neighboring planets, the more we wonder if our good fortune is not a result as well as the cause of life on the earth," Furthermore, the variability in ET at a particular aridity index appears related to variability in actual root architecture (its mass fractal dimensionality). This work thus suggests that the relationship of hydrology with biota is so intertwined that the basic partitioning of water at the terrestrial Earth's surface is only properly understood in biological terms, namely that evolution favors those ecosystems that maximize their productivity with respect to the available water and energy fluxes.

Even from the perspective of soil ecology and biogeochemistry, Fierer et al. (2009) cite Kuhn (1962) to emphasize the importance of fundamental unifying principles of study, compared with a simple categorization of distinctions between specific systems and processes. They note the relatively advanced states of aquatic (citing the trophic cascade theory of Carpenter et al., 1985, and ecological stoichiometry of Elser et al., 2000) and plant ecology (structuring of plant diversity and plant community dynamics across spatial scales, e.g. Grime, 1977; Tilman, 1994; Hubbell, 2001) compared with soil ecology. Yet these same authors cite Dokuchaev (1880/1948) and Jenny (1941) as authors helping to provide a basis for the study of soil ecology. They also suggest that there are similarities across ecosystems that may warrant formulation of more general principles: "Even where disturbances such as agricultural conversion or plant invasions have altered soil properties, the underlying processes often remain remarkably similar (Haas et al., 1957; Mann, 1986; Lauber et al., 2008)." They report that the observation that "all compounds that get metabolized in soil must pass through the same physiological 'funnel' that constrains decomposition to a shared set of biochemical pathways (McGill, 2007) … may partially explain why parameters such as litter C:N ratio and lignin:N ratio can often predict decomposition rates across a range of ecosystem types."

In conclusion, it is suggested that a combination of techniques should be utilized, involving everything from advances in fundamental research in physics to experimental techniques in measurement and interpretation, classification, and generalization. Advances in one relevant discipline must be communicated to the other related disciplines. Understanding of the relationships between micro- and macrobiota will be essential, and how the soil constrains these relationships. In this process, both universal tendencies and specific distinctions must be accounted for. Presumably only then will it be possible to disentangle the effects of the multiple influences on ecosystem stability, adaptability, and vulnerability, together with their interactions with solar variability (early weak sun paradox), astronomical events (possible bolide collisions), tectonic developments, and volcanism (e.g. development of supercontinents, or release of CO_2 by the Siberian traps).

REFERENCES

Amundson, R., Heimsath, A. M., Owen, J. J., Yoo, K., & Dietrich, W. E. (2015). Hillslope soils and vegetation. *Geomorphology*, *234*, 122–132.

Anderson, R. S., & Anderson, S. P. (2010). *Geomorphology: The mechanics and chemistry of landscapes*. New York: Cambridge University Press.

Anderson, S. P., Kelly, P. J., Hoffman, N., Barnhart, K., Befus, K., & Ouimet, W. (2021). Is this steady state? Weathering and critical zone architecture in Gordon Gulch, Colorado Front Range. In A. Hunt et al. (Eds.), *Hydrogeology, chemical weathering, and soil formation* (chap. 13). Hoboken, NJ: AGU/Wiley.

Bandopadhyay, A., Le Borgne, T., Meheust, Y., & Dentz, M. (2017). Enhanced reaction kinetics and reactive mixing scale dynamics in mixing fronts under shear flow for arbitrary Damköhler numbers. *Advances in Water Resources*, *100*, 78–95.

Benson, D. A., Wheatcraft, S. W., & Meerschaert, M. M. (2000a). Application of a fractional advection-dispersion equation. *Water Resources Research*, *36*(6), 1403–1412.

Benson, D. A., Wheatcraft, S. W., & Meerschaert, M. M. (2000b). The fractional-order governing equation of Lévy motion. *Water Resources Research*, *36*(6), 1413–1423.

Berkowitz, B., Klafter, J., Metzler, R., & Scher, H. (2002). Physical pictures of transport in heterogeneous media: Advection-dispersion, random-walk, and fractional derivative formulations, *Water Resour. Res*. *38*. doi: 10.1029/2001WR001030

Berkowitz , B., & Scher, H. (1995). On characterization of anomalous dispersion in porous and fractured media, *Water Resour. Res.*, *31*, 1461–1466.

Berner, R. A. (1992). Weathering, plants, and the long-term carbon-cycle, *Geochim. Cosmochim. Acta*, *56*(8), 3225–3231.

Bestland, E. A., Retallack, G. J., Rice, A. E., & Mindszenty, A. (1996). Late Eocene detrital laterites in central Oregon, mass balance geochemistry depositional setting, and landscape evolution. *GSA Bulletin*, *108*, 285–302.

Blanco, H., & Lal, R. (2010). *Principles of soil conservation and management*. Heidelberg: Springer.

Bockheim, J. G., Gennadiyev, A. N., Hammer, R. D., & Tandarich, J. P. (2005). Historical development of key concepts in pedology. *Geoderma*, *124*, 23–36.

Boulange, B., & Carvalho, A. (1989). The genesis and evolution of the Porto Trombetas deposits in Amazon basin, Para, Brazil. *Trav. ICSOBA*, *22*, 71–79.

Brantley, S. L., Eissenstat, D. M., Marshall, J. A., Godsey, S. A., Balogh-Brunstad, Z., Karwan, D. L., et al. (2017a). Reviews and syntheses: On the roles trees play in building and plumbing the critical zone. *Biogeosciences*, *14*, 5115–5142.

Brantley, S. L., Goldhaber, M. B., & Ragnarsdottir, K. V. (2007). Crossing disciplines and scales to understand the Critical Zone. *Elements*, *3*, 307–314. doi: 10.2113/gselements.3.5.307

Brantley, S. L., McDowell, W. H., Dietrich, W. E., White, T. S., Kumar, P., Anderson, S. P., et al. (2017b). Designing a network of critical zone observatories to explore the living skin of the terrestrial Earth, *Earth Surf. Dynam., 5*, 841–860.

Budyko, M. I. (1958). *The heat balance of the earth's surface*. Washington, DC: US Dept. of Commerce, Weather Bureau.

Budyko, M. I. (1974). *Climate and life*, English ed., San Diego: Academic Press.

Burke, B. C., Heimsath, A. M., Dixon, J. L., Chappell, J., & Yoo, K. (2009). Weathering the escarpment: Chemical and physical rates and processes, southeastern Australia. *Earth Surface Processes and Landforms*, *34*, 765–785.

Burke, B. C., Heimsath, A. M., & White, A. F. (2006). Coupling chemical weathering with soil production across soil-mantled landscapes. *Earth Surf. Proc. Landf.*, *32*(6), 853–873. doi: 10.1002/esp.1443

Carpenter, S. R., Kitchell, J. F., & Hodgson, J. R. (1985). Cascading trophic interactions and lake productivity. *Bioscience*, *35*, 634–639.

Certini, G., & Scalenghe, R. (2011). Anthropogenic soils are the golden spikes for the Anthropocene. *The Holocene*, *21*, 1269–1274.

Cleaves, E. T., Fisher, D. W., & Bricker, O. P. (1974). Chemical weathering of serpentinite in the eastern piedmont of Maryland. *GSA Bulletin*, *85*, 437–444.

Cline, M. L. (1961). The changing model of soil. *Soil Science Society of America Proc*, *25*, 442– 446. doi:10.2136/sssaj1961.03615995002500060009x

Coffey, G. N. (1912). A study of the soils of the United States. *USDA Bur. of Soils Bull., 85*. Washington, DC: U.S. Govt. Print. Office.

Cooper, W.G.G. (1936). The bauxite deposits of the gold coast. *Gold Coast Geology Survey Bulletin*, *7*.

Cortis, A., & Berkowitz, B. (2004). Anomalous transport in "classical" soil and sand columns, *Soil Sci. Soc. Am. J.*, *68*, 1539–1548.

Costantini, E. (2018). Paleosols and pedostratigraphy. *Applied Soil Ecology*, *123*, 597–600.

Crutzen, P. J. (2002). The geology of mankind. *Nature*, *415*, 23–23.

Crutzen, P. J., & Stoermer, E. F. (2000). The Anthropocene. *Global Change Newsletter*, *41*, 17–18.

Cushman, J. H., & O'Malley, D. (2015). Fickian dispersion is anomalous. *J. Hydrol.* doi:10.1016/j.jhydrol.2015.06.036

Darwin, C. R. (1881). *The formation of vegetable mould through the action of worms, with observations on their habits*. London: John Murray.

DiBiase, R. A., Heimsath, A. M., & Whipple, K. X. (2012). Hillslope response to tectonic forcing in threshold landscapes. *Earth Surface Processes and Landforms*, *37*, 855–865.

Dixon, J. L., Hartshorn, A. S., Heimsath, A. M., DiBiase, R. A., Whipple, K. X. (2012). Chemical weathering response to tectonic forcing: A soils perspective from the San Gabriel Mountains, California. *Earth and Planetary Science Letters*, *323–324*, 40–49.

Dixon, J. L., Heimsath, A. M., Kaste, J., & Amundson, R. (2009). Climate-driven processes of hillslope weathering. *Geology*, *37*, 975–978.

Dixon, J. L., & von Blanckenburg, F. (2012). Soils as pacemakers and limiters of global silicate weathering. *C. R. Geosci.*, *344*, 596–609.

Dokuchaev, V. V. (1880/1948). *Russian chernozem: Selected works of V. V. Dokuchaev*, vol. I. Moskva, 1948. Translated from the Russian by Israel Program for Scientific Translations, Jerusalem, 1967.

Driese, S. G., Medaris Jr, L. G., Kirsimäe, K., Somelar, P., & Stinchcomb, G. E. (2018). Oxisolic processes and geochemical constraints on duration of weathering for Neoproterozoic Baltic paleosol. *Precambrian Research*, *310*, 165–178.

Driese, S. G., Nordt, L. C., & Stinchcomb, G. E. (2021). Soils, chemical weathering, and climate change in Earth history. In A. Hunt et al. (Eds.), *Hydrogeology, chemical weathering, and soil formation* (chap. 2). Hoboken, NJ: AGU/Wiley.

Edgeworth, M., Richter, D. D., Waters, C., Haff, P., Neal, C., & Price, S. J. (2015). Diachronous beginnings of the Antropocene: The stratigraphic bounding surface between anthropogenic and non-antthropogenic deposits. *The Anthropocene Review*, *2*, 33–58.

Egli, M., Dahms, D., & Norton, K. (2014). Soil formation rates on silicate parent material in alpine environments: Different approaches–different results? *Geoderma*, *213*, 320–333. doi: 10.1016/j.geoderma.2013.08.016

Egli, M., Hunt, A., Dahms, D., Raab, G., Derungs, C., Raimondi, S., & Fang, Y. (2018). Prediction of soil formation as a function of age using the percolation theory approach. *Frontiers in Environmental Science*, *6*, 108. doi: 10.3389/fenvs.2018.00108

Egli, M. & Mirabella, A. (2021). The origin and formation of clay minerals in Alpine soils. In A. Hunt et al. (Eds.), *Hydrogeology, chemical weathering, and soil formation* (chap. 6). Hoboken, NJ: AGU/Wiley.

Elser, J. J., Fagan, W. F., Denno, R. F., Dobberfuhl, D. R., Folarin, A., Huberty, A., et al. (2000). Nutritional constraints in terrestrial and freshwater food webs. *Nature*, *408*, 578–580.

Eppes, M. C., & Keanini, R. (2017). Peering into the cracks, *Eos*, *98*. https://doi.org/10.1029/2018EO078321. Published on 23 August 2017.

Falster, D. S., Duursma, R. A., Ishihara, M. I., Barneche, D. R., Fitzjohn, R. G., Varhammar, A., et al. (2015). BAAD, a biomass and allometry database for woody plants. *Ecological Archives*, *HO96-128*. http://esapubs.org/archive

Fan, Y., Miguez-Macho, G., Jobbágy, E. G., Jackson, R. B., & Otero-Casal, C. (2017). Hydrologic regulation of plant rooting depth. *Proceedings of the National Academy of Sciences*, *114*, doi/10.1073/pnas.1712381114

Fatt, I. (1956a). The network model of porous media. I. Capillary pressure characteristics. *Petr. Trans. AIME*, *207*, 144–159.

Fatt, I. (1956b). The network model of porous media. II. Dynamic properties of a single size tube network. *Trans. AIME*, *207*, 160–163.

Fatt, I. (1956c). The network model of porous media. III. Dynamic properties of networks with tube radius distribution. *Trans. AIME*, *207*, 164–177.

Faybishenko, B., (2010). Fuzzy-probabilistic calculations of water-balance uncertainty. *Stochastic Environmental Research and Risk Analysis*, *24*, 939–952.

Faybishenko, B., & Molz, F. (2013). Nonlinear rhizosphere dynamics yields synchronized oscillations of microbial populations, carbon and oxygen concentrations, induced by root exudation *Procedia Environmental Sciences*, *Four Decades of Progress in Monitoring and Modeling of Processes in the Soil-Plant-Atmosphere System: Applications and Challenges*, *19*, 681–690.

Felix-Henningsen, P. (2018). Field Trip D 9/27, Characteristics and development of the Mesozoic-Tertiary weathering mantle and Pleistocene periglacial slope deposits in the Hintertaunus mountainous region. *DEUQUA Spec. Pug., 1*, 53–77.

Ferrier, K. L., & Kirchner, J. W. (2008). Effects of physical erosion on chemical denudation rates: a numerical modeling study of soil-mantled hillslopes. *Earth Planet. Sci. Lett.*, *272*, 591–599.

Fierer, N., Grandy, A. S., Six, J., & Paul, E. A. (2009). Searching for unifying principles in soil ecology. *Soil Biology & Biochemistry*, *11*, 2249–2256.

Finke, P. A., Ranathunga, N., Verdoodt, A., Yu, Y. Y., & Yin, Q. Z. (2021). Unraveling loess records of climate change from the Chinese loess plateau using precess-based models. In A. Hunt et al. (Eds.), *Hydrogeology, chemical weathering, and soil formation* (chap. 8). Hoboken, NJ: AGU/Wiley.Forman, S. L., & Stinchcomb, G. E. (2015,).Views on grand research challenges for Quaternary geology, geomorphology and environments. *Frontiers in Earth Science, 3,* Article 47 doi. org/10.3389/feart.2015.00047

Freyssinet, P., & Farah, A. S. (1997). Geochemical mass balance and weathering rates of ultra-mafic rocks in Amazonian rainforest: insights from field data. *30th Int. Geological Congress, Beijing, abstract book*, p. 111.

Garcia-Fresca, B. (2007). Urban-enhanced groundwater recharge: Review and case study of Austin, Texas, USA in Urban Groundwater, Meeting the Challenge. In K.W.F. Howard (Ed.), *IAH Selected Papers on Hydrogeology, 8*. London: Taylor & Francis.

Gelhar, L. W., Welty, C., & Rehfeldt, K. R. (1992). A critical review of data on field-scale dispersion in aquifers. *Water Resour Res.*, *28*, 1955–1974.

Gentine, P., D'Pdorico, Linter, B. R., Sivandran, G., & Salvucci, G. (2012). Interdependence of climate, soil, and vegetation as constrained by the Budyko curve. *Geophys. Res. Lett.*, *39*, L19404. doi:10.1029/2012GL053492

Gilbert, G. K. (1877). *Report on the geology of Henry Mountains*. US Geological and Geographical Survey of the Rock Mountain Region. Washington, DC: U.S. Government of Printing Office.

Grime, J. (1977). Evidence for the existence of three primary strategies in plants and its relevance to ecological and evolutionary theory. *American Naturalist*, *111*, 1169–1197.

Haas, H., Evans, C., & Miles, E. (1957). Nitrogen and carbon changes in Great Plains soils as influenced by cropping and soil treatments. *Technical Bulletin #1164*. USDA State Agricultural Experiment Stations.

Hacking, I. (2012). Introduction. In T. Kuhn, *The structure of scientific revolutions*. University of Chicago Press.

Haff, P. K. (2014a). Technology as a geological phenomenon: Implications for human well-being. In C. N. Waters, Z. J. Zalasiewic, M. Williams, M. A. Ellis, & A. Snelling (Eds.), *A stratigraphical basis for the Anthropocene* (Special Publications 395, pp. 301–330). London: Geological Society.

Haff, P. K. (2014b). Humans and technology in the Anthropocene: Six rules. *The Anthropocene Review*, *1*. https://doi.org/10.1177/2053019614530575

Harris, E. C. (1979). The laws of archaeological stratigraphy. *World Archaeology*, *11*, 111–117.

Harris, E. C. (2014). Principles of archaeological stratigraphy, 2nd ed. London: Academic Press.

Hartmann, J., Moosdorf, N., Lauerwald, R., Hinderer, M., & West, J. A. (2014). Global chemical weathering and associated P-release: The role of lithology, temperature and soil properties. *Chemical Geology*, *363*, 145–163. doi: 10.1016/j.chemgeo.2013.10.025

Heimsath, A. M., Dietrich, W. E., Nishiizumi, K., & Finkel, R. C. (1997). The soil production function and landscape equilibrium. *Nature*, *388*, 358–361. doi:10.1038/41056

Heimsath, A. M., Dietrich, W. E., Nishiizumi, K., & Finkel, R. C. (1999). Cosmogenic nuclides, topography, and the spatial variation of soil depth. *Geomorphology*, *27*, 151–172. doi: 10.1016/S0169-555X(98)00095-6

Heimsath, A. M., Fink, D., & Hancock, G.R. (2009). The 'humped' soil production function: Eroding Arnhem Land, Australia. *Earth Surf. Process. Landforms*, *34*, 1674–1684. doi: 10.1002/esp.1859

Hilgard, E. W. (1860). *Report on the geology and agriculture of Mississippi*. Jackson, Mississippi: E. Barksdale, State Printer.

Hilgard, E. W. (1906). *Soils: Their formation, properties, composition, and relations to climate and plant growth in the humid and arid regions*. New York: Macmillan.

Hill, I. G., Worden, R. H., Meighan, I. G. (2000). Geochemical evolution of a palaeolaterite: The Interbasaltic Formation, Northern Ireland. *Chemical Geology*, *166*, 65–84.

Hillel, D. (2005). Soil: Crucible of life. *J. Nat. Resour. Life Sci. Educ.*, *34*, 60–61.

Horn, R. F., & Lal, R. (2021). Soils in agricultural engineering: Effect of land-use management systems on mechanical soil processes. In A. Hunt et al. (Eds.), *Hydrogeology, chemical weathering, and soil formation* (chap. 10). Hoboken, NJ: AGU/Wiley.

Hubbell, S. (2001). *The unified neutral theory of biodiversity and biogeography*. Princeton, NJ: Princeton University Press.

Huggett, R. J. (2021). Soil as a system: A history. In A. Hunt et al. (Eds.), *Hydrogeology, chemical weathering, and soil formation* (chap. 1). Hoboken, NJ: AGU/Wiley.

Humphreys, G. S., & Wilkinson, M. T. (2007). The soil production function: A brief history. *Geoderma*, *129*, 75–78.

Hunt, A. G. (2017). Spatio-temporal scaling of vegetation growth and soil formation: Explicit predictions, *Vadose Zone Journal.* doi:10.2136/vzj2016.06.0055

Hunt, A. (2021). Soil formation, vegetation growth, and water balance: A theory for Budyko. In A. Hunt et al. (Eds.),

Hydrogeology, chemical weathering, and soil formation (chap. 3). Hoboken, NJ: AGU/Wiley.

Hunt, A. G, & Ewing, R. P. (2016). Scaling. In J. H. Cushman & D. Tartakovsky (Eds.), *Handbook of groundwater engineering*, 3rd ed. Taylor & Francis.

Hunt, A. G., Ewing, R. P., & Horton, R. (2013). What's wrong with soil physics? *Soil Science Society of America Journal*, *77*(6), 1877–1887.

Hunt, A. G., & Ghanbarian, B. (2016). Percolation theory for solute transport in porous media: Geochemistry, geomorphology, and carbon cycling. *Water Resource Research*, *52*, 7444–7459. doi: 10.1002/2016WR019289

Hunt, A. G., & Sahimi, M. (2017). Flow, transport, and reaction in porous media: Percolation scaling, critical path analysis and effective-medium approximation. *Reviews of Geophysics*, *55*, 993–1078. doi: 10.1002/2017RG000558

Hunt, A. G., Skinner, T. E., Ewing, R. P., & Ghanbarian-Alavijeh, B. (2011). Dispersion of solutes in porous media, *Eur. Phys. J. B, 80*, 411–432.

Jenny, H. (1941). *Factors of soil formation: A system of quantitative pedology*. New York: Dover.

Joffe, J. S. (1936). *Pedology*. New Brunswick, NJ: Rutgers University Press.

Johnson, D. L., & Schaetzl, R. J. (2015). Differing views of soil and pedogenesis by two masters, Darwin and Dokuchaev. *Geoderma*, *237–238*, 176–189.

Kuhn, T. (1962). *The structure of scientific revolutions*. Chicago: Univ. of Chicago Press.

Lal, R. (2004). Soil carbon sequestration impacts on global climate change and food security. *Science*, *304*, 1623–1627. doi: 10.1126/science.1097396

Larsen, I. J., Almond, P. C., Eger, A., Stone, J. O., Montgomery, D. R., & Malcolm, B. (2014). Rapid soil production and weathering in the Southern Alps, New Zealand. *Science*, *343*, 637–640. doi: 10.1126/science.1244908

Lauber, C. L., Strickland, M. S., Bradford, M. A., & Fierer, N. (2008). The influence of soil properties on the structure of bacterial and fungal communities across land-use types. *Soil Biology & Biochemistry*, *40*, 2407–2415.

Le Bayon, R.-C., Bullinger, G., Schomburg, A., Turberg, P., Brunner, P., Schlaepfer, R., & Guenat, C. (2021). Earthworms, plants, and soils. In A. Hunt et al. (Eds.), *Hydrogeology, chemical weathering, and soil formation* (chap. 4). Hoboken, NJ: AGU/Wiley.

Liivamägi, S., Somelar, P., Mahaney, W. C., Kirs, J., Vircava, I., & Kirsimäe, K. (2014). Late Neoproterozoic Baltic paleosol: Intense weathering at high latitude? *Geology*, *42*(4), 323–326.

Liu, C., Shi, Z., & Zachara, J. M. (2009). Kinetics of Uranium(VI) desorption from contaminated sediments: Effect of geochemical conditions and model evaluation. *Environ. Sci. Technol.*, *43*, 6560–6566.

Liu, C., Zachara, J. M., Qafoku, N. P., & Wang, Z. (2008). Scale-dependent desorption of uranium from contaminated subsurface sediments. *Water Resour. Res.*, *44*, W08413.

Lukens, C. E., & Norton, K. E. (2021). Tephra for the trees? Geochemical constraints on weathering and tephra inputs to soils on New Zealand's North Island. In A. Hunt et al. (Eds.), *Hydrogeology, chemical weathering, and soil formation* (chap. 5). Hoboken, NJ: AGU/Wiley.

Lvovitch, M. I. (1973). The global water balance: U.S. National Committee for the International Hydrological Decade. *U.S. National Committee for the International Hydrological Decade Bulletin*, *23*, 28–42. doi: 10.1029/EO054i001p00028

Lyon, T. L., & Buckman, H. O. (1922). *The nature and properties of soils: A textbook of edaphology*. New York: Macmillan.

Lyons, W. B., Leslie, D. L., & Gooseff, M. N. (2021). Chemical weathering in the McMurdo dry valleys, Antarctica. In A. Hunt et al. (Eds.), *Hydrogeology, chemical weathering, and soil formation* (chap. 11). Hoboken, NJ: AGU/Wiley.

Maher, K. (2010). The dependence of chemical weathering rates on fluid residence time. *Earth and Planetary Science Letters*, *294*, 101–110.

Mann, L. K. (1986). Changes in soil carbon storage after cultivation. *Soil Science*, *142*, 279–288.

McGill, W. (2007). The physiology and biochemistry of soil organisms. In E. A. Paul (Ed.), *Soil microbiology, ecology, and biochemistry*. New York: Academic Press.

Migon, P., & Lidmar-Bergstro, K. (2002). Deep weathering through time in central and northwestern Europe: Problems of dating and interpretation of geological record. *Catena*, *49*, 25–40.

Montgomery, D. (2007a). Soil erosion and agricultural sustainability. *Proceedings of the National Academy of Sciences 104*, 13268–13272. doi: 10.1073/pnas.0611508104

National Research Council. (1991). *Opportunities in the hydrologic sciences*. Washington, DC: The National Academies Press. https://doi.org/10.17226/1543.

National Research Council. (2001). *Basic research opportunities in earth science*. Washington, DC: National Academies Press.

Nicolis, G., & Prigogine, I. (1989). *Exploring complexity*. New York: W.H. Freeman.

Pavich, M. J. (1986). Processes and rates of saprolite production and erosion on a foliated granitic rock of the Virginia Piedmont. In S. M. Colman & D. P. Dethier (Eds.), *Rates of chemical weathering of rocks and minerals* (pp. 551–590). New York: Academic Press.

Pavich, M. J. (1989). Regolith residence time and the concept of surface age of the Piedmont "peneplain," *Geomorphology*, *2*, 181–196.

Pavich, M. J., Brown, L., Valette-Silver, J. N., Klein, J., & Middleton, R. (1989). 10Be analysis of a Quaternary weathering profile in the Virginia piedmont. *Geomorphology*, *2*, 181–196.

Peng, S., Hu, Q., Ewing, R. P., Liu, C., & Zachara, J. M. (2012). Quantitative 3-D elemental mapping by LA-ICP-MS of a basaltic clast from the Hanford 300 area, Washington, USA. *Envir. Sci. Technol.*, *46*, 2025–2032.

Price, J. R., Velbel, M. A., & Patino, L. (2005). Rates and time scales of clay-mineral formation by weathering in saprolitic regoliths of the southern Appalachians from geochemical mass balance. *GSA Bulletin*, *117*, 783–794.

Prigogine, I. (1980). *From being to becoming: Time and complexity in the physical sciences*. New York: W.H. Freeman.

Ramann, E. (1911). *Bodenkunde*. Berlin: Verlag Julius Springer.

Ramann, E. (1928). *The evolution and classification of soils*. London: W. Heffer & Sons Limited.

Rasmussen, T. C., Foroughi, M., & Markewitz, D. (2021). Carbon and nutrient fluxes within southeastern Piedmont

critical zones. In A. Hunt et al. (Eds.), *Hydrogeology, chemical weathering, and soil formation* (chap. 12). Hoboken, NJ: AGU/Wiley.

Redfield, A. C. (1958). The biological control of chemical factors in the environment. *American Scientist*, Contribution No. 976, 205–221. Woods Hole Oceanographic Institution.

Reeves, D., & Rothman, D. H. (2014). Diffusion and kinetic control of weathering layer development. *Geofluids*, *14*, 128–142.

Reiners, P. W., Ehlers, T. A., Mitchell, S. G., Montgomery, D. R. (2003). Coupled spatial variations in precipitation and long-term erosion rates across the Washington Cascades. *Nature*, *426*, 645–647.

Richter, D. D., & Markewitz, D. (1995). How deep is soil? *Bioscience*, *45*, 600–609.

Richter, D. D., & Yaalon, D. H. (2012). "The Changing Model of Soil" revisited. *Soil Science Society of America Journal*, *76*, 766–778.

Sak, P. B. (2021). Weathering rinds as tools for constraining reaction kinetics and duration of weathering at the clast-scale. In A. Hunt et al. (Eds.), *Hydrogeology, chemical weathering, and soil formation* (chap. 7). Hoboken, NJ: AGU/Wiley.

Salehikhoo, F., Li, L., & Brantley, S. (2013). Magnesite dissolution rates at different spatial scales: The role of mineral spatial distribution and flow velocity. *Geochimica et Cosmochimica Acta*, *108*, 91–106.

Scheidegger, A. E. (1959). An evaluation of the accuracy of the diffusivity equation for describing miscible displacement in porous media. In *Proc. Theory of Fluid Flow in Porous Media Conf.,* Univ. Oklahoma. pp. 101–116.

Schlesinger, W. H., Jasechko, S. (2014). Transpiration in the global water cycle. *Agr. Forest. Meteorol.*, *189*, 115–117.

Sheldon, N. D., Retallack, G. J., & Tanaka, S. (2002). Geochemical climofunctions from North American soils and application to paleosols across the Eocene-Oligocene boundary in Oregon. *The Journal of Geology*, *110*(6), 687–696.

Steffen, W., Richardson, K., Rockström, J., Cornell, S. E., Fetzer, I., Bennett, E. M., et al. (2015). Planetary boundaries: Guiding human development on a changing planet. *Science*, *347*, 736. doi: 10.1126/science.1259855

Taha, H. (1997). Albedo, evapotranspiration, and anthropogenic heat. *Energy and Buildings*, *25*, 99–103.

Taylor, G., Eggleton, R. A., Holzhauer, C. C., Maconachie, L. A., Gordon, M., Brown, M. C., McQueen, K. G. (1992). Cool climate lateritic and bauxitic weathering. *The Journal of Geology*, *100*, 669–677.

Taylor, L. L., Quirk, J., Thorley, R.M.S., Kharecha, P. A., Hansen, J., Ridgwell, A., et al. (2016). *Nature Climate Change*, *6*, 402–406.

Temme, A.J.A.M. (2021). Relations between soil development and landslides. In A. Hunt et al. (Eds.), *Hydrogeology, chemical weathering, and soil formation* (chap. 9). Hoboken, NJ: AGU/Wiley.

Tian, H., Chen, G., Zhang, C., Melillo, J. M., & Hall, C.A S. (2010). Pattern and variation of C:N:P ratios in China's soils: A synthesis of observational data. *Biogeochemistry*, *98*, 139–151.

Tilman, D. (1994). Competition and biodiversity in spatially structured habitats. *Ecology*, *75*, 2–16.

Vernadsky, V. I. (1926). *Biosphere*. Leningrad: Chem-Tech. Publ. House.

West, A. J., Galy, A., & Bickle, M. (2005). Tectonic and climatic controls on silicate weathering. *Earth Planet. Sci. Lett.*, *235*, 211–228.

Wilcove, D. S., Giam, X., Edwards, D. P., Fisher, B., & Koh, L. P. (2013). Navjot's nightmare revisited: Logging, agriculture, and biodiversity loss in Southeast Asia. *Trends in Ecology and Evolution*, *28*, 531–540.

White, A. F., & Brantley, S. L. (2003). The effect of time on the weathering of silicate minerals: Why do weathering rates differ in the laboratory and field? *Chemical Geology*, *202*, 479–506.

Williams, C. A., Reichstein, M., Buchmann, N., Baldocchi, D., Beer, C., Schwalm, C., et al. (2012). Climate and vegetation controls on the surface water balance: Synthesis of evapotranspiration measured across a global network of flux towers. *Water Resources Research*, *48*, W06523. doi:10.1029/2011WR011586

Wright, V. P. (1994). Losses and gains in weathering profiles and duripans. In A. Parker, B. W. Sellwood (Eds.), *Quantitative diagenesis: Recent developments and applications to reservoir geology*, NATO ASI series. Series C, Mathematical and Physical Sciences, *453*, 95–123.

Young, I. M., & Crawford, J. W. (2004). Interactions and self-organization in the soil-microbe complex. *Science*, *304*, 1634–1637.

Yu, F., Faybishenko, B., Hunt, A. G., & Ghanbarian-Alavijeh, B. (2017). A simple model of the variability of soil depths. *Water*, *9*, 460. doi: 10.3390/w9070460

Yu, F., & Hunt, A. G. (2017a). An examination of the steady-state assumption in soil development models with application to landscape evolution. *Earth Surface Processes and Landforms*, *42*, 2599–2610. doi: 10.1002/esp.4209

Yu F., & Hunt, A. G. (2017b). Damköhler number input to transport-limited chemical weathering calculations. *ACS Earth and Space Chemistry*, *1*, 30–38. doi: 10.1021/acsearthspacechem.6b00007

Yu F., & Hunt, A. G. (2017c). Predicting of soil formation on the basis of transport-limited chemical weathering. *Geomorphology*, *201*, 21–27. doi: 10.1016/j.geomorph.2017.10.027

Yu, F., Hunt, A., Egli, M., & Raab, G. (2019). Comparison and contrast in soil depth evolution for steady-state and stochastic erosion processes: Possible implications for landslide prediction. *Geochemistry, Geophysics, Geosystems G³*, *20*, 2886–2906. https://doi.org/10.1029/2018GC008125

Zhong, L., Liu, C., Zachara, J. M., Kennedy, D. W., Scezcody, J. E., & Wood, B. (2005). Oxidative remobilization of biogenic Uranium(IV) precipitates: Effects of iron(II) and pH. *J. Environmental Quality*, *34*, 1763–1771.

INDEX

Hydrogeology, Chemical Weathering, and Soil Formation, Geophysical Monograph 257, First Edition.
Edited by Allen Hunt, Markus Egli, and Boris Faybishenko.

DOI: 10.1002/9781119563952.index

WILEY END USER LICENSE AGREEMENT

Go to www.wiley.com/go/eula to access Wiley's ebook EULA.